Marcelo Di Carli · Maurizio Dondi
Raffaele Giubbini · Diana Paez
Paolo Raggi · Michelle Williams
Editors

IAEA Atlas of Cardiac PET/CT

A Case-Study Approach

Second Edition

IAEA
International Atomic Energy Agency

OPEN ACCESS

Springer

Marcelo Di Carli • Maurizio Dondi
Raffaele Giubbini • Diana Paez
Paolo Raggi • Michelle Williams
Editors

IAEA Atlas of Cardiac PET/CT

A Case-Study Approach

Second Edition 2027

Springer

IAEA
International Atomic Energy Agency

Editors
Marcelo Di Carli
Brigham and Women's Hospital
Boston, MA, USA

Raffaele Giubbini
Nuclear Medicine
International Specialized Hospital
of Uganda (ISHU)
Kampala, Uganda

Paolo Raggi
Division of Cardiology
University of Alberta
Edmonton, AB, Canada

Maurizio Dondi
Division of Human Health
International Atomic Energy Agency
Vienna, Austria

Diana Paez
Division of Human Health
International Atomic Energy Agency
Vienna, Austria

Michelle Williams
British Heart Foundation Centre for Research
Excellence, Institute for Neuroscience and
Cardiovascular Research
University of Edinburgh
Edinburgh, United Kingdom



ISBN 978-3-662-74187-0 ISBN 978-3-662-74188-7 (eBook)
https://doi.org/10.1007/978-3-662-74188-7

This work was supported by International Atomic Energy Agency.

1st edition: © IAEA: International Atomic Energy Agency 2022
2nd edition: © IAEA: International Atomic Energy Agency 2027. This book is an open access publication.

The opinions expressed in this publication are those of the authors/editors and do not necessarily reflect the views of the IAEA: International Atomic Energy Agency, its Board of Directors, or the countries they represent.
Open Access This book is licensed under the terms of the Creative Commons Attribution 3.0 IGO license (http://creativecommons.org/licenses/by/3.0/igo/), which permits use, sharing, adaptation, distribution and reproduction in any medium or format, as long as you give appropriate credit to the IAEA: International Atomic Energy Agency, provide a link to the Creative Commons license and indicate if changes were made.
Any dispute related to the use of the works of the IAEA: International Atomic Energy Agency that cannot be settled amicably shall be submitted to arbitration pursuant to the UNCITRAL rules. The use of the IAEA: International Atomic Energy Agency's name for any purpose other than for attribution, and the use of the IAEA: International Atomic Energy Agency's logo, shall be subject to a separate written license agreement between the IAEA: International Atomic Energy Agency and the user and is not authorized as part of this CC-IGO license. Note that the link provided above includes additional terms and conditions of the license.
The images or other third party material in this book are included in the book's Creative Commons license, unless indicated otherwise in a credit line to the material. If material is not included in the book's Creative Commons license and your intended use is not permitted by statutory regulation or exceeds the permitted use, you will need to obtain permission directly from the copyright holder.
Unless otherwise expressly agreed by the Publisher in writing, the Publisher does not authorize use or reproduction of all or any part of this work in any manner for the purpose of training, fine-tuning, evaluating, or developing artificial intelligence models, technologies, or systems. In accordance with Article 4(3) of the EU Directive 2019/790 on copyright and related rights in the Digital Single Market, the Publisher expressly reserves all rights with respect to this work under the text and data mining exception of the directive.
The use of general descriptive names, registered names, trademarks, service marks, etc. in this publication does not imply, even in the absence of a specific statement, that such names are exempt from the relevant protective laws and regulations and therefore free for general use.
The publisher, the authors and the editors are safe to assume that the advice and information in this book are believed to be true and accurate at the date of publication. Neither the publisher nor the authors or the editors give a warranty, expressed or implied, with respect to the material contained herein or for any errors or omissions that may have been made. The publisher remains neutral with regard to jurisdictional claims in published maps and institutional affiliations.

This Springer imprint is published by the registered company Springer-Verlag GmbH, DE, part of Springer Nature.
The registered company address is: Heidelberger Platz 3, 14197 Berlin, Germany

If disposing of this product, please recycle the paper.

Preface

Cardiovascular diseases (CVDs) remain the leading cause of death globally, with over 18 million deaths annually, and ischemic heart disease (IHD) accounting for approximately 16% of all global mortality. Despite progress in prevention and treatment, disparities persist, particularly in low- and middle-income countries.

Among the 17 million premature deaths (under age 70) due to noncommunicable diseases (NCDs), CVDs account for 37%, underscoring their impact on younger populations. Regional variations in risk factor prevalence, healthcare infrastructure, and socioeconomic conditions continue to influence outcomes.

In alignment with the United Nations Sustainable Development Goals (SDGs), particularly Goal 3.4, which aims to reduce premature mortality from NCDs by 30% by 2030, the International Atomic Energy Agency (IAEA) supports Member States through initiatives that strengthen medical imaging services. The Nuclear Medicine and Diagnostic Imaging Section within the Division of Human Health plays a pivotal role in promoting nuclear cardiology, ensuring appropriate use, and maintaining high standards of clinical practice.

Cardiac PET/CT is a powerful non-invasive imaging modality that enables accurate diagnosis, risk stratification, and management of various cardiac conditions. While SPECT myocardial perfusion imaging (MPI) remains widely available and accepted, the adoption of PET/CT has been slower due to cost, limited scanner availability, and its predominant use in oncology. According to the IAEA Medical imAGIng and Nuclear Medicine global resources database (IMAGINE), over 5,600 PET/CT scanners are installed worldwide, primarily used for oncological indications. Expanding their use to cardiology requires targeted education, policy support, and increased awareness among referring physicians.

Addressing these challenges requires a multi-faceted approach involving cost-effectiveness analyses, industry collaboration, and tailored educational initiatives. Regional differences further influence adoption: while usage is increasing in the United States, Europe faces slower transitions from SPECT to PET due to ownership models and educational gaps. In other regions, resource constraints and funding limitations remain significant obstacles.

In response to this global challenge, the IAEA continues to support Member States in strengthening nuclear cardiology services. The first edition of the *IAEA Atlas of Cardiac PET/CT: A Case-Based Approach*, published in April 2022, has been downloaded over 36,000 times, reflecting its value to practitioners worldwide. This second edition builds upon that foundation, offering an expanded and updated collection of case studies that illustrate the clinical utility of cardiac PET/CT across a wide spectrum of indications.

The Atlas is organized to reflect the breadth of cardiac PET/CT applications across clinical scenarios. It begins with foundational principles and artifact recognition, followed by cases addressing ischemic heart disease, coronary microvascular dysfunction, myocardial viability, heart failure, heart transplantation, inflammatory and infiltrative cardiomyopathies, infectious processes, vasculitides, and cardiotoxicity related to cancer therapies. The final chapter explores emerging directions in cardiac PET/CT, including plaque imaging and theranostic approaches.

Each case is presented in a structured format, including clinical history, imaging findings, teaching points, and suggested management. This case-based approach aims to equip practitioners with practical insights to enhance clinical decision-making and patient care across diverse healthcare settings.

References

- International Atomic Energy Agency, IAEA Atlas of Cardiac PET/CT: A Case-Study Approach. Springer, Berlin (2022).
- World Health Organization. (n.d.-a). Global health estimates: Leading causes of death. https://www.who.int/data/gho/data/themes/mortality-and-global-health-estimates/ghe-leading-causes-of-death. Accessed October 10, 2025.
- World Health Organization. (n.d.-b). Cardiovascular diseases. https://www.who.int/news-room/fact-sheets/detail/cardiovascular-diseases-(cvds). Accessed October 10, 2025.
- IAEA Medical imaging and nuclear medicine global resources database (IMAGINE). (n.d.). https://humanhealth.iaea.org/HHW/DBStatistics/IMAGINEMaps.html. Accessed October 10, 2025.
- International Atomic Energy Agency, Nuclear Cardiology: Guidance on the Implementation of SPECT Myocardial Perfusion Imaging, IAEA Human Health Series No. 23 (Rev. 1), IAEA, Vienna (2016)
- Arumugam P, Better N, Keng FY, Allam A, Gimelli A, et al. Current state and challenges of implementing a cardiac positron emission tomography program outside North America. J Nucl Cardiol. 2024 Jan; 31:101788. doi:10.1016/j.nuclcard.2023.101788. Epub 2023 Dec 12. PMID: 38215599.
- Peix A, Mesquita CT, Gutiérrez C, Puente A, Dueñas-C KA, et al. Current status of nuclear cardiology practice in Latin America and the Caribbean, in the era of multimodality cardiac imaging approach: 2022 update. Nucl Med Commun. 2022 Dec 1;43(12):1163-1170.

Vienna, Austria Diana Paez

Acknowledgments

The editors would like to thank Mr Selemo Craviolatti and Ms. Erika Minoshima for their assistance during the meetings and for their contribution to the language editing.

Contents

1 Basic Principles of Cardiac PET 1
Paolo Raggi, Marcelo Di Carli, Michelle Williams, Raffaele Giubbini, Diana Paez, Maurizio Dondi, and Marina Piccinelli

1.1 PET Radiotracers for Myocardial Perfusion Imaging 2
1.1.1 ^{82}Rubidium 2
1.1.2 ^{13}N-Ammonia 3
1.1.3 ^{15}O-Labeled H_2O 3
1.1.4 ^{18}F-Flurpiridaz 3
1.2 Perfusion Imaging Protocols 4
1.3 Image Reorientation and Display 5
1.4 Quantitative Nuclear Cardiology 6
1.4.1 Relative Perfusion Quantification and Segmental Scoring 6
1.5 Myocardial Blood Flow Quantification 7
1.5.1 Global Left Ventricular Function 10
1.6 Cardiac PET/CT for Metabolic and Inflammation Imaging 11
1.6.1 Myocardial Viability Imaging Protocol 11
1.6.2 Cardiac Sarcoidosis Imaging Protocol 12

2 Artifacts 15
Marcelo Di Carli, Raffaele Giubbini, Michelle Williams, Diana Paez, Maurizio Dondi, Paolo Raggi, Erick Alexanderson, Isabel Carvajal, Elisa Milan, and Carole Kounga

2.1 Misregistration: Case 1 15
2.2 Patient Motion: Case 2 17
2.3 Cardiac Motion Artifacts: Case 3 19
2.4 Ammonia Lateral Defect: Case 4 22
2.5 Nonresponder to Coronary Vasodilators: Case 5 23
2.6 Vasodilator Non-responsiveness Mimic: Case 6 25
2.7 Metal Artifact in Hot Spot Imaging: Case 7 29
2.8 Recognizing and Troubleshooting Artifacts with Flow Quantification 31
2.8.1 Radiotracer Injection 31
2.8.2 Problems with the Timing of the Arterial Blood Input Curve 32
2.8.3 Patient Motion 32
2.8.4 Residual Activity Correction 33
2.8.5 Vasodilator Non-responsiveness 33
2.8.6 Vasodilator Non-responsiveness Mimic 37

3 Evaluation of Ischemic Heart Disease 39
Marcelo Di Carli, Raffaele Giubbini, Michelle Williams, Paolo Raggi, Vasvi Singh, Erick Alexanderson, Isabel Carvajal, Andrew Thornton, Raymond Endozo, Carlo Rodella, Diana Paez, and Maurizio Dondi

3.1 Multi-parametric Evaluation of Ischemic Heart Disease 40
3.1.1 Normal PET MPI: Case 8 40
3.1.2 Single-Vessel Disease: Case 9 41

3.1.3 Single-Vessel Disease: Case 10 . . . 43
3.1.4 Single-Vessel Obstructive Disease MPI: Case 11 . . . 46
3.1.5 Multivessel Disease: Case 12 . . . 47
3.1.6 No Coronary Artery Calcium with Abnormal PET: Case 13 . . . 49
3.1.7 High Coronary Artery Calcium Score with Normal PET: Case 14 . . . 51
3.1.8 Very High Coronary Artery Calcium Score with Normal MBF: Case 15 . . . 53
3.1.9 Abnormal PET MPI in a Patient with Typical Chest Pain and Normal SPECT: Case 16 . . . 54
3.1.10 Multivessel Disease: Case 17 . . . 57
3.1.11 High-Risk Scan: Case 18 . . . 59
3.1.12 Reclassification to Multivessel Disease by Integrating Flow Quantification: Case 19 . . . 61
3.2 Challenging Cases Integrating Perfusion CAC and Flow . . . 62
3.2.1 High-Risk Scan Myocardial Perfusion PET Scan: Case 20 . . . 62
3.2.2 Investigating Angina Post Percutaneous Coronary Intervention: Case 21 . . . 65
3.2.3 Equivocal Coronary CT Angiography and Normal PET: Case 22 . . . 68
3.3 Patient with Known Coronary Artery Disease . . . 70
3.3.1 Prior PCI: Case 23 . . . 70
3.3.2 Prior CABG: Case 24 . . . 72
3.3.3 Evaluation of a Patient with Prior Myocardial Infarction: Case 25 . . . 73
3.3.4 Evaluation of a Patient with Prior Myocardial Infarction: Case 26 . . . 74
3.3.5 Evaluation of Chest Pain in a Patient Post PCI: Case 27 . . . 77
3.3.6 Example of a Case with ^{15}Oxygen Water PET/CT: Case 28 . . . 79
3.4 Evaluation of Medical Therapy . . . 80
3.4.1 Reassessment After Optimized Medical Therapy: Case 29 . . . 80

4 Coronary Microvascular Disease . . . 85
Marcelo Di Carli, Raffaele Giubbini, Paolo Raggi, Michelle Williams, Diana Paez, Maurizio Dondi, Vasvi Singh, and Zhiyuan Ou
4.1 Without Atherosclerosis . . . 85
4.1.1 Hypertensive Heart Disease: Case 30 . . . 85
4.1.2 Aortic Stenosis: Case 31 . . . 87
4.1.3 Septal Hypertrophic Cardiomyopathy: Case 32 . . . 88
4.1.4 Apical Hypertrophic Cardiomyopathy: Case 33 . . . 90
4.1.5 Stress Cardiomyopathy: Takotsubo: Case 34 . . . 92
4.2 Nonobstructive Atherosclerosis . . . 95
4.2.1 Diabetes Mellitus: Case 35 . . . 95
4.2.2 Obesity and Coronary Microvascular Dysfunction: Case 36 . . . 97
4.2.3 Heart Failure with Preserved Ejection Fraction (HFpEF): Case 37 . . . 99
4.2.4 Coronary Microvascular Dysfunction in Systemic Inflammatory Disorders: Case 38 . . . 100

5 Heart Failure and Myocardial Viability . . . 103
Marcelo Di Carli, Paolo Raggi, Raffaele Giubbini, Michelle Williams, Diana Paez, Maurizio Dondi, and Carlo Rodella
5.1 Mismatch SPECT/CT Perfusion-PET/CT FDG: Case 39 . . . 103
5.2 Mismatch PET/CT Perfusion-PET/CT FDG: Case 40 . . . 106
5.3 Match PET/CT Perfusion-PET/CT FDG: Case 41 . . . 107
5.4 Rest-Stress Perfusion and Viability Imaging: Case 42 . . . 108
5.5 End-Stage Ischemic Cardiomyopathy: Case 43 . . . 110
5.6 Severe Left Ventricular Dysfunction and Unknown CAD: Case 44 . . . 111
5.7 Incremental Value of Stress Testing to Differentiate Ischemic vs. Nonischemic CM in a Patient with CAD: Case 45 . . . 112

6 Heart Transplantation . . . 115
Marcelo Di Carli, Paolo Raggi, Michelle Williams, Raffaele Giubbini, Diana Paez, and Maurizio Dondi
6.1 Evaluation of Possible Coronary Allograft Vasculopathy (CAV) . . . 115
6.1.1 Without CAV: Case 46 . . . 115
6.2 Mild CAV: Case 47 . . . 117
6.3 Severe CAV: Case 48 . . . 119

7 Inflammatory and Infiltrative Cardiomyopathies . . . 123
Marcelo Di Carli, Raffaele Giubbini, Paolo Raggi, Michelle Williams, Diana Paez, Maurizio Dondi, and Sanjay Divakaran
7.1 Cardiac Sarcoidosis: Likelihood . . . 124
7.1.1 Low Probability of Cardiac Sarcoidosis: Case 49 . . . 124
7.1.2 Possible Cardiac Sarcoidosis: Case 50 . . . 126
7.1.3 Probable Isolated Cardiac Sarcoidosis: Case 51 . . . 127
7.1.4 Highly Probable Cardiac Sarcoidosis: Case 52 . . . 129
7.2 Cardiac Sarcoidosis: Complementary Value of 18F-FDG PET and MRI . . . 131
7.2.1 Cardiac Sarcoidosis and Coronary Artery Disease: Case 53 . . . 131
7.2.2 Cardiac Sarcoidosis on PET/MRI: Case 54 . . . 134
7.3 Differential Diagnosis: Sarcoidosis Mimic . . . 136
7.3.1 Arrhythmogenic Cardiomyopathy: Case 55 . . . 136
7.4 Risk Stratification by ^{18}F-FDG PET . . . 138
7.4.1 Possible Cardiac Sarcoidosis: Case 56 . . . 138
7.4.2 Highly Probable Cardiac Sarcoidosis: Case 57 . . . 139
7.5 Evaluation of Response to Therapy . . . 140
7.5.1 Evaluation of Response to Therapy: Case 58 . . . 140
7.5.2 Evaluation of Response to Therapy: Case 59 . . . 142
7.6 Fabry's Disease . . . 143
7.6.1 Fabry's Disease: Not Yet Diagnosed: Case 60 . . . 143
7.6.2 Fabry's Disease: Case 61 . . . 145
7.7 Amyloidosis . . . 149
7.7.1 Amyloidosis: Case 62 . . . 149

8 Infection . . . 153
Marcelo Di Carli, Raffaele Giubbini, Paolo Raggi, Michelle Williams, Elisa Milan, Ayaz Aghayev, Nazarena Pizzi, Albert Roque, Paola Anna Erba, Roberto Boni, Antonio Celestino, Elena Busnardo, Marianna Spallino, Irene Gotuzzo, Diana Paez, and Maurizio Dondi
8.1 Suspected Prosthetic Valve Endocarditis (PVE) . . . 153
8.1.1 Prosthetic Valve Endocarditis: Case 63 . . . 153
8.1.2 Prosthetic Valve Endocarditis with Contrast CT: Case 64 . . . 155
8.1.3 Prosthetic Valve Endocarditis After Mechanical Valve Replacement: Case 65 . . . 157
8.1.4 Prosthetic Valve Endocarditis in TAVI: Case 66 . . . 158
8.1.5 Bioprosthetic Pulmonary-Valved Graft Infection in a Patient with CHD: Case 67 . . . 159
8.1.6 Aortic Graft Infection: Case 68 . . . 161
8.1.7 Native Valve Endocarditis: Case 69 . . . 162
8.1.8 Native Valve Endocarditis in a Pediatric Patient: Case 70 . . . 164
8.1.9 Focal Abscess Before and After Antibiotic Therapy: Case 71 . . . 166
8.2 Device Infection . . . 168
8.2.1 Generator Pocket and Lead Infection: Case 72 . . . 168
8.2.2 Device Infection in Patient with Amyloidosis: Case 73 . . . 169
8.2.3 Generator Pocket Infection, Cardiac Device Infection: Case 74 . . . 171

8.2.4 Identifying Source of Infection with Whole-Body PET/CT (False Positive with and Without Attenuation Correction): Case 75 173
8.2.5 Left Ventricular Assist Device (LVAD) Driveline Infection: Case 76 . . . 175
8.2.6 Assessing Infection in a Left Ventricular Assist Device: Case 77 177

9 Vasculitides 181
Paolo Raggi, Marcelo Di Carli, Michelle Williams, Raffaele Giubbini, Diana Paez, Maurizio Dondi, Erick Alexanderson, Isabel Carvajal, Ayaz Aghayev, Alison Clifford, Dan Pugh, and Neeraj Dhaun
9.1 Assess Response to Therapy in Vasculitis: Case 78. 182
9.2 Large Vessel Vasculitis: Case 79 185
9.3 Immunoglobulin G4 Vasculitis: Case 80 186
9.4 Takayasu Arteritis: Case 81 188
9.5 Giant Cell Arteritis: Case 82 190
9.6 Multimodality Imaging in Giant Cell Arteritis: Case 83 191
9.7 PET/MRI for Diagnosis and Monitoring of Large Vessel Vasculitis: Case 84. . . 193

10 Cardiac Toxicity After Chemo/Radiation 197
Raffaele Giubbini, Paolo Raggi, Marcelo Di Carli, Michelle Williams, Diana Paez, Maurizio Dondi, Elisa Milan, Francesco Lanfranchi, Matteo Bauckneht, and Gianmario Sambuceti
10.1 After Chemotherapy for Hodgkin's Lymphoma: Case 85 197
10.2 Pericarditis After Chemotherapy: Case 86. 199
10.3 Incidental Findings of Cardiac Masses 200
10.3.1 Cardiac Metastasis from Prostate Cancer Detected with 18F-PSMA-1007: Case 87. 200
10.4 ^{68}Ga-DOTATOC PET/CT in Metastatic Neuroendocrine Tumors: Case 88 . . . 202

11 Future Directions 205
Michelle Williams, Marcelo Di Carli, Paolo Raggi, Raffaele Giubbini, Diana Paez, Maurizio Dondi, Mouaz Al-Mallah, Olivier Clerc, Sharmila Dorbala, Jason Zelt, Christiane Wiefels, Rob de Kemp, Yoshito Kadoya, Neil Craig, Marc R. Dweck, Beth Whittington, Anna Barton, Marta Peverelli, Christopher Wall, Jason M. Tarkin, Andrej Ćorović, Craig Balmforth, and David Newby
11.1 NEW TRACER for Myocardial Perfusion Imaging 206
11.1.1 ^{18}F-Flurpiridaz 206
11.1.2 Example of Case with Flurpiridaz: Case 89 206
11.2 Molecular Radiotracers for Cardiovascular Imaging. 209
11.2.1 ^{18}F-Sodium Fluoride. 209
11.2.2 ^{68}Gallium-DOTATATE. 209
11.2.3 ^{18}Fluoride-GP1. 209
11.2.4 ^{68}Gallium-FAPI 209
11.2.5 ^{11}Carbon-Meta-hydroxyephedrine 210
11.3 Cardiac Amyloidosis 210
11.3.1 Differentiating Transthyretina Amyloidosis (ATTR) from Light Chain Amyloidosis (AL) Amyloidosis with SPECT/CT and PET/CT: Case 90. 210
11.3.2 Cardiac Imaging in AL Amyloidosis: Case 91 212
11.3.3 ^{124}I-Evumetazide Targeted Tracer: Case 92 214
11.4 Molecular Imaging. 215
11.4.1 ^{18}F-Sodium Fluoride in Coronary Artery Disease: Case 93. 215
11.4.2 1^{18}F-Sodium Fluoride in Aortic Valve Disease: Case 94 216

11.5 Thrombus Imaging 218
11.5.1 Thrombus Imaging of Pulmonary Embolism: Case 95 218
11.5.2 Apical Left Ventricle Thrombus Post-Myocardial Infarction: Case 96 219
11.5.3 Thrombus Imaging of Prosthetic Material: Case 97 221
11.5.4 Thrombus Imaging of Prosthetic Valves with ^{18}F-GP1: Case 98 222
11.6 Fibrosis Imaging 224
11.6.1 ^{68}Ga-FAPI Fibrosis Imaging in Aortic Valve Disease: Case 99 224
11.6.2 ^{68}Ga-FAPI Imaging of Fibrosis Post-Myocardial Infarction: Case 100 226
11.7 Vascular Inflammation Imaging 227
11.7.1 Takayasu Arteritis PET/MRI Imaging: Case 101 227
11.7.2 Inflammation After Myocardial Infarction: Case 102 228
11.7.3 Lymphocitic Myocarditis: Case 103 230
11.8 Imaging of Cardiac Sympathetic Innervation 231
11.8.1 Denervation in Large Anterior Infarction and Ischemic Cardiomyopathy: Case 104 231
11.8.2 Denervation in Medium-Size Infero-lateral Myocardial Infarction: Case 105 233
11.9 Total Body PET 234
11.9.1 Cardioembolic Stroke: Case 106 234

Contributors

Ayaz Aghayev Brigham and Women's Hospital, Boston, MA, USA

Erick Alexanderson Instituto Nacional de Cardiologia Ignacio Chavex, Mexico City, Mexico

Mouaz Al-Mallah De Bakey Heart and Vascular Center, Houston, TX, USA

Craig Balmforth British Heart Foundation Centre for Research Excellence, University of Edinburgh, Edinburgh, UK

Anna Barton Heart & Lung Research Institute, University of Cambridge, Cambridge, UK

Matteo Bauckneht Department of Health Sciences (DISSAL), University of Genova, Genoa, Italy

Roberto Boni Nuclear Medicine, ASST Papa Giovanni XXIII Bergamo and University of Milano Bicocca, Milan, Italy

Elena Busnardo Nuclear Medicine Department – San Raffaele Hospital, Milan, Italy

Isabel Carvajal Instituto Nacional de Cardiologia Ignacio Chavex, Mexico City, Mexico

Antonio Celestino Nuclear Medicine, ASST Papa Giovanni XXIII Bergamo and University of Milano Bicocca, Milan, Italy

Olivier Clerc Brigham and Women's Hospital, Boston, MA, USA

Alison Clifford University of Alberta, Edmonton, AB, Canada

Andrej Ćorović Heart & Lung Research Institute, University of Cambridge, Cambridge, UK

Neil Craig British Heart Foundation Centre for Research Excellence, University of Edinburgh, Edinburgh, UK

Rob de Kemp University of Ottawa Heart Institute, Ottawa, ON, Canada

Neeraj Dhaun British Heart Foundation Centre for Research Excellence, University of Edinburgh, Edinburgh, UK

Marcelo Di Carli Brigham and Women's Hospital, Boston, MA, USA

Sanjay Divakaran Brigham and Women's Hospital, Boston, MA, USA

Maurizio Dondi Division of Human Health, International Atomic Energy Agency, Vienna, Austria

Sharmila Dorbala Brigham and Women's Hospital, Boston, MA, USA

Marc R. Dweck British Heart Foundation Centre for Research Excellence, University of Edinburgh, Edinburgh, UK

Raymond Endozo Institute of Nuclear Medicine, University College London Hospital, London, UK

Paola Anna Erba Nuclear Medicine, ASST Papa Giovanni XXIII Bergamo and University of Milano Bicocca, Milan, Italy

Raffaele Giubbini Nuclear Medicine, International Specialized Hospital of Uganda (ISHU), Kampala, Uganda

Irene Gotuzzo Nuclear Medicine, ASST Papa Giovanni XXIII Bergamo and University of Milano Bicocca, Milan, Italy

Yoshito Kadoya University of Ottawa Heart Institute, Ottawa, ON, Canada

Carole Kounga Brigham and Women's Hospital, Boston, MA, USA

Francesco Lanfranchi Department of Health Sciences (DISSAL), University of Genova, Genoa, Italy

Elisa Milan Nuclear Cardiology Lab and PET Centre, Treviso Hospital, Treviso, Italy

David Newby British Heart Foundation Centre for Research Excellence, University of Edinburgh, Edinburgh, UK

Zhiyuan Ou University of Alberta, Edmonton, AB, Canada

Diana Paez Division of Human Health, International Atomic Energy Agency, Vienna, Austria

Marta Peverelli Heart & Lung Research Institute, University of Cambridge, Cambridge, UK

Marina Piccinelli Emory School of Medicine, Department of Radiology and Imaging Sciences, Atlanta, GA, USA

Nazarena Pizzi Vall d'Hebron University Hospital, Barcelona, Spain

Dan Pugh British Heart Foundation Centre for Research Excellence, University of Edinburgh, Edinburgh, UK

Paolo Raggi Division of Cardiology, University of Alberta, Edmonton, AB, Canada

Carlo Rodella Department of Medical Physics, Spedali Civili Brescia, Brescia, Italy

Albert Roque Vall d'Hebron University Hospital, Barcelona, Spain

Gianmario Sambuceti Department of Health Sciences (DISSAL), University of Genova, Genoa, Italy

Vasvi Singh Midwest Heart and Vascular Specialists, HCA Midwest Health, Kansas City, MO, USA

Marianna Spallino Nuclear Medicine, ASST Papa Giovanni XXIII Bergamo and University of Milano Bicocca, Milan, Italy

Jason M. Tarkin Heart & Lung Research Institute, University of Cambridge, Cambridge, UK

Andrew Thornton Institute of Nuclear Medicine, University College London Hospital, London, UK

Christopher Wall Heart & Lung Research Institute, University of Cambridge, Cambridge, UK

Beth Whittington British Heart Foundation Centre for Research Excellence, University of Edinburgh, Edinburgh, UK

Christiane Wiefels University of Ottawa Heart Institute, Ottawa, ON, Canada

Michelle Williams British Heart Foundation Centre for Research Excellence, Institute for Neuroscience and Cardiovascular Research, University of Edinburgh, Edinburgh, United Kingdom

Jason Zelt Department of Medicine, University of Ottawa, Ottawa, ON, Canada

List of Abbreviations

^{11}C-HED	^{11}Carbon-meta-hydroxyephedrine
^{13}NH3	^{13}Nitrogen-Ammonia
^{15}O-H2O	^{15}Oxygen-Labeled Water
^{18}F-Flu	^{18}Fluorine-flurpiridaz
^{18}F-GP1	^{18}Fluoride-GP1
^{18}F-NaF	^{18}F-Sodium Fluoride
^{68}GA	^{68}Gallium
^{68}Ga-DOT	^{68}Gallium-Dotatate
^{82}Rb	^{82}Rubidium
AAV	Antineutrophil Cytoplasmic Antibody Associated Vasculitis
AC	Attenuation Correction
AICD	Automatic Implantable Cardioverter Defibrillator
AIF	Arterial Input Function
AL	Light Chain
ANCA	Antineutrophil Cytoplasmic Antibody
ARB	Angiotensin II Receptor Blocker
BD	Behcet's Disease
CACS	Coronary Artery Calcium Score
CAD	Coronary Artery Disease
CAV	Coronary Allograft Vasculopathy
CCTA	Coronary CT Angiography
CDRIE	Cardiac Device Related Infective Endocarditis
CFC	Coronary Flow Capacity
CFR	Coronary Flow Reserve
CMD	Coronary Microvascular Dysfunction
CRP	C-reactive Protein
CS	Cardiac Sarcoidosis
CT	Computed Tomography
CV	Cryoglobulinemic Vasculitis
CVDs	Cardiovascular Diseases
ECG	Electrocardiogram
ED	End Diastole
EDV	End Diastolic Volume
EF	Ejection Fraction
ENT	Ear, Nose and Throat
ES	End Systole
ESR	Erythrocyte Sedimentation Rate
ESV	End Systolic Volume
FAP	Fibroblast Activation Protein
FAPI	Fibroblast activation Protein-specific Inhibitors
FDG	F-fluorodeoxyglucose
FFR	Fractional Flow Reserve

GBM	Glomerular Basement Membrane
GCA	Giant Cell Arteritis
G-CSF	Granulocyte Colony Stimulating Factor
GLA	Galactosidase Alpha
GLS	Global longitudinal Strain
GPA	Granulomatosis with Polyangiitis
HFpEF	Heart Failure with preserved Ejection Fraction
HL	Hodgkin's Lymphoma
HLA	Horizontal Long Axis
HUV	Hypocomplementemia Urticarial Vasculitis
IAEA	International Atomic Energy Agency
IF	Input Function
IHDs	Ischemic Heart Disease
KD	Kawasaki's Disease
LAD	Left Anterior Descending artery
LCX	Left Circumflex
LM	Left Main coronary artery
LOR	Line Of Response
LV	Left Ventricle
LVAD	Left Ventricular Assist Device
LVEDV	Left Ventricular End-Diastolic Volume
LVEF	Left Ventricular Ejection Fraction
LVV	Large Vessel Vasculitides
MBF	Myocardial Blood Flow
MC1	Mitochondrial-Complex 1
MFR	Myocardial Flow Reserve
MPA	Microscopic Polyangiitis
MPI	Myocardial Perfusion Imaging
MRI	Magnetic Resonance Imaging
MVV	Medium Vessel Vasculitides
NCDs	Noncommunicable Diseases
NET	Neuroendocrine Tumor
NET-1	Norepinephrine Reuptake Transporter
NMC	Non-motion Corrected
PAN	Polyarteritis Nodosa
PET/CT	Positron Emission Tomography/Computed Tomography
PET/CTA	Positron Emission Tomography with Computed Tomography Angiography
PET-MPI	Positron Emission Tomography Myocardial Perfusion Imaging
PFR	Peak Filling Rate
PVE	Prosthetic Valve Endocarditis
RA	Rheumatoid Arthritis
RCA	Right Coronary Artery
RF	Retention Fraction
RFR	Relative Flow Reserve
ROIs	Regions Of Interest
RPP	Rate-Pressure Product
SA	Short Axis
SDGs	Sustainable Development Goals
SDS	Summed Difference Score
SLE	Systemic Lupus Erythematosus
SPECT	Single-Photon Emission Computed Tomography
SRS	Summed Rest Score
SSS	Summed Stress Score

SST2	Somatostatin Receptor 2
STIR	Short-Tau-Inversion-Recovery
SUV	Standardized Uptake Value
SV	Stroke Volume
SVV	Small Vessel Vasculitides
TACs	Time Activity Curves
TAK	Takayasu Arteries
TAVI	Transcatheter Aortic Valve Implantation
TAVI-IE	Transcatheter Aortic Valve Implantation Infective Endocarditis
TID	Transient Ischemic Dilation
TNF	Tumour Necrosis Factor
TOCA	Tyrosine^3-octreotate
TOE	Transoesophageal Echocardiography
TPD	Total Perfusion Deficit
VAC	Vacuum-Assisted Closure
VLA	Vertical Long Axis
WHO	World Health Organization

Basic Principles of Cardiac PET

1

Paolo Raggi, Marcelo Di Carli, Michelle Williams, Raffaele Giubbini, Diana Paez, Maurizio Dondi, and Marina Piccinelli

Objectives

- To understand the fundamental principles of positron emission tomography (PET) technology and its application in cardiac imaging.
- To recognize the advantages of PET imaging, including its quantitative nature, superior sensitivity, and higher spatial and temporal resolution, compared with other nuclear modalities.
- To learn about the integration of PET with computed tomography (CT) and its impact on cardiovascular imaging.
- To comprehend the process of positron emission, annihilation, and detection of γ-rays in PET imaging.
- To explore the main clinical applications of PET in assessing myocardial perfusion, viability, metabolism, and innervation.

Positron emission tomography (PET) has significantly advanced the understanding of cardiac anatomy, biology, and pathophysiology. Given its inherently quantitative nature, superior sensitivity, and higher spatial and temporal resolution when compared with other nuclear modalities, it is widely considered the "gold standard" for noninvasive assessments of various cardiovascular functions such as myocardial perfusion, viability, metabolism, and innervation. Hybrid devices combining PET technology and computed tomography (CT) imaging have rapidly spread worldwide, a success that originated in oncology but soon extended to cardiovascular imaging. In this chapter, we provide an overview of the physical principles behind PET technology and image formation and introduce its main clinical applications.

Specific to PET imaging, during decay, PET radiotracers emit positrons: a positively charged subatomic particle also known as the positive electron. After emission, a positron travels a short distance, known as *positron range*, before colliding with an electron. The higher the positron energy, the longer the distance it travels before annihilation, and the lower the image resolution. The collision of a positron with an electron causes annihilation of the positron, and it is followed by the release of a pair of 511 keV photons (γ-rays) that travel in opposite directions along what is commonly called *the line of response* (LOR). These high-energy photons are captured in coincidence by opposing detectors organized in rings around the patient (Fig. 1.1).

All authors have no conflict of interest to disclose.

P. Raggi
Division of Cardiology, University of Alberta, Edmonton, AB, Canada

M. Di Carli
Brigham and Women's Hospital, Boston, MA, USA
e-mail: mdicarli@bwh.harvard.edu

M. Williams
British Heart Foundation Centre for Research Excellence, Institute for Neuroscience and Cardiovascular Research, University of Edinburgh, Edinburgh, United Kingdom
e-mail: michelle.williams@ed.ac.uk

R. Giubbini
Nuclear Medicine, International Specialized Hospital of Uganda (ISHU), Kampala, Uganda
e-mail: raffaele.giubbini@unibs.it

D. Paez · M. Dondi (✉)
Division of Human Health, International Atomic Energy Agency, Vienna, Austria
e-mail: d.paez@iaea.org; m.dondi@iaea.org

M. Piccinelli
Emory School of Medicine, Department of Radiology and Imaging Sciences, Atlanta, GA, USA

© The Author(s) 2027
M. Di Carli et al. (eds.), *IAEA Atlas of Cardiac PET/CT*, https://doi.org/10.1007/978-3-662-74188-7_1

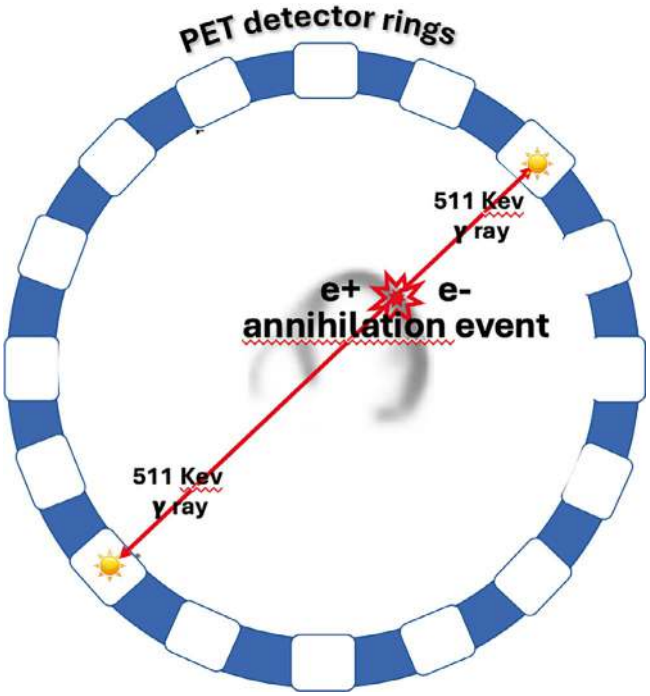


Fig. 1.1 PET imaging technology: the diagram depicts the principles of annihilation and coincidence detection

Table 1.1 Basic PET and SPECT characteristics

	PET	SPECT
Routine attenuation correction	+++	+
Spatial resolution	4–7 mm	12–15 mm
Radiation dose	1.5–4 mSv	3–11 mSv
Study duration	25–90 min	1–3 h
Absolute MBF quantification	+++	Ongoing research
Feasibility with exercise stress	+	+++
Cost	+++	+
Availability	+	+++

MBF myocardial blood flow

The goal of PET imaging is to accurately detect (spatially and temporally) all γ-rays that have arisen during annihilation and reconstruct the distribution of radioactivity inside the body. Data is initially displayed in sinograms but are subsequently reconstructed in 2D or 3D images.

Compared with single photon emission computed tomography (SPECT), PET systems demonstrate enhanced sensitivity, advanced image reconstruction techniques with noise reduction, and routinely applied correction algorithms (Table 1.1).

These factors translate into higher spatial and contrast resolution, a decrease in the radiation dose administered to the patient, and shorter acquisition times. Additionally, due to its high temporal resolution, PET can generate dynamic sequences to track tracer kinetics through the myocardium and compute absolute myocardial blood flow (MBF) in mL/min/gram of tissue. Extensive literature has demonstrated that MBF and myocardial flow reserve (MFR), computed as stress over rest flow, provide insights into early stages of coronary artery disease (CAD), coronary microvascular dysfunction, and long-term prognosis.

1.1 PET Radiotracers for Myocardial Perfusion Imaging

PET radiotracers have a relatively short half-life, and for many of them, an on-site cyclotron is required for production and prompt utilization. In PET, the most commonly used myocardial perfusion imaging (MPI) radiotracers are rubidium-82 (^{82}Rb), nitrogen-13 ammonia (^{13}NH3), and oxygen-15 labeled water (^{15}O-H_2O). Additionally, fluorine-18 flurpiridaz (^{18}F-Flu) was recently introduced to the market.

In addition to their physical characteristics (such as half-life or positron range), two additional parameters describe the physiologic properties of a perfusion radiotracer: the extraction fraction (EF) of the tracer from blood to tissue and retention fraction (RF) of the tracer into the myocardium. The ideal perfusion tracer exhibits 100% EF and 100% RF over a wide range of blood flow values indicating a linear relationship between true MBF and measured tracer activity. All currently available PET tracers have suboptimal EF (particularly at higher flow rates) and RF, and corrections are necessary during absolute MBF calculations.

Table 1.2 summarizes the basic properties and physical characteristics of the most commonly used PET MPI radiotracers.

1.1.1 ^{82}Rubidium

^{82}Rb is the most frequently used tracer for PET MPI (it accounts for over 90% of PET studies performed in North America), and it does not require an on-site cyclotron. The radiotracer can be produced by a relatively small ^{82}Sr/^{82}Rb generator coupled to an elution system with a life of 4–8 weeks depending on the commercial supplier. ^{82}Rb is a potassium analog and is similarly taken up by myocytes by active transport via the Na+/K+ ATPase pump. It has a short half-life of 75.5 s and a positron range of 8.6 mm, resulting in lower image spatial resolution when compared with other PET MPI radiotracers. ^{82}Rb has a moderate stress EF ~35% (which increases at resting conditions) and moderate stress RF ~25% due to early washout. Nevertheless, reliable correction methods have been implemented and tested, and ^{82}Rb PET-derived MBF has been shown to provide significant incremental diagnostic and prognostic information over relative perfusion assessment. Given its short half-life, ^{82}Rb is not compatible with exercise stress, and hyperemic conditions are induced with a pharmacological stress agent. The

Table 1.2 Basic properties of PET MPI tracers

	^{82}Rubidium	^{13}N Ammonia	^{15}O-water	^{18}F Flurpiridaz
Production method	Generator	On-site or nearby cyclotron	On-site cyclotron	Regional cyclotron
Positron range (mm)	8.6	2.53	4.14	1.03
Half-life (min)	1.25	9.96	2.06	110
Image/contrast resolution	Lowest	Intermediate-high	Intermediate	Highest
Stress/rest extraction fraction (%)	35/70	90/100	100/100	95/100
Stress/rest retention fraction (%)	25/70	50/90	0/0	55/90
Dosage per study (MBq)	925–1850	740	370–740	92–111 (rest) 222–240 (pharmacological stress) 333–351 (exercise stress)

injected activity is typically the same for rest and stress imaging and ranges between 925 and 1850 MBq per study resulting in an effective radiation dose to the patient of <5.0 mSv.

1.1.2 ^{13}N-Ammonia

^{13}NH3 is taken up by the myocytes through a passive mechanism of free diffusion across cell membranes as NH3 reaches equilibrium with its charged version (NH4) and gets trapped inside the cell after conversion to ^{13}N-glutamine. It has a physical half-life of 9.96 min, and it requires an on-site or nearby cyclotron. Its positron range is 2.53 mm resulting in intermediate-to-high image spatial resolution and quality. ^{13}NH3 exhibits favorable kinetic properties with a stress EF > 90% over a wide range of flow values, so that only small corrections are necessary for accurate MBF quantification. Stress RF is ~50% due to relatively rapid washout. Due to its longer half-life and smaller positron range, ^{13}NH3 images are of higher quality compared with ^{82}Rb, with higher spatial and contrast resolution. Conversely, image quality can be degraded by liver and lung uptake; lung activity in particular can interfere with CT image co-registration for attenuation correction. The diagnostic performance of ^{13}NH3 for the detection of obstructive CAD is similar to that of ^{82}Rb PET. While the physical characteristics of the tracer are compatible with exercise stress, pharmacological stress is primarily performed. The injected dose activity is commonly set at 740 MBq per study with a radiation dose to the patient of <5.0 mSv.

1.1.3 ^{15}O-Labeled H_2O

Water behaves as a freely diffusible inert gas. It crosses capillary and cell membranes and quickly reaches equilibrium between blood and myocardial tissue. These characteristics make it the ideal agent for blood flow quantification with an EF = 100%. However, it is not metabolically retained in tissues (RF = 0%), and consequently it is not used for conventional perfusion imaging. Similarly, the creation of gated images for the investigation of cardiac function is also not commonly performed with this tracer. ^{15}O-H_2O has been primarily used as the tracer of reference to validate accurate measurements of MBF in a variety of pathophysiological conditions, including cardiovascular diseases. Its physical half-life is 2.06 min, requiring an on-site cyclotron. Its positron range is 4.14 mm, resulting in intermediate image resolution between ^{13}NH3 and ^{82}Rb. The fusion of ^{15}O-H_2O PET-derived MBF maps and coronary CT angiography has shown very high diagnostic power for the detection of obstructive CAD. Due to its short life, stress MPI is usually performed with a pharmacologic agent. Injected activity ranges between 370 and 740 MBq per study with an effective radiation dose to the patient of 1–2 mSv.

1.1.4 ^{18}F-Flurpiridaz

^{18}F-Flurpiridaz is the newest PET MPI radiotracer, which the FDA approved after the completion of a phase III clinical trial. The tracer binds to the mitochondrial complex 1 (MC1). Animal as well as human studies showed a very rapid myocardial uptake and a relatively slow washout. ^{18}F-Flurpiridaz shows very favorable kinetics with an EF >95% during stress, slightly higher than ^{13}NH3, and stable retention in the tissue with RF ~ 55%. It has a half-life of 110 min, allowing production in regional cyclotrons and delivery to imaging centers as unit doses. The positron range of ^{18}F-Flurpiridaz is 1.03 mm, which leads to higher spatial image resolution, image quality and contrast, and increased confidence in image interpretation compared with other radiotracers. In a seminal phase III trial, ^{18}F-flurpiridaz showed better sensitivity for detection of coronary artery stenosis ≥50% than Tc-99 m SPECT (72% vs 54%, $p < 0.001$), but similar specificity (76.2 vs 86.6%, P = NS)[41]. ^{18}F-Flurpiridaz's half-life is compatible with exercise stress, at the expense of measuring MBF, which relies on the quantification of tracer concentration in the blood from the time of injection. Injected activity is 92.5–111 MBq for rest, 222–240.5 MBq for pharmacological stress, and 333–351.2 MBq for exercise stress, with an average effective radiation dose to patients of 4.8–6.4 mSv.

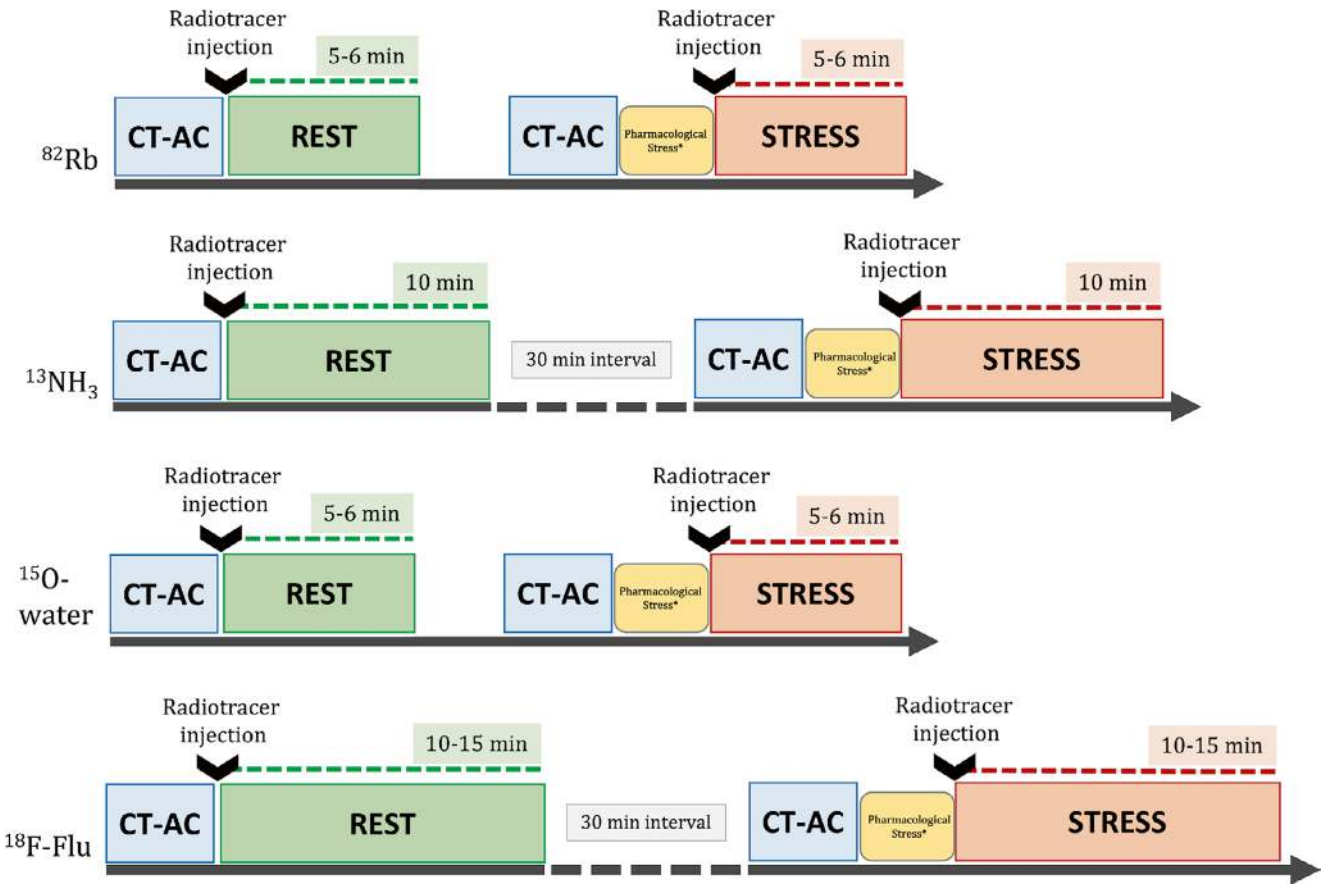


Fig. 1.2 Image acquisition protocols for PET/CT myocardial perfusion imaging with common tracers and pharmacological stress: ^{82}rubidium, ^{13}N ammonia, ^{15}O-water, and ^{18}F-flurpiridaz. Modalities to induce hyperemic conditions vary depending on the stressor selected (see text). The diagram highlights differences in timing and intervals for each tracer's imaging protocol, important for planning cardiac stress tests. *AC* attenuation correction, *CT* computed tomography

1.2 Perfusion Imaging Protocols

The protocols for image acquisition with each of the tracers discussed in the previous section are summarized in Fig. 1.2.

Patient preparation is the same as for MPI using SPECT: fasting for at least 4 h, no smoking for at least 4 h, and avoidance of caffeine intake for at least 12 h prior to the test. PET MPI is commonly conducted as a same-day rest-stress study sequence. Isolated stress imaging is rarely performed. The total acquisition time varies depending on the radiotracer and on the necessary time interval between rest and stress, but a complete study can usually be conducted in less than 1 h. While the physical properties of some tracers may be compatible with exercise, pharmacological stress is commonly required for MBF quantification as image acquisition should start at the time of tracer injection (or a few seconds earlier) to properly reconstruct the time-dependent changes of tracer concentration in the blood and myocardium. Common pharmacological stressors are dipyridamole (intravenous infusion of 0.56 mg/kg for 4 min, followed by radiotracer injection 3–5 min after completion of stressor infusion), adenosine (intravenous infusion of 140 μg/kg/min for 4–6 min and radiotracer injection at mid infusion), and regadenoson (single intravenous bolus injection of 0.4 mg followed by 10 mL of saline flush and the radiotracer). The first step consists in the acquisition of a low-dose non-contrast CT transmission scan to be used for tissue attenuation correction, followed by the injection of a rest dose of the selected radiotracer. The imaging acquisition usually starts a few seconds before radiotracer injection. Acquisition time varies according to the radiotracer used: 5–6 min for ^{82}Rb and ^{15}O-water, 10 min for $^{13}NH_3$, and 10–15 min for ^{18}F-Flu. When using ^{82}Rb and ^{15}O-water, the stress phase can be started right after the rest acquisition. Due to the longer half-life of $^{13}NH_3$ and ^{18}F-Flu, the stress acquisition is routinely delayed for 30 min to allow for tracer decay. Prior to the stress phase, a second attenuation CT scan is acquired, followed by vasodilator stress or physical stress depending on radiotracer selection and preference to perform or not perform MBF quantification. Image acquisition should start a few seconds before the injection of the stress dose of radiotracer. With recent PET/CT scanners, raw data is commonly collected from the

PET scanner in list mode, which keeps track of time and position of each coincidence event and its occurrence on the electrocardiogram (ECG) signal.

The data are used to reconstruct retrospectively static, gated, and dynamic images. Static images are high-count statistic reconstructions obtained by summing all data after a predefined delay following radiotracer injection to focus on the myocardial tissue phase of the acquisition; they are commonly used for relative perfusion assessment. Gated images are created at multiple phases of the cardiac cycle by combining data from ECG information; they provide data on cardiac function and wall motion. Dynamic images are obtained by serial temporal sampling at different times after injection; they are used to compute absolute MBF. The temporal sampling scheme should be carefully selected as it allows to properly track the time-dependent changes of tracer concentration throughout the arterial and tissue phases: Intervals are usually shorter at the beginning of the acquisition to capture the rapidly evolving arterial phase and the peak in blood tracer concentration, while they are longer during the more slowly changing migration of the radiotracer into the myocardium.

1.3 Image Reorientation and Display

Images should be reoriented and displayed as follows:

A short-axis (SA) view, by slicing perpendicular to the long axis of the left ventricle (LV) from the apex to the base

A vertical long-axis (VLA) view, by slicing vertically from the septum to the lateral wall

A horizontal long-axis (HLA) view, by slicing from the inferior to the anterior wall

For a correct interpretation of stress/rest image sets of SA, VLA and HLA images are displayed aligned and next to each other (Fig. 1.3).

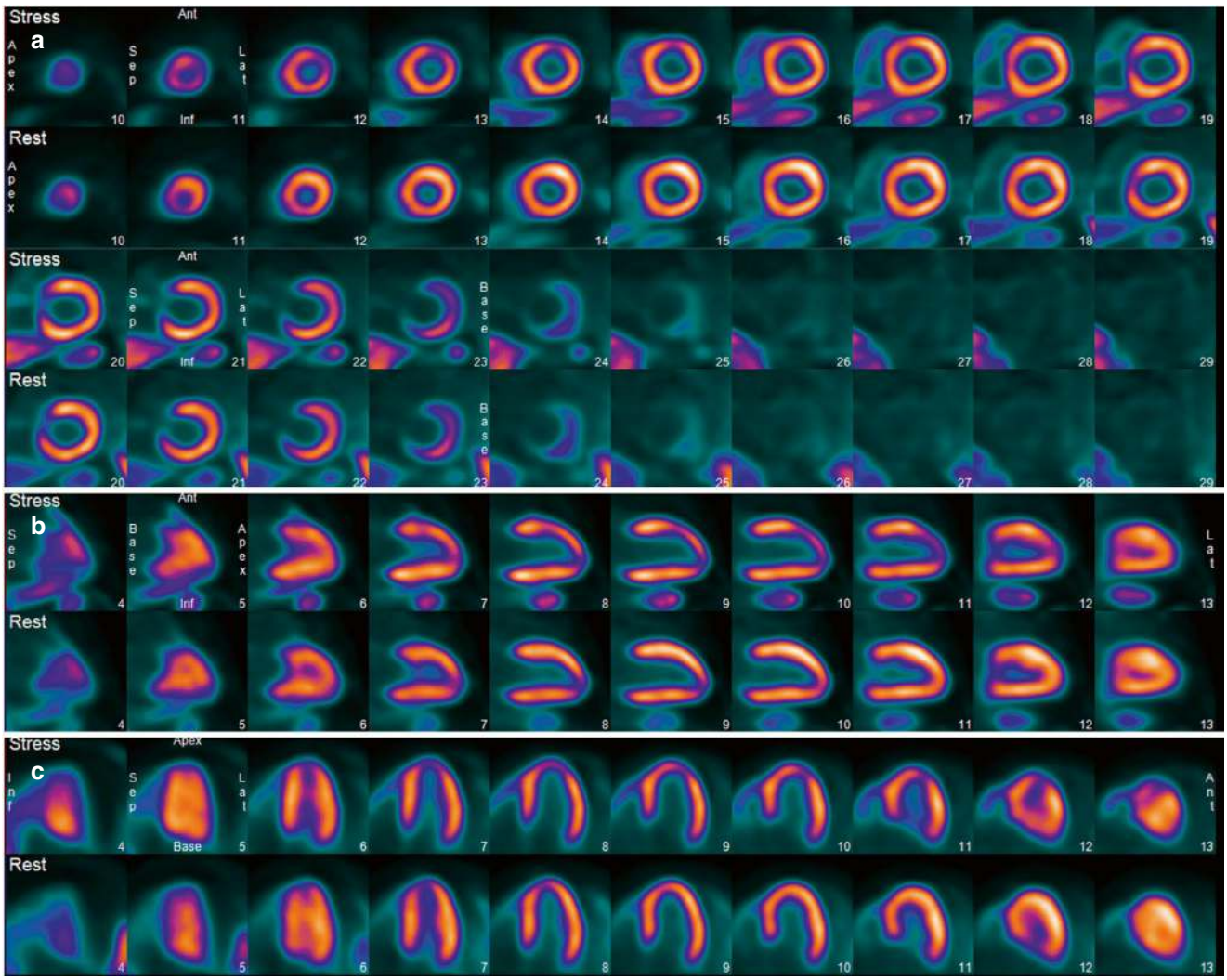


Fig. 1.3 Standard views for reorientated cardiac nuclear images. Stress images are displayed in the top row, and rest images in the bottom row of each set

1.4 Quantitative Nuclear Cardiology

1.4.1 Relative Perfusion Quantification and Segmental Scoring

Perfusion quantification is typically performed for the diagnosis and/or risk stratification of obstructive CAD. It relies on the identification of a relative difference between stress and rest images and on their comparison to normal limits created from perfusion studies of subjects with low likelihood of disease. The first step is the extraction of the perfusion distribution from each SA image as circumferential profiles extracted as mid wall maximal counts. The concentric profiles are mapped onto the rings of a 2D polar map that concisely represents the entire LV, with the external rings of the polar map representing the counts distribution at the base, while the center of the polar map is obtained from the LV apex. Crucial in the creation of the relative perfusion map is the identification of areas with the highest tracer uptake as the most normal and the normalization of all other LV regions to this value. The polar map is further subdivided into standard vascular territories and segments, according to the widely used 17-segment model. While it is recognized that the anatomy of the coronary tree varies among individuals, the model proposes a fixed assignment of segments to the three major vascular territories: the left anterior descending artery (LAD), the left circumflex (LCX), and the right coronary artery (RCA). Figure 1.4 shows the mapping of 3D perfusion data onto a bidimensional polar map representation; the generic 17-segment model and its subdivision in standard vascular territories are also displayed.

To detect areas of hypoperfusion, a patient's normalized 3D perfusion distribution is compared with the lower limits of normal quantified in terms of mean and standard deviation on the normal database. To quantify the degree of abnormality, each segment's perfusion is scored with a value from 0 (normal) to 4 (absent). Global indexes of LV perfusion have been developed and validated and are routinely used by physicians: summed stress score (SSS) and summed rest score (SRS), obtained by adding all individual scores on the 17-segment map of the LV, and the percentage of LV at risk, obtained as SSS divided by the maximum summed value (4x17 = 68). From a clinical perspective, a SSS <4 suggests a mild and likely insignificant abnormality; increasing SSS values reflect greater perfusion defects with SSS > 13 denoting a severe abnormality. These quantifications are fully automated: individual segment scores and global indexes are typically reported on the polar map.

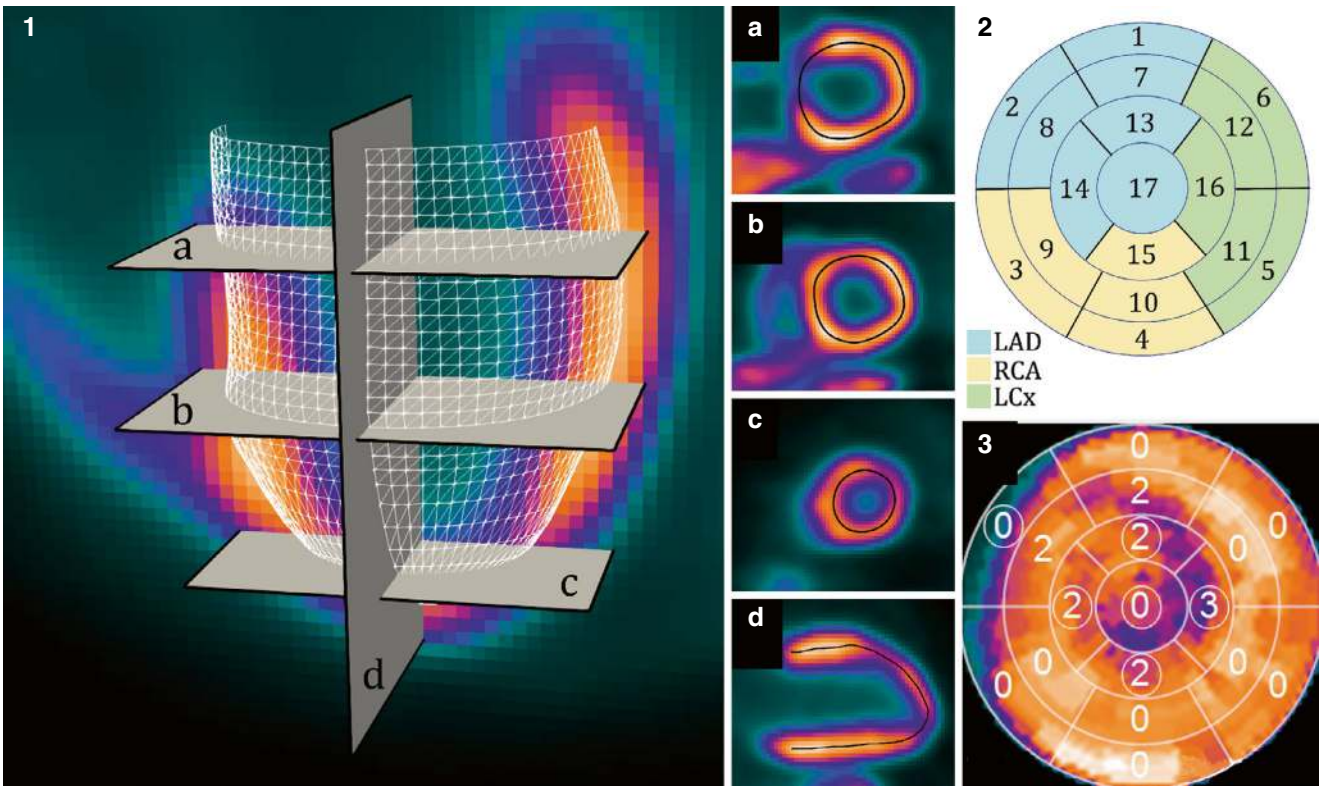


Fig. 1.4 Mapping of myocardial perfusion distributions into polar maps. 1) mid-wall maximum count circumferential distribution profiles are extracted from SA images base to apex (**a**–**c**) and mapped into concentric rings in a 2D polar map from outer to inner layers; apical is distribution obtained from long-axis views (**d**) and mapped onto the central element. 2) Generic 17-segment. 3) Example of polar map

The extent of hypoperfusion is commonly displayed on blackout polar maps, where the areas that fall below the lower limits of normality are highlighted in black. Another recently introduced index is the total perfusion deficit (TPD) which combines perfusion defect extent and severity. Comparison between rest and stress perfusion maps define the concept of reversibility, which refers to the extent and magnitude of improved perfusion at rest compared with values under pharmacological or physical stress. The summed difference score (SDS)—computed as SSS minus SRS—quantifies the extent of reversible myocardium, also referred to as ischemic myocardium or ischemic burden once converted to percentage of LV involvement. Clinical studies have extensively investigated these indexes and have identified a 10% LV ischemic burden as the value differentiating patients that will benefit from revascularization (≥10%) from those who may be treated with guideline-directed medical therapy alone (<10%). Figure 1.5 displays different indexes of perfusion abnormality, reversibility, and ischemic burden.

1.5 Myocardial Blood Flow Quantification

The need for normalization of LV perfusion maps to areas with the highest tracer uptake is a limitation of relative MPI. In fact, in cases with globally reduced LV perfusion or left main coronary artery obstruction, relative perfusion may not accurately identify the presence, severity, and extent of CAD. PET/CT systems overcome these limitations by computing regional and global absolute MBF in mL/min/g of tissue.

The quantification of myocardial blood flow (MBF) depends on the accurate measurement of the total activity injected into the circulation and transported to the myocardium over time. This is obtained by way of dynamic acquisitions that collect all events after radiotracer injection and reorganize them into sequential time-framed images, which are collected in shorter intervals during the radiotracer first-pass transit through the heart (5–10 s), and longer intervals during the tissue phase when the radiotracer is delivered to the myocardium (1–3 min). Regions of interest (ROIs) are used to sample radiotracer activity providing time-dependent profiles called time activity curves (TACs; Fig. 1.6). To calculate MBF, at least two ROIs are necessary: one in the arterial pool, called arterial input function (IF), and one in the myocardium. Different regions have been used to extract the IF, the most common being the LV, the left atrium, or the aorta. Several tissue TACs are routinely extracted: the entire LV for a global assessment and the standard vascular territories and segments for a regional evaluation. TACs are used as input data for mathematical models that describe the tracer kinetics and compute MBF.

Two main modeling techniques are currently used in clinical practice: tissue compartmental model and the retention model. In compartmental techniques, myocardial radiotracer uptake is described as a sequence of compartments exchanging radiotracer. The concentration in each compartment is extracted from PET images as TACs, while the rate of radiotracer exchange with adjacent compartments is modeled in terms of ordinary differential equations. MBF (i.e., the exchange of radiotracer between blood pool and myocardium) is estimated by fitting the measured TACs to the equations. The retention model can be considered a simplified version of the compartmental models wherein the radiotracer washout (i.e., the exchange from the myocardium to the blood pool) is disregarded. With retention models, only the input function during the arterial phase and one image of the late tissue phase are necessary to estimate MBF. Irrespective of the selected approach, since MPI radiotracers are imperfect perfusion agents (with extraction fraction <100% that decreases at hyperemic rates), numerical corrections are necessary and routinely implemented, with approaches varying between models, radiotracers, and software.

Once rest and stress dynamic acquisitions are processed and analyzed, MBF values are reported in tabulated form, or more commonly as polar maps. Normal stress flow values are generally >1.8 mL/min/g, while normal resting flows range between 0.4 and 1.2 mL/min/g. Rest MBF is a measure of myocardial oxygen demand and depends upon blood pressure and heart rate. Rest MBF can be normalized by the rate-pressure product (RPP, heart rate x systolic blood pressure) using the following formula: $MBF_{rest}^{adj} = \left(\frac{MBF_{rest}}{RPP_{rest}} \right) * RPP_{ref}$ with RPP_{ref} = 8,500 as a reference value. However, there is new evidence that adjustment of rest MBF by the RPP is not helpful as patients with increased rest MBF remain high risk even after RPP adjustment. Thus, the elevated rest MBF is a marker of risk that is associated with comorbid conditions that elevate myocardial oxygen demand (e.g., atrial fibrillation, uncontrolled hypertension, anemia, etc.) and by themselves confer higher clinical risk. In patients with normal perfusion scans with elevated rest MBF and reduced MFR, one should consider using the stress MBF as a marker of flow-limiting CAD instead of MFR.

From resting and hyperemic values, several other parameters can be derived. Myocardial flow reserve (MFR) is computed as the ratio of stress over rest MBF and is the most widely used parameter as it has recognized diagnostic and prognostic value. MFR measures the ability of the myocardium to effectively respond to an increase in energy demands. It is considered an index of overall vascular health and is dependent upon the presence of coronary luminal obstruction and/or increased microvascular resistance (coronary microvascular dysfunction, CMD). The threshold for normal

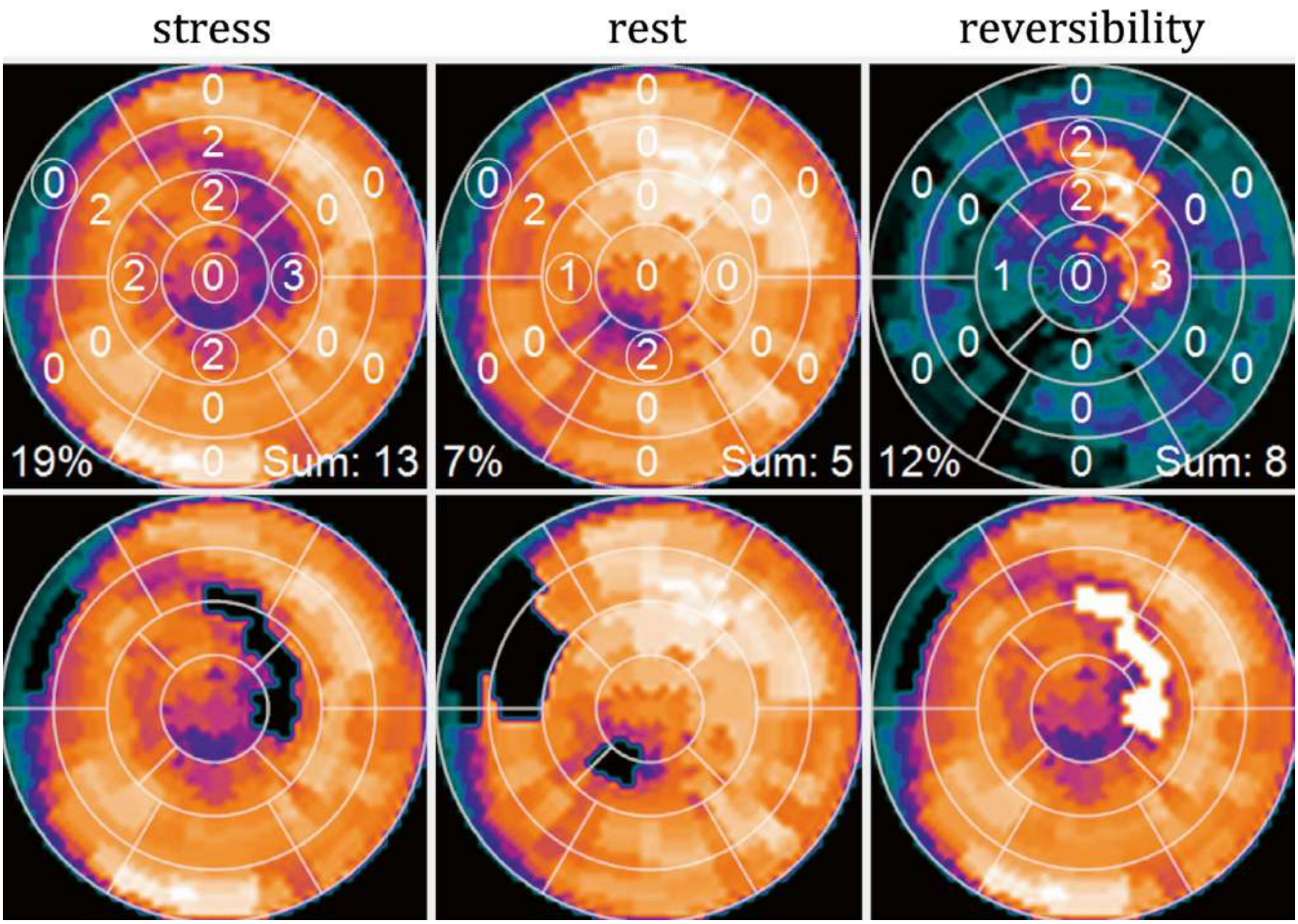
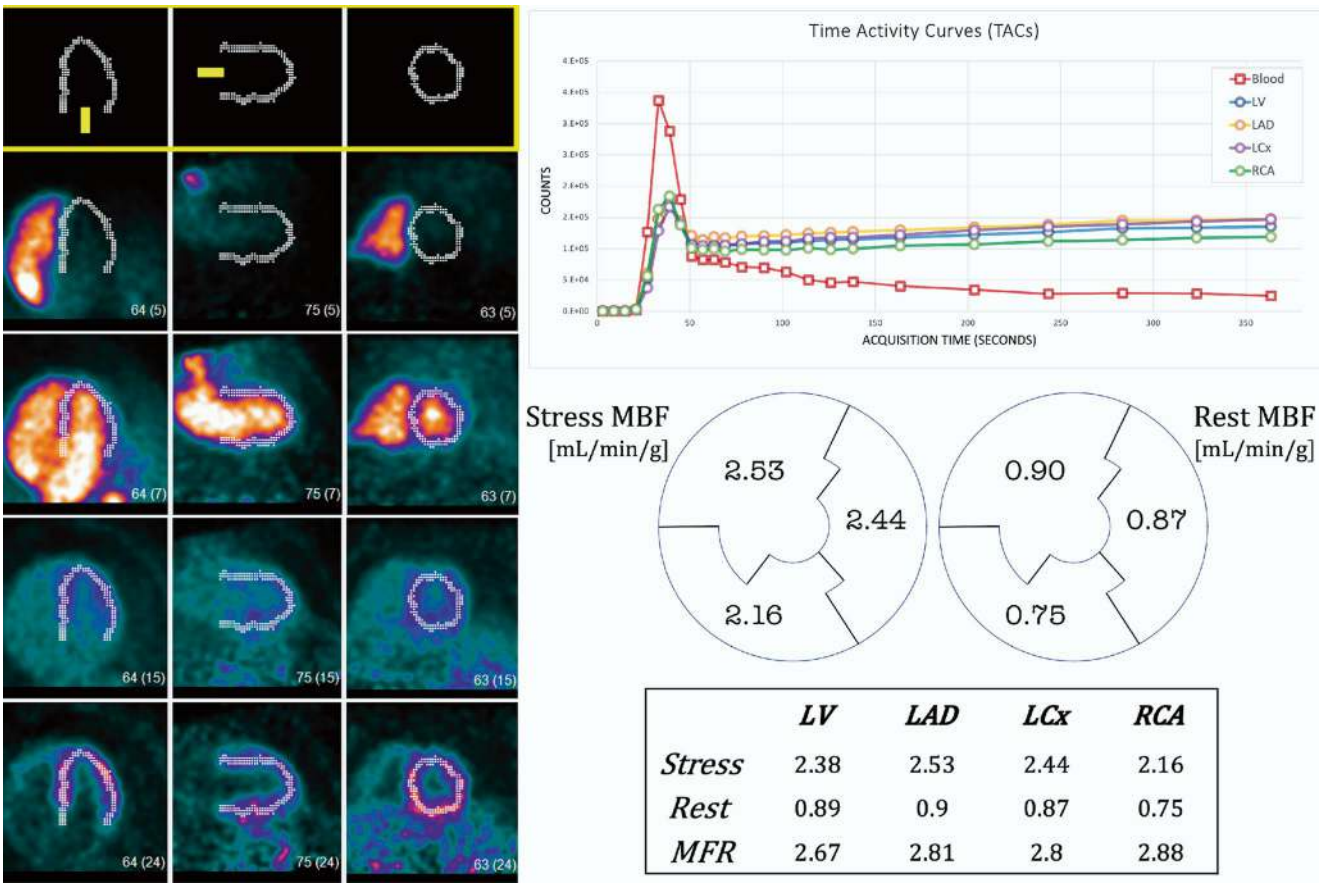


Fig. 1.5 *Top row*—polar maps of stress, rest, and reversibility. Each segment is scored (0–4) to quantify the degree of abnormality compared with a normal database. Global indexes SSS (13), SRS (5), and SDS (8) are reported with corresponding % of LV involvement (19%, 7% and 12%). With an ischemic burden >10%, this patient may be a good candidate for revascularization. *Bottom row*—blackout maps representing areas of difference (i.e., below lower limit of normality) between patient's distribution and a normal database. *SSS* summed stress score, *SRS* summed rest score, *SDS* summed difference score

MFR is typically set at >2.0. A high resting MBF may result in an erroneously calculated low MFR. In this instance, the RPP-adjusted resting MBF may be used instead. A second derived index is relative flow reserve (RFR). It is calculated as the hyperemic MBF in a specific area under investigation divided by the maximum hyperemic MBF measured in a remote and normally perfused area of the myocardium. RFR does not have the same clinical relevance as MFR, but it is widely considered the closest noninvasive approximation to invasive fractional flow reserve (FFR) for the identification of obstructive CAD.

The concept of coronary flow capacity (CFC) was recently introduced. CFC is a categorical classification of coronary flow based on a combined assessment of hyperemic MBF and MFR. Since MFR depends on both baseline and hyperemic flows, physiological alterations of both components may limit the ability of the index to identify flow abnormalities. The CFC index assumes that regions with severely impaired hyperemic flow and exhausted vasodilator capacity will develop ischemia; conversely, regions with high maximal flow and high flow reserve will unlikely exhibit ischemic changes.Originally introduced by Johnsons and Gould, CFC classification can be simplified in four subgroups, as detailed below, using a limit of 1.8 mL/min/g to define preserved versus reduced myocardial stress flow and 2.0 to delineate preserved versus low myocardial flow reserve (see Fig 1.7 and Chap. 3 for several examples).

1. **Concordant abnormal:** These patients have reduced myocardial stress flow and flow reserve and represent the



	LV	LAD	LCx	RCA
Stress	2.38	2.53	2.44	2.16
Rest	0.89	0.9	0.87	0.75
MFR	2.67	2.81	2.8	2.88

Fig. 1.6 *Left, top row*—definition of ROIs for the extraction of the IF (yellow marker) and LV (white outline) TACs. *Left, from second to last row*—ROIs are overlaid on dynamic images and used to extract time-dependent radiotracer concentrations. The second row shows the radiotracer reaching the RV; the third row shows the radiotracer reaching the LV; the 4th and 5th row show the radiotracer uptake by the myocardium. *Right, top*—TACs for IF, LV (shown on the left), and the standard territories which can be similarly obtained by subdividing the LV mask in LAD, LCX, and RCA regions (not shown). *Right, bottom*—Stress and rest MBF values displayed as polar map and in a table; MFR is computed as stress/rest MBF. Legend: *IF* input function, *LAD* left anterior descending coronary artery, *LCX* left circumflex coronary artery, *LV* left ventricle, *MBF* myocardial blood flow, *MFR* myocardial flow reserve, *RCA* right coronary artery, *ROIs* regions of interest, *TACs* time activity curves

highest risk subgroup with an annualized risk of cardiac death >3%/year. Patients in this category represent a heterogeneous group of patients including those with multivessel obstructive CAD, diffuse coronary microvascular dysfunction, or some combination of the two. The MBF and flow reserve data should be interpreted in the context of other important imaging findings including extent/severity of perfusion defects, change in left ventricular ejection fraction (LVEF) with stress, transient cavity dilatation, severity of coronary artery calcification, etc. Because clinical risk is very high in this subgroup, correlation with angiographic information is necessary to determine the predominant phenotype (obstructive vs nonobstructive CAD) that will inform patient management.

2. **Concordant/normal:** These patients have preserved stress flow and flow reserve and represent the lowest-risk subgroup with an annualized risk of cardiac death <0.5%/year. Most of these patients do not have obstructive CAD or coronary microvascular dysfunction. There is no need for angiographic assessment in most of these patients.
3. **Discordant/reduced stress flow and preserved MFR:** These patients have reduced myocardial stress flow and preserved flow reserve and represent a low-intermediate risk subgroup with an annualized risk of cardiac death ~1%/year. In the absence of regional perfusion abnormalities, the discordant information in this group reflects primarily patients with diffuse nonobstructive CAD. When a perfusion defect is present, it usually reflects a combination of low risk obstructive and nonobstructive CAD.

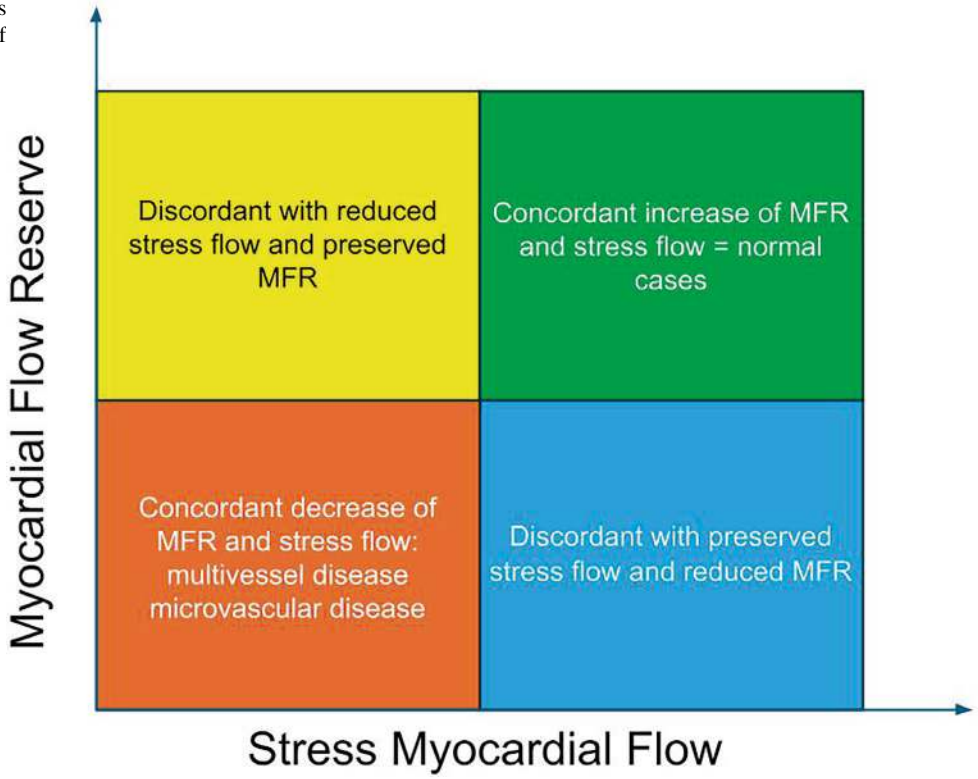


Fig. 1.7 The four patient subgroups resulting from the combination of stress flow and flow reserve

4. **Discordant/preserved stress flow and reduced MFR:** These patients have preserved stress flow and reduced flow reserve usually related to increased rest myocardial blood flow (denominator of the flow reserve calculation) and represent an intermediate-risk subgroup with an annualized risk of cardiac death ~2%/year. Because stress flow is preserved, most of these patients do not have obstructive CAD. However, they frequently include patients with comorbid conditions that increase myocardial oxygen demand at rest (e.g., atrial fibrillation, uncontrolled hypertension, anemia, etc.), which in turn increase rest flow. Since myocardial perfusion is almost always normal and the stress flow is preserved, most patients do not need additional coronary angiography. Management is usually directed to the underlying cardiometabolic abnormality.

The added clinical value of MBF quantification is undeniable. It has entered clinical practice, and various software provide a fully automated calculation. Nevertheless, assessment of absolute MBF, MFR, and CFC remains technically demanding, including challenges of image acquisition, image processing, radiotracer kinetic modeling, corrections, and finally result interpretation. Several publications from the Society of Nuclear Medicine and Molecular Imaging (SNMMI) Cardiovascular Council and American Society of Nuclear Cardiology (ASNC) have addressed these issues and underlined the importance of carefully reviewing both data and results prior to reporting and making management decisions.

1.5.1 Global Left Ventricular Function

Several parameters are routinely extracted from gated rest/stress PET MPI acquisitions to measure left ventricular function. The most common are myocardial thickening, end-systolic (ESV), end-diastolic (EDV) volumes, LV ejection fraction ($LVEF = \frac{(EDV - ESV)}{EDV}$), myocardial mass, peak filling rate (PFR), and other indexes specific to diastolic function (Fig. 1.8).

The algorithms used to extract these indexes vary depending on the software being used. They are mostly based on the automated identification of LV endo- and epicardial borders throughout the cardiac cycle. Regional wall thickening from end diastole to end systole is extracted based on the principle that the relative change in peak myocardial intensity is directly related to the change in myocardial thickness. Wall thickening is commonly displayed on a polar map, while 2D cinematic rendering displays SA, VLA, and HLA slices with moving LV wall borders for a comprehensive analysis of thickening and motion.

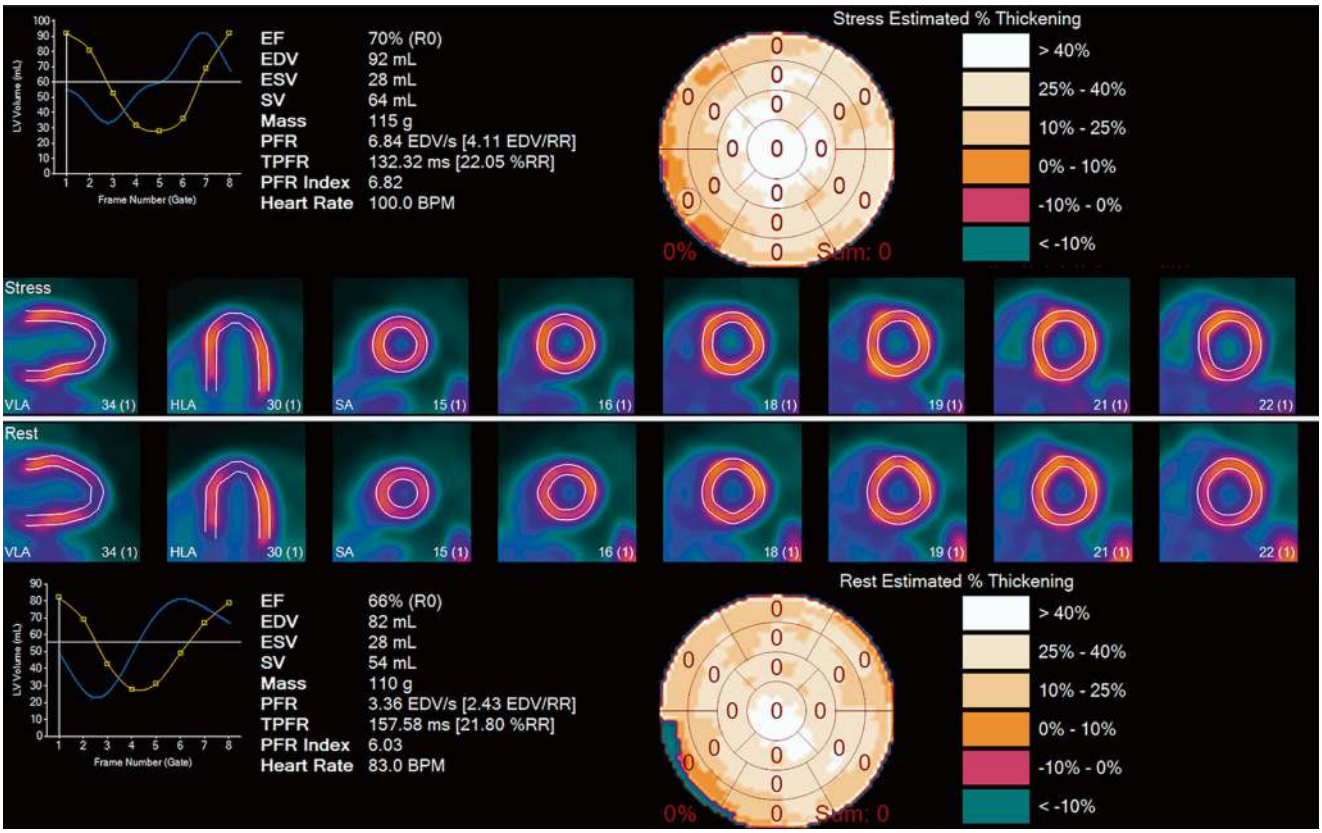


Fig. 1.8 Various indexes of cardiac function obtained from fully automated analysis of a gated myocardial perfusion study. The parameters reported are rest and stress EF, EDV, ESV, SV, and PFR. LV wall thickening is commonly conveyed in polar maps and wall motion through moving renderings of segmented LV endo- and epicardial borders. Legend: *EF* ejection fraction, *EDS* end-diastolic volume, *ESV* end-systolic volume, *PFR* peak filling rate, *LV* left ventricle, *SV* stroke volume

1.6 Cardiac PET/CT for Metabolic and Inflammation Imaging

Besides the performance of MPI studies, PET imaging is extensively employed to investigate myocardial metabolism. Notable applications are the assessment of myocardial viability and the study of inflammatory cardiomyopathies with the tracer ^{18}F-fluorodeoxyglucose (FDG). FDG crosses cell membranes through glucose transporters such as GLUT-4 and is rapidly phosphorylated to ^{18}F-FDG-6 phosphate. This compound cannot undergo further modification and is trapped within the cells. The ^{18}F isotope is produced in a cyclotron, has a half-life of ~110 min (making delivery from regional sites of production feasible), and has a relatively low energy.

As a glucose analog, FDG is taken up by cells with increased metabolic activity. Healthy myocytes consume mostly free fatty acids (70–90% of ATP production), followed by glucose and lactate (10–30% of total ATP production), and small quantities of amino acids and ketones. In a state of ischemia, viable myocardial cells switch to glucose metabolism. This feature is exploited by implementing specific FDG preparation protocols that combine fasting with dietary modifications, to optimize metabolic signaling and favor image interpretation. Viability imaging is performed with a combination of resting MPI and FDG PET to determine whether patients will benefit from revascularization. Among inflammatory diseases, the most frequently investigated with FDG PET imaging is cardiac sarcoidosis (CS). Sarcoidosis is a multi-system granulomatous disease that may involve many organs including the eye, skin, lungs, and heart and it can cause conduction abnormalities, heart failure, arrhythmias, and sudden cardiac death. FDG PET is utilized to detect active metabolic processes (in this case from increased glucose utilization by macrophages, T and B lymphocytes) and monitor treatment effects. Similar to the identification of viable myocardium, the imaging protocol for CS has also been carefully designed to direct substrate utilization and suppress physiological background of FDG uptake.

1.6.1 Myocardial Viability Imaging Protocol

Under aerobic conditions, myocytes consume fatty acids for energy production, but they transition to glucose in anaero-

bic or ischemic conditions. The goal of the FDG protocol for viability imaging is to switch the metabolism of the heart to glucose metabolism, hence maximizing radiotracer uptake. This is commonly performed with dietary patient preparation in the hours and minutes prior to radiotracer injection. While not strictly necessary, FDG images are typically compared with a resting perfusion scan acquired with either $^{13}NH_3$ or ^{82}Rb and attenuation corrected. Patient preparation consists of 6–12 h fasting. On the day of imaging, patients first undergo a rest MPI scan followed by glucose loading. This is usually achieved with an oral administration of 25–100 g of glucose. Intravenous administration may also be used. The rapidly raised glucose plasma concentration stimulates insulin release which, in turn, favors the glucose-based metabolism of ischemic but viable myocytes. Once the target blood concentration of glucose is reached (100–140 mg/dL), FDG is injected intravenously. Typical injected activity ranges between 185 and 555 MBq. Image acquisition starts 45–60 min after the injection of FDG and lasts 10–30 min depending on the PET scanner. Longer delays may result in images with better blood pool clearance. The resting PET perfusion scan can be replaced with a SPECT scan (preferably with attenuation correction), although differences in spatial resolution may complicate scan comparisons. Specific preparations may be necessary for patients with diabetes as the simple oral glucose load may be insufficient to provide good quality images. A technique known as the euglycemic-hyperinsulinemic clamp is usually applied consisting of an infusion of insulin and glucose to maintain the desired level of both. Figure 1.9 (A) summarizes the FDG viability protocol.

Comparison of the perfusion and the metabolic images highlights the presence of viable and nonviable myocardium. Four possible patterns may arise from the comparison: i) normal myocardial perfusion and normal FDG uptake indicate normally perfused and viable myocardium; ii) concordant areas of reduced perfusion and reduced FDG uptake indicate scarred myocardium (matched pattern), unlikely to benefit from revascularization; iii) abnormal perfusion with normal FDG uptake (mismatched pattern), indicates viable myocardium that is likely to recover from revascularization; iv) normal perfusion with abnormal FDG uptake (reverse mismatched pattern) occurring in instances of left bundle branch block, severe resistance to insulin, and myocardial stunning (impaired contractile function due to repetitive hypoperfusion episodes).

1.6.2 Cardiac Sarcoidosis Imaging Protocol

Similar to viability imaging, a sequence of two scans (resting MPI followed by FDG) is recommended for a comprehensive CS diagnosis and treatment monitoring. Dietary indications and restrictions are imperative to suppress glucose metabolism and shift to free fatty acids for normal myocardium. Most commonly, patients are instructed to follow a high-fat, high-protein, and low-carbohydrate diet the day before imaging followed by a 12-h fast. Although not consistently performed, injection of unfractionated heparin has also been used to increase serum free fatty acid levels. The typical heparin dose is 50 IU/Kg to be administered approximately 15 min prior to FDG injection. The day of imaging, a resting MPI is performed first, typically with $^{13}NH_3$ or ^{82}Rb and attenuation correction. The resting PET perfusion scan may be replaced with a SPECT (preferably with attenuation correction). After perfusion imaging, FDG is injected intravenously. Typical radiation activity ranges between 370 and 444 MBq. Image acquisition starts 60–90 min after injection and may last 10–30 min depending on the PET scanner. Figure 1.10 summarizes the sarcoidosis FDG protocol.

Interpretation of the images is done side-by-side with qualitative or semiquantitative approaches. Patterns of FDG uptake are usually conveyed as no uptake, diffuse uptake, focal uptake, and focal on diffuse uptake. A normal study for CS will show no perfusion defect on the MPI and no FDG uptake, indicating the absence of inflammation. Diffuse homogeneous FDG uptake may be the result of suboptimal patient preparation. Areas with focal FDG uptake with or without corresponding perfusion defects indicate the presence of active inflammation. Other approaches include the degree of perfusion defect to distinguish different CS stages: early, progressive, progressive myocardial impairment and fibrosis.

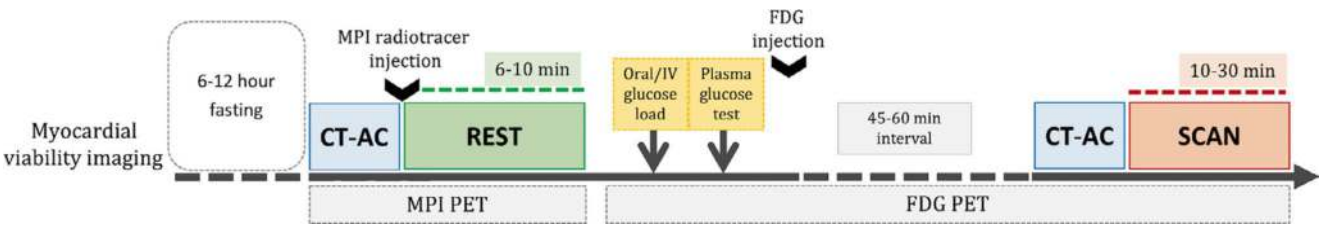


Fig. 1.9 Imaging acquisition protocols for the assessment of myocardial with FDG PET. Legend: *FDG* ^{18}F-fluorodeoxyglucose, *MPI* myocardial perfusion imaging, *AC* attenuation correction, *CT* computed tomography

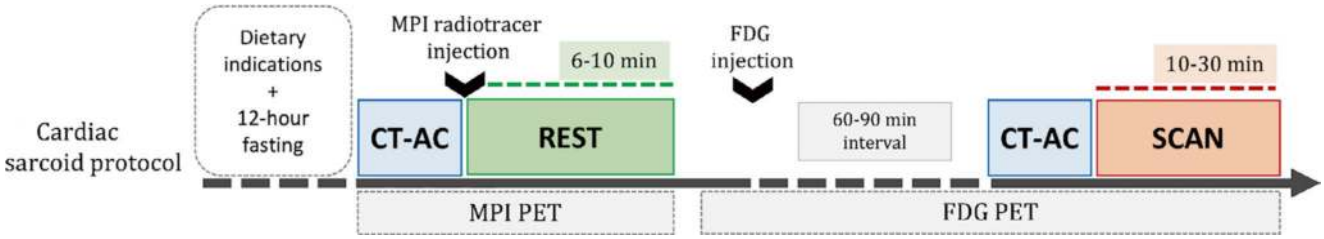


Fig. 1.10 Imaging acquisition protocols for the assessment of cardiac sarcoid with FDG PET. Legend: *FDG* ^{18}F-fluorodeoxyglucose, *MPI* myocardial perfusion imaging, *AC* attenuation correction, *CT* computed tomography

Further Reading

- Garcia EV. Cardiac PET and SPECT instrumentation. J Nucl Cardiol, 2015, 22:563–70.
- Townsend DW. Physical principle and technology of clinical PET imaging. Ann Acad Med Sing, 2004, 33:133–45.
- Bateman TM, Dilsizian V, Beanlands RS, et al. American Society Nuclear Cardiology and Society of Nuclear Medicine and Molecular Imaging joint position statement on the clinical indications for myocardial perfusion PET. J Nucl Med, 2016, 57:1654–6.
- Murthy VL, Bateman TM, Beanlands RS, et al. Clinical quantification of myocardial blood flow using PET: joint position paper of the SNMMI cardiovascular council and the ASNC. J Nucl Med, 2018, 59:273–93.
- Patel KK, Spertus JA, Chan PS, et al. Myocardial blood flow reserve assessed by positron emission tomography myocardial perfusion imaging identifies patients with a survival benefit from early revascularization. Eur Heart J, 2020, 41:759–68.
- Gould KL, Johnson NP, Bateman TM, et al. Anatomic versus physiologic assessment of coronary artery disease. Role of coronary flow reserve, fractional flow reserve and positron emission tomography imaging in revascularization decision making. J Am Coll Cardiol, 2013, 62:1639–53.
- Schindler TH, Fearon WF, Pelletier-Galarneau M, et al. Myocardial perfusion PET for the detection and reporting of coronary microvascular dysfunction. J Am Coll Cardiol Img, 2023, 16:536–48.
- Slart RHJA, Glaudemans AWJM, Gheysens O, et al. Procedural recommendation of cardiac PET/CT imaging: standardization in inflammatory-, infective-, infiltrative-, and innervation- (4Is) related cardiovascular diseases: joint collaboration of the EACVI and the EANM: summary. Eur Heart J – Cardiovasc Imaging, 2020, 21:1320–30.
- Celiker-Guler E, Ruddy TD, Wells RG. Acquisition, processing and interpretation of PET 18-FDG viability and inflammation. Curr Cardiol Rep, 2021, 23:124. https://doi.org/10.1007/s11886-021-01555-7.
- Maddahi J, Lazewatsky J, Udelson JE, et al. Phase-III clinical trial of fluorine-18 Flurpiridaz positron emission tomography for evaluation of coronary artery disease. J Am Coll Cardiol, 2020, 4:391–401.
- Johnson NP, Gould KL. Integrating noninvasive absolute flow, coronary flow reserve, and ischemic thresholds into a comprehensive map of physiological severity. JACC Cardiovasc Imaging. 2012, 5:430–40
- Huck DM, Weber BN, Brown JM, Lopez D, Hainer J, Blankstein R, Dorbala S, Divakaran S, Di Carli MF. Prognostic value of myocardial flow reserve vs corrected myocardial flow reserve in patients without obstructive coronary artery disease. J Nucl Cardiol. 2024 Jul;37:101854
- Bateman TM, Heller GV, Beanlands R, et al. Practical guide for interpreting and reporting cardiac PET measurements of myocardial blood flow: an information statement from the American Society of Nuclear Cardiology and the Society of Nuclear Medicine and Molecular imaging. J Nucl Med, 2021, 62:1599–1615.
- Gupta A, Taqueti VR, van de Hoef TP, Bajaj NS, Bravo PE, Murthy VL, Osborne MT, Seidelmann SB, Vita T, Bibbo CF, Harrington M, Hainer J, Rimoldi O, Dorbala S, Bhatt DL, Blankstein R, Camici PG, Di Carli MF. Integrated noninvasive physiological assessment of coronary circulatory function and impact on cardiovascular mortality in patients with stable coronary artery disease. Circulation. 2017;136(24):2325–2336.

The opinions expressed in this chapter are those of the author(s) and do not necessarily reflect the views of the IAEA: International Atomic Energy Agency, its Board of Directors, or the countries they represent.

Open Access This chapter is licensed under the terms of the Creative Commons Attribution 3.0 IGO license (http://creativecommons.org/licenses/by/3.0/igo/), which permits use, sharing, adaptation, distribution and reproduction in any medium or format, as long as you give appropriate credit to the IAEA: International Atomic Energy Agency, provide a link to the Creative Commons license and indicate if changes were made.

Any dispute related to the use of the works of the IAEA: International Atomic Energy Agency that cannot be settled amicably shall be submitted to arbitration pursuant to the UNCITRAL rules. The use of the IAEA: International Atomic Energy Agency's name for any purpose other than for attribution, and the use of the IAEA: International Atomic Energy Agency's logo, shall be subject to a separate written license agreement between the IAEA: International Atomic Energy Agency and the user and is not authorized as part of this CC-IGO license. Note that the link provided above includes additional terms and conditions of the license.

The images or other third party material in this chapter are included in the chapter's Creative Commons license, unless indicated otherwise in a credit line to the material. If material is not included in the chapter's Creative Commons license and your intended use is not permitted by statutory regulation or exceeds the permitted use, you will need to obtain permission directly from the copyright holder.



Artifacts

2

Marcelo Di Carli, Raffaele Giubbini, Michelle Williams, Diana Paez, Maurizio Dondi, Paolo Raggi, Erick Alexanderson, Isabel Carvajal, Elisa Milan, and Carole Kounga

Objectives

- To recognize and develop skills to troubleshoot artifacts caused by incorrect emission-transmission alignment, patient or cardiac motion, and other sources of attenuation correction errors.
- To recognize normal variants associated with different radiotracers on myocardial perfusion PET imaging.
- To develop skills to perform quality control of PET images, verify accuracy of time activity curves, and quantitative data.

Artifacts in positron emission tomography (PET) imaging can significantly impact the accuracy and reliability of diagnostic results. Understanding and troubleshooting these artifacts is crucial for ensuring high-quality images and accurate clinical interpretations. This chapter delves into the common sources of artifacts in cardiac PET imaging, including incorrect emission-transmission alignment, patient or cardiac motion, and attenuation correction errors.

All authors have no conflict of interest to disclose.

M. Di Carli · C. Kounga
Brigham and Women's Hospital, Boston, MA, USA
e-mail: mdicarli@bwh.harvard.edu; Ckounga@bwh.harvard.edu

R. Giubbini
Nuclear Medicine, International Specialized Hospital of Uganda (ISHU), Kampala, Uganda
e-mail: raffaele.giubbini@unibs.it

M. Williams
British Heart Foundation Centre for Research Excellence, Institute for Neuroscience and Cardiovascular Research, University of Edinburgh, Edinburgh, United Kingdom
e-mail: michelle.williams@ed.ac.uk

D. Paez · M. Dondi (✉)
Division of Human Health, International Atomic Energy Agency, Vienna, Austria
e-mail: d.paez@iaea.org; m.dondi@iaea.org

P. Raggi
Division of Cardiology, University of Alberta, Edmonton, AB, Canada

E. Alexanderson · I. Carvajal
Instituto Nacional de Cardiologia Ignacio Chavex, Mexico City, Mexico

E. Milan
Nuclear Cardiology Lab and PET Centre, Treviso Hospital, Treviso, Italy
e-mail: elisa.milan@aulss2.veneto.it

2.1 Misregistration: Case 1

Key Points

- Careful inspection of the emission/CT transmission alignment is a critical quality control step in the assessment of cardiac PET/CT images.
- Misalignment should be corrected and images re-reconstructed with the proper alignment before clinical interpretation.
- The perfusion defect is caused by incorrectly applying attenuation coefficients corresponding to lung tissue (air), resulting in under-correction of attenuation in the misregistered region that appears cold compared to the rest of the heart corrected with soft tissue attenuation coefficients.

History

- A 57-year-old man without a history of coronary artery disease was referred for a rest/stress myocardial perfusion PET/CT to evaluate for atypical angina (Figs. 2.1 and 2.2).

PET/CT Images

© The Author(s) 2027

M. Di Carli et al. (eds.), *IAEA Atlas of Cardiac PET/CT*, https://doi.org/10.1007/978-3-662-74188-7_2

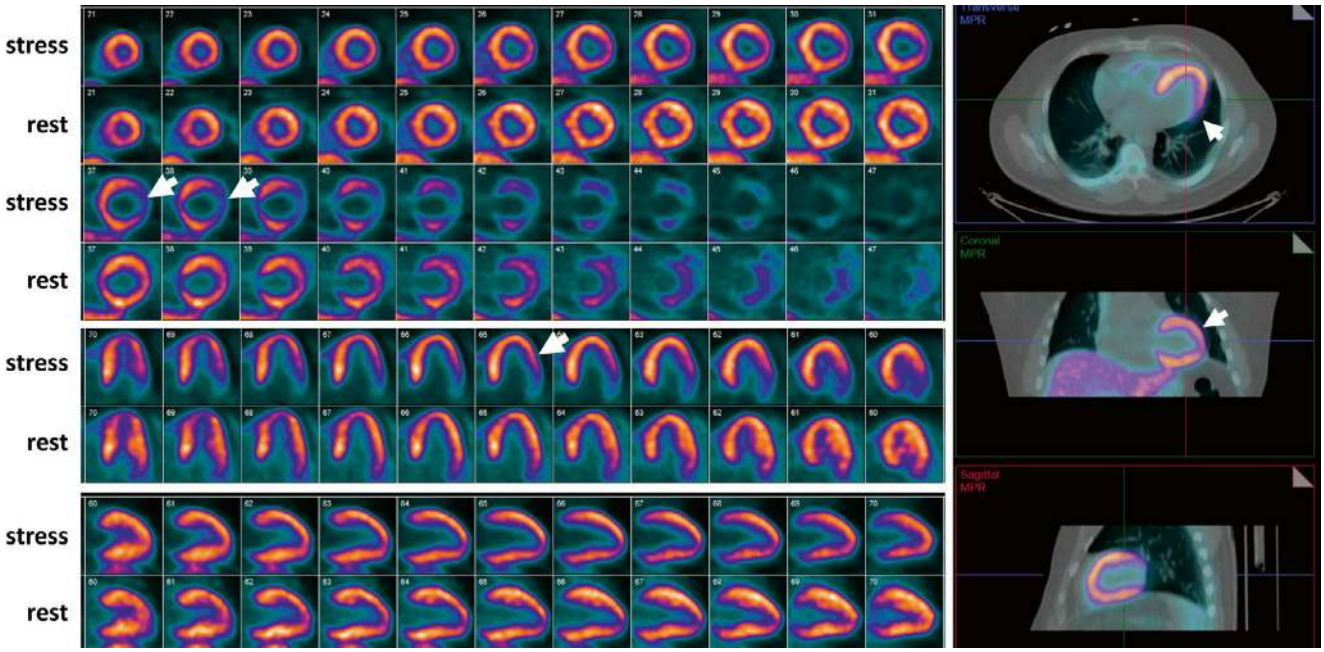


Fig. 2.1 **Left panel**: Regadenoson stress myocardial and rest perfusion PET/CT images obtained with ^{13}N-ammonia. The images demonstrate a medium-sized perfusion defect of severe intensity involving the mid and basal anterolateral and inferolateral LV segments (arrows), showing complete reversibility. **Right panel**: The fused perfusion/CT transmission images demonstrate misregistration of the lateral and anterolateral walls on the stress images, which are overlapping the left lung field on the CT (arrows). This misalignment leads to an artifact, resulting in an apparent perfusion defect

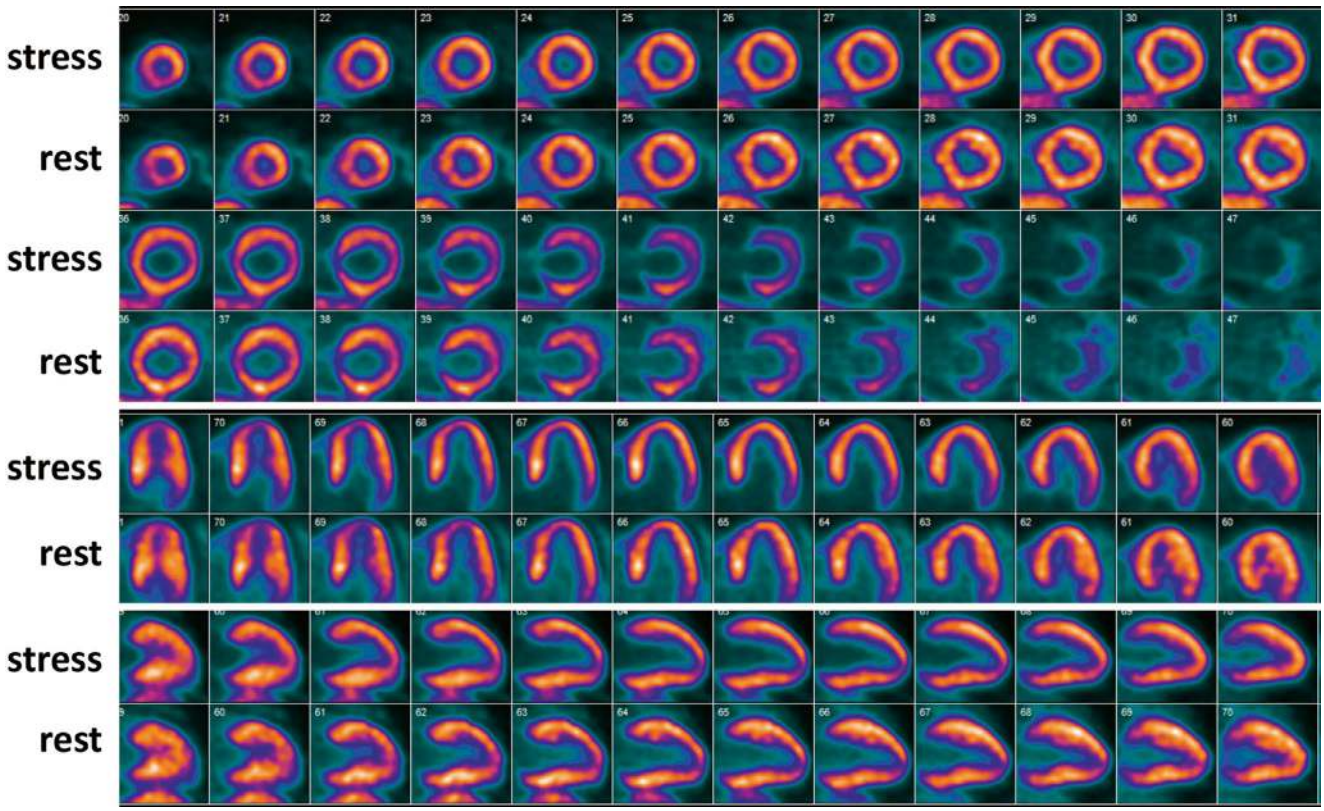


Fig. 2.2 Regadenoson stress myocardial and rest myocardial perfusion PET/CT images of the same patient *after correction of the misregistration* between the perfusion and CT transmission images. The images now demonstrate normal myocardial perfusion and a normal scan

Findings
- The original reconstructed stress images demonstrate a medium-sized perfusion defect of severe intensity involving the anterolateral wall (arrows), showing complete reversibility.
- However, inspection of the fused PET emission/CT transmission images demonstrated misalignment between the two datasets with the anterolateral wall overlapping the lung field on the CT images.
- Correction of the PET emission/CT transmission misalignment resulted in resolution of the perfusion defect and a normal scan.

Imaging Diagnosis
- Normal perfusion of the left ventricle.

Differential Diagnosis
- Obstructive coronary artery disease with single-vessel myocardial ischemia.

Correlative Imaging
- None.

Management
- Reassurance and risk factor management.

Further Reading

- Bettinardi V, Gilardi MC, Lucignani G, Landoni C, Rizzo G, Striano G, et al. A procedure for patient repositioning and compensation for misalignment between transmission and emission data in PET heart studies. Journal of Nuclear Medicine. 1993;34:137–42.
- McCord ME, Bacharach SL, Bonow RO, Dilsizian V, Cuocolo A, Freedman N. Misalignment between PET transmission and emission scans: its effect on myocardial imaging. Journal of Nuclear Medicine. 1992;33:1209–1214.
- Loghin C, Sdringola S, Gould KL. Common artifacts in PET myocardial perfusion images due to attenuation-emission misregistration: clinical significance, causes, and solutions. Journal of Nuclear Medicine. 2004;45:1029–39.

2.2 Patient Motion: Case 2

Key Points
- The distortion of the LV shape on the stress and/or rest images associated with perfusion defects which are exactly opposite to each other should raise the suspicion of an artifact from patient motion.

History
- A 37-year-old man with no known coronary artery disease was referred for a regadenoson myocardial perfusion PET study to evaluate for chest pain.
- He has a strong family history of premature coronary artery disease.

PET/CT Images (Fig. 2.3)

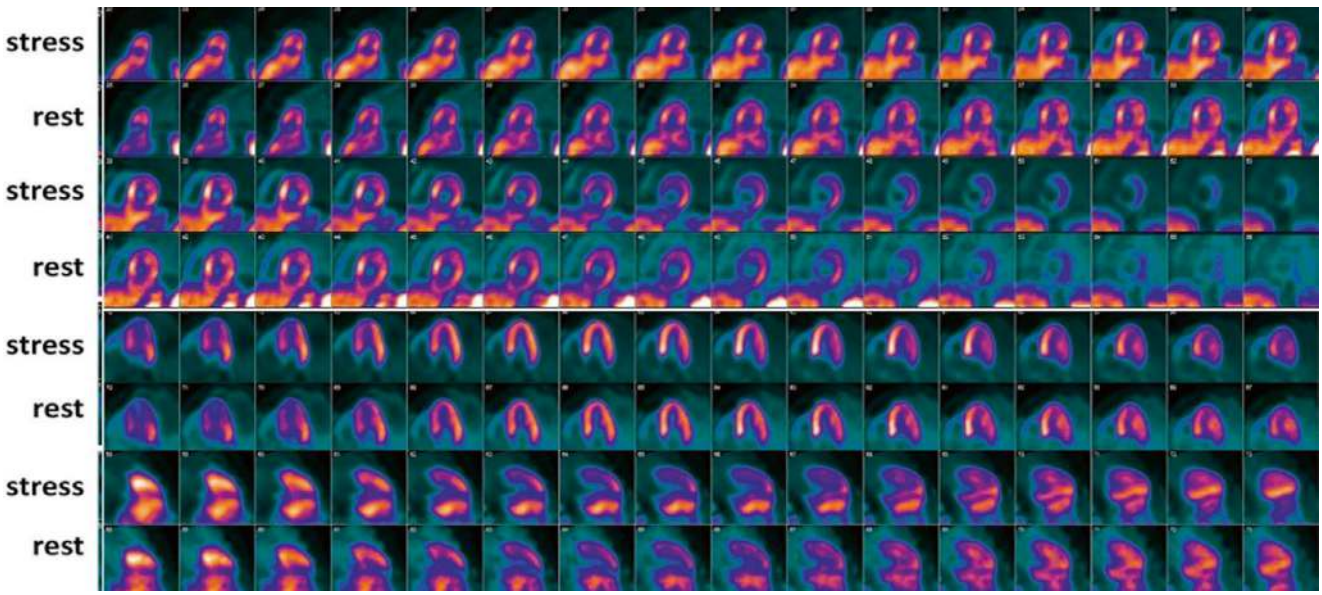


Fig. 2.3 Stress and rest ^{82}Rubidium myocardial perfusion PET study. The stress images demonstrate medium-sized perfusion defects involving the anterior and inferior walls, showing moderate reversibility at rest

Findings

- The stress images demonstrate medium-sized perfusion defects involving the anterior and inferior walls, showing moderate reversibility at rest.
- The distortion of the LV shape on the stress and rest images associated with perfusion defects exactly opposite to each other should raise the suspicion of an artifact from patient motion.
- Motion correction was then performed for the ^{82}Rubidium myocardial perfusion PET study (Figs. 2.4 and 2.5).

Findings After Motion Correction

- There are no regional perfusion defects on the stress or rest images after motion correction.
- Normal LV shape on the stress and rest images.

Imaging Diagnosis

- Normal myocardial perfusion study demonstrating no evidence of flow-limiting coronary artery disease.

Differential Diagnosis

- Patient motion artifact.

Correlative Imaging

- None.

Management

- Careful review of the images is necessary to identify common sources of artifact, including patient motion.

Further Reading

- Rubeaux M, Doris MK, Alessio A, Slomka PJ. Enhancing Cardiac PET by Motion Correction Techniques. Curr Cardiol Rep. 2017;19(2):14.
- Garcia EV, Nye JA. Moving forward with motion reduction, detection and correction in cardiac PET. J. Nucl. Cardiol. 2022; 29:1607–1610.

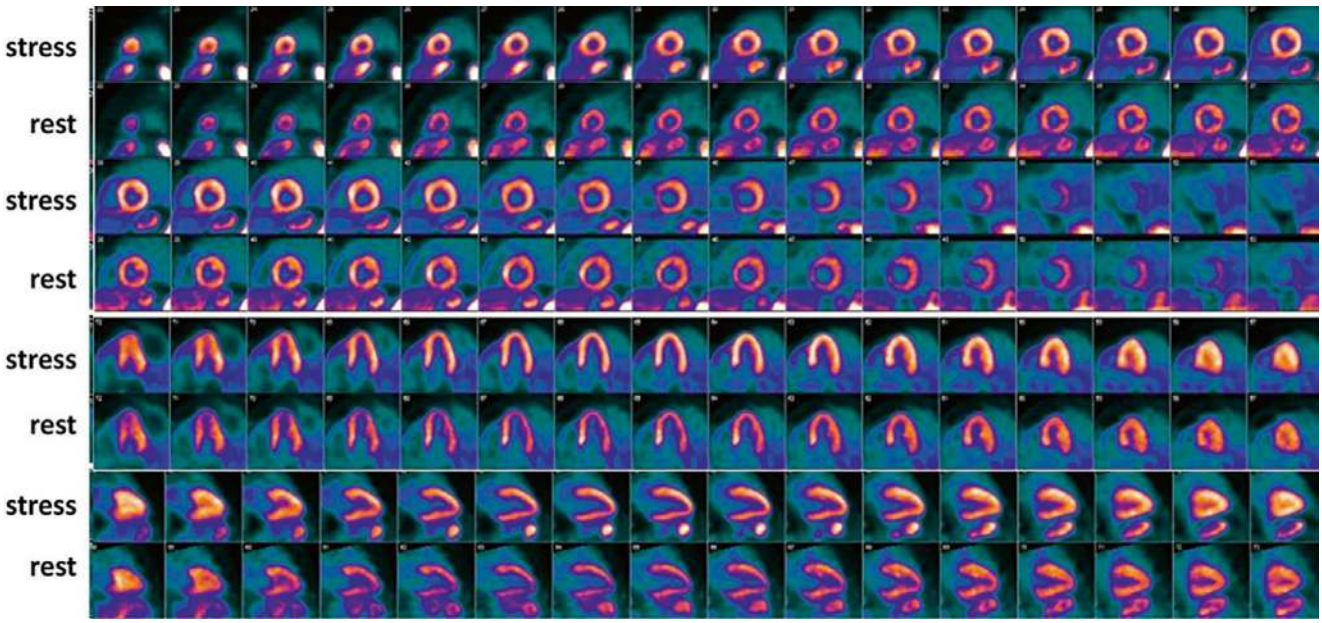


Fig. 2.4 Stress and rest ^{82}Rubidium myocardial perfusion PET study of the same patient *after motion correction*. There are no regional perfusion defects on the stress or rest images

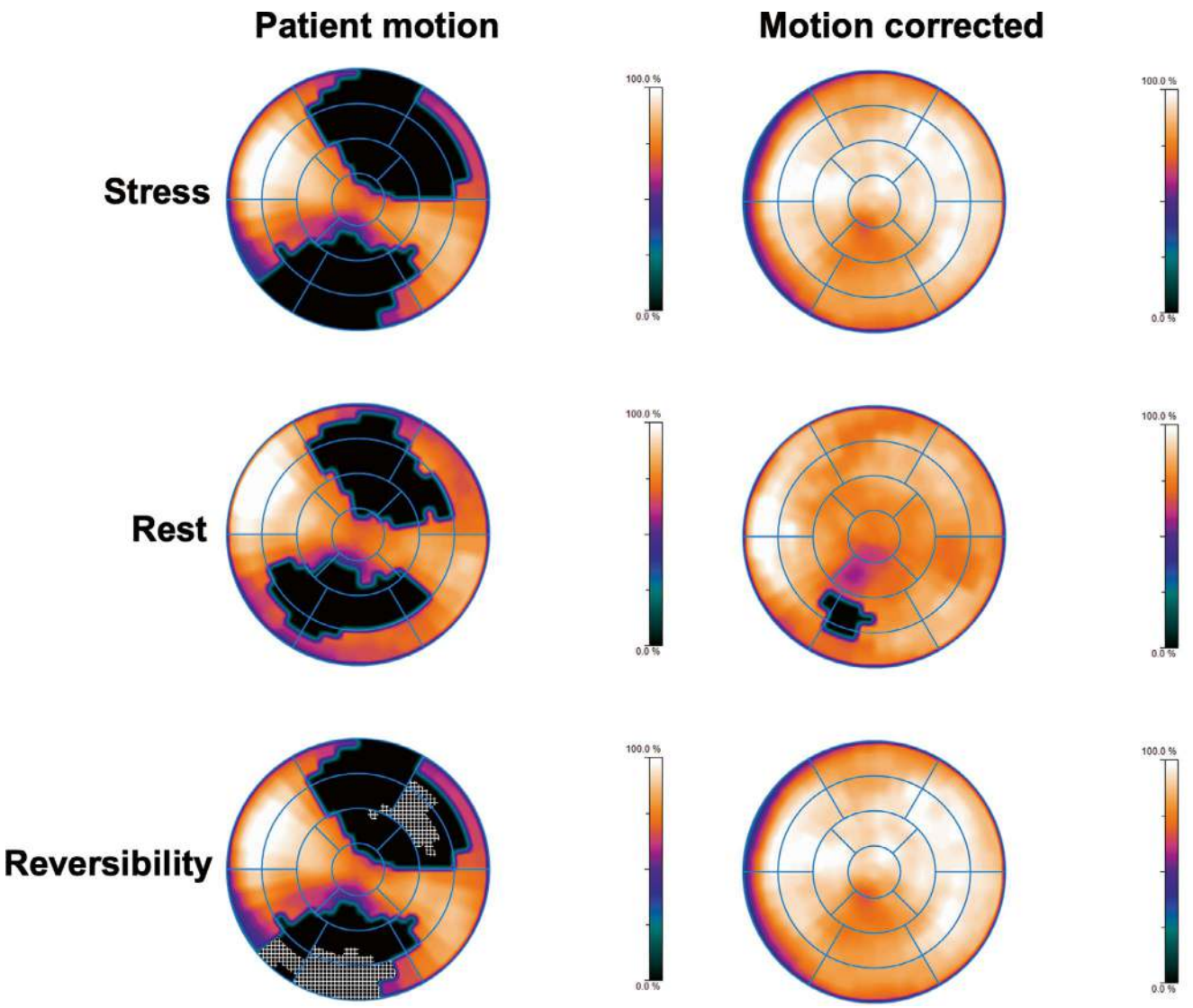


Fig. 2.5 Stress, rest, and reversibility polar maps before and after motion correction. With patient motion, there are medium-sized perfusion defects involving the anterior and inferior walls, showing moderate reversibility at rest. After motion correction, there is no evidence of perfusion abnormalities

2.3 Cardiac Motion Artifacts: Case 3

Key Points

- A quality control of patient motion during acquisition is mandatory as it can affect results.
- After Regadenoson injection, an increase in breathing excursion and, consequently, a cardiac upward shift is commonly observed.

History

- A 63-year-old man with no risk factors.
- Non-anginal chest pain.

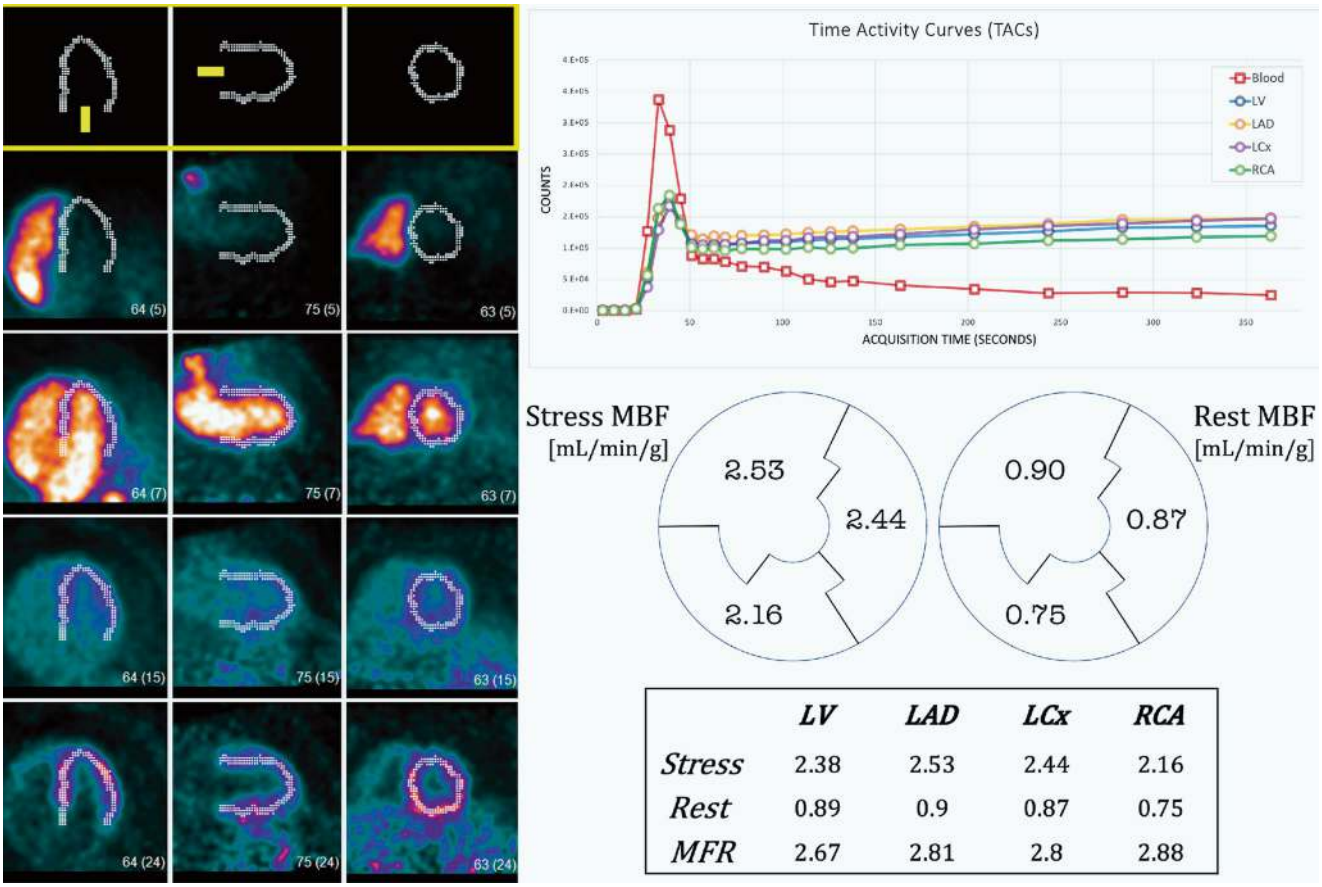
PET/CT Images (Fig. 2.6)

A downshift of the LV during the LV cavity filling at rest and an upshift of myocardial wall in the stress study is detected after quality check for LV motion during acquisition, as shown in Fig. 2.7.

After correction for patient movements, both myocardial blood flow (MBF) and myocardial flow reserve (MFR) values normalize (Table 2.1).

Findings

- In the originally reconstructed images, MPI shows mild reversible perfusion defect in the inferoapical segments.



	LV	LAD	LCx	RCA
Stress	2.38	2.53	2.44	2.16
Rest	0.89	0.9	0.87	0.75
MFR	2.67	2.81	2.8	2.88

Fig. 2.6 The study shows a mild reversible perfusion defect of the apical region. The quantitative values (see Table 2.1; non-motion corrected data (NMC data)) show an abnormal (too high) MBF at rest in the RCA territory resulting in an impairment of the MFR in the same territory

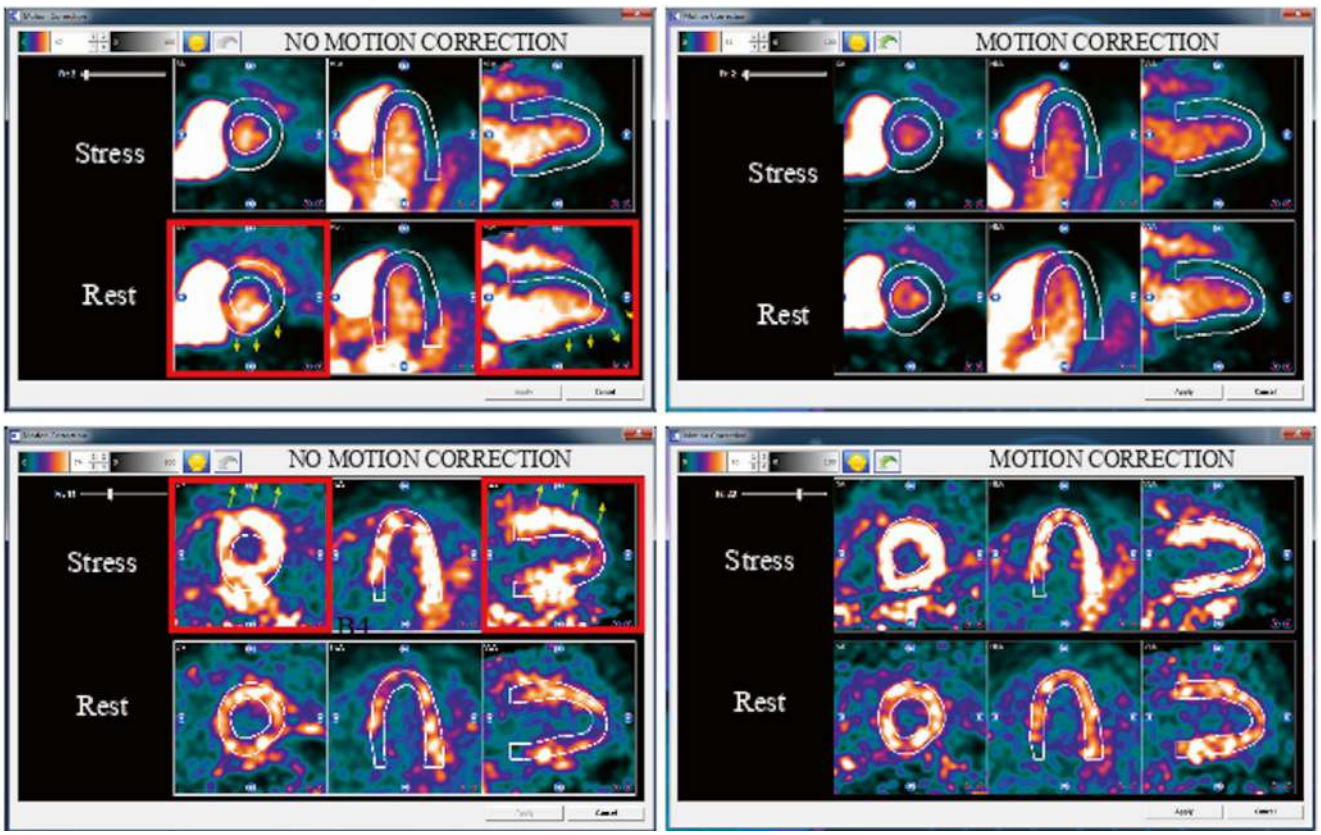


Fig. 2.7 Downshift of the LV during the LV cavity filling at rest (upper left panel; lower row; red boxes) and an upshift of myocardial wall in the stress study (lower left panel; upper row; red boxes). The upper right and lower right panels show the motion corrected studies

Table 2.1 MBF and MFR values before (NMC) and after motion correction (MC). Quantitative values show an abnormal (too high) MBF at rest in the RCA territory and impairment of the MFR in the same territory due to an abnormally high MBF at rest. MBF normalizes (3.21) after MC

Quantitative myocardial blood flow						
	MBF rest (ml/min/g)		MBF stress (ml/min/g)		MFR (stress/rest)	
LAD	NMC	0.76	NMC	1.87	NMC	2.46
	MC	0.70	MC	1.96	MC	2.79
LCX	NMC	1.09	NMC	2.30	NMC	2.11
	MC	0.93	MC	2.08	MC	2.22
RCA	NMC	1.53	NMC	1.75	NMC	1.15
	MC	0.55	MC	1.77	MC	3.21
Global LV	NMC	0.85	NMC	1.97	NMC	2.31
	MC	0.71	MC	1.95	MC	2.73

Legend: *LCX* left circumflex artery, *MBF* myocardial blood flow, *MFR* myocardial flow reserve, *NMC* no motion correction, *MC* motion correction, *RCA* right coronary artery

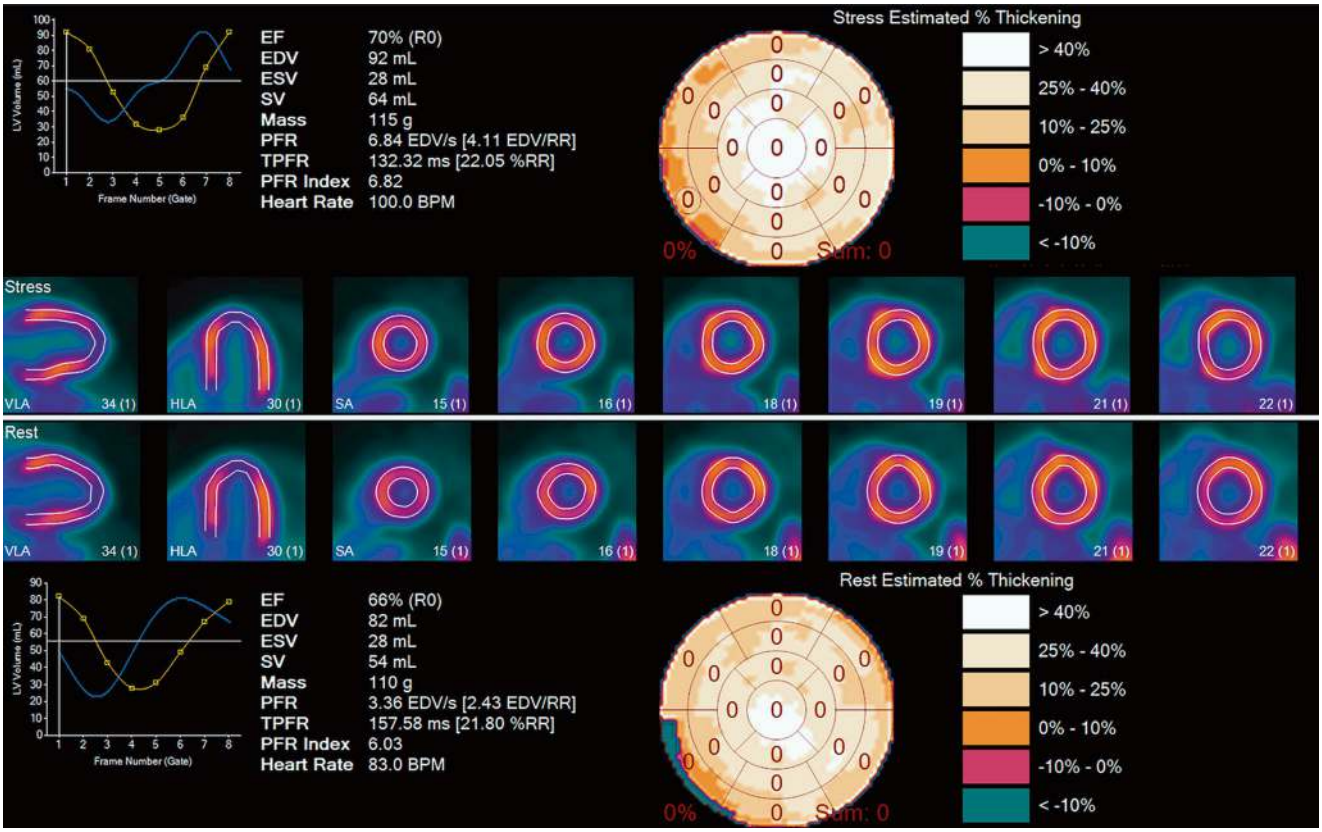


Fig. 2.8 Selected views of the right and left coronary arteries show normal coronary anatomy of both RCA (left panel) and left coronary system (right panel)

- In the study non-corrected for motion, MFR appears severely impaired in the right coronary artery (RCA) territory (Regadenoson stress test) due to abnormally elevated rest MBF.
- Study reconstructed after motion correction shows values within normal limits.

Imaging Diagnosis

- Normal study.

Differential Diagnosis

- Obstructive coronary artery disease with single-vessel myocardial ischemia.

Correlative Imaging

- Coronary angiography showing normal coronary anatomy (Fig. 2.8).

Management
- Reassurance and risk factor management.

Further Reading
- Vleeming E, Lazarenko S, van der Zant F, Pan X, Declerck J, Wondergem M, et al. Cardiac Displacement During13N-Ammonia Myocardial Perfusion PET/CT: Comparison Between Adenosine- and Regadenoson-Induced Stress. Journal of Nuclear Medicine Technology. 2017;46:114–122.
- Schleyer P, O'Doherty M, Barrington S, Morton G, Marsden P. Comparing approaches to correct for respiratory motion in NH3 PET-CT cardiac perfusion imaging. Nuclear Medicine Communications. 2013; 34:1174–1184.

2.4 Ammonia Lateral Defect: Case 4

Key Points
- Decreased counts in the lateral wall of the left ventricle with ^{13}N-ammonia PET/CT occurs frequently. Misalignment of the PET and CT images should always be considered and checked.
- The challenge is to differentiate between a real perfusion defect vs artifact.

History
- A 40-year-old woman.
- Asymptomatic. No cardiovascular risk factors. Presurgical (kidney donor).

PET/CT Images (Fig. 2.9)

Findings
- Decreased perfusion in the lateral wall of the left ventricle at rest and stress.
- Normal thickening, normal LV function with a rest LVEF of 79% up to 87% at peak stress; MBF and MFR.

Imaging Diagnosis
- Normal study.

Differential Diagnosis
- Ischemic disease in the left circumflex territory.

Correlative Imaging
- Coronary CT angiography (Fig. 2.10).

Management
- None.

Further Reading
- Klingensmith W, Noonan C, Goldberg J, Buchwald D, Kimball J, Manson S. Decreased Perfusion in the Lateral Wall of the Left Ventricle in PET/CT Studies with 13 N-Ammonia: Evaluation in Healthy Adults. Journal of Nuclear Medicine Technology. 2009;37:215–219.
- Nakazato R, Berman D, Alexanderson E, Slomka P. Myocardial perfusion imaging with PET. Imaging in Medicine. 2013;5:35–46.

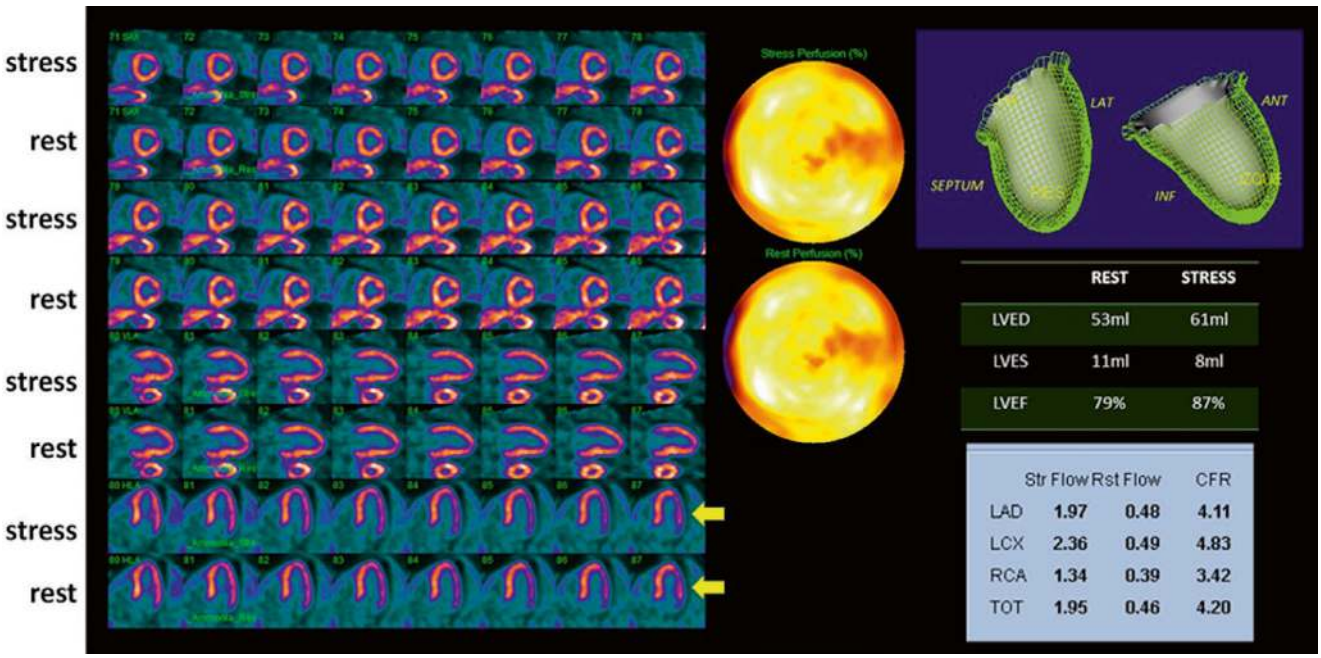


Fig. 2.9 Summed Regadenoson stress and rest myocardial perfusion PET/CT images obtained with ^{13}N-ammonia. Fixed perfusion defect in the lateral wall (arrows). Normal left ventricular systolic function and normal MFR

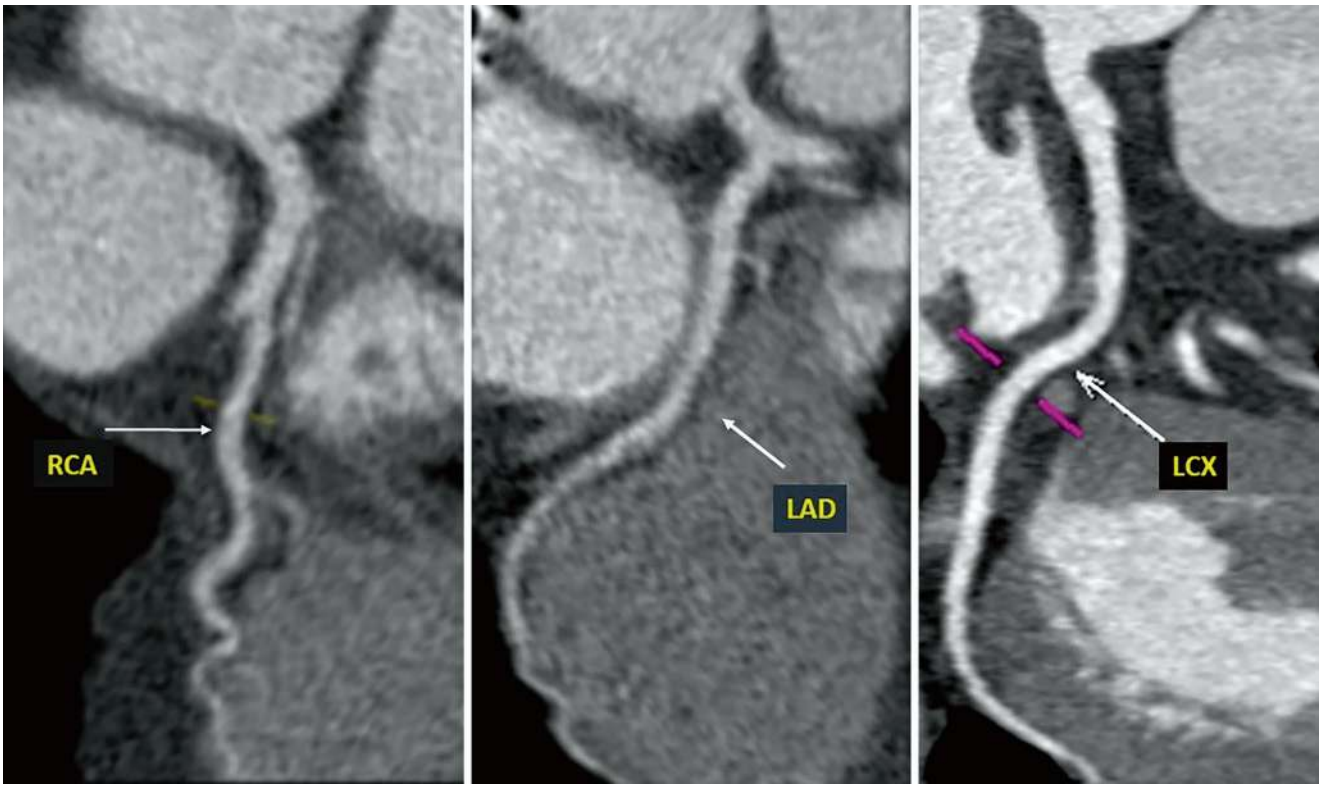


Fig. 2.10 Normal coronary CT angiography, without evidence of obstructive lesions

2.5 Nonresponder to Coronary Vasodilators: Case 5

Key Points

- Even low levels of serum caffeine may considerably worsen global and regional perfusion heterogeneity, leading to false positive and false negative perfusion results, and potentially impairing optimal patient risk stratification and management.
- Current guidelines recommend avoidance of adenosine, dipyridamole, and regadenoson if caffeine has been consumed within 12 h.
- Patients should be strictly reminded to avoid caffeine and xanthine (coffee, tea, etc.) when pharmacologic stress testing is planned.
- Personnel should inquire at reception if instructions have been complied with.

History

- A 67-year-old man with type 2 diabetes.
- Risk factors: dyslipidemia, hypertension.
- At the age of 35, multivessel revascularization by coronary artery bypass graft (CABG).
- At the age of 57, percutaneous coronary intervention (PCI) on multiple vessels.
- $^{13}NH_3$ PET/CT requested for evaluation of residual ischemia.

PET/CT Images

- A first study showed normal perfusion both at stress and rest, but low MFR values (Fig. 2.11).

Enquired after completion of the imaging procedure, the patient admitted having had a cup of coffee 30 min before the stress test, despite detailed instructions given at registration. The patient was instructed to avoid caffeine, and the study was repeated the following day (Fig. 2.12).

Findings

- No reversible perfusion defects on initial MPI.
- No flow reserve after dipyridamole infusion.
- The first test deemed falsely negative due to caffeine intake.

Imaging Diagnosis

- Vasodilator non-responsiveness.

Differential Diagnosis

- Vasodilator non-responsiveness.
- Multivessel obstructive coronary artery disease.
- Diffuse microvascular dysfunction.

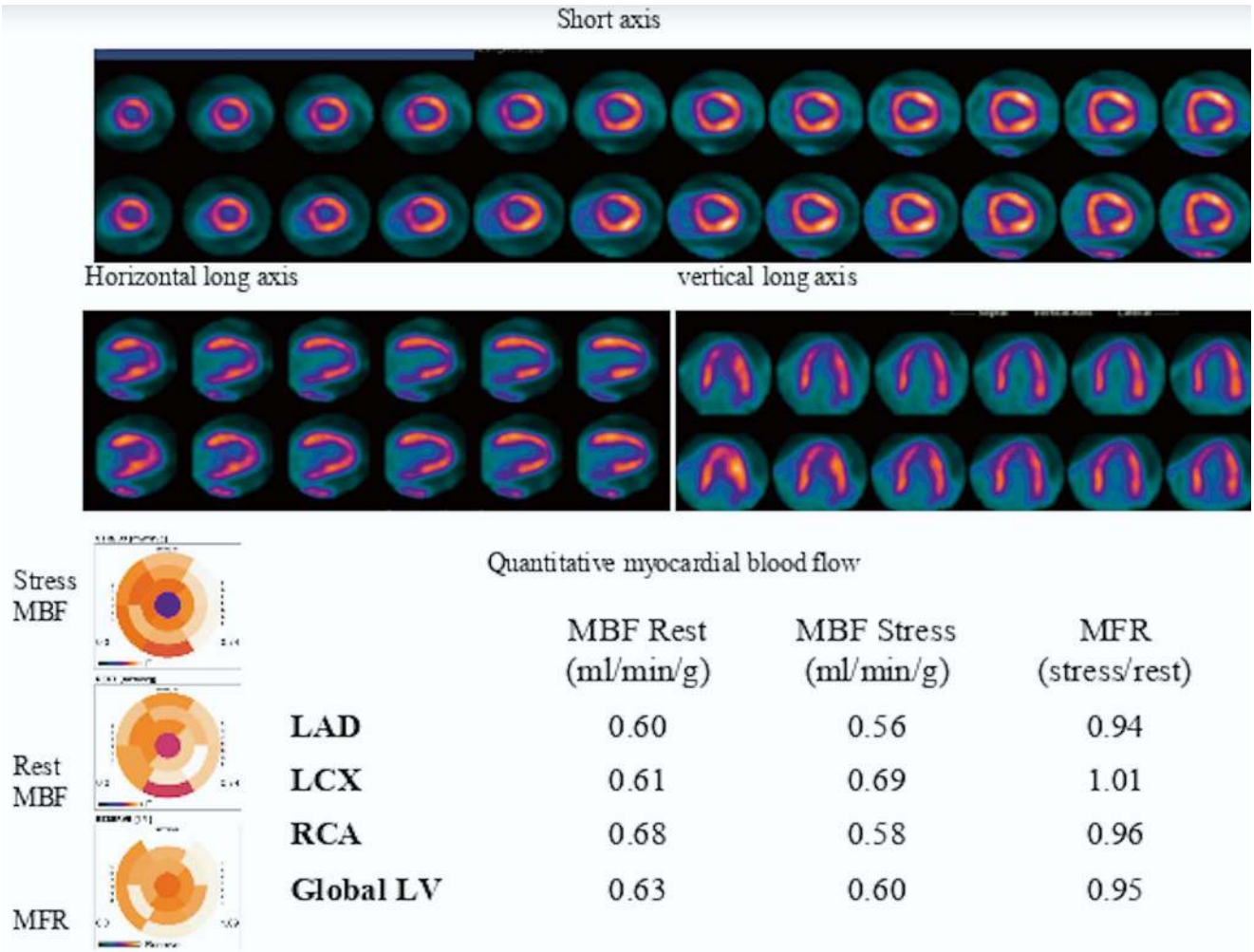


Fig. 2.11 The first MPI shows normal perfusion. MFR values, however, are below normal for all coronary territories

Management

- Repetition of the study after instructions to the patient to avoid caffeine.

Further Reading

- Kitkungvan D, Bui L, Johnson N, Patel M, Roby A, Vejpongsa P, et al. Quantitative myocardial perfusion positron emission tomography and caffeine revisited with new insights on major adverse cardiovascular events and coronary flow capacity. European Heart Journal - Cardiovascular Imaging. 2019;20:751–762.
- Dorbala S, Ananthasubramaniam K, Armstrong I, Chareonthaitawee P, DePuey E, Einstein A, et al. Single Photon Emission Computed Tomography (SPECT) Myocardial Perfusion Imaging Guidelines: Instrumentation, Acquisition, Processing, and Interpretation. Journal of Nuclear Cardiology. 2018;25:1784–1846.

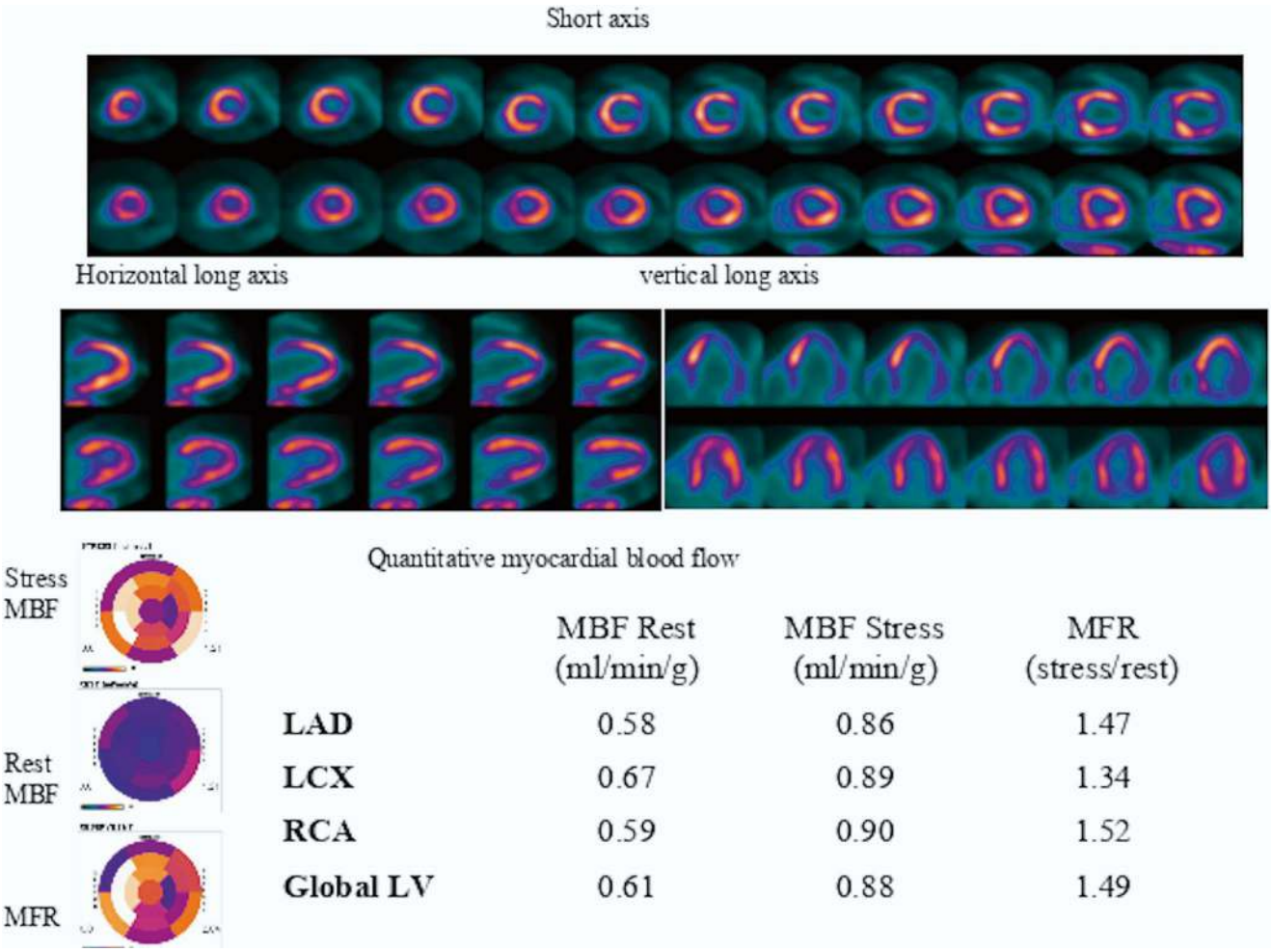


Fig. 2.12 The repeated study shows a severe, reversible perfusion defect in the left circumflex artery (LCX) territory and posteroseptal segment after dipyridamole infusion, together with transient ischemic dilation (TID). MFR calculation show reduced values for all coronary arteries, more prominent for the LCX

2.6 Vasodilator Non-responsiveness Mimic: Case 6

Key Points

- During maximal hyperemia, stress MBF augmentation is directly related to the coronary perfusion pressure, therefore marked hypotension during vasodilator stress can mimic vasodilator non-responsiveness.
- Reviewing changes in heart rate and blood pressure and assessing the presence of an appropriate *splenic switch off* during vasodilator stress can help differentiate non-responsiveness due to caffeine intake or theophylline-containing medications from other problems that can mimic non-responsiveness especially marked hypotension.
- If vasodilator non-responsiveness mimic is suspected, repeating the stress MPI study with dobutamine can help unmask possible underlying multivessel coronary artery disease or microvascular dysfunction.

History

- An 86-year-old woman with no known coronary artery disease was referred for a myocardial perfusion PET/CT study to evaluate for dyspnea.
- She had a history of hypertension and dyslipidemia.

PET/CT Images

Findings

- No evidence of regional perfusion defects on the stress or rest images.
- Severely blunted stress MBF and MFR.
- The transmission CT scan shows severe multivessel coronary artery calcium (CAC).

Differential Diagnosis and Management After Regadenoson Stress Study:

- The myocardial perfusion study is normal, and there are no ancillary markers of clinical risk including transient ischemic dilation (TID), drop in LVEF, or transient increase in RV tracer uptake.
- However, the blunted stress MBF and MFR in the context of severe CAC raises the concern of multivessel coronary artery disease.
- In this setting, the differential diagnoses include non-responsiveness to vasodilator stress, multivessel coronary artery disease, and severe coronary microvascular dysfunction.
- The nearly identical rest and stress MBF in all coronary territories strongly suggest non-responsiveness to Regadenoson.
- Vasodilator non-responsiveness can be assessed by reviewing changes in heart rate and blood pressure. An additional clue is to examine the radiotracer retention in the spleen. In the setting of an adequate vasodilator response, the tracer retention in the spleen during stress is typically lower than that at rest (so-called *splenic switch off*).
- Review of the radiotracer retention in the spleen demonstrated an appropriate "splenic switch off" suggesting an adequate response to regadenoson (Figs. 2.13 and 2.14, Table 2.2).
- However, review of her systemic hemodynamics (Table 2.3) revealed a marked hypotensive response to regadenoson. During maximal hyperemia, coronary autoregulation is abolished, and myocardial flow is entirely dependent on the coronary driving pressure. Consequently,

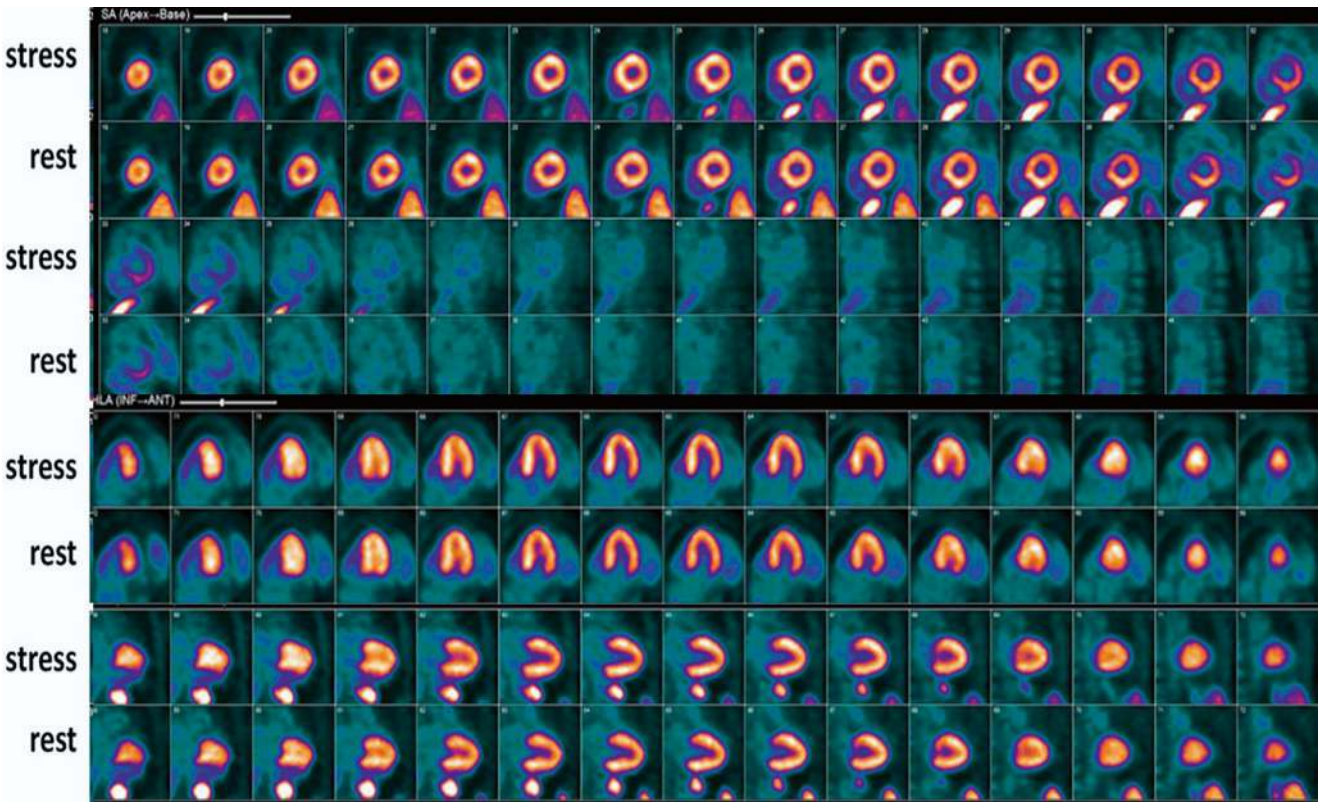


Fig. 2.13 Regadenoson stress and rest ^{82}Rubidium myocardial perfusion PET study. There are no perfusion defects on the stress or rest images

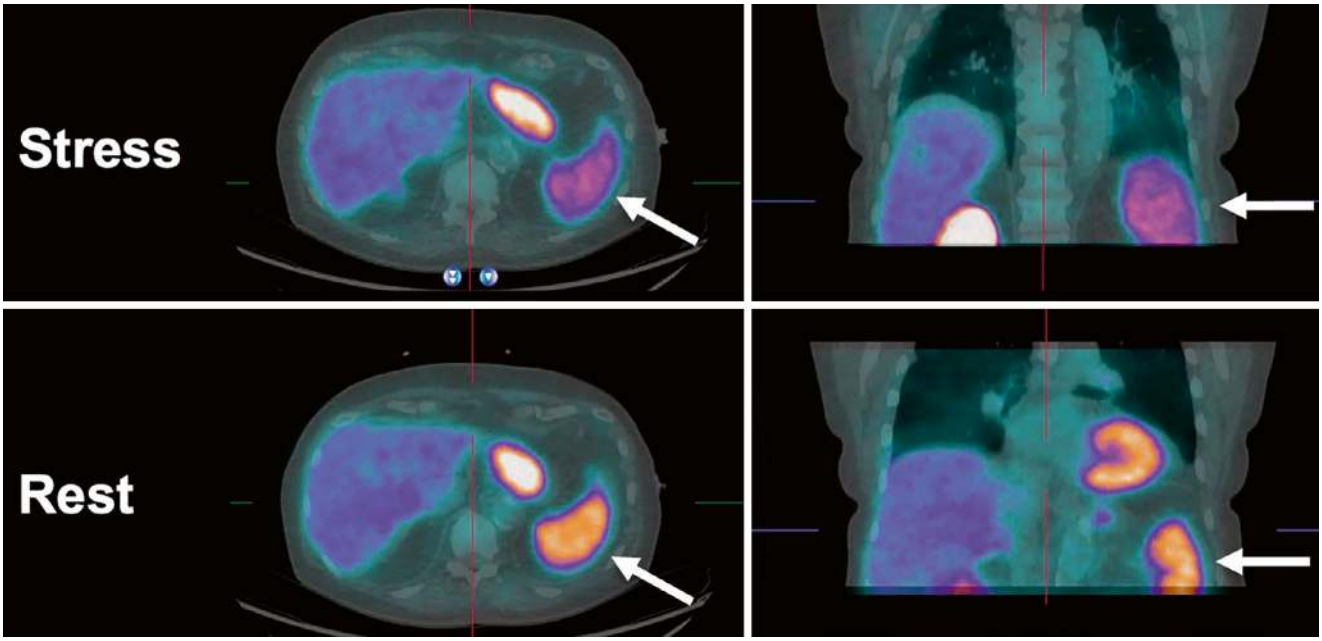


Fig. 2.14 Selective transaxial and coronal fused PET/CT images at rest and during stress. Counts in the spleen decreased appropriately during stress (arrows) consistent with an appropriate response to Regadenoson

Table 2.2 Summary of changes MBF and MFR with Regadenoson

	MBF rest (ml/min/g)	MBF stress (ml/min/g)	MFR (stress/rest)
LAD	0.86	0.96	1.12
LCX	0.91	0.96	1.05
RCA	0.86	1.02	1.18
Global LV	0.87	0.97	1.12

Table 2.3 Systemic hemodynamics at rest and during regadenoson PET MPI

	Heart rate (beats per minute)	Systolic blood pressure (mmHg)	Diastolic blood pressure (mmHg)	Mean arterial pressure (MAP)
Rest	56	155	83	107
Stress (Regadenoson)	74	98	48	65

the blunted stress MBF and MFR are likely caused by the marked drop in the MAP (noninvasive proxy for coronary pressure) (Fig. 2.15 and Table 2.4).

- The decision was to repeat the stress MPI study with dobutamine (Fig. 2.16).

Findings After Dobutamine Stress

- No evidence of regional perfusion defects on the stress or rest images.
- Normal stress MBF and MFR indicate no evidence of flow-limiting coronary artery disease or microvascular dysfunction.

Final Imaging Diagnosis

- Normal myocardial perfusion study demonstrating no evidence of flow-limiting coronary artery disease or microvascular dysfunction.

Differential Diagnosis

- None.

Correlative Imaging

- None.

Management

- The study ruled out flow-limiting coronary artery disease and microvascular dysfunction as potential reasons for her symptoms.
- She received optimization of risk factor management, including blood pressure control.

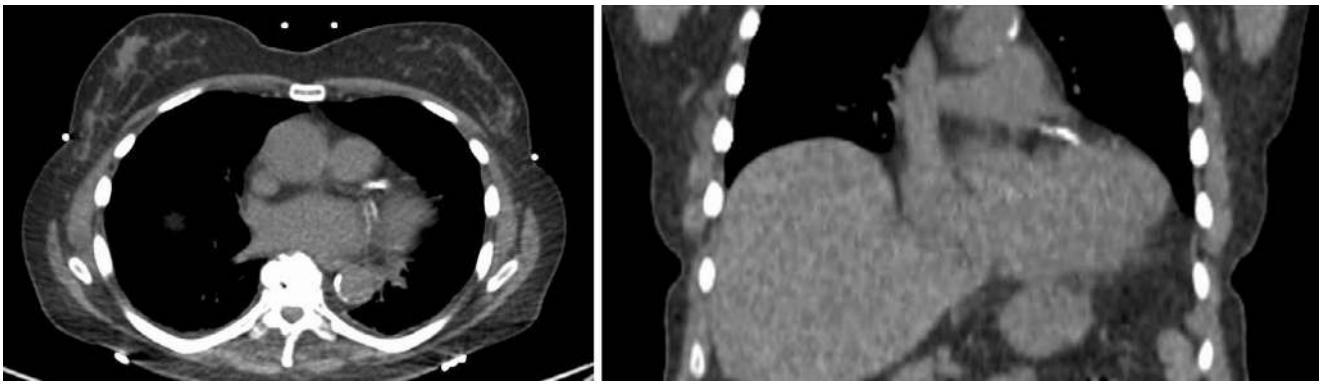


Fig. 2.15 Axial and coronal attenuation correction CT images showing coronary artery calcification

Table 2.4 Summary of changes MBF and MFR with dobutamine

	MBF rest (ml/min/g)	MBF stress (ml/min/g)	MFR (stress/rest)
LAD	1.04	2.38	2.30
LCX	1.01	2.42	2.41
RCA	1.09	2.62	2.42
Global LV	1.03	2.44	2.38

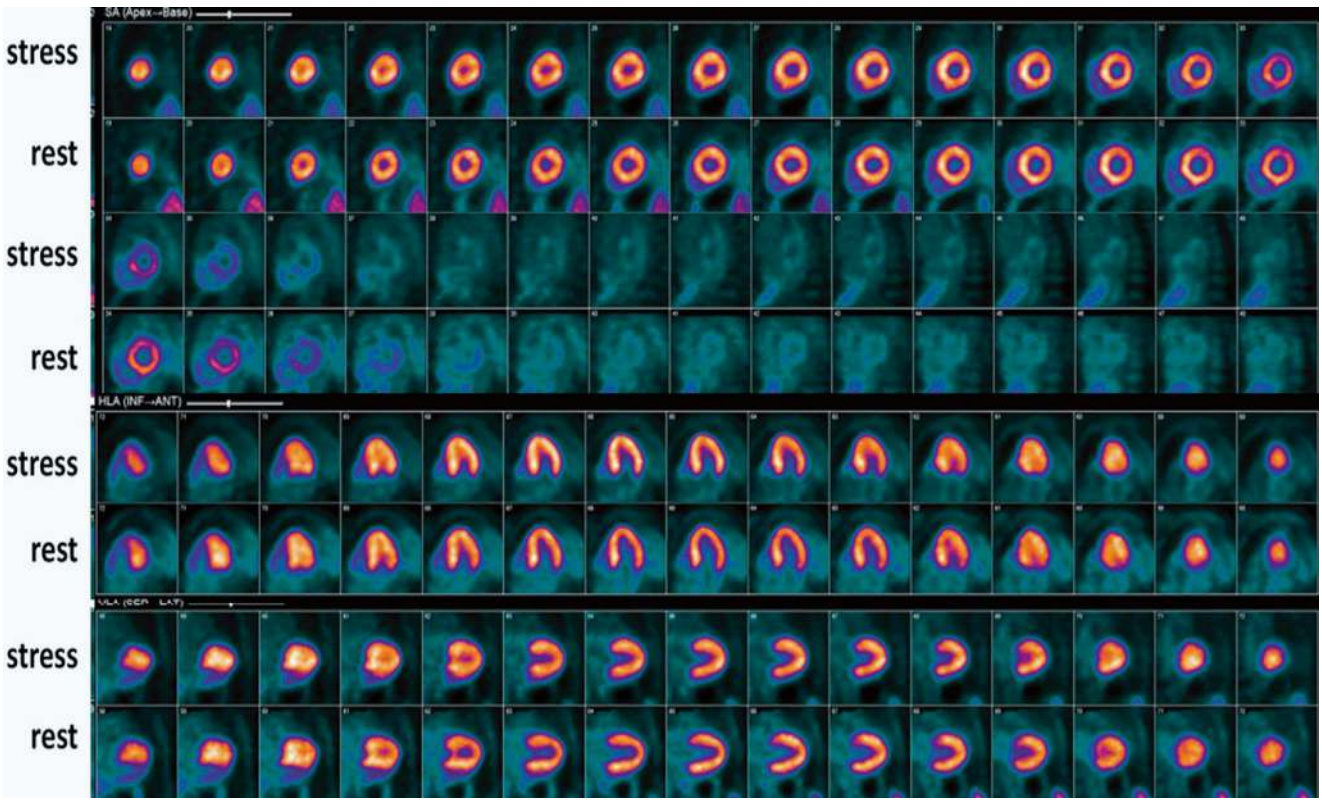


Fig. 2.16 Dobutamine stress and rest ^{82}Rubidium myocardial perfusion PET study. There are no perfusion defects on the stress or rest images

Further Reading

- Saad JM, et al. Journal of Nuclear Cardiology. 2023;30(4):1484–96.

2.7 Metal Artifact in Hot Spot Imaging: Case 7

Key Points

- ^{18}F-FDG PET/CT is a useful imaging technique in the evaluation of patients with fever of unknown origin. It is considered highly sensitive, but specificity is moderate. In equivocal cases, radiolabeled white blood cell imaging can be considered
- Dense calcification and metal can lead to artificially high ^{18}F-FDG uptake on attenuation correction images. It is always recommended that both the attenuation corrected and non-attenuation corrected images be evaluated.

History

- An 85-year-old woman with chronic atrial fibrillation and pacemaker implantation.
- She had a recent fall with displacement of the left hip and a peritrochanteric hematoma.
- She was being evaluated for fever of unknown origin and positive blood cultures which identified *Staphylococcus aureus*.
- Transesophageal echocardiography was negative for endocarditis.
- She was referred for ^{18}F-FDG PET/CT for the identification of possible infectious foci.

PET/CT Images (Fig. 2.17, 2.18, and 2.19)

Findings

- The ^{18}F-FDG PET/CT showed high tracer uptake in the left hip suggestive of peritrochanter infection or inflammation.
- There is a second focus of focal ^{18}F-FDG uptake at the level of the left subclavian vein, corresponding to the pacemaker lead. This is present on both the attenuation-corrected and uncorrected PET images.
- There is an additional focus of intense ^{18}F-FDG accumulation in the area of dense mitral annular calcification, which almost completely disappears in the non-attenuation correction PET images.

Imaging Diagnosis

- Focal areas of increased ^{18}F-FDG uptake consistent with infection including the left hip and pacemaker lead.



Fig. 2.17 Coronal ^{18}F-FDG PET image demonstrating intense glucose uptake around the left hip

Differential Diagnosis

- Infection
- Nonspecific inflammation
- Artifact

Management

- The presence of focal ^{18}F-FDG uptake in the pacemaker leads that persisted in the uncorrected PET images in the clinical context of a patient with fever and bacteremia with positive blood cultures is consistent with an infected pacemaker lead.
- The pacemaker lead was removed. Culture of the device was positive for *Staphylococcus aureus*.
- Systemic broad-spectrum antibiotic therapy was initiated.
- The ^{18}F-FDG focus around the dense mitral annular calcification was an attenuation correction artifact.

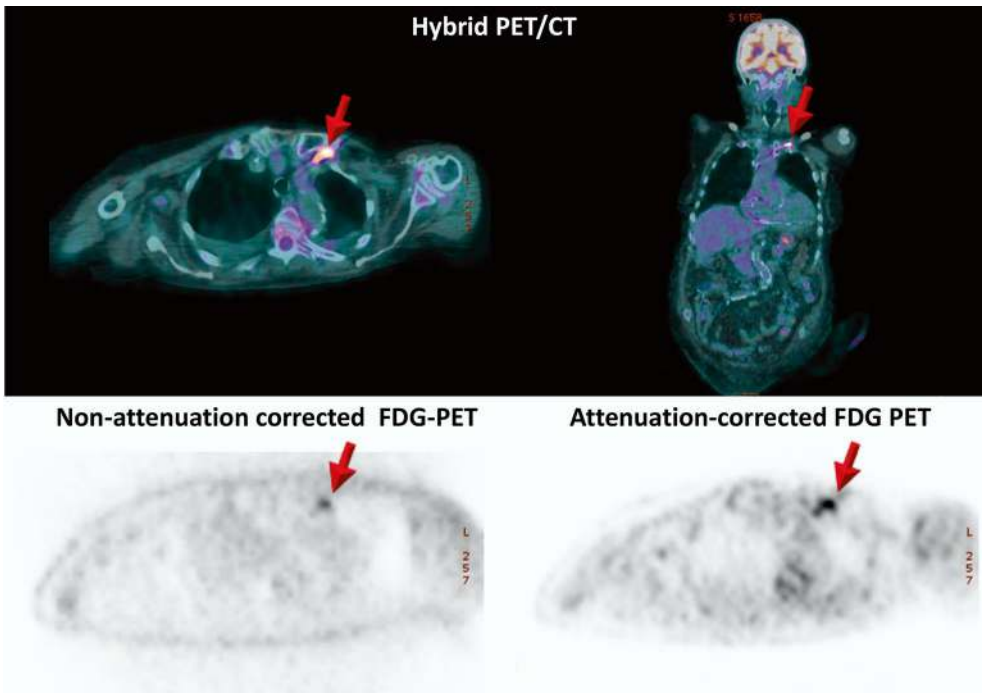


Fig. 2.18 ^{18}F-FDG PET/CT images demonstrating intense focal uptake around the pacemaker lead on attenuation corrected images (arrow, top panel), which persists on the non-attenuation corrected images (arrow, lower panel)

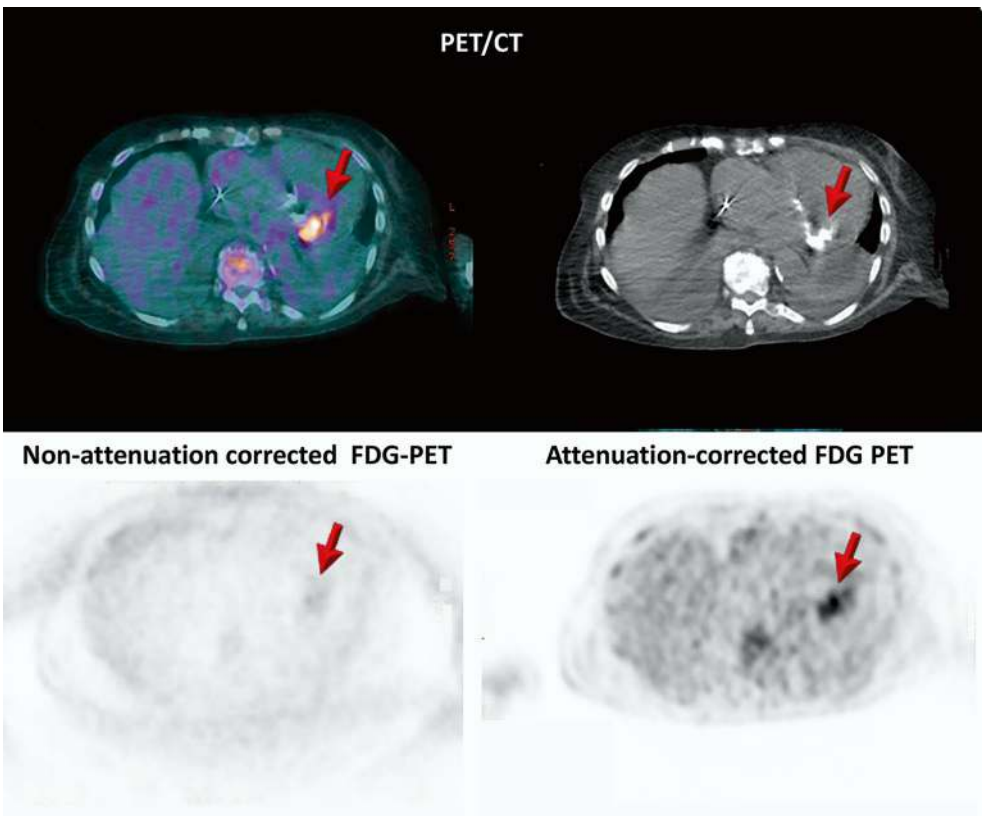


Fig. 2.19 ^{18}F-FDG PET/CT images showing intense ^{18}F-FDG accumulation in the area corresponding to intense mitral annular calcification (arrow, top panel). This almost completely disappears on non-attenuation correction images suggesting that it is an artifact (arrow, lower panel)

Further Reading

- Kouijzer I, Mulders-Manders C, Bleeker-Rovers C, Oyen W. Fever of Unknown Origin: the Value of FDG-PET/CT. Seminars in Nuclear Medicine. 2018;48:100–107.
- Diemberger I, Bonfiglioli R, Martignani C, Graziosi M, Biffi M, Lorenzetti S, et al. Contribution of PET imaging to mortality risk stratification in candidates to lead extraction for pacemaker or defibrillator infection: a prospective single center study. European Journal of Nuclear Medicine and Molecular Imaging. 2018;46:194–205.

2.8 Recognizing and Troubleshooting Artifacts with Flow Quantification

2.8.1 Radiotracer Injection

To ensure accurate estimates of MBF and MFR, it is critical to verify that each dynamic series is acquired and analyzed correctly, with thorough review of quality assurance information. Please refer to Chap. 1 (Fig. 1.6) for a detailed discussion of the placement of regions of interest and the construction of time-activity curves. The peak height of blood pool time-activity curves at rest and stress should be comparable (or slightly lower at stress) if similar radiotracer activities are injected (Fig. 2.20). If there are substantial differences, extravasation or incomplete delivery of tracer may have occurred and may result in inaccurate MBF estimates.

A good quality AIF has a sharp rise and a narrow peak followed by a sharp decline in counts in arterial blood. The integral of the area under the AIF will be used as the denominator of the MBF calculation so it is critically important to capture the true peak height of the counts in arterial blood. As counts in arterial blood decline, there is a rise in tissue counts representing the myocardial retention phase (red line). Since the injected doses of Rubidium-82 are typically similar at rest and during stress, the peak height of arterial blood pool curve at rest is comparable or can be slightly higher than that at stress. However, the peak height of the blood pool curve will be substantially different with imaging protocols using a low-dose rest/high-dose stress radiotracer injection (e.g., N-13 ammonia, F-18 flurpiridaz) (Fig. 2.21).

The shape of the blood input function should also be standardized as much as possible, as variations in tracer injection profile have been shown to adversely affect MBF accuracy and test-retest repeatability. Arterial blood pool time-activity curves should also be visually examined for multiple peaks or broad peaks, which may suggest poor-quality injections due to poor-quality intravenous catheters, arm positioning, or other factors.

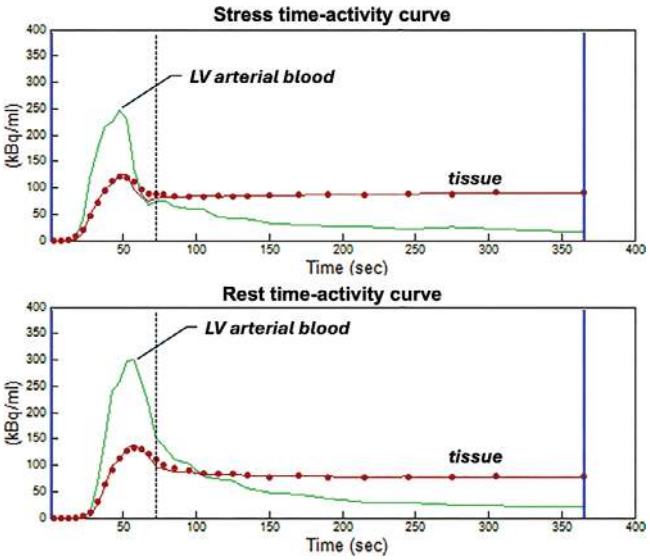


Fig. 2.20 Stress and rest Rubidium-82 time-activity curves. The light green curve represents the change in radioactivity concentration in the arterial LV blood pool over time. Imaging begins prior to the arrival of the radioactive bolus (note the absence of counts in the first two to three frames). The light green line illustrates the change in radioactivity concentration over time also known as the arterial input function (AIF) and represents the first pass of the radioactive bolus through the LV cavity

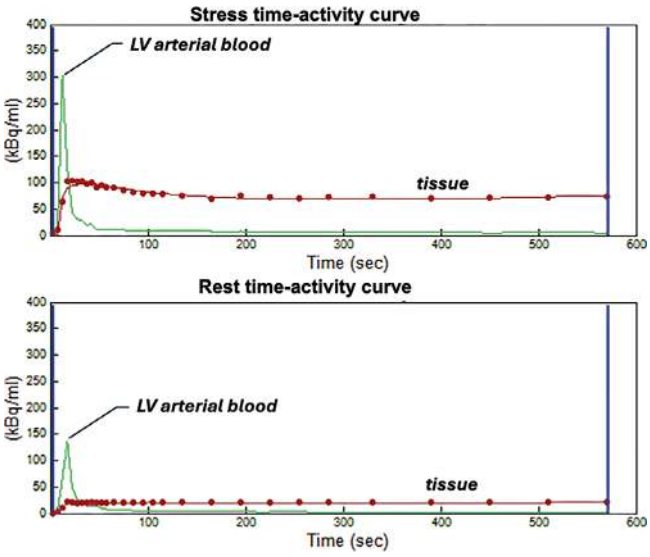


Fig. 2.21 Stress and rest N-13 ammonia time-activity curves obtained with a low-dose rest and high-dose stress injection protocol. As the injected dose at rest is at least three times lower than that injected at stress, the peak height of the AIF at rest is expected to be substantially lower than that during stress

2.8.2 Problems with the Timing of the Arterial Blood Input Curve

For adequate quantification of myocardial blood flow, dynamic time-activity curves must include at least one background frame to ensure adequate sampling of the complete arterial blood input function (Fig. 2.20 and 2.21). A late start of image acquisition relative to radiotracer injection can result in an incomplete or completely missed arterial blood input function (Fig. 2.22). In such cases, blood flow quantification will be inaccurate (partial capture of the arterial blood input curve) or not possible at all (complete miss of the arterial blood input curve).

2.8.3 Patient Motion

Assessment and correction of patient motion during the first-pass arterial phase are essential, as this can otherwise introduce a large bias in the estimated MBF values (Figs. 2.23 and 2.24). All commercially available software packages provide automated and manual options for motion correction of the multi-frame dynamic flow series. Appropriate motion correction is necessary to accurately quantify myocardial blood flow.

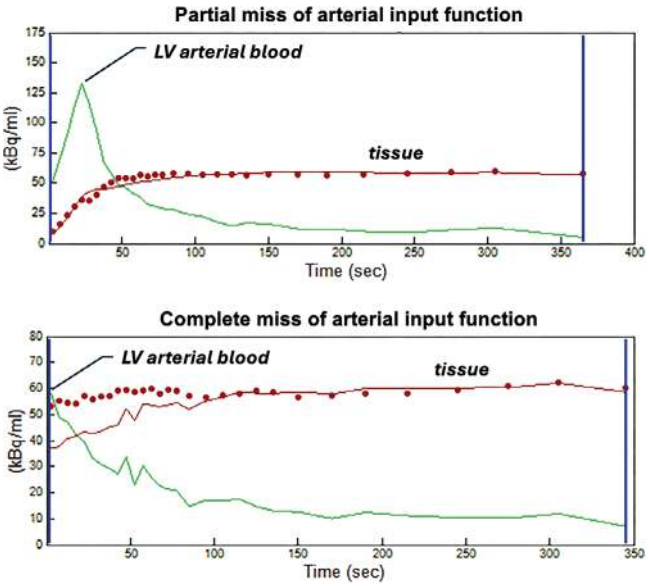


Fig. 2.22 Examples of a partial (top panel) or a complete (lower panel) miss of the upstroke of the AIF caused by delays in the start of imaging relative to the radiotracer injection. In both cases, computation of MBF will be inaccurate and should not be used for imaging interpretation or reporting. If MBF quantification is critical to the case (i.e., investigation of coronary microvascular disease), the patient should undergo a repeat study

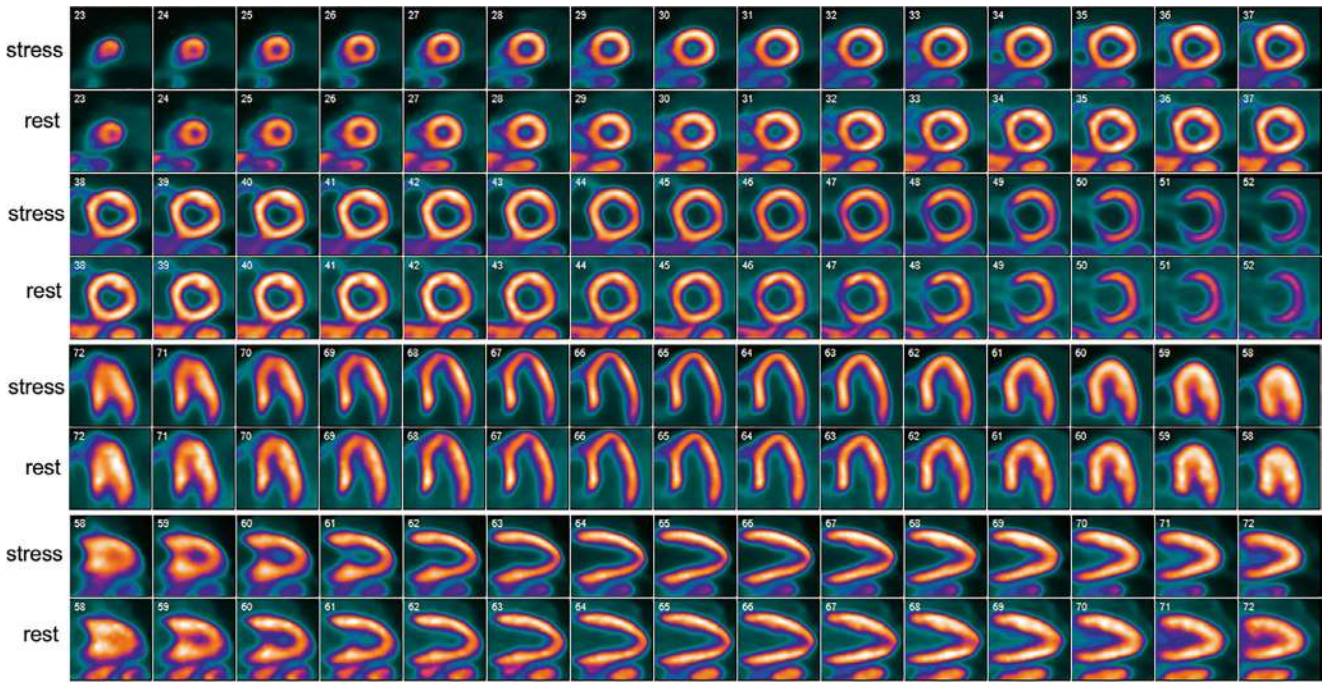


Fig. 2.23 Stress and rest ^{82}Rubidium PET images demonstrating no evidence of regional perfusion defects

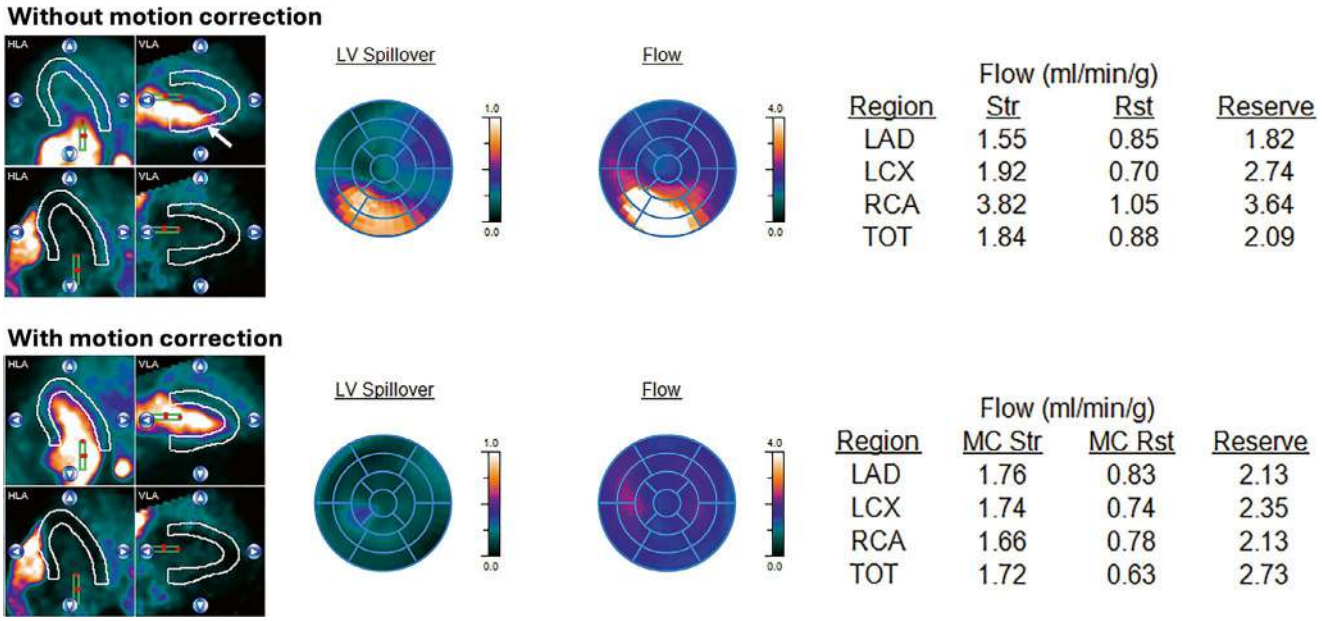


Fig. 2.24 First-pass transit of the ^{82}Rubidium bolus through the heart during rest and stress without and with motion correction (left panel). Without motion correction, the LV blood pool frame in the VLA image is misaligned and overlapping the inferior LV wall (arrow), resulting in increased spillover of LV blood pool counts onto the inferior wall (middle panel, LV spillover polar map) and the corresponding increase in myocardial blood flow (middle panel, flow polar map) with a stress myocardial blood flow in the RCA territory of 3.82 mL/min/g. After motion correction, the LV blood pool is now aligned within the LV cavity which in turn corrected the increased spillover fraction in the inferior wall, resulting in a more accurate myocardial blood flow estimation in the RCA territory of 1.66 mL/min/g consistent with stress flows in the other vascular territories

It is important to keep in mind that severe patient motion resulting in visible reconstruction artifacts on the static (late phase) myocardial perfusion images will often result in inaccurate MBF estimations even after ways to correct reconstruction artifacts from severe patient motion in the dynamic flow series. Consequently, one cannot rely on MBF values to troubleshoot motion artifacts on the static myocardial perfusion images. Figures 2.25 and 2.26 illustrate this point. This patient has a visible motion artifact on the static perfusion images, resulting in an inferior wall defect (Fig. XX, left panel). Despite adequate motion correction of the dynamic flow series, MBF is severely reduced in the inferior wall (Fig. XX, stress MBF in RCA territory: 1.41 mL/min/g). Using the MBF data to troubleshoot the interpretation of the static images would have resulted in the conclusion that this was an abnormal study, which would have been incorrect since there is no evidence of perfusion abnormalities after motion correction of the static images. The key point is that one should not use or report MBF quantification to overcome visible motion artifacts on the static images. In such cases, motion correction and a new reconstruction of the static images should be performed, and the motion corrected images should be used for the final report.

2.8.4 Residual Activity Correction

Compared to short-lived PET myocardial perfusion imaging radiotracers (e.g., Rubidium-82, ^{15}O water), the longer half-life of those radiolabeled with ^{18}F (e.g., flurpiridaz) or even ^{13}N ammonia (when used without delay between the stress and rest injections) necessitates correction of the residual radioactivity originating from the rest injection in stress scans when a rest/stress imaging sequence is used. As shown in Fig. 2.27, the residual activity correction is a critical quality control step for the accurate quantification of MBF, which improves diagnostic accuracy.

2.8.5 Vasodilator Non-responsiveness

Vasodilator non-responsiveness resulting in a blunted flow augmentation during stress markedly affects the accuracy of myocardial perfusion imaging (please also refer to *case # 5* earlier in this chapter). In this situation, myocardial perfusion images are nearly identical at rest and stress. Stress MBF is typically blunted similarly in all coronary vascular territories, resulting in severely reduced flow reserve (typi-

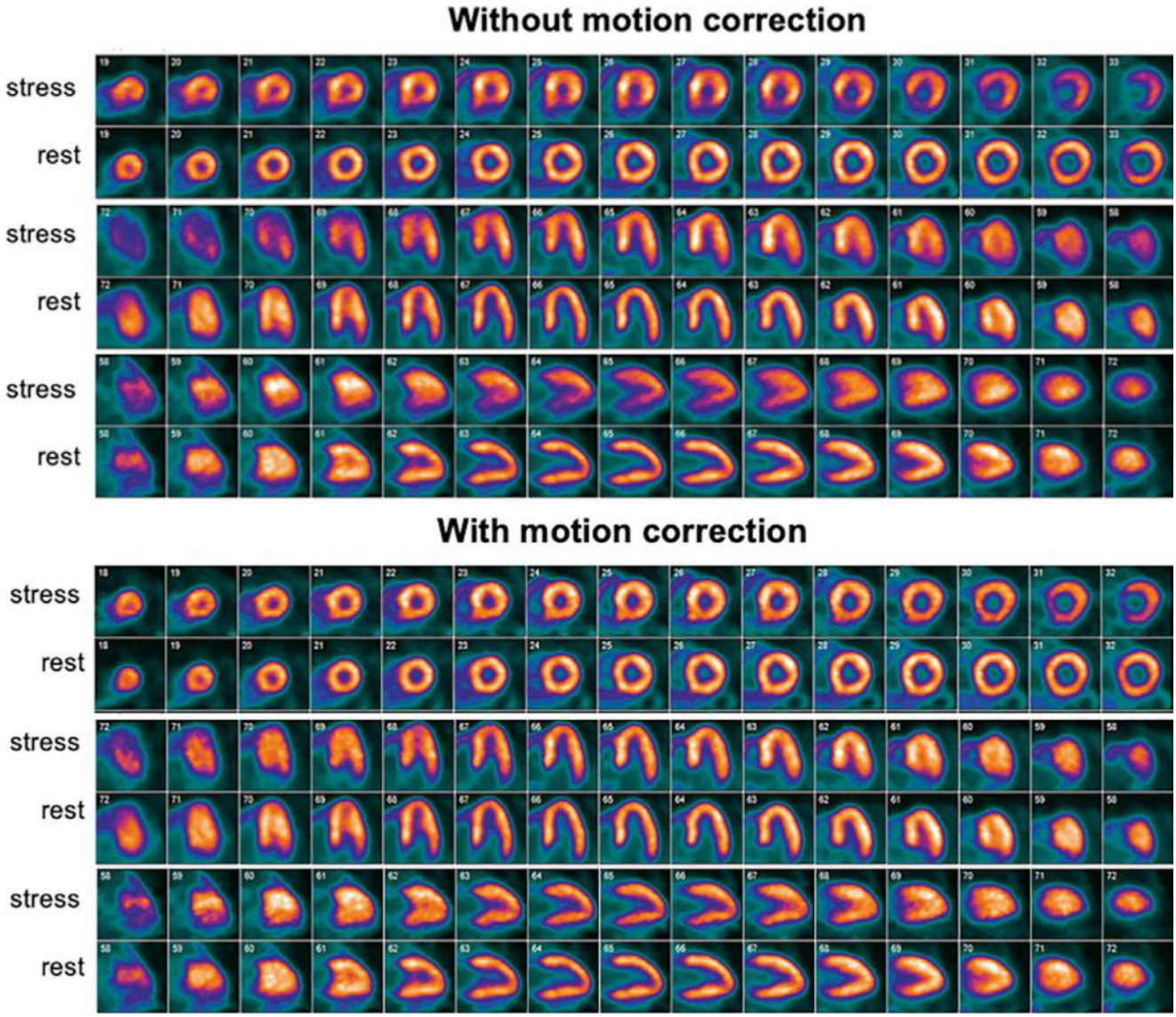


Fig. 2.25 Stress and rest ^{82}Rubidium PET images with motion artifact and an inferior wall defect (upper half), which is resolved after motion correction (lower half)

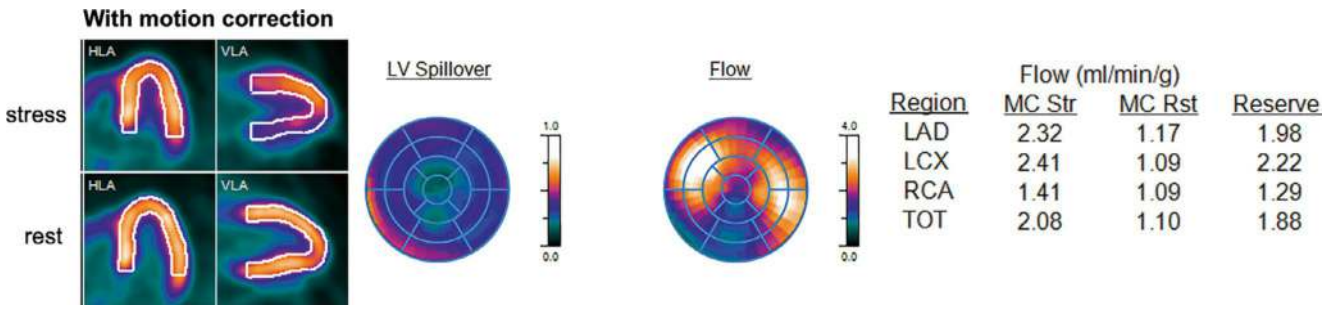


Fig. 2.26 First-pass transit of the ^{82}Rubidium bolus through the heart during rest and stress after motion correction (Left panel). Despite motion correction of the frames in the dynamic flow series, there is a visible flow abnormality in the inferior wall (middle panel, flow polar map) and the corresponding reduction in stress MBF in the RCA territory of 1.41 mL/min/g

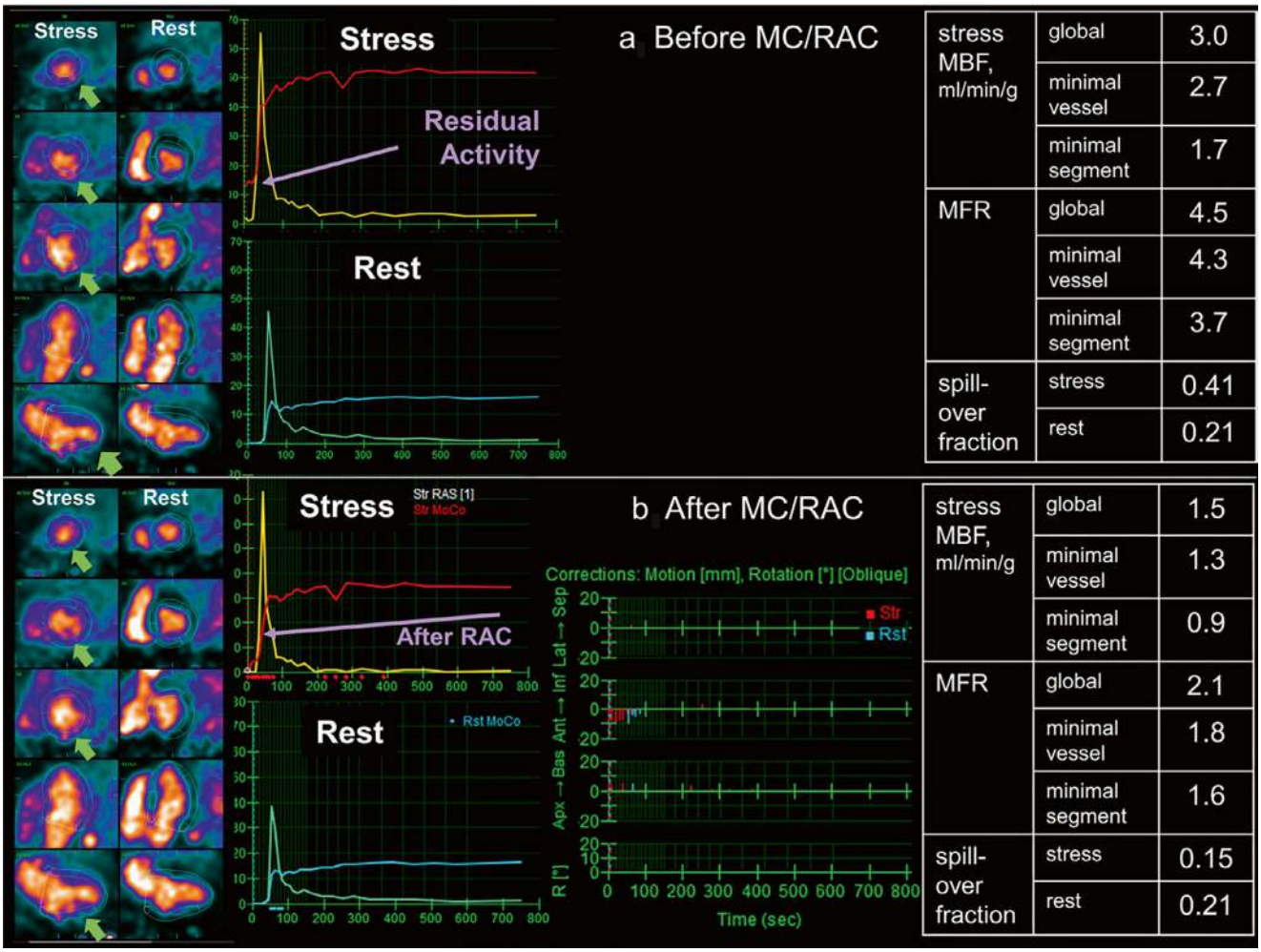


Fig. 2.27 Case example of a rest/stress ^{18}F flurpiridaz study. A 59-year-old male with multiple cardiovascular risk factors who had mild stenosis in LAD and total occlusion in distal RCA and LCX. MBF, MFR, and spillover fraction before (**a**) and after (**b**) motion correction and residual activity correction (RAC). The green arrows show the part where the blood pool is not aligned inside of myocardial contour, which implies there is a shift due to patient motion. Please note the nonzero baseline of the myocardial tissue curve before RAC and its correction to a zero baseline after RAC (purple arrows), and their large impact on the MBF estimation. MBF myocardial blood flow, MC motion correction, MFR myocardial flow reserve, LAD left anterior descending artery, LCX left circumflex coronary artery, RCA right coronary artery. Reproduced from Otaki Y, et al. Improved myocardial blood flow estimation with residual activity correction and motion correction in 18F-flurpiridaz PET myocardial perfusion imaging. (European Journal of Nuclear Medicine and Molecular Imaging (2022) 49:1881–1893)

cally close to 1). Differentiation between vasodilator nonresponsiveness from severe multivessel CAD or coronary microvascular dysfunction is of utmost clinical importance. One practical clue to differentiate between these conditions is to examine the change in counts from rest to stress in the spleen. Patients who responded to the vasodilator stress show a visible reduction in spleen counts from rest to stress (so-called splenic switch-off) (Figs. 2.28 and 2.29).

This patient was brought back for repeat vasodilator stress ^{82}Rubidium PET myocardial perfusion imaging. The stress and rest images are normal (Fig. 2.30). However, a review of the fused CT and PET images shows an appropriate reduction in spleen counts from rest to stress (Fig. 2.31), with the associated augmentation in MBF and a normal myocardial flow reserve.

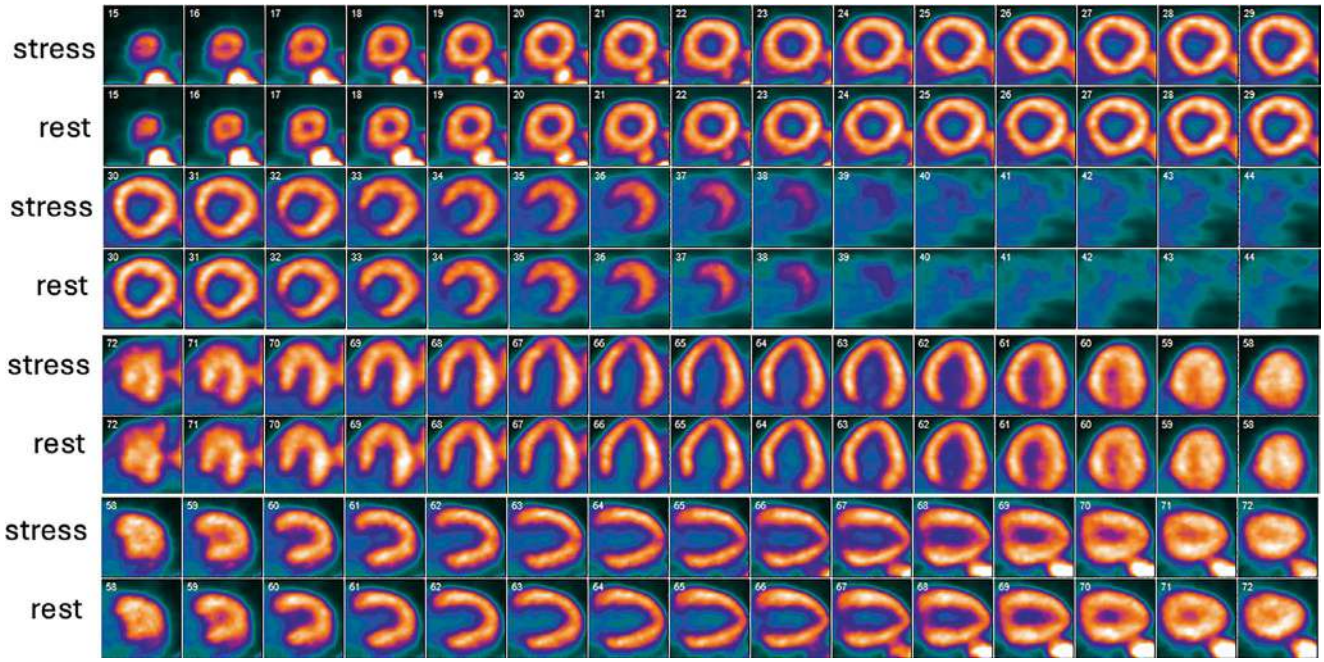


Fig. 2.28 Regadenoson stress and rest Rubidium-82 PET images showing no evidence of regional perfusion defects

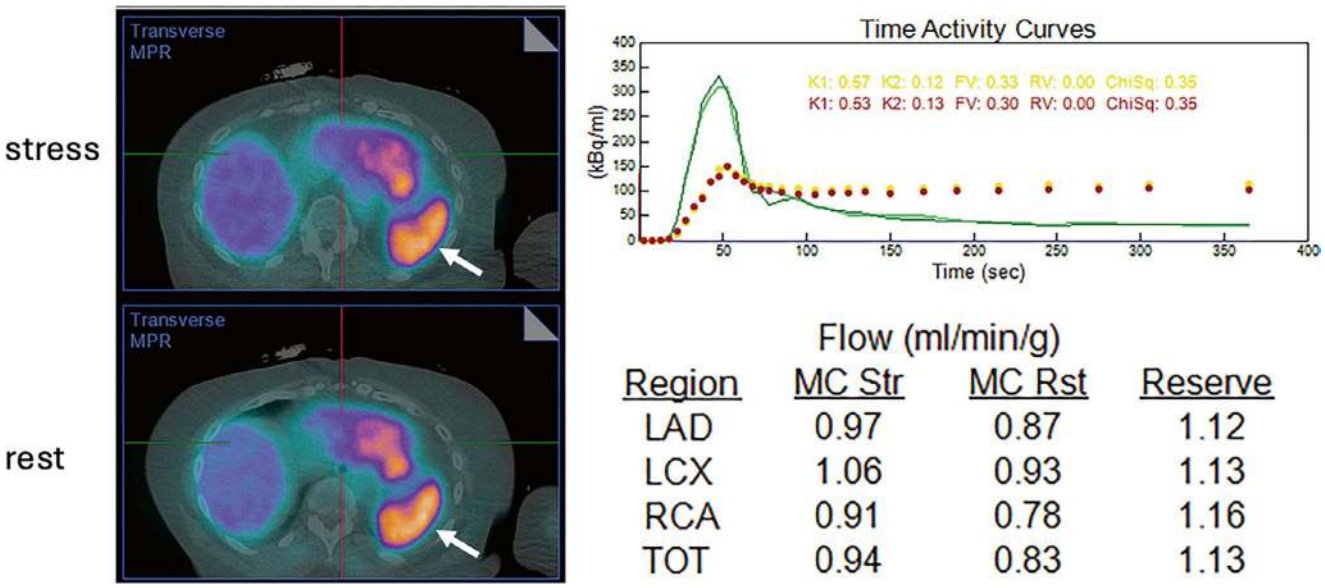


Fig. 2.29 Axial fused CT and ^{82}Rubidium PET images showing a lack of splenic switch-off (left panel, arrows showing no change in spleen counts from rest to stress). There is virtually no augmentation of myocardial blood flow during stress in all vascular territories resulting in a severely blunted flow reserve

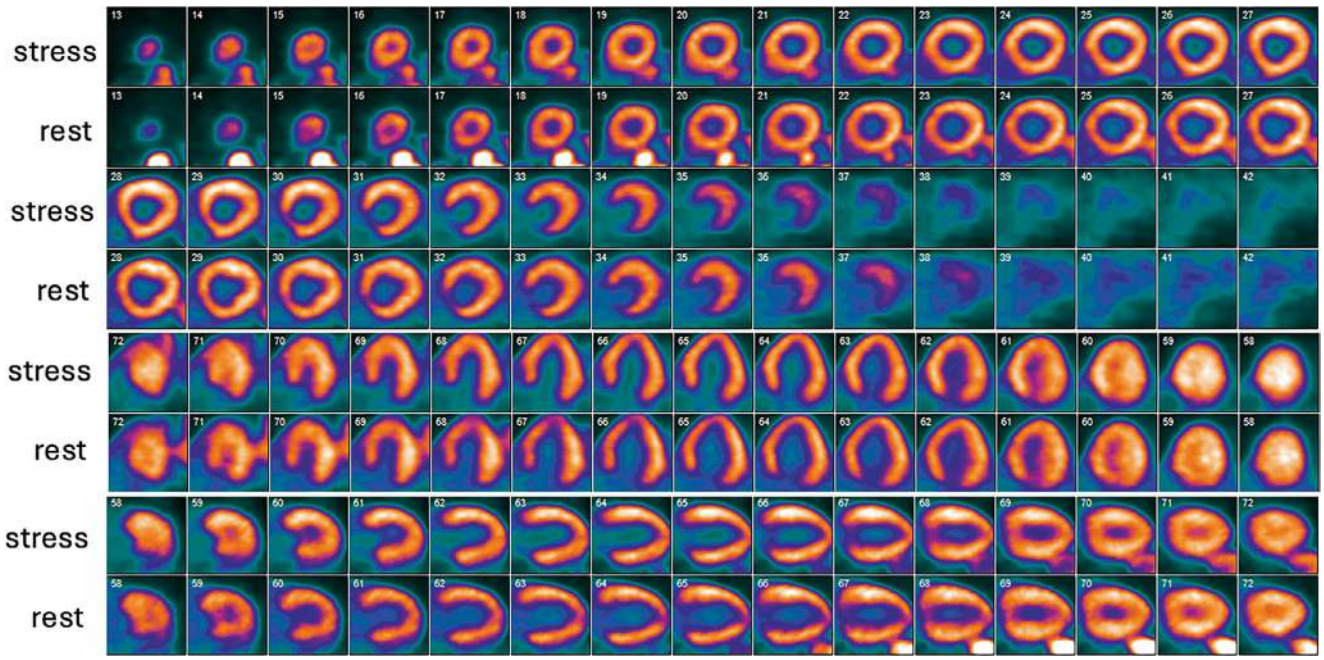


Fig. 2.30 Repeat Regadenoson stress and rest ^{82}Rubidium PET images showing no evidence of regional perfusion defects

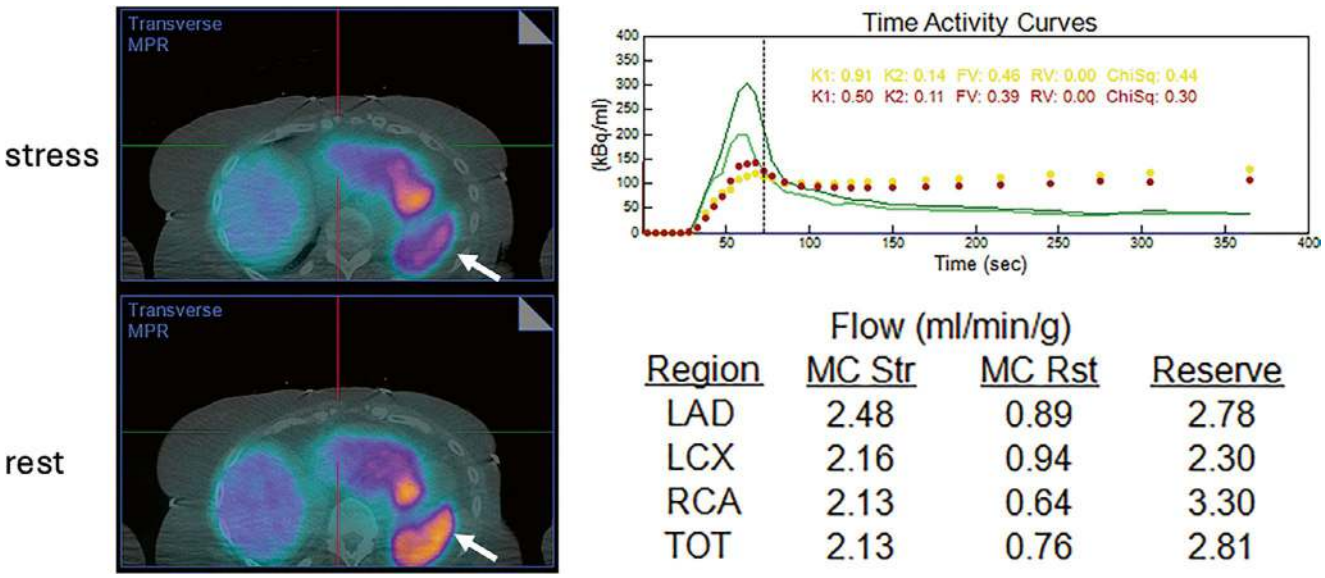


Fig. 2.31 Axial fused CT and ^{82}Rubidium PET images showing an appropriate splenic switch-off (left panel, arrows showing reduced spleen counts from rest to stress). There is normal rise of stress myocardial blood flow with normal flow reserve

2.8.6 Vasodilator Non-responsiveness Mimic

Marked hypotension during vasodilator stress can mimic vasodilator non-responsiveness. Reviewing changes in heart rate and blood pressure and assessing the presence of an appropriate splenic switch-off during vasodilator stress can help differentiate non-responsiveness due to caffeine intake or theophylline-containing medications from other problems that can mimic non-responsiveness especially marked hypotension. Please refer to ***case # 6*** (earlier in this chapter) for a more detailed discussion about this problem.

The opinions expressed in this chapter are those of the author(s) and do not necessarily reflect the views of the IAEA: International Atomic Energy Agency, its Board of Directors, or the countries they represent.

Open Access This chapter is licensed under the terms of the Creative Commons Attribution 3.0 IGO license (http://creativecommons.org/licenses/by/3.0/igo/), which permits use, sharing, adaptation, distribution and reproduction in any medium or format, as long as you give appropriate credit to the IAEA: International Atomic Energy Agency, provide a link to the Creative Commons license and indicate if changes were made.

Any dispute related to the use of the works of the IAEA: International Atomic Energy Agency that cannot be settled amicably shall be submitted to arbitration pursuant to the UNCITRAL rules. The use of the IAEA: International Atomic Energy Agency's name for any purpose other than for attribution, and the use of the IAEA: International Atomic Energy Agency's logo, shall be subject to a separate written license agreement between the IAEA: International Atomic Energy Agency and the user and is not authorized as part of this CC-IGO license. Note that the link provided above includes additional terms and conditions of the license.

The images or other third party material in this chapter are included in the chapter's Creative Commons license, unless indicated otherwise in a credit line to the material. If material is not included in the chapter's Creative Commons license and your intended use is not permitted by statutory regulation or exceeds the permitted use, you will need to obtain permission directly from the copyright holder.



Evaluation of Ischemic Heart Disease

3

Marcelo Di Carli, Raffaele Giubbini, Michelle Williams, Paolo Raggi, Vasvi Singh, Erick Alexanderson, Isabel Carvajal, Andrew Thornton, Raymond Endozo, Carlo Rodella, Diana Paez, and Maurizio Dondi

Objectives

- To learn how to recognize a normal myocardial perfusion study.
- To recognize common patterns of myocardial perfusion imaging for one, two, and multivessel diseases.
- To learn how to quantify the extent and severity of myocardial ischemia and scar.
- To recognize artifacts from different radiotracers that may mimic coronary artery disease.
- To understand how to integrate ancillary information (e.g., rest and stress left ventricular (LV) function, coronary artery calcium, and myocardial blood flow) to make an accurate diagnosis.
- To recognize how to differentiate predominantly obstructive coronary artery disease from coronary microvascular disease.

The use of hybrid imaging using positron emission tomography/computed tomography (PET/CT) in ischemic heart disease; integrating information from PET and CT, has grown in the last decade, particularly because of its capacity of quantifying myocardial perfusion, allowing the assessment of myocardial blood flow (MBF) and myocardial flow reserve (MFR). This feature makes PET/CT the best technique to detect multivessel coronary artery disease, which might not be identified with Single-photon Emission Computed Tomography (SPECT) due to its inherent limitation in cases of balanced ischemia. Additionally, the CT component of these hybrid imaging systems allows the calculation of coronary artery calcium score (CACS) and the visualization of the epicardial coronary arteries with coronary CT angiography (CCTA). PET/CT has therefore great potential in the diagnosis and management of coronary artery disease. This chapter covers several clinical cases, illustrating many different clinical applications in ischemic heart disease.

All authors have no conflict of interest to disclose.

M. Di Carli
Brigham and Women's Hospital, Boston, MA, USA
e-mail: mdicarli@bwh.harvard.edu

R. Giubbini
Nuclear Medicine, International Specialized Hospital of Uganda (ISHU), Kampala, Uganda
e-mail: raffaele.giubbini@unibs.it

M. Williams
British Heart Foundation Centre for Research Excellence, Institute for Neuroscience and Cardiovascular Research, University of Edinburgh, Edinburgh, United Kingdom
e-mail: michelle.williams@ed.ac.uk

P. Raggi
Division of Cardiology, University of Alberta, Edmonton, AB, Canada

V. Singh
Midwest Heart and Vascular Specialists, HCA Midwest Health, Kansas City, MO, USA
e-mail: vasvi.singh@hcahealthcare.com

E. Alexanderson · I. Carvajal
Instituto Nacional de Cardiologia Ignacio Chavex, Mexico City, Mexico

A. Thornton · R. Endozo
Institute of Nuclear Medicine, University College London Hospital, London, UK
e-mail: andrew.thornton11@nhs.net; raymond.endozo@nhs.net

C. Rodella
Department of Medical Physics, Spedali Civili Brescia, Brescia, Italy
e-mail: carlo.rodella@asst-spedalicivili.it

D. Paez · M. Dondi (✉)
Division of Human Health, International Atomic Energy Agency, Vienna, Austria
e-mail: d.paez@iaea.org; m.dondi@iaea.org

© The Author(s) 2027
M. Di Carli et al. (eds.), *IAEA Atlas of Cardiac PET/CT*, https://doi.org/10.1007/978-3-662-74188-7_3

3.1 Multi-parametric Evaluation of Ischemic Heart Disease

3.1.1 Normal PET MPI: Case 8

Key Points

- Normal myocardial perfusion with ^{82}rubidium PET with normal stress myocardial blood flow and flow reserve has a very high sensitivity and negative predictive value for excluding flow-limiting coronary artery disease.
- Normal myocardial flow reserve excludes the possibility of coronary microvascular dysfunction.
- For further discussion of interpretation of myocardial blood flow, see Chap. 1, Fig. 1.7.

History

- A 72-year-old man with exertional dyspnea with a history of hypertension, diabetes mellitus, and obesity was referred for a rest/stress myocardial perfusion PET/CT to evaluate possible flow-limiting coronary artery disease (Figs. 3.1 and 3.2).

PET/CT Images

Findings

- The rest and stress myocardial perfusion images demonstrate no evidence of regional perfusion abnormalities.
- The quantitative myocardial blood flow and flow reserve (MFR: normal values >2) are normal both regionally and globally.
- Myocardial blood flow (MBF) measurements (in mL/min/g) at rest and during regadenoson stress for each coronary artery territory and for the entire left ventricle are shown. The myocardial flow reserve (stress over rest MBF) is also shown.

Imaging Diagnosis

- Normal myocardial perfusion study.

Differential Diagnosis

- None.

Correlative Imaging

- None.

Management

- Reassurance and risk factor management.

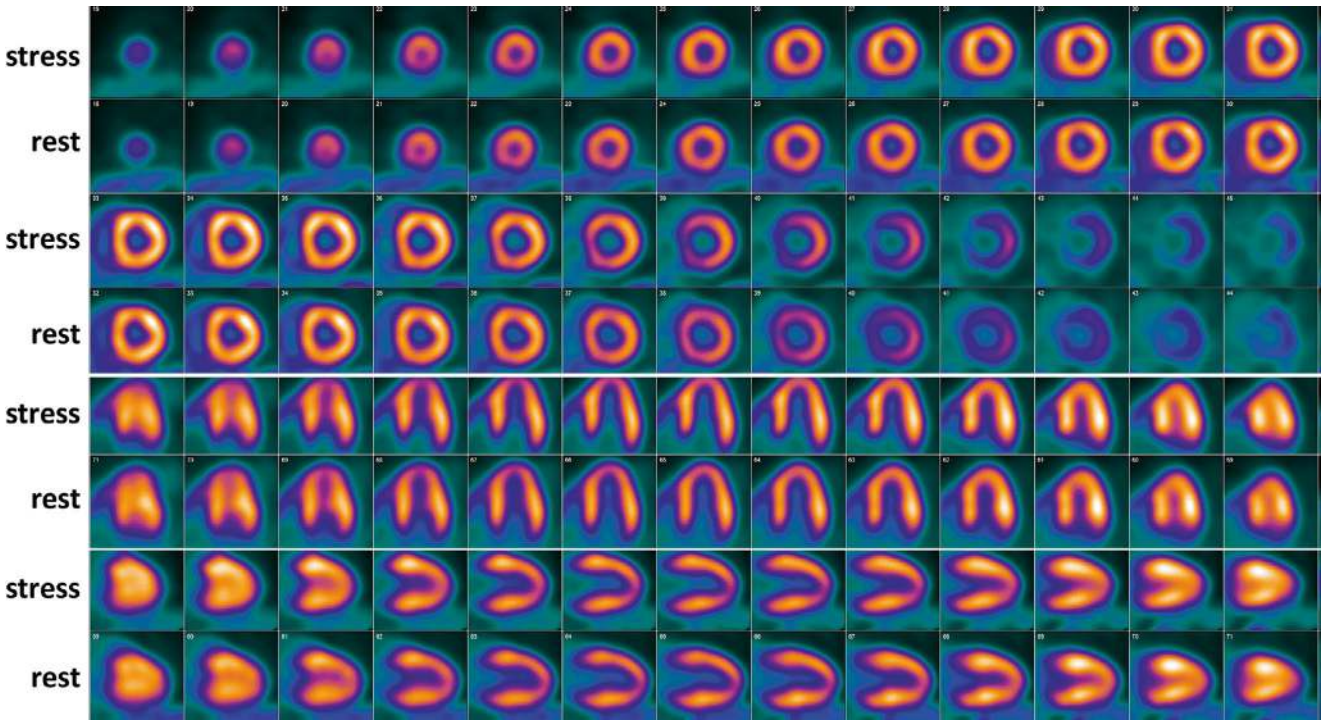


Fig. 3.1 Regadenoson stress and rest myocardial perfusion images obtained with ^{82}Rubidium as the perfusion tracer. Images are displayed in the short axis (top), horizontal long axis (middle), and vertical long axis (bottom) of the heart with the stress images on the top of each pair. The images demonstrate normal and homogeneous distribution of the radiotracer throughout the LV without regional perfusion defects



Fig. 3.2 The results show normal maximal MBF at stress (>1.8 mL/min/g) and flow reserve (>2) in all coronary territories and for the entire left ventricle

Further Reading

- McArdle B, Dowsley T, deKemp R, Wells G, Beanlands R. Does Rubidium-82 PET Have Superior Accuracy to SPECT Perfusion Imaging for the Diagnosis of Obstructive Coronary Disease?. Journal of the American College of Cardiology. 2012;60:1828–1837.
- Parker M, Iskandar A, Limone B, Perugini A, Kim H, Jones C, et al. Diagnostic accuracy of cardiac positron emission tomography versus single photon emission computed tomography for coronary artery disease: a bivariate meta-analysis. Circulation Cardiovascular Imaging. 2020;5:700–707.
- Neglia D, Rovai D, Caselli C, Pietila M, Teresinska A, Aguadé-Bruix S, et al. Detection of Significant Coronary Artery Disease by Noninvasive Anatomical and Functional Imaging. Circulation: Cardiovascular Imaging. 2015;8.
- Takx R, Blomberg B, Aidi H, Habets J, de Jong P, Nagel E, et al. Diagnostic Accuracy of Stress Myocardial Perfusion Imaging Compared to Invasive Coronary Angiography With Fractional Flow Reserve Meta-Analysis. Circulation: Cardiovascular Imaging. 2015;8.

Acknowledgment ^{82}Rubidium images are courtesy of Dr. Mouaz Al-Mallah, Methodist Hospital, Houston, Texas.

3.1.2 Single-Vessel Disease: Case 9

Key Points

- The presence of a regional perfusion defect with associated abnormality in quantitative MBF and MFR identifies the presence of hemodynamically significant coronary artery disease.
- Preserved hyperemic MBF and MFR in the LAD and left circumflex artery (LCX) territories help exclude multivessel flow-limiting coronary artery disease.
- A normal rest and stress left ventricular ejection fraction (LVEF) is also consistent with low-risk ischemia in a single vascular territory.
- For further discussion of interpretation of myocardial blood flow, see Chap. 1, Fig. 1.7.

History

- A 78-year-old man with typical angina with a history of dyslipidemia and hypertension.
- The patient was referred for PET/CT to assess for obstructive coronary artery disease (Tables 3.1 and 3.2).

PET/CT Images

Table 3.1 Summary of the quantitative blood flow data demonstrating reduced MFR in the RCA territory but preserved in the left anterior descending artery (LAD) and left circumflex aartery (LCX) territories

	MBF rest (ml/min/g)	MBF stress (ml/min/g)	MFR (stress/rest)
LAD	0.77	1.83	2.37
LCX	0.84	1.98	2.43
RCA	0.86	1.38	1.74
Global LV	0.82	1.75	2.22

Table 3.2 Left ventricular volumes and function

	EDV	ESV	EF	TID	LV mass
Rest	110 ml	39 ml	65%		153 g
Vasodilation	137 ml	47 ml	66%	–	172 g

Findings

- MPI shows a reversible perfusion defect in the right coronary artery (RCA) territory (Fig. 3.3).
- The rest LVEF was 65%, and it remained almost unchanged during stress at 66%.
- Stress MBF and MFR were reduced in the RCA territory.

Imaging Diagnosis

- Abnormal study consistent with moderate stress-induced ischemia in the RCA territory.

Differential Diagnosis

- None.

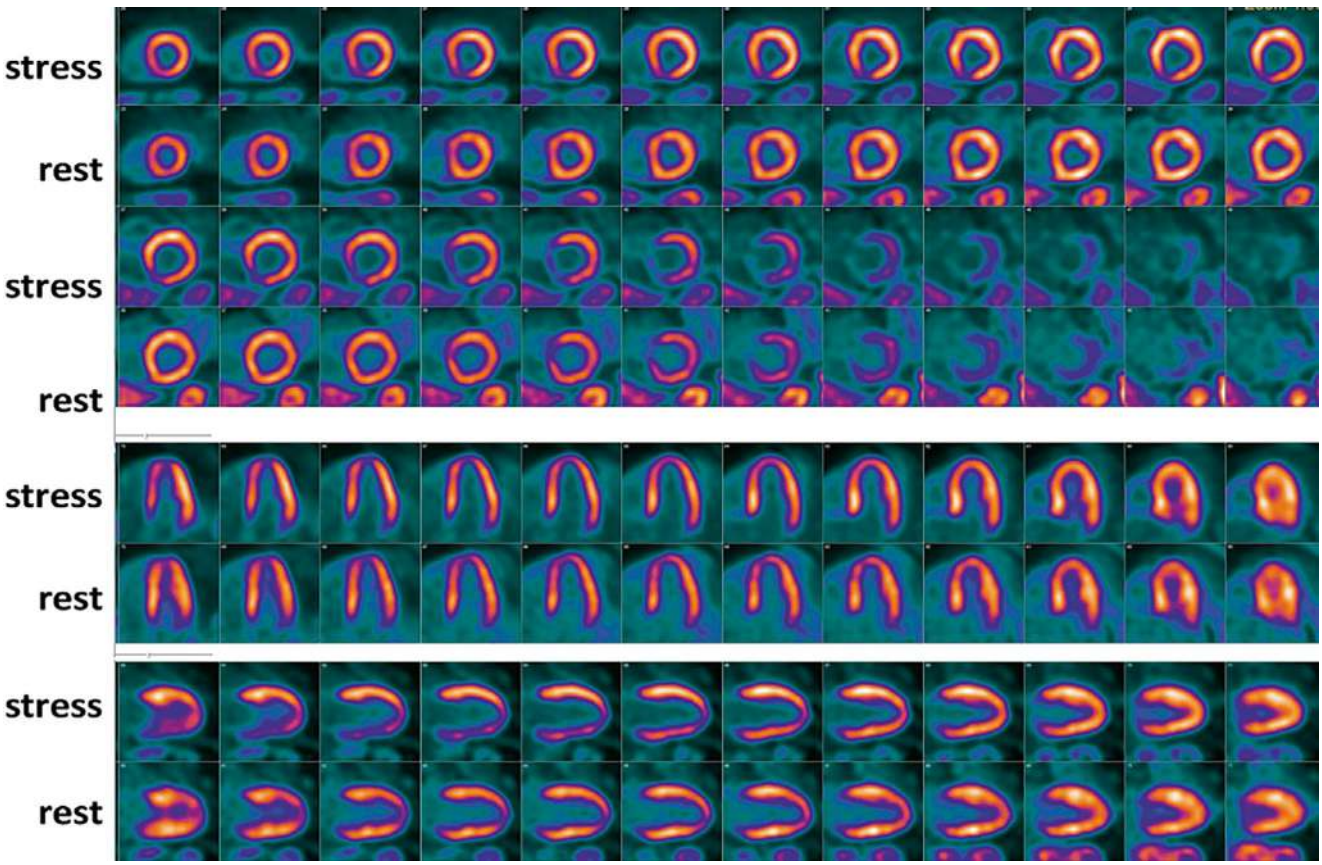


Fig. 3.3 Summed rest and adenosine stress myocardial perfusion ^{13}N ammonia PET images demonstrate severe perfusion defect involving the inferior wall with complete reversibility

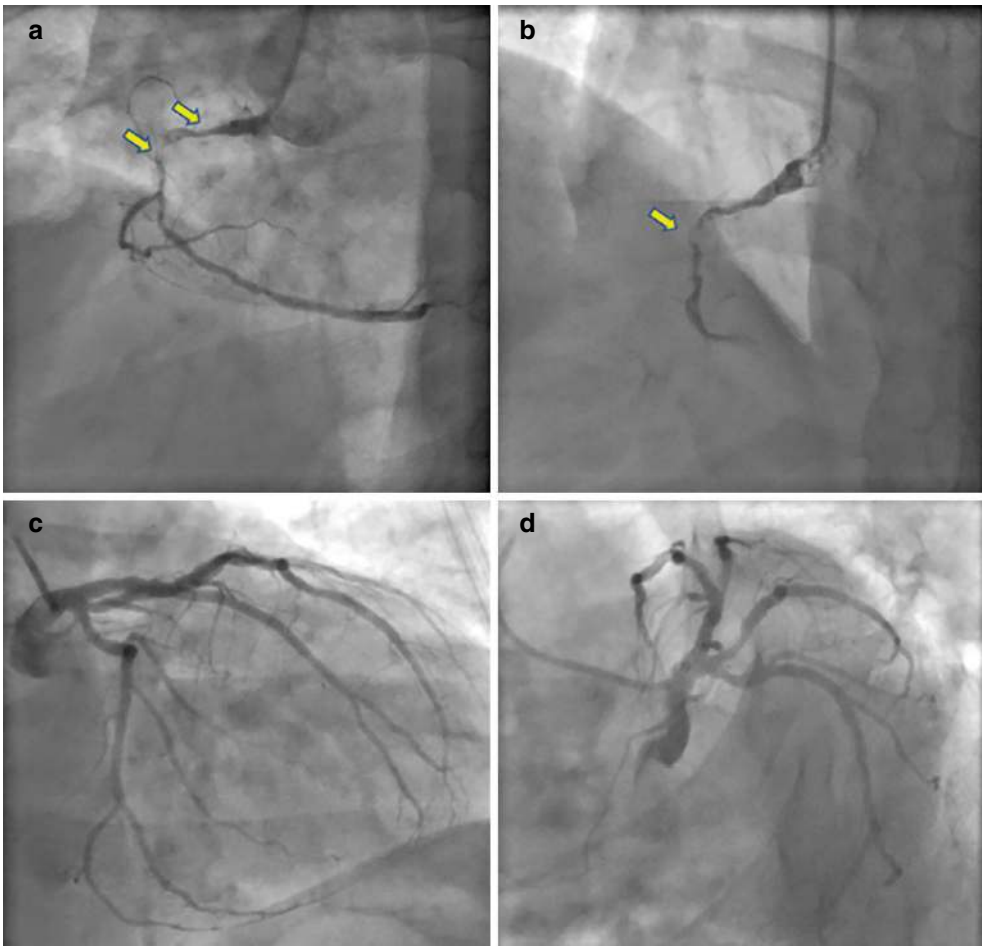


Fig. 3.4 Selective view of the right (**a**, **b**) and left (**c**, **d**) coronary arteries demonstrating an 80% RCA stenosis (yellow arrows), mild irregularities in the LAD without stenoses and LCX without stenoses

Correlative Imaging
- Invasive coronary angiography (Fig. 3.4).

Management
- Single-vessel disease with normal LV function.
- Revascularization may be performed to improve symptoms.

Further Reading

- Naya M, Murthy V, Blankstein R, Sitek A, Hainer J, Foster C, et al. Quantitative Relationship Between the Extent and Morphology of Coronary Atherosclerotic Plaque and Downstream Myocardial Perfusion. Journal of the American College of Cardiology. 2011;58:1807–1816.
- Ziadi M, deKemp R, Williams K, Guo A, Renaud J, Chow B, et al. Does quantification of myocardial flow reserve using rubidium-82 positron emission tomography facilitate detection of multivessel coronary artery disease? Journal of Nuclear Cardiology. 2012;19:670–680.

3.1.3 Single-Vessel Disease: Case 10

Key Points
- A large perfusion defect combined with transient LV dilation with stress suggests multivessel coronary artery disease.
- However, the preserved flow and flow reserve in the other territories suggests single-vessel ischemia in the LAD territory.
- For further discussion of interpretation of myocardial blood flow, see Chap. 1, Fig. 1.6.

History
- A 64-year-old woman and former smoker was referred to PET/CT for the evaluation of atypical chest pain.
- She did not have any other cardiovascular risk factors (Fig. 3.5 and Table 3.3).

PET/CT Images

This patient also underwent CCTA fused with PET image (Fig. 3.6a and b).

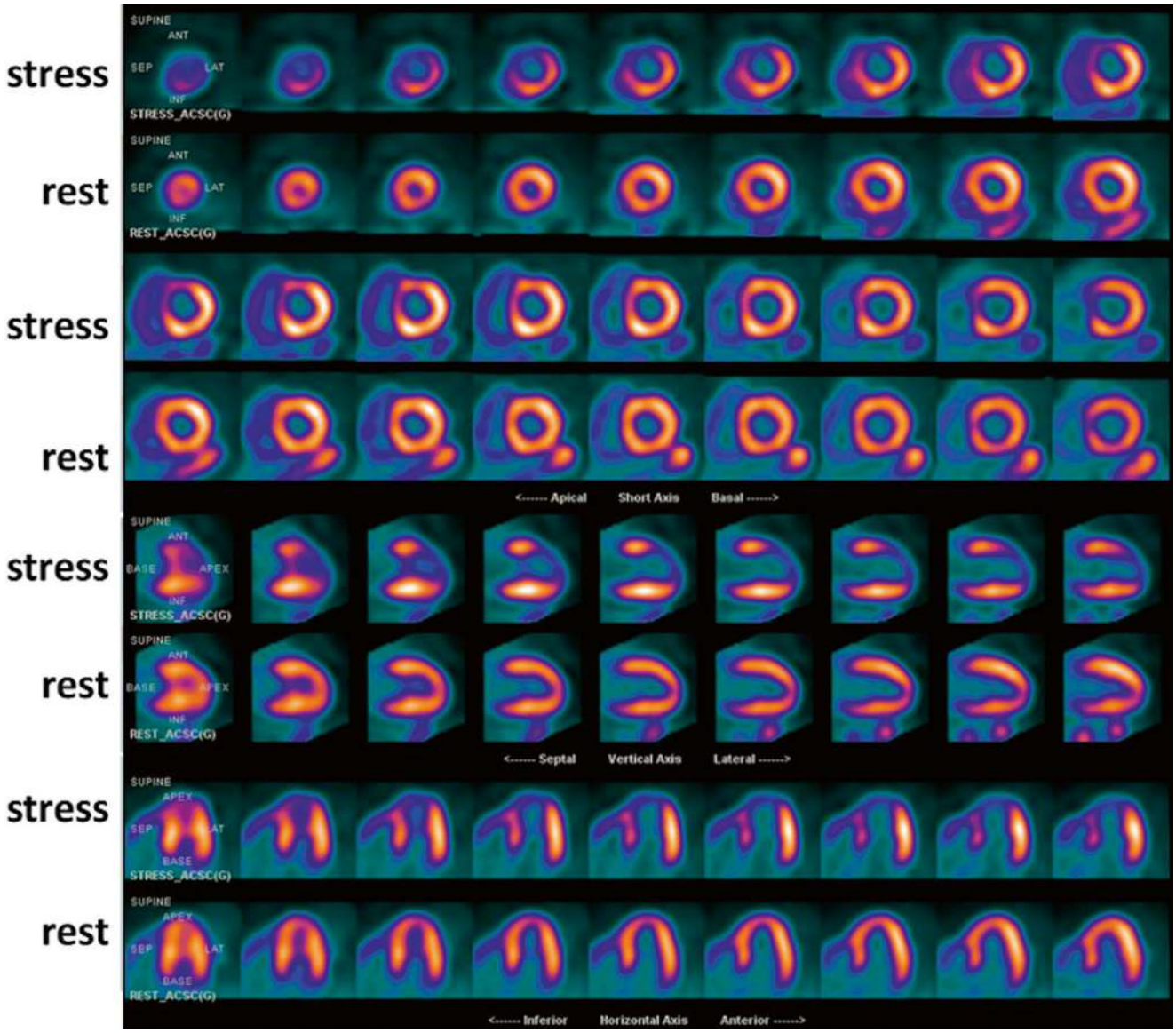


Fig. 3.5 Summed rest and vasodilator stress myocardial perfusion PET images with ^{82}Rubidium show a large-size perfusion defect of severe intensity involving the mid-anteroseptal wall, the apical LV segments, and the LV apex with complete reversibility. There is also evidence of transient LV dilatation with stress

Table 3.3 Summary of the quantitative blood flow data demonstrating high MBF at rest, with good augmentation during stress albeit lower in the LAD territory. The MFR is reduced in the LAD territory but preserved in the LCX and RCA territories

	MBF rest (ml/min/g)	MBF stress (ml/min/g)	MFR (stress/rest)
LAD	1.30	2.05	1.58
LCX	1.39	3.05	2.19
RCA	1.19	2.35	2.09
Global LV	1.30	2.39	1.97

Findings

- The PET images demonstrate transient LV dilatation and a large-sized perfusion defect of severe intensity involving the mid-anteroseptal wall, the apical LV segments and the LV apex with complete reversibility.
- The quantitative blood flow data demonstrates high MBF at rest, with good augmentation during stress albeit lower in the LAD territory. The MFR is reduced in the LAD territory but preserved in the LCX and RCA territories.
- The coronary CTA shows subtotal occlusion of the mid LAD coronary artery which seems to also involve the takeoff of a first diagonal branch.

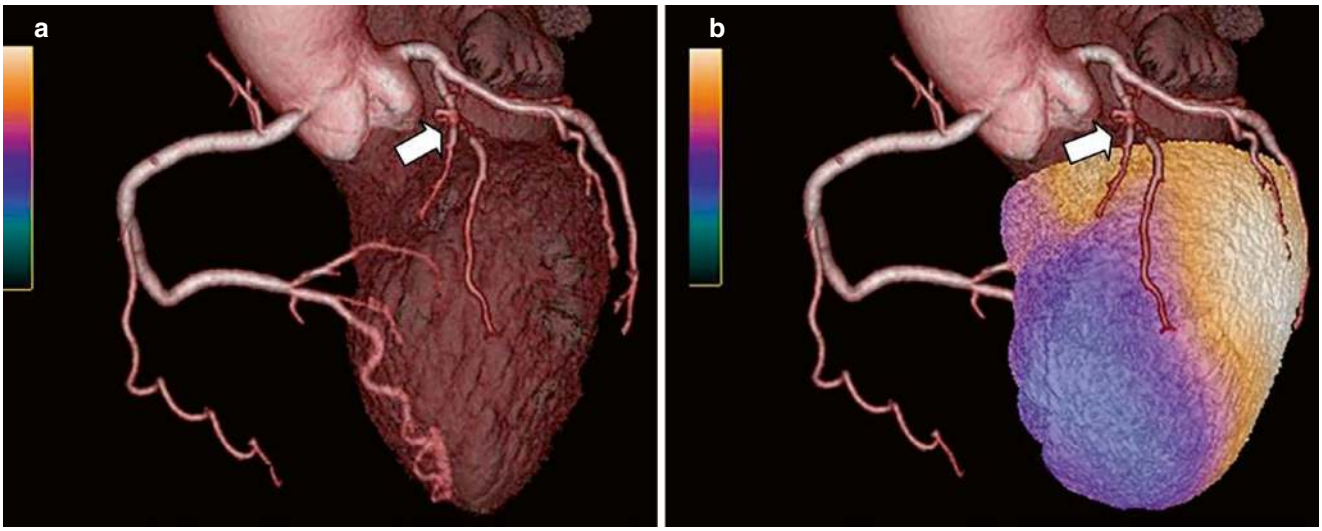


Fig. 3.6 The fused myocardial perfusion PET/CCTA demonstrates severe stenosis of the mid-LAD coronary artery involving the proximal first diagonal branch (arrows)

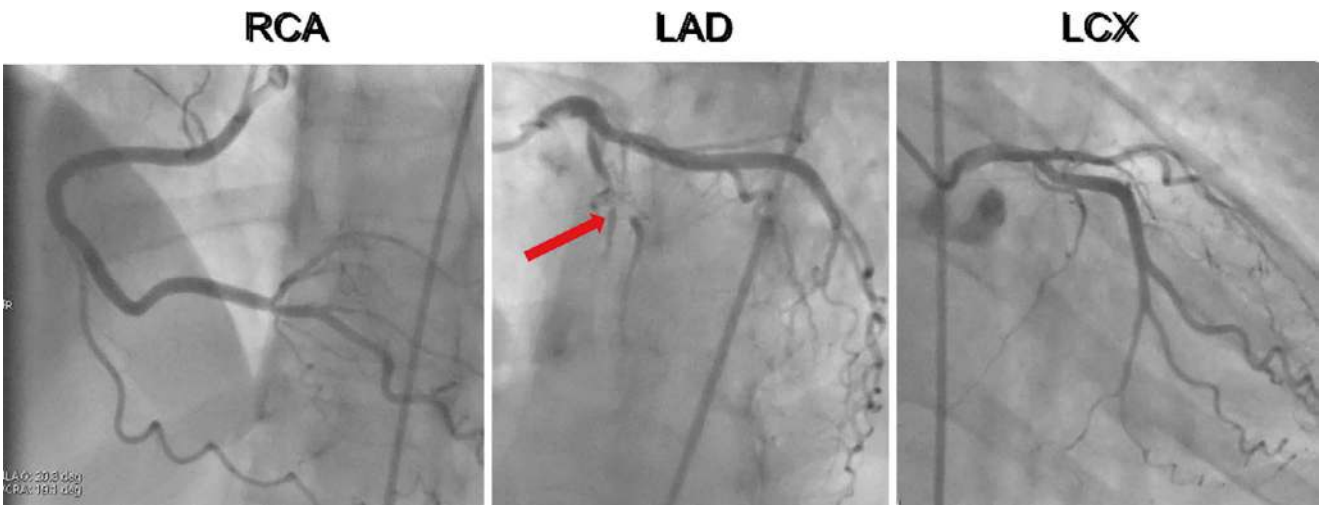


Fig. 3.7 Selective views from coronary angiography demonstrating a complex critical stenosis of the mid LAD and diagonal coronary arteries (red arrow)

Imaging Diagnosis

- Abnormal study consistent with severe stress-induced ischemia in the proximal LAD territory.

Differential Diagnosis

- None.

Correlative Imaging

- Invasive coronary angiography (Fig. 3.7).

Management

- The patient underwent successful PCI of the LAD/diagonal arteries.

Further Reading

- Johnson N, Gould K, Di Carli M, Taqueti V. Invasive FFR and Noninvasive CFR in the Evaluation of Ischemia: What is the Future?. Journal of the American College of Cardiology. 2016;67:2772–2788.
- Taqueti V, Di Carli M. Coronary Microvascular Disease Pathogenic Mechanisms and Therapeutic Options: JACC State-of-the-Art Review. Journal of the American College of Cardiology. 2018;72(21):2625–2641.
- Ziadi M, deKemp R, Williams K, Guo A, Renaud J, Chow B, et al. Does quantification of myocardial flow reserve using rubidium-82 positron emission tomography facilitate detection of multivessel coronary artery disease?. Journal of Nuclear Cardiology. 2012;19:670–680.

3.1.4 Single-Vessel Obstructive Disease MPI: Case 11

Key Points

- The presence of a perfusion defect in a single territory associated with preserved flow reserve in the remote myocardial territories helps identify single-vessel obstructive coronary artery disease.
- For further discussion of interpretation of myocardial blood flow, see Chap. 1, Fig. 1.7.

History

- A 52-year-old man with hypercholesterolemia, HIV, hepatitis B, previous Burkitt's lymphoma, and typical angina was referred for myocardial perfusion PET/CT (Fig. 3.25) with quantitation of MBF.

PET/CT Images

Coronary CT angiography was also performed and fused with PET (Fig. 3.9).

Findings

- The myocardial perfusion PET images demonstrate a medium-sized perfusion defect of severe intensity throughout the inferior wall with complete reversibility.
- The quantitative flow data demonstrate severe diffuse reduction in stress MBF in all coronary territories with focal reduction in MFR only in the RCA territory.
- The fused PET/CCTA data confirmed the presence of a total occlusion of the RCA, corresponding to the perfusion defect and the reduction in stress MBF and MFR.
- The reduction in stress MBF with preserved MFR in the LAD and LCX territories correlated with the presence of diffuse coronary calcifications in those vessels.

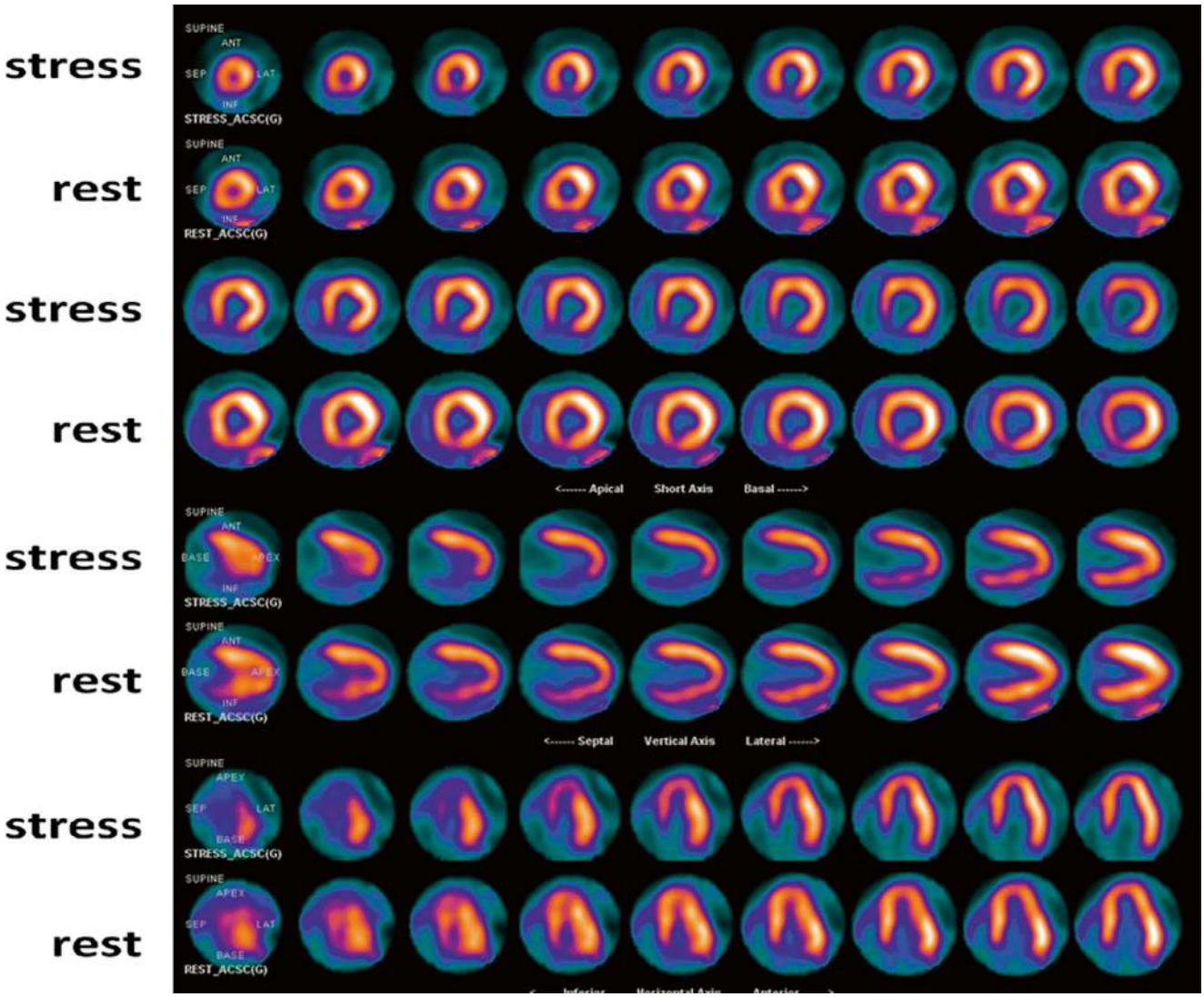


Fig. 3.8 Stress and rest ^{82}Rubidium myocardial perfusion PET/CT demonstrated a medium-sized perfusion defect of severe intensity throughout the inferior wall with complete reversibility

Table 3.4 Summary of the quantitative blood flow data demonstrating severe reduction in stress myocardial blood flow in all coronary artery territories and globally (normal value >1.8 mL/min/g). Myocardial flow reserve is only impaired in the RCA territory (normal value >2.0)

	MBF rest (ml/min/g)	MBF stress (ml/min/g)	MFR (stress/rest)
LAD	0.49	1.20	2.47
LCX	0.47	1.06	2.17
RCA	0.46	0.53	1.17
Global LV	0.48	1.00	2.08

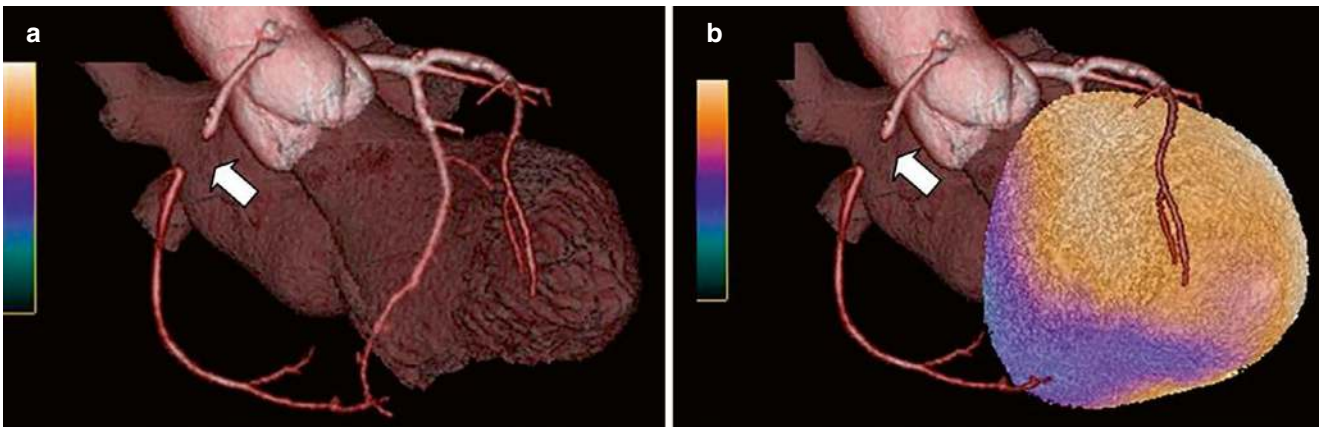


Fig. 3.9 Fused myocardial perfusion PET/coronary CT angiography (PET/CCTA). The coronary CT angiogram images demonstrate a total occlusion of the proximal dominant RCA. There is also evidence of diffuse coronary artery calcifications on the LAD and LCX arteries

Imaging Diagnosis
Single-vessel obstructive coronary artery disease.

Differential Diagnosis
- Obstructive coronary artery disease.
- Diffuse nonobstructive atherosclerosis.
- Coronary microvascular dysfunction.

Correlative Imaging
- Invasive coronary angiography (not shown) confirmed the presence of an occluded RCA.

Further Reading
- Bateman TM, et al. Practical guide for interpreting and reporting cardiac PET measurements of myocardial blood flow: an information statement from the American Society of Nuclear Cardiology, and the Society of Nuclear medicine and molecular imaging. JNC 2021:28(2);768–87.

3.1.5 Multivessel Disease: Case 12

Key Points
- The presence of large multivessel perfusion defects, transient LV cavity dilatation with stress, and severe reduction in MBF and MFR identify high-risk ischemia associated with multivessel coronary artery disease.
- For further discussion of interpretation of myocardial blood flow, see Chap. 1, Fig. 1.7.

History
- An asymptomatic 79-year-old man with a history of dyslipidemia and hypertension was referred for PET/CT (Fig. 3.10) for the evaluation of new onset LV dysfunction which was identified on echocardiography (not shown) (Table 3.5).

PET/CT Images

Findings
- The myocardial perfusion PET images demonstrate severe transient ischemic dilation (TID) during stress. There is a medium-sized perfusion defect of severe intensity involving the apical LV segments and the LV apex with complete reversibility. In addition, there is a large perfusion defect of severe intensity throughout the inferior and basal inferoseptal and inferolateral walls, also showing complete reversibility.
- The quantitative flow data demonstrated diffuse and severe reduction in stress MBF and MFR in all three coronary territories.

Imaging Diagnosis
- Multivessel obstructive coronary disease.

Differential Diagnosis
- None.

Correlative Imaging
- Invasive coronary angiography (Fig. 3.11).

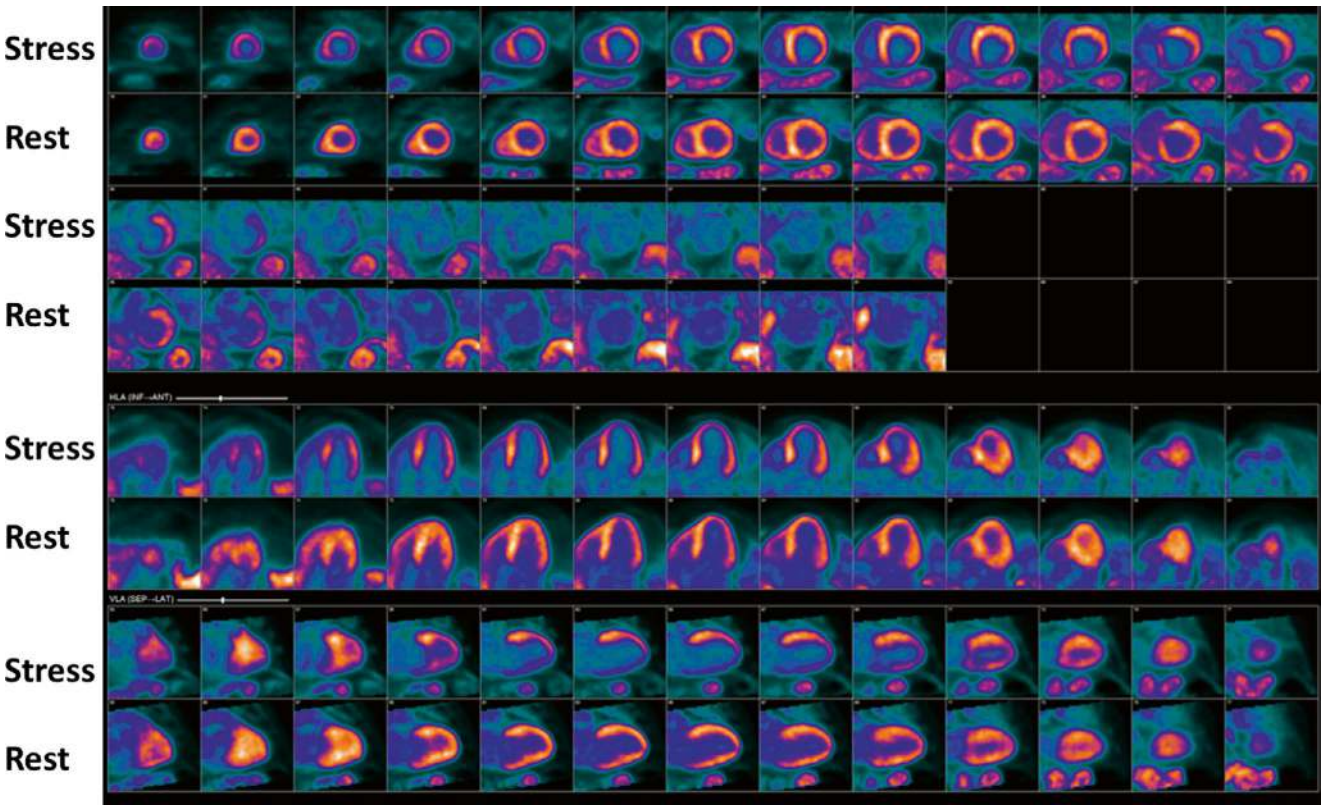


Fig. 3.10 Images show medium-sized severe perfusion defect involving the apical LV segments and the LV apex with complete reversibility. Large severe perfusion defect throughout the inferior and basal inferoseptal and inferolateral walls, also showing complete reversibility

Table 3.5 Summary of rest and stress MBF and myocardial flow reserve showing a global severe reduction in stress MBF and MFR

	MBF rest (ml/min/g)	MBF stress (ml/min/g)	MFR (stress/rest)
LAD	0.65	1.06	1.64
LCX	0.64	1.09	1.71
RCA	0.59	0.69	1.17
Global LV	0.63	0.96	1.54

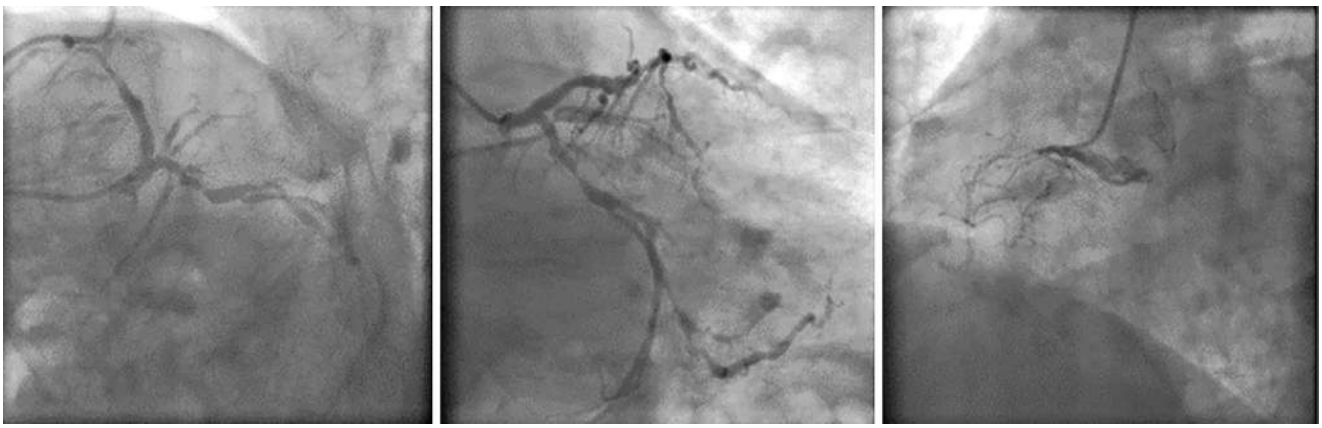


Fig. 3.11 Selective coronary angiographic views demonstrate severe three-vessel obstructive coronary artery disease including a long and severe stenosis in the mid LAD, a severe stenosis in the proximal LCX artery, and a total occlusion of a dominant RCA

Management
- The patient underwent coronary artery bypass grafting (CABG).

Further Reading

- Sambuceti G, Marzullo P, Giorgetti A, Neglia D, Marzilli M, Salvadori P, et al. Global alteration in perfusion response to increasing oxygen consumption in patients with single-vessel coronary artery disease. Circulation. 1994;90:1696–1705.
- Naya M, Murthy V, Blankstein R, Sitek A, Hainer J, Foster C, et al. Quantitative Relationship Between the Extent and Morphology of Coronary Atherosclerotic Plaque and Downstream Myocardial Perfusion. Journal of the American College of Cardiology. 2011;58:1807–1816.

3.1.6 No Coronary Artery Calcium with Abnormal PET: Case 13

Key Points
- The absence of coronary artery calcification (CAC) is associated with a high probability of normal perfusion on stress testing, since only 3–7% of the subjects without CAC have obstructive CAD.
- Obstructive coronary artery disease due to noncalcified plaques occurs mostly in young individuals, especially women and smokers.
- For further discussion of interpretation of myocardial blood flow, see Chap. 1, Fig. 1.7.

History
- A 57-year-old woman with no known risk factors for atherosclerosis, and prior history of hepatitis B and heavy alcohol use, was referred for cardiac PET/CT for pre-liver transplant risk assessment (Figs. 3.12 and 3.13).

Fused PET/CT Images (Fig. 3.14 and Table 3.6)

Findings
- There is an intermediate-size perfusion defect of mild severity involving the mid and basal inferolateral wall of the LV. The LV cavity size is normal.
- The flow maps confirm that there has been an appropriate increase in MFR after dobutamine injection. The rest flows are severely increased in the context of end-stage liver disease.
- There was adequate registration of the transmission and emission maps without motion artifacts.
- There is no coronary artery calcium in the transmission CT images used for attenuation correction.

Imaging Diagnosis
- Inducible ischemia of the inferolateral wall of the LV in keeping with coronary artery disease.

Differential Diagnosis
- Misregistration artifact.

Correlative Imaging
- None.

Management
- Patient was managed medically with anti-ischemic medications and lipid lowering drugs. Eight months later, she underwent a successful liver transplant.

Further Reading

- Esteves FP, Khan A, Correia LC, Nye JA, Halkar RK, Schuster DM, et al. Absent coronary artery calcium excludes inducible myocardial ischemia on computed tomography/positron emission tomography. Int J Cardiol. 2011;147(3):424–7.
- Bavishi C, Argulian E, Chatterjee S, Rozanski A. CACS and the frequency of stress-induced myocardial ischemia during MPI: A Meta-Analysis. JACC Cardiovasc Imaging. 2016;9(5):580–9.
- Osborne-Grinter M, Kwiecinski J, Doris M, McElhinney P, Cadet S, Adamson PD, Moss AJ, et al. Association of coronary artery calcium score with qualitatively and quantitatively assessed adverse plaque on coronary CT angiography in the SCOT-HEART trial. Eur Heart J Cardiovasc Imaging. 2022;23(9):1210–1221.

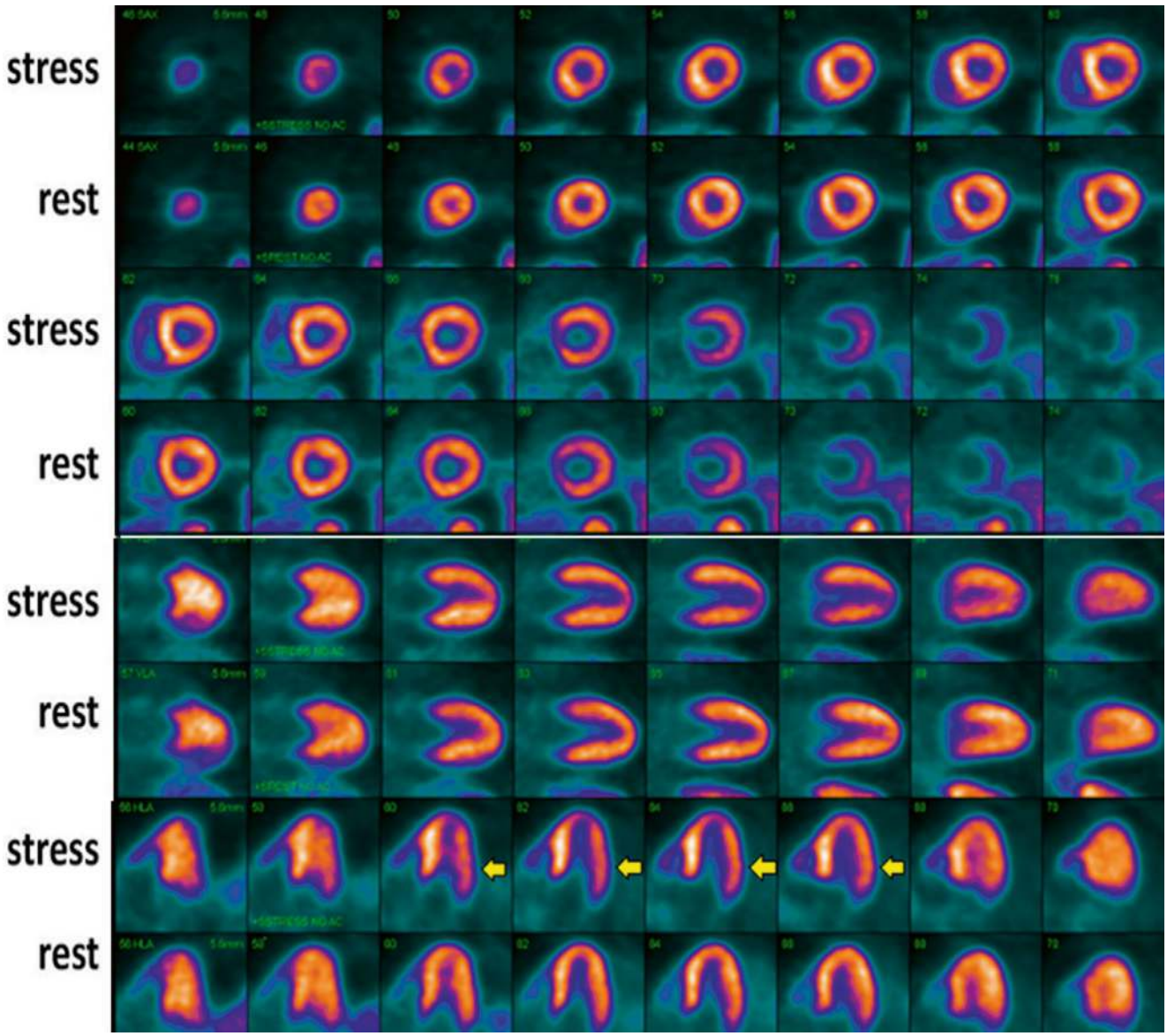


Fig. 3.12 ^{82}Rubidium dobutamine stress and rest myocardial perfusion PET/CT images. There is a small-sized perfusion defect of mild intensity in the mid and basal inferolateral wall of the LV visible during stress (arrows) which is completely reversible at rest



Fig. 3.13 Axial chest CT image showing no evidence of coronary artery calcium

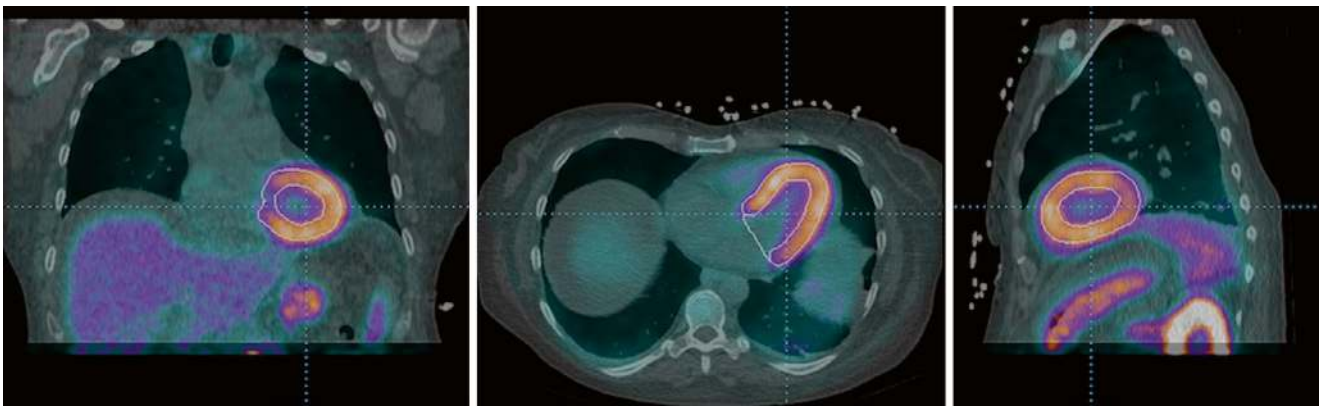


Fig. 3.14 Fused PET/CT images show optimal registration, therefore excluding the possibility that the inferolateral perfusion defect may have been due to a motion artifact

Table 3.6 MFR and flow reserve measurements

	MBF rest (ml/min/g)	MBF stress (ml/min/g)	MFR (stress/rest)
LAD	2.10	3.99	1.96
LCX	1.89	3.04	1.85
RCA	1.91	3.74	1.96
Global LV	1.97	3.71	1.92

3.1.7 High Coronary Artery Calcium Score with Normal PET: Case 14

Key Points

- Extensive coronary atherosclerosis by coronary CT angiography without evidence of flow-limiting stenoses or coronary microvascular dysfunction.
- Absence of ischemia excludes the need for coronary intervention, but the presence of high-risk factors and severe coronary calcification requires secondary prevention by optimized medical therapy (OMT).
- For further discussion of interpretation of myocardial blood flow, see Chap. 1, Fig. 1.7.

History

- A 58-year-old man with a history of dyslipidemia, hypertension, and type 2 diabetes mellitus was admitted to the emergency room with vertigo, nausea, and excessive sweating.
- Echocardiogram showed mild LV hypertrophy, mild valvular fibrosis, and normal LV function.
- Exercise ECG was negative for ischemia at 80% of maximal predicted heart rate.
- A previous coronary CT angiogram showed a CACS of 956 Agatston units and multiple stenotic lesions (Fig. 3.15).
- The patient was referred for myocardial perfusion PET to assess the functional significance of coronary artery disease (Fig. 3.16).

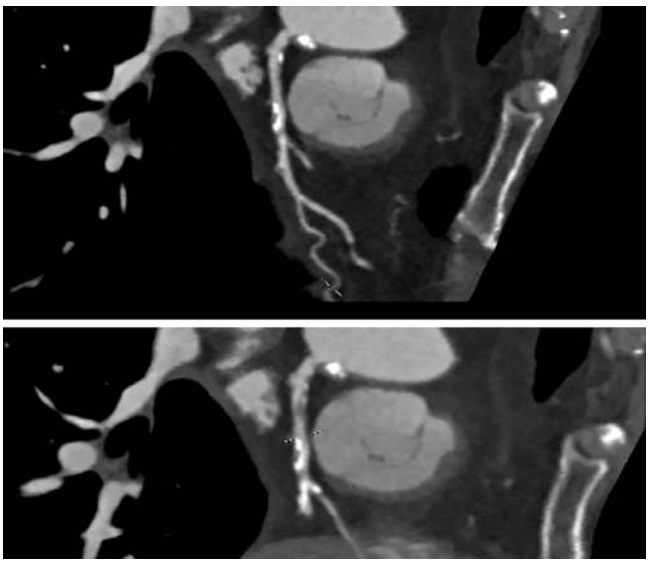


Fig. 3.15 Coronary CT angiography showing 30% occlusion of LM and proximal LAD and 50–70% stenosis after the first diagonal branch

Myocardial blood flow (MBF) and myocardial flow reserve (MFR) were also calculated (Table 3.7).

Findings

- Normal regional myocardial perfusion.
- Normal MBF and MFR after regadenoson stress in all three coronary vascular territories.

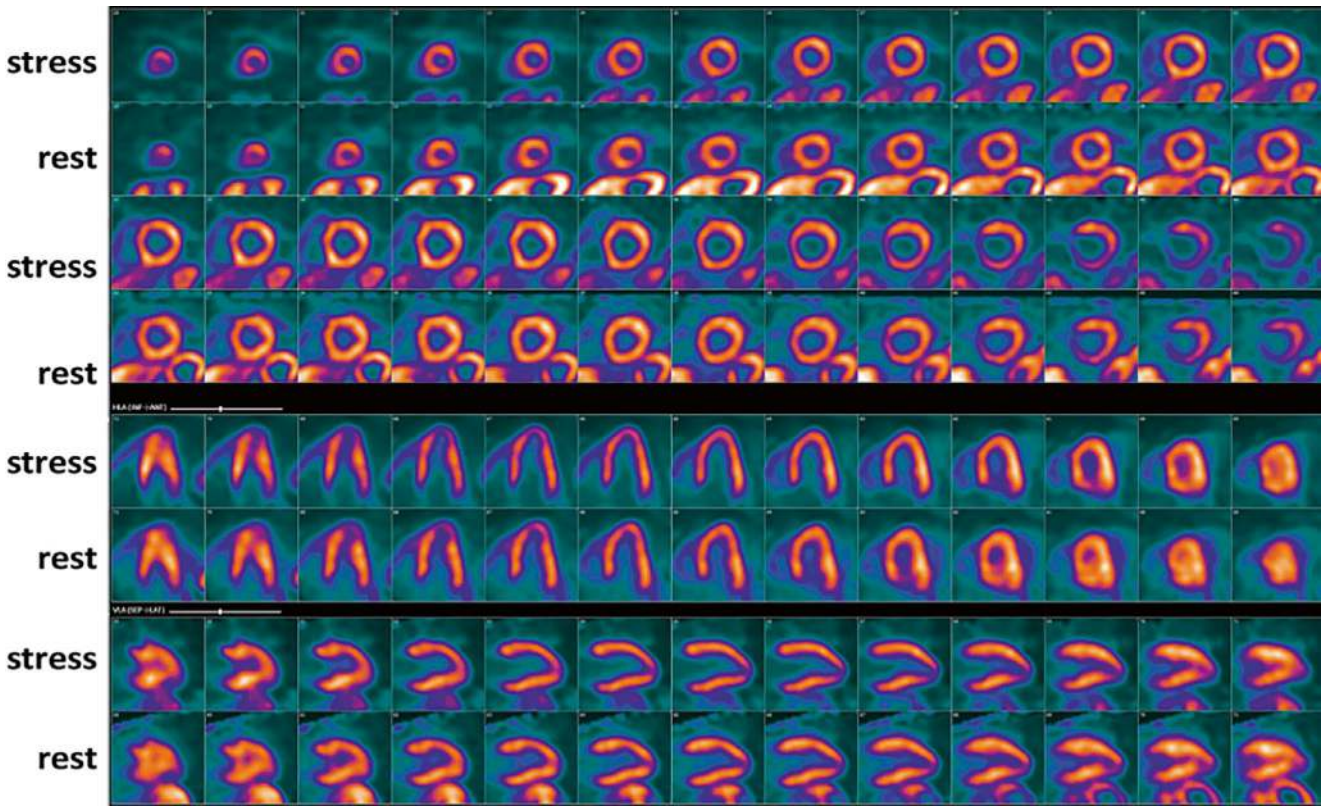


Fig. 3.16 Summed rest and regadenoson stress myocardial perfusion PET/CT images obtained with ^{13}N-ammonia showing normal perfusion

Table 3.7 Normal MBF and MFR after regadenoson in all three coronary vascular territories

	MBF rest (ml/min/g)	MBF stress (ml/min/g)	MFR (stress/rest)
LAD	0.72	2.46	3.43
LCX	0.88	2.71	3.10
RCA	0.75	2.22	2.97
Global LV	0.76	2.46	3.23

Imaging Diagnosis

- Severe calcified coronary atherosclerosis without evidence of flow-limiting coronary artery disease.

Differential Diagnosis

- None.

Management

- Optimal medical therapy.

Further Reading

- Santana C, Garcia E, Faber T, Sirineni G, Esteves F, Sanyal R, et al. Diagnostic performance of fusion of myocardial perfusion imaging (MPI) and computed tomography coronary angiography. Journal of Nuclear Cardiology. 2009;16:201–211.
- Gaemperli O, Schepis T, Kalff V, Namdar M, Valenta I, Stefani L, et al. Validation of a new cardiac image fusion software for three-dimensional integration of myocardial perfusion SPECT and stand-alone 64-slice CT angiography. European Journal of Nuclear Medicine and Molecular Imaging. 2007;34:1097–1106.
- Piccinelli M, Santana C, Sirineni G, Folks R, Cooke C, Arepalli C, et al. Diagnostic performance of the quantification of myocardium at risk from MPI SPECT/CTA 2G fusion for detecting obstructive coronary disease: A multicenter trial. Journal of Nuclear Cardiology. 2018;25:1376–1386.

3.1.8 Very High Coronary Artery Calcium Score with Normal MBF: Case 15

Key Points

- The presence of severe coronary artery calcification is associated with an increased likelihood of obstructive coronary artery disease.
- Normal regional and global stress MBF and MFR increase reader confidence to rule out high-risk obstructive coronary artery disease.
- For further discussion of interpretation of myocardial blood flow, see Chap. 1, Fig. 1.7.

History

- A 60-year-old woman with no known coronary artery disease was referred for a regadenoson stress myocardial perfusion PET study to evaluate for non-anginal chest pain.
- She has a history of controlled hypertension, dyslipidemia, and diabetes (Figs. 3.17, 3.18 and Table 3.8).

PET/CT Images

Findings

- Normal LV size.
- There was no evidence of regional perfusion defects on the stress or rest images (Fig. 3.16).
- Mildly reduced regional and global stress MBF with normal MFR.
- Rest LVEF: 63% with normal LV volumes. Stress LVEF: increased to 66% with normal LV volumes. There is normal regional wall motion and thickening.
- Severe coronary artery calcification (Fig. 3.18).

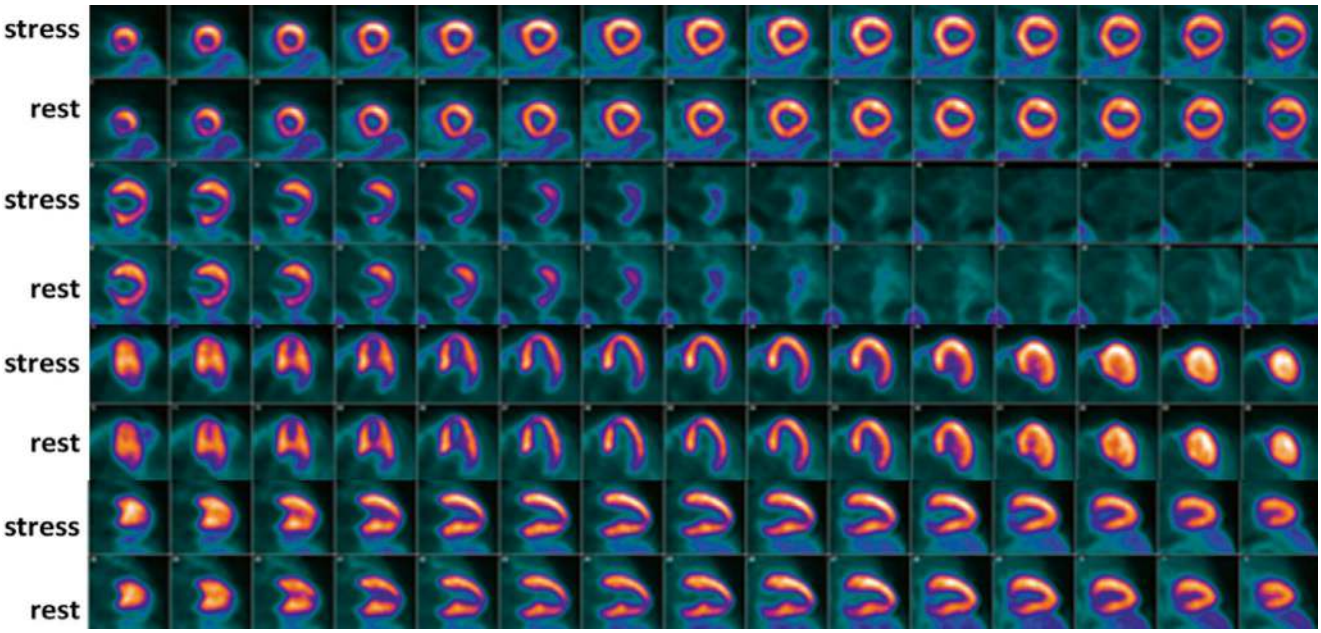


Fig. 3.17 Regadenoson stress and rest ^{13}N ammonia myocardial perfusion study. The LV is normal in size. There is no evidence of regional perfusion defects on the stress or rest images



Fig. 3.18 The transmission CT scan demonstrates severe coronary artery calcification

Table 3.8 Summary of rest and stress MBF and MFR

	MBF rest (ml/min/g)	MBF stress (ml/min/g)	MFR (stress/rest)
LAD	0.84	1.73	2.05
LCX	0.84	1.84	2.19
RCA	0.76	1.64	2.15
Global LV	0.82	1.72	2.11

Imaging Diagnosis
- Severe calcified atherosclerosis without evidence of flow-limiting coronary artery disease.

Differential Diagnosis
- None.

Correlative Imaging
- None.

Management
- Given the absence of flow-limiting coronary artery disease, there is no need for invasive coronary angiography at this time.
- Aggressive management of her risk factors given the evidence of severe nonobstructive coronary atherosclerosis.

Further Reading

- Piccinelli M, Santana C, Sirineni G, Folks R, Cooke C, Arepalli C, et al. Diagnostic performance of the quantification of myocardium at risk from MPI SPECT/CTA 2G fusion for detecting obstructive coronary disease: A multicenter trial. Journal of Nuclear Cardiology. 2018;25:1376–1386.
- Osborne-Grinter M, Kwiecinski J, Doris M, McElhinney P, Cadet S, Adamson PD, Moss AJ, et al. Association of coronary artery calcium score with qualitatively and quantitatively assessed adverse plaque on coronary CT angiography in the SCOT-HEART trial. Eur Heart J Cardiovasc Imaging. 2022;23(9):1210–1221.

3.1.9 Abnormal PET MPI in a Patient with Typical Chest Pain and Normal SPECT: Case 16

Key Points
- A strongly positive exercise treadmill test for ischemia with a normal myocardial perfusion SPECT study should prompt additional investigations to exclude obstructive coronary artery disease.
- A possible explanation for the absence of perfusion defects in a patient with known coronary artery disease is balanced reduction in myocardial blood flow, which limits flow heterogeneity and leads to relatively normal myocardial perfusion with SPECT.
- The improved first-pass extraction of PET tracers makes the test more sensitive to detect obstructive coronary stenosis.
- For further discussion of interpretation of myocardial blood flow, see Chap. 1, Fig. 1.7.

History
- A 74-year-old man with known coronary artery disease and prior PCI was referred for an exercise myocardial perfusion SPECT study to evaluate for typical chest pain and dyspnea.
- His cardiac risk factors include hypertension and dyslipidemia.

Exercise Stress Test
- The patient exercised for 10:00 min of a Bruce protocol.
- The heart rate increased from 58 bpm at rest to a peak heart rate of 134 bpm (92% age predicted maximal heart rate).
- The blood pressure increased from 130/64 mmHg at rest to 148/62 mmHg at peak exercise (Rate Pressure Product: 19832).
- Exercise was terminated due to fatigue.
- The symptomatic response to exercise was ischemic due to typical chest pain.
- The blood pressure response was normal.
- The ECG response to exercise (Fig. 3.19) was ischemic due to 3 mm horizontal ST segment depression in leads II, III, aVF, and V3-V6. ST depressions began 9:00 min into the test at a heart rate of 136 bpm and resolved 11:00 min into recovery.
- No exercise-induced arrhythmia was observed.

SPECT Images

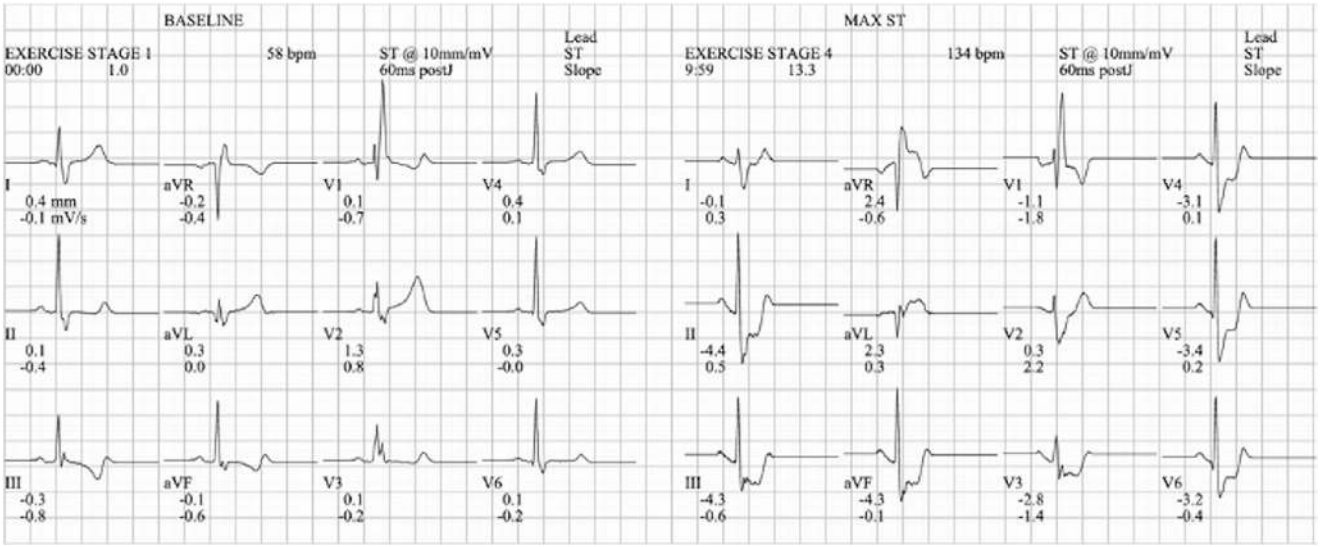


Fig. 3.19 Rest and peak exercise ECGs demonstrating 3 mm ST segment depression in leads II, III, aVF, and V3–V6

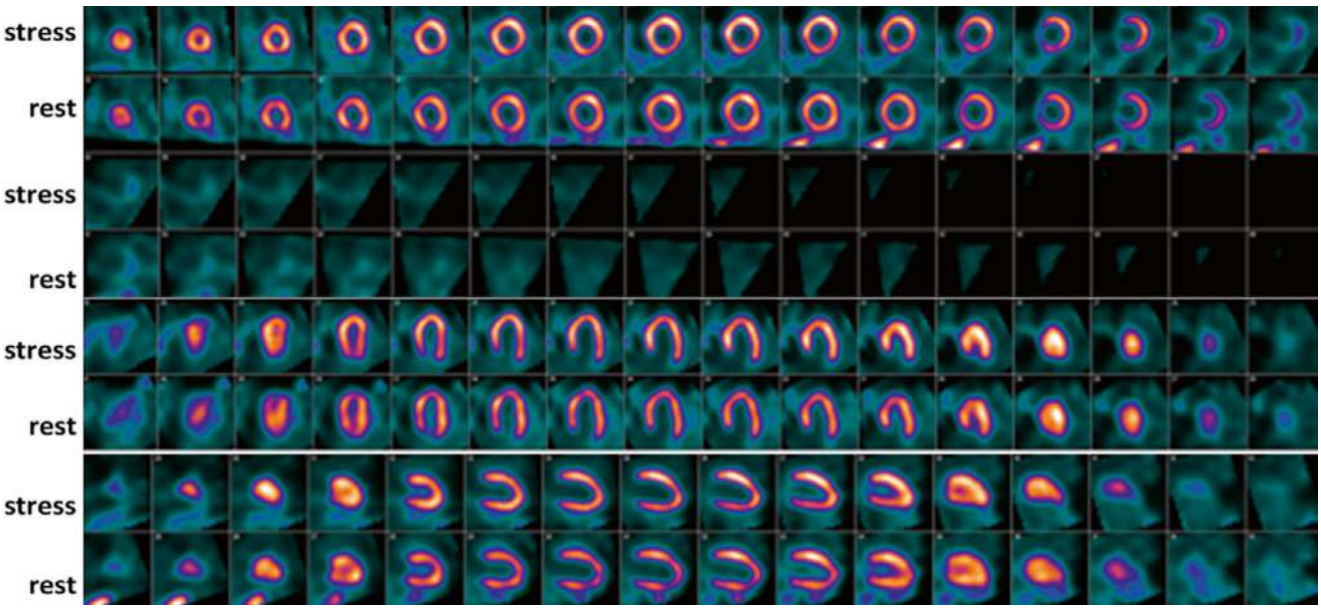


Fig. 3.20 Stress and rest ^{99m}Tc sestamibi SPECT study. There is no evidence of regional perfusion defect on the stress or rest images

Findings

- There is no evidence of regional perfusion defect on the stress or rest images at SPECT (Fig. 3.20).
- The post-stress LVEF was 66% with normal LV volumes. There were normal regional wall motion and thickening.

Imaging Diagnosis

- Normal myocardial perfusion SPECT study.
- Markedly positive ECG response to exercise.

Differential Diagnosis

- Obstructive coronary artery disease.

Management

- Given the history of coronary artery disease and the strongly positive clinical response to exercise (chest pain and ECG changes), the patient was referred for a myocardial perfusion PET/CT study (Fig. 3.21 and Table 3.9).

PET/CT Images

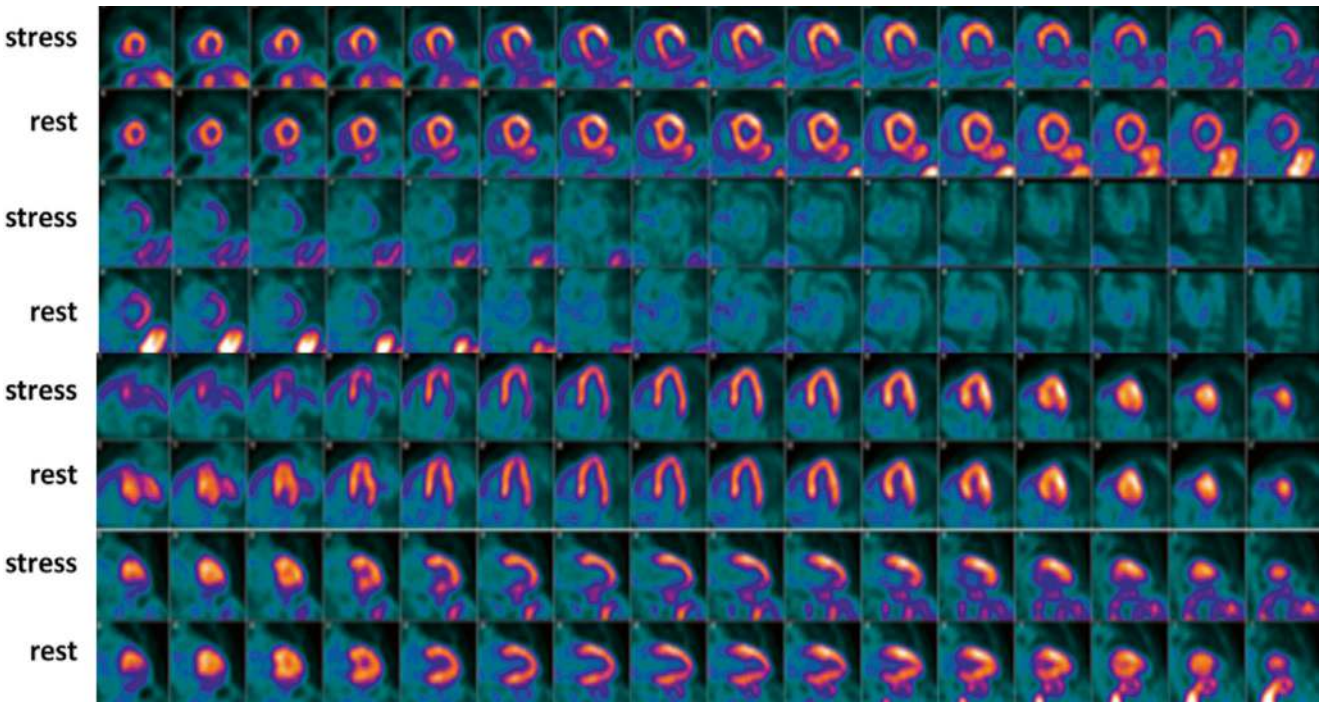


Fig. 3.21 Regadenoson stress and rest ^{82}Rubidium myocardial perfusion PET study. There is a large and severe perfusion defect throughout the inferior and inferolateral walls during stress, showing complete reversibility at rest

Table 3.9 Summary of rest and stress MBF and MFR

	MBF rest (ml/min/g)	MBF stress (ml/min/g)	MFR (stress/rest)
LAD	0.78	1.52	1.95
LCX	0.74	1.19	1.61
RCA	0.73	0.91	1.25
Global LV	0.74	1.17	1.58

Findings

- There is a large and severe perfusion defect throughout the inferior and inferolateral walls during stress, showing complete reversibility at rest (Fig. 3.20).
- Severe reduction in stress MBF and MFR in the RCA territory.
- Moderate reduction in stress MBF and MFR in the LAD and LCX consistent with nonobstructive diffuse atherosclerosis and microvascular dysfunction.

Imaging Diagnosis

- Large area of severe stress-induced ischemia in the RCA territory consistent with flow-limiting coronary artery stenosis in the RCA territory.

Correlative Imaging

- Invasive coronary angiography (Figs. 3.21 and 3.22).

Differential Diagnosis

- None.

Management

- The patient underwent successful drug-eluting stent placement in the RCA.
- A repeat PET study (not shown) demonstrated complete resolution of perfusion abnormalities and improvement in MBF and MFR.

Further Reading

- Patel FS et al. Reclassification of severe ischaemia on PET versus SPECT MPI using a same-patient simultaneous imaging protocol JACC CVI 2022:15(6);1158–59.

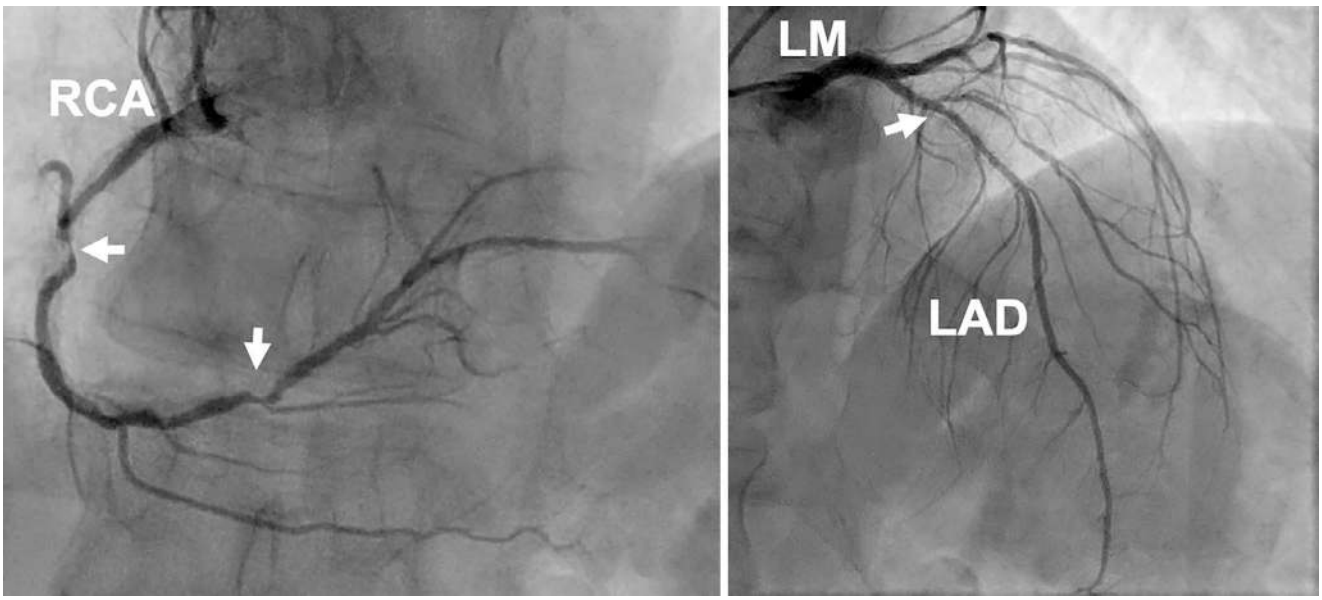


Fig. 3.22 Selective views of the right and left coronary system demonstrating a severe stenosis of the mid RCA. There is also a nonobstructive stenosis in the mid portion of the LAD coronary artery

3.1.10 Multivessel Disease: Case 17

Key Points

- The presence of transient LV dilatation, RV tracer uptake, and large multivessel perfusion abnormalities along with the reduced MFR in multiple territories identify patients with multivessel coronary artery disease at very high risk of adverse cardiac events.
- For further discussion of interpretation of myocardial blood flow, see Chap. 1, Fig. 1.7.

History

- A 78-year-old woman with a history of dyslipidemia, hypertension, diabetes mellitus type 2 and Crohn's disease was referred for vasodilator PET/CT with ^{82}Rubidium, after suffering a prolonged episode of chest pain (Figs. 3.8, 3.23 and Table 3.4).

PET Images (Table 3.10)

Findings

- Transient ischemic dilatation of the left ventricle during stress.
- Transiently increased uptake of the free wall of the right ventricle during stress.
- Large, severe and reversible perfusion defect involving the mid-anteroseptal wall, apical LV segments and LV apex, showing complete reversibility.
- Medium-sized perfusion defect of moderate severity throughout the inferolateral wall, also showing complete reversibility.
- Regionally and globally reduced stress myocardial blood flow and flow reserve.
- LVEF at rest was 69% and it dropped to 57% during peak stress.

Imaging Diagnosis

- Severe multivessel obstructive coronary disease.

Differential Diagnosis

- None.

Correlative Imaging

- Invasive coronary angiography (Fig. 3.24).

Management

- This patient was deemed at high risk and in line with the best current evidence for treatment of multivessel disease in patients with diabetes mellitus was referred for coronary artery by-pass surgery.

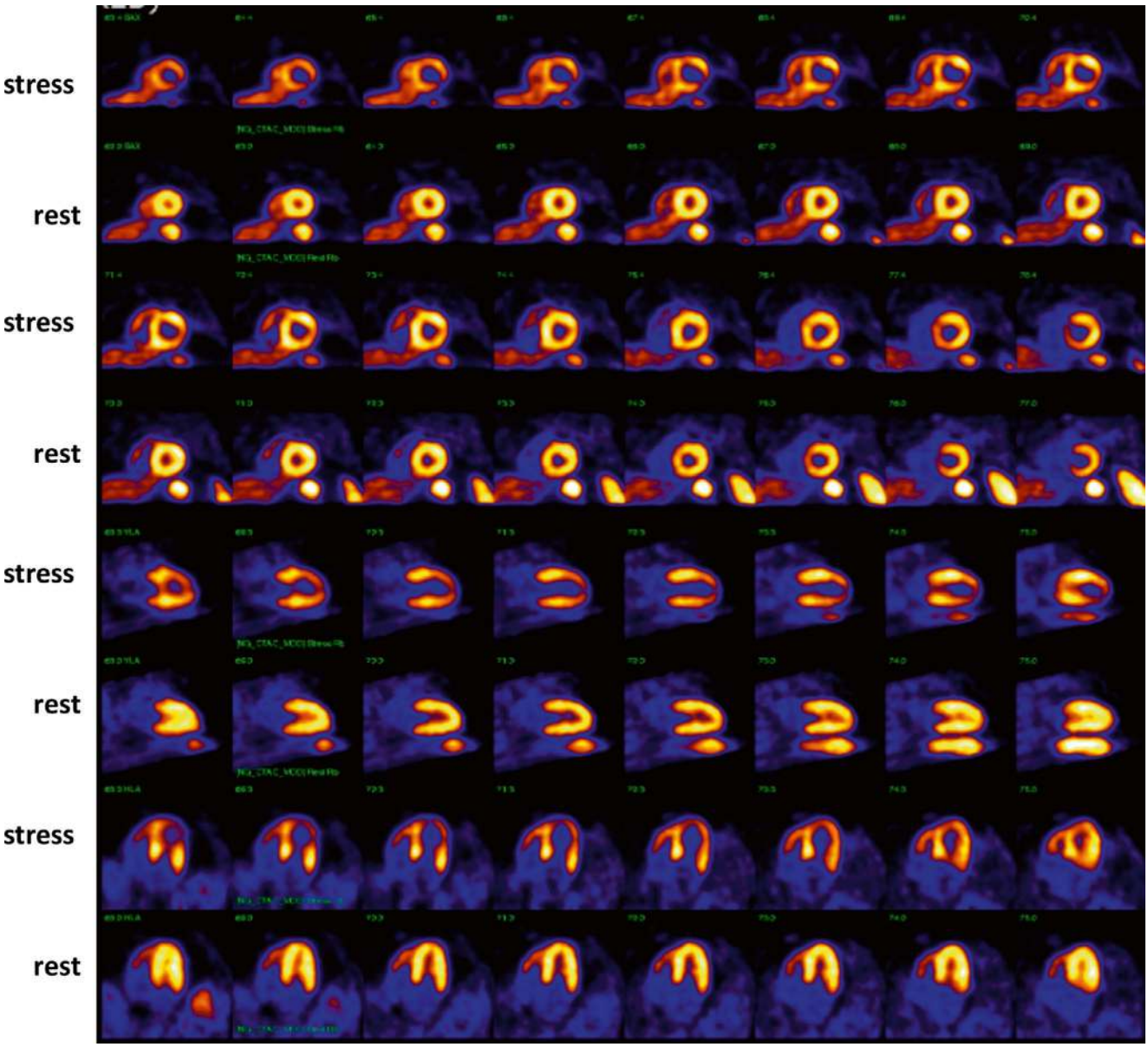


Fig. 3.23 Stress and rest ^{82}Rubidium myocardial perfusion PET images. There is transient ischemic dilatation of the left ventricle during stress. Also, there is increased tracer uptake of the free wall of the right ventricle, more pronounced during stress. There is a large, severe, and reversible perfusion defect involving the mid-anteroseptal wall, apical LV segments and LV apex, showing complete reversibility. In addition, there is a medium-sized perfusion defect of moderate severity throughout the inferolateral wall, also showing complete reversibility

Table 3.10 Summary of the quantitative blood flow data demonstrating severe reduction in stress myocardial blood flow in all coronary artery territories and globally (normal value >1.8 mL/min/g). MFR is impaired in the RCA and LAD territories (normal value >2.0)

	MBF rest (ml/min/g)	MBF stress (ml/min/g)	MFR (stress/rest)
LAD	0.76	1.03	1.35
LCX	0.86	1.23	1.43
RCA	0.92	1.21	1.31
Global LV	0.83	1.13	1.36

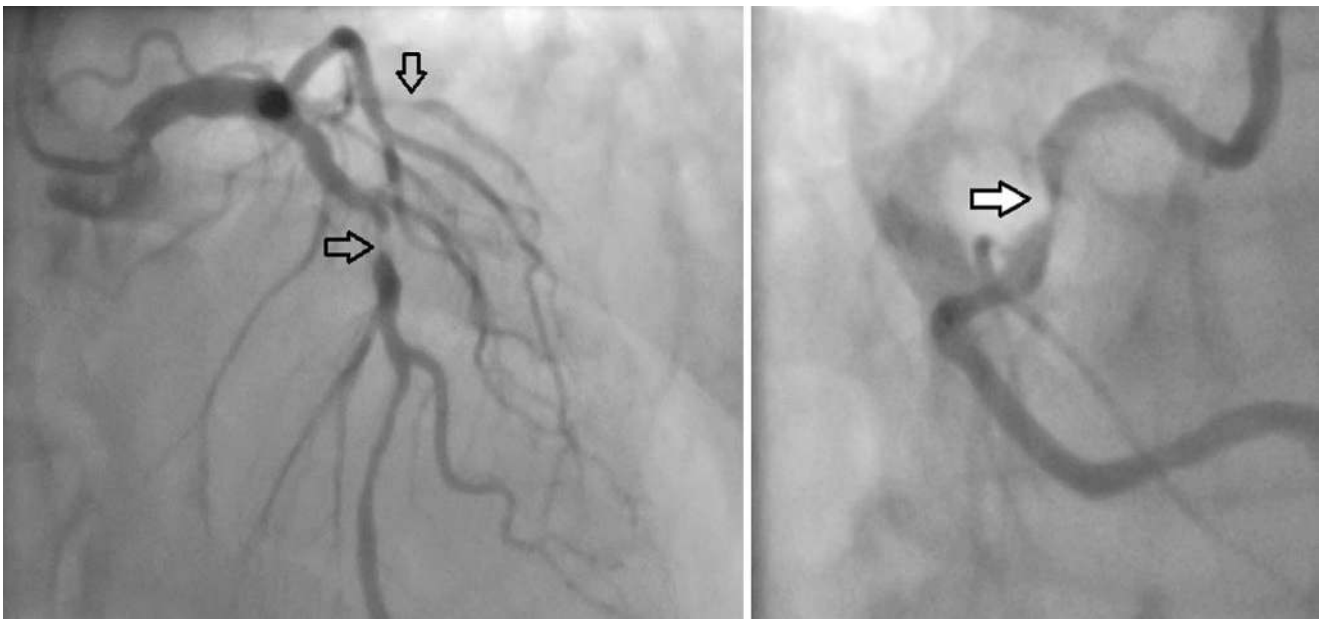


Fig. 3.24 Selective angiographic views of the coronary arteries: RAO cranial projection showing a high-degree stenosis of the mid LAD (left panel: arrow) and proximal obtuse marginal coronary artery (arrow). Right panel: LAO view showing a high-degree stenosis of the proximal to mid RCA (arrow)

Further Reading

- BARI 2D Study Group, Frye RL, August P, Brooks MM, Hardison RM, Kelsey SF, et al. A randomized trial of therapies for type 2 diabetes and coronary artery disease. The New England Journal of Medicine. 2009;360:2503–2515.
- Farkouh ME, Domanski M, Sleeper LA, Siami FS, Dangas G, Mack M, et al. Strategies for multivessel revascularization in patients with diabetes. The New England Journal of Medicine. 2012;367:2375–2384.

3.1.11 High-Risk Scan: Case 18

Key Points

- Large area of myocardial ischemia throughout the proximal LAD territory associated with reduced myocardial blood flow and flow reserve, consistent with single-vessel disease.
- For further discussion of interpretation of myocardial blood flow, see Chap. 1, Fig. 1.7.

History

- An 84-year-old man with no cardiovascular risk factors presented with atypical angina and exertional dyspnea.
- Referred for regadenoson stress ^{13}N-ammonia myocardial perfusion PET/CT (Table 3.11).

PET/CT Images

Findings

- Myocardial perfusion imaging showed a large, severe and reversible perfusion defect in the LAD territory.
- Transiently increase in RV tracer uptake with stress.
- Reduced stress MBF and MFR were identified in LAD territory.
- Normal LV function at rest (55%) with a drop in LVEF during peak stress (48%), consistent with large ischemic burden.

Imaging Diagnosis

- Severe myocardial ischemia in the LAD territory.

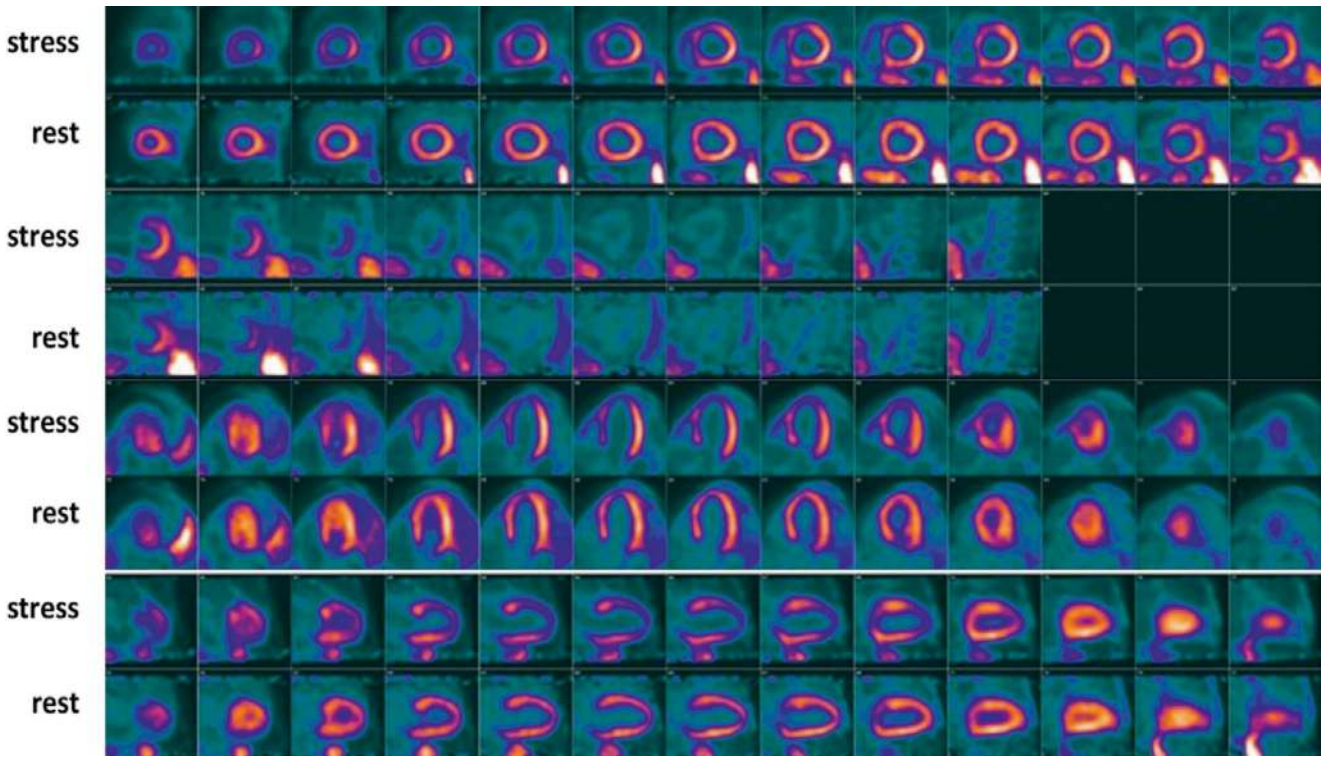


Fig. 3.25 Regadenoson stress and rest ^{13}N-ammonia myocardial perfusion PET/CT images demonstrate dilated LV and a large and severe perfusion defect throughout the mid and distal anterior and anteroseptal walls, LV apical segments, and the LV apex, showing complete reversibility

Table 3.11 Summary of the quantitative blood flow data demonstrating MBF and MFR impairment during regadenoson in LAD and RCA territories and globally (normal value >1.8 mL/min/g). Myocardial flow reserve is impaired in the RCA and LAD territories (normal value >2.0)

	MBF rest (ml/min/g)	MBF stress (ml/min/g)	MFR (stress/rest)
LAD	0.80	1.28	1.62
LCX	0.84	1.80	2.15
RCA	0.72	1.32	1.84
Global LV	0.79	1.44	1.83

Differential Diagnosis

- None.

Correlative Imaging

- Invasive coronary angiography (Fig. 3.26).

Management

- The patient underwent coronary artery bypass grafting of the LAD.

Further Reading

- Kobayashi N, Maehara A, Brener S, Généreux P, Witzenbichler B, Guagliumi G, et al. Usefulness of the Left Anterior Descending Coronary Artery Wrapping Around the Left Ventricular Apex to Predict Adverse Clinical Outcomes in Patients With Anterior Wall ST-Segment Elevation Myocardial Infarction (from the Harmonizing Outcomes With Revascularization and Stents in Acute Myocardial Infarction Trial). The American Journal of Cardiology. 2015;116:1658–1665.
- Sapin P, Musselman D, Dehmer G, Cascio W. Implications of inferior ST-segment elevation accompanying anterior wall acute myocardial infarction for the angiographic morphology of the left anterior descending coronary artery morphology and site of occlusion. The American Journal of Cardiology. 1992;69:860–865.
- Peters S. Takotsubo cardiomyopathy and structural abnormalities of the left anterior descending coronary artery. International Journal of Cardiology. 2016;223:510–511.

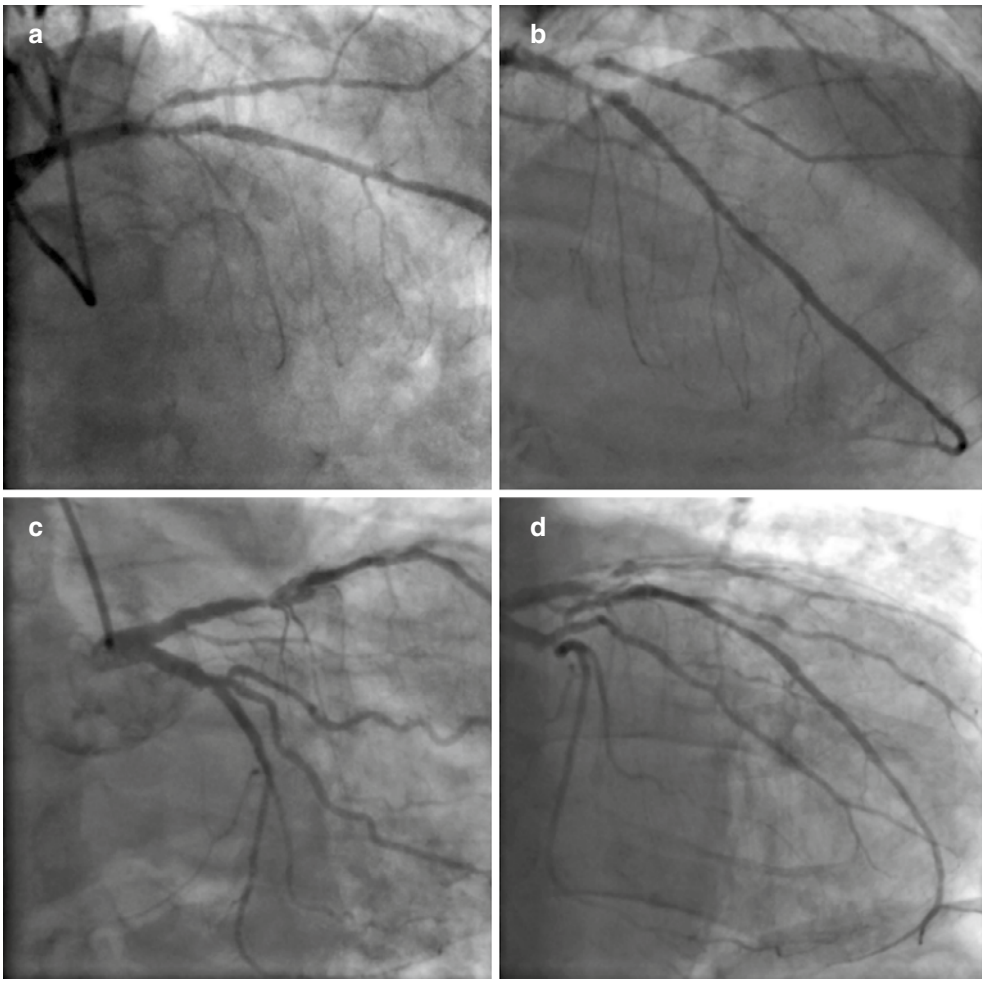


Fig. 3.26 Selective angiographic views of the coronary arteries showed a severe stenosis of the proximal LAD with post-stenotic aneurysm and > 90 stenosis of the first diagonal branch (A, B). A long LAD wraps around the apex and supplies the mid to distal inferior wall of the left ventricle (B and D). The LCX and RCA show luminal irregularities without focal stenosis (C, D)

3.1.12 Reclassification to Multivessel Disease by Integrating Flow Quantification: Case 19

Key Points

- Severely reduced stress MBF and MFR in all territories in a patient with a single perfusion abnormality helps to reclassify the diagnosis from single to multivessel coronary artery disease.
- Large perfusion defects associated with LV dilatation, TID and a drop in LVEF with stress, and severe reduction of stress MBF and MFR are all markers of high-risk coronary artery disease.
- For further discussion of interpretation of myocardial blood flow, see Chap. 1, Fig. 1.7.

History

- A 68-year-old woman with no known coronary artery disease was referred for a regadenoson myocardial perfusion PET study for preoperative evaluation.
- She has a history of controlled hypertension (Fig. 3.27 and Table 3.12).

PET/CT Images

Findings

- There is transient LV dilatation during stress.
- There is a large and severe perfusion defect involving the mid and basal inferior and inferolateral walls during stress with near complete reversibility at rest.
- Severe reduction in stress MBF and MFR in all coronary territories, more marked in the RCA territory.
- LVEF at rest is 44% with moderately dilated LV volumes. The peak stress LVEF dropped to 39% with transient dilatation of the LV end systolic volume. There is moderate global LV hypokinesis and akinesis of the inferior and inferolateral walls.
- The coronary artery calcium core score was 333 Agatston units, which is >90th percentile for sex and age.

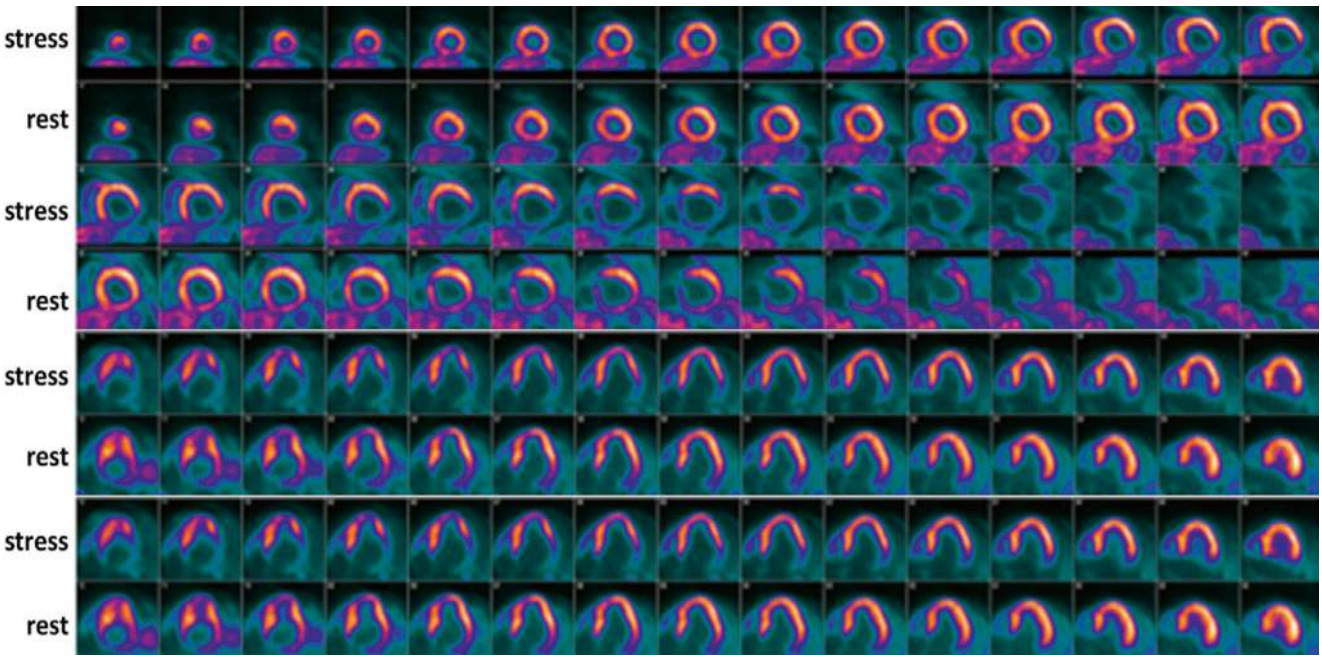


Fig. 3.27 Regadenoson stress and rest ^{13}N-ammonia PET study. There is moderate LV dilatation with mild TID during stress. There is a large and severe perfusion defect involving the mid and basal inferior and inferolateral walls during stress with near complete reversibility at rest

Table 3.12 Summary of stress and rest MBF and MFR

	MBF rest (ml/min/g)	MBF stress (ml/min/g)	MFR (stress/rest)
LAD	0.70	1.21	1.72
LCX	0.82	1.20	1.47
RCA	0.68	0.99	1.45
Global LV	0.72	1.14	1.57

Imaging Diagnosis
- Abnormal myocardial perfusion study consistent with a medium-sized area of severe stress-induced ischemia in the RCA territory.
- Severely reduced stress MBF and MFR in all territories is consistent with multivessel obstructive coronary artery disease.

Differential Diagnosis
- None.

Correlative Imaging
- Invasive coronary angiography report:
- Proximal RCA is 100% stenosed.
- Ostial first marginal is 80% stenosed.
- Proximal LCX is 80% stenosed.
- Ostial left main is 70% stenosed.

Management
- The patient underwent CABG without complications.

Further Reading

- Bateman TM, et al. Practical guide for interpreting and reporting cardiac PET measurements of myocardial blood flow: an information statement from the American Society of Nuclear Cardiology, and the Society of Nuclear medicine and molecular imaging. JNC 2021:28(2);768–87.

3.2 Challenging Cases Integrating Perfusion CAC and Flow

3.2.1 High-Risk Scan Myocardial Perfusion PET Scan: Case 20

Key Points
- A relatively normal rest flow reserve does not exclude high-risk ischemia in a patient with multi-territorial ischemia and very diminished stress flow.

- All available imaging information should be considered in the interpretation of myocardial perfusion imaging, including visual and quantitative information.
- For further discussion of interpretation of myocardial blood flow, see Chap. 1, Fig. 1.7.

History

- A 74-year-old man with a history of dyslipidemia, hypertension, and former tobacco use.
- Referred for PET/CT to assess postprandial episodes of angina (Figs. 3.28, 3.29 and Table 3.13).

PET/CT Images

Findings

- The myocardial perfusion PET images demonstrate TID during stress (TID ratio: 1.42).
- There is a large perfusion defect of severe intensity throughout the mid-anterior and anteroseptal walls, the apical LV segments and the LV apex, showing complete reversibility. In addition, there is a medium-sized defect of moderate intensity throughout the inferior and basal inferolateral walls, also showing complete reversibility.
- The quantitative flow data shows severe and diffuse reduction in stress MBF and relatively preserved MFR due to a low rest flow.

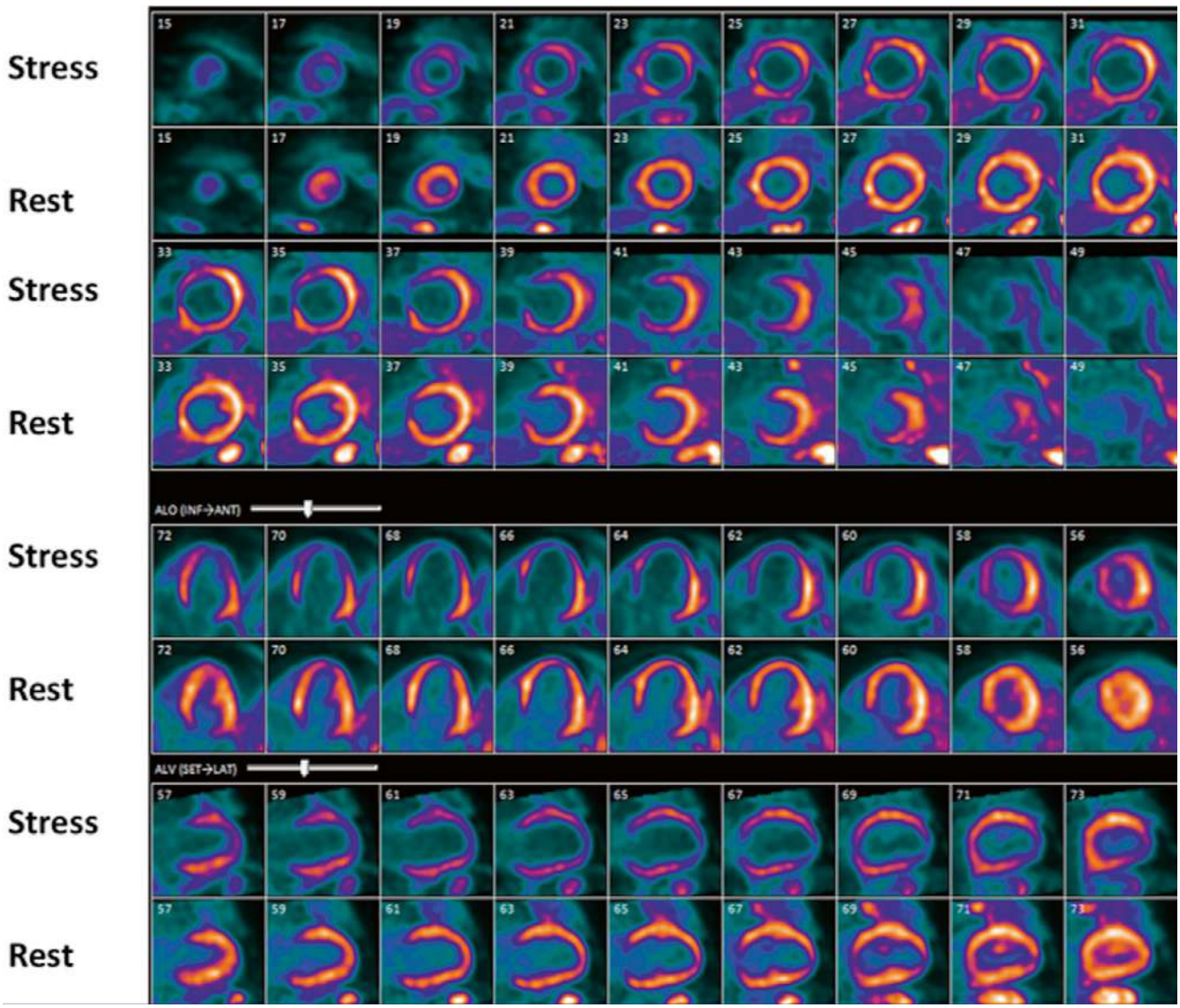


Fig. 3.28 Stress rest ^{13}N-ammonia PET images demonstrate TID at peak stress and a large and severe defect, completely reversible at rest, involving the mid-anterior and anteroseptal walls, the apical LV segments and the LV apex. In addition, there is a medium-sized defect of moderate intensity throughout the inferior and basal inferolateral walls, also showing complete reversibility

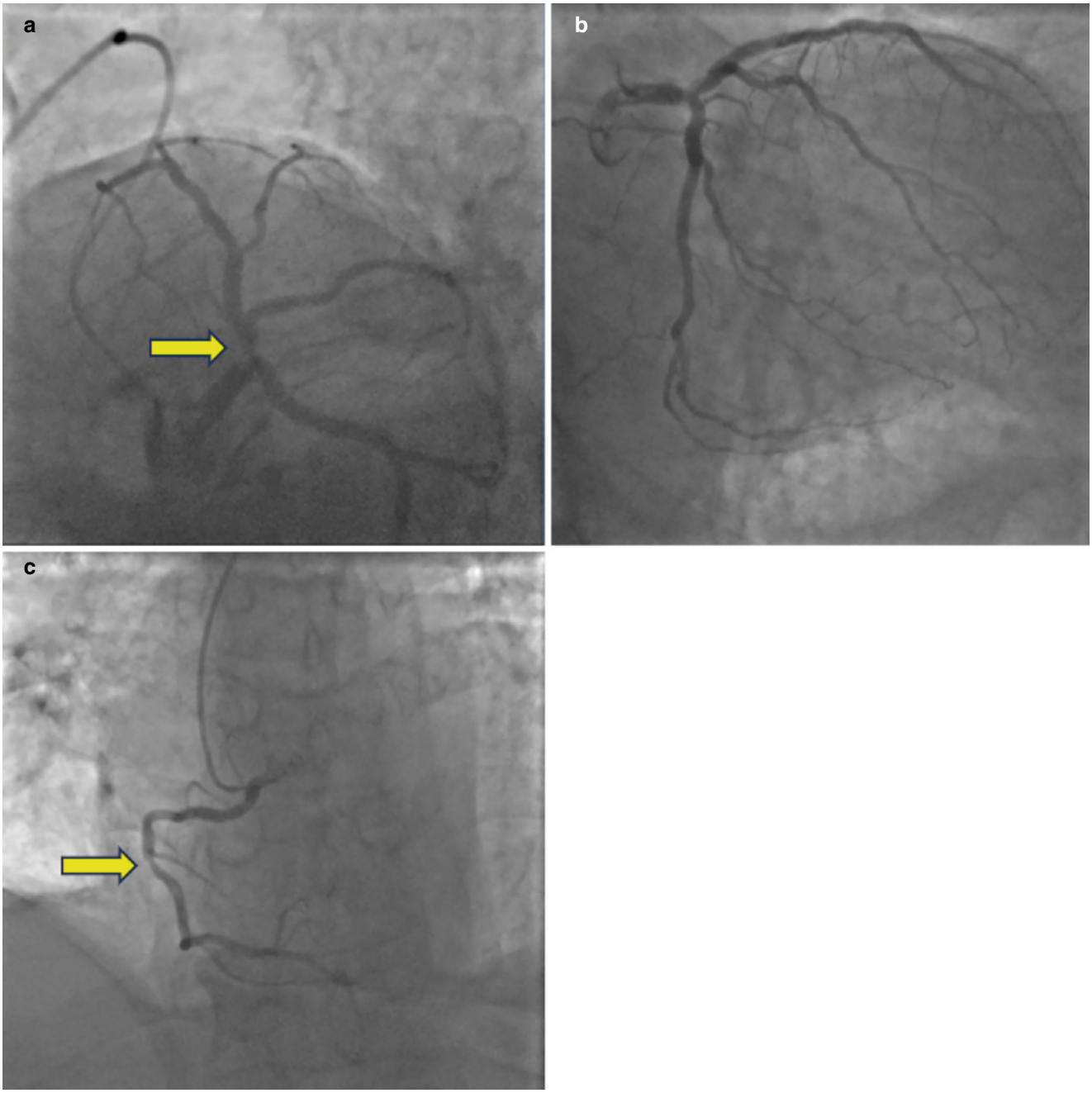


Fig. 3.29 Selective view of the left coronary system demonstrating (A) a 70% left main stenosis, (B) 70% ostial LAD stenosis, and (C) 70% stenosis of the mid RCA

Table 3.13 Summary of the quantitative blood flow data demonstrating severe reduction in stress myocardial blood flow in all coronary artery territories and globally (normal value >1.8 mL/min/g), with relatively normal myocardial flow reserve (normal value >2.0)

	MBF rest (ml/min/g)	MBF stress (ml/min/g)	MFR (stress/rest)
LAD	0.53	1.17	2.20
LCX	0.72	1.74	2.42
RCA	0.47	1.15	2.43
Global LV	0.56	1.31	2.35

- LV systolic function was severely reduced with an LVEF of 21% on both the rest and stress images with severe global hypokinesis and LV dilatation (end-systolic volume: 190 mL) that worsened with stress.

Imaging Diagnosis
- Severe multivessel obstructive coronary artery disease.

Differential Diagnosis
- Severe multivessel obstructive coronary artery disease.
- Mixed ischemic and nonischemic cardiomyopathy.

Correlative Imaging
- Invasive coronary angiography.

Management
- The patient underwent high-risk CABG.

Further Reading

- Johnson N, Gould K, Di Carli M, Taqueti V. Invasive FFR and Noninvasive CFR in the Evaluation of Ischemia: What is the Future? Journal of the American College of Cardiology. 2016;67:2772–2788.
- Ziadi M, deKemp R, Williams K, Guo A, Renaud J, Chow B, et al. Does quantification of myocardial flow reserve using rubidium-82 positron emission tomography facilitate detection of multivessel coronary artery disease? Journal of Nuclear Cardiology. 2012;19:670–680.
- Valenta I, Quercioli A, Schindler TH. Diagnostic value of PET-measured longitudinal flow gradient for the identification of coronary artery disease. JACC Cardiovasc Imaging 2014;7:387–96.
- Gould KL, Johnson NP, Bateman TM, Beanlands RS, Bengel FM, Bober R et al.. Anatomic versus physiologic assessment of coronary artery disease. Role of coronary flow reserve, fractional flow reserve, and positron emission tomography imaging in revascularization decision-making. J Am Coll Cardiol 2013;62:1639–53.
- Valenta I, Antoniou A, Marashdeh W, Leucker T, Kasper E, Jones SR, Dannals RF, Solnes L, Pomper MG, Schindler TH. PET-measured longitudinal flow gradient correlates with invasive fractional flow reserve in coronary artery disease patients. Eur Heart J Cardiovasc Imaging. 2017 May 1;18(5):538–548.

3.2.2 Investigating Angina Post Percutaneous Coronary Intervention: Case 21

Key Points
- The PET scan confirmed that the patient's recurrent angina was due to an area of severe myocardial ischemia.
- Assignment of coronary vascular distribution when reporting myocardial perfusion imaging is based on a standard model of coronary artery distribution.
- However, nonstandard coronary artery branching patterns may cause perfusion abnormalities in other territories. For example, a wraparound RCA artery causing ischemia in the LAD territory.
- For further discussion of interpretation of myocardial blood flow, see Chap. 1, Fig. 1.7.

History
- A 67-year-old man on peritoneal dialysis due to chronic renal insufficiency.
- He presented with an inferior-posterior STEMI (TnI max 90.2 ng/ml, CK-MB 183.4 ng/ml), which was treated with primary PCI (Fig. 3.30a and b).
- The invasive coronary angiogram demonstrated additional disease in the LCX and LAD coronary arteries (Fig. 3.30c and d). Two months after the index STEMI, he underwent percutaneous coronary intervention (PCI) of the LCX artery (Fig. 3.30e).

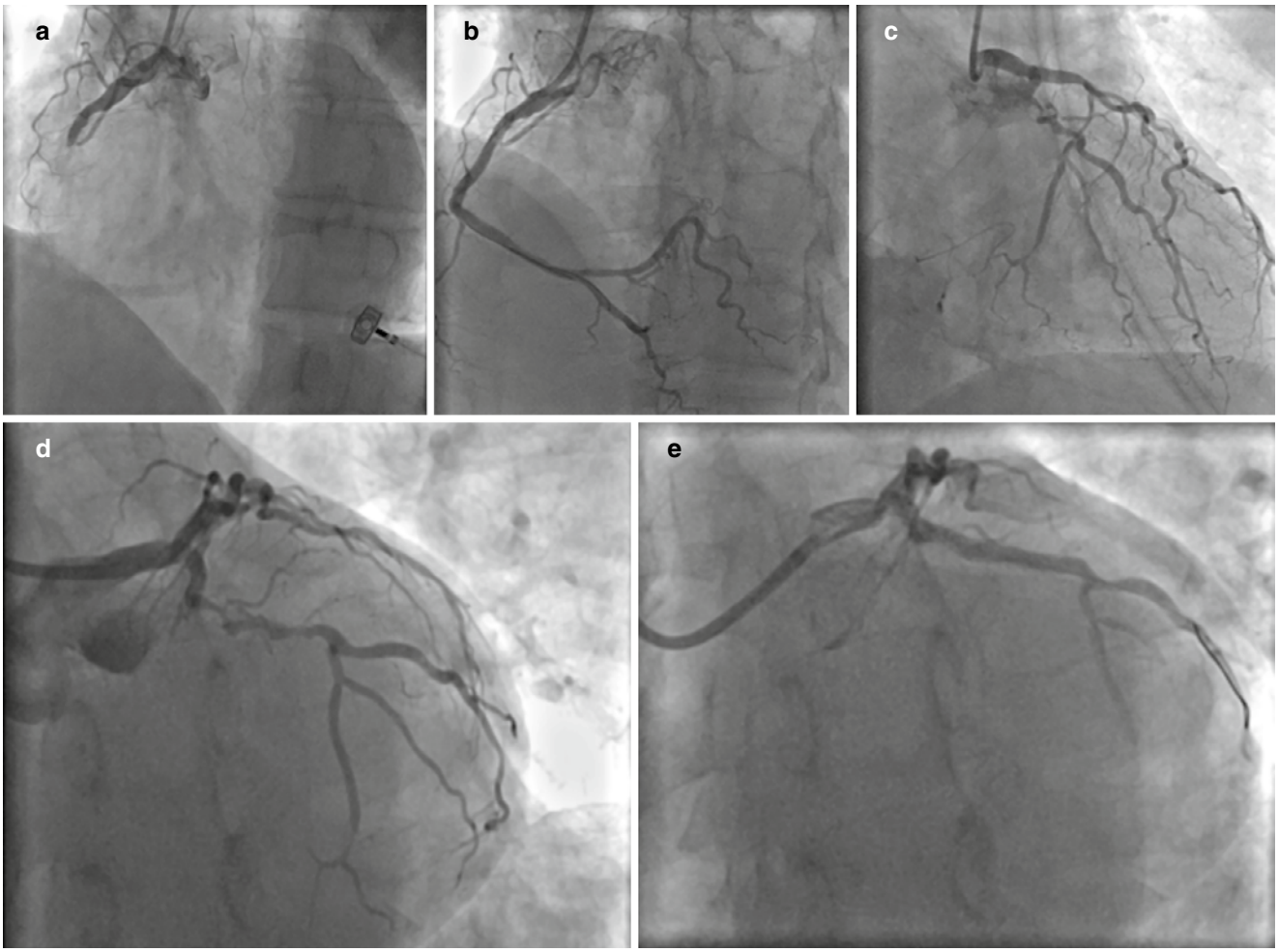


Fig. 3.30 Invasive coronary angiography showing occlusion of the RCA before primary PCI (**a**) and patent vessel (**b**) after PCI. Additional disease is present on LCX and LAD (**c**). LCX is treated with staged PCI (**d**, **e**)

- Nine months later, the patient was readmitted to the emergency room due to recurrent chest pain.
- The cardiac enzymes were negative.
- He was referred for myocardial perfusion PET (Fig. 3.31 and Table 3.14).

PET/CT Images

Findings

- The stress PET images revealed a severe perfusion defect involving the apical LV segments and the LV apex, with good reversibility at rest.
- The stress MBF was reduced in all vascular territories but MFR was reduced only in the LAD and LCX territories.

Imaging Diagnosis

- Moderate ischemia in the distal LAD territory.

Management

- This patient was referred for invasive coronary angiography (Fig. 3.32).

Further Reading

- Shibutani H, Akita Y, Yutaka K, Yamamoto S, Matsui Y, Yoshinaga M, et al. Acute myocardial infarction with "wrap around" right coronary artery mimicking Takotsubo cardiomyopathy: a case report. BMC Cardiovascular Disorders. 2016;16:16–71.

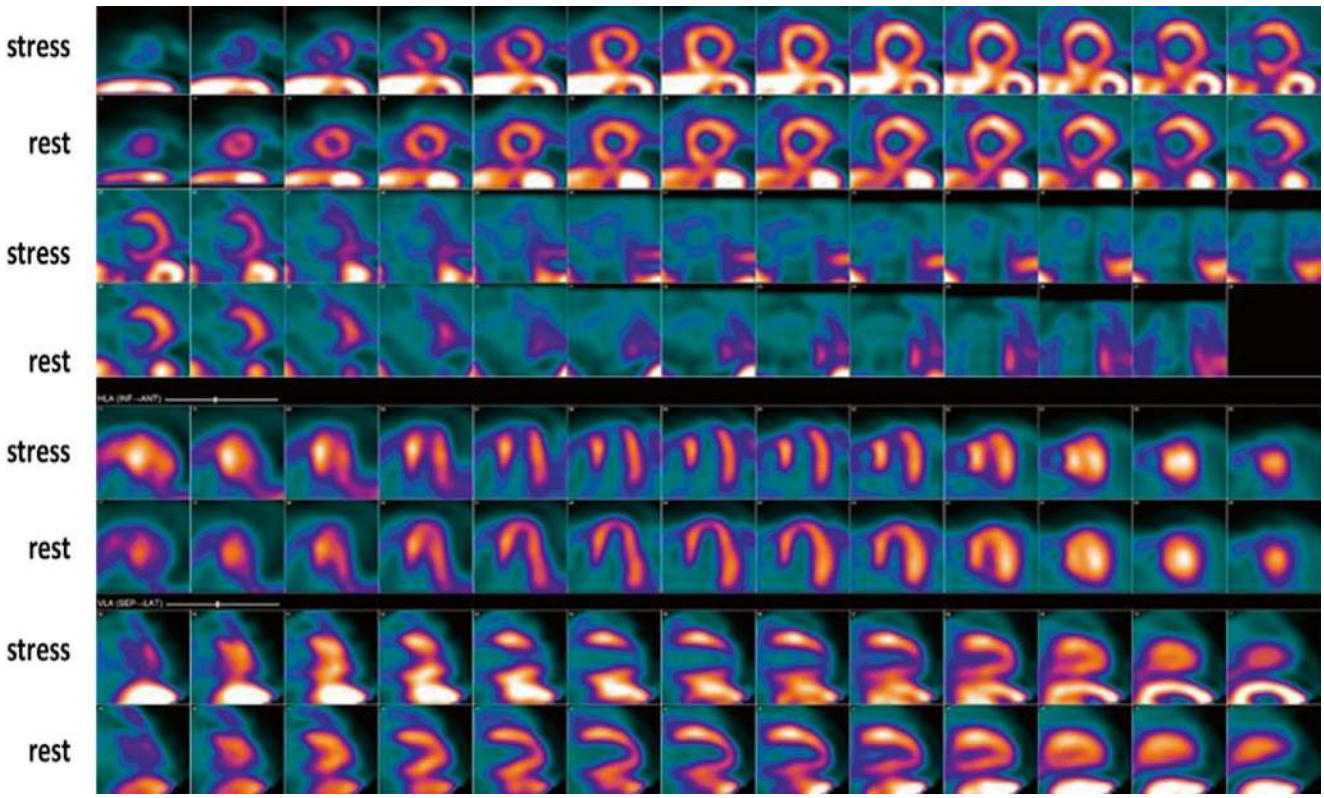


Fig. 3.31 Stress-rest ^{13}N-ammonia PET images demonstrate a reversible perfusion defect involving the apical LV segments and the LV apex

Table 3.14 Summary of the quantitative blood flow data demonstrating reduced MBF in all vascular territories with MFR reduction only in the LAD and LCX territories

	MBF rest (ml/min/g)	MBF stress (ml/min/g)	MFR (stress/rest)
LAD	0.73	1.20	1.65
LCX	0.84	1.47	1.76
RCA	0.64	1.38	2.16
Global LV	0.74	1.75	1.61

- Naya M, Murthy V, Blankstein R, Sitek A, Hainer J, Foster C, et al. Quantitative Relationship Between the Extent and Morphology of Coronary Atherosclerotic Plaque and Downstream Myocardial Perfusion. Journal of the American College of Cardiology. 2011;58:1807–1816.
- Gaemperli O, Schepis T, Valenta I, Husmann L, Scheffel H, Duerst V, et al. Cardiac Image Fusion from Stand-Alone SPECT and CT: Clinical Experience. Journal of Nuclear Medicine. 2007;48(5):696–703.
- Javadi M, Lautamaki R, Merrill J, Voicu C, Epley W, McBride G, et al. Definition of Vascular Territories on Myocardial Perfusion Images by Integration with True Coronary Anatomy: A Hybrid PET/CT Analysis. Journal of Nuclear Medicine. 2010;51:198–203.

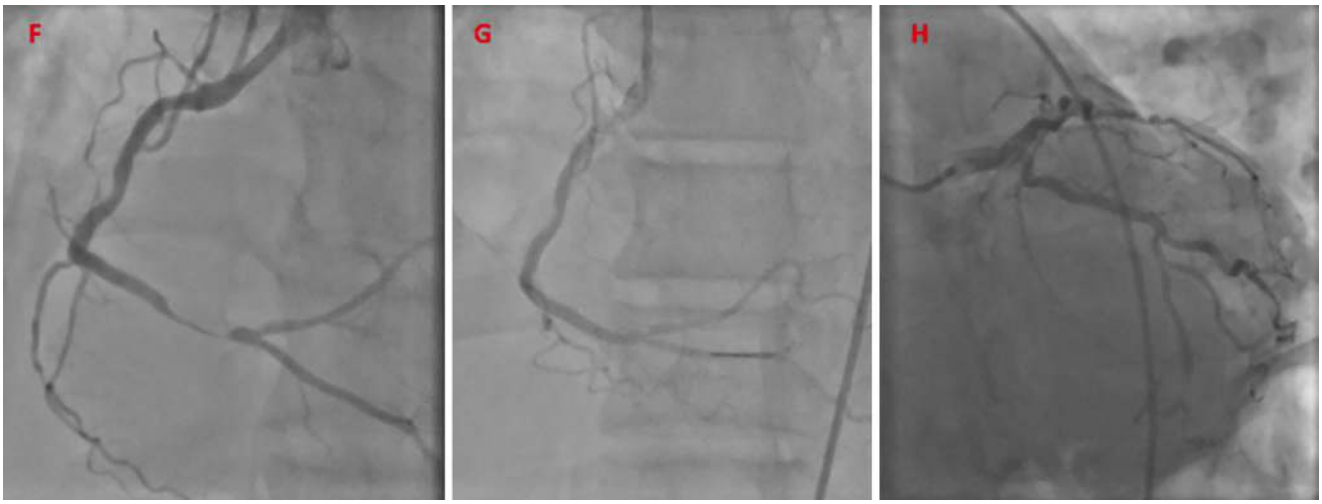


Fig. 3.32 The new invasive coronary angiography documented a tight stenosis of the distal RCA (panel F—before, panel G after PCI) with a wraparound distribution to the apical LV segments and LV apex, which explains the distribution of the perfusion abnormality and MFR data. Invasive coronary angiography of the left coronary system demonstrated a persistent good result of previous PCI (panel H)

3.2.3 Equivocal Coronary CT Angiography and Normal PET: Case 22

Key Points

- Extensive atherosclerosis on coronary CT angiography (CCTA) without regional perfusion abnormalities on PET myocardial perfusion imaging.
- Low short-term risk of cardiovascular events (< 1% cardiac death rate/year). However, high long-term risk of events based on the presence of severe nonobstructive atherosclerosis.
- This requires aggressive management of cardiovascular risk factors.
- For further discussion of interpretation of myocardial blood flow, see Chap. 1, Fig. 1.7.

History

- A 68-year-old man with a history of hypertension. He underwent recent coronary CT angiography, which demonstrated extensive coronary atherosclerosis including severe calcified and partially calcified stenoses in the LCX and LAD (Fig. 3.33).
- He was referred for PET/CT for the evaluation of exertional dyspnea and chest pain (Fig. 3.34).

PET/CT Images (Table 3.15)

Findings

- The images demonstrated normal LV size. There was normal regional myocardial perfusion on both the stress and rest imaging.
- The ECG-gated images demonstrated a rest LV ejection fraction of 52% which increased to 60% post stress with normal LV volumes. There was normal regional wall motion and thickening.
- The maximal stress myocardial blood flow was moderately reduced in all coronary territories and globally, but myocardial flow reserve was normal.

Imaging Diagnosis

- No evidence of flow-limiting coronary artery disease.

Differential Diagnosis

- None.

Correlative Imaging

- None.

Management

- Aggressive risk factor management.

Further Reading

- Gupta A, Taqueti VR, van de Hoef TP, Bajaj NS, Bravo PE, Murthy VL, et al. Integrated Non-invasive Physiological Assessment of Coronary Circulatory Function and Impact on Cardiovascular Mortality in Patients with Stable Coronary Artery Disease. Circulation. 2017;136:2325–2336.
- SCOT-HEART Investigators, Newby DE, Adamson PD, Berry C, Boon NA, Dweck MR, et al. Coronary CT Angiography and 5-Year Risk of Myocardial Infarction. New England Journal of Medicine. 2018;379:924–933.

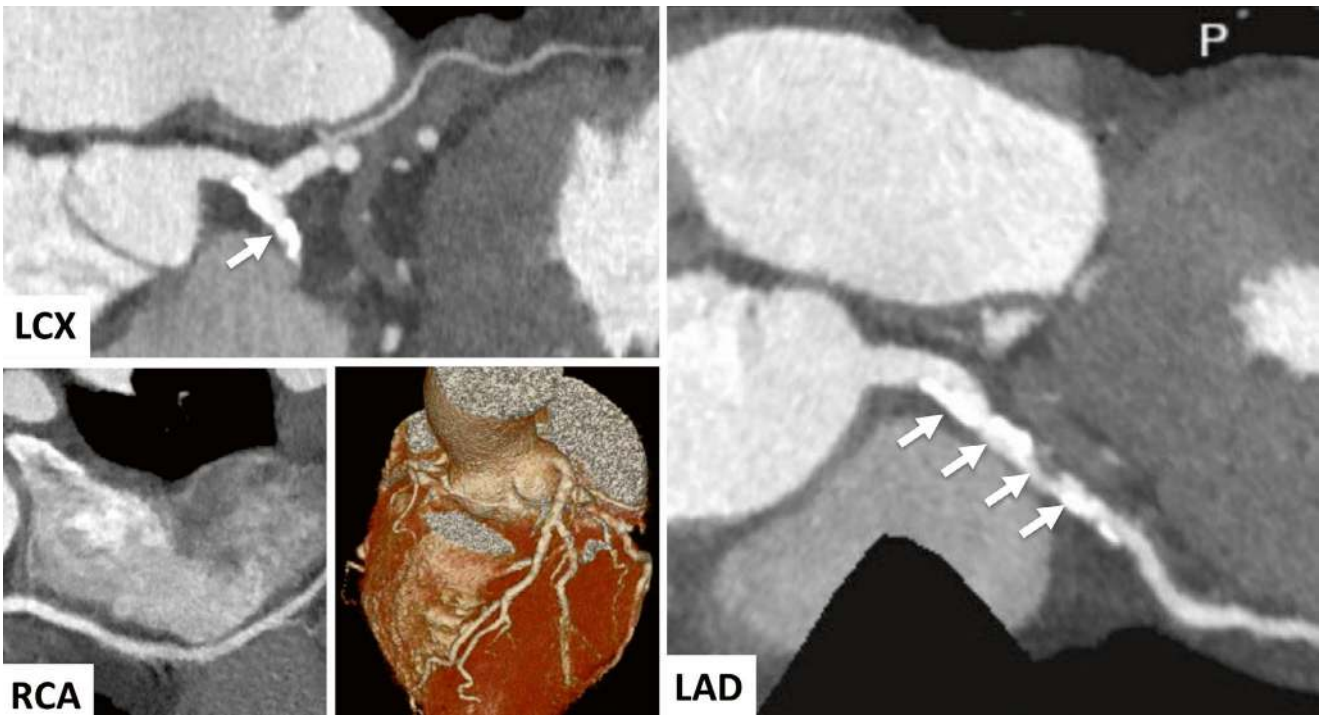


Fig. 3.33 Coronary CT angiography showing extensive coronary atherosclerosis including severe calcified and partially calcified stenoses in the LAD and LCX (arrows)

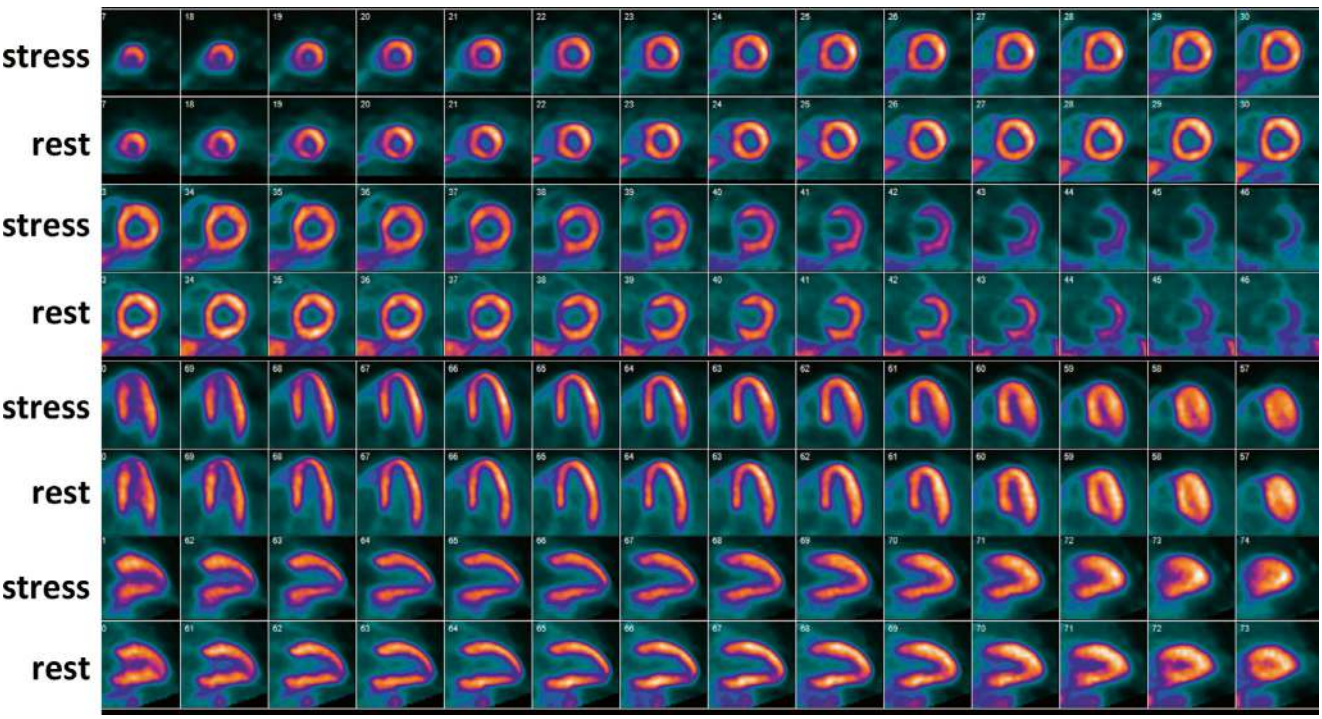


Fig. 3.34 Stress rest ^{13}N-ammonia PET images demonstrate normal myocardial perfusion

Table 3.15 Summary of the quantitative blood flow data demonstrating a moderate reduction in stress myocardial blood flow (normal value >1.8 mL/min/g) with preserved myocardial flow reserve (normal value >2.0) in all coronary artery territories and globally

	Rest (ml/min/g)	Stress (ml/min/g)	MFR (stress/rest)
LAD	0.45	1.48	3.29
LCX	0.51	1.89	3.17
RCA	0.47	1.47	3.13
Global LV	0.47	1.58	3.36

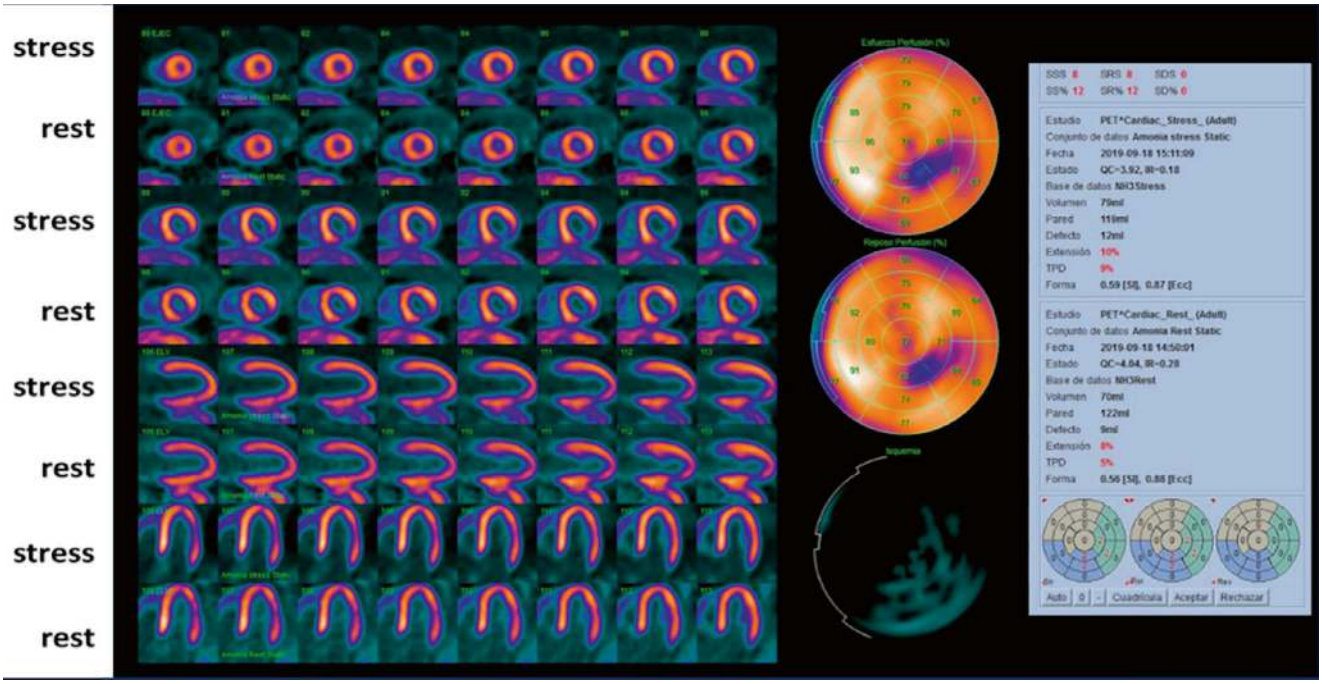


Fig. 3.35 Stress-rest ^{13}N ammonia PET MPI demonstrating a small and severe perfusion defect in the mid and basal inferolateral wall, which is fixed

3.3 Patient with Known Coronary Artery Disease

3.3.1 Prior PCI: Case 23

Key Points

- Myocardial perfusion PET imaging with quantitative flow information can help guide diagnosis and management of patients with known coronary artery disease and prior revascularization with recurrent symptoms.
- Preserved MBF and MFR help exclude the presence of obstructive coronary artery disease and microvascular dysfunction.
- For further discussion of interpretation of myocardial blood flow, see Chap. 1, Fig. 1.7.

History

- A 76-year-old man with a history of hypertension, smoking, and dyslipidemia. He had known coronary artery disease with prior STEMI followed by PCI of the LCX.
- The patient was referred for cardiac imaging with PET/CT (Fig. 3.35) for the evaluation of recurrent atypical angina (Table 3.16).

PET/CT Images

Findings

- A small area of prior myocardial infarction throughout the mid and basal inferolateral wall without residual stress-induced ischemia (Fig. 3.36).

Table 3.16 There is mildly reduced stress MBF in the RCA territory. MFR is preserved in all coronary territories and globally

	Rest (ml/min/g)	Stress (ml/min/g)	MFR (stress/rest)
LAD	0.71	2.19	3.05
LCX	0.68	1.86	2.72
RCA	0.71	1.67	2.33
Global LV	0.70	1.99	2.80

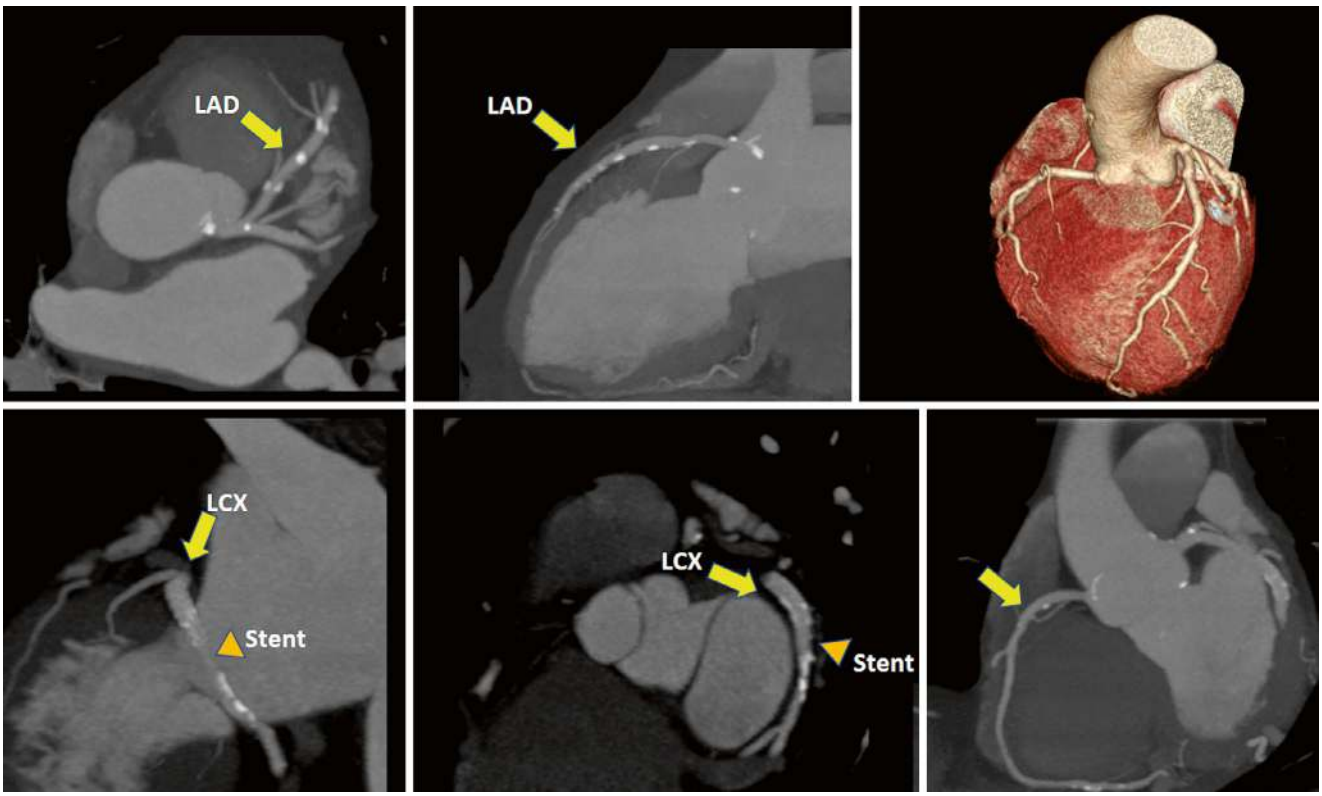


Fig. 3.36 Multiplanar reformatted coronary CT angiogram images and a three-dimensional reconstruction of the heart and vessels. Scattered calcified plaques in all three coronary arteries without obstructive stenosis. The stent in the LCX was patent

- The LVEF was 63% at rest and 61% during peak stress.
- Preserved stress MBF and MFR in the LCX and LAD territories.

Imaging Diagnosis
- Small prior myocardial infarction in the mid and basal inferolateral wall without evidence of stress-induced ischemia.
- No evidence of coronary microvascular dysfunction.

Differential Diagnosis
- Noncardiac chest pain.

Correlative Imaging
- Coronary CT angiography.

Management
- Optimization of medical therapy.

Further Reading

- Murthy V, Bateman T, Beanlands R, Berman D, Borges-Neto S, Chareonthaitawee P, et al. Clinical Quantification of Myocardial Blood Flow Using PET: Joint Position Paper of the SNMMI Cardiovascular Council and the ASNC. Journal of Nuclear Cardiology. 2017;25:269–297.
- Patel KK, Spertus JA, Chan PS, Sperry BW, Thompson RC, Al Badarin F et al. Extent of Myocardial Ischemia on Positron Emission Tomography and Survival Benefit With Early Revascularization. J Am Coll Cardiol. 2019 Oct 1;74(13):1645–1654.

3.3.2 Prior CABG: Case 24

Key Points

- Quantitative PET MPI is helpful to localize the culprit vessel and assess the magnitude of myocardial ischemia post-coronary artery bypass grafting (CABG).
- Stress myocardial blood flow after CABG tends to be reduced even in asymptomatic patients. This is likely related to the fact that the native coronary arteries typically developed diffuse atherosclerosis and calcifications.
- Reporting of myocardial perfusion images in patients post CABG should be ideally performed with knowledge of the operative report to better guide the localization of the culprit artery in cases with documented ischemia undergoing repeat angiography.
- For further discussion of interpretation of myocardial blood flow, see Chap. 1, Fig. 1.7.

History

- A 40-year-old woman with known coronary artery disease and prior CABG (left internal mammary artery to LAD) and end-stage renal disease in the setting of lupus nephritis.
- She has a history of a mechanical mitral valve replacement for severe calcific mitral stenosis and tricuspid repair for severe tricuspid insufficiency.
- She was referred for a regadenoson myocardial perfusion PET study (Fig. 3.37) for pre-renal transplant evaluation (Table 3.17).

PET/CT Images

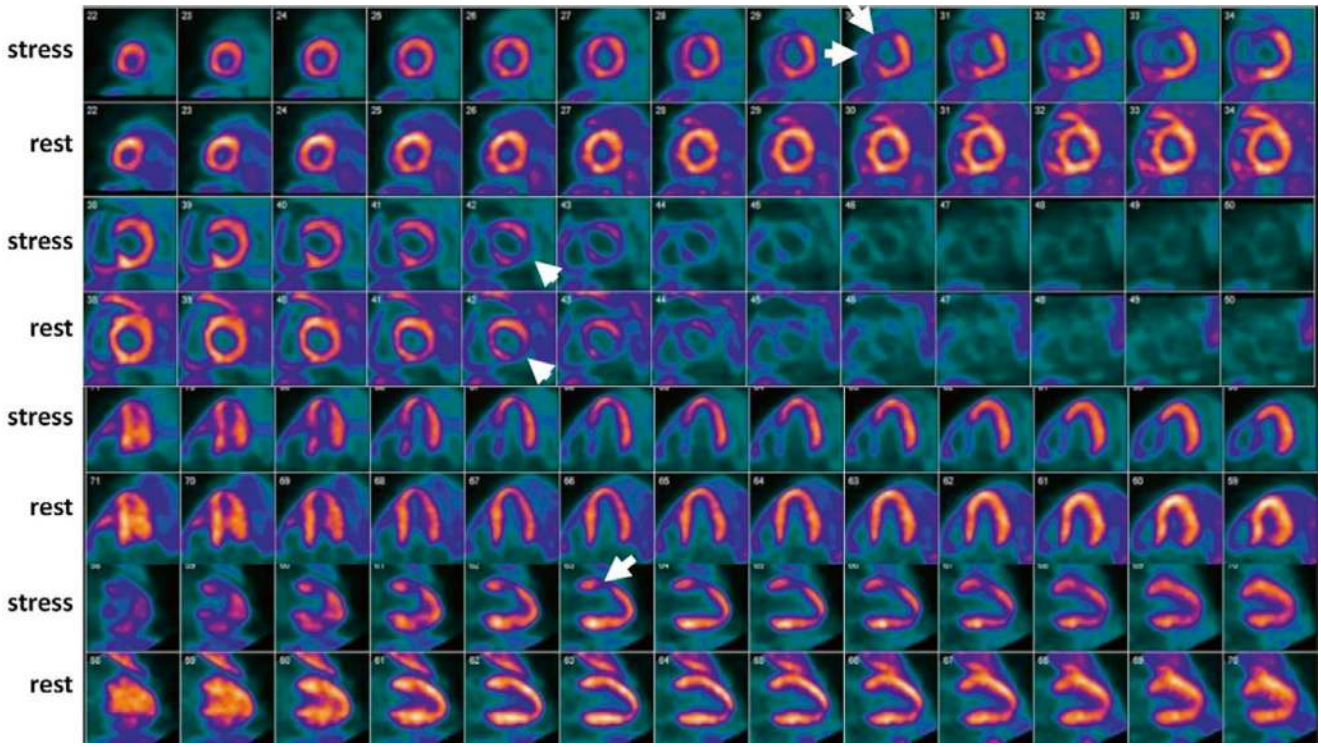


Fig. 3.37 Stress/rest ^{13}N-ammonia PET myocardial perfusion images demonstrate a medium-sized perfusion defect of severe intensity involving the mid and basal anterior and anteroseptal walls (arrows), showing complete reversibility. The apical LV segments and the LV apex have relatively preserved myocardial perfusion during stress. In addition, there is a small and severe perfusion defect involving the basal inferolateral wall (arrows), which is fixed

Table 3.17 Summary of quantitative flow data demonstrating moderate diffuse reduction in stress myocardial blood flow in all territories, more severe in the proximal LAD territory. MFR regionally reduced in the area of the myocardial perfusion defect

	MBF rest (ml/min/g)	MBF stress (ml/min/g)	MFR (stress/rest)
LAD	0.82	1.45	1.76
LCX	0.72	1.68	2.35
RCA	0.75	1.50	2.00
Global LV	0.76	1.52	2.00

Findings

- There is a medium-sized perfusion defect of severe intensity involving the mid and basal anterior and anteroseptal walls, showing complete reversibility. The apical LV segments and the LV apex have relatively preserved myocardial perfusion during stress.
- In addition, there is a small and severe perfusion defect involving the basal inferolateral wall, which is fixed.
- The ECG-gated images demonstrated a normal LVEF calculated at 56% at rest with paradoxical septal motion, consistent with prior open heart surgery.
- The quantitative flow data demonstrated a moderate diffuse reduction in stress myocardial blood flow, more severe in the proximal LAD territory. The flow reserve is regionally reduced in the area of the myocardial perfusion defect.

Imaging Diagnosis

- Medium-sized area of severe ischemia in the anterobasal area of the LV consistent with obstructive disease of proximal LAD proximal to anastomosis of left internal mammary graft to LAD.
- Small area of scar in the inferobasal area of the LV.

Differential Diagnosis

- None.

Correlative Imaging

Follow-up invasive coronary angiography demonstrated**:**

- Proximal 100% LAD occlusion, with collateral flow from the RCA.
- The LCX has a 95% midlesion and is occluded distally.
- The left internal mammary graft to the mid LAD is patent.
- The RCA is without significant disease.

Management

- The area of moderate ischemia in the proximal LAD territory with preservation of perfusion in the distal part of the territory is caused by progression of disease in the native LAD proximal to the anastomosis of the left internal mammary graft.
- The small fixed defect in the LCX/obtuse marginal territory corresponds to a totally occluded LCX. She was continued on dual antiplatelet therapy and antianginal therapy was intensified. On a follow-up office visit, she remains angina free.

Further Reading

- Murthy V, Bateman T, Beanlands R, Berman D, Borges-Neto S, Chareonthaitawee P, et al. Clinical Quantification of Myocardial Blood Flow Using PET: Joint Position Paper of the SNMMI Cardiovascular Council and the ASNC. Journal of Nuclear Cardiology. 2017;25:269–297.

3.3.3 Evaluation of a Patient with Prior Myocardial Infarction: Case 25

Key Points

- The presence of mild TID with diffuse reduction in MBF and MFR in the non-infarcted territories illustrates that diffuse atherosclerosis and coronary microvascular disease (CMD) are prevalent in patients with known coronary artery disease. This affects the magnitude of myocardial ischemia and the quantitative imaging pattern can look like multivessel obstructive coronary artery disease.
- In patients with stable coronary artery disease, reduction in microcirculatory reserve exacerbates the functional significance of upstream coronary stenosis and may magnify the severity of inducible myocardial ischemia.
- For further discussion of interpretation of myocardial blood flow, see Chap. 1, Fig. 1.7.

History

- A 59-year-old woman with known coronary artery disease and prior inferior myocardial infarction (MI) was referred for a regadenoson stress myocardial perfusion PET (Fig. 3.38) to evaluate symptoms of atypical chest pain.
- Her cardiac risk factors include hypertension, dyslipidemia, tobacco use, and obesity (Table 3.18).

PET/CT Images

Findings

- There is mild TID of the LV cavity during stress. There is a medium-sized perfusion defect of severe intensity throughout the inferior wall, showing only mild reversibility. In addition, there is a small perfusion defect of severe intensity involving the LV apex, which shows complete reversibility.
- The ECG-gated images demonstrated a mild reduction in global LV systolic function with severe hypokinesis of the inferior wall and an LVEF at rest of 47%.
- The quantitative flow data demonstrates marked reduction in stress myocardial blood flow and moderate reduction in flow reserve in all coronary artery territories.

Imaging Diagnosis

- Medium-sized area of scar in the RCA territory with evidence of mild residual stress-induced ischemia.
- Mild TID associated with reduced stress MBF and MFR represent diffuse subendocardial ischemia.

Differential Diagnosis

- Multivessel obstructive coronary artery disease.
- Coronary microvascular dysfunction.

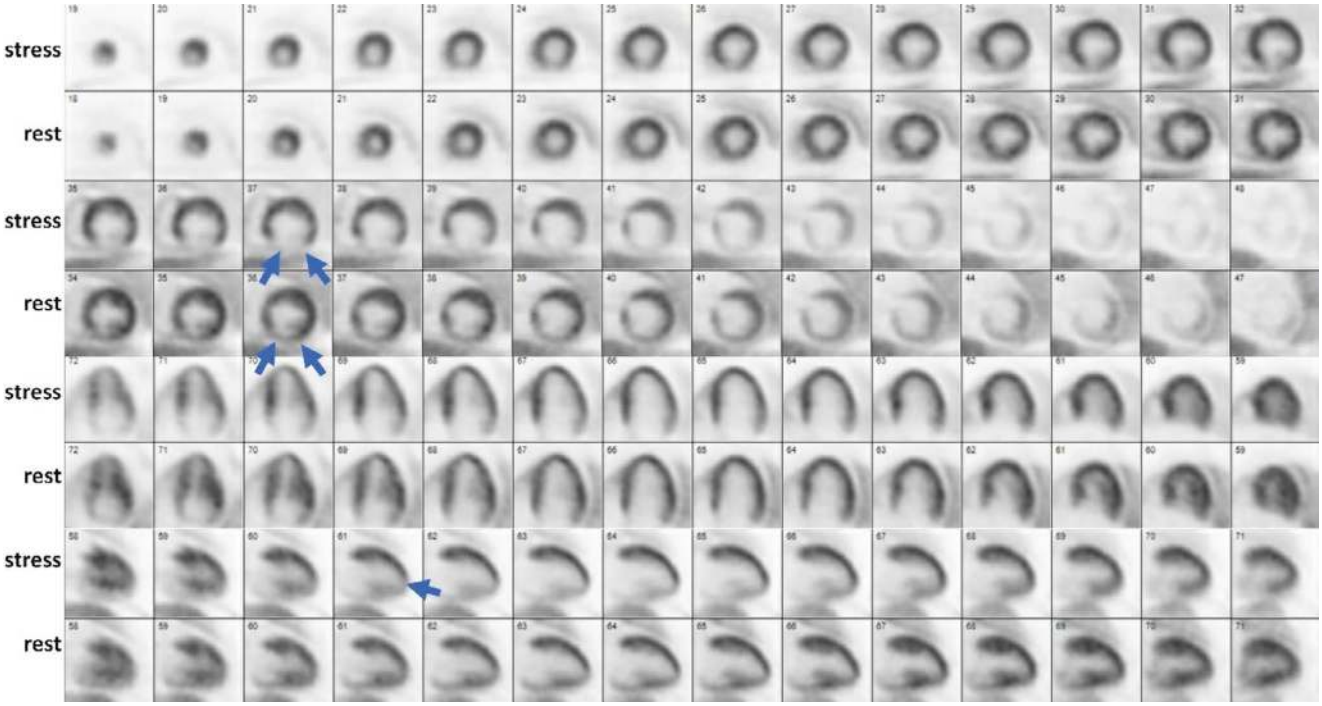


Fig. 3.38 Stress/rest ^{13}N-ammonia PET myocardial perfusion images. There is mild transient ischemic dilation of the LV cavity during stress. There is a medium-sized perfusion defect of severe intensity throughout the inferior wall, showing only mild reversibility (arrows). In addition, there is a small perfusion defect of severe intensity involving the LV apex, which shows complete reversibility (arrow)

Table 3.18 Summary of the quantitative blood flow data demonstrating marked reduction in stress MBF and moderate reduction in MFR in all coronary artery territories

	MBF rest (ml/min/g)	MBF stress (ml/min/g)	MFR (stress/rest)
LAD	0.72	1.33	1.84
LCX	0.84	1.42	1.70
RCA	0.74	1.18	1.61
Global LV	0.75	1.29	1.72

Correlative Imaging

- Follow-up invasive coronary angiography demonstrated a total occlusion of the mid RCA with moderate right-to-right collaterals. The left main and LAD arteries had mild irregularities. The LCX has a moderate stenosis (Figs. 3.39 and 3.40).

Management

- The patient underwent PCI of the total mid RCA occlusion and intensification of medical therapy of myocardial ischemia.

Further Reading

- Taqueti V, Di Carli M. Coronary Microvascular Disease Pathogenic Mechanisms and Therapeutic Options: JACC State-of-the-Art Review. Journal of the American College of Cardiology. 2018;72:2625–2641.
- Johnson N, Gould K, Di Carli M, Taqueti V. Invasive FFR and Noninvasive CFR in the Evaluation of Ischemia: What is the Future?. Journal of the American College of Cardiology. 2016;67:2772–2788.

3.3.4 Evaluation of a Patient with Prior Myocardial Infarction: Case 26

Key Points

- In patients with known CAD and recurrent symptoms, PET MPI can help delineate the presence and severity of myocardial ischemia and guide management.
- The quantitative flow data helps uncover extensive balanced ischemia in patients with multivessel coronary artery disease and exclude microvascular dysfunction as a potential source of recurrent symptoms.
- For further discussion of interpretation of myocardial blood flow, see Chap. 1, Fig. 1.7.

History

- A 33-year-old man with a history of premature coronary artery disease with prior myocardial infarction and PCI of the LAD coronary artery.
- He has a history of controlled hypertension and hyperlipidemia. Due to his past history and recurrent symptoms, he underwent a new invasive coronary angiography (Fig. 3.40),

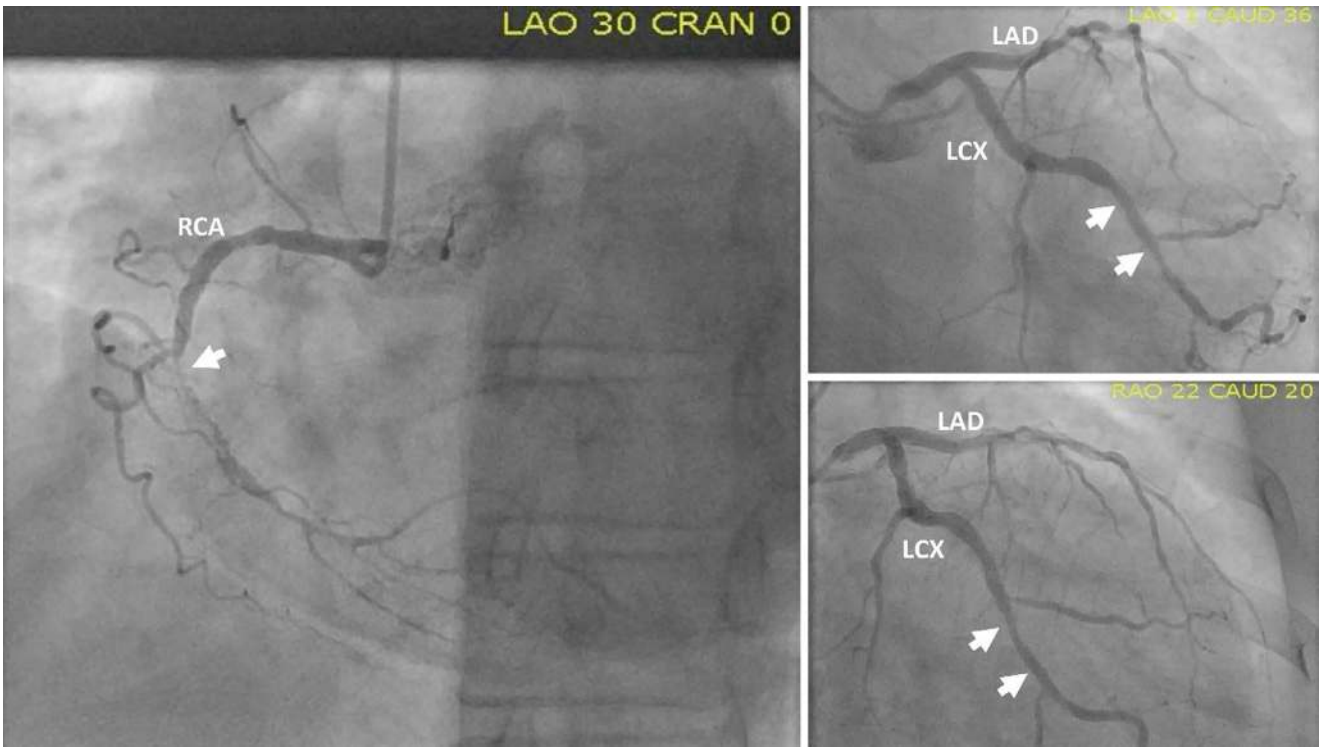


Fig. 3.39 Selective invasive coronary angiographic views demonstrating a total occlusion of the RCA (arrow) with right-to-tight collaterals and moderate diffuse nonobstructive atherosclerosis of the LCX and LAD coronary arteries (arrows)

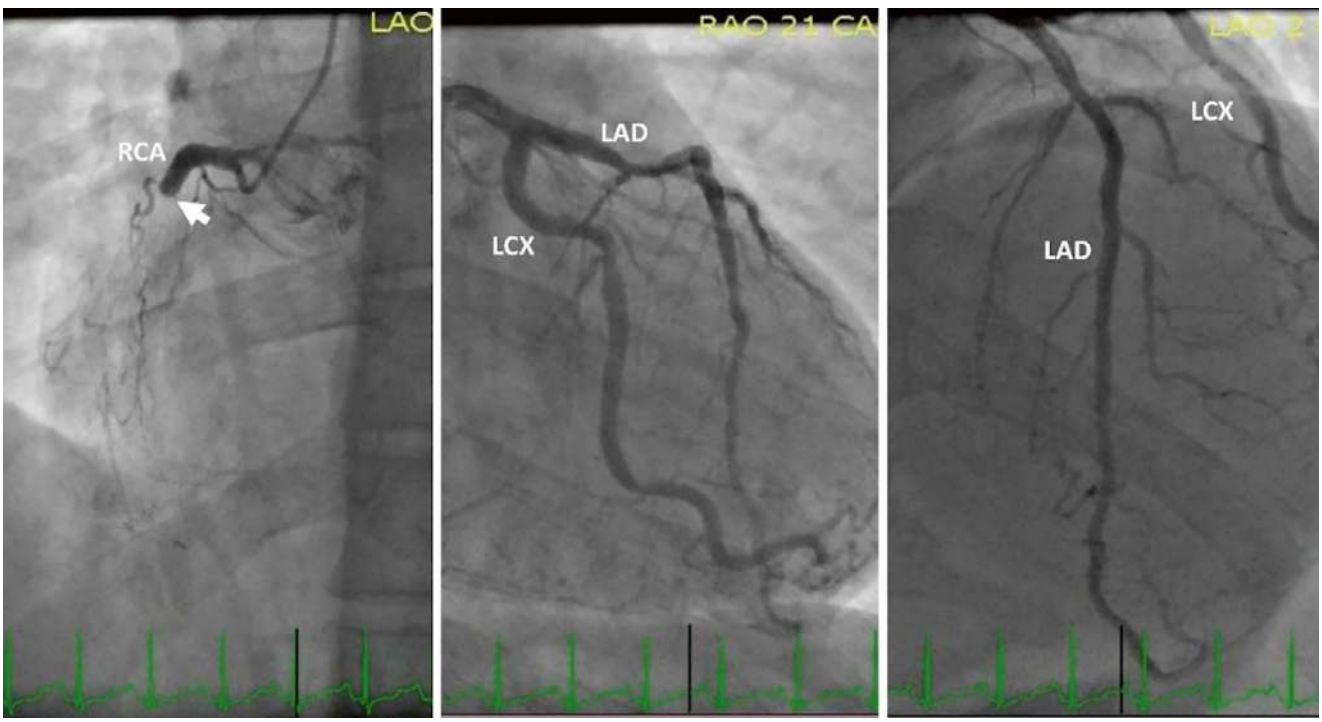


Fig. 3.40 Selective invasive coronary angiographic views demonstrating a total occlusion of the RCA (left panel, arrow) with right-to-right collaterals and moderate diffuse nonobstructive atherosclerosis of the LCX and LAD coronary arteries

which demonstrated a widely patent LAD stent and a total occlusion of the RCA, which was essentially unchanged since his first invasive coronary angiogram.
- He was referred to PET/CT MPI (Fig. 3.41) for the evaluation of recurrent atypical angina to assess the extent and severity of myocardial ischemia (Table 3.19).

PET/CT Images

Findings
- Large and severe perfusion defect throughout the inferior, inferoseptal, and inferolateral walls, showing moderate reversibility.
- Medium-sized perfusion defect involving the mid-anteroseptal LV segment, and the apical segments, showing complete reversibility.
- The ECG-gated images demonstrated a rest LV ejection fraction of 38% that increased to 44% post-stress. The LV volumes appeared mildly dilated. There was akinesis of the inferior and inferoseptal walls.
- The quantitative flow data demonstrates markedly reduced stress myocardial blood flow in the infarct-related territory of the occluded RCA. Stress myocardial blood flow and flow reserve are mildly reduced in the LAD territory and preserved in the LCX territory.

Imaging Diagnosis
- Medium-sized area of prior scar in the RCA territory with evidence of moderate residual stress-induced peri-infarct ischemia.
- Medium-sized area of moderate stress-induced ischemia in mid- to distal LAD territory.

Differential Diagnosis
- None.

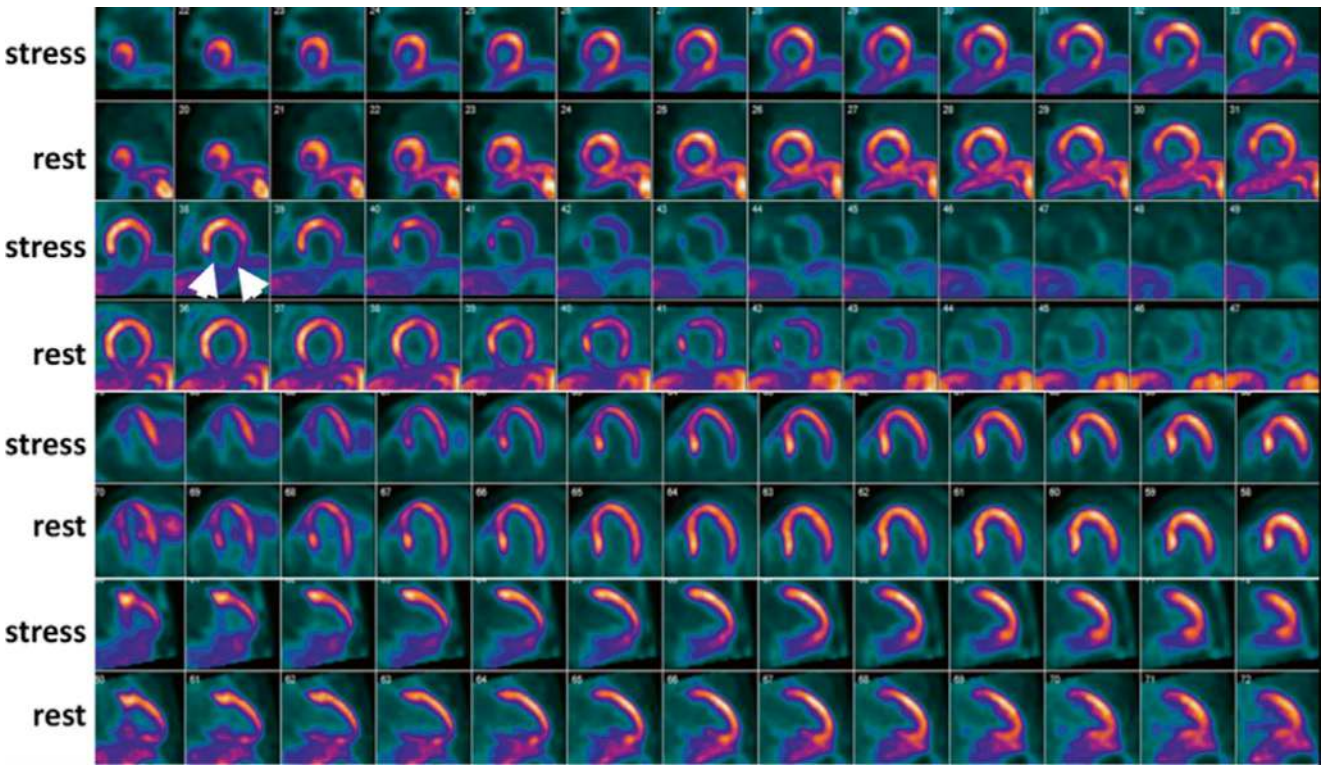


Fig. 3.41 Stress/rest ^{13}N-ammonia PET myocardial perfusion images. There is a large-sized and severe perfusion defect throughout the inferior, inferoseptal, and inferolateral walls, showing moderate reversibility (arrows). In addition, there is a medium-sized perfusion defect involving the mid-anteroseptal LV segment, and the apical segments, showing complete reversibility

Table 3.19 The summary of the quantitative blood flow data demonstrates markedly reduced stress myocardial blood flow in the infarct-related territory of the RCA, which is expected. Stress myocardial blood flow and flow reserve are preserved in the LAD and LCX territories

	MBF rest (ml/min/g)	MBF stress (ml/min/g)	MFR (stress/rest)
LAD	0.61	2.13	3.50
LCX	0.60	2.78	4.63
RCA	0.64	1.36	2.06
Global LV	0.62	2.01	3.24

Correlative Imaging
- None.

Management
- This patient was managed medically by intensifying his anti-anginal regimen with good symptomatic response.

Further Reading

- Murthy V, Bateman T, Beanlands R, Berman D, Borges-Neto S, Chareonthaitawee P, et al. Clinical Quantification of Myocardial Blood Flow Using PET: Joint Position Paper of the SNMMI Cardiovascular Council and the ASNC. Journal of Nuclear Cardiology. 2017;25:269–297.
- Galassi A, Brilakis E, Boukhris M, Tomasello S, Sianos G, Karmpaliotis D, et al. Appropriateness of percutaneous revascularization of coronary chronic total occlusions: an overview. European Heart Journal. 2015; 37:2692–2700.

3.3.5 Evaluation of Chest Pain in a Patient Post PCI: Case 27

Key Points
- Quantitative myocardial perfusion PET imaging is useful in the management of symptomatic patients with complex coronary artery disease.
- The relatively mild amount of ischemia and normal MFR supported the conservative management of this patient.
- For further discussion of interpretation of myocardial blood flow, see Chap. 1, Fig. 1.7.

History
- A 63-year-old man with a history of type 2 diabetes mellitus, hypertension, a former tobacco user presenting with typical angina.
- He had previous PCI of the left main coronary artery.
- He was referred to PET/CT for assessing the physiologic significance of the remaining angiographic stenosis for potential staged PCI (Fig. 3.42 and Table 3.20).

PET/CT Images

Findings
- Small area of moderate ischemia involving the distal LAD territory.
- Normal LV function at rest and during maximal vasodilation.
- Diffuse reduction of stress MBF in all three vascular territories with normal MFR.

Imaging Diagnosis
- Small area of moderate stress induced ischemia in the distal LAD territory.

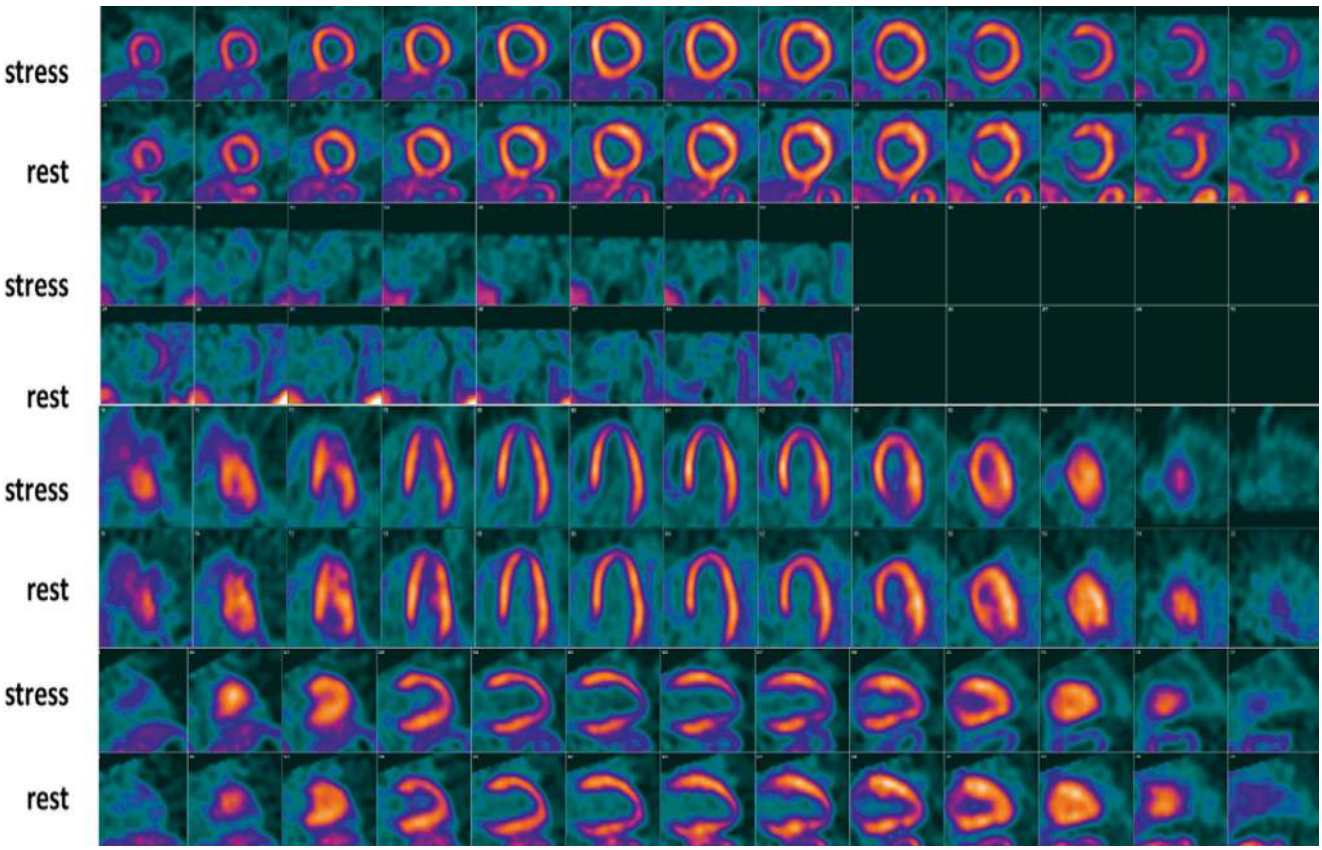


Fig. 3.42 Small perfusion defect of moderate intensity involving the LV apex and inferoapical segment showing complete reversibility

Table 3.20 Summary of the quantitative blood flow data demonstrates a reduction of stress MBF in all coronary territories with preserved MFR

	MBF rest (ml/min/g)	MBF stress (ml/min/g)	MFR (stress/rest)
LAD	0.58	1.46	2.53
LCX	0.68	1.62	2.37
RCA	0.62	1.40	2.26
Global LV	0.62	1.49	2.41

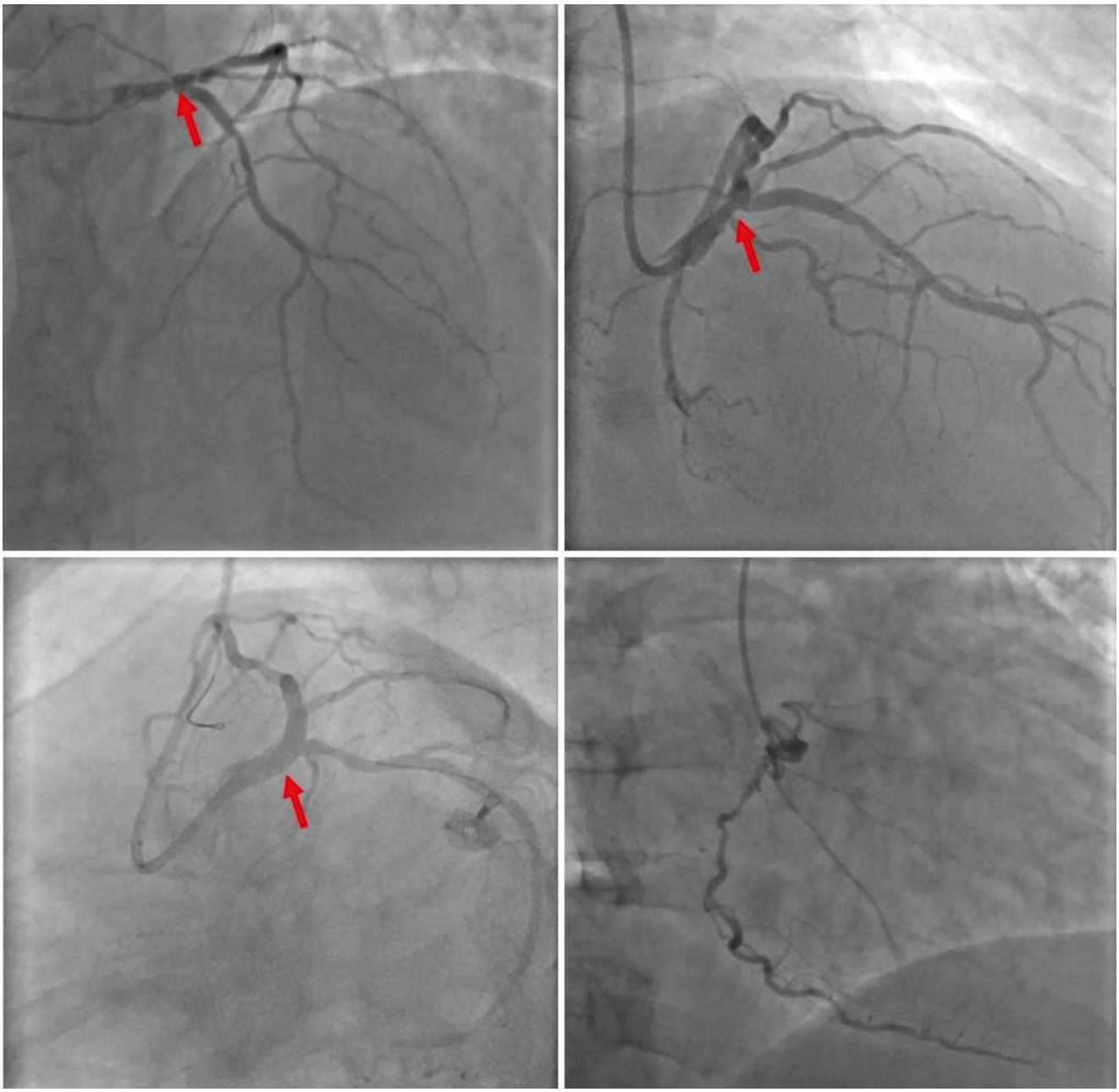


Fig. 3.43 Selective angiographic images demonstrating severe left main stenosis before and after stent placement (red arrows). Additionally, there is diffuse atherosclerosis of the RCA, distal LAD, and LCX coronary arteries

Differential Diagnosis

- None.

Correlative Imaging

- Invasive coronary angiography (Fig. 3.43).

Management

- The patient was managed by optimization of anti-ischemic therapy.

Further Reading

- DePuey E, Roubin G, Depasquale E, Nody A, Garcia E, King S, et al. Sequential multivessel coronary angioplasty assessed by thallium-201 tomography. Catheterization and Cardiovascular Diagnosis. 1989;18:213–221.
- Nikolsky E, Halabi M, Roguin A, Zdorovyak A, Gruberg L, Hir J, et al. Staged versus one-step approach for multivessel percutaneous coronary interventions. American Heart Journal. 2002;143:1017–1026.
- Patel K, Spertus J, Chan P, Sperry B, Al Badarin F, Kennedy K, et al. Myocardial blood flow reserve assessed by positron emission tomography myocardial perfusion imaging identifies patients with a survival benefit from early revascularization. European Heart Journal. 2019;41:751–759.

3.3.6 Example of a Case with ^{15}Oxygen Water PET/CT: Case 28

Key Points

- ^{15}Oxygen water can be used to measure myocardial blood flow with PET.
- Water is freely diffusible so ^{15}Oxygen water has nearly 100% myocardial extraction at any flow rate. Therefore, it is considered the gold standard for flow quantification.
- It is a cyclotron-produced radiotracer with a short half-life (2 min).

History

- A 75-year-old man presented with symptoms of typical angina.
- He had a history of hypertension and hypercholesterolemia.
- An exercise tolerance test was normal.
- He underwent ^{15}Oxygen water PET/CT as part of a research study (Fig. 3.44 and Table 3.21).

PET/CT Images

Findings

- The Global MBF was suppressed at rest and during adenosine stress.
- The MBF in the LAD territory was particularly reduced at rest and decreased during stress.
- During stress the LCX and RCA MBF failed to increase as much as usual.

Imaging Diagnosis

- Globally reduced myocardial blood flow with particularly reduced myocardial blood flow in the LAD territory.

Differential Diagnosis

- None.

Correlative Imaging

- Invasive coronary angiography (Fig. 3.45).

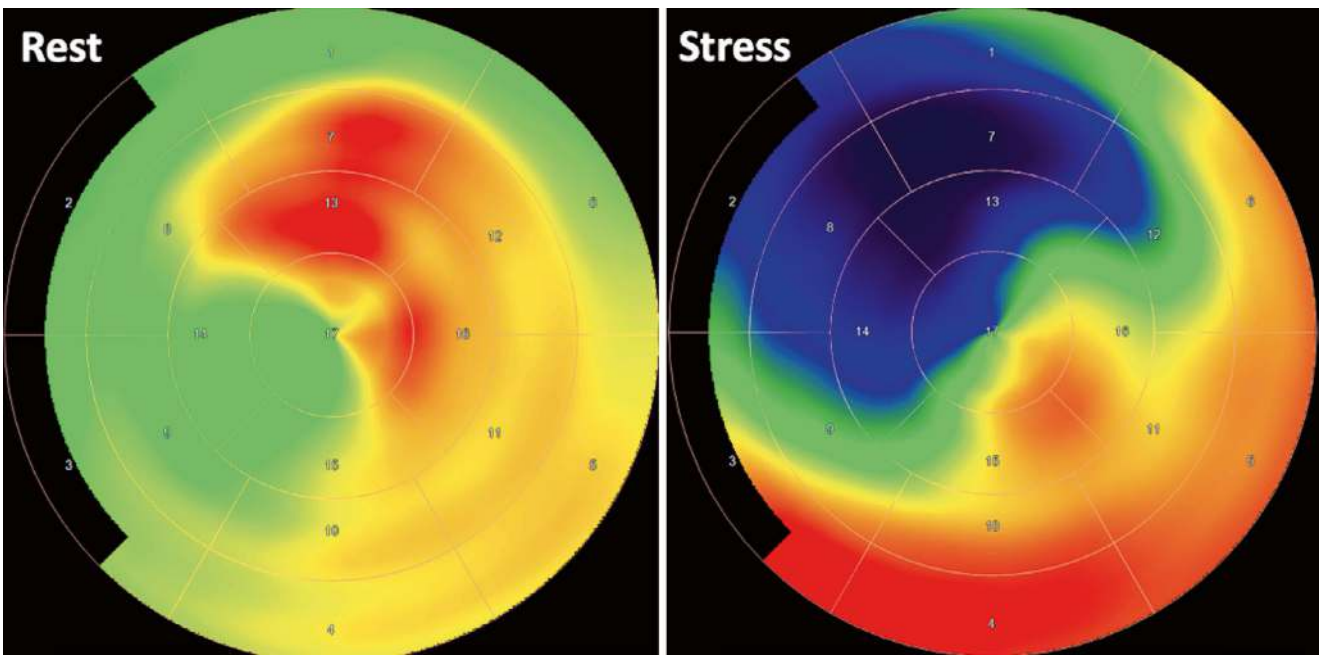


Fig. 3.44 Rest and adenosine stress ^{15}Oxygen water positron emission tomography. Bullseye plots of the LV myocardial showed globally reduced myocardial blood flow during stress, which was particularly reduced in the LAD territory

Table 3.21 Summary of the rest and stress MBF and MFR

	MBF rest (ml/min/g)	MBF stress (ml/min/g)	MFR (stress/rest)
LAD	0.93	0.64	0.69
LCX	0.99	1.50	1.55
RCA	0.97	1.10	1.11
Global LV	0.95	0.99	1.04

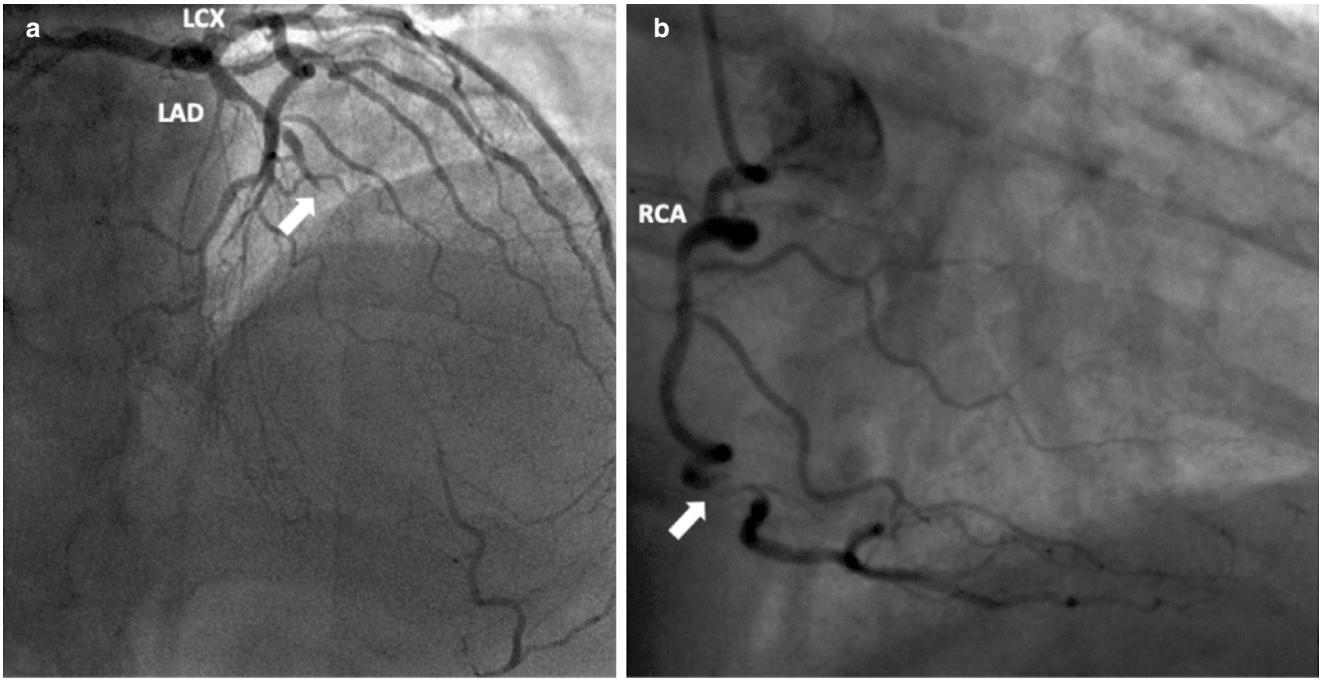


Fig. 3.45 Invasive coronary angiography images showing an occlusion in the mid LAD (A, arrow) and severe stenosis in the mid RCA (B, arrow)

Management

- The right and left coronary artery lesions were treated with drug-eluting stents.
- The patient has remained symptom-free since the procedure.

Further Reading

- Danad I, Uusitalo V, Kero T, Saraste A, Raijmakers PG, Lammertsma AA, et al. Quantitative assessment of myocardial perfusion in the detection of significant coronary artery disease: cutoff values and diagnostic accuracy of quantitative [(15)O]H2O PET imaging. J Am Coll Cardiol. 2014 Oct 7;64(14):1464–75.
- Danad I, Raijmakers PG, Driessen RS, Leipsic J, Raju R, Naoum C, et al. Comparison of Coronary CT Angiography, SPECT, PET, and Hybrid Imaging for Diagnosis of Ischemic Heart Disease Determined by Fractional Flow Reserve. JAMA Cardiol. 2017 Oct 1;2(10):1100–1107.

3.4 Evaluation of Medical Therapy

3.4.1 Reassessment After Optimized Medical Therapy: Case 29

Key Points

- The advantage of perfusion imaging with PET is to be able to measure not only the benefits on MBF brought about by mechanical revascularization interventions, but also those related to optimized medical therapy (OMT).

History

- A 64-year-old man with a history of type 2 diabetes mellitus and hypercholesterolemia admitted for atrial fibrillation with rapid ventricular response.
- He is undergoing hormonal replacement following surgery for a pituitary adenoma.

- His coronary angiogram demonstrated total occlusions of the RCA and LCX coronary arteries and an intermediate stenosis of the mid LAD artery. He underwent successful PCI of the occluded LCX artery (Fig. 3.46).
- He was referred for a myocardial perfusion PET scan for the evaluation of viability and residual ischemia (Fig. 3.47 and Table 3.22).

Findings

- The myocardial perfusion PET scan demonstrated a moderate amount of stress induced ischemia with complete viability in the territory of the occluded RCA, with relatively preserved stress MBF and MFR in the LAD and LCX territories.

Management

- The patient underwent optimization of medical therapy.
- He returned a year after the index PET scan for reassessment of ischemic burden for potential myocardial revascularization (Fig. 3.48 and Table 3.23).

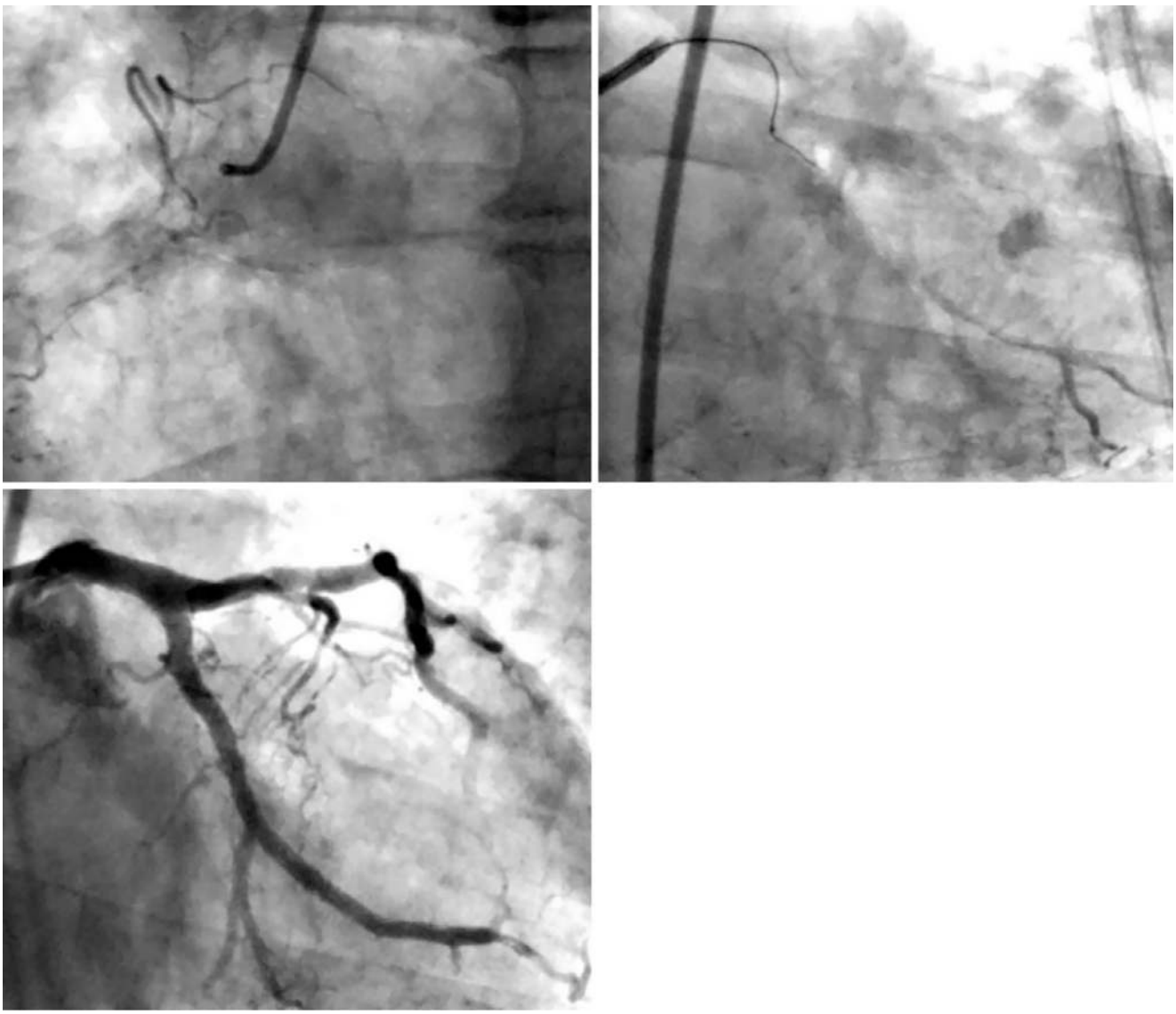


Fig. 3.46 Selective coronary angiographic views demonstrating total occlusion of RCA (left panel) and LCX (middle panel), and successful recanalization of the LCX total occlusion (right panel)

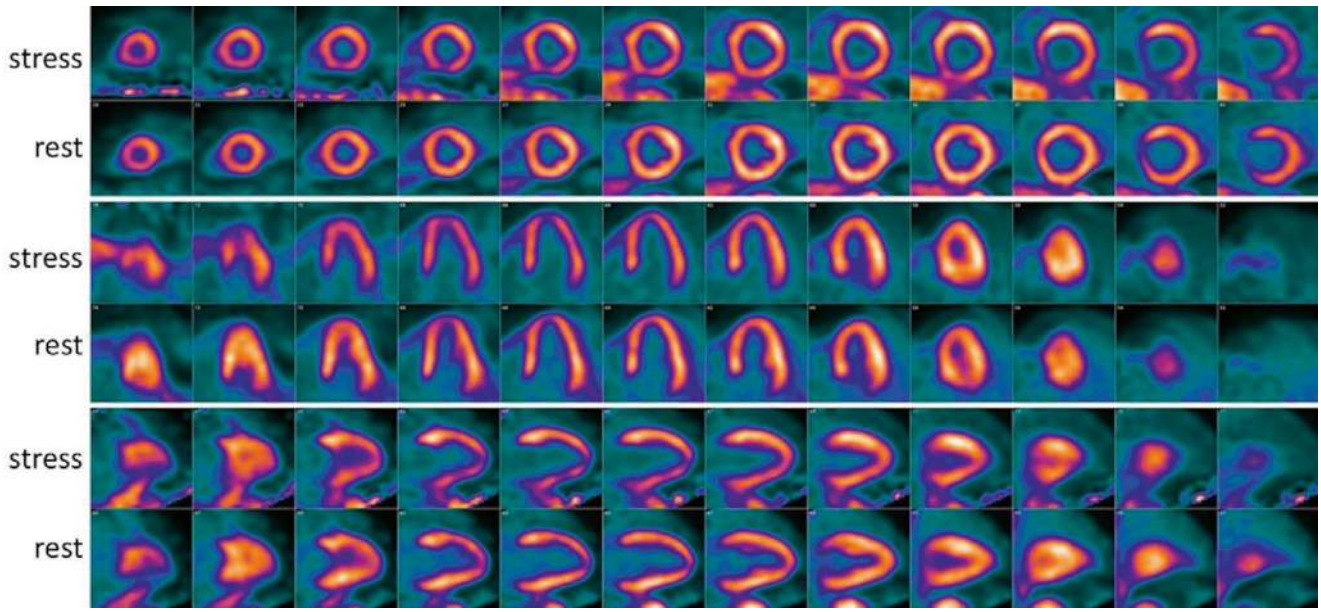


Fig. 3.47 Stress-rest ^{13}N-ammonia PET images demonstrating a medium-sized perfusion defect of moderate severity in the inferior wall showing complete reversibility

Table 3.22 Quantitative analysis shows relatively preserved stress MBF and normal MFR in the LAD and LCX territories. Stress MBF and MFR are both reduced in the RCA territory

	MBF rest (ml/min/g)	MBF stress (ml/min/g)	MFR (stress/rest)
LAD	0.84	1.77	2.11
LCX	0.93	1.93	1.96
RCA	0.87	1.32	1.52
Global LV	0.88	1.66	1.89

Findings

- The follow-up PET myocardial perfusion scan a year after OMT demonstrates significant interval improvement in myocardial perfusion in all vascular territories including near complete resolution of the area of ischemic in the territory of the occluded RCA.

Differential Diagnosis

- None.

Management

- Given the results of the follow-up PET scan, consideration for PCI of the RCA was deferred.

Teaching Points

- This case illustrates the benefits of optimal medical therapy for the management of ischemic heart disease.
- The addition of the quantitative blood flow data by PET permits the assessment of treatment efficacy, especially in areas that do not show regional perfusion deficit.

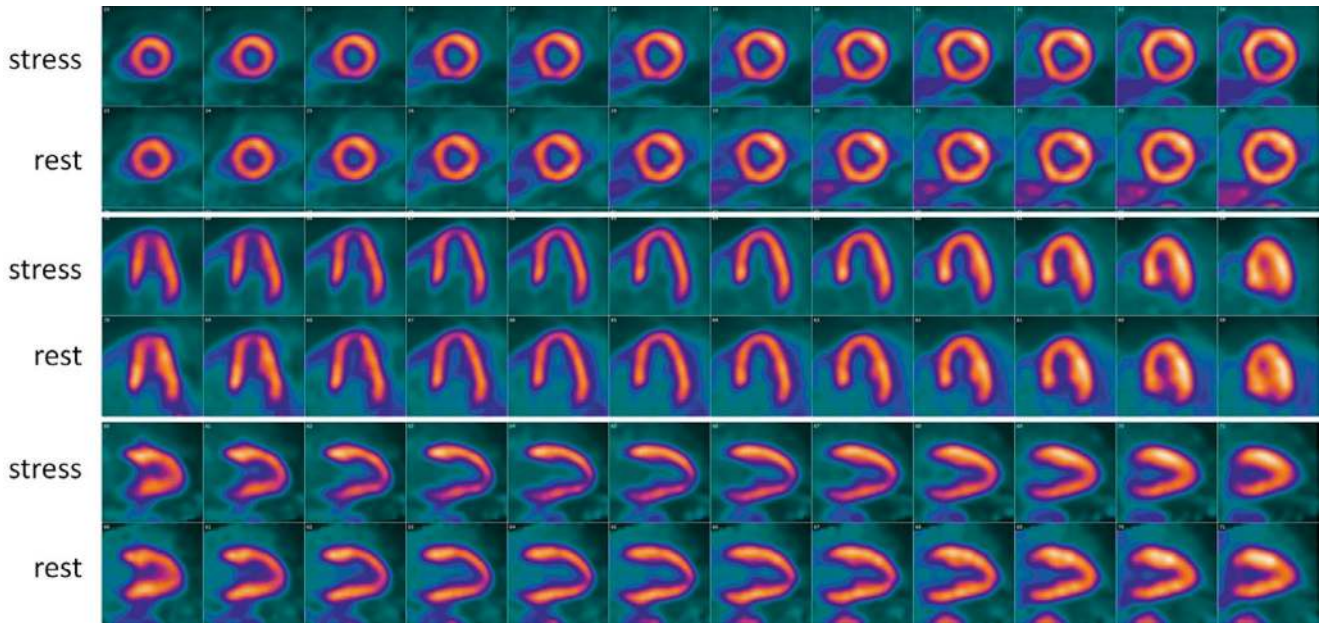


Fig. 3.48 Stress-rest ^{13}N-ammonia PET images demonstrating near complete resolution of the inferior perfusion defect seen on the index PET scan

Table 3.23 Summary of quantitative blood flow data showing normal stress and MFR in the LAD and LCX territories, with mild reduction of stress MBF with normal MFR in the RCA territory

	MBF rest (ml/min/g)	MBF stress (ml/min/g)	MFR (stress/rest)
LAD	0.76	2.09	2.73
LCX	0.79	2.24	2.83
RCA	0.70	1.70	2.43
Global LV	0.75	2.03	2.69

Further Reading

- Ohira H, Dowsley T, Dwivedi G, deKemp R, Chow B, Ruddy T, et al. Quantification of myocardial blood flow using PET to improve the management of patients with stable ischemic coronary artery disease. Future Cardiology. 2014;10:611–631.

The opinions expressed in this chapter are those of the author(s) and do not necessarily reflect the views of the IAEA: International Atomic Energy Agency, its Board of Directors, or the countries they represent.

Open Access This chapter is licensed under the terms of the Creative Commons Attribution 3.0 IGO license (http://creativecommons.org/licenses/by/3.0/igo/), which permits use, sharing, adaptation, distribution and reproduction in any medium or format, as long as you give appropriate credit to the IAEA: International Atomic Energy Agency, provide a link to the Creative Commons license and indicate if changes were made.

Any dispute related to the use of the works of the IAEA: International Atomic Energy Agency that cannot be settled amicably shall be submitted to arbitration pursuant to the UNCITRAL rules. The use of the IAEA: International Atomic Energy Agency's name for any purpose other than for attribution, and the use of the IAEA: International Atomic Energy Agency's logo, shall be subject to a separate written license agreement between the IAEA: International Atomic Energy Agency and the user and is not authorized as part of this CC-IGO license. Note that the link provided above includes additional terms and conditions of the license.

The images or other third party material in this chapter are included in the chapter's Creative Commons license, unless indicated otherwise in a credit line to the material. If material is not included in the chapter's Creative Commons license and your intended use is not permitted by statutory regulation or exceeds the permitted use, you will need to obtain permission directly from the copyright holder.



Coronary Microvascular Disease

4

Marcelo Di Carli, Raffaele Giubbini, Paolo Raggi, Michelle Williams, Diana Paez, Maurizio Dondi, Vasvi Singh, and Zhiyuan Ou

Objectives

- To learn how to recognize coronary microvascular disease in the absence of obstructive epicardial coronary disease.
- To learn how to identify coronary microvascular disease in different disease states and patient groups.
- To appreciate prognostic significance of coronary microvascular disease.

Coronary microvascular disease (CMD) is a critical yet often overlooked component of cardiovascular health. Unlike obstructive epicardial coronary disease, CMD affects the smaller vessels within the heart, leading to impaired blood flow and contributing to various cardiac conditions. This chapter provides a detailed exploration of CMD, focusing on its recognition in the absence of atherosclerosis and nonobstructive atherosclerosis.

Through a series of case studies, this chapter examines CMD in different contexts, including hypertensive heart disease, aortic stenosis, hypertrophic cardiomyopathy, stress cardiomyopathy, diabetes mellitus, obesity, heart failure with preserved ejection fraction, and systemic inflammatory disorders.

4.1 Without Atherosclerosis

4.1.1 Hypertensive Heart Disease: Case 30

Key Points

- Widespread, homogeneous reduction of both hyperemic myocardial blood flow (MBF) and myocardial flow reserve (MFR) with mild transient ischemic dilatation (TID) and absence of perfusion abnormalities may reflect concentric subendocardial ischemia from diffuse atherosclerosis and coronary microvascular dysfunction.
- This is commonly seen in patients with hypertensive heart disease and other forms of left ventricular hypertrophy (LVH).

History

- A 78-year-old man, former smoker with atypical angina, chronic renal failure, dyslipidemia, and hypertension.

All authors have no conflict of interest to disclose.

M. Di Carli
Brigham and Women's Hospital, Boston, MA, USA
e-mail: mdicarli@bwh.harvard.edu

R. Giubbini
Nuclear Medicine, International Specialized Hospital of Uganda (ISHU), Kampala, Uganda
e-mail: raffaele.giubbini@unibs.it

P. Raggi
Division of Cardiology, University of Alberta, Edmonton, AB, Canada

M. Williams
British Heart Foundation Centre for Research Excellence, Institute for Neuroscience and Cardiovascular Research, University of Edinburgh, Edinburgh, United Kingdom
e-mail: michelle.williams@ed.ac.uk

D. Paez · M. Dondi (✉)
Division of Human Health, International Atomic Energy Agency, Vienna, Austria
e-mail: d.paez@iaea.org; m.dondi@iaea.org

V. Singh
Midwest Heart and Vascular Specialists, HCA Midwest Health, Kansas City, MO, USA
e-mail: vasvi.singh@hcahealthcare.com

Z. Ou
University of Alberta, Edmonton, AB, Canada
e-mail: zo2@ualbera.ca

© The Author(s) 2027
M. Di Carli et al. (eds.), *IAEA Atlas of Cardiac PET/CT*, https://doi.org/10.1007/978-3-662-74188-7_4

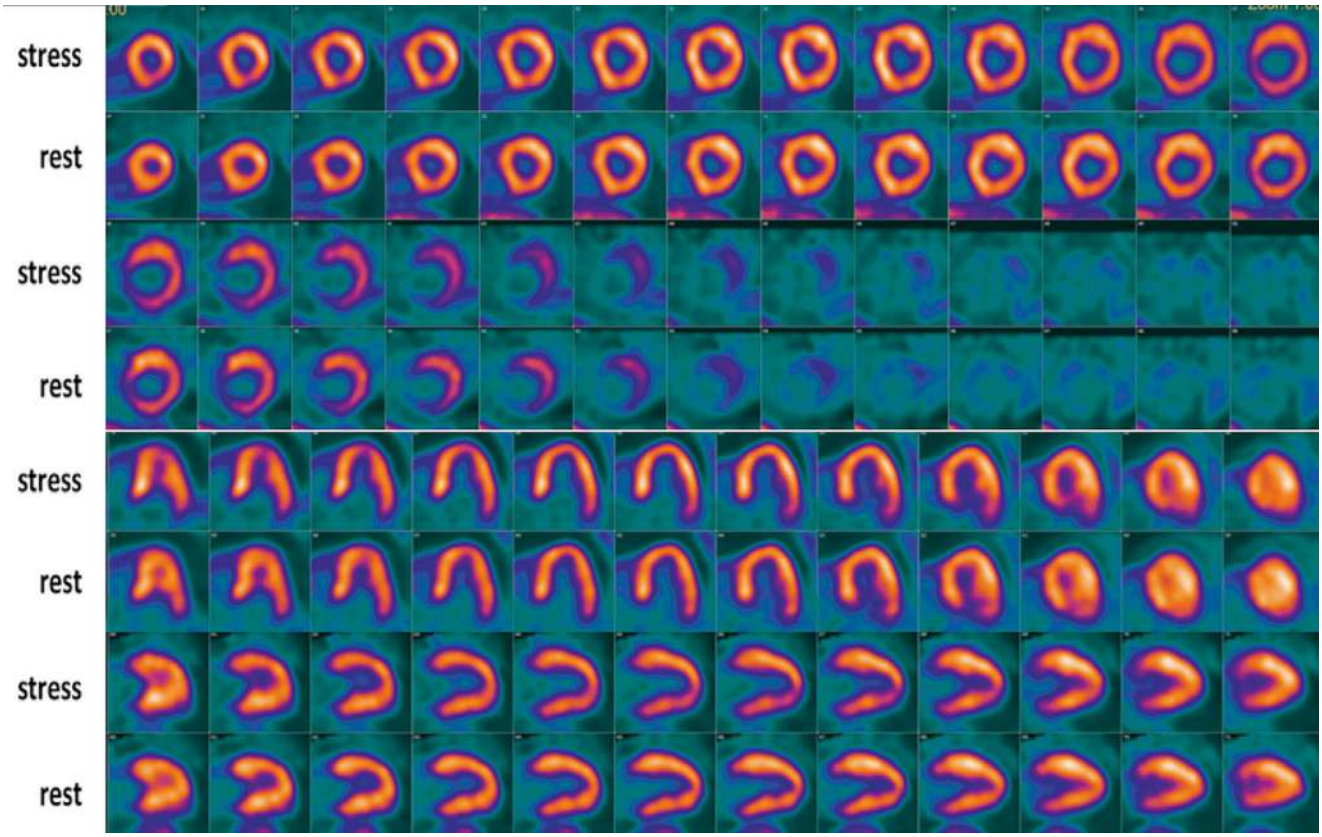


Fig. 4.1 Stress-rest ^{13}N-ammonia PET images demonstrate transient LV dilatation during stress (TID ratio = 1.27) without evidence of regional perfusion defects

- Referred to positron emission tomography (PET)/computed tomography (CT) for angina assessment (Fig. 4.1 and Table 4.1).

PET/CT Images

Findings

- On myocardial perfusion imagng (MPI), there was evidence of transient LV dilatation during stress (TID ratio = 1.27) without evidence of regional perfusion defects.
- There was diffuse reduction of stress MBF and MFR.
- LVEF was mild reduction at stress (67%) compared to rest (69%).

Imaging Diagnosis

- Transient LV dilatation during stress without evidence of regional perfusion defects.

Differential Diagnosis

- Obstructive coronary artery disease vs microvascular disease.

Table 4.1 Summary of rest and stress MBF and myocardial flow reserve showing diffuse reduction of stress MBF

	MBF rest (ml/min/g)	MBF stress (ml/min/g)	MFR (stress/rest)
LAD	0.95	1.56	1.65
LCX	0.88	1.64	1.88
RCA	0.81	1.40	1.73
Global LV	0.89	1.54	1.73

Management

- Follow-up coronary angiography demonstrated no evidence of obstructive coronary artery disease.
- The patient underwent aggressive risk factor management.

Further Reading

- Fukushima K, Javadi M, Higuchi T, Bravo P, Chien D, Lautamaki R, et al. Impaired Global Myocardial Flow Dynamics Despite Normal Left Ventricular Function and Regional Perfusion in Chronic Kidney Disease: A

Quantitative Analysis of Clinical 82Rb PET/CT Studies. Journal of Nuclear Medicine. 2012;53:887–893.
- Koivuviita N, Tertti R, Jarvisalo M, Pietila M, Hannukainen J, Sundell J, et al. Increased basal myocardial perfusion in patients with chronic kidney disease without symptomatic coronary artery disease. Nephrology Dialysis Transplantation. 2009;24:2773–2779.

4.1.2 Aortic Stenosis: Case 31

Key Points
- Severe aortic stenosis can be associated with myocardial ischemia from a high transvalvular gradient leading to reduced coronary pressure and hyperemic blood flow, and coronary microvascular dysfunction.

History
- A 72-year-old woman with a history of hypertension, dyslipidemia, and aortic stenosis.
- She was referred for a rest/adenosine stress PET/CT for evaluation of coronary artery disease after a positive exercise treadmill test (Fig. 4.2 and Table 4.2).

PET/CT Images

Findings
- Marked transient LV cavity dilatation with stress.
- Small and reversible perfusion defect involving the LV apex.
- Normal LVEF (73%) and volumes at rest with a drop in LVEF with stress (53%) and marked enlargement of end-systolic volume.

Imaging Diagnosis
- Severe multivessel myocardial ischemia.

Differential Diagnosis
- Multivessel obstructive coronary disease.
- Diffuse coronary microvascular dysfunction.

Table 4.2 Summary of rest and stress MBF and myocardial flow reserve showing diffuse reduction of stress MBF

	MBF rest (ml/min/g)	MBF stress (ml/min/g)	MFR (stress/rest)
LAD	0.80	1.32	1.66
LCX	0.89	1.41	1.58
RCA	0.78	1.20	1.53
Global LV	0.82	1.29	1.58

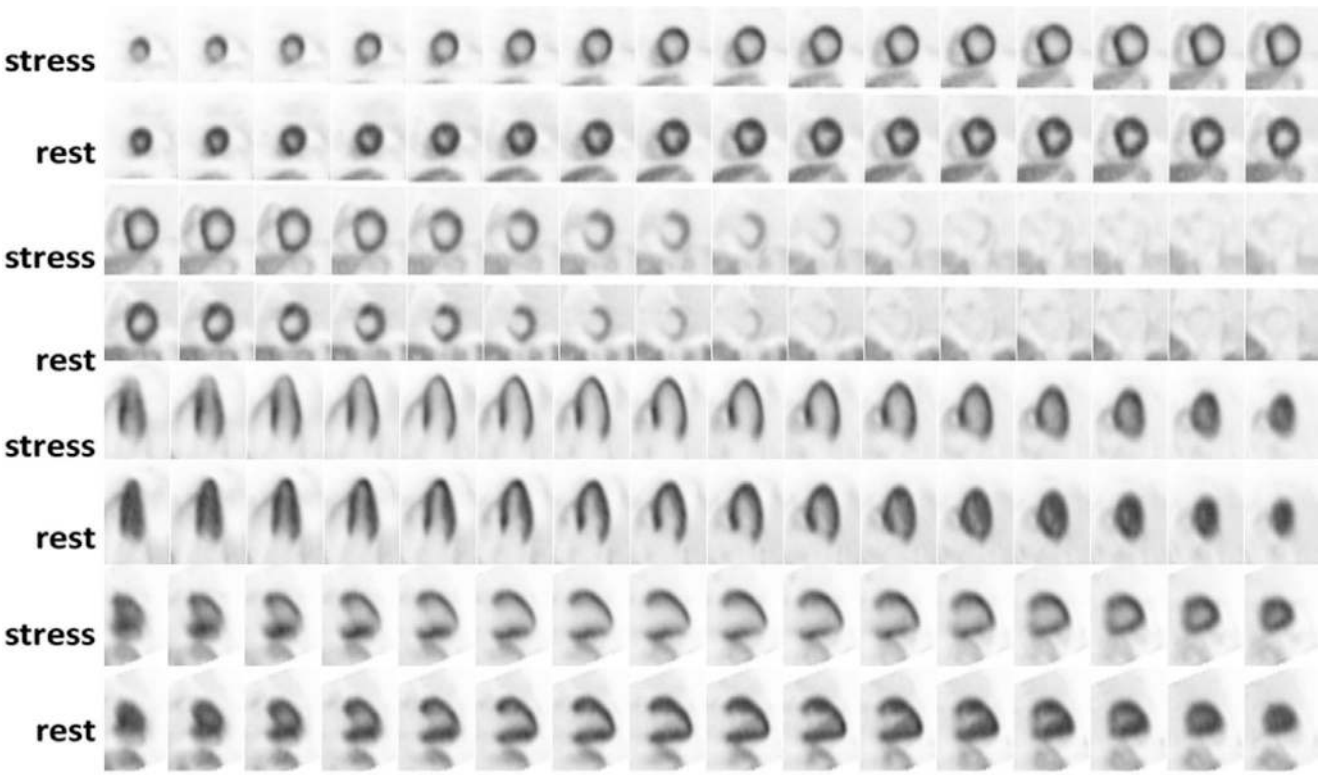


Fig. 4.2 Stress-rest ^{13}N-ammonia PET images. Marked transient LV cavity dilatation with stress. Small and reversible perfusion defect involving the LV apex

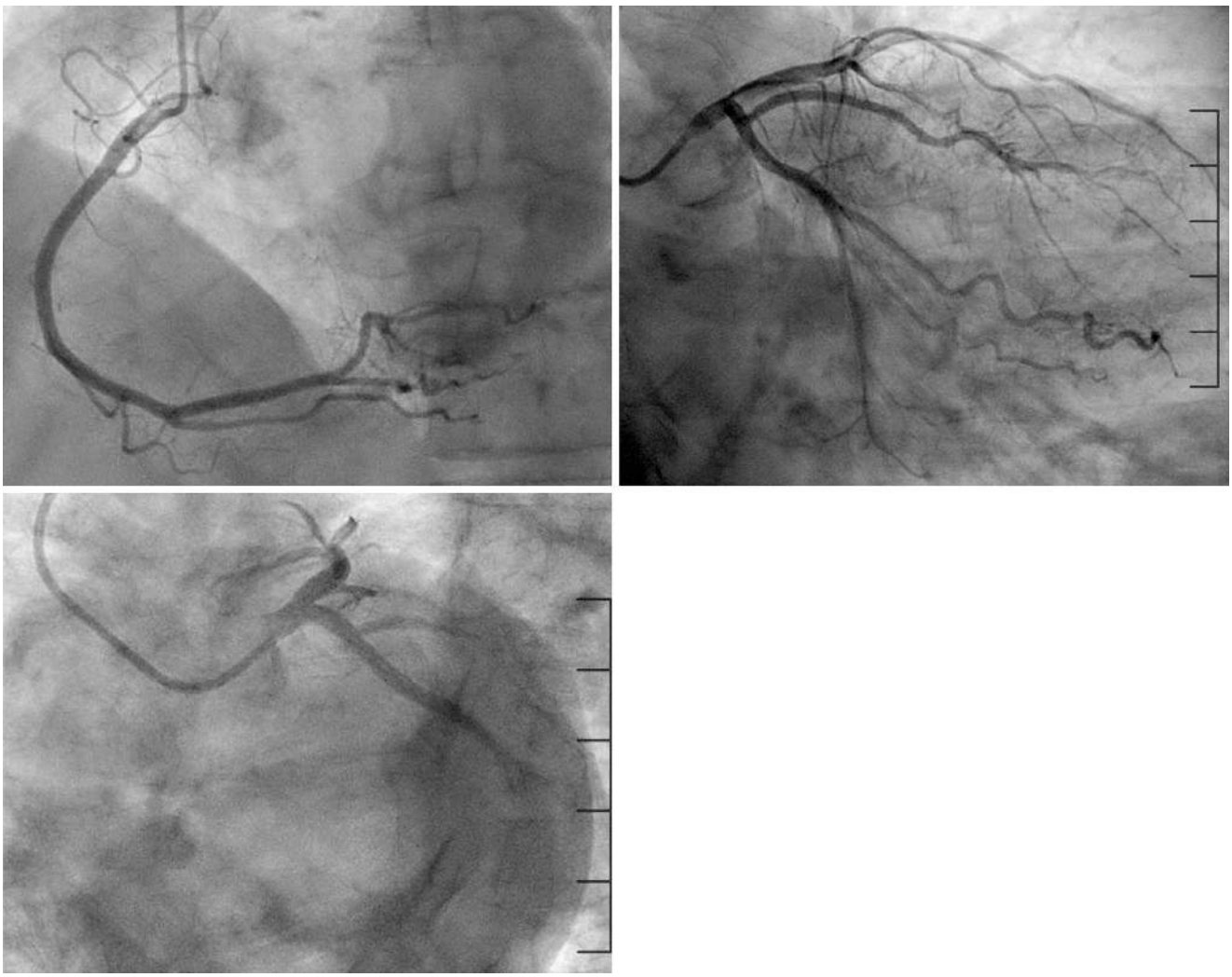


Fig. 4.3 Selective views of the right and left coronary system demonstrating no evidence of obstructive coronary artery disease

Correlative Imaging

- Invasive coronary angiography (Fig. 4.3).

Management

- The patient underwent transcatheter aortic valve replacement.

Further Reading

- Zhou W, et al. Association of Myocardial Blood Flow Reserve With Adverse Left Ventricular Remodeling in Patients With Aortic Stenosis: The Microvascular Disease in Aortic Stenosis (MIDAS) Study. JAMA Cardiol. 2022:7(1);93–99.

4.1.3 Septal Hypertrophic Cardiomyopathy: Case 32

Key Points

- Hypertrophic cardiomyopathy consists of a disorderly microarray of myofibrils which is frequently associated with microvascular remodeling causing altered myocardial perfusion that can be demonstrated by quantitative PET.
- PET/CT can provide prognostic stratification in patients with hypertrophic cardiomyopathy by identifying patients with microvascular perfusion abnormalities.

History

- A 63-year-old man presented with inverted T waves in the inferior electrocardiogram (ECG) leads and asymmetric hypertrophic cardiomyopathy on echocardiography.
- He underwent ^{13}N-ammonia PET/CT at rest and after pharmacological stress with dipyridamole (Figs. 4.4, 4.5 and Table 4.3).

PET/CT Images

Findings

- Asymmetric LV septal hypertrophy.
- Medium-sized perfusion defect during stress throughout the anterior wall showing complete reversibility at rest.
- Mild TID of the LV cavity during stress.
- Reduced stress myocardial blood flow (MBF) and MFR in the left anterior descending artery (LAD) territory.

Imaging Diagnosis

- Hypertrophic cardiomyopathy with evidence of anterior wall ischemia.

Differential Diagnosis

- Hypertrophic cardiomyopathy.
- Obstructive coronary artery disease.

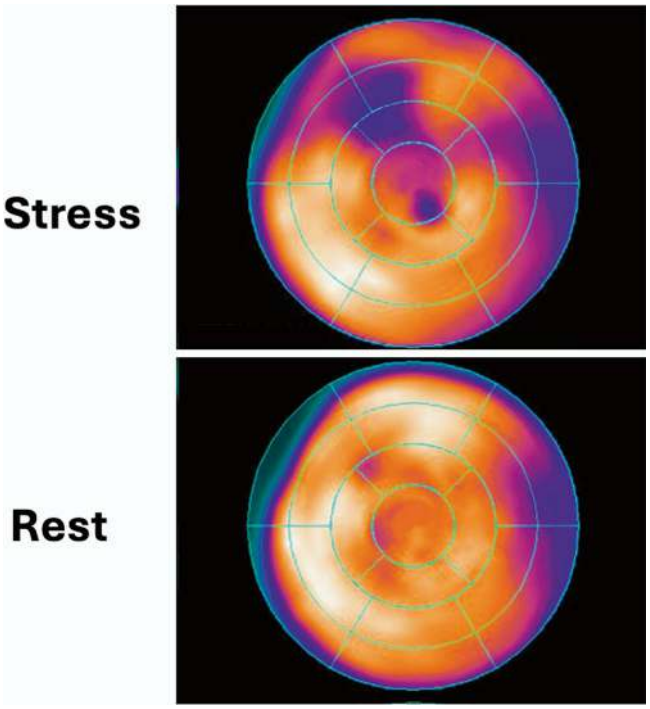


Fig. 4.5 Polar map image confirmed a moderate perfusion defect involving the anterior wall which was completely reversible at rest

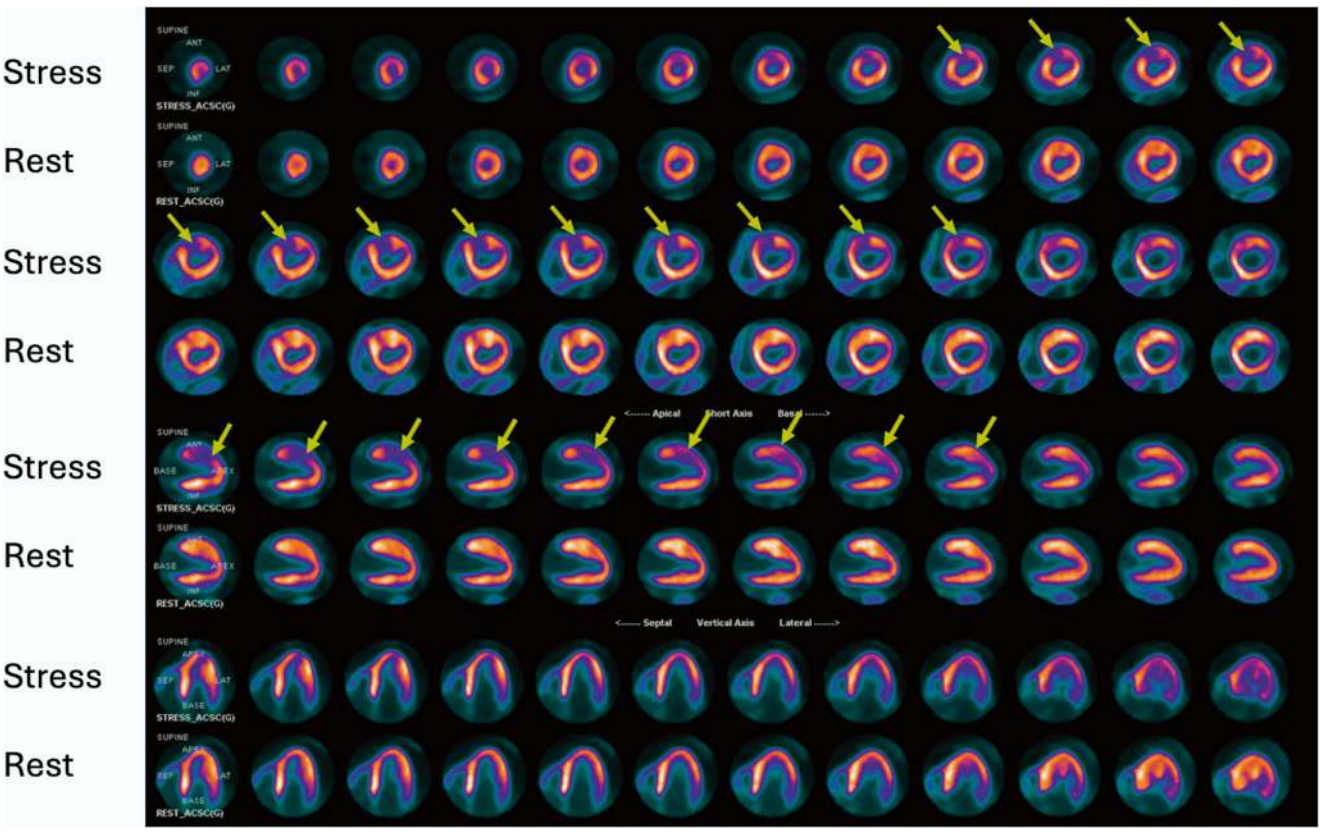


Fig. 4.4 Rest and dipyridamole-stress ^{13}N-ammonia PET/CT images. The stress images show a medium-sized perfusion defect throughout the anterior wall (yellow arrows), with complete reversibility. There is evidence of asymmetric anterior hypertrophy

Table 4.3 Summary of the quantitative blood flow data demonstrating diffuse reduction of global stress MBF which was more severe in the LAD territory, as well as of MFR

	MBF rest (ml/min/g)	MBF stress (ml/min/g)	MFR (stress/rest)
LAD	0.81	1.11	1.37
LCX	0.90	2.14	2.37
RCA	0.81	2.20	2.72
Global LV	0.80	1.79	2.23

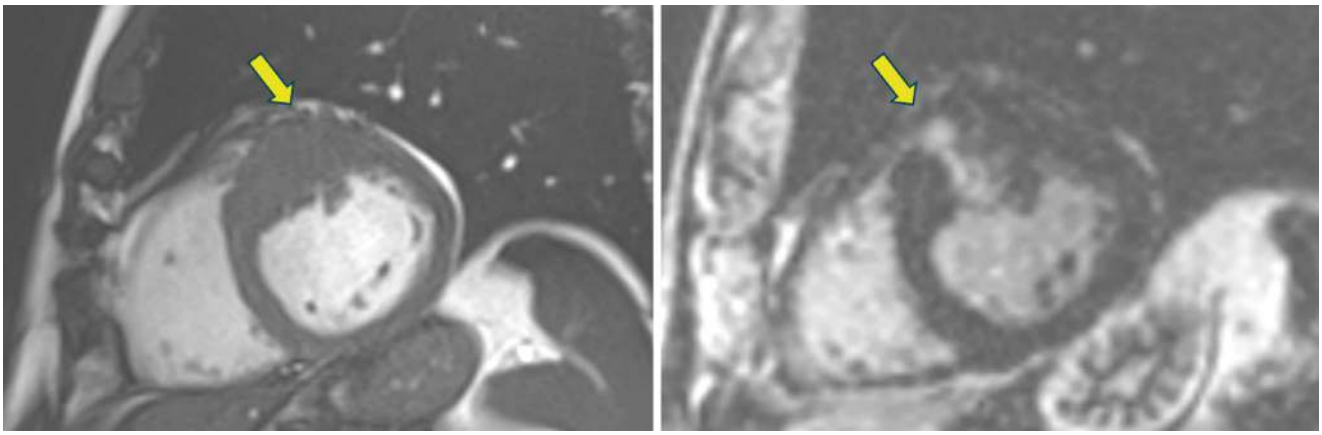


Fig. 4.6 Two-chamber contrast-enhanced cardiac MRI images showed severe left ventricular hypertrophy, more pronounced in the anterior wall where a patchy mid-myocardial late gadolinium enhancement is displayed (yellow arrows). Findings are consistent with asymmetric hypertrophic cardiomyopathy

Correlative Imaging

- Cardiac MRI showed severe left ventricular hypertrophy, more evident in the anterior wall, matched by patchy mid-myocardial late gadolinium enhancement (Fig. 4.6).

Management

- The patient underwent medical treatment for microvascular disease.

Further Reading

- PG Camici, Carsten Tschope et Al. Coronary microvascular dysfunction in hypertrophy and heart failure. Cardiovascular Research 2020 116, 806–816.
- PG Camici, I. Olivotto, O. Rimoldi. The coronary circulation and blood flow in left ventricular hypertrophy. J Mol Cell Cardiol 2012 52(4):857–64.
- H. Castagnoli, C. Ferrantini. Role of quantitative myocardial positron emission tomography for risk stratification in patients with hypertrophic cardiomyopathy: a 2016 reappraisal. Eur J Nucl Med Mol Imaging (2016) 43:2413–2422.

Acknowledgment

Cardiac MR images courtesy of Prof. Francesco Secchi, Institute of Cardiovascular MR/CT Imaging Unit of Radiology IRCCS Policlinico San Donato Milan, Italy.

4.1.4 Apical Hypertrophic Cardiomyopathy: Case 33

Key Points

- Coronary microvascular dysfunction is prevalent in patients with hypertrophic cardiomyopathy (HCM).
- In patients with HCM and coronary artery disease, interpretation of severely impaired stress MBF and MFR is challenging as it is difficult to differentiate multivessel obstructive disease from severe coronary microvascular dysfunction. This distinction often needs anatomic investigation with coronary angiography.

History

- A 79-year-old man with known apical hypertrophic cardiomyopathy and coronary artery disease with prior percutaneous coronary intervention (PCI) was referred for a myocardial perfusion PET study (Fig. 4.7) to evaluate for chest pain.
- His cardiac risk factors include hypertension and dyslipidemia (Table 4.4).

PET/CT Images

Findings

- There is transient LV dilatation with stress.

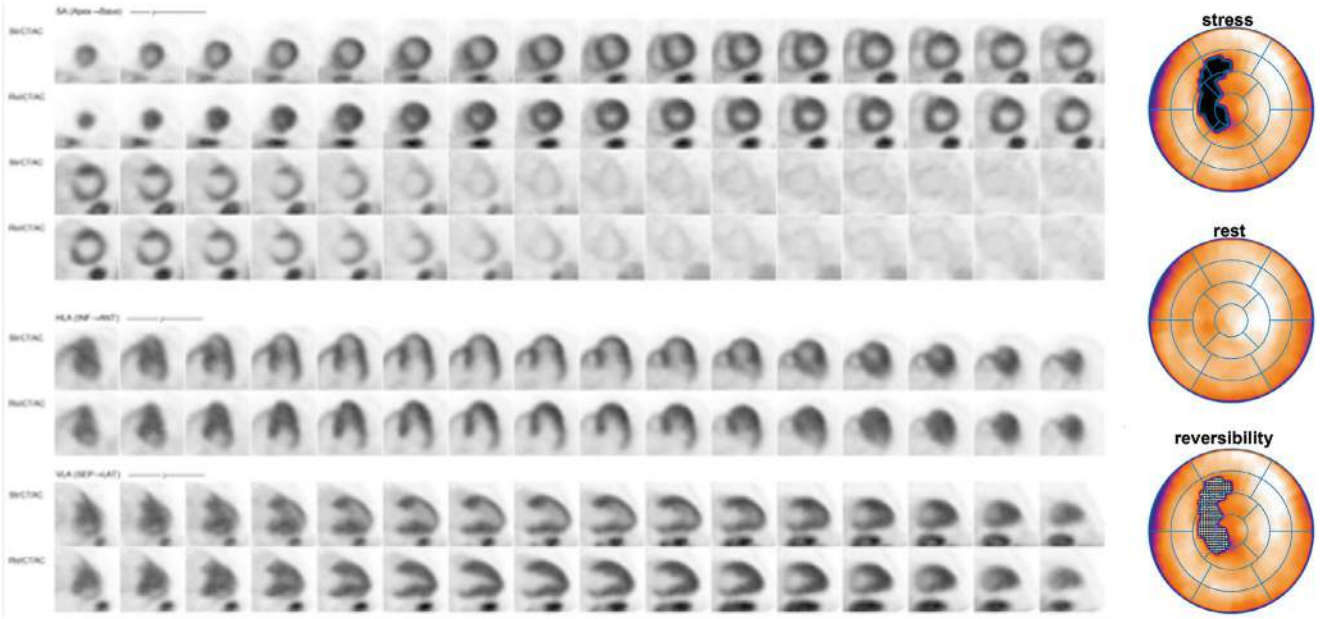


Fig. 4.7 Regadenoson-stress and rest ^{82}Rubidium myocardial perfusion study. There is a small perfusion defect of severe intensity involving the mid and apical anterior wall during stress showing complete reversibility at rest. There is also evidence of marked concentric subendocardial hypoperfusion in the mid and apical LV segments. *On the right side*: corresponding stress, rest, and reversibility polar maps demonstrating the small reversible perfusion defect in the mid and apical anterior wall

Table 4.4 Summary of rest and stress MBF and MFR

	MBF rest (ml/min/g)	MBF stress (ml/min/g)	MFR (stress/rest)
LAD	0.92	0.85	0.92
LCX	1.07	1.14	1.07
RCA	0.88	0.95	1.08
Global LV	0.95	0.93	0.98

- There is a small-sized perfusion defect of severe intensity involving the mid and apical anterior wall during stress showing complete reversibility.
- There is also evidence of marked concentric subendocardial hypoperfusion in the mid and apical LV segments.
- Severe reduction in regional and global stress MBF and MFR in all coronary territories.
- Rest LVEF: 56% with normal LV volumes. Peak stress LVEF declined to 51% with transiently increased LV ESV. There is severe hypokinesis of the LV apex and apical LV segments with stress.

Imaging Diagnosis

- Abnormal myocardial perfusion study consistent with a small area of moderate ischemia in the LAD territory.
- There is evidence of severe concentric subendocardial ischemia involving the mid and apical LV myocardium, associated with severe reduction in regional and global stress MBF and MFR.
- Normal global LV systolic function at rest with a significant drop in LVEF with stress.
- While this may represent microvascular dysfunction in the setting of HCM, severe multivessel obstructive disease cannot be excluded especially considering the history of coronary artery disease and prior PCI.

Differential Diagnosis

- Multivessel obstructive coronary artery disease.
- Severe coronary microvascular dysfunction in the setting of atherosclerosis and HCM.

Correlative Imaging

- Invasive coronary angiography (Fig. 4.8).

Management

- Overall, the findings are consistent with severe coronary microvascular dysfunction associated with diffuse nonobstructive coronary artery disease and HCM.
- He underwent optimization of anti-ischemic therapy and aggressive management of risk factors.

Further Reading

- Camici PG et al. Coronary microvascular dysfunction in hypertrophy and heart failure. Cardiovasc. Res. 2020:116(4);806–816.

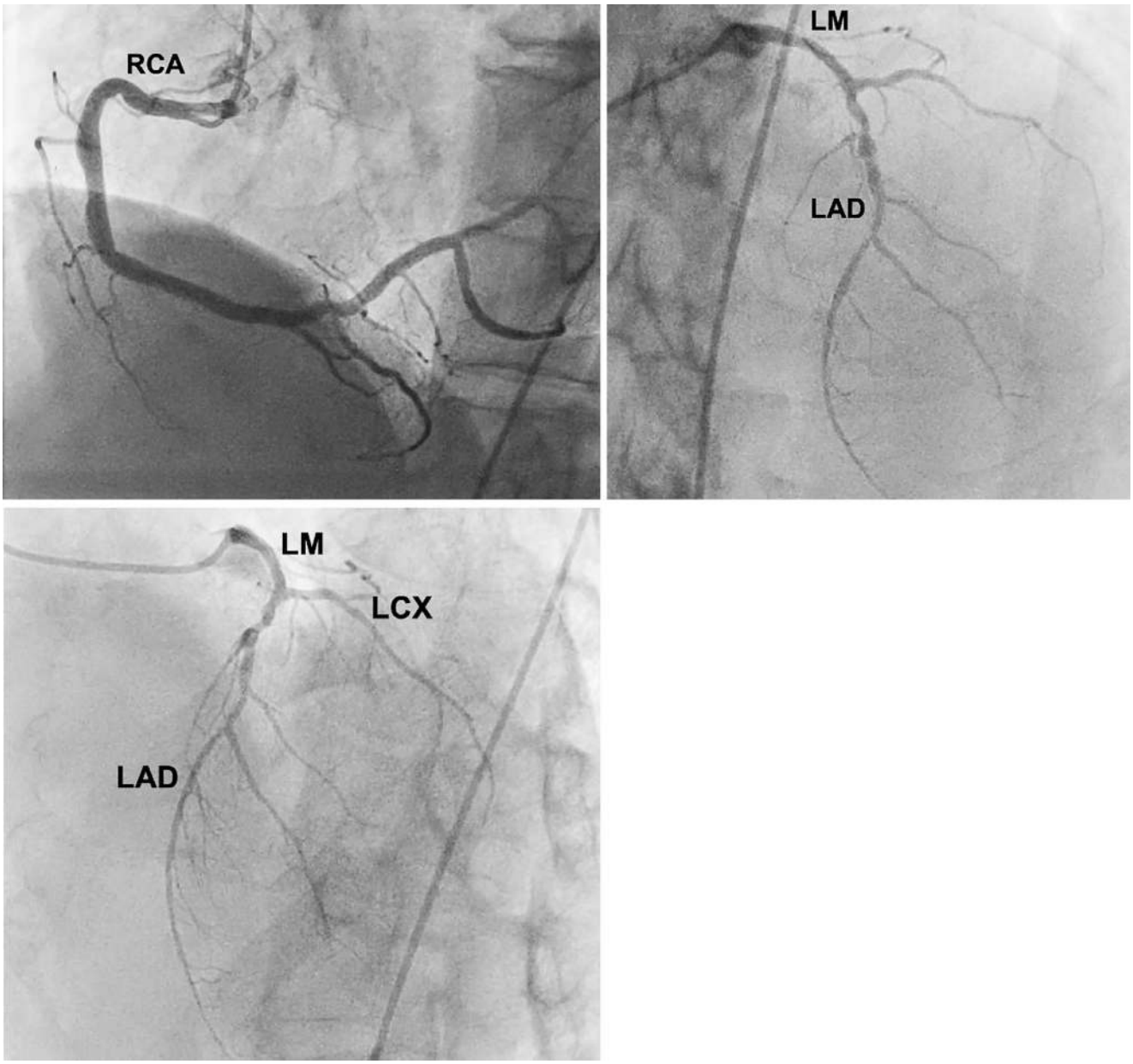


Fig. 4.8 Selective views of the right and left coronary systems demonstrating diffuse atherosclerosis without focally obstructive coronary artery disease

4.1.5 Stress Cardiomyopathy: Takotsubo: Case 34

Key Points

- A new wall motion abnormality in the context of an acute illness may prompt the performance of an imaging test to exclude the presence of coronary artery disease.
- A fixed perfusion defect on nuclear imaging suggests the occurrence of a myocardial infarction and is usually followed by the performance of an invasive coronary angiogram.
- The absence of obstructive coronary artery disease on invasive coronary angiography suggests severe coronary microvascular dysfunction in the context of stress cardiomyopathy.

History

- A 79-year-old woman with a history of chronic kidney disease and systemic hypertension was admitted to the hospital with high fever, low blood pressure, and profuse sweating. She was diagnosed with acute community pneumonia and sepsis.

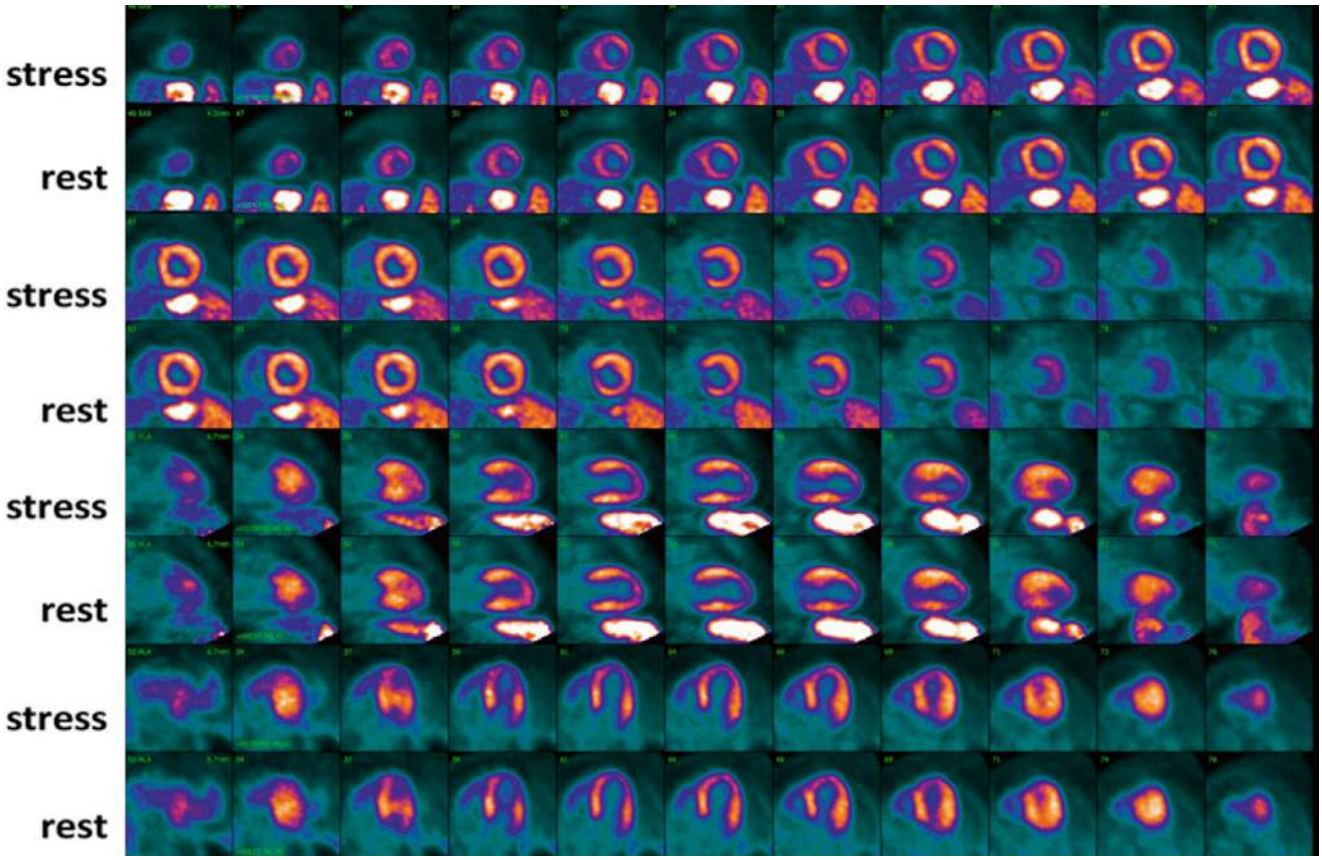


Fig. 4.9 Dipyridamole stress/rest ^{82}Rb-PET myocardial perfusion imaging demonstrating a large, severe, and fixed perfusion defect of the anterior wall and apex of the LV with apical aneurysmal dilatation

- Her initial blood tests revealed an elevated white cell count, hyperglycemia, severely elevated serum creatinine, and mildly to moderately elevated high sensitivity troponin T three consecutive times.
- A transthoracic echocardiogram revealed a reduced LV ejection fraction estimated at 30–35% with akinesis of the mid to distal anterior wall and apex.
- She was referred for a vasodilator PET myocardial perfusion study for risk assessment of coronary artery disease (Fig. 4.9).

PET Images

Correlative Imaging

- Invasive cardiac catheterization (Fig. 4.10).

Findings

- The stress/rest PET myocardial perfusion images demonstrate aneurysmal dilatation of the LV associated with a large perfusion defect of severe intensity from the mid anterior wall to the apex and apical segments of the LV, which is fixed.
- The ECG-gated images demonstrated severe LV dilatation (ESV: 125 ml) and global systolic dysfunction with akinesia of the apex and apical segments.
- An invasive angiogram revealed patent epicardial coronary arteries and ballooning of the peri-apical segments and apex of the left ventricle without evidence of atherosclerosis or dissection, confirming the diagnosis of Takotsubo cardiomyopathy.

A follow-up ^{82}Rb-PET myocardial perfusion study was performed 4 months later (Fig. 4.11).

PET/CT Images (Follow-Up)

Figure 4.12 compares the end-systolic frames of the original PET scan (baseline) performed for cardiac risk assessment at hospitalization and the follow-up scan (repeat study) 4 months later. The gated study obtained during the first study showed akinesia of the anterior wall, as well as of the apical segments, while in the second study, the same segments are hypercontractile. There is also a marked reduction in end-systolic volume between acute and follow-up scan (from 125 ml to 59 ml, respectively).

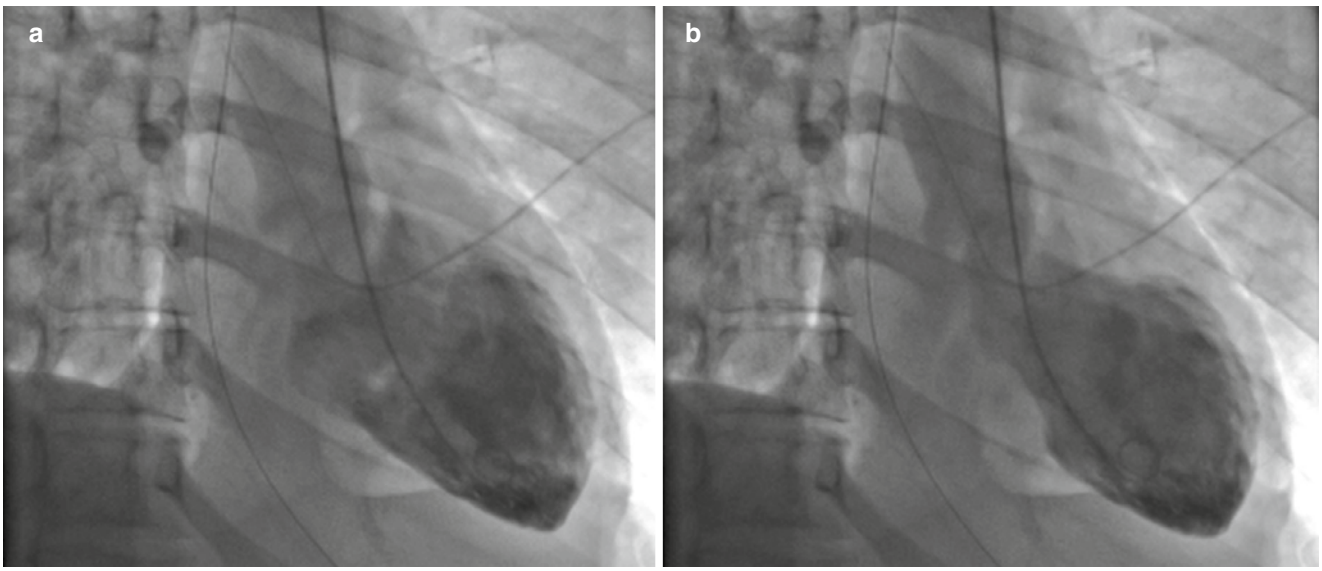


Fig. 4.10 Selective views of left ventriculogram obtained during invasive cardiac catheterization: (**a**) end-diastolic frame showing the size of the left ventricle at peak filling. (**b**) End-systolic frame showing ballooning of the peri-apical segments and apex of the left ventricle

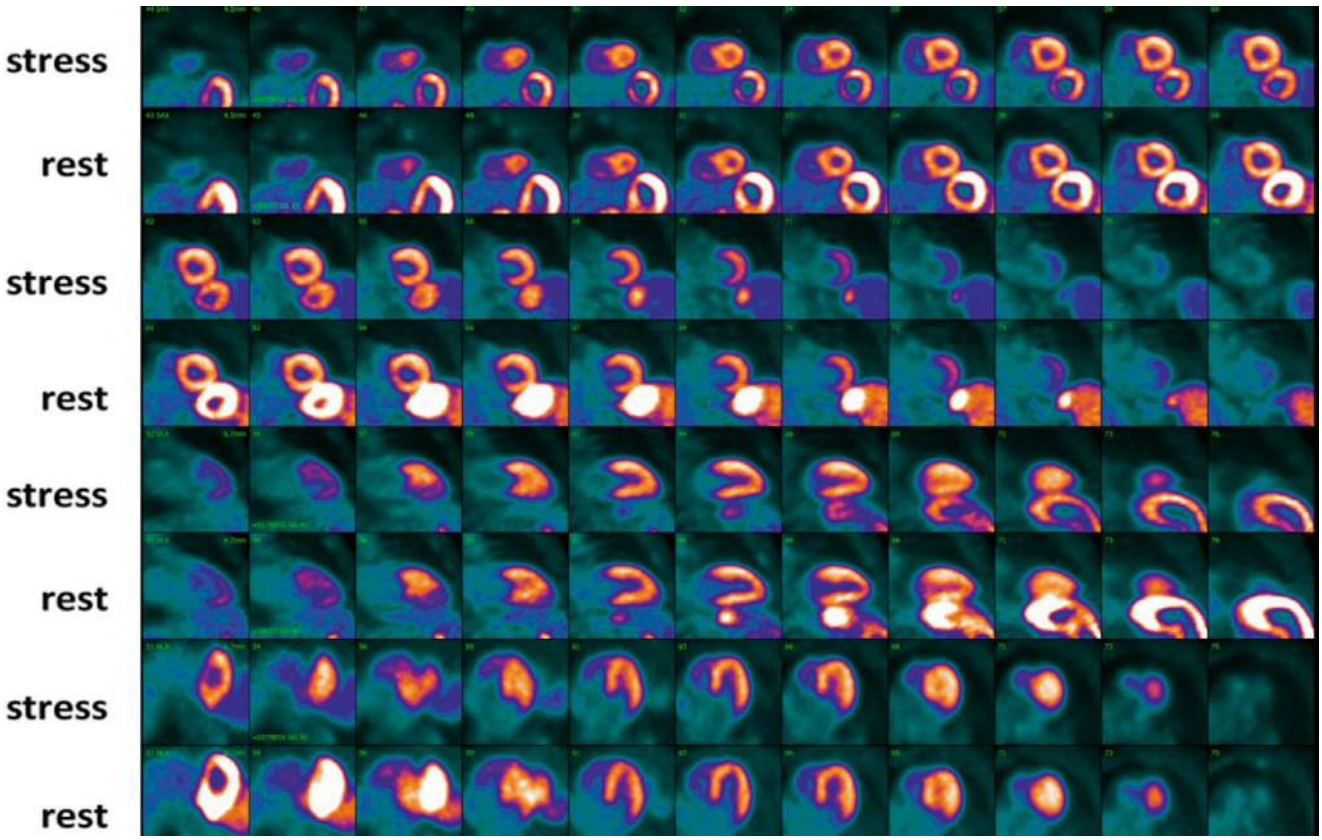


Fig. 4.11 Dipyridamole stress/rest ^{82}Rb-PET study demonstrating completely normal myocardial perfusion and resolution of the apical aneurysmatic dilatation of the LV

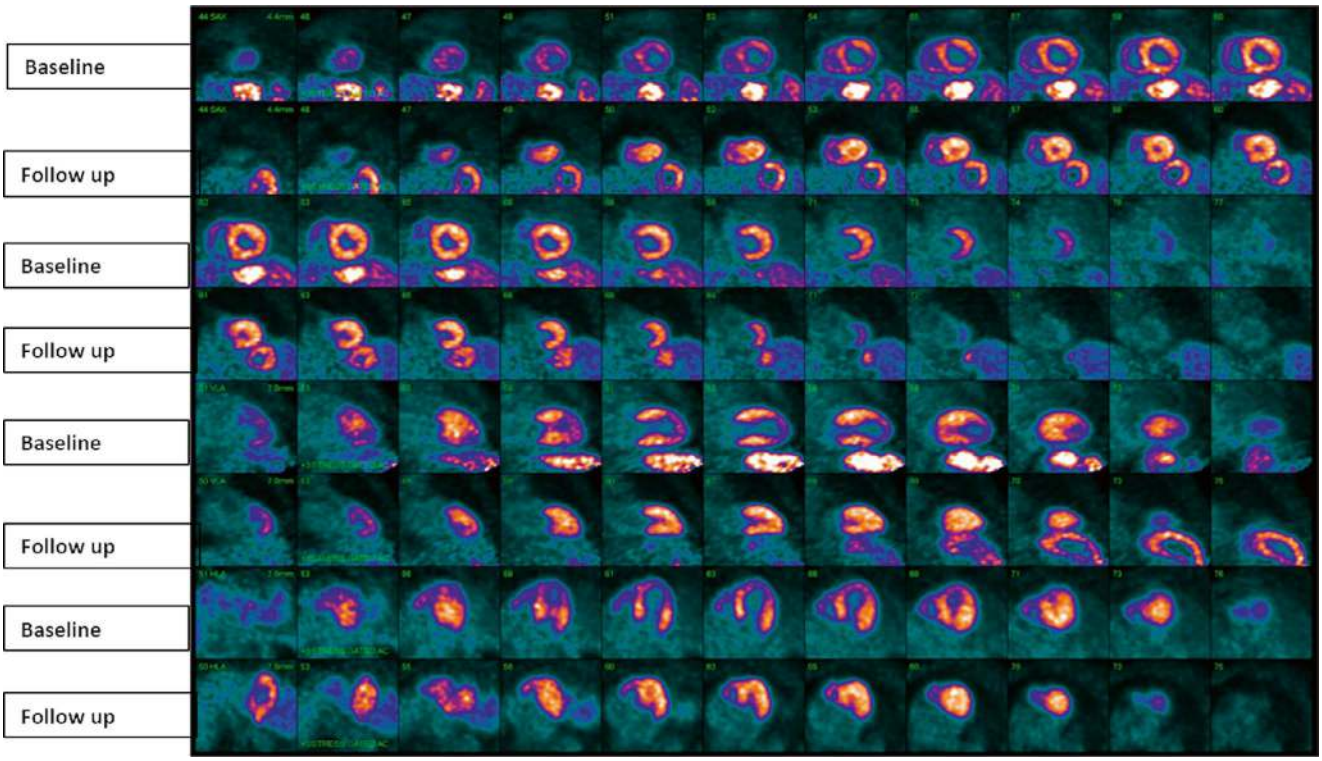


Fig. 4.12 End-systolic frames of the first set of stress images (baseline) are compared with the stress images of the repeat study (follow-up). In the baseline scan, the anterior wall, apex, and apical segments are akinetic, while in the second study, the same segments are hypercontractile

Findings at Follow-Up
- There is normalization of perfusion throughout all LV segments, consistent with full perfusion recovery.
- Full recovery of systolic function with reduction in LV volumes and resolution of apical aneurysmal dilation.
- The gated study during the original scan showed that the anterior wall, apex, and apical segments were akinetic, while in the second study, the same segments are hypercontractile.
- There is a dramatic reduction in end-systolic volume between acute and follow-up scan (from 125 ml to 59 ml).

Imaging Diagnosis at Follow-Up
- Normal stress/rest ^{82}Rb-PET perfusion study.

Differential Diagnosis
- Anterior myocardial infarction with antero-apical aneurysm.
- Takotsubo stress cardiomyopathy with transient perfusion abnormality and LV dysfunction.

Correlative Imaging
- Invasive coronary angiography demonstrated no evidence of luminal stenoses.

Management
- She was subsequently discharged home on optimal medical therapy (OMT) for ischemic heart failure including beta blocker, angiotensin receptor blockers, loop diuretic, acetylsalicylic acid, and statins.

Further Reading

- Pelliccia F, Kaski J, Crea F, Camici P. Pathophysiology of Takotsubo Syndrome. Circulation. 2017;135:2426–2441.
- Templin C, Ghadri J, Diekmann J, Napp L, Bataiosu D, Jaguszewski M, et al. Clinical Features and Outcomes of Takotsubo (Stress) Cardiomyopathy. New England Journal of Medicine. 2015;373:929–938.

4.2 Nonobstructive Atherosclerosis

4.2.1 Diabetes Mellitus: Case 35

Key Points
- Normal myocardial perfusion PET images associated with the absence of coronary calcification and reduced stress MBF suggest a low likelihood of flow-limiting CAD.

- This phenotype is common among women who typically have a low prevalence of obstructive atherosclerosis and has been linked to microvascular disease, which may be the source of their symptoms.

History

- An 86-year-old woman with a history of hypertension, dyslipidemia, diabetes mellitus, and obesity but no known coronary artery disease underwent evaluation for dyspnea and palpitations.
- She was referred for PET/CT to assess myocardial perfusion (Fig. 4.13 and Table 4.5).

PET/CT Images

Findings

- The images demonstrate normal LV size. There is mild RV dilatation with moderate increased tracer uptake during stress. There are no regional perfusion defects on the stress and rest images.
- The ECG-gated images demonstrated a rest LV ejection fraction of 52% with minimal increase during stress to 54% with normal LV volumes. There was normal regional wall motion and thickening.
- The maximal stress MBF and MFR are severely reduced in all coronary territories.
- The CT scan demonstrated no evidence of coronary artery calcification.

Imaging Diagnosis

- No evidence of obstructive CAD.
- Probable microvascular dysfunction.

Differential Diagnosis

- Multivessel obstructive coronary artery disease.
- Coronary microvascular dysfunction.

Correlative Imaging

- Invasive coronary angiography (Fig. 4.14).

Management

- Management of risk factors and anti-ischemic therapy.

Table 4.5 Summary of the quantitative blood flow data demonstrating severe reduction in stress MBF (normal value >1.8 mL/min/g) and MFR (normal value >2.0) in all coronary artery territories and globally

	MBF rest (ml/min/g)	MBF stress (ml/min/g)	MFR (stress/rest)
LAD	0.63	0.99	1.58
LCX	0.72	1.23	1.70
RCA	0.68	1.12	1.65
Global LV	0.67	1.09	1.63

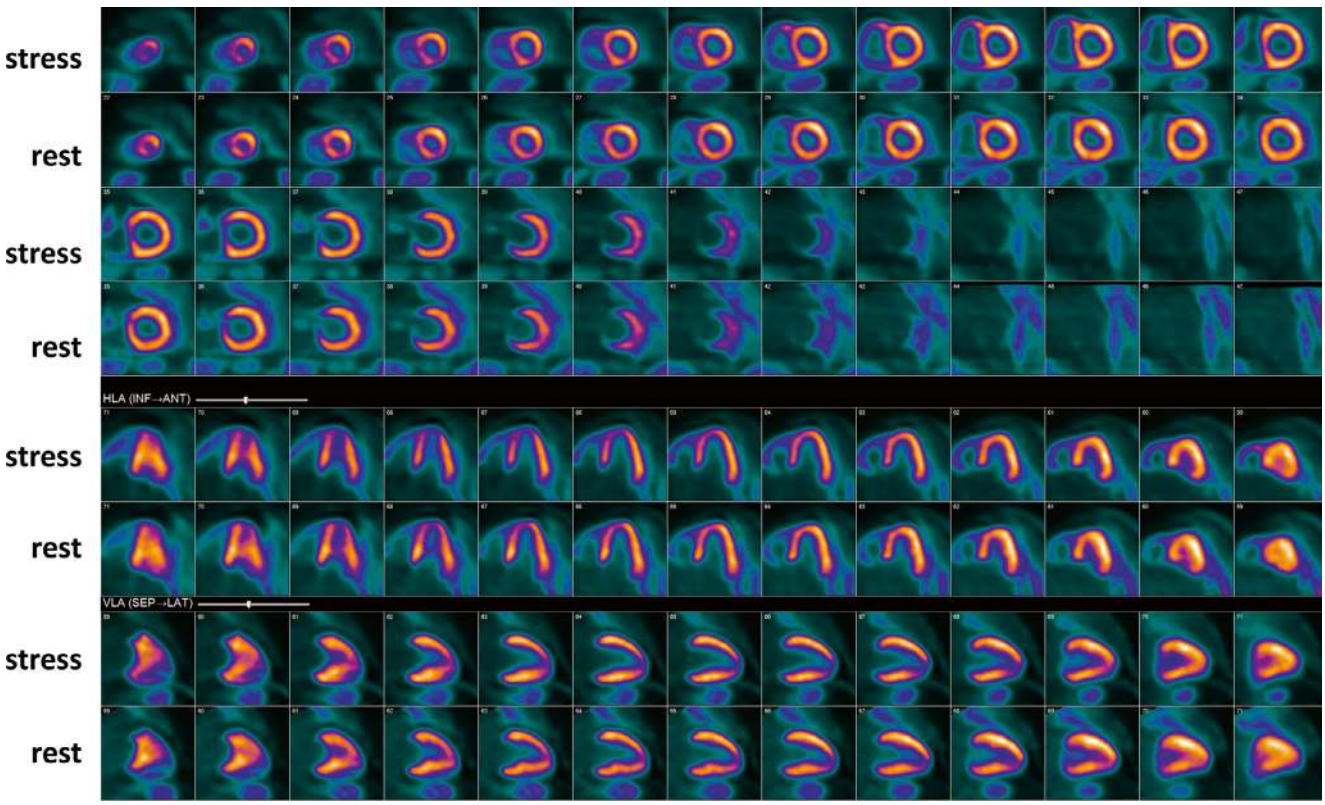


Fig. 4.13 Adenosine stress and rest ^{13}N-ammonia myocardial perfusion PET/CT images demonstrate normal LV size. There is mild RV dilatation with moderate increase tracer uptake during stress. There are no regional perfusion defects on the stress and rest images

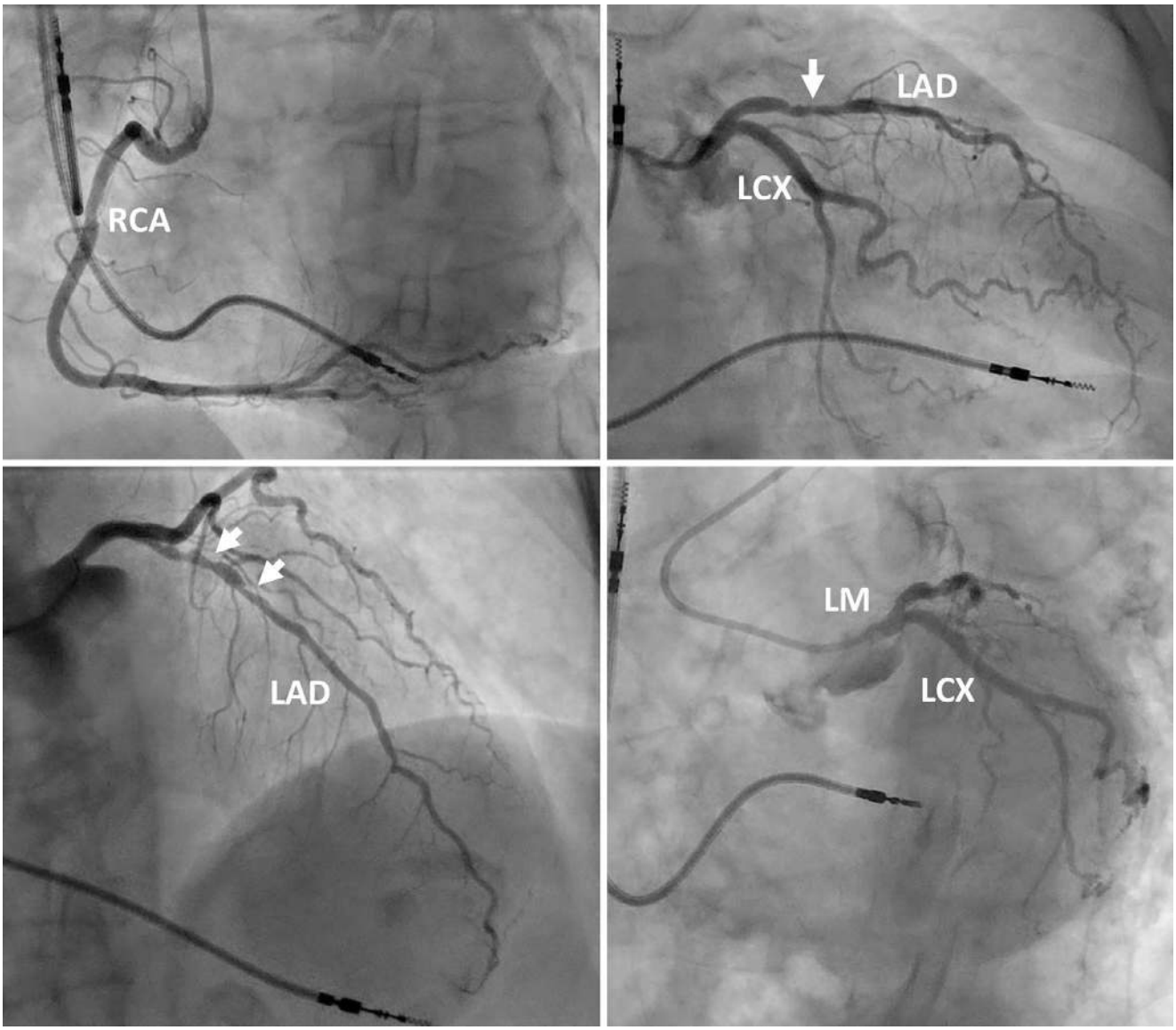


Fig. 4.14 Selective coronary angiographic views demonstrate nonobstructive CAD. The moderate stenosis in the proximal LAD (arrows) was associated with an fractional flow reserve (FFR) of 0.87, indicating no evidence of flow-limiting disease

Further Reading

- Gupta A, Taqueti VR, van de Hoef TP, Bajaj NS, Bravo PE, Murthy VL, et al. Integrated Non-invasive Physiological Assessment of Coronary Circulatory Function and Impact on Cardiovascular Mortality in Patients with Stable Coronary Artery Disease. Circulation. 2017;136:2325–2336.
- Taqueti V, Shaw L, Cook N, Murthy V, Shah N, Foster C, et al. Excess Cardiovascular Risk in Women Relative to Men Referred for Coronary Angiography Is Associated With Severely Impaired Coronary Flow Reserve, Not Obstructive Disease. Circulation. 2017;135:566–577.
- Murthy V, Naya M, Taqueti V, Foster C, Gaber M, Hainer J, et al. Effects of Sex on Coronary Microvascular Dysfunction and Cardiac Outcomes. Circulation. 2014;129:2518–2527.

4.2.2 Obesity and Coronary Microvascular Dysfunction: Case 36

Key Points

- Reduced stress MBF and MFR in the absence of flow-limiting coronary artery disease is consistent with coronary microvascular dysfunction.

- This imaging phenotype is prevalent in patients with cardiometabolic disease, including morbid obesity.
- The presence of coronary microvascular dysfunction identifies patients at increased risk of adverse cardiovascular events including heart failure and death.

History

- A 65-year-old man with morbid obesity was referred for a coronary computed tomography angiography (CCTA) after an episode of atypical chest pain. This revealed only minimal coronary calcification.
- Due to ongoing symptoms, he was then referred for a quantitative PET MPI (Fig. 4.15) to assess for microvascular dysfunction (Table 4.6).

PET/CT Images

Findings

- The PET scan demonstrates normal regional myocardial perfusion on both the rest and stress images.
- The ECG-gated images demonstrated an LVEF of 59% at rest and 63% post stress with normal LV volumes.
- The stress MBF is markedly reduced, and the MFR is moderately reduced both regionally and globally.

Imaging Diagnosis

- Coronary microvascular dysfunction.

Differential Diagnosis

- None.

Correlative Imaging

- None.

Management

- Counseling on lifestyle modifications and weight loss.

Table 4.6 Summary of the quantitative blood flow data demonstrating a diffuse and severe reduction in stress myocardial blood flow (normal value >1.8 mL/min/g) with moderate reduction in myocardial flow reserve (normal value >2.0) in all coronary artery territories and globally

	MBF rest (ml/min/g)	MBF stress (ml/min/g)	MFR (stress/rest)
LAD	0.47	0.83	1.77
LCX	0.52	0.96	1.84
RCA	0.49	0.86	1.77
Global LV	0.48	0.87	1.80

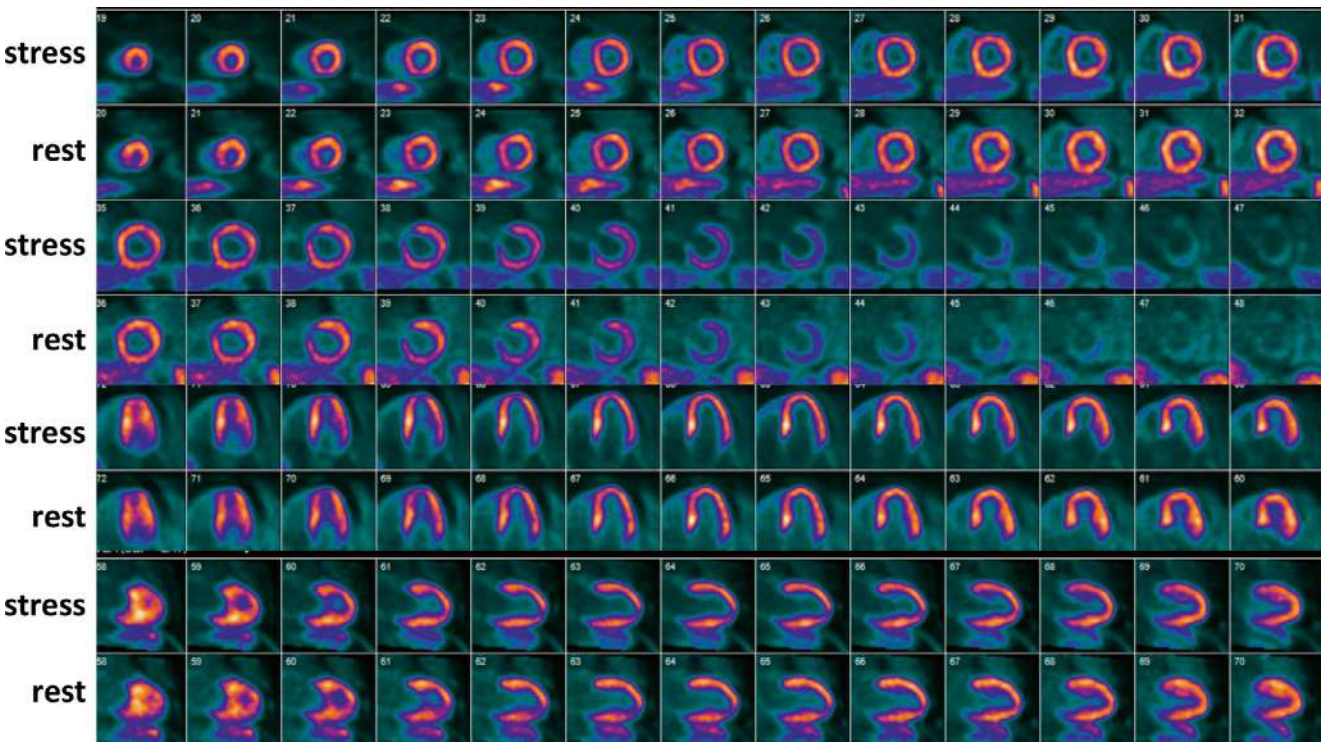


Fig. 4.15 Stress/rest ^{13}N-ammonia PET myocardial perfusion images. There is normal regional myocardial perfusion on both the stress and rest images

Further Reading

- Schindler T, Cardenas J, Prior J, Facta A, Kreissl M, Zhang X, et al. Relationship Between Increasing Body Weight, Insulin Resistance, Inflammation, Adipocytokine Leptin, and Coronary Circulatory Function. Journal of the American College of Cardiology. 2006;47:1188–1195.
- Tona F, Serra R, Di Ascenzo L, Osto E, Scarda A, Fabris R, et al. Systemic inflammation is related to coronary microvascular dysfunction in obese patients without obstructive coronary disease. Nutrition, Metabolism and Cardiovascular Diseases. 2014;24:447–453.
- Bajaj N, Osborne M, Gupta A, Tavakkoli A, Bravo P, Vita T, et al. Coronary Microvascular Dysfunction and Cardiovascular Risk in Obese Patients. Journal of the American College of Cardiology. 2018;72:707–717.

4.2.3 Heart Failure with Preserved Ejection Fraction (HFpEF): Case 37

Key Points

- The presence of extensive multivessel ischemia in the absence of flow-limiting coronary artery disease reflects the presence of severe microvascular dysfunction.
- CMD is frequently associated with cardiomyocyte injury (troponin elevation without obstructive coronary artery disease) and abnormal myocardial mechanics, which is likely to play a role in the pathophysiology of HFpEF.

History

- A 51-year-old man with known coronary artery disease and a prior ST-elevated myocardial infarction (STEMI) with stenting of the proximal LAD 3 months prior to the current hospitalization presented with chest pain, dyspnea, and heart failure. He had type 1 diabetes mellitus, complicated by peripheral neuropathy and nephropathy with a renal transplant in 2008. He also has hypertension and hyperlipidemia.
- The patient was referred for a myocardial perfusion PET scan to assess for obstructive coronary artery disease (Fig. 4.16 and Table 4.7).

PET/CT Images

Findings

- There is evidence of TID.
- There is a medium-sized perfusion defect of moderate intensity involving the LV apex, apical LV segments, the mid and basal anterior wall, showing complete reversibility. There is a medium-size perfusion defect of moderate severity throughout the inferoseptal wall, also showing complete reversibility.
- The ECG-gated images demonstrate an LVEF of 62% at rest that drops to 45% with transient enlargement of the end-systolic volume.
- The stress MBF and MFR are markedly reduced both regionally and globally.

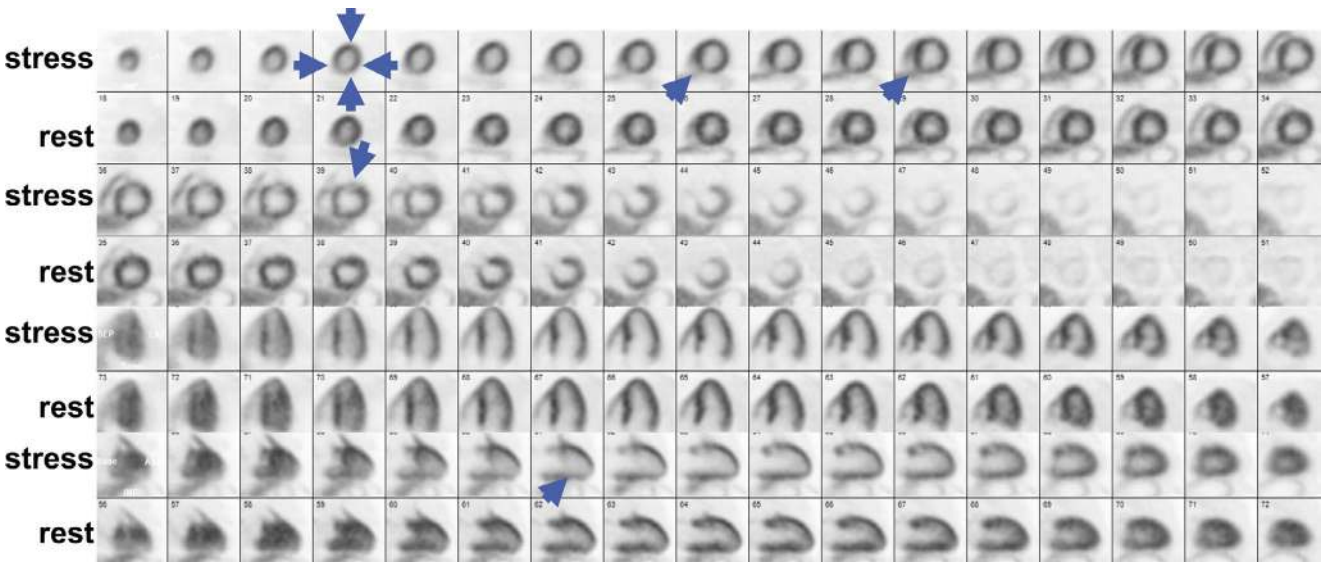


Fig. 4.16 Stress/rest ^{13}N-ammonia PET myocardial perfusion images. The images demonstrate transient ischemic dilatation (TID). There is a medium-sized perfusion defect of moderate intensity involving the LV apex, apical LV segments, and the mid and basal anterior wall, showing complete reversibility. In addition, there is a medium-sized perfusion defect of moderate severity throughout the inferoseptal wall, also showing complete reversibility

Table 4.7 Summary of the quantitative blood flow data demonstrating a diffuse and severe reduction in stress myocardial blood flow (normal value >1.8 mL/min/g) with moderate reduction in myocardial flow reserve (normal value >2.0) in all coronary artery territories and globally

	MBF rest (ml/min/g)	MBF stress (ml/min/g)	MFR (stress/rest)
LAD	0.82	1.23	1.50
LCX	0.83	1.34	1.62
RCA	0.81	1.13	1.39
Global LV	0.82	1.23	1.50

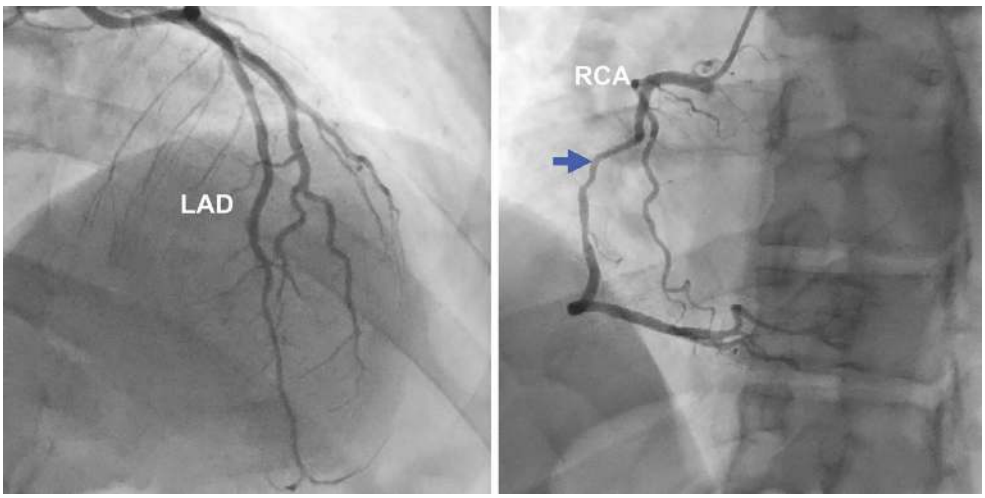


Fig. 4.17 Selective invasive coronary angiographic views demonstrating a patent LAD stent with diffuse nonobstructive coronary artery disease and a long 70% stenosis in the mid RCA (blue arrow) with an associated FFR of 0.78, which is borderline abnormal

Imaging Diagnosis
- Severe multivessel myocardial ischemia.

Differential Diagnosis
- Multivessel obstructive coronary artery disease.
- Coronary microvascular dysfunction.

Correlative Imaging
- Invasive coronary angiography (Fig. 4.17).

Management
- Medical management of myocardial ischemia and heart failure.

Further Reading

- Shah S, Lam C, Svedlund S, Saraste A, Hage C, Tan R, et al. Prevalence and correlates of coronary microvascular dysfunction in heart failure with preserved ejection fraction: PROMIS-HFpEF. European Heart Journal. 2018;39:3439–3450.
- Taqueti V, Solomon S, Shah A, Desai A, Groarke J, Osborne M, et al. Coronary microvascular dysfunction and future risk of heart failure with preserved ejection fraction. European Heart Journal. 2017;39:840–849.
- Taqueti V, Di Carli M. Coronary Microvascular Disease Pathogenic Mechanisms and Therapeutic Options: JACC State-of-the-Art Review. Journal of the American College of Cardiology. 2018;72:2625–2641.

4.2.4 Coronary Microvascular Dysfunction in Systemic Inflammatory Disorders: Case 38

Key Points
- Coronary microvascular dysfunction (CMD) is common in patients with systemic inflammatory disorders, including systemic lupus erythematosus (SLE), rheumatoid arthritis (RA), psoriasis, and others.
- Presenting symptoms are not always typical and one needs to keep a high index of suspicion.
- Quantitative PET is a powerful noninvasive tool to diagnose coronary microvascular dysfunction. In the absence of obstructive CAD, a myocardial flow reserve (MFR) < 2.0 reflects CMD and a marker of increased risk. Since MFR declines with age, an MFR between 2–2.5 in young patients (< 50) reflects coronary vascular dysfunction suggestive of CMD. Thus, the diagnostic threshold for abnormal MFR in young patients is higher than in older individuals.

History
- A 34-year-old female patient with recent diagnosis of SLE complicated by lupus nephritis, cytopenia, and cutaneous lupus referred for a myocardial perfusion PET/CT for the evaluation of atypical angina. She has hyperlipidemia including high cholesterol and triglycerides (Fig. 4.18 and Table 4.8).

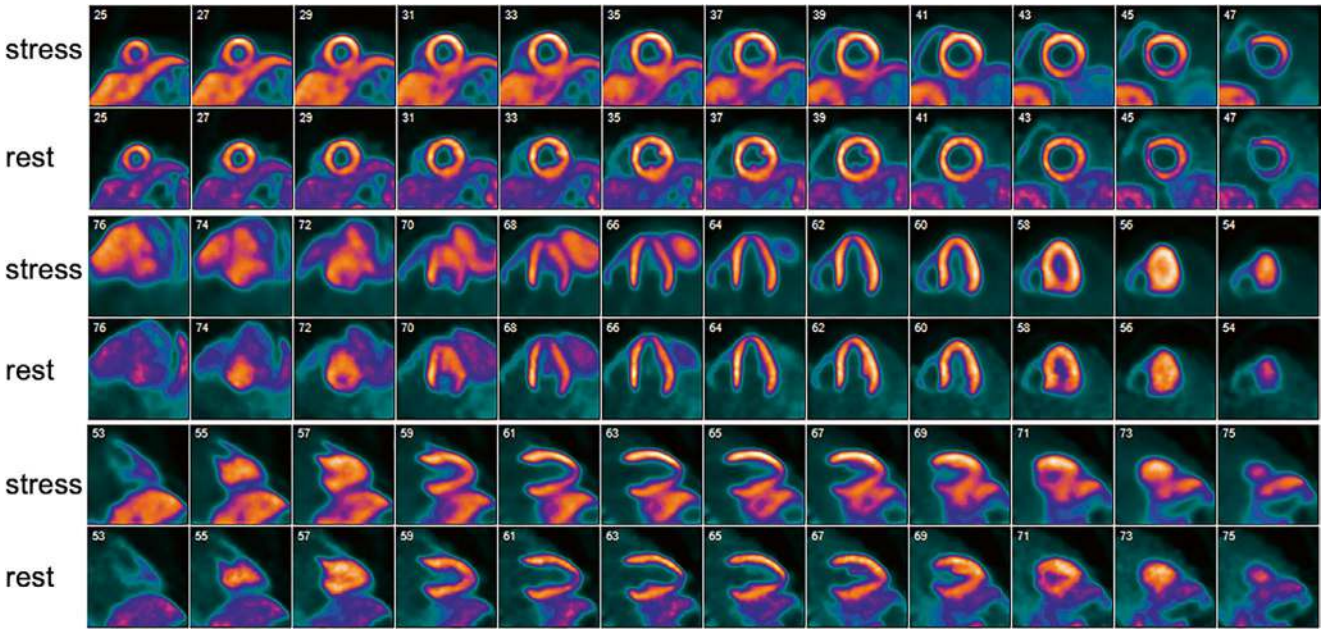


Fig. 4.18 Regadenoson stress and rest N-^{13} ammonia myocardial perfusion PET study. There is no evidence of perfusion abnormalities on the rest or stress images

Table 4.8 Summary of rest and stress MBF and MFR

	MBF rest (ml/min/g)	MBF stress (ml/min/g)	MFR (stress/rest)
LAD	1.10	1.98	1.80
LCX	1.05	2.03	1.93
RCA	1.09	2.02	1.85
Global LV	1.08	2.01	1.86

PET/CT images

Findings

- There is no evidence of regional perfusion defects on the rest or stress images.
- Moderate reduction (for age) in stress MBF and MFR in all coronary territories and globally.
- She had no evidence of coronary artery calcification.
- LV ejection fraction was normal at rest (59%) and showed a normal rise during vasodilator stress (to 64%), with normal LV volumes and no evidence of regional wall motion abnormalities.

Imaging Diagnosis

- Findings are consistent with moderate coronary microvascular dysfunction.

Correlative Imaging

- Invasive coronary angiography (Fig. 4.19).

Differential Diagnosis

- None.

Management

- She was placed on a moderate dose statin and diet to control lipids.

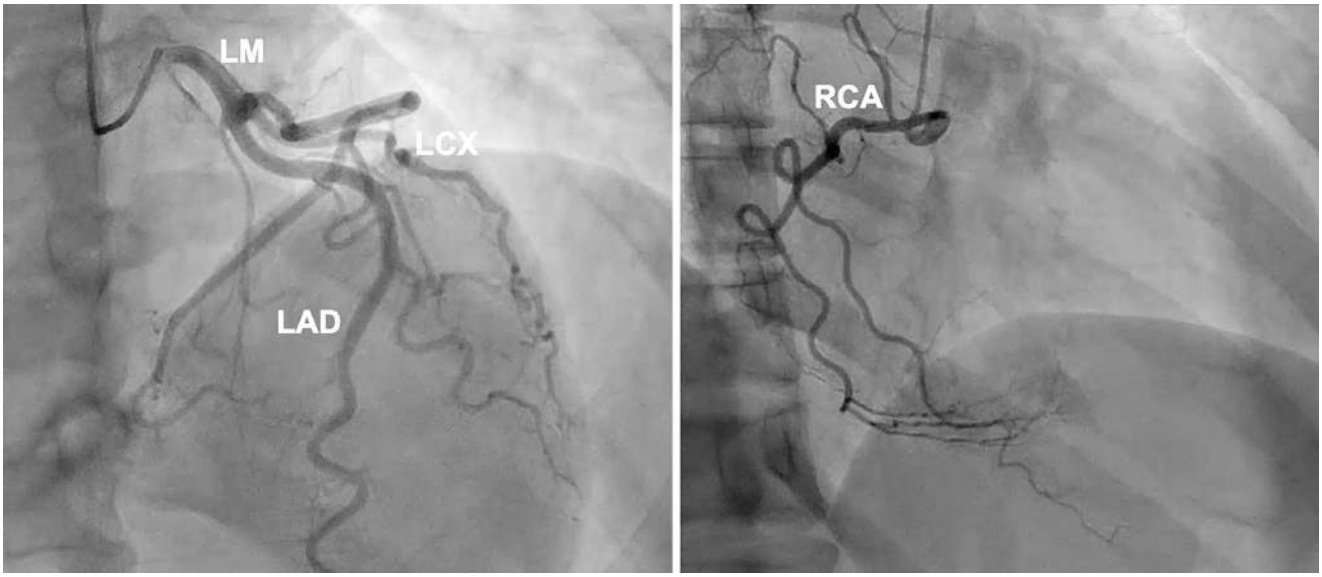


Fig. 4.19 Selective views of the right and left coronary system demonstrating no evidence of obstructive CAD

Further Reading

- Taqueti VR, Di Carli MF. Coronary Microvascular Disease Pathogenic Mechanisms and Therapeutic Options: JACC State-of-the-Art Review. J Am Coll Cardiol. Nov 27 2018;72(21):2625–2641. https://doi.org/10.1016/j.jacc.2018.09.042
- Weber BN, Paik JJ, Aghayev A, et al. Novel Imaging Approaches to Cardiac Manifestations of Systemic Inflammatory Diseases: JACC Scientific Statement. J Am Coll Cardiol. Nov 28 2023;82(22):2128–2151. https://doi.org/10.1016/j.jacc.2023.09.819

The opinions expressed in this chapter are those of the author(s) and do not necessarily reflect the views of the IAEA: International Atomic Energy Agency, its Board of Directors, or the countries they represent.

Open Access This chapter is licensed under the terms of the Creative Commons Attribution 3.0 IGO license (http://creativecommons.org/licenses/by/3.0/igo/), which permits use, sharing, adaptation, distribution and reproduction in any medium or format, as long as you give appropriate credit to the IAEA: International Atomic Energy Agency, provide a link to the Creative Commons license and indicate if changes were made.

Any dispute related to the use of the works of the IAEA: International Atomic Energy Agency that cannot be settled amicably shall be submitted to arbitration pursuant to the UNCITRAL rules. The use of the IAEA: International Atomic Energy Agency's name for any purpose other than for attribution, and the use of the IAEA: International Atomic Energy Agency's logo, shall be subject to a separate written license agreement between the IAEA: International Atomic Energy Agency and the user and is not authorized as part of this CC-IGO license. Note that the link provided above includes additional terms and conditions of the license.

The images or other third party material in this chapter are included in the chapter's Creative Commons license, unless indicated otherwise in a credit line to the material. If material is not included in the chapter's Creative Commons license and your intended use is not permitted by statutory regulation or exceeds the permitted use, you will need to obtain permission directly from the copyright holder.



Heart Failure and Myocardial Viability

5

Marcelo Di Carli, Paolo Raggi, Raffaele Giubbini, Michelle Williams, Diana Paez, Maurizio Dondi, and Carlo Rodella

Objectives

- To learn how to use stress myocardial perfusion imaging to differentiate ischemic from nonischemic cardiomyopathy.
- To learn how to protocol exams to assess the extent and severity of ischemia and viability.
- To learn how to recognize patterns of myocardial viability.
- To learn how to integrate ancillary information into ischemia/viability exams to guide management.

Dysfunctional, but viable myocardium that can fully or partially recover its contractile function after mechanical revascularization is characterized by perfusion defects associated with preserved metabolic activity as evidenced by positron emission tomography (PET) with ^{18}F-fluordeoxyglucose (FDG). Therefore, a viability study using a metabolic tracer is typically combined with a perfusion study using PET flow tracers (^{13}NH3, ^{15}O-labeled H_2O, ^{82}Rb) or, alternatively, with single-photon emission computed tomography (SPECT) tracers (^{99m}Tc-MIBI, ^{99m}Tc-tetrofosmin, ^{201}Tl).

Of particular interest is combining the PET metabolic study with ^{18}F-FDG and the SPECT flow study with technetium-labeled tracers, as this methodology allows the vitality study to be performed even in centers not equipped with a cyclotron or rubidium generator.

5.1 Mismatch SPECT/CT Perfusion-PET/CT FDG: Case 39

Key Points

- The presence of fixed perfusion defects in a patient with a subacute myocardial infarction should always prompt the consideration of assessing residual myocardial viability.
- Identification of significant viable but hibernating myocardium identifies not only patients who may benefit from revascularization but also a high-risk cohort for adverse cardiac events.
- The absence of obstructive CAD on coronary angiography suggests that severe coronary microvascular dysfunction is the underlying pathophysiology for the extensive area of hibernating myocardium in the left anterior descending artery (LAD) territory and, likely, for the acute presentation with cardiac arrest. The clinical presentation and imaging findings are consistent with stress cardiomyopathy.
- The absence of revascularizable disease poses a management challenge as there is residual ischemic myocardium.

All authors have no conflict of interest to disclose.

M. Di Carli
Brigham and Women's Hospital, Boston, MA, USA
e-mail: mdicarli@bwh.harvard.edu

P. Raggi
Division of Cardiology, University of Alberta, Edmonton, AB, Canada

R. Giubbini
Nuclear Medicine, International Specialized Hospital of Uganda (ISHU), Kampala, Uganda
e-mail: raffaele.giubbini@unibs.it

M. Williams
British Heart Foundation Centre for Research Excellence, Institute for Neuroscience and Cardiovascular Research, University of Edinburgh, Edinburgh, United Kingdom
e-mail: michelle.williams@ed.ac.uk

D. Paez · M. Dondi (✉)
Division of Human Health, International Atomic Energy Agency, Vienna, Austria
e-mail: d.paez@iaea.org; m.dondi@iaea.org

C. Rodella
Department of Medical Physics, Spedali Civili Brescia, Brescia, Italy
e-mail: carlo.rodella@asst-spedalicivili.it

© The Author(s) 2027
M. Di Carli et al. (eds.), *IAEA Atlas of Cardiac PET/CT*, https://doi.org/10.1007/978-3-662-74188-7_5

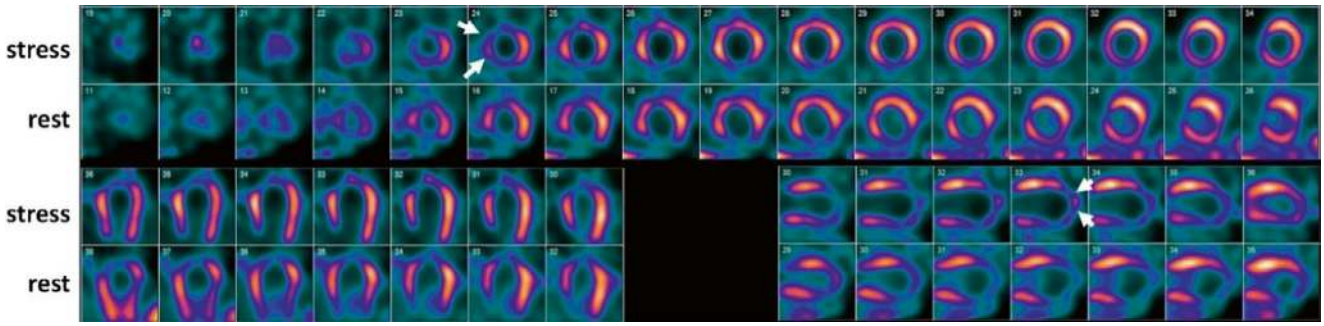


Fig. 5.1 Stress/rest ^{99m}Tc-sestamibi SPECT myocardial perfusion images demonstrate aneurysmal dilatation of the LV associated with a large perfusion defect of severe intensity throughout the mid-anteroseptal wall, apical LV segments, and the LV apex, which was essentially fixed

History

- A 69-year-old female with a history of breast cancer and bioprosthetic aortic valve replacement in 2017 presented with out-of-hospital cardiac arrest. Her cardiac risk factors included hypertension, dyslipidemia, diabetes, and obesity.
- She was found to have a new left bundle branch block, and a transthoracic echocardiogram revealed newly reduced left ventricle (LV) ejection fraction of 35%. There was global hypokinesis with akinesis of the apex and septum.
- She was referred for a regadenoson SPECT myocardial perfusion study to evaluate for CAD (Fig. 5.1).

SPECT Imaging

Imaging Findings

- The stress/rest SPECT myocardial perfusion images demonstrate aneurysmal dilatation of the LV associated with a large perfusion defect of severe intensity throughout the mid-anteroseptal wall, apical LV segments, and the LV apex, which is essentially fixed.
- The electrocardiogram (ECG) gated images demonstrated severe global LV systolic dysfunction with akinesis of the LV apex and apical LV segments.
- A follow-up PET with FDG was recommended to assess myocardial viability and paired with rest SPECT (Fig. 5.2). The results were consistent with the presence of combined nonviable and viable but hibernating myocardium throughout the mid LAD territory involving approximately 38% of the LV mass (perfusion-FDG mismatch).

FDG PET/CT Imaging

Imaging Findings

- There is significant FDG uptake throughout all hypoperfused LV segments (perfusion-FDG mismatch), consistent with the presence of combined nonviable and viable but hibernating myocardium throughout the mid LAD territory involving approximately 38% of the LV mass.

Imaging Diagnosis

- Combined nonviable and viable but hibernating myocardium in the mid LAD territory.

Differential Diagnosis

- Subacute anterior myocardial infarction with significant residual viable but hibernating myocardium due to obstructive CAD.

Correlative Imaging

- Invasive coronary angiography (Fig. 5.3).

Management

- She underwent a secondary prevention automatic implantable cardioverter defibrillator (AICD) placement.
- She was subsequently discharged home on optimal medical therapy for ischemic heart failure including beta blocker, angiotensin-receptor blocker (ARB), loop diuretic, acetylsalicilic acid, and statin therapy.

Further Reading

- Pelliccia F, Kaski J, Crea F, Camici P. Pathophysiology of Takotsubo Syndrome. Circulation. 2017;135:2426–2441.
- Templin C, Ghadri J, Diekmann J, Napp L, Bataiosu D, Jaguszewski M, et al. Clinical Features and Outcomes of Takotsubo (Stress) Cardiomyopathy. New England Journal of Medicine. 2015;373:929–938.

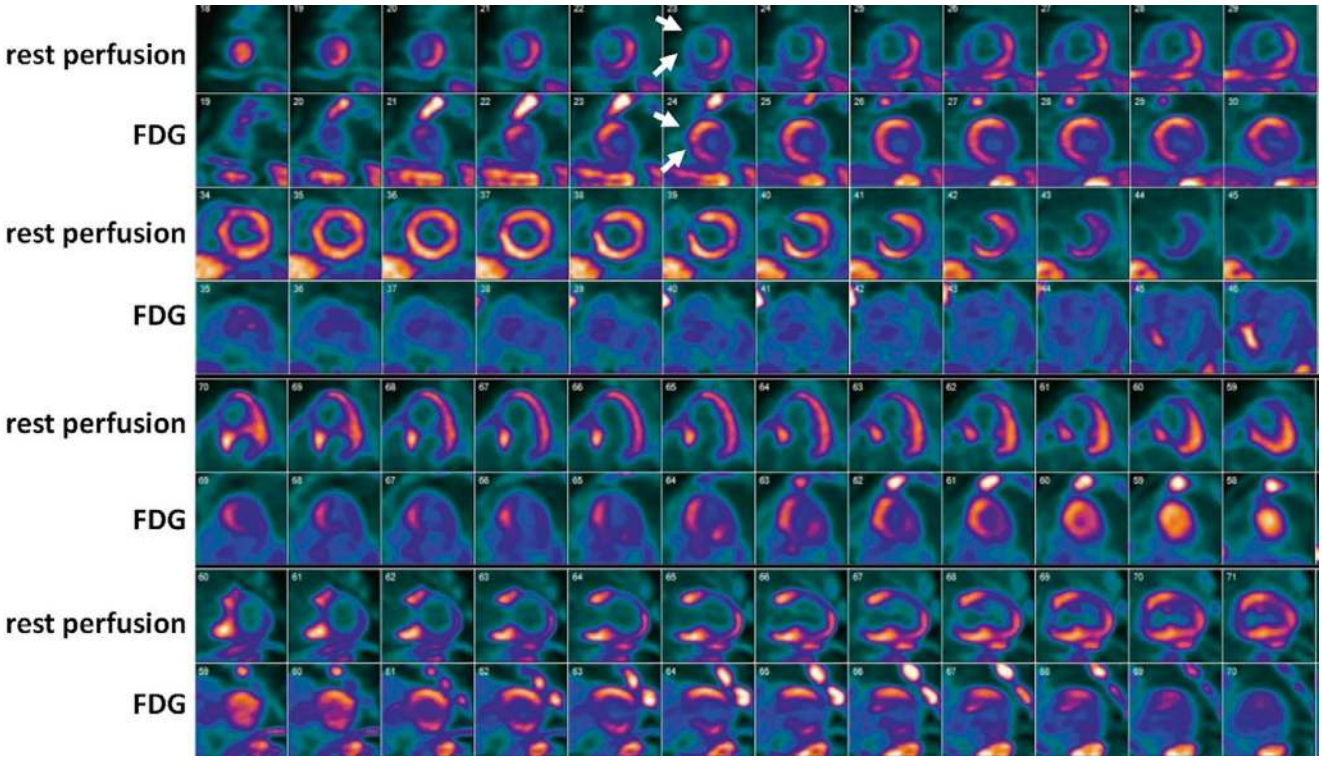


Fig. 5.2 Rest ^{99m}Tc-sestamibi SPECT myocardial perfusion (rest perfusion rows) and ^{18}F-FDG PET images (FDG rows) demonstrating significant FDG uptake throughout all hypoperfused LV segments (perfusion-FDG mismatch), consistent with the presence of combined nonviable and viable but hibernating myocardium throughout the mid LAD territory involving approximately 38% of the LV mass

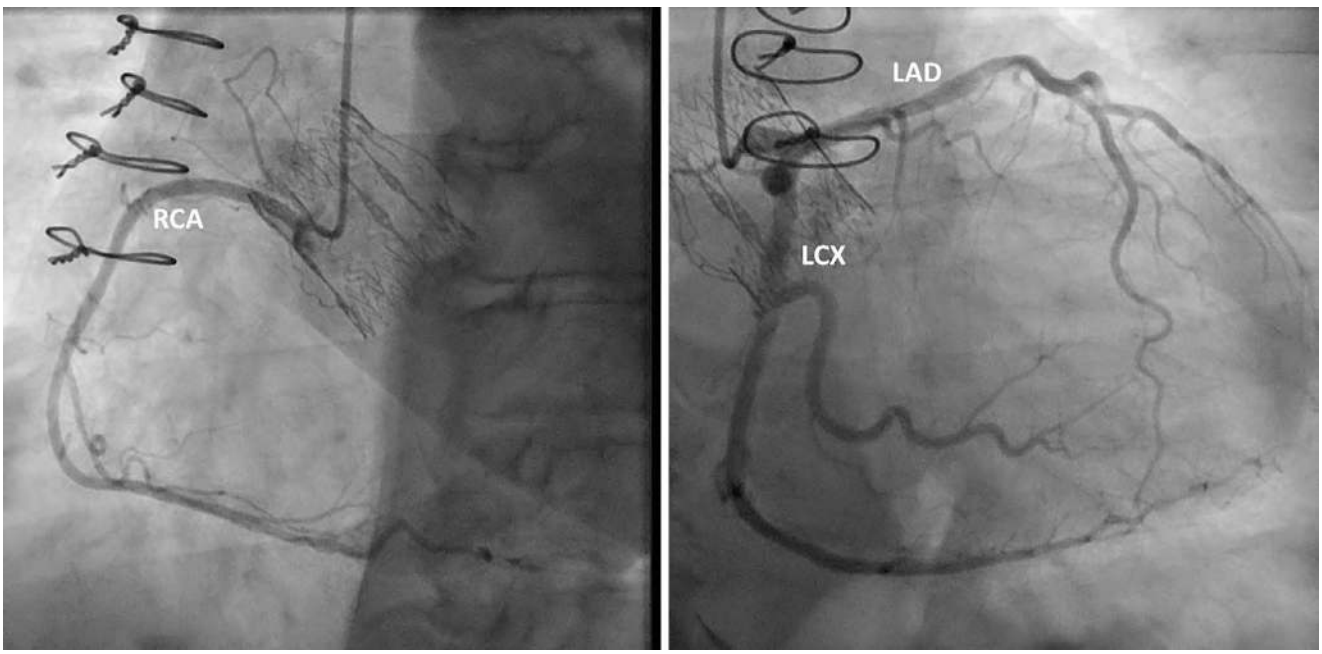


Fig. 5.3 Invasive coronary angiography with no evidence of obstructive coronary artery disease

5.2 Mismatch PET/CT Perfusion-PET/CT FDG: Case 40

Key Points

- Preservation of glucose uptake in hypoperfused myocardium (perfusion-FDG mismatch) with severe systolic dysfunction identifies evidence of myocardial viability.
- The perfusion-FDG mismatch reflects myocardial hibernation, which is generally associated with improved systolic function after revascularization.

History

- A 57-year-old man was admitted to the hospital for an episode of septic arthritis and bacteremia.
- While in the hospital, he had a witnessed loss of consciousness while attempting to get out of bed. Heart rhythm evaluation on the telemetry monitor revealed polymorphic ventricular tachycardia for which he was shocked with return of spontaneous circulation after 4 min of cardiopulmonary resuscitation.
- Echocardiography showed severe LV dysfunction and an LVEF of 25%.
- Invasive coronary angiography demonstrated a complete occlusion of the LAD coronary artery with collaterals. Given his complex hospital course, intervention was deferred pending myocardial viability assessment (Fig. 5.4).

PET/CT Images

Findings

- Moderate LV dilatation and intense lung uptake.
- Large and severe perfusion defect throughout the anterior and anteroseptal walls, the apical LV segments, and the LV apex.
- Relatively preserved ^{18}F-FDG uptake in all hypoperfused LV segments (perfusion-FDG mismatch).
- Rest LVEF is 36% with moderately dilated LV volumes. There is akinesis of the LV apex and severe hypokinesis of the apical LV segments and mid-anterior and anteroseptal walls.

Imaging Diagnosis

- Large area of viable but hibernating myocardium throughout the LAD territory.

Differential Diagnosis

- None.

Management

- Given the extensive area of viable but hibernating myocardium, he underwent percutaneous coronary intervention (PCI) of the totally occluded LAD coronary artery.

Correlative Imaging

- Invasive coronary angiography (Fig. 5.5).

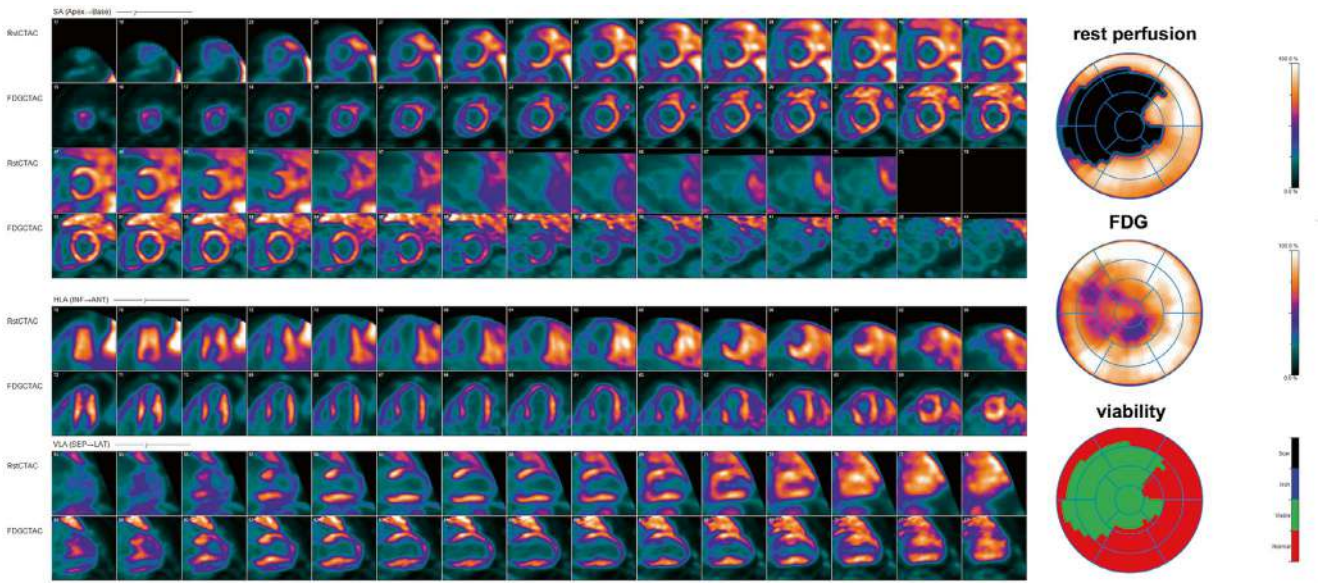


Fig. 5.4 Rest ^{13}N-ammonia and ^{18}F-FDG PET images. There is moderate LV dilatation and intense lung uptake. There is a large and severe perfusion defect throughout the anterior and anteroseptal walls, the apical LV segments, and the LV apex. There is relatively preserved ^{18}F-FDG uptake in all hypoperfused LV segments (perfusion-FDG mismatch). The corresponding perfusion and ^{18}F-FDG polar maps on the right demonstrate the large perfusion abnormality with preserved metabolic activity consistent with viable myocardium

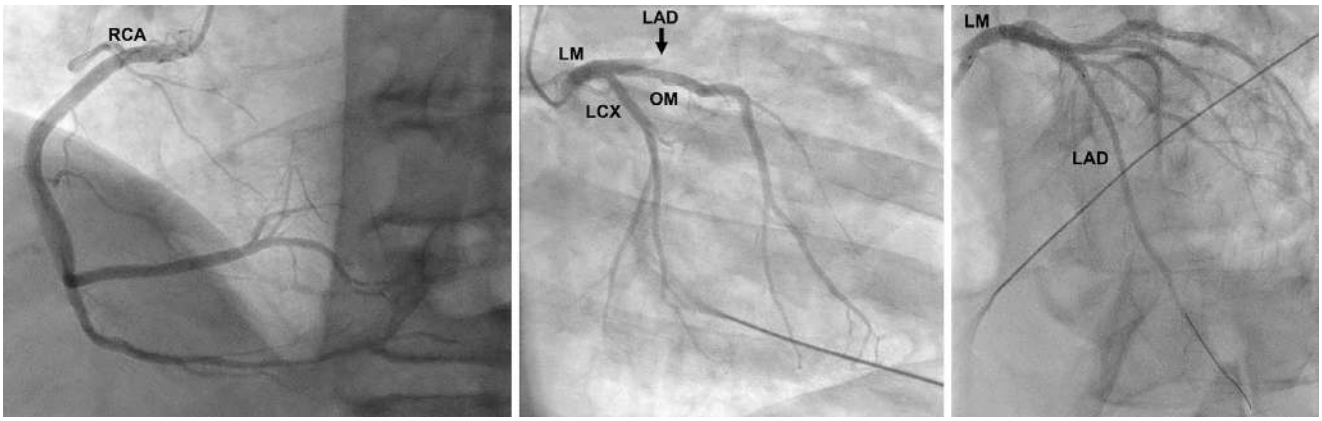


Fig. 5.5 Selective views of the right left coronary systems before (left and middle panels) and after (right panel) PCI of the LAD coronary artery

Further Reading
- Bax J, Di Carli M, Narula J, Delgado V. Multimodality imaging in ischaemic heart failure. Lancet 2019:393;1056–70.

5.3 Match PET/CT Perfusion-PET/CT FDG: Case 41

Key Points
- Glucose uptake in dysfunctional myocardium with a perfusion defect is indicative of viability, whereas the absence of ^{18}F-FDG uptake is consistent with nonviable myocardium.
- A perfusion-FDG match has a high negative predictive value for predicting functional recovery after revascularization.

History
- A 69-year-old man with ischemic cardiomyopathy and prior coronary artery bypass graft (CABG) presenting with dyspnea was referred for a PET scan to assess for myocardial viability. His cardiac risk factors include hypertension, dyslipidemia, and a family history of ischemic heart disease (Fig. 5.6).

  PET/CT Images

Findings
- The images demonstrate a severely dilated LV. The rest perfusion images show a large and severe perfusion defect throughout the inferior and inferolateral walls.
- On the ^{18}F-FDG images, glucose uptake is concordantly reduced in all hypoperfused LV segments (perfusion-FDG matched defect), consistent with nonviable myocardium in the left circumflex artery (LCX)/obtuse marginal territory.
- Rest myocardial perfusion and ^{18}F-FDG uptake are normal in the LAD and right coronary artery (RCA) territories.
- The ECG-gated images demonstrated a rest LV ejection fraction of 34% with severely dilated LV volumes. There was moderate global hypokinesis with akinesis of the inferior and inferolateral walls.

Imaging Diagnosis
- Large area of myocardial scar in the left circumflex artery (LCX)/RCA territory.
- Preserved viability in the LAD territory.

Differential Diagnosis
- None.

Correlative Imaging
- None.

Management
- He continued to be managed medically.

Further Reading
- Mc Ardle B, Shukla T, Nichol G, deKemp R, Bernick J, Guo A, et al. Long-Term Follow-Up of Outcomes With F-18-Fluorodeoxyglucose Positron Emission Tomography Imaging–Assisted Management of Patients With Severe Left Ventricular Dysfunction Secondary to Coronary Disease. Circulation: Cardiovascular Imaging. 2016;9.
- Bax J, Di Carli M, Narula J, Delgado V. Multimodality imaging in ischaemic heart failure. The Lancet. 2019;393:1056–1070.

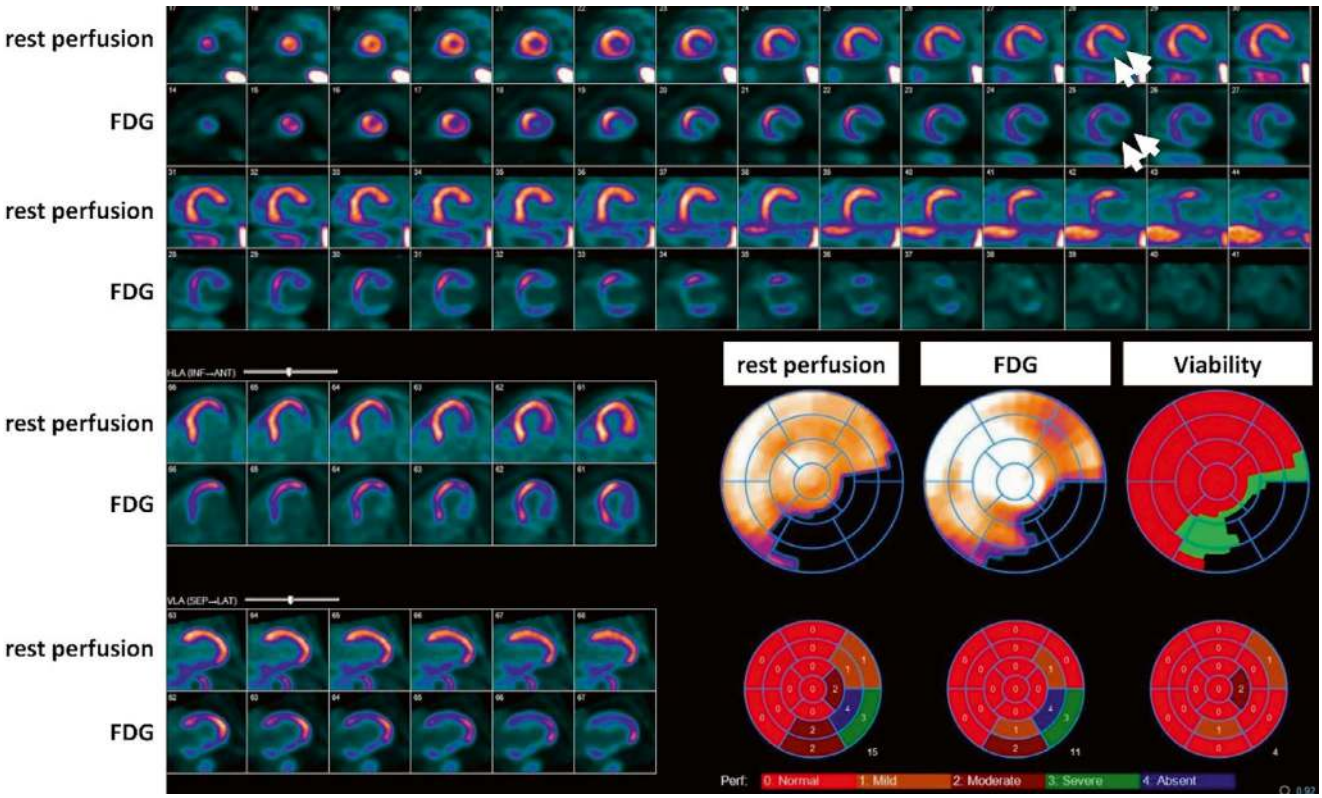


Fig. 5.6 Rest ^{13}N-ammonia myocardial perfusion and ^{18}F-FDG PET images. The images demonstrate a severely dilated LV. The rest perfusion images show a large and severe perfusion defect throughout the inferior and inferolateral walls with concordantly reduced ^{18}F-FDG uptake (perfusion-FDG matched defect), consistent with nonviable myocardium (arrows). Rest myocardial perfusion and ^{18}F-FDG uptake are normal in the LAD and right coronary artery (RCA) territories. The polar maps for myocardial perfusion (left), ^{18}F-FDG (middle), and viability (right) confirm the extent of nonviable myocardium

5.4 Rest-Stress Perfusion and Viability Imaging: Case 42

Key Points

- Comprehensive evaluation of patients with ischemic cardiomyopathy often requires stress perfusion and viability imaging.
- If there are no contraindications for stress testing, stress imaging should always be considered as part of the myocardial viability evaluation.
- The presence of myocardial viability can be associated with different patterns of metabolic activity; perfusion-FDG mismatch (reflecting hibernation) or reversed perfusion-FDG mismatch (reflecting myocardial stunning).

History

- A 71 year-old man with a history of ischemic cardiomyopathy, remote multivessel CABG, and implantable cardioverter-defibrillator (ICD) placement for sustained ventricular tachycardia presented with congestive heart failure and recurrent ventricular arrhythmias.
- He was referred for a PET/CT scan to assess the degree of stress induced ischemia and myocardial viability (Fig. 5.7).

PET/CT Images

Findings

- There is severe LV dilatation and increased lung uptake on both the rest and stress images.
- The stress perfusion images demonstrate a large-sized perfusion defect of severe intensity throughout the inferior and inferolateral and basal inferoseptal walls, which is essentially fixed. ^{18}F-FDG uptake in this area is concordantly reduced (perfusion-FDG matched defect).
- In addition, there is a large perfusion defect of severe intensity involving the mid-anterior, anterolateral, and anteroseptal walls, the apical LV segments, and the LV apex, which shows near complete reversibility. ^{18}F-FDG uptake in this area is normal, except in the anteroseptal

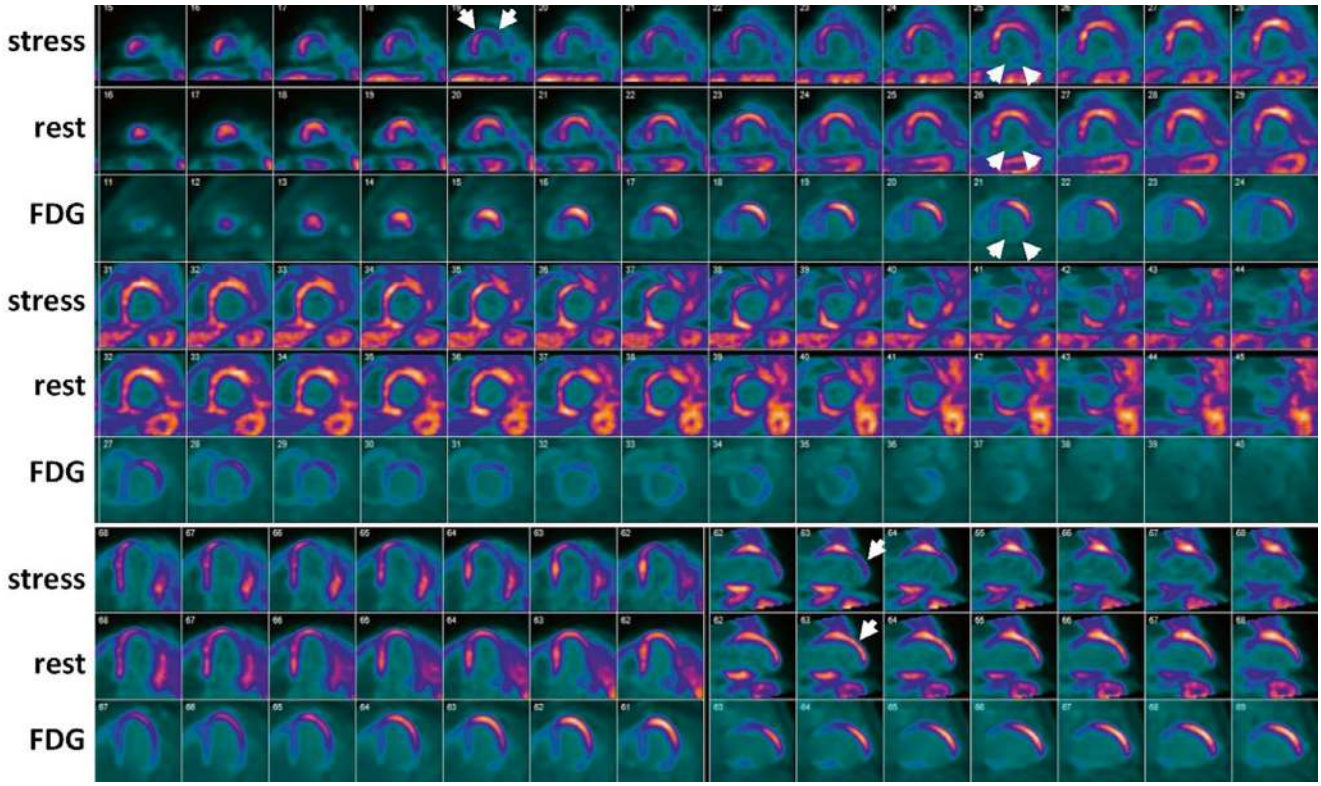


Fig. 5.7 Stress-rest ^{13}N-ammonia myocardial perfusion and rest ^{18}F-FDG PET images. There is severe LV dilatation and increased lung uptake on both the rest and stress images. There is a large perfusion defect of severe intensity involving the mid-anterior, anterolateral, and anteroseptal walls, the apical LV segments, and the LV apex, showing near complete reversibility. ^{18}F-FDG uptake in this area is normal, except in the anteroseptal wall, which is reduced compared to perfusion (so-called reversed perfusion-FDG mismatched defect)

wall, which is reduced compared to perfusion (so-called reversed perfusion-FDG mismatched defect).

- The ECG-gated images demonstrated a rest LV ejection fraction of 12% with minimal change post stress. There was severe global hypokinesis with akinesis of the inferior and inferolateral walls. Perfusion-reversed mismatched defects in the septum can be seen in the context of conduction abnormalities with left bundle branch block (LBBB). This patient did not have a LBBB.

Imaging Diagnosis

- Large area of severe stress induced ischemia (viability) in the LAD territory.
- Large myocardial infarction in the RCA territory.

Differential Diagnosis

- None.

Correlative Imaging

- None.

Management

- Invasive coronary angiography (not shown) demonstrated:
  - Left main: focal 80% stenosis.
  - Proximal LAD: focal 90% stenosis.
  - First obtuse marginal branch: focal 100% stenosis.
  - Mid RCA is totally occluded.
  - The left internal mammary graft to mid LAD: patent.
- In view of the PET scan results and his ventricular arrhythmias and worsening heart failure, the patient underwent PCI of his native LAD.

Further Reading

- Bax J, Di Carli M, Narula J, Delgado V. Multimodality imaging in ischaemic heart failure. The Lancet. 2019;393:1056–1070.
- Di Carli M, Prcevski P, Singh TP, Janisse J, Ager J, Muzik O, et al., Myocardial blood flow, function, and metabolism in repetitive stunning. J Nucl Med. 2000;41:1227–1234.

5.5 End-Stage Ischemic Cardiomyopathy: Case 43

Key Points

- PET myocardial perfusion imaging can be useful in delineating the extent and severity of myocardial ischemia to differentiate ischemic from nonischemic cardiomyopathy.
- Extensive areas of severe stress-induced ischemia are consistent with ischemic cardiomyopathy.

History

- A 79-year-old man with a history of chronic kidney disease and unexplained cardiomyopathy referred for a myocardial perfusion PET study (Fig. 5.8) to evaluate for coronary artery disease in the setting of dyspnea and heart failure.
- He was obese and had a history of obstructive sleep apnea.

PET/CT Images

Findings

- Severe LV dilatation.
- Moderate RV dilatation with severely increased RV tracer uptake on both the rest and stress images.
- Medium-sized perfusion defect of severe intensity involving the LV apex, apical LV segments, and mid-anteroseptal walls, showing near complete reversibility.
- Large and severe perfusion defect throughout the inferior and inferoseptal walls, with complete reversibility.
- Rest LVEF: 20% with severely dilated LV volumes (ESV indexed: 106 ml/m2). Peak stress LVEF: 24%. There is severe global LV hypokinesis and akinesis of the inferior, inferoseptal, and inferolateral walls.
- Marked reduction of stress MBF and MFR in all coronary territories (Table 5.1).

Imaging Diagnosis

- Severe multivessel ischemia consistent with ischemic cardiomyopathy.

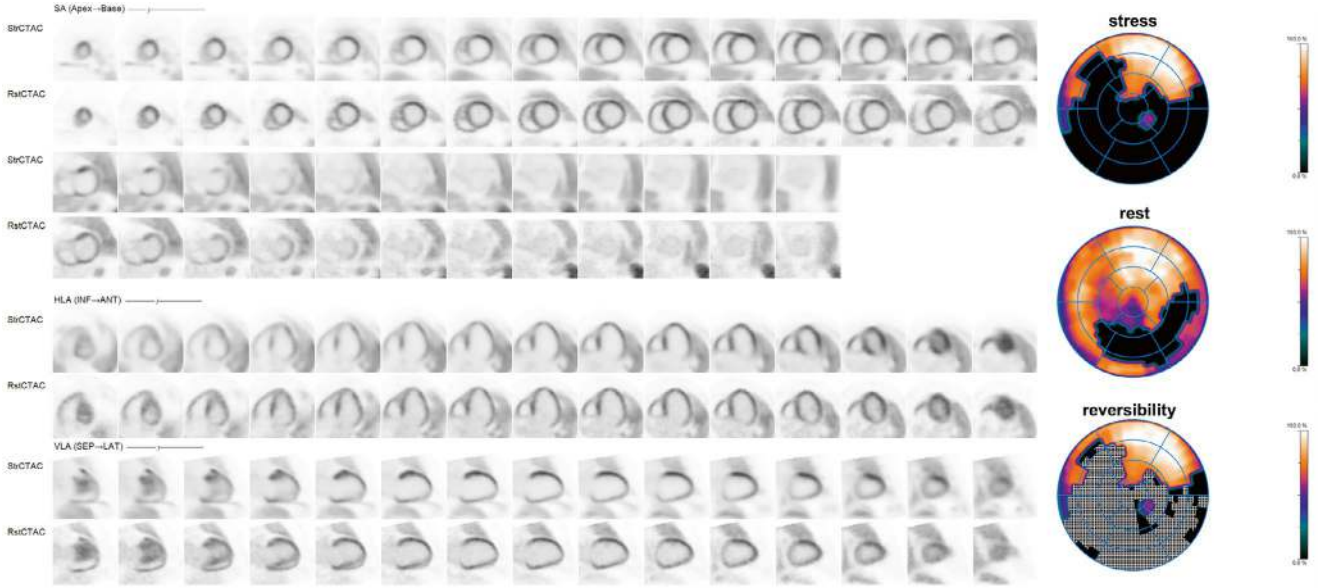


Fig. 5.8 ^{13}N-ammonia PET/CT images. Severe LV dilatation. Moderate RV dilatation with severely increased RV tracer uptake on both the rest and stress images. Medium-sized perfusion defect of severe intensity involving the LV apex, apical LV segments, and mid-anteroseptal wall, showing near complete reversibility. Large and severe perfusion defect throughout the inferior and inferoseptal walls, with complete reversibility

Table 5.1 Summary of stress and rest MBF and MFR

	MBF rest (ml/min/g)	MBF stress (ml/min/g)	MFR (stress/rest)
LAD	0.91	0.78	0.86
LCX	0.70	0.65	0.93
RCA	0.64	0.41	0.64
Global LV	0.76	0.63	0.83

- End-stage LV remodeling.
- Increased RV tracer uptake consistent with pulmonary hypertension.

Differential Diagnosis
- None.

Correlative Imaging
- Invasive coronary angiography showed:
- LAD: diffuse 50% proximal disease and 85% diffuse mid-vessel disease.
- Diagonal 2 is long with 90% diffuse disease.
- LCX: large vessel with 90% long proximal lesion.
- Obtuse marginal 1 is proximally occluded and fills via left-to-left collaterals.
- RCA: occluded proximally.

Management
- Extensive areas of severe myocardial ischemia, consistent with advanced ischemic cardiomyopathy.
- The patient refused surgical or percutaneous intervention.
- He was managed medically and died a year after the PET scan.

Further Reading
- Bax J, Di Carli M, Narula J, Delgado V. Multimodality imaging in ischaemic heart failure. Lancet 2019:393;1056–70.

5.6 Severe Left Ventricular Dysfunction and Unknown CAD: Case 44

Key Points
- Coronary microvascular dysfunction (CMD) is prevalent in several clinical conditions where atherosclerosis plays little or no role in its pathogenesis. These conditions include arterial hypertension, aortic stenosis, and non-ischemic cardiomyopathies.
- CMD has been documented in several nonischemic cardiomyopathies such as idiopathic, hypertrophic, infiltrative, and stress cardiomyopathies.
- Whether CMD in nonischemic cardiomyopathies is a cause or effect of the underlying myopathic process is unknown.

History
- A 78-year-old woman with a history of hypertension and diabetes mellitus presenting with new onset heart failure, reduced left ventricular (LV) systolic function, and ventricular arrhythmias. Her ECG shows a LBBB. She was referred for PET/CT (Fig. 5.9 and Table 5.2).

PET/CT Images

Findings
- The images demonstrate a severely dilated LV. There is also normal RV size with moderately increased RV tracer

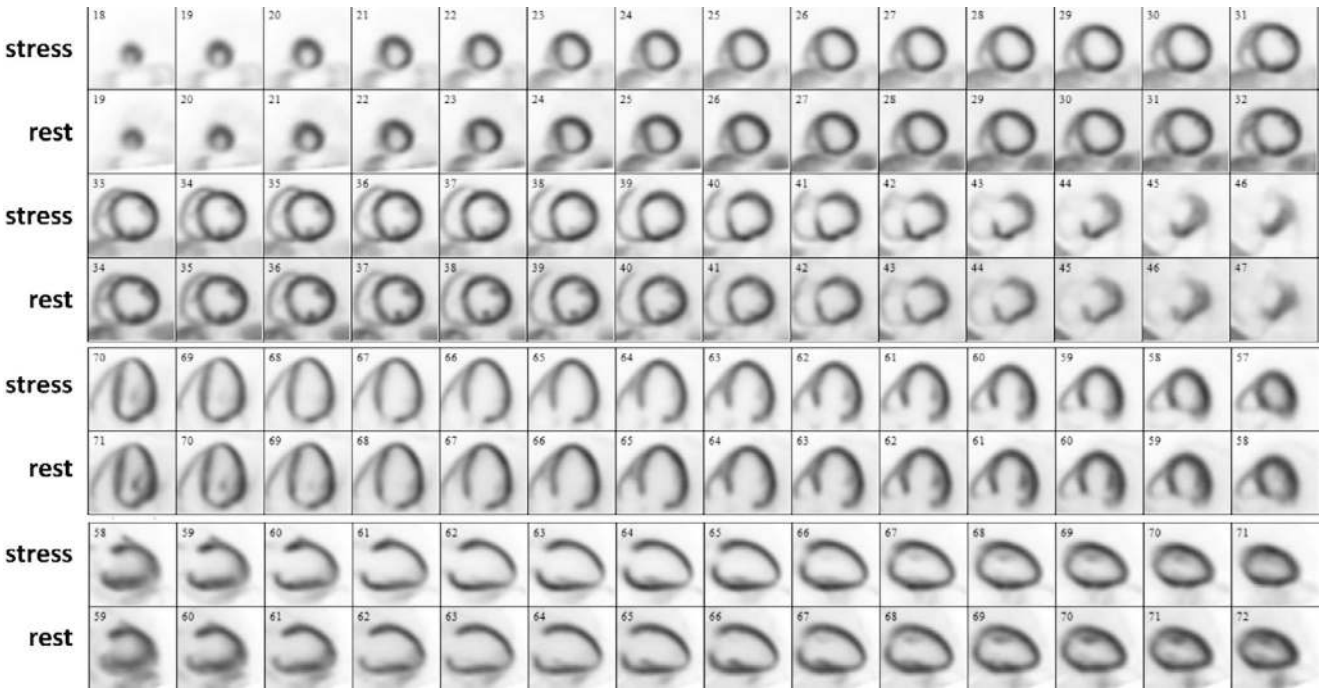


Fig. 5.9 Stress and rest adenosine ^{13}N-ammonia myocardial perfusion PET/CT images. There is severe LV dilatation and moderately increased RV tracer uptake on both the stress and rest images. There is mildly reduced tracer uptake in the septum on both stress and rest imaging, which is consistent with her LBBB. The fixed defect involving the LV apex is consistent with apical thinning and resulting partial volume effect

Table 5.2 Summary of the quantitative blood flow data demonstrating a moderate reduction in stress myocardial blood flow (normal value >1.8 mL/min/g) and myocardial flow reserve (normal value >2.0) in all coronary artery territories and globally

	MBF rest (ml/min/g)	MBF stress (ml/min/g)	MFR (stress/rest)
LAD	0.92	1.56	1.69
LCX	0.87	1.57	1.80
RCA	0.89	1.54	1.73
Global LV	0.89	1.55	1.74

uptake on the rest and stress images. The myocardial perfusion images demonstrate no evidence of regional perfusion defects.
- The maximal stress myocardial blood flow and myocardial flow reserve are moderately reduced both regionally and globally.
- The ECG-gated images demonstrated a rest LVEF of 15% increasing to 20% post stress with severely dilated LV volumes. There was paradoxical septal motion consistent with a LBBB on her rest ECG.

Imaging Diagnosis
- Nonischemic cardiomyopathy with coronary microvascular dysfunction.

Differential Diagnosis
- Severe obstructive multivessel coronary artery disease.

Correlative imaging
- None.

Management
- Invasive coronary angiography demonstrated normal coronary arteries.
- Medical therapy for heart failure and management of ventricular arrhythmias.

Further Reading

- Majmudar M, Murthy V, Shah R, Kolli S, Mousavi N, Foster C, et al. Quantification of coronary flow reserve in patients with ischaemic and non-ischaemic cardiomyopathy and its association with clinical outcomes. European Heart Journal—Cardiovascular Imaging. 2015;16:900–909.
- Neglia D, Michelassi C, Trivieri M, Sambuceti G, Giorgetti A, Pratali L, et al. Prognostic Role of Myocardial Blood Flow Impairment in Idiopathic Left Ventricular Dysfunction. Circulation. 2002;105(2): 186–193.
- Taqueti V, Di Carli M. Coronary Microvascular Disease Pathogenic Mechanisms and Therapeutic Options: JACC State-of-the-Art Review. Journal of the American College of Cardiology. 2018;72(21):2625–2641.

5.7 Incremental Value of Stress Testing to Differentiate Ischemic vs. Nonischemic CM in a Patient with CAD: Case 45

Key Points
- Stress nuclear imaging can be useful to differentiate ischemic from nonischemic or mixed cardiomyopathies.
- LV dysfunction and severe LV dilation disproportionate to the degree of obstructive coronary artery disease suggest a mixed pathogenetic mechanism.
- In cases with severe LV dilation where a combined pathogenesis of severe LV dysfunction is suspected, patients may not benefit from revascularization.

History
- A 73-year-old man with a history of hypertension, dyslipidemia, and type 2 diabetes mellitus presented to the emergency department after 3 h of severe retrosternal chest pain.
- On arrival, the ECG revealed an inferior ST-elevated myocardial infarction (STEMI), and he was given thrombolysis with tenecteplase.
- Due to only partial resolution of the ST elevation and continuing chest pain, he was referred for invasive coronary angiography (Figs. 5.10 and 5.11).

He was referred for PET/CT to assess myocardial ischemia and viability.

PET/CT Images

Imaging Diagnosis
- Viable myocardium throughout with no evidence of inducible ischemia.
- Dilated cardiomyopathy.

Differential Diagnosis
- Mixed ischemic and nonischemic cardiomyopathy.

Correlative Imaging
- Transthoracic echocardiogram showed an enlarged heart (ESLVD: 6.8 cm), global LV hypokinesis with akinesis of the inferior wall, and an estimated LVEF of 20%.

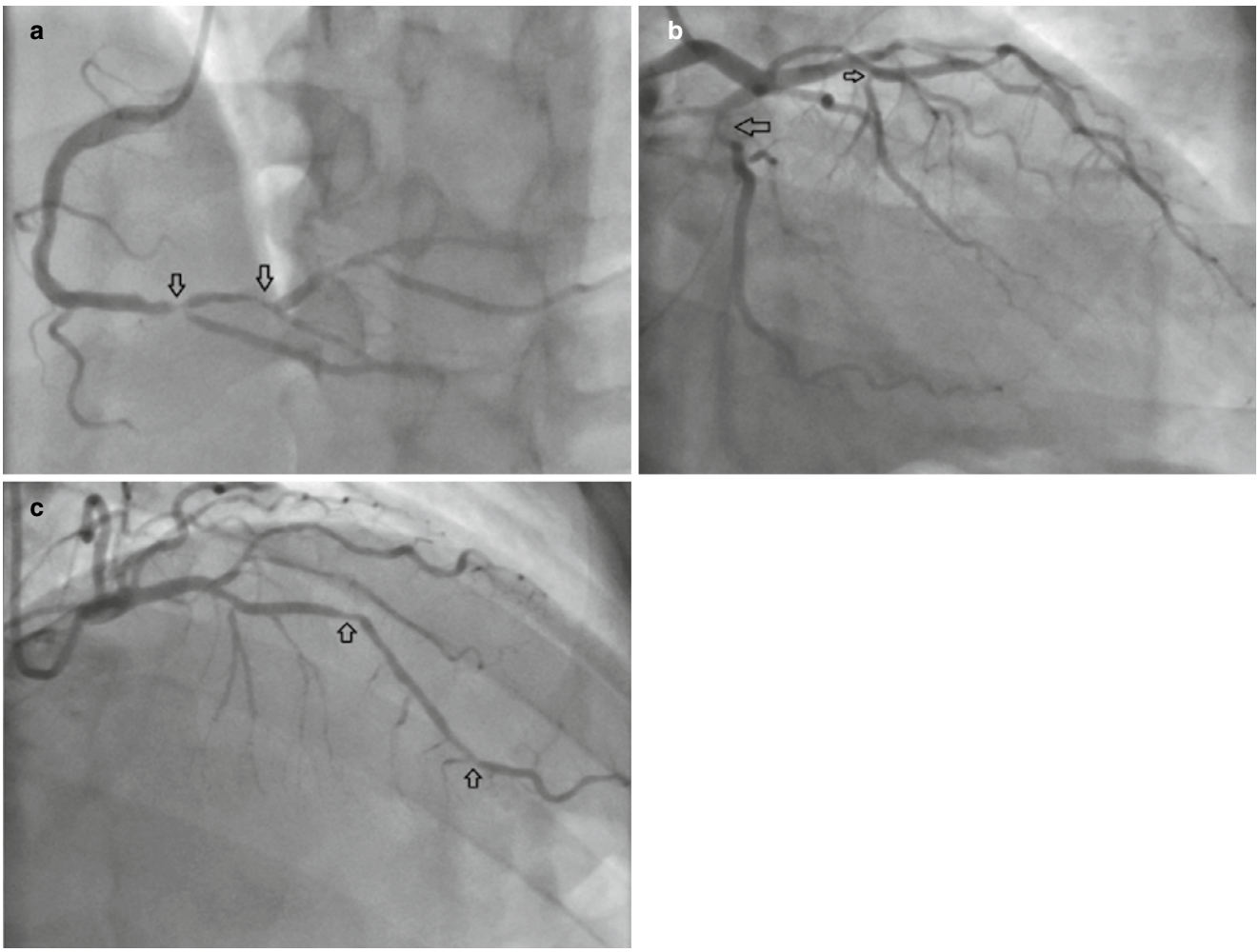


Fig. 5.10 Selective views of the right and left coronary arteries showing moderate to severe triple-vessel coronary artery disease (A-C), with diffuse narrowing of the mid to distal LAD (panel C)

Management

- The patient was managed with optimal medical therapy per current guidelines on treatment of heart failure with reduced ejection fraction, and antianginal and lipid lowering therapies.

Further Reading

- Singh P, Bhatt B, Pawar SU, Kamra A, Shetye S, Ghorpade M. Role of Myocardial Perfusion Study in Differentiating Ischemic versus Nonischemic Cardiomyopathy Using Quantitative Parameters. Indian J Nucl Med. 2018 Jan-Mar;33(1):32–38.
- Parag Bawaskar, Nicholas Thomas, Khaled Ismail, Yugene Guo, Sanya Chhikara, Pal Satyajit Singh Athwal, Alison Ranum, Achal Jadhav, Abel Hooker Mendez, Ishan Nadkarni, Dominic Frerichs, Pratik Velangi, Tesfatsiyon Ergando, Hassan Akram, Adinan Kanda and Chetan Shenoy. Nonischemic or Dual Cardiomyopathy in Patients With Coronary Artery Disease. Circulation. 2024;149:807–821.
- Cleland JG, Calvert M, Freemantle N, Arrow Y, Ball SG, Bonser RS, Chattopadhyay S, Norell MS, Pennell DJ, Senior R. The Heart Failure Revascularisation Trial (HEART). Eur J Heart Fail. 2011 Feb;13(2):227–33.
- Petrie MC, Jhund PS, She L, et al. Ten-year outcomes after coronary artery bypass grafting according to age in patients with heart failure and left ventricular systolic dysfunction: an analysis of the extended follow-up of the STICH Trial (Surgical Treatment for Ischemic Heart Failure). Circulation 2016;134:1314–24.
- Lopes RD, Alexander KP, Stevens SR, et al. Initial invasive versus conservative management of stable ischemic heart disease patients with a history of heart failure or left ventricular dysfunction: insights from the ISCHEMIA trial. Circulation. 2020 Nov 3;142(18):1725–1735.

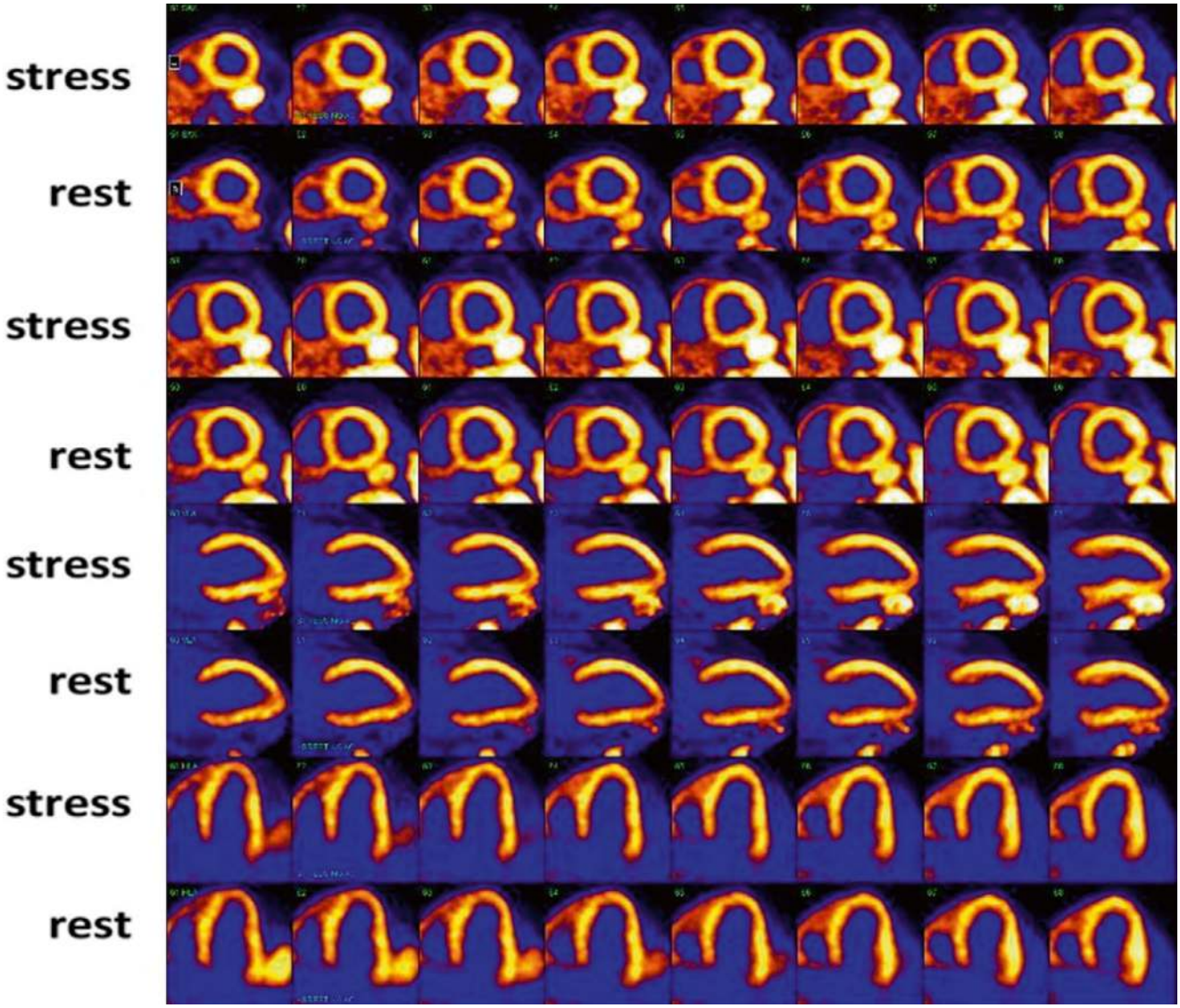


Fig. 5.11 Stress and rest ^{82}rubidium myocardial perfusion images showing homogeneous myocardial radiotracer uptake throughout the LV. There is severe LV dilation. Gated images showed an LV end-diastolic volume of 290 cc and an end-systolic volume of 238 cc, with a calculated LVEF of 18%

The opinions expressed in this chapter are those of the author(s) and do not necessarily reflect the views of the IAEA: International Atomic Energy Agency, its Board of Directors, or the countries they represent.

Open Access This chapter is licensed under the terms of the Creative Commons Attribution 3.0 IGO license (http://creativecommons.org/licenses/by/3.0/igo/), which permits use, sharing, adaptation, distribution and reproduction in any medium or format, as long as you give appropriate credit to the IAEA: International Atomic Energy Agency, provide a link to the Creative Commons license and indicate if changes were made.

Any dispute related to the use of the works of the IAEA: International Atomic Energy Agency that cannot be settled amicably shall be submitted to arbitration pursuant to the UNCITRAL rules. The use of the IAEA: International Atomic Energy Agency's name for any purpose other than for attribution, and the use of the IAEA: International Atomic Energy Agency's logo, shall be subject to a separate written license agreement between the IAEA: International Atomic Energy Agency and the user and is not authorized as part of this CC-IGO license. Note that the link provided above includes additional terms and conditions of the license.

The images or other third party material in this chapter are included in the chapter's Creative Commons license, unless indicated otherwise in a credit line to the material. If material is not included in the chapter's Creative Commons license and your intended use is not permitted by statutory regulation or exceeds the permitted use, you will need to obtain permission directly from the copyright holder.



Heart Transplantation

6

Marcelo Di Carli, Paolo Raggi, Michelle Williams, Raffaele Giubbini, Diana Paez, and Maurizio Dondi

Objectives

- To recognize normal positron emission tomography (PET) imaging appearances after heart transplantation.
- To learn how to integrate myocardial perfusion imaging, left ventricular (LV) function and quantitative blood flow to ascertain the presence of coronary allograft vasculopathy (CAV).

Heart transplantation is a life-saving procedure for patients with end-stage heart failure, offering them a chance for improved quality of life and survival. However, posttransplant care involves meticulous monitoring to ensure the health and function of the transplanted heart. One of the critical aspects of this monitoring is the evaluation for coronary allograft vasculopathy (CAV), a form of chronic rejection that affects the coronary arteries of the transplanted heart. This chapter provides an in-depth look at the normal positron emission tomography (PET) imaging appearances after heart transplantation and the methods to integrate myocardial perfusion imaging, left ventricular (LV) function, and quantitative blood flow to detect and assess the severity of CAV.

6.1 Evaluation of Possible Coronary Allograft Vasculopathy (CAV)

6.1.1 Without CAV: Case 46

Key Points

- Posttransplant surveillance for coronary allograft vasculopathy (CAV) and risk stratification guide clinical care decisions such as immunotherapy, revascularization for focal disease, and re-transplantation in selected patients with associated graft dysfunction.
- PET myocardial perfusion imaging with quantitative myocardial bood flow (MBF) is one of the most accurate noninvasive techniques to monitor for CAV and one of the safest alternatives to coronary angiography in the setting of renal dysfunction—a frequent complication of immunosuppressive therapy posttransplant.
- The most recent International Society for Heart and Lung Transplantation incorporated a new class IIa recommendation for PET MBF quantification and perfusion imaging for noninvasive detection of CAV and for providing prognostic information.

History

- A 37-year-old woman with a history of end-stage arrhythmogenic right ventricle (RV) cardiomyopathy underwent cardiac transplantation 2 years prior to the current examination.
- She has tacrolimus-induced chronic kidney impairment (glomerular filtration rate: 15 mL/min).

All authors have no conflict of interest to disclose.

M. Di Carli
Brigham and Women's Hospital, Boston, MA, USA
e-mail: mdicarli@bwh.harvard.edu

P. Raggi
Division of Cardiology, University of Alberta, Edmonton, AB, Canada

M. Williams
British Heart Foundation Centre for Research Excellence, Institute for Neuroscience and Cardiovascular Research, University of Edinburgh, Edinburgh, United Kingdom
e-mail: michelle.williams@ed.ac.uk

R. Giubbini
Nuclear Medicine, International Specialized Hospital of Uganda (ISHU), Kampala, Uganda
e-mail: raffaele.giubbini@unibs.it

D. Paez · M. Dondi (✉)
Division of Human Health, International Atomic Energy Agency, Vienna, Austria
e-mail: d.paez@iaea.org; m.dondi@iaea.org

© The Author(s) 2027
M. Di Carli et al. (eds.), *IAEA Atlas of Cardiac PET/CT*, https://doi.org/10.1007/978-3-662-74188-7_6

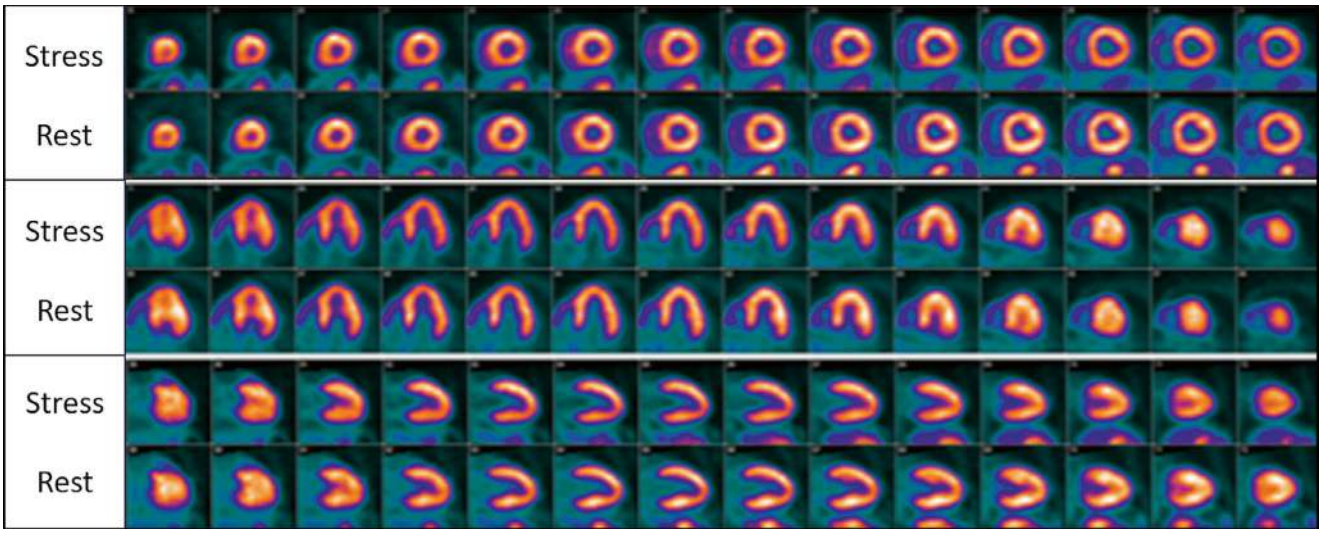


Fig. 6.1 Regadenoson stress and rest ^{82}rubidium myocardial perfusion PET study. There is normal myocardial perfusion on the rest and stress images

Table 6.1 Summary of the quantitative blood flow data demonstrating normal values of stress and rest MBF and MFR

	MBF rest (ml/min/g)	MBF stress (ml/min/g)	MFR (stress/rest)
LAD	1.10	2.67	2.42
LCX	1.19	2.26	1.90
RCA	1.09	2.44	2.13
Global LV	1.12	2.44	2.17

- A recent endomyocardial biopsy demonstrated no evidence of allograft rejection.
- She was referred for a PET myocardial perfusion study (Fig. 6.1) for routine surveillance of cardiac allograft vasculopathy.

PET/CT Images

Findings

- Normal LV size.
- There is no evidence of regional perfusion defects on the stress or rest images.
- Preserved stress myocardial bood flow (MBF) and myocardial flow reserve (MFR) (Table 6.1).
- Rest LVEF: 68% with normal LV volumes. Peak-stress LVEF increased to 74%. Normal regional and global LV wall motion and thickening.

Imaging Diagnosis

- No evidence of cardiac allograft vasculopathy.

Correlative Imaging

- None.

Differential Diagnosis

- None.

Management

- Continue current immunosuppressive regimen and risk factor management.

Further Reading

- Ajluni SC, Jr., Mously H, Chami T, Hajjari J, Stout A, Zacharias M et al. Non-invasive Imaging in the Evaluation of Cardiac Allograft Vasculopathy in Heart Transplantation: A Systematic Review. Curr Probl Cardiol 2022;47:101103.
- Bravo PE, Bergmark BA, Vita T, Taqueti VR, Gupta A, Seidelmann S et al. Diagnostic and prognostic value of myocardial blood flow quantification as non-invasive indicator of cardiac allograft vasculopathy. Eur Heart J 2018;39:316–23.
- Abadie BQ, Chan N, Sharalaya Z, Bhat P, Harb S, Jacob M et al. Negative Predictive Value and Prognostic Associations of Rb-82 PET/CT with Myocardial Blood Flow in CAV. JACC Heart Fail 2022;11:555–65.
- Chih S, Chong AY, Erthal F, deKemp RA, Davies RA, Stadnick E et al. PET Assessment of Epicardial Intimal Disease and Microvascular Dysfunction in Cardiac Allograft Vasculopathy. J Am Coll Cardiol 2018;71:1444–56.

6.2 Mild CAV: Case 47

Key Points

- Quantitative MBF and MFR increase the sensitivity of PET myocardial perfusion imaging to detect coronary allograft vasculopathy (CAV).
- It is important to examine both regional and global MBF. In this case, stress MBF and MFR are markedly reduced compared to the other vascular territories. This regional difference should raise the suspicion of obstructive coronary artery disease.

History

- A 67-year-old man with a history of heart transplantation 17 years prior to the current visit.
- Referred for evaluation of cardiac allograft vasculopathy for a recent presyncopal episode. He has controlled hypertension.
- He underwent PET/CT myocardial perfusion imaging (Fig. 6.2).

PET/CT Images (Table 6.2)

Findings

- The ^{13}N-ammonia PET myocardial perfusion scan demonstrates normal regional myocardial perfusion without definitive defects.
- The ECG-gated images demonstrated an LVEF of 64% at rest that increased to 67% with normal LV volumes.
- The stress myocardial blood flow and flow reserve are markedly reduced in the left anterior descending artery (LAD) coronary artery territory and normal in the left circumflex artery (LCX) and right coronary artery (RCA) territories.

Table 6.2 Summary of the quantitative blood flow data demonstrating a severe reduction in stress myocardial blood flow (normal value >1.8 mL/min/g) in the LAD territory with normal stress flow in flow reserve in the LCX and RCA territories (normal value >2.0)

	MBF rest (ml/min/g)	MBF stress (ml/min/g)	MFR (stress/rest)
LAD	**1.05**	**1.48**	**1.40**
LCX	**0.89**	2.22	**2.49**
RCA	**0.96**	1.99	**2.08**
Global LV	**0.98**	1.75	**1.79**

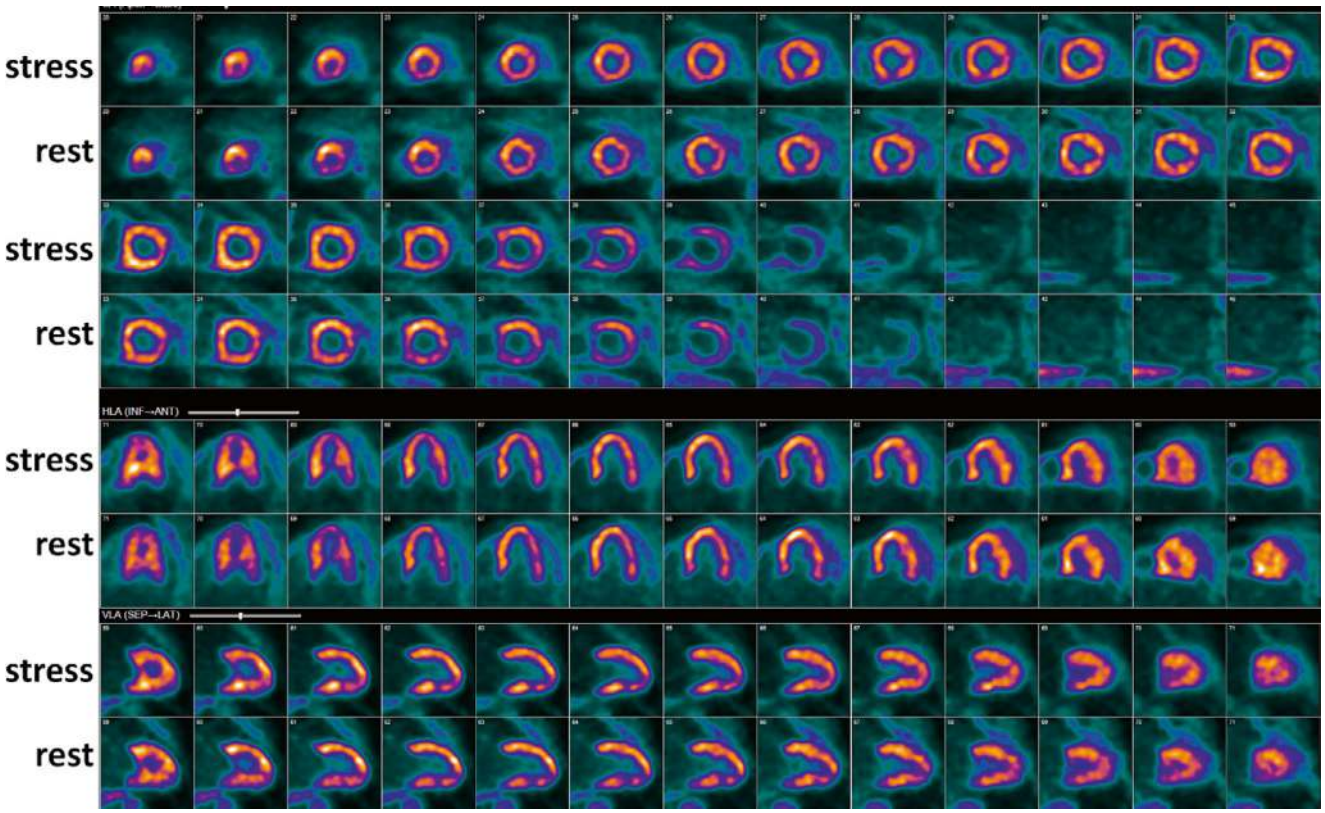


Fig. 6.2 Stress/rest ^{13} N-ammonia PET myocardial perfusion images. There is evidence of apical thinning, but overall, the images demonstrate normal myocardial perfusion without definitive regional defects. The electrocardiogram (ECG)-gated images demonstrated an LVEF of 64% at rest that increased to 67% with normal LV volumes

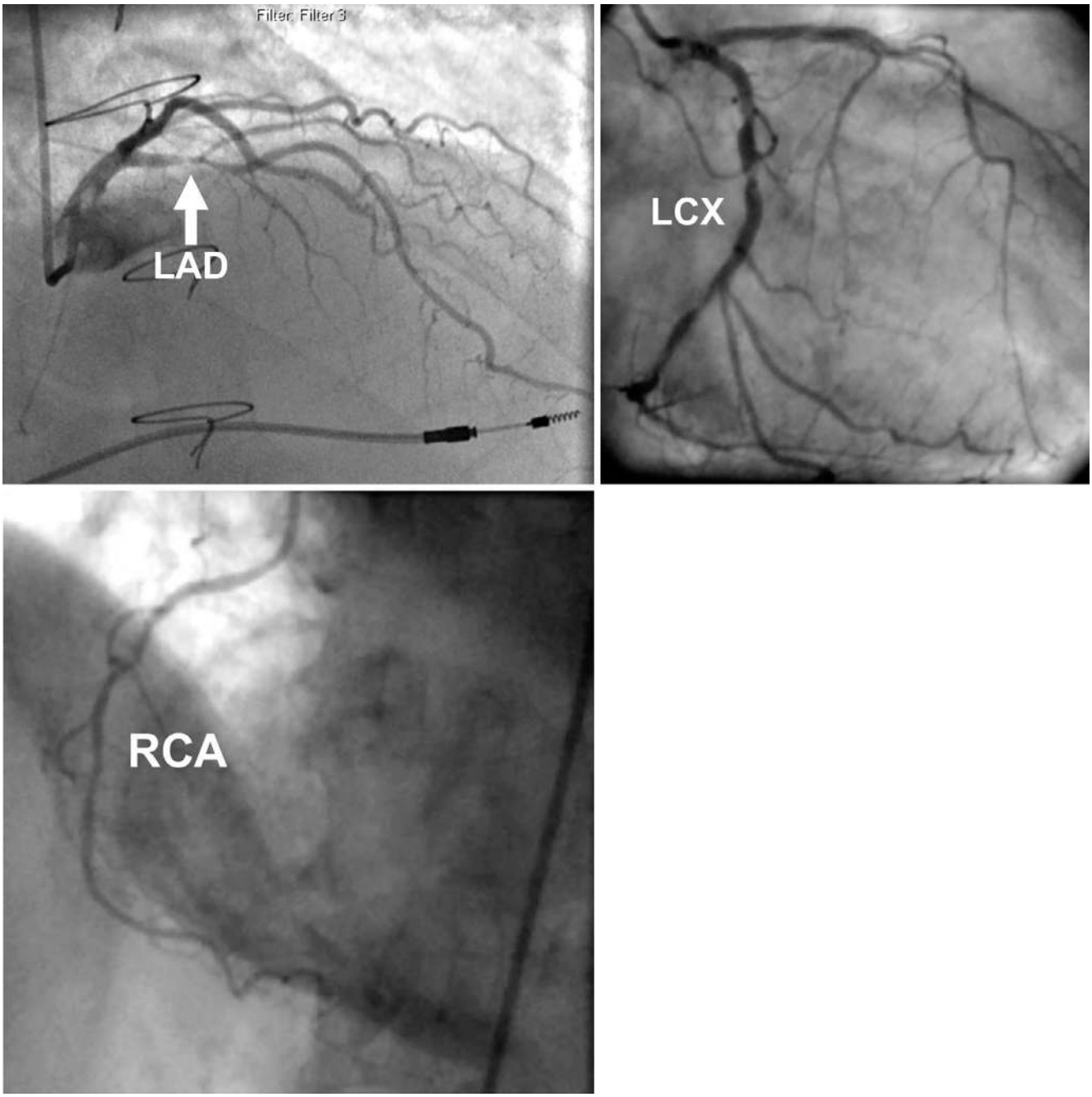


Fig. 6.3 Selective invasive coronary angiographic views demonstrating a severe stenosis in the proximal LAD coronary artery (arrow). There is mild diffuse allograft vasculopathy in the LCX and RCA arteries

Imaging Diagnosis
- Flow-limiting CAV in the LAD territory.

Differential Diagnosis
- None.

Correlative Imaging
- Invasive coronary angiography (Fig. 6.3).

Management
- The patient was referred to invasive coronary angiography which confirmed a severe stenosis in the proximal LAD coronary artery, which was subsequently stented.

Further Reading
- Driessen R, Danad I, Stuijfzand W, Raijmakers P, Schumacher S, van Diemen P, et al. Comparison of

Coronary Computed Tomography Angiography, Fractional Flow Reserve, and Perfusion Imaging for Ischemia Diagnosis. Journal of the American College of Cardiology. 2019;73:161–173.
- Ziadi M, deKemp R, Williams K, Guo A, Renaud J, Chow B, et al. Does quantification of myocardial flow reserve using rubidium-82 positron emission tomography facilitate detection of multivessel coronary artery disease?. Journal of Nuclear Cardiology. 2012;19:670–680.
- Naya M, Murthy V, Taqueti V, Foster C, Klein J, Garber M, et al. Preserved Coronary Flow Reserve Effectively Excludes High-Risk Coronary Artery Disease on Angiography. Journal of Nuclear Medicine. 2014;55:248–255.

6.3 Severe CAV: Case 48

Key Points
- Quantitative PET is a useful alternative to invasive coronary angiography to delineate the presence of CAV, especially in patients with renal dysfunction.
- The presence of RV tracer uptake is common in heart transplantation recipients due to their restrictive physiology and increased pulmonary vascular resistance.
- The relatively normal flow reserve in the LCX territory is caused by a very low rest flow in this patient with a prior infarction in this area.

History
- A 51-year-old man with prior orthotopic heart transplantation 14 years prior for severe idiopathic dilated cardiomyopathy. He had diabetes mellitus and end-stage kidney disease on hemodialysis for the past 12 years. He was an active smoker.
- A recent transthoracic echocardiogram demonstrated a new wall motion abnormality in the anterior wall.
- Because of unresponsiveness to vasodilator stress on a prior study, he was referred for dobutamine-stress ^{82}Rb PET/CT to assess for CAV (Fig. 6.4).

PET/CT Images (Table 6.3)

Findings
- Transient ischemic dilation (TID) of the left ventricle during stress.
- Increased uptake of the RV free wall on both stress and rest images.
- A large-sized perfusion defect of severe intensity involving the anterolateral and anterior walls, and the LV apex, showing complete reversibility.
- Small-sized perfusion defect of moderate intensity in the mid lateral wall with minimal reversibility.
- Normal LV systolic function with a rest LVEF of 53% with normal LV volumes which increased to 56% during stress.
- MFR is reduced in the LAD. The relatively preserved MFR in the LCX territory is due to the presence of a prior scar in this area. Stress MBF and MFR were normal in the RCA territory.

Imaging Diagnosis
- Grade 3 cardiac allograft vasculopathy.

Differential Diagnosis
- None.

Correlative Imaging
- Invasive coronary angiography (Fig. 6.5).

Management
- Patient was referred for revascularization of the LAD and LCX coronary arteries.

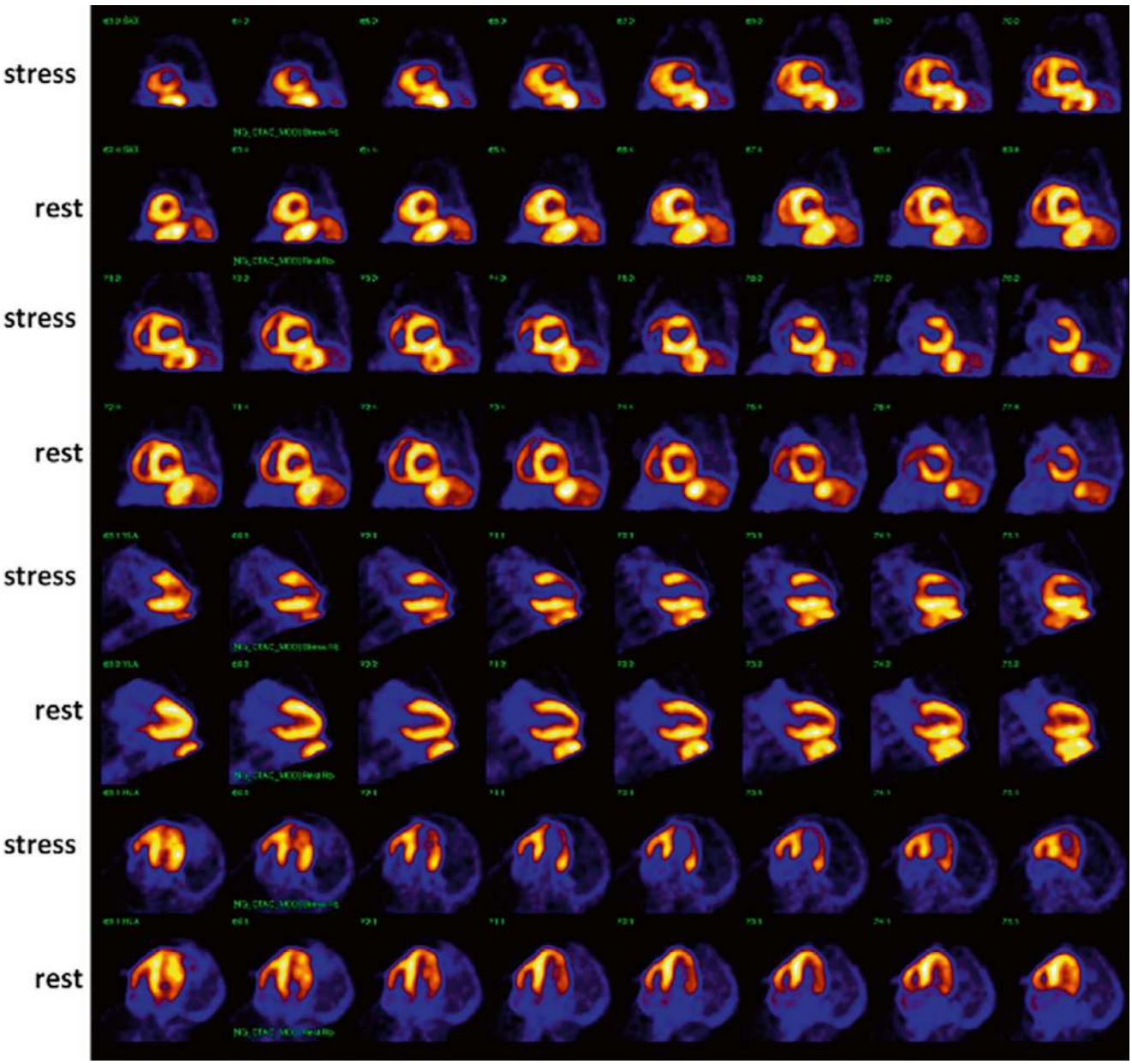


Fig. 6.4 Dobutamine stress and rest ^{82}Rb myocardial perfusion PET images. There is transient ischemic dilatation of the left ventricle during stress. There is increased tracer uptake of the RV free on both stress and rest images. The stress images show a large perfusion defect of severe intensity involving the mid and apical anterolateral and anterior walls, and the LV apex, showing complete reversibility. In addition, there is a small-sized perfusion defect of moderate intensity in the mid lateral wall with minimal reversibility

Table 6.3 Summary of quantitative flow data showing severely reduced stress flows in the LCX and LAD territories

	MBF rest (ml/min/g)	MBF stress (ml/min/g)	MFR (stress/rest)
LAD	0.97	1.36	1.40
LCX	0.58	1.31	2.25
RCA	1.02	2.48	2.43
Global LV	0.88	1.64	1.86

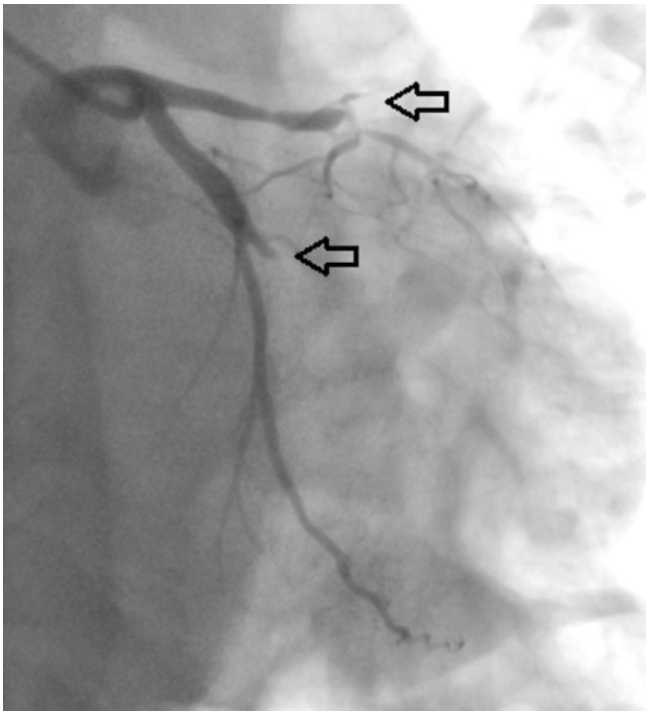


Fig. 6.5 Selective view from invasive coronary angiography showing complete occlusion of the mid LAD and proximal first obtuse marginal coronary artery

Further Reading

- Michael Weis and Wolfgang von Scheidt. Cardiac Allograft Vasculopathy. A Review. Circulation. 1997; 96:2069–2077.
- Mc Ardle B, Dowsley T, Cocker M, Ohira H, deKemp R, DaSilva J. et al. Cardiac PET: Metabolic and Functional Imaging of the Myocardium. Seminars in Nuclear Medicine. 2013;43:434–448.
- Bravo P, Bergmark B, Vita T, Taqueti V, Gupta A, Seidelmann S. et al. Diagnostic and prognostic value of myocardial blood flow quantification as non-invasive indicator of cardiac allograft vasculopathy. European Heart Journal. 2017;39:316–323.

The opinions expressed in this chapter are those of the author(s) and do not necessarily reflect the views of the IAEA: International Atomic Energy Agency, its Board of Directors, or the countries they represent.

Open Access This chapter is licensed under the terms of the Creative Commons Attribution 3.0 IGO license (http://creativecommons.org/licenses/by/3.0/igo/), which permits use, sharing, adaptation, distribution and reproduction in any medium or format, as long as you give appropriate credit to the IAEA: International Atomic Energy Agency, provide a link to the Creative Commons license and indicate if changes were made.

Any dispute related to the use of the works of the IAEA: International Atomic Energy Agency that cannot be settled amicably shall be submitted to arbitration pursuant to the UNCITRAL rules. The use of the IAEA: International Atomic Energy Agency's name for any purpose other than for attribution, and the use of the IAEA: International Atomic Energy Agency's logo, shall be subject to a separate written license agreement between the IAEA: International Atomic Energy Agency and the user and is not authorized as part of this CC-IGO license. Note that the link provided above includes additional terms and conditions of the license.

The images or other third party material in this chapter are included in the chapter's Creative Commons license, unless indicated otherwise in a credit line to the material. If material is not included in the chapter's Creative Commons license and your intended use is not permitted by statutory regulation or exceeds the permitted use, you will need to obtain permission directly from the copyright holder.



Inflammatory and Infiltrative Cardiomyopathies

7

Marcelo Di Carli, Raffaele Giubbini, Paolo Raggi, Michelle Williams, Diana Paez, Maurizio Dondi, and Sanjay Divakaran

Objectives

- To identify patterns of myocardial perfusion and inflammation to establish the likelihood of active cardiac sarcoidosis.
- To learn how to quantify the extent and severity of cardiac inflammation for risk stratification and to guide response to therapy.
- To identify the pattern of myocardial ischemia in patients with infiltrative cardiomyopathies and provide a list of differential diagnoses.

Sarcoidosis is a multisystem disorder that is characterized histologically by noncaseating, non-necrotic granulomas. Although it most commonly manifests in the lungs or with lymphadenopathy, it can affect any organ. Only 40–50% of patients with cardiac sarcoidosis (CS) diagnosed at autopsy had the diagnosis made during their lifetime.

Areas of active cardiac inflammation demonstrated increased glucose metabolism and therefore increased fluorodeoxyglucose (FDG) uptake on PET. On the contrary, myocardial perfusion imaging (MPI) (by single-photon emission computed tomography (SPECT) or positron emission tomography (PET) with perfusion tracers) can show areas of hypoperfusion due to inflammation and vascular compression due to edema or myocardial fibrosis and scar. Depending on the degree of active inflammation on FDG-PET and resting perfusion defects on MPI, the disease can be staged as no evidence of activity (no inflammation or scar); early stage (active inflammation with mild or no scar); progressive disease (active inflammation with moderate scar); or fibrous disease (minimal or no inflammation with severe scar).

The evaluation of myocardial uptake of ^{18}F-FDG PET in cardiac sarcoidosis is not simple as the metabolic utilization of glucose can be physiological, and ischemia may affect myocardial uptake. Therefore, adequate patient preparation aimed to suppress myocardial utilization is mandatory.

The presence of obstructive coronary disease and myocardial ischemia should be excluded by stress imaging, computed tomography (CT) angiography, or, when needed, invasive coronary angiography.

Evaluation of myocardial uptake requires an accurate quality control to exclude attenuation artifacts due to misalignment between PET and CT or presence of attenuators (devices, prosthetic valves, coronary calcification). Both attenuations corrected and uncorrected images should be considered. Semiquantitative measurements can be helpful in serial follow-up after appropriate treatment, as it is in other noncardiac localizations. Integrated PET/magnetic resonance (MR) or PET/CT and MR fusion imaging could be useful to increasing specificity of MR findings and for follow-up.

All authors have no conflict of interest to disclose.

M. Di Carli · S. Divakaran
Brigham and Women's Hospital, Boston, MA, USA
e-mail: mdicarli@bwh.harvard.edu; sdivakaran@bwh.harvard.edu

R. Giubbini
Nuclear Medicine, International Specialized Hospital of Uganda (ISHU), Kampala, Uganda
e-mail: raffaele.giubbini@unibs.it

P. Raggi
Division of Cardiology, University of Alberta, Edmonton, AB, Canada

M. Williams
British Heart Foundation Centre for Research Excellence, Institute for Neuroscience and Cardiovascular Research, University of Edinburgh, Edinburgh, United Kingdom
e-mail: michelle.williams@ed.ac.uk

D. Paez · M. Dondi (✉)
Division of Human Health, International Atomic Energy Agency, Vienna, Austria
e-mail: d.paez@iaea.org; m.dondi@iaea.org

© The Author(s) 2027
M. Di Carli et al. (eds.), *IAEA Atlas of Cardiac PET/CT*, https://doi.org/10.1007/978-3-662-74188-7_7

7.1 Cardiac Sarcoidosis: Likelihood

7.1.1 Low Probability of Cardiac Sarcoidosis: Case 49

Key Points

- Presence of late gadolinium enhancement on cardiac magnetic resonance imaging (MRI) with absence of metabolic activity on ^{18}F-FDG indicates a low probability of active cardiac sarcoidosis.

History

- A 61-year-old woman with a remote history of biopsy-proven pulmonary sarcoidosis was referred for ^{18}F-FDG cardiac PET due to new left bundle branch block (LBBB) on electrocardiogram (ECG) (Figs. 7.1 and 7.2).

PET/CT Images

Findings

- Rest myocardial perfusion images demonstrate no evidence of regional perfusion defects.
- There is adequate suppression of ^{18}F-FDG uptake in the normal myocardium. The ^{18}F-FDG images demonstrate no evidence of focal glucose uptake.
- The ECG-gated images demonstrated moderate left ventricle (LV) dysfunction with a rest left ventricle ejection fraction (LVEF) of 42% and mildly enlarged volumes and paradoxical septal motion consistent with LBBB.
- There is no evidence of metabolically active extracardiac sarcoidosis.

Imaging Diagnosis

- No evidence of active cardiac sarcoidosis.

Differential Diagnosis

- None.

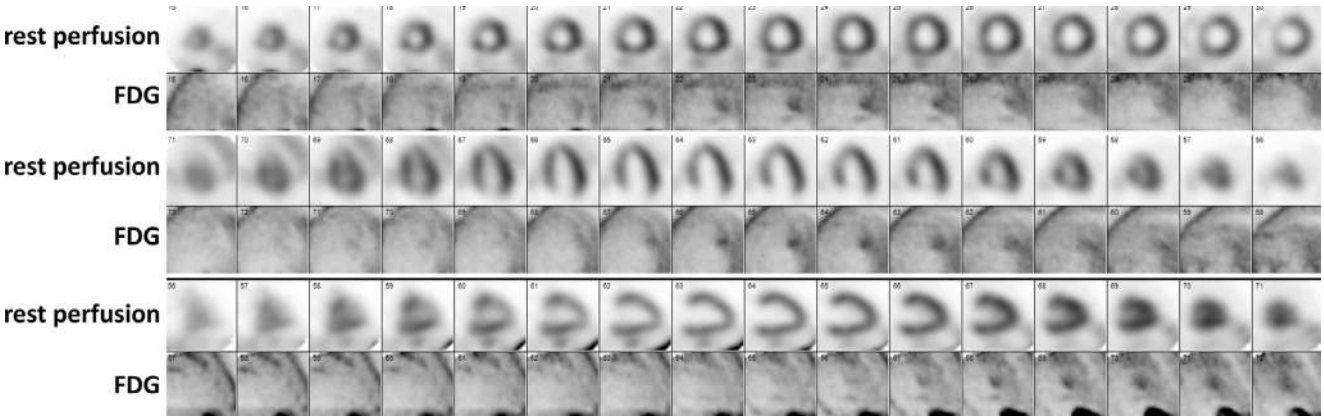


Fig. 7.1 Myocardial studies at rest with both ^{99m}Tc-sestamibi SPECT and ^{18}F-FDG PET/CT. There was no evidence of regional perfusion defects. There was adequate suppression of physiological ^{18}F-FDG uptake in the normal myocardium. The ^{18}F-FDG images demonstrate no evidence of focal glucose uptake in the heart

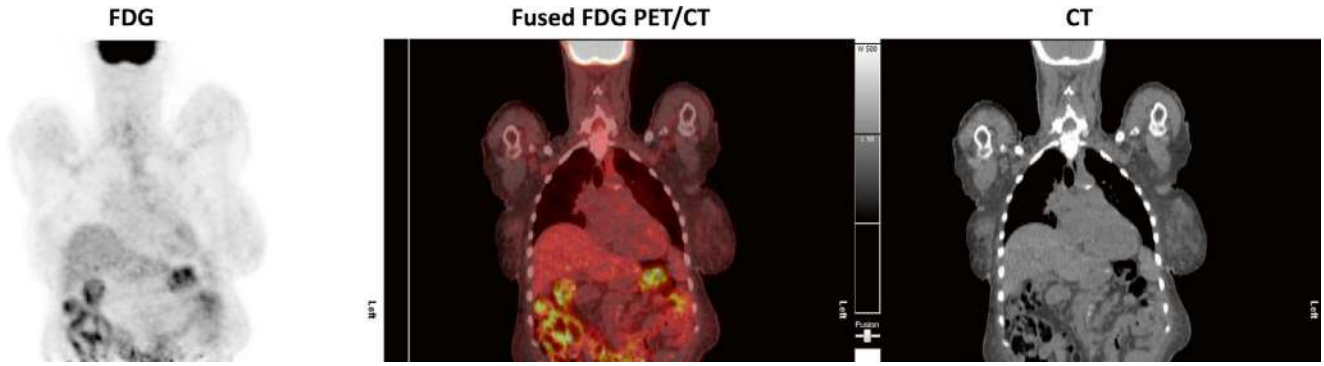


Fig. 7.2 Limited whole-body ^{18}F-FDG PET/CT images demonstrated no evidence of metabolically active extracardiac sarcoidosis

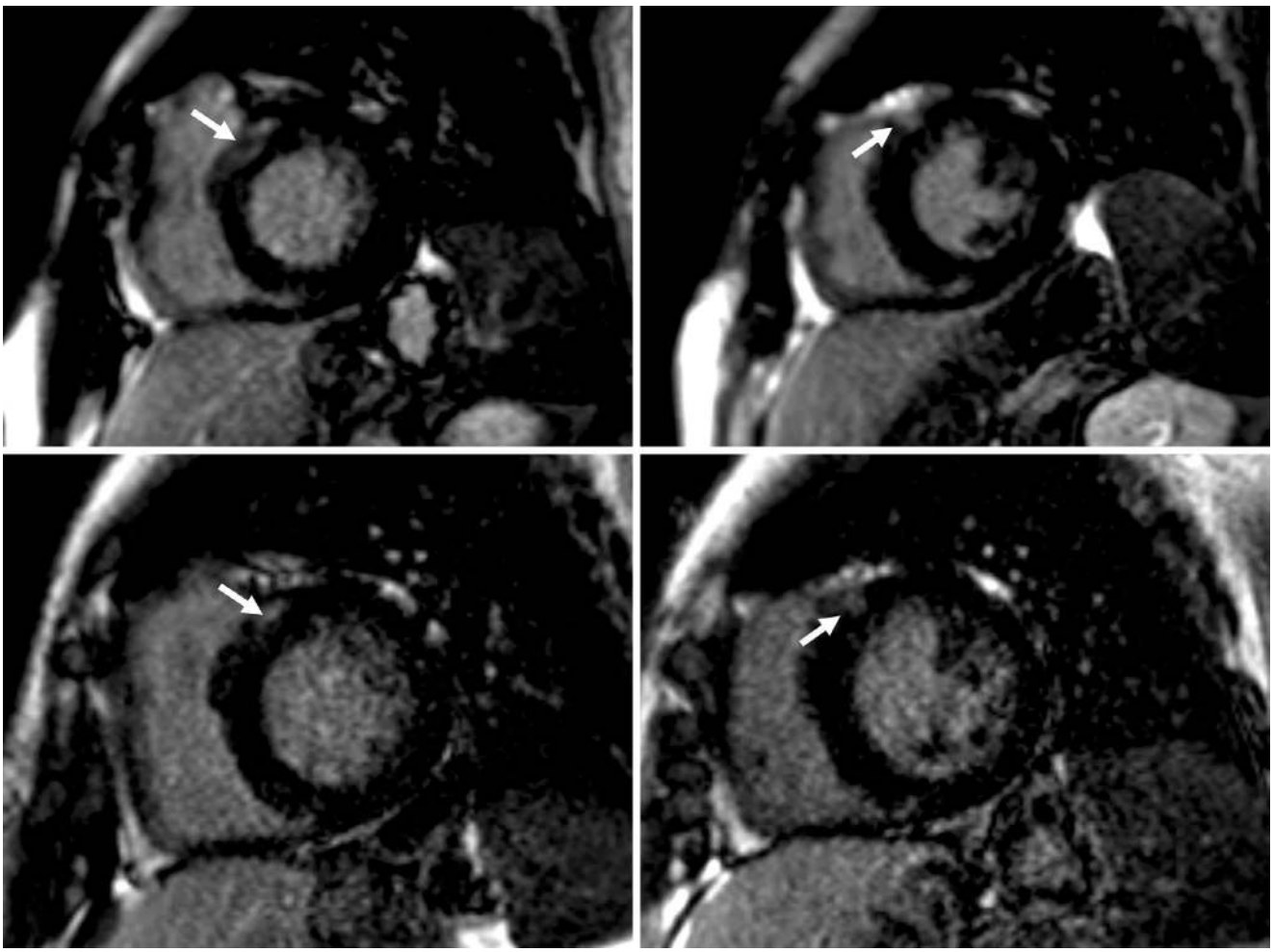


Fig. 7.3 Selective short-axis views of the contrast enhanced cardiac MRI demonstrate patchy subepicardial late gadolinium enhancement in the basal anteroseptum (arrows)

Correlative Imaging

- Cardiac MRI revealed patchy subepicardial late gadolinium enhancement in the basal anteroseptum (Fig. 7.3).
- The cine MRI images demonstrated a left ventricular ejection fraction of 35% with abnormal septal motion in keeping with the already known LBBB.

Management

- The cardiac sarcoidosis likelihood by cardiac MRI was deemed possible (10–50%) due to one focal area of late gadolinium enhancement.
- The absence of regional perfusion defects on ^{18}F-FDG is consistent with a PET likelihood of active cardiac sarcoidosis categorized as unlikely (<10%).
- Initiation of immunosuppressive therapy for the patient was deferred as the patient did not have evidence of active inflammation, even though there was some suspicion of cardiac involvement given the cardiac MRI findings.
- She underwent vasodilator stress myocardial perfusion imaging, which was normal, to explore ischemia as the cause of her LBBB.

Further Reading

- Vita T, et al. Complementary value of cardiac magnetic resonance imaging and positron emission tomography/computed tomography in the assessment of cardiac sarcoidosis. Circ Cardiovasc Imaging. 2018;11:e007030.
- Divakaran S, et al. Diagnostic accuracy of advanced imaging in cardiac sarcoidosis: an imaging-histologic correlation study in patients undergoing cardiac transplantation. Circ Cardiovasc Imaging. 2019 Jun;12(6):e008975.
- Chareonthaitawee P, et al. Joint SNMMI-ASNC Expert Consensus Document on the Role of 18F-FDG PET/CT in Cardiac Sarcoid Detection and Therapy Monitoring. J Nucl Med. 2017 Aug;58(8):1341–1353.

7.1.2 Possible Cardiac Sarcoidosis: Case 50

Key Points

- Diffuse ^{18}F-FDG uptake in a patient without evidence of extracardiac sarcoidosis is generally a nonspecific finding and in keeping with a low probability of active myocardial inflammation.
- The use of ^{18}F-FDG PET to detect inflammation may be limited in cases of severe heart failure and/or recurrent ventricular tachycardia due to preferential and physiologic glucose utilization by the myocardium despite adequate diet preparation.
- Severe diffuse isolated cardiac sarcoidosis in this patient is also less likely as LV function was normal.

History

- A 69-year-old man without obstructive coronary artery disease by angiography was referred for a cardiac PET to evaluate for cardiac sarcoidosis due to recurrent ventricular tachycardia (Figs. 7.4 and 7.5).

PET/CT Images

Findings

- There is no evidence of regional perfusion defects on the rest images.
- There is inadequate suppression of ^{18}F-FDG uptake in the heart. The ^{18}F-FDG images demonstrate diffuse myocardial glucose uptake.

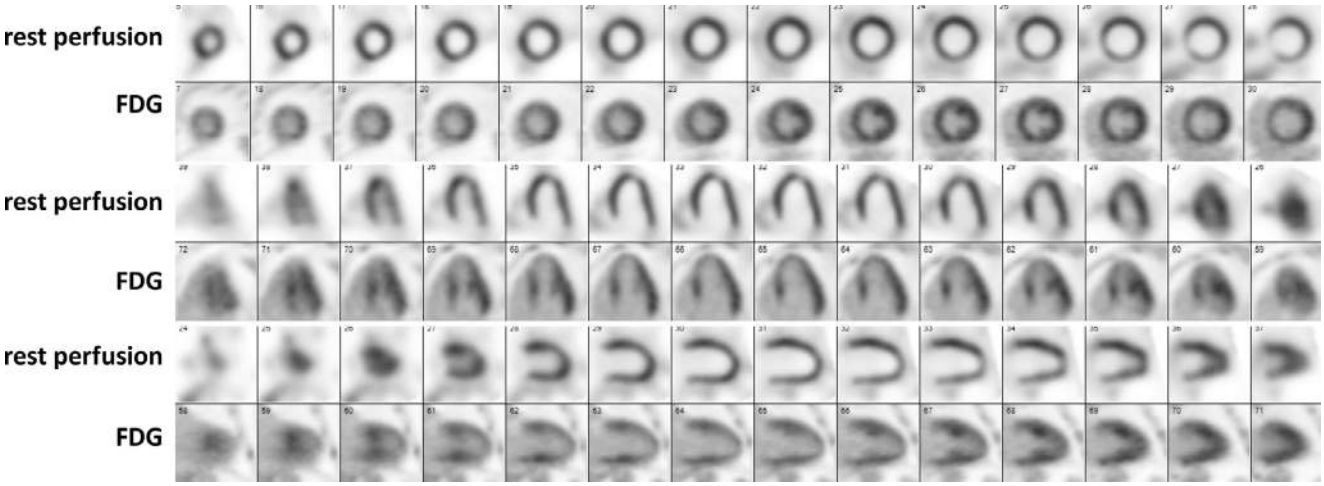


Fig. 7.4 Myocardial studies at rest with both ^{99m}Tc-sestamibi SPECT and ^{18}F-FDG PET/CT. There is no evidence of regional perfusion defects. There is inadequate suppression of ^{18}F-FDG uptake in the normal myocardium. The ^{18}F-FDG images demonstrate mild-moderate diffuse glucose uptake in the heart

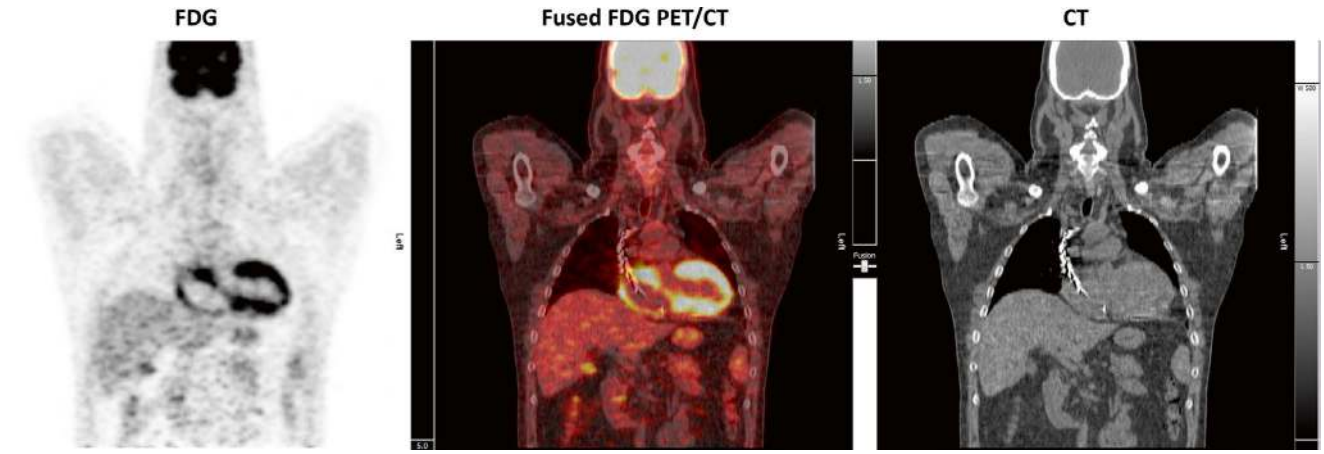


Fig. 7.5 Limited whole-body ^{18}F-FDG PET/CT images demonstrate no evidence of metabolically active extracardiac sarcoidosis

- The ECG-gated images demonstrated normal LV function with a rest LVEF of 57% with normal volumes and regional wall motion and thickening.
- The limited whole-body PET/CT images demonstrate no evidence of abnormal extracardiac ^{18}F-FDG uptake.

Imaging Diagnosis
- No evidence of active myocardial inflammation.

Differential Diagnosis
- Poor diet preparation.
- Heart failure and ventricular tachycardia resulting in myocardial glucose utilization despite adequate diet preparation.

Correlative Imaging
- None.

Management
- The patient underwent an electrophysiology study where three ventricular tachycardia morphologies were identified. Two were ablated, and one was not due to proximity to the conduction system. His ventricular tachycardia has remained controlled since then with antiarrhythmic drug therapy.
- ^{18}F-FDG PET likelihood of cardiac sarcoidosis is possible (10–50%) when there is a single perfusion defect without associated ^{18}F-FDG uptake OR no perfusion defects but nonspecific ^{18}F-FDG uptake (diffuse ^{18}F-FDG uptake of the left ventricular myocardium or focal ^{18}F-FDG uptake with signal intensity that is only mildly increased when compared with background/blood pool uptake), like in this case.

Further Reading

- Vita T, Okada D, Veillet-Chowdhury M, Bravo P, Mullins E, Hulten E, et al. Complementary Value of Cardiac Magnetic Resonance Imaging and Positron Emission Tomography/Computed Tomography in the Assessment of Cardiac Sarcoidosis. Circulation: Cardiovascular Imaging. 2018;11.
- Divakaran S, Stewart G, Lakdawala N, Padera R, Zhou W, Desai A, et al. Diagnostic Accuracy Of Advanced Imaging In Cardiac Sarcoidosis: An Imaging-Histologic Correlation Study In Patients Undergoing Cardiac Transplantation. Journal of the American College of Cardiology. 2019;73:934.
- Chareonthaitawee P, Beanlands R, Chen W, Dorbala S, Miller E, Murthy V, et al. Joint SNMMI–ASNC Expert Consensus Document on the Role of 18 F-FDG PET/CT in Cardiac Sarcoid Detection and Therapy Monitoring. Journal of Nuclear Medicine. 2017;58:1341–1353.

7.1.3 Probable Isolated Cardiac Sarcoidosis: Case 51

Key Points
- The pattern of multiple patchy perfusion defects not following a normal coronary distribution with evidence of ^{18}F-FDG uptake is characteristic of "probable" cardiac sarcoidosis.

History
- A 45-year-old man with a history of cardiac arrest one year prior with no coronary artery disease by invasive coronary angiography (Fig. 3.6) and implantation of an implantable cardioverter defribillator (ICD) for secondary prevention.
- He was referred for a PET/CT for evaluation for cardiac sarcoidosis due to a recent diagnosis of biopsy-proven reticuloendothelial sarcoidosis (Figs. 7.6, 7.7 and 7.8).

PET/CT Images

Findings
- Rest myocardial perfusion imaging revealed a medium-sized perfusion defect of severe intensity in the mid and basal inferior and the basal inferoseptal walls. In addition, there were patchy areas of perfusion deficit in the mid and apical anterior and anteroseptal walls.
- The cardiac ^{18}F-FDG images demonstrate predominantly matched reduction in perfusion and ^{18}F-FDG uptake except for the mid and basal anteroseptal wall that shows increased glucose uptake (perfusion-FDG mismatched defect).
- The ECG-gated images demonstrated severely reduced LV function with a rest LVEF of 35% with moderately enlarged volumes and severe global hypokinesis.
- The limited whole-body images demonstrated no evidence of abnormal extracardiac ^{18}F-FDG uptake.

Imaging Diagnosis
- Probable isolated cardiac sarcoidosis.

Differential Diagnosis
- Cardiac sarcoidosis.
- Myocarditis.
- Arrhythmogenic cardiomyopathy.
- Idiopathic dilated cardiomyopathy.

Management
- The patient was treated with prednisone for immunosuppression, but without improvement in his heart failure. He eventually underwent a successful heart transplantation. Explant histology confirmed the presence of cardiac sarcoidosis.

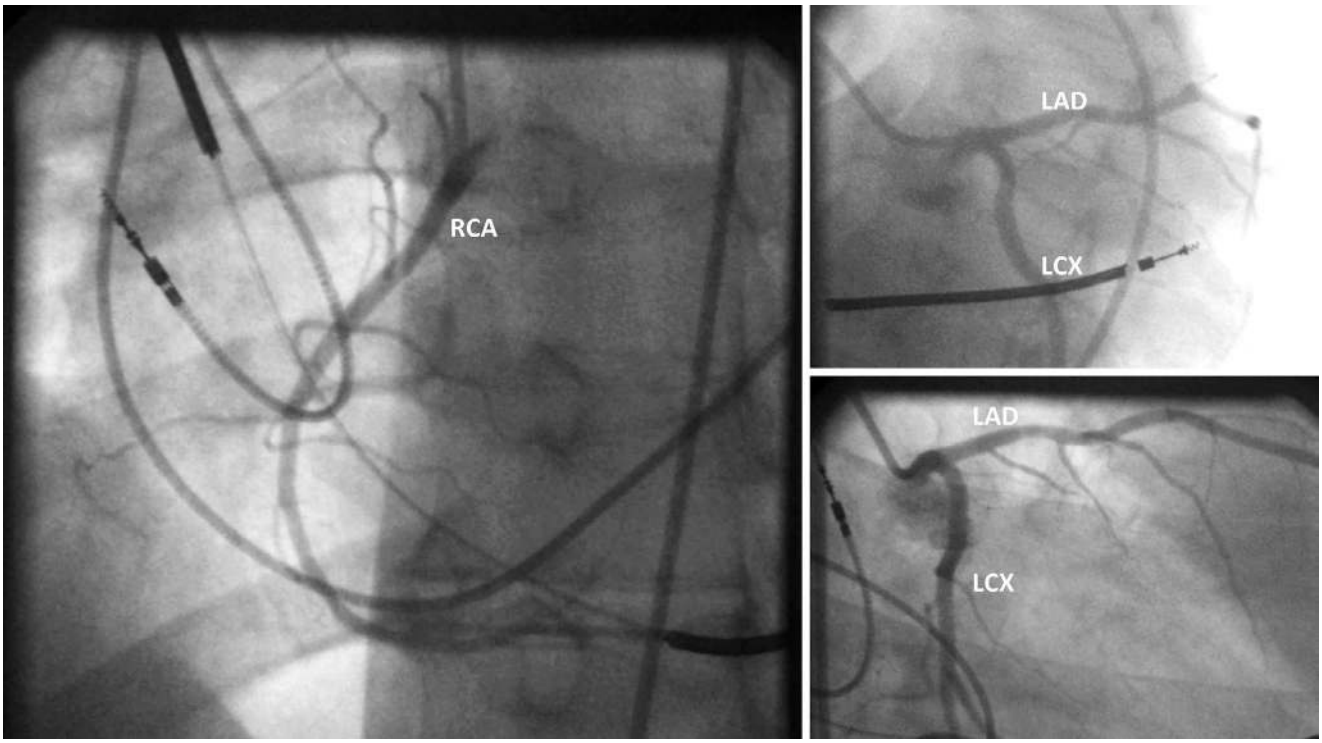


Fig. 7.6 Selective invasive coronary angiographic views demonstrating normal coronary arteries

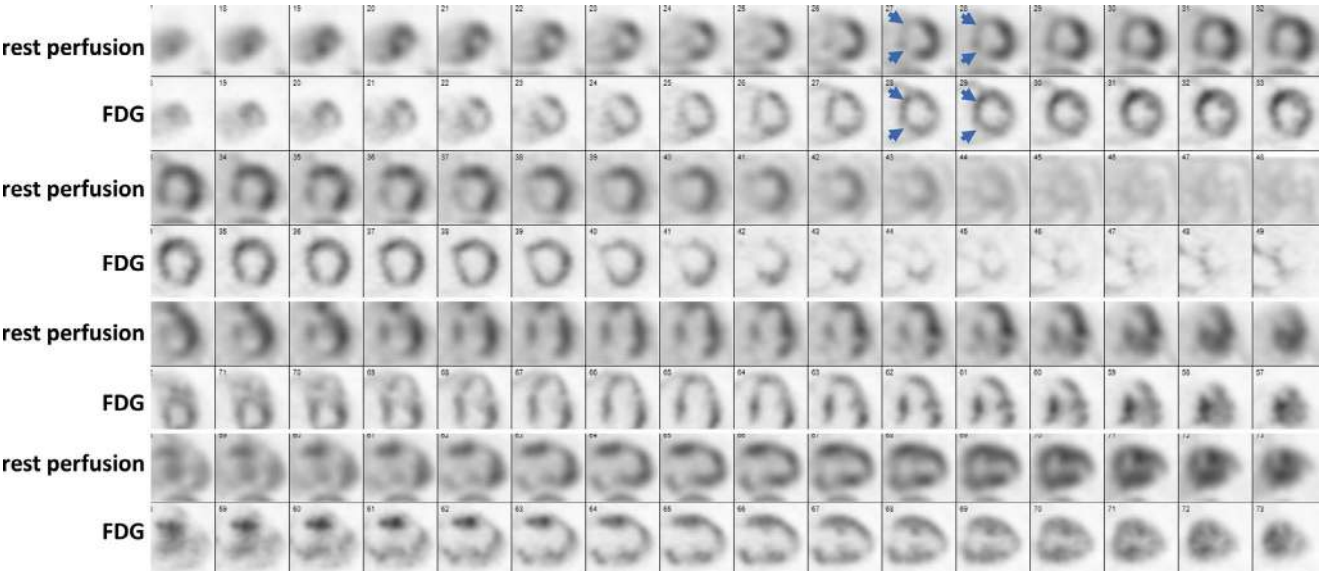


Fig. 7.7 Myocardial studies at rest with both ^{99m}Tc-sestamibi SPECT and ^{18}F-FDG PET/CT. The cardiac ^{18}F-FDG images demonstrate adequate suppression of glucose uptake. There is predominantly matched reduction in perfusion and FDG uptake except for the mid and basal anteroseptal wall that shows increased glucose uptake (perfusion-FDG mismatched defect, arrows)

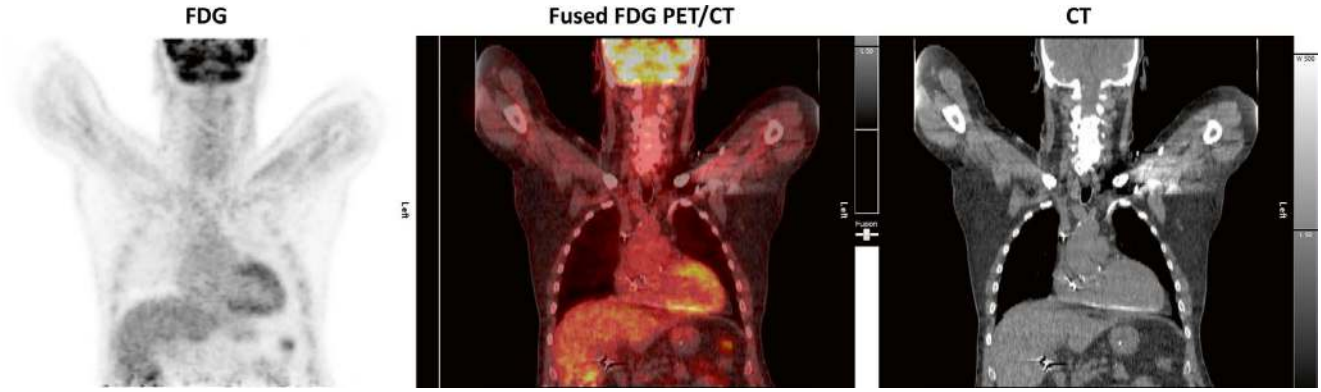


Fig. 7.8 Limited whole-body ^{18}F-FDG PET/CT images demonstrate no evidence of metabolically active extracardiac sarcoidosis

Further Reading

- Vita T, Okada D, Veillet-Chowdhury M, Bravo P, Mullins E, Hulten E, et al. Complementary Value of Cardiac Magnetic Resonance Imaging and Positron Emission Tomography/Computed Tomography in the Assessment of Cardiac Sarcoidosis. Circulation: Cardiovascular Imaging. 2018;11.
- Divakaran S, Stewart G, Lakdawala N, Padera R, Zhou W, Desai A, et al. Diagnostic Accuracy Of Advanced Imaging In Cardiac Sarcoidosis: An Imaging-Histologic Correlation Study In Patients Undergoing Cardiac Transplantation. Journal of the American College of Cardiology. 2019;73:934.

7.1.4 Highly Probable Cardiac Sarcoidosis: Case 52

Key Points

- ^{18}F-FDG PET likelihood of cardiac sarcoidosis is highly probably (>90%) when there are multiple, noncontiguous perfusion defects with associated ^{18}F-FDG uptake or multiple areas of focal ^{18}F-FDG uptake and extracardiac ^{18}F-FDG uptake is present.

History

- A 55-year-old man with a history of biopsy-proven extracardiac sarcoidosis and recent diagnosis of nonischemic cardiomyopathy was referred to evaluate for cardiac sarcoidosis.
- He underwent both rest ^{99m}Tc-sestamibi SPECT myocardial perfusion and ^{18}F-FDG PET/CT (Figs. 7.9 and 7.10).

SPECT and PET/CT Images

Findings

- There is a medium-sized and severe perfusion defect involving the mid and basal anteroseptal, inferoseptal, and inferior walls.
- The cardiac ^{18}F-FDG images show increased glucose uptake in almost all hypoperfused regions (perfusion-FDG mismatched defect).
- The limited whole-body PET/CT imaging shows multiple ^{18}F-FDG-avid bilateral mediastinal, hilar, and upper abdominal lymph nodes.

Imaging Diagnosis

- Active myocardial inflammation consistent with cardiac sarcoidosis.

Differential Diagnosis

- None.

Correlative Imaging

- Gross photograph of a four-chamber view of the explanted heart shows diffuse involvement of the myocardium by sarcoid. The right ventricle is extensively involved, as is the interventricular septum, with more patchy involvement of the left ventricle.

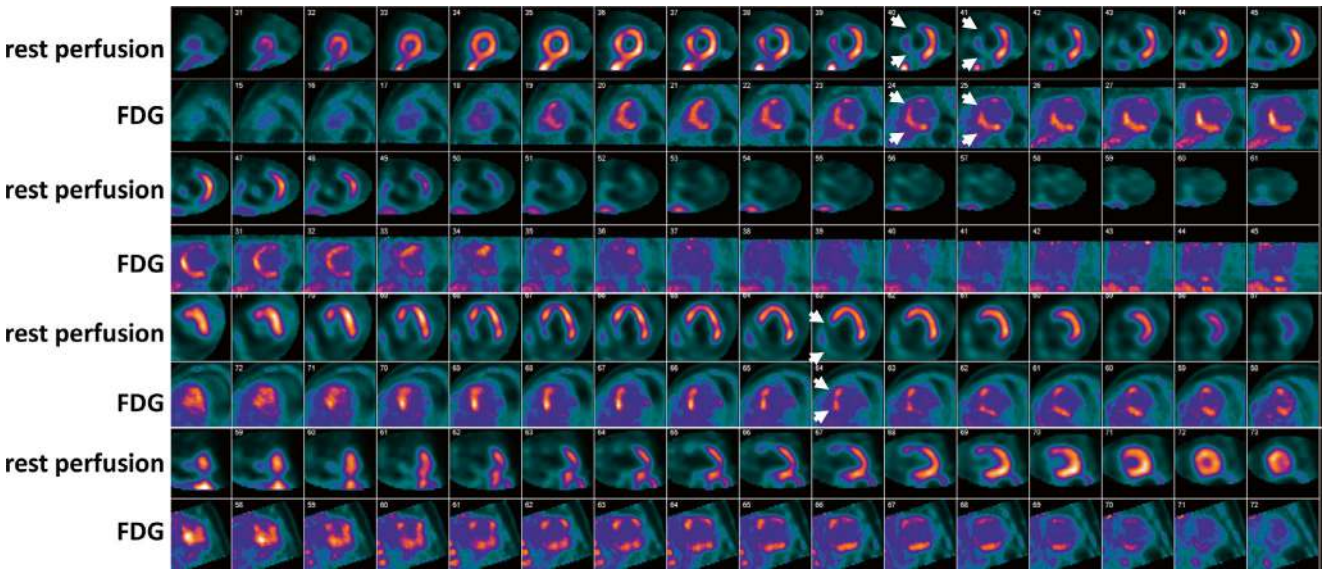


Fig. 7.9 Myocardial studies at rest with both ^{99m}Tc-sestamibi SPECT and ^{18}F-FDG PET/CT. There is a medium-sized and severe perfusion defect involving the mid and basal anteroseptal, inferoseptal, and inferior walls, with intense ^{18}F-FDG uptake (perfusion-FDG mismatched defect)

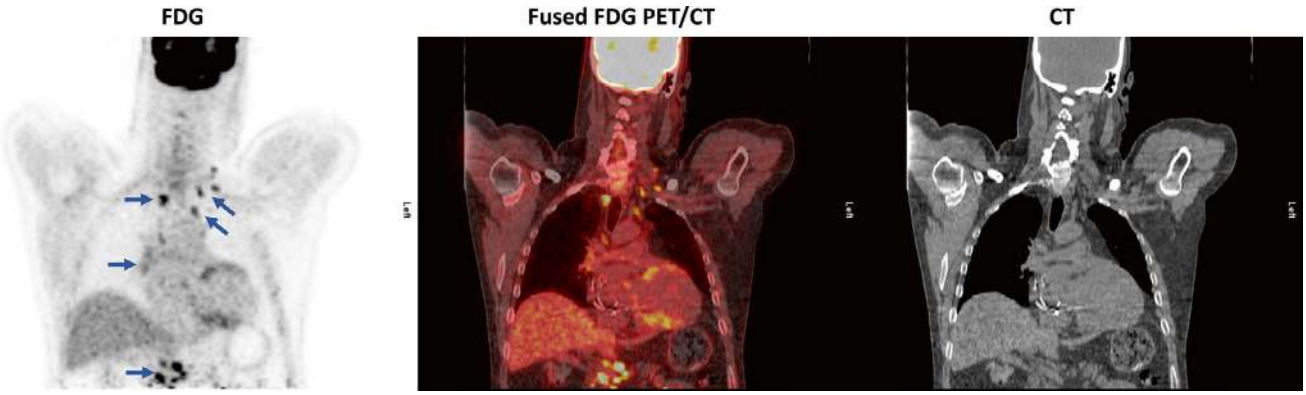


Fig. 7.10 Limited whole-body PET/CT imaging shows multiple ^{18}F-FDG-avid bilateral mediastinal, hilar, and upper abdominal lymph nodes (arrows)

- Photomicrograph of hematoxylin and eosin (H&E)-stained section showing myocardium with a non-necrotizing granuloma containing abundant giant cells. There is fibrosis and a lymphocytic infiltrate at the periphery of the granuloma (200x original magnification) (Fig. 7.11).

Management

- The patient eventually underwent left ventricular assist device placement and subsequent successful cardiac transplantation for end-stage sarcoid cardiomyopathy.

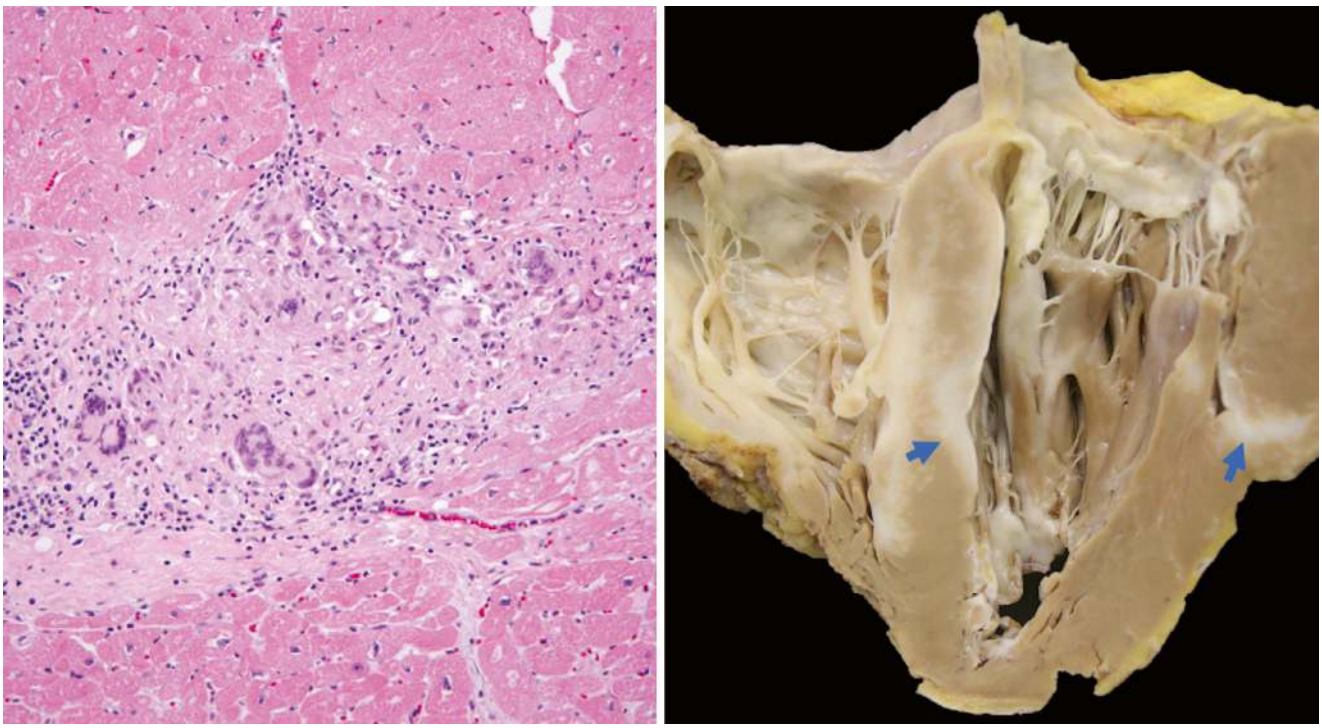


Fig. 7.11 *Right panel:* Gross photograph of a four-chamber view of the explanted heart shows diffuse involvement of the myocardium by sarcoidosis (arrows). The right ventricle is extensively involved, as is the interventricular septum, with more patchy involvement of the left ventricle. *Left panel:* Photomicrograph of hematoxylin and eosin (H&E)-stained section showing myocardium with a non-necrotizing granuloma containing abundant giant cells. There is fibrosis and a lymphocytic infiltrate at the periphery of the granuloma (200x original magnification)

Further Reading

- Vita T, Okada D, Veillet-Chowdhury M, Bravo P, Mullins E, Hulten E, et al. Complementary Value of Cardiac Magnetic Resonance Imaging and Positron Emission Tomography/Computed Tomography in the Assessment of Cardiac Sarcoidosis. Circulation: Cardiovascular Imaging. 2018;11.
- Divakaran S, Stewart G, Lakdawala N, Padera R, Zhou W, Desai A, et al. Diagnostic Accuracy Of Advanced Imaging In Cardiac Sarcoidosis: An Imaging-Histologic Correlation Study In Patients Undergoing Cardiac Transplantation. Journal of the American College of Cardiology. 2019;73:934.
- Chareonthaitawee P, Beanlands R, Chen W, Dorbala S, Miller E, Murthy V, et al. Joint SNMMI–ASNC Expert Consensus Document on the Role of 18 F-FDG PET/CT in Cardiac Sarcoid Detection and Therapy Monitoring. Journal of Nuclear Medicine. 2017;58:1341–1353.
- Images are reproduced with permission from Divakaran S, Stewart GC, Lakdawala NK, Padera RF, Zhou W, Desai AS, Givertz MM, Mehra MR, Kwong RY, Ghoshhajra BB, Taqueti VR, Skali H, Dorbala S, Blankstein R, Di Carli MF. Diagnostic accuracy of advanced imaging in cardiac sarcoidosis: an imaging-histologic correlation study in patients undergoing cardiac transplantation. Circ Cardiovasc Imaging. 2019 Jun;12(6):e008975.

7.2 Cardiac Sarcoidosis: Complementary Value of 18F-FDG PET and MRI

7.2.1 Cardiac Sarcoidosis and Coronary Artery Disease: Case 53

Key Points

- ^{18}F-FDG PET and MRI have complementary value in the evaluation of patients with suspected cardiac sarcoidosis. Both have very high sensitivity and negative predictive value.

- In the setting of a positive MRI, like in this case vignette, the metabolic signal from ^{18}F-FDG PET provides an indication of active inflammation and the potential need to consider immunosuppressive therapy.
- When immunosuppressive therapy is started, ^{18}F-FDG PET is then used to monitor treatment response.

History

- A 60-year-old woman with biopsy-proven pulmonary sarcoidosis and known coronary artery disease with prior remote PCI to the mid LAD presented with excessive fatigue and was found to have episodes of recurrent ventricular tachycardia.
- An invasive coronary angiogram demonstrated a patent LAD stent and minimal luminal irregularities in the other coronary arteries.
- She was referred for advanced imaging to evaluate for cardiac sarcoidosis with cardiac MRI. Based on these findings and recurrent symptomatic episodes of ventricular tachycardia, she underwent ICD placement.
- A few months post ICD placement, she was referred for rest ^{99m}Tc-sestamibi SPECT myocardial perfusion and ^{18}F-FDG PET/CT for the evaluation of active cardiac sarcoidosis (Figs. 7.12, 7.13 and 7.14).

MR Image

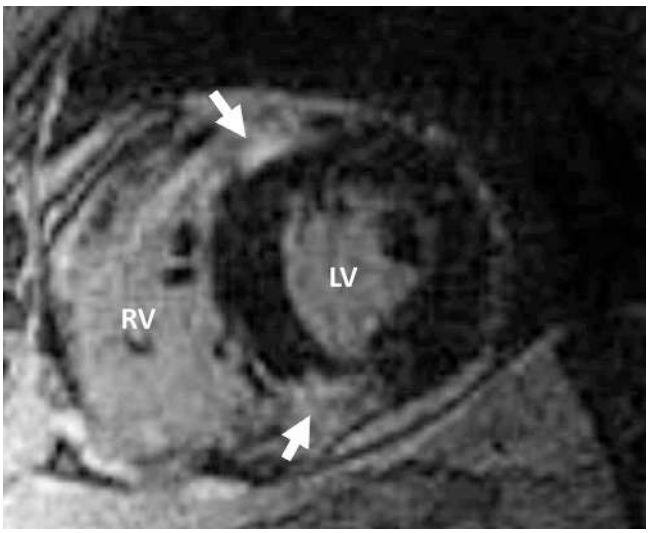


Fig. 7.12 Selective mid short-axis slice of the patient's contrast-enhanced cardiac MRI. There is dense subepicardial late gadolinium enhancement involving the basal and mid inferoseptal and to a lesser extent the anterior and anteroseptal walls (arrows). There is additional subepicardial late gadolinium enhancement in the apical inferoseptal segment at the inferior RV insertion site (not shown)

PET/CT Images

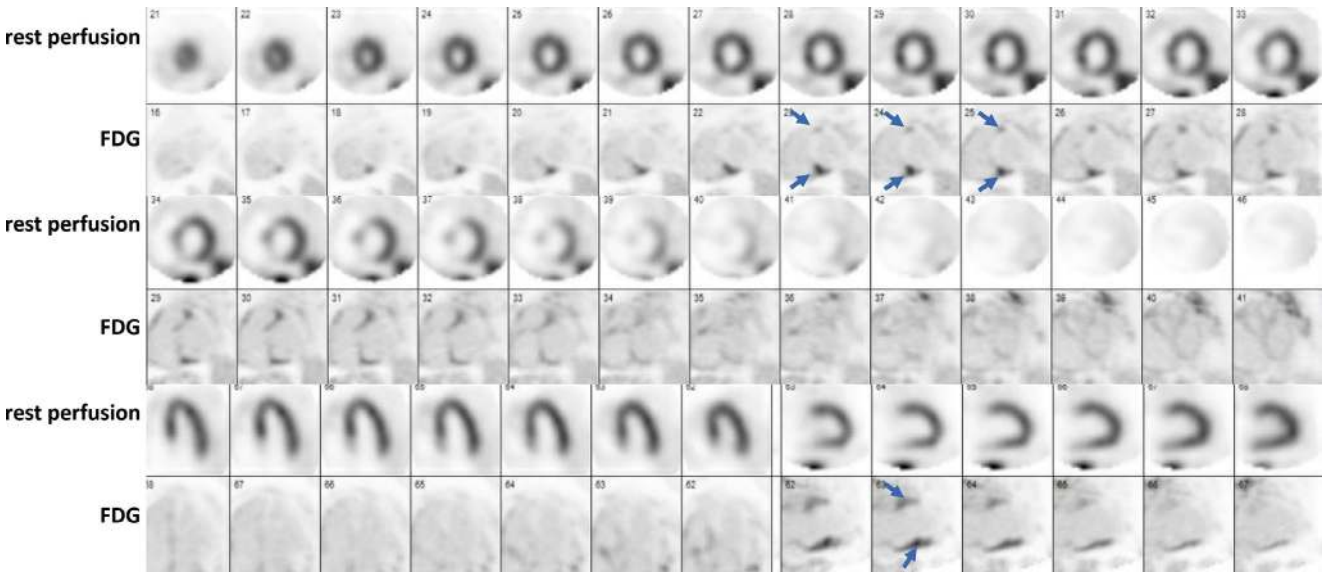


Fig. 7.13 Myocardial studies at rest with both ^{99m}Tc-sestamibi SPECT and ^{18}F-FDG PET/CT. The rest perfusion images showed a small and severe perfusion defect involving the mid and basal inferoseptal and basal anteroseptal LV segments. The ^{18}F-FDG images demonstrate adequate suppression of glucose uptake by normal myocardium. There is intense focal ^{18}F-FDG uptake in the mid and basal inferoseptal wall and mild uptake in the basal anteroseptal wall (perfusion-FDG mismatched defect, arrows)

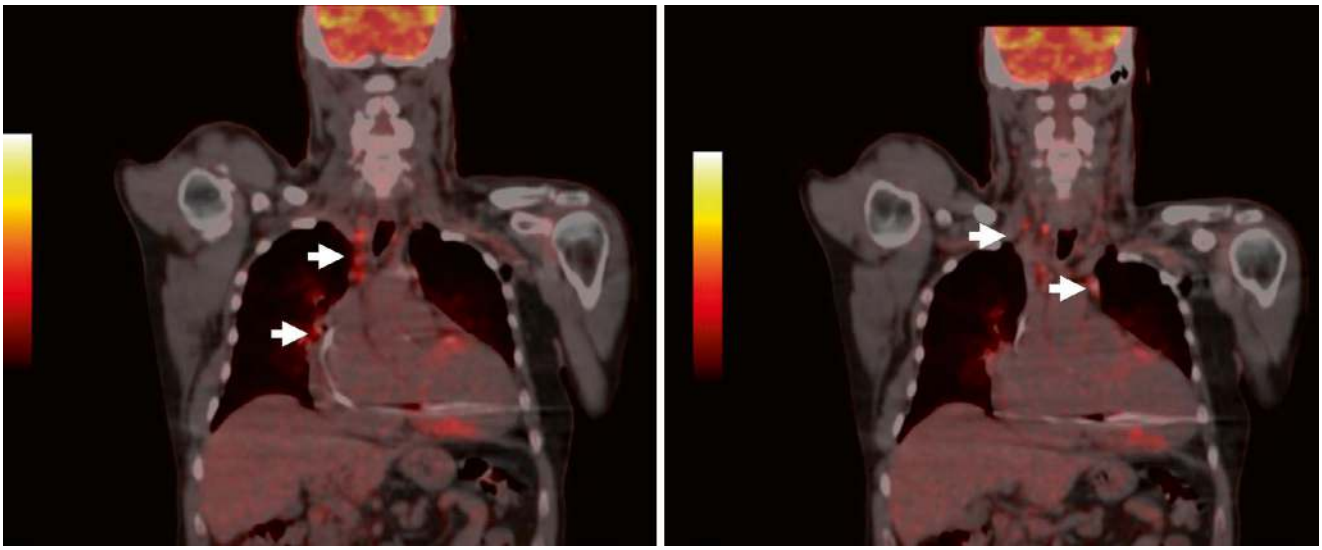


Fig. 7.14 Limited whole-body PET/CT images demonstrating increased ^{18}F-FDG uptake in upper mediastinal and hilar nodes, consistent with active extracardiac sarcoidosis (arrows)

Findings

MRI

- There is dense subepicardial late gadolinium enhancement involving the basal and mid inferoseptal and to a lesser extent the anterior and anteroseptal walls. There is additional subepicardial late gadolinium enhancement in the apical inferoseptal segment at the inferior RV insertion site.
- Global LV function was mildly reduced.

PET/CT Imaging

- There was adequate suppression of ^{18}F-FDG uptake by normal myocardium.
- The rest perfusion images showed a small and severe perfusion defect involving the mid and basal inferoseptal and basal anteroseptal LV segments.
- The ^{18}F-FDG images demonstrate intense focal glucose uptake in the mid and basal inferoseptal wall and mild uptake in the basal anteroseptal wall (perfusion-FDG mismatched defect).
- The ECG-gated images demonstrated mildly reduced LV function with a rest LVEF of 48% and mild global hypokinesis.
- The limited whole-body PET/CT images demonstrate increased ^{18}F-FDG uptake in upper mediastinal and hilar nodes, consistent with active extracardiac sarcoidosis.

Imaging Diagnosis

- Active myocardial inflammation consistent with cardiac sarcoidosis.

Differential Diagnosis

- Myocarditis: Given clinical presentation and absence of troponin elevation, this diagnosis was considered less likely.

Management

- Given the absence of recurrent ventricular arrhythmias and after detailed discussion with the patient regarding potential benefit vs risk of immunosuppressive therapy, it was decided to perform watchful waiting and eventually repeat the ^{18}F-FDG PET scan during follow-up to look for signs of disease progression.

Further Reading

- Vita T, Okada D, Veillet-Chowdhury M, Bravo P, Mullins E, Hulten E, et al. Complementary Value of Cardiac Magnetic Resonance Imaging and Positron Emission Tomography/Computed Tomography in the Assessment of Cardiac Sarcoidosis. Circulation: Cardiovascular Imaging. 2018;11.
- Chareonthaitawee P, Beanlands R, Chen W, Dorbala S, Miller E, Murthy V, et al. Joint SNMMI–ASNC Expert Consensus Document on the Role of 18 F-FDG PET/CT in Cardiac Sarcoid Detection and Therapy Monitoring. Journal of Nuclear Medicine. 2017;58:1341–1353.

7.2.2 Cardiac Sarcoidosis on PET/MRI: Case 54

Key Points

- For the assessment of cardiac sarcoidosis, ^{18}F-FDG PET/MRI can provide combined information on myocardial disease activity and the impact of this on the function and presence of scarring in the myocardium.
- Combined PET/MRI has a lower radiation dose, shorter imaging time, and higher diagnostic accuracy compared to imaging with separate cardiac MRI, PET/CT, and SPECT (Figs. 7.15 and 7.16).

History

- A 47-year-old woman with known pulmonary sarcoidosis presented with ongoing breathlessness and limited exercise capacity.
- Transthoracic echocardiography showed a moderate reduction in LV systolic function with an LVEF of 40%.
- She was referred for ^{18}F-FDG PET/MRI for the assessment of cardiac sarcoidosis.

PET/MRI Images

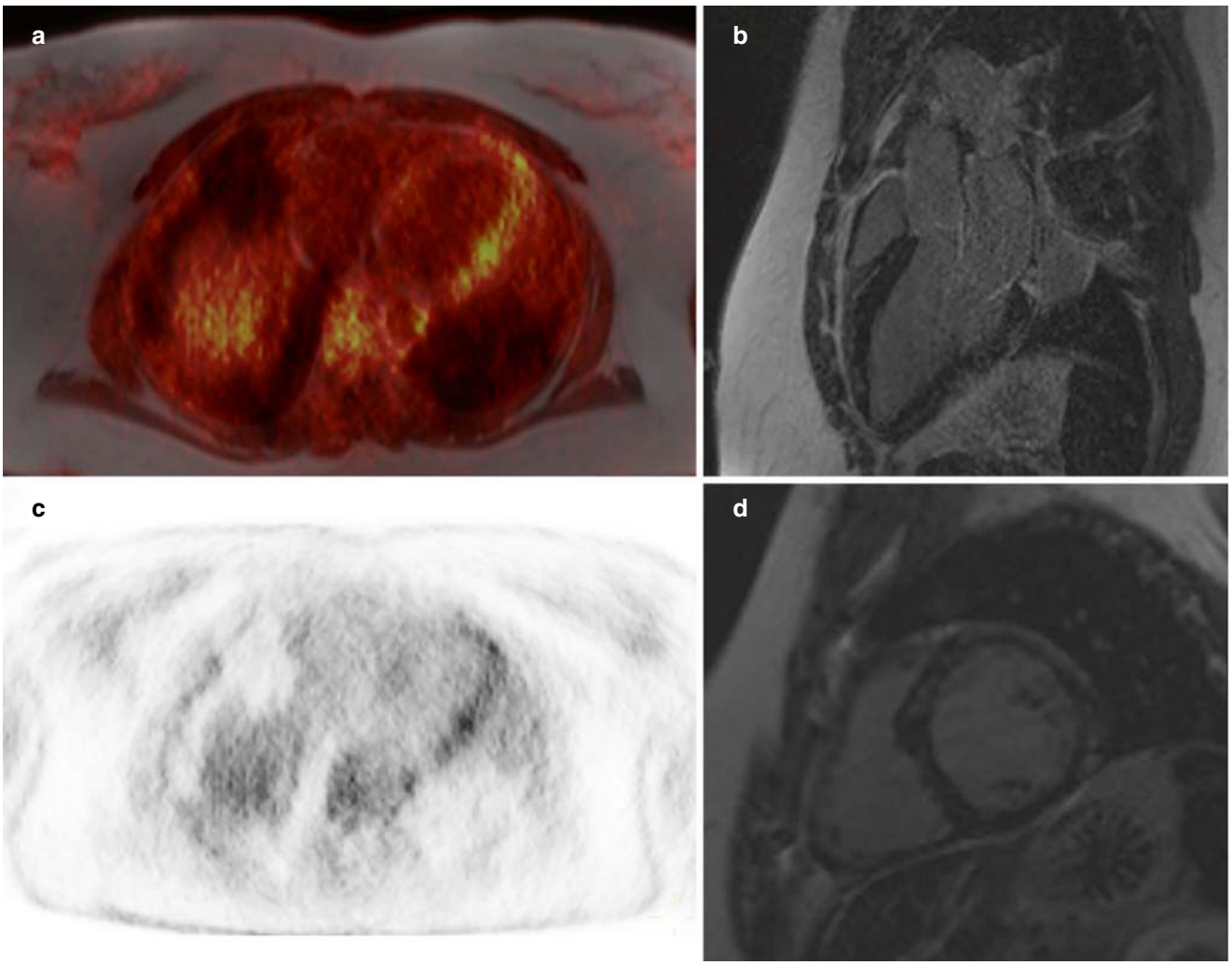


Fig. 7.15 ^{18}F-FDG PET/MRI images with axial fused PET/MRI (**a**), axial PET (**c**), and MRI late gadolinium enhancement images (**b**, **d**). These show patchy ^{18}F-FDG uptake in the LV myocardium in keeping with active sarcoidosis. There was patchy late gadolinium enhancement in a noncoronary distribution affecting around 20% of the LV myocardium

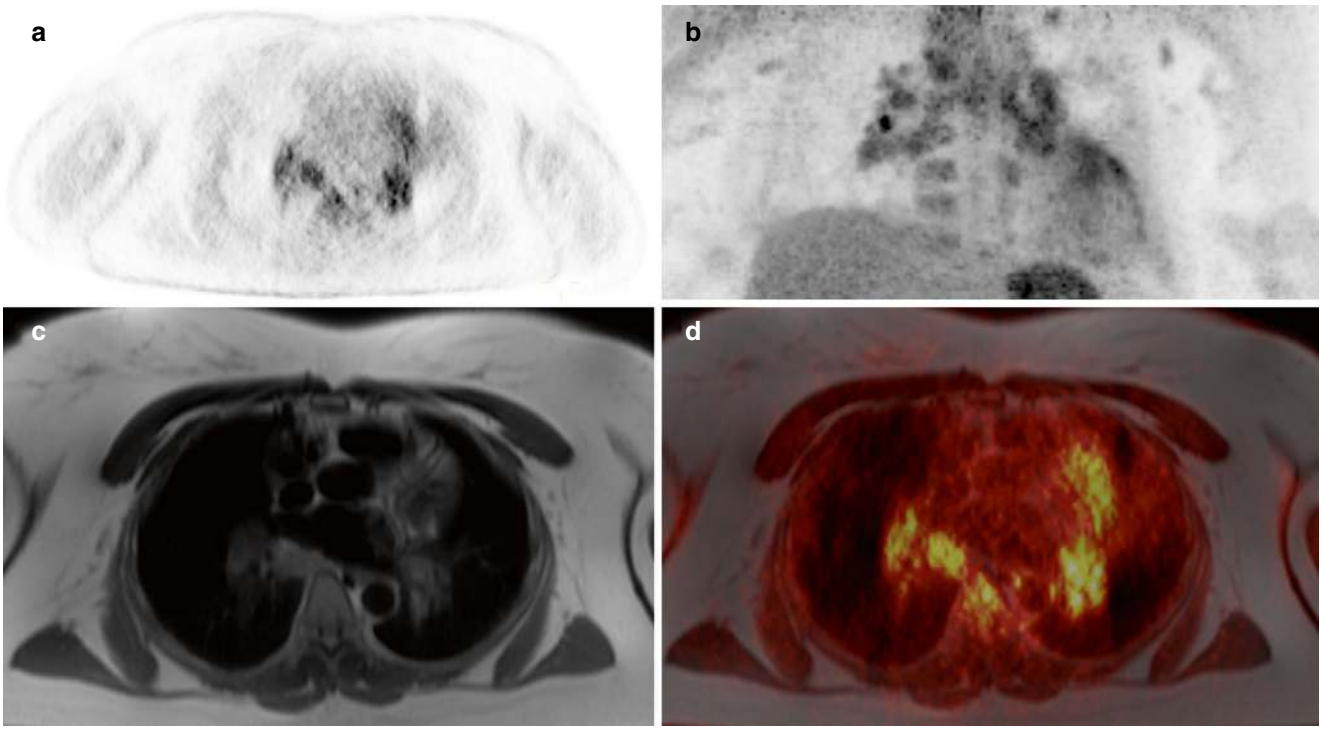


Fig. 7.16 ^{18}F-FDG PET/MRI images with axial PET (**a**), MIP PET (**b**), axial MRI (**c**), and axial fused PET/MRI (**d**) images showing enlarged mediastinal and hilar lymph nodes with associated ^{18}F-FDG uptake in keeping with active sarcoidosis

Findings

- ^{18}F-FDG PET/MRI showed patchy ^{18}F-FDG uptake in the LV myocardium in keeping with active cardiac sarcoidosis.
- There was patchy late gadolinium enhancement in a non-coronary distribution affecting around 20% of the LV myocardium.
- MRI also showed a moderately reduced LV systolic function with an LVEF of 40%. There was mild hypokinesis in the mid anterior and inferolateral segments and in the basal to mid inferolateral segments.

Imaging Diagnosis

- Active pulmonary and cardiac sarcoidosis.

Differential Diagnosis

- Myocarditis.

Correlative Imaging

- None.

Management

- She was commenced on oral steroids.
- She was referred for ICD implantation due to the high volume of scar identified on MRI.

Further Reading

- Cheung E, Ahmad S, Aitken M, Chan R, Iwanochko RM, Balter M, et al. Combined simultaneous FDG-PET/MRI with T1 and T2 mapping as an imaging biomarker for the diagnosis and prognosis of suspected cardiac sarcoidosis Eur J Hybrid Imaging. 2021 Dec; 5: 24. Published online 2021 Dec 16. https://doi.org/10.1186/s41824-021-00119-w.
- Subramanian K, Martinez J, Osborne J, Nicholson S, Van Parys J, Singh P, et al. Access to Cardiac PET/CT by Sarcoidosis Patients and Cost-Effectiveness Analysis of Cardiac PET/MR compared to the Standard of Care Clin Imaging. Author manuscript; available in PMC 2024 Feb 1.
- Published in final edited form as: Clin Imaging. 2023 Feb; 94: 50–55. Published online 2022 Dec 2. https://doi.org/10.1016/j.clinimag.2022.11.021

7.3 Differential Diagnosis: Sarcoidosis Mimic

7.3.1 Arrhythmogenic Cardiomyopathy: Case 55

Key Points

- The pattern of perfusion abnormalities and nonmatching focal ^{18}F-FDG uptake is equivocal for cardiac sarcoidosis, especially in the absence of extracardiac evidence of sarcoidosis.

History

- A 47-year-old man with a history of cardiomyopathy and no evidence of coronary artery disease by invasive angiography was referred to evaluate for cardiac sarcoidosis due to diffuse hypokinesis of a non-dilated left ventricle on echocardiogram.
- She underwent rest SPECT myocardial perfusion imaging with ^{99m}Tc-sestamibi and ^{18}F-FDG PET/CT (Figs. 7.17 and 7.18).

SPECT and PET/CT Imaging

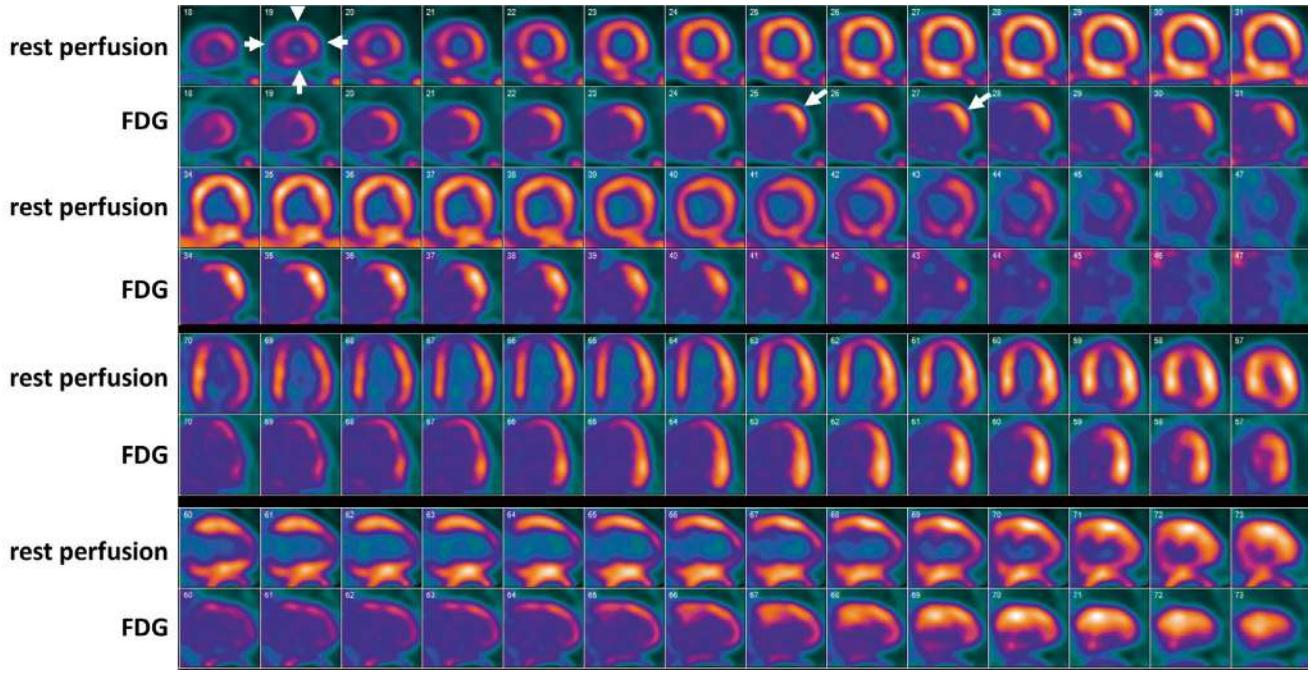


Fig. 7.17 Rest SPECT ^{99m}Tc-sestamibi myocardial perfusion study shows a medium-sized perfusion defect in the apical LV segments and apex. PET/CT shows intense ^{18}F-FDG uptake in the apical lateral and the mid and basal anterolateral walls

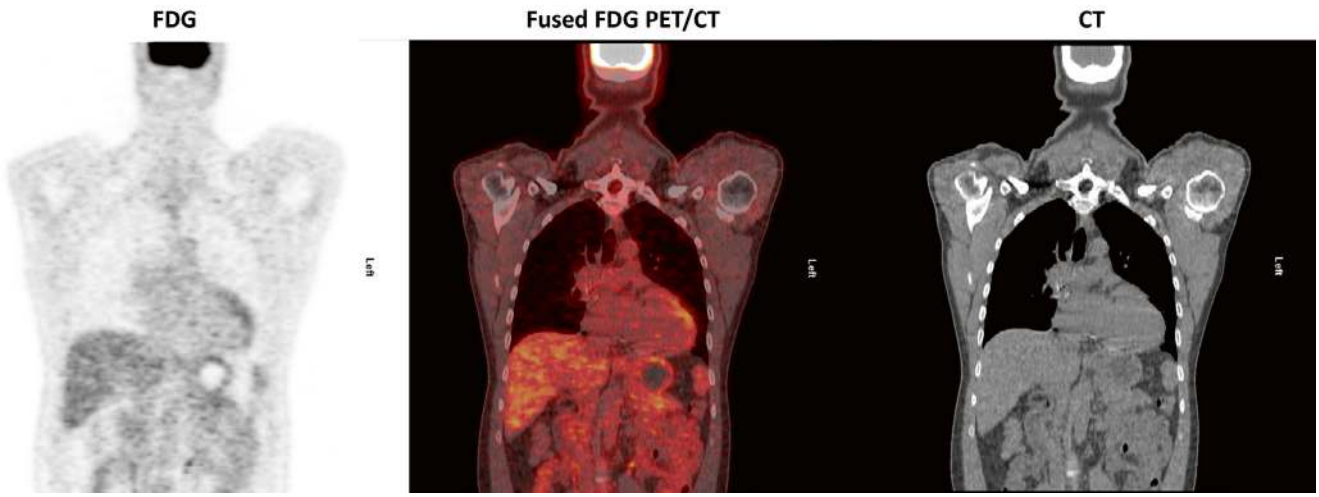


Fig. 7.18 Limited whole-body PET/CT images demonstrating no evidence of abnormal extracardiac ^{18}F-FDG uptake

Imaging findings

- The rest myocardial perfusion images show a medium-sized perfusion defect in the apical LV segments and apex. There is also a small-sized perfusion defect in the basal inferolateral wall.
- On the ^{18}F-FDG images, there is intense ^{18}F-FDG uptake in the apical lateral and the mid and basal anterolateral walls.
- The ECG-gated images demonstrated severe LV systolic dysfunction with a rest LVEF of 35% and severe global hypokinesis.
- On the whole-body PET/CT images, there is no evidence of abnormal extracardiac ^{18}F-FDG uptake.

Imaging Diagnosis

- Patchy myocardial scar in the apical anterior wall and equivocal evidence of myocardial inflammation of the lateral wall.

Differential Diagnosis

- Cardiac sarcoidosis.
- Myocarditis.
- Arrhythmogenic cardiomyopathy.
- Idiopathic dilated cardiomyopathy.

Management

- The patient underwent genetic testing which revealed a disease-causing mutation in the phospholamban gene (c.40_42delAGA) consistent with the diagnosis of arrhythmogenic cardiomyopathy. His heart failure progressed and required left ventricular assist device placement, and he eventually underwent successful cardiac transplantation.

Correlative Imaging (Fig. 7.19)

- Gross photograph of four-chamber view of the explanted heart showing fatty replacement of the right ventricular free wall characteristic of arrhythmogenic cardiomyopathy. An ICD lead is seen in the right heart along with evidence of an apically placed left ventricular assist device (**left panel**).
- Photomicrograph of hematoxylin and eosin (H&E)-stained section demonstrating transmural fibrofatty infiltration of the right ventricular free wall without other significant pathology. Occasional islands of viable myocardium remain. (40x original magnification) (**right panel**).

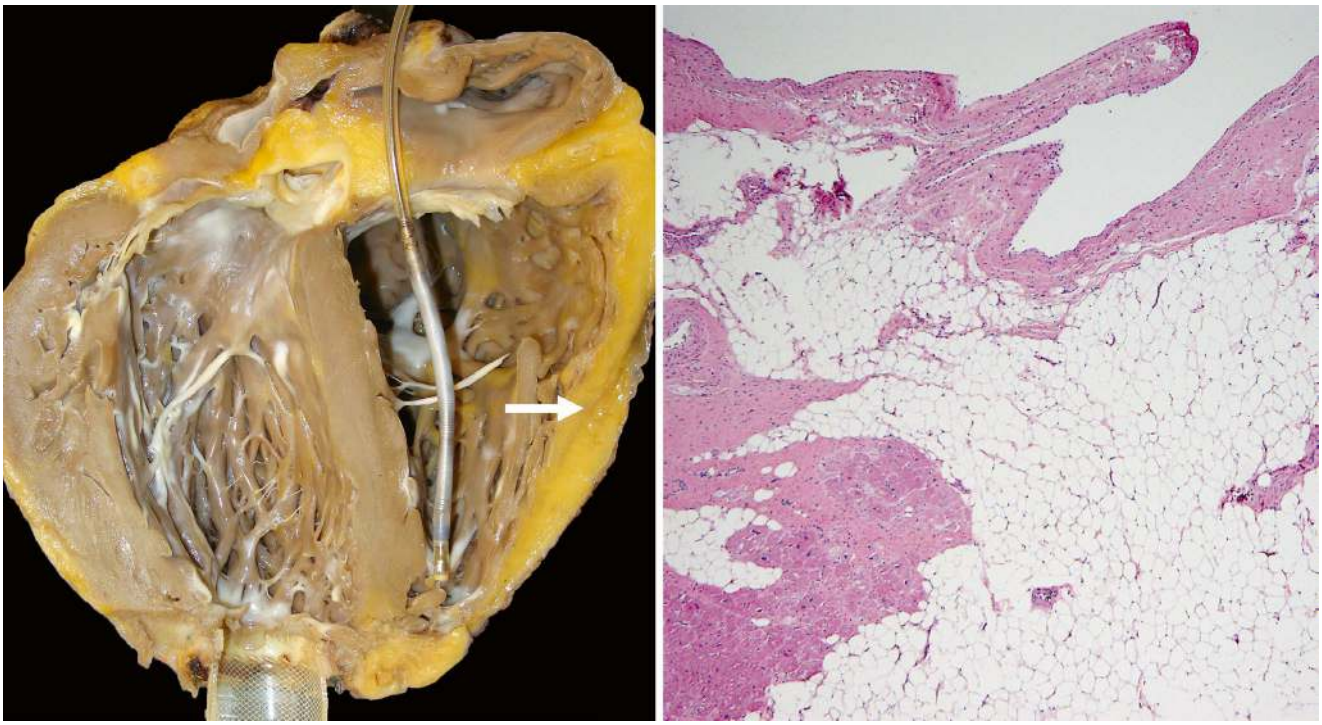


Fig. 7.19 *Left panel:* Gross photograph of four-chamber view of the explanted heart showing fatty replacement of the right ventricular free wall characteristic of arrhythmogenic cardiomyopathy (AC). An ICD lead is seen in the right heart along with evidence of an apically placed left ventricular assist device. *Right panel:* Photomicrograph of hematoxylin and eosin (H&E)-stained section demonstrating transmural fibrofatty infiltration of the right ventricular free wall without other significant pathology. Occasional islands of viable myocardium remain. (40x original magnification)

Further Reading

- Divakaran S, Stewart G, Lakdawala N, Padera R, Zhou W, Desai A, et al. Diagnostic Accuracy Of Advanced Imaging In Cardiac Sarcoidosis: An Imaging-Histologic Correlation Study In Patients Undergoing Cardiac Transplantation. Journal of the American College of Cardiology. 2019;73:934.
- Protonotarios A, Wicks E, Ashworth M, Stephenson E, Guttmann O, Savvatis K, et al. Prevalence of 18F-fluorodeoxyglucose positron emission tomography abnormalities in patients with arrhythmogenic right ventricular cardiomyopathy. International Journal of Cardiology. 2019;284:99–104.
- Images are reproduced with permission from Divakaran S, Stewart GC, Lakdawala NK, Padera RF, Zhou W, Desai AS, Givertz MM, Mehra MR, Kwong RY, Ghoshhajra BB, Taqueti VR, Skali H, Dorbala S, Blankstein R, Di Carli MF. Diagnostic accuracy of advanced imaging in cardiac sarcoidosis: an imaging-histologic correlation study in patients undergoing cardiac transplantation. Circ Cardiovasc Imaging. 2019 Jun;12(6):e008975.

7.4 Risk Stratification by ^{18}F-FDG PET

7.4.1 Possible Cardiac Sarcoidosis: Case 56

Key Points

- Isolated lateral wall FDG uptake without associated perfusion abnormalities or extracardiac uptake is nonspecific for myocardial inflammation.
- In patients with equivocal evidence of active myocardial inflammation, follow-up imaging may be helpful to ascertain progression or resolution of scan findings, which would be especially helpful in patients with recurrent symptoms or changes in LV function.

History

- A 43-year-old man with a history of ventricular tachycardia status post ICD implantation was referred for ^{18}F-FDG PET to evaluate for possible cardiac sarcoidosis (Figs. 7.20 and 7.21).

SPECT and PET/CT Images

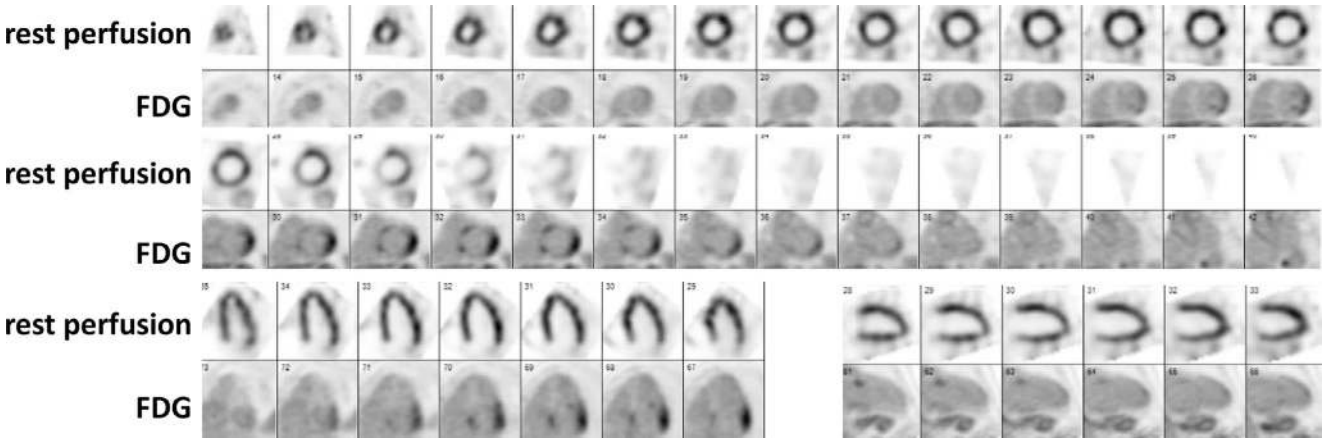


Fig. 7.20 Rest ^{99m}Tc-sestamibi SPECT perfusion and ^{18}F-FDG PET scan. The rest myocardial perfusion images demonstrated no regional perfusion abnormalities. The cardiac ^{18}F-FDG images demonstrated moderate focal glucose uptake in the basal lateral wall

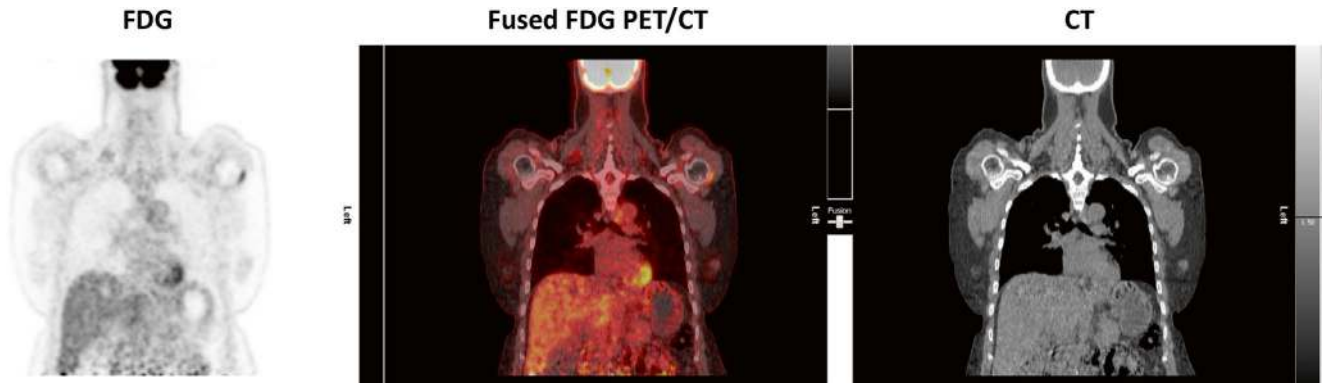


Fig. 7.21 Limited whole-body PET/CT images showing no evidence of metabolically active extracardiac sarcoidosis

Findings
- The rest myocardial perfusion images demonstrated no regional perfusion defects.
- The cardiac ^{18}F-FDG images demonstrated moderate focal glucose uptake in the basal lateral wall.
- The ECG-gated images demonstrated normal LV systolic function with a rest LVEF of 51% with normal volumes and regional wall motion and thickening.
- On the whole-body PET/CT images, there was no evidence of metabolically active extracardiac sarcoidosis.

Imaging Diagnosis
- No definitive evidence of active myocardial inflammation.

Differential Diagnosis
- Partial suppression of ^{18}F-FDG uptake.
- Cardiac sarcoidosis.
- Myocarditis.

Correlative Imaging
- None.

Management
- Initiation of immunosuppressive therapy for the patient was deferred as the patient did not have definitive evidence of active inflammation.

Further Reading

- Blankstein R, Osborne M, Naya M, Waller A, Kim C, Murthy V, et al. Cardiac Positron Emission Tomography Enhances Prognostic Assessments of Patients With Suspected Cardiac Sarcoidosis. Journal of the American College of Cardiology. 2014;63:329–336.

7.4.2 Highly Probable Cardiac Sarcoidosis: Case 57

Key Points
- ^{18}F-FDG PET likelihood of cardiac sarcoidosis is highly probable when there are multiple, noncontiguous perfusion defects with associated ^{18}F-FDG uptake OR multiple areas of focal ^{18}F-FDG uptake and extracardiac ^{18}F-FDG uptake present.
- The presence of a perfusion-FDG mismatched defect associated with focal ^{18}F-FDG uptake in the RV free wall identifies patients at high risk for ventricular arrhythmias and death.

History
- A 75-year-old woman with known pulmonary sarcoidosis presented with ventricular tachycardia/cardiac arrest. She received a secondary prevention ICD and was subsequently referred for an ^{18}F-FDG PET/CT to evaluate for cardiac sarcoidosis (Fig. 7.22).

SPECT and PET/CT Images

Findings
- Rest myocardial perfusion images demonstrated a small-sized perfusion defect of severe intensity involving the basal anteroseptal wall.
- There was adequate suppression of ^{18}F-FDG uptake in the normal myocardium. The ^{18}F-FDG images demonstrate intense focal glucose uptake involving the mid and basal anterior and septal walls. There is also focal ^{18}F-FDG uptake in the RV free wall.
- The ECG-gated images demonstrated normal LV systolic function with a rest LVEF of 60% and normal volumes and regional wall motion and thickening.
- There was no evidence of metabolically active extracardiac sarcoidosis.

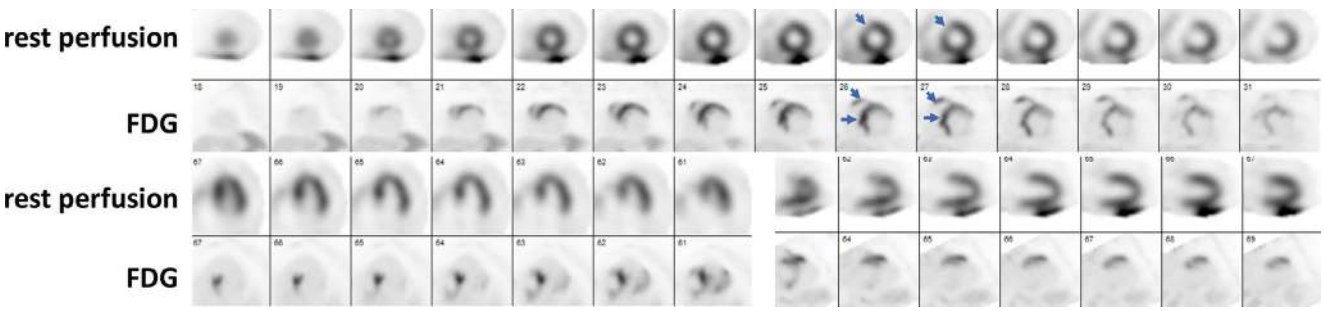


Fig. 7.22 Rest ^{99m}Tc-sestamibi SPECT myocardial perfusion and ^{18}F-FDG PET/CT images. Rest myocardial perfusion images demonstrate a small-sized perfusion defect of severe intensity involving the basal anteroseptal wall. There was adequate suppression of ^{18}F-FDG uptake in the normal myocardium. The ^{18}F-FDG images demonstrate intense focal glucose uptake involving the mid and basal anterior and septal walls. There is also focal ^{18}F-FDG uptake in the RV free wall

Imaging Diagnosis
- Active myocardial inflammation in keeping with sarcoidosis.

Differential Diagnosis
- None.

Correlative Imaging
- None.

Management
- The patient was started on anti-inflammatory therapy including corticosteroids.

Further Reading

- Blankstein R, Osborne M, Naya M, Waller A, Kim C, Murthy V, et al. Cardiac Positron Emission Tomography Enhances Prognostic Assessments of Patients With Suspected Cardiac Sarcoidosis. Journal of the American College of Cardiology. 2014;63:329–336.
- Vita T, Okada D, Veillet-Chowdhury M, Bravo P, Mullins E, Hulten E, et al. Complementary Value of Cardiac Magnetic Resonance Imaging and Positron Emission Tomography/Computed Tomography in the Assessment of Cardiac Sarcoidosis. Circulation: Cardiovascular Imaging. 2018;11.
- Chareonthaitawee P, Beanlands R, Chen W, Dorbala S, Miller E, Murthy V, et al. Joint SNMMI–ASNC Expert Consensus Document on the Role of 18 F-FDG PET/CT in Cardiac Sarcoid Detection and Therapy Monitoring. Journal of Nuclear Medicine. 2017;58:1341–1353.

7.5 Evaluation of Response to Therapy

7.5.1 Evaluation of Response to Therapy: Case 58

Key Points
- ^{18}F-FDG PET/CT is currently the standard of care for the evaluation of response to anti-inflammatory therapy in patients with cardiac sarcoidosis.
- A decreased burden of inflammation helps with decisions regarding tapering/discontinuation of immunosuppressive therapy.
- Adding objective quantitative analysis of the intensity and extent of ^{18}F-FDG uptake to the qualitative interpretation is recommended to track response to therapy. The use of maximum standardized uptake value (SUVmax) is recommended to monitor the intensity of inflammation in response to therapy. Additionally, some measure of extent of active inflammation is also recommended.

History
- A 68-year-old man with a history of biopsy-proven cardiac sarcoidosis status post anti-inflammatory therapy was referred for ^{18}F-FDG PET/CT to evaluate response to immunosuppressive therapy.
- He had ^{18}F-FDG PET/CT before and after therapy.

SPECT and PET/CT Images (Baseline study Fig. 7.23**)**
SPECT and PET/CT Images (Follow-Up Study Fig. 7.24**)**

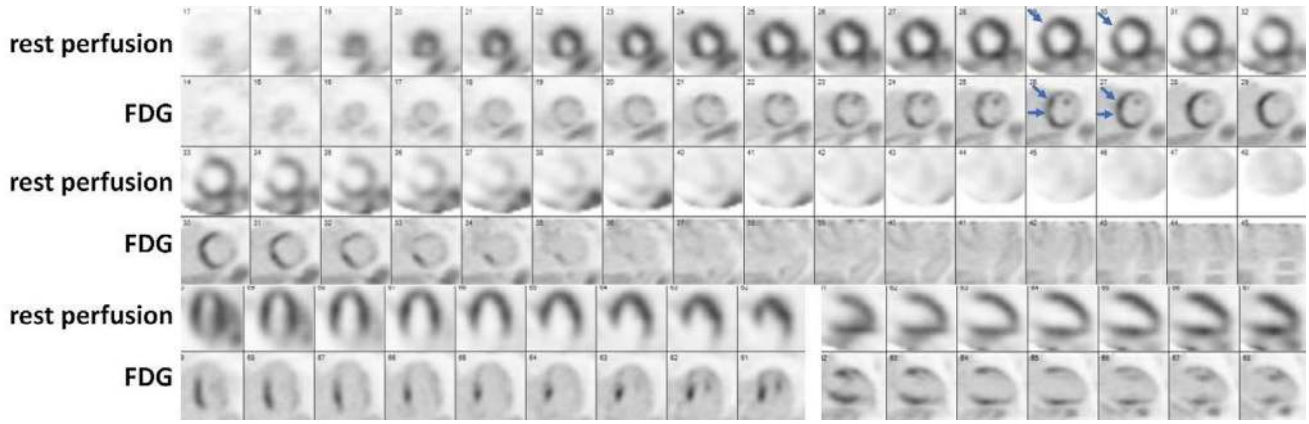


Fig. 7.23 Rest ^{99m}Tc-sestamibi myocardial perfusion and ^{18}F-FDG PET/CT. The rest perfusion images demonstrate a small-sized perfusion defect of severe intensity involving the mid and basal anteroseptal wall. The ^{18}F-FDG PET/CT study demonstrates adequate suppression of glucose uptake in normal myocardium. There is a focus of intense ^{18}F-FDG uptake involving the mid and basal interventricular septum (perfusion-FDG mismatched defect)

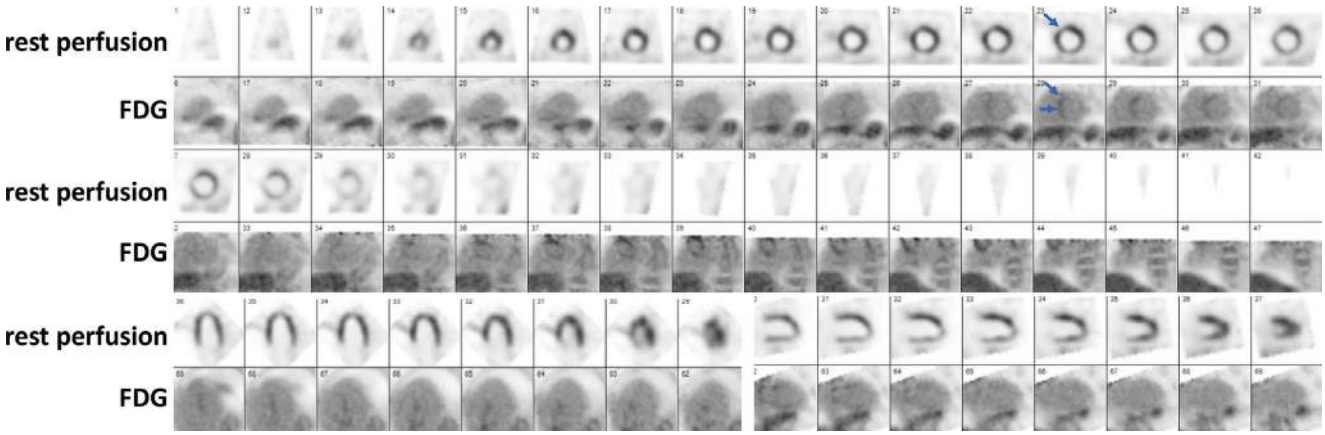


Fig. 7.24 Rest ^{99m}Tc-sestamibi myocardial perfusion SPECT and ^{18}F-FDG PET/CT. The rest perfusion images demonstrate a small-sized perfusion defect of mild intensity involving the basal anteroseptal wall, which appears decreased in size and intensity compared to the baseline study. The ^{18}F-FDG PET/CT study demonstrates adequate suppression of glucose uptake in normal myocardium. There is minimal ^{18}F-FDG uptake involving the basal interventricular septum

Findings

Baseline study (Fig. 7.23):

- The rest perfusion images demonstrate a small-sized perfusion defect of severe intensity involving the mid and basal anteroseptal wall.
- The ^{18}F-FDG PET/CT study demonstrates adequate suppression of glucose uptake in normal myocardium. There is a focus of intense ^{18}F-FDG uptake involving the mid and basal interventricular septum (perfusion-FDG mismatched defect).
- The ECG-gated images demonstrated moderate LV systolic dysfunction and a rest LVEF of 42% with mildly enlarged volumes and moderate global hypokinesis.

Follow-up study (7 months after baseline) (Fig. 7.24):

- The rest perfusion images demonstrate a small-sized perfusion defect of mild intensity involving the basal anteroseptal wall, which appears decreased in size and intensity compared to the baseline study.
- The ^{18}F-FDG PET/CT study demonstrates adequate suppression of glucose uptake in normal myocardium. There is minimal ^{18}F-FDG uptake involving the basal interventricular septum.
- The ECG-gated images demonstrated normal LV systolic function and a rest LVEF of 52% with normal volumes and regional wall motion, which had improved compared to the previous imaging.

Quantitative analysis of the intensity and extent of ^{18}F-FDG uptake shows a decrease of both SUVmax and volume of ^{18}F-FDG uptake (Table 7.1).

Table 7.1 Quantitative analysis of ^{18}F-FDG PET/CT

Exam sequence	Myocardial SUVmax	Volume of ^{18}F-FDG uptake (SUVmax >2.7 mL)
Baseline	5.9	22.63
Follow-up	1.6	0.91

Imaging Diagnosis

- Active myocardial inflammation in keeping with active cardiac sarcoidosis, which improved after immunosuppressive therapy.

Differential Diagnosis

- None.

Correlative Imaging

- None.

Management

- After the baseline scan, the patient was started on prednisone (20 mg/day) and methotrexate (20 mg/week). Following the results of the second scan, the patient began tapering immunosuppressive therapy.

Further Reading

- Chareonthaitawee P, Beanlands R, Chen W, Dorbala S, Miller E, Murthy V, et al. Joint SNMMI–ASNC Expert Consensus Document on the Role of 18 F-FDG PET/CT in Cardiac Sarcoid Detection and Therapy Monitoring. Journal of Nuclear Medicine. 2017;58:1341–1353.
- Gillmore JD, Maurer MS, Falk RH, Merlini G, Damy T, Dispenzieri A et al. Nonbiopsy Diagnosis of Cardiac Transthyretin Amyloidosis. Circulation 2016;133:2404–12.

- Dorbala S, Ando Y, Bokhari S, Dispenzieri A, Falk R, Ferrari V, et al. ASNC/AHA/ASE/EANM/HFSA/ISA/SCMR/SNMMI expert consensus recommendations for multimodality imaging in cardiac amyloidosis: Part 1 of 2—evidence base and standardized methods of imaging. Journal of Nuclear Cardiology. 2019;26:2065–2123.

7.5.2 Evaluation of Response to Therapy: Case 59

Key Points

- ^{18}F-FDG PET/CT is currently the standard of care for the evaluation of response to anti-inflammatory therapy in patients with cardiac sarcoidosis.
- An increased burden of inflammation indicates progression of disease and helps with decisions regarding increasing intensity of immunosuppressive therapy or a change in therapy.
- As discussed in case #59, adding objective quantitative analysis of the intensity and extent of ^{18}F-FDG uptake to the qualitative interpretation is recommended to track response to therapy.

History

- A 58-year-old man with a history of ventricular arrhythmias and biopsy proven cardiac sarcoidosis was referred to assess response to immunosuppressive therapy.
- He had ^{18}F-FDG PET/CT before and after therapy.

SPECT and PET/CT Images (Baseline study, Fig. 7.25)

SPECT and PET/CT Images (Follow-up study, Fig. 7.26)

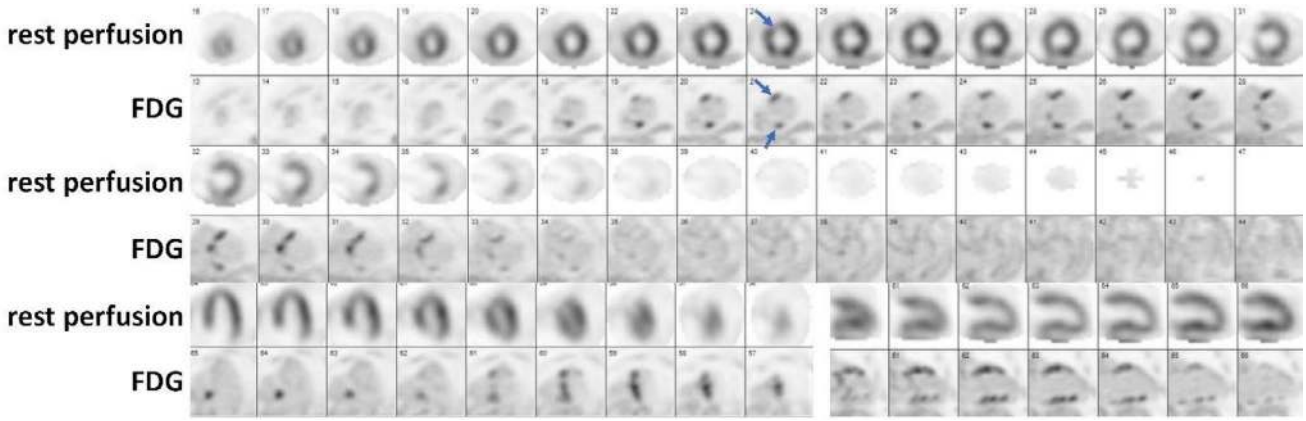


Fig. 7.25 *Baseline study*. Rest myocardial perfusion SPECT with ^{99m}Tc-sestamibi and ^{18}F-FDG PET/CT. The rest perfusion images show a small-sized perfusion defect of moderate intensity involving the mid and apical anterior wall. The ^{18}F-FDG images demonstrate adequate suppression of glucose uptake in normal myocardium. There is intense focal glucose uptake in the mid and basal anteroseptal and inferoseptal LV segments

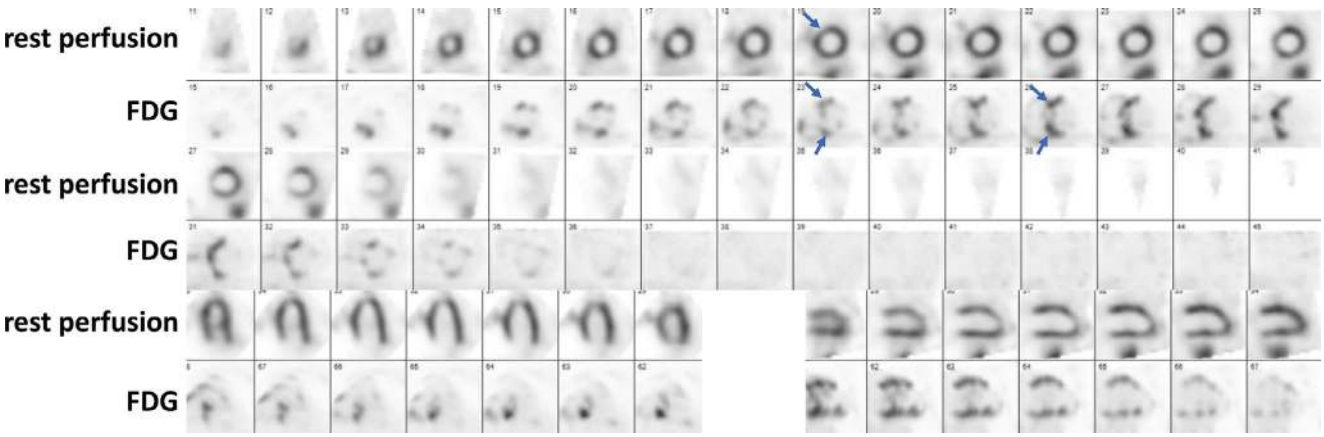


Fig. 7.26 *Follow-up study*. Rest ^{99m}Tc-sestamibi myocardial perfusion SPECT and ^{18}F-FDG PET/CT. The rest perfusion images show a small-sized perfusion defect of moderate intensity involving the mid and apical anterior wall, which is essentially unchanged compared to his baseline study. The ^{18}F-FDG images demonstrate adequate suppression of glucose uptake in normal myocardium. Compared to his baseline scan, there is more intense and extensive focal glucose uptake in the mid and basal anteroseptal and inferoseptal LV segments

Findings

Baseline study (Fig. 7.25)

- The rest perfusion images show a small-sized perfusion defect of moderate intensity involving the mid and apical anterior wall.
- The ^{18}F-FDG images demonstrate adequate suppression of glucose uptake in normal myocardium. There is intense focal glucose uptake in the mid and basal anteroseptal and inferoseptal LV segments.
- The ECG-gated images demonstrated normal LV systolic function and a rest LVEF of 57% with normal volumes and regional wall motion.
- There was mild extracardiac ^{18}F-FDG uptake in diaphragmatic and abdominal lymph nodes, scattered bilateral pulmonary nodules, and osseous uptake.

Follow-up study (Fig. 7.26)

- Six months after baseline scan, the rest perfusion images show a small-sized perfusion defect of moderate intensity involving the mid and apical anterior wall, which is essentially unchanged compared to his baseline study.
- The ^{18}F-FDG images demonstrate adequate suppression of glucose uptake in normal myocardium. Compared to his baseline scan, there is more intense and extensive focal glucose uptake in the mid and basal anteroseptal and inferoseptal LV segments.
- The ECG-gated images demonstrated mildly reduced LV systolic function and a rest LVEF of 47% with normal volumes and mild global hypokinesis.
- Similar ^{18}F-FDG avid extracardiac sarcoidosis involving lymph nodes, spleen and bones as compared to his baseline scan.

Quantitative analysis of the intensity and extent of ^{18}F-FDG uptake (Table 7.2).

Imaging Diagnosis

- Interval worsening of myocardial inflammation.

Differential Diagnosis

- None.

Correlative Imaging

- None.

Table 7.2 Quantitative analysis of ^{18}F-FDG PET/CT

Exam sequence	Myocardial SUVmax	Volume of ^{18}F-FDG uptake (SUVmax >2.7 mL)
Baseline	6.1	10.28
Follow-up	14.0	110

Management

- After the baseline scan, the patient was started on prednisone (20 mg/day) and methotrexate (15 mg/week). Following the results of the second scan, the patient underwent intensification of immunosuppressive therapy.

Further Reading

- Chareonthaitawee P, et al. Joint SNMMI-ASNC Expert Consensus Document on the Role of 18F-FDG PET/CT in Cardiac Sarcoid Detection and Therapy Monitoring. J Nucl Med. 2017 Aug;58(8):1341–1353.
- Jamar F., Buscombe J., Chiti A., Christian PE, Delbeke D et al. EANM/SNMMI Guideline for 18F-FDG Use in Inflammation and Infection. JOURNAL OF NUCLEAR MEDICINE 54: 647–658; 2012.
- OSBORNE MT, et al. Reduction in ^{18}F-fluorodeoxyglucose uptake on serial cardiac positron emission tomography is associated with improved left ventricular ejection fraction in patients with cardiac sarcoidosis. J Nucl Cardiol. 2014;21(1):166–74. PMID: 24307261.

7.6 Fabry's Disease

7.6.1 Fabry's Disease: Not Yet Diagnosed: Case 60

Key Points

- Anderson-Fabry's disease is a rare genetic disorder that can affect many organs, including kidneys, heart, brain, and skin. It is a lysosomal storage disease caused by a compromised alpha-galactosidase enzyme with abnormal lysosomal accumulation of a sphingolipid called globotriaosyl ceramide, predominantly in endothelial cells.
- Coronary microvascular dysfunction is common in Fabry's disease and develops early in the natural history of the disease, preceding the development of LV hypertrophy.

History

- A 67-year-old woman with a history of hypercholesterolemia, controlled hypertension, and active smoker. She was admitted to the hospital for dyspnea and atypical angina.
- She underwent invasive coronary angiography which showed patent epicardial coronary arteries.
- She was referred for PET myocardial perfusion imaging to assess for microvascular dysfunction (Figs. 7.27, 7.28, 7.29 and Table 7.3).

Correlative Imaging

- Invasive coronary angiography.

PET/CT Images

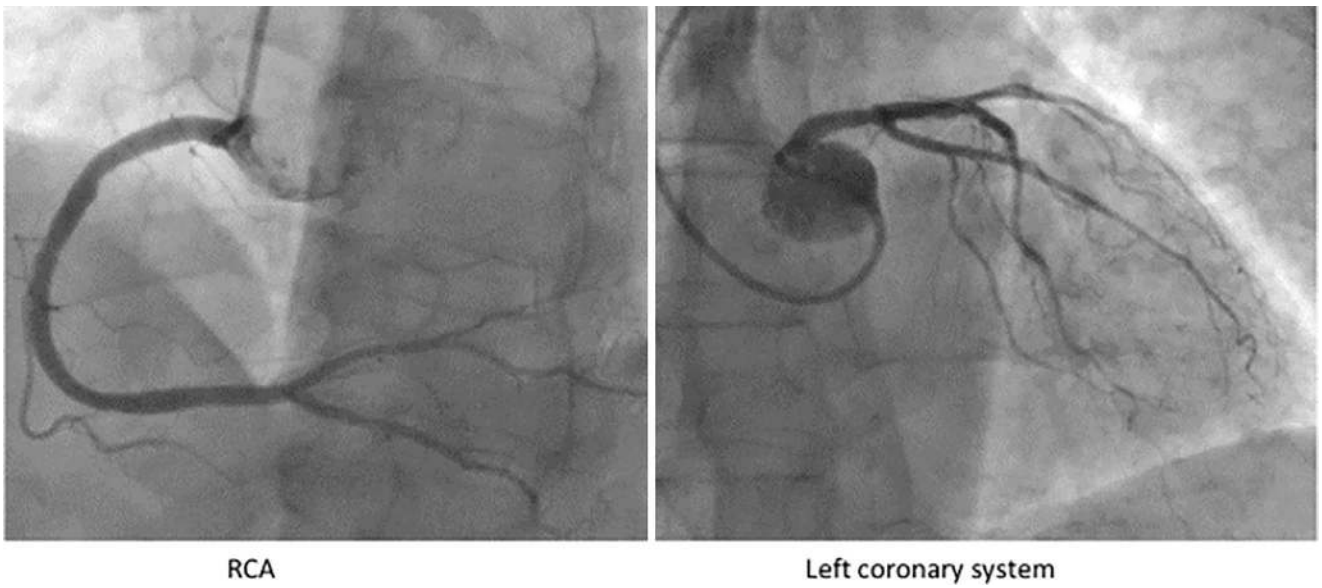


Fig. 7.27 Selective views of invasive coronary angiography showing patent epicardial coronary arteries with diffuse distal tapering of the LAD and LCX

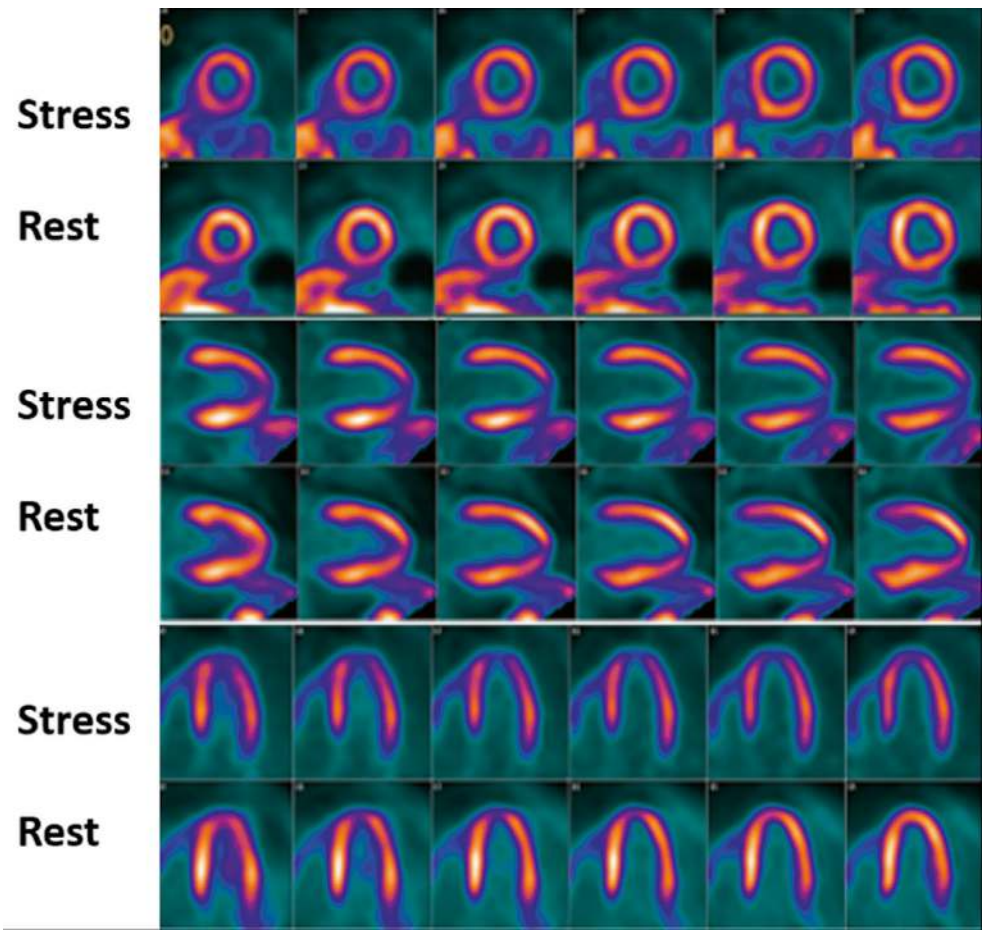


Fig. 7.28 Regadenoson stress and rest ^{13}N-ammonia PET imaging, showing mild LV dilatation during stress. Mild reduction in myocardial perfusion during stress (upper rows in each section) involving the apical LV segments and the LV apex



Fig. 7.29 ECG at rest (panel on the left) and 2 min after regadenoson infusion (panel on the right), showing ischemic changes during vasodilator stress

Table 7.3 Summary of the quantitative blood flow data demonstrating severe and diffuse reductions in stress myocardial blood flow (MBF) and myocardial flow reserve (MFR) impairment

	MBF rest (ml/min/g)	MBF stress (ml/min/g)	MFR (stress/rest)
LAD	1.06	1.31	1.24
LCX	1.02	1.42	1.40
RCA	1.15	1.53	1.33
Global LV	1.07	1.40	1.32

Findings
- Mild LV dilatation during stress.
- Mild reduction in myocardial perfusion during stress involving the apical LV segments and the LV apex.
- Severe and diffuse reduction in stress MBF and MFR impairment.
- Normal LV function with an LVEF of 64% at rest and during peak stress.
- Ischemic ECG changes during vasodilator stress.

Imaging Diagnosis
- Normal stress perfusion with mild LV dilation and abnormal MBF and MFR.

Differential Diagnosis
- Hypertensive heart disease.
- Hypertrophic cardiomyopathy.
- Infiltrative cardiomyopathy.

Correlative Imaging
- Cardiac MRI (Figs. 7.30 and 7.31).

Management
- Based on PET and cardiac MRI results, the patient was evaluated for Fabry's disease. She had a negative enzyme assay for alpha-galactosidase.
- Molecular genetic analysis was positive for the galactosidase alpha (*GLA*) gene.
- She was started on enzyme replacement therapy.

Further Reading

- Tomberli B, Cecchi F, Sciagrà R, Berti V, Lisi F, Torricelli F, et al. Coronary microvascular dysfunction is an early feature of cardiac involvement in patients with Anderson-Fabry disease. European Journal of Heart Failure. 2013;15:1363–1373.

Acknowledgment Cardiac MR images courtesy of Prof Davide Farina and Dr. Emanuele Gavazzi, Institute of Radiology, University of Brescia.

7.6.2 Fabry's Disease: Case 61

Key Points
- On PET/CT, hypertrophic cardiomyopathy and Anderson-Fabry's disease may have a similar appearance.
- Diagnosis of Anderson-Fabry's disease usually requires MRI and genetic testing.

History
- A 54-year-old woman with a diagnosis of Anderson-Fabry's disease (molecular genetic analysis positive for GLA gene).
- She was not yet on enzyme replacement therapy.
- She was referred for PET/CT for the evaluation of myocardial perfusion and function (Figs. 7.32 and Table 7.4).

PET/CT Images

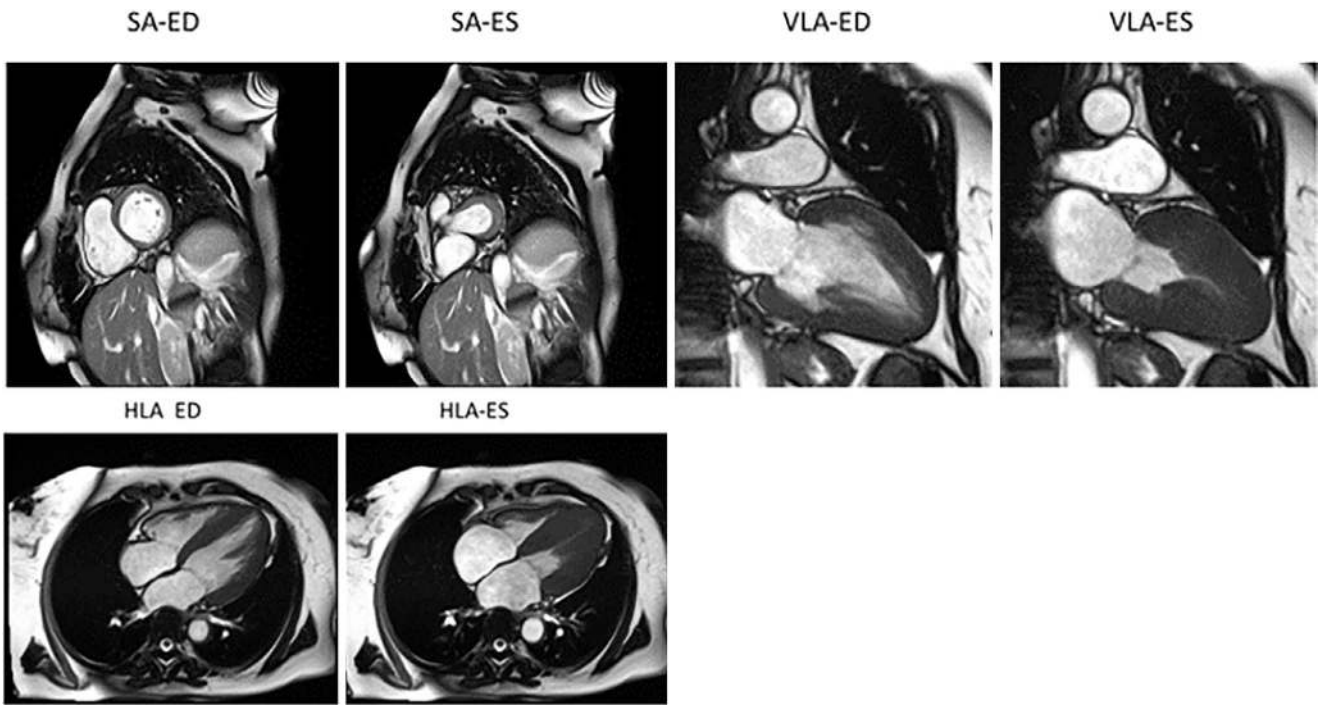


Fig. 7.30 Cardiac MRI with short-axis (SA), vertical long-axis (VLA), and horizontal long-axis (HLA) images at end diastole (ED) and end systole (ES). These show LV hypertrophy

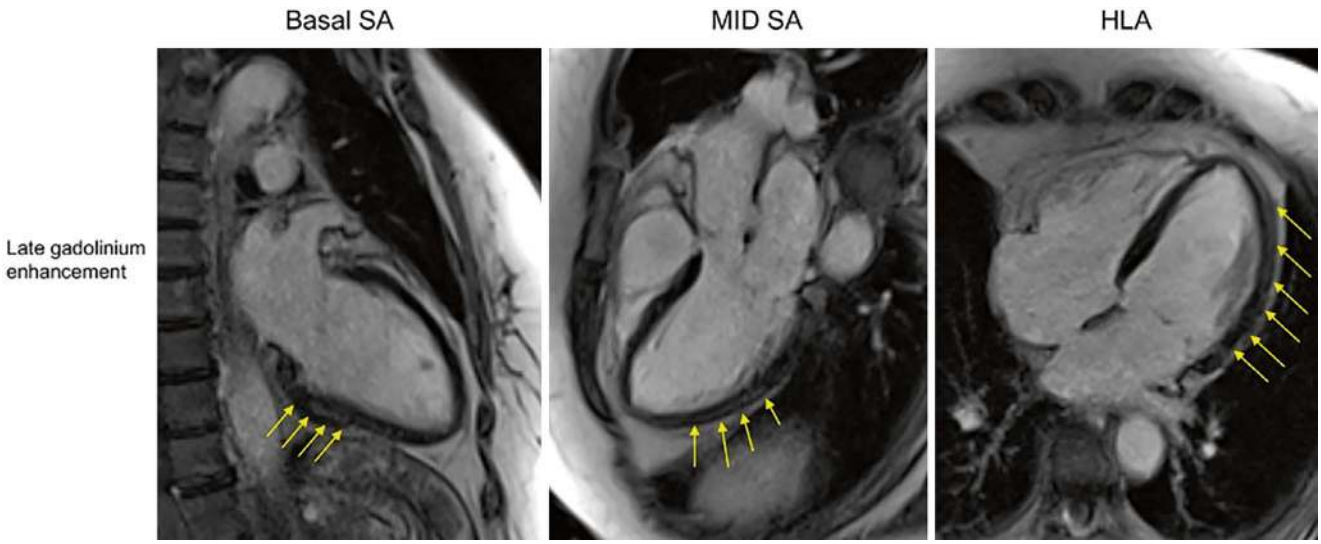


Fig. 7.31 Cardiac MRI with short-axis (SA) and horizontal long-axis (HLA) late gadolinium enhancement images. These show mild subepicardial late gadolinium enhancement in the inferior and lateral walls (arrows)

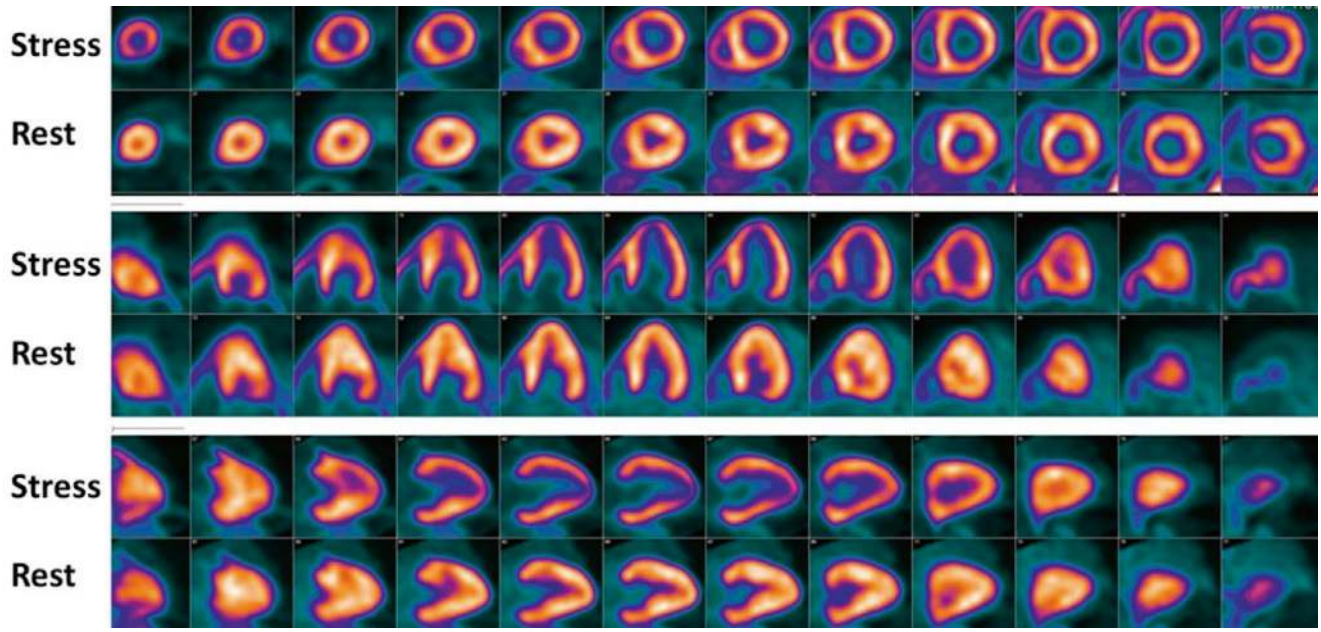


Fig. 7.32 Regadenoson stress and rest ^{13}N-ammonia PET images showing severe TID of the LV during stress with increased RV tracer uptake. There were no regional perfusion abnormalities. At rest, there was evidence of LV hypertrophy

Table 7.4 Summary of the quantitative blood flow data demonstrating diffuse reduction in stress MBF regionally and globally, as well as of MFR

	MBF rest (ml/min/g)	MBF stress (ml/min/g)	MFR (stress/rest)
LAD	0.70	1.29	1.84
LCX	0.72	1.51	2.08
RCA	0.70	1.24	1.76
Global LV	0.71	1.33	1.88

Findings
- MPI: Severe TID of the LV during stress with increased RV tracer uptake, without regional perfusion defects. Evidence of LV hypertrophy.
- Diffuse reduction in stress MBF regionally and globally.
- On ECG-gated images, there was a low normal LVEF at rest measured at 50% with a significant drop to 37% at stress along with severe enlargement of the LV ESV.

Imaging Diagnosis
- Microvascular dysfunction due associated with LV hypertrophy, in the context of known Anderson-Fabry's disease.

Differential Diagnosis
- Obstructive coronary artery disease.

Correlative Imaging
- Cardiac MRI (Figs. 7.33 and 7.34).

Management
- Invasive coronary angiography demonstrated normal coronary arteries.
- The patient was placed on enzyme replacement therapy.

Further Reading

- El Dib R, Gomaa H, Ortiz A, Politei J, Kapoor A, Barreto F. Enzyme replacement therapy for Anderson-Fabry disease: A complementary overview of a Cochrane publication through a linear regression and a pooled analysis of proportions from cohort studies. PLOS ONE. 2017;12.
- Simonetta I, Tuttolomondo A, Di Chiara T, Miceli S, Vogiatzis D, Corpora F, et al. Genetics and Gene Therapy of Anderson-Fabry Disease. Current Gene Therapy. 2018;18:96–106.

Acknowledgment Cardiac MRI images courtesy of Prof Davide Farina and Dr. Emanuele Gavazzi, Institute of Radiology, University of Brescia.

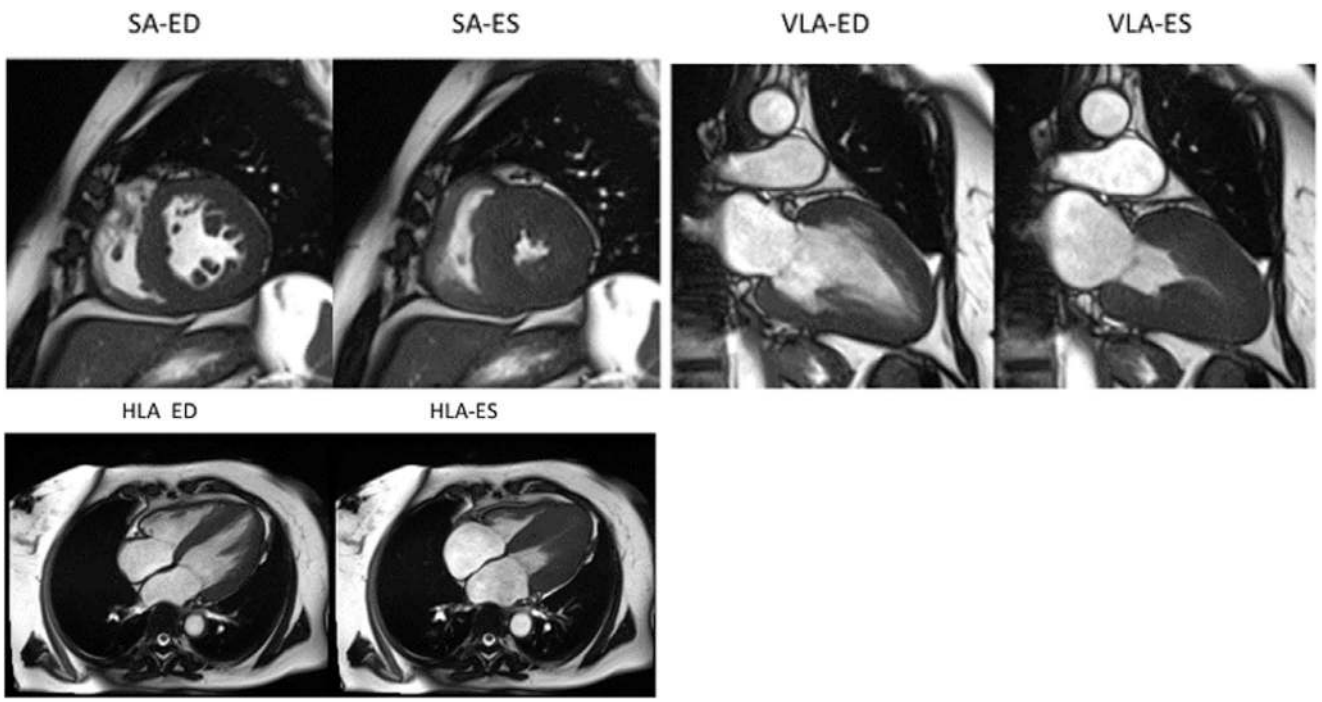


Fig. 7.33 Cardiac MRI with short-axis (SA) images, vertical long-axis images (VLA), and horizontal long-axis images (HLA), during end diastole (ED) and end systole (ES). These show severe LV hypertrophy

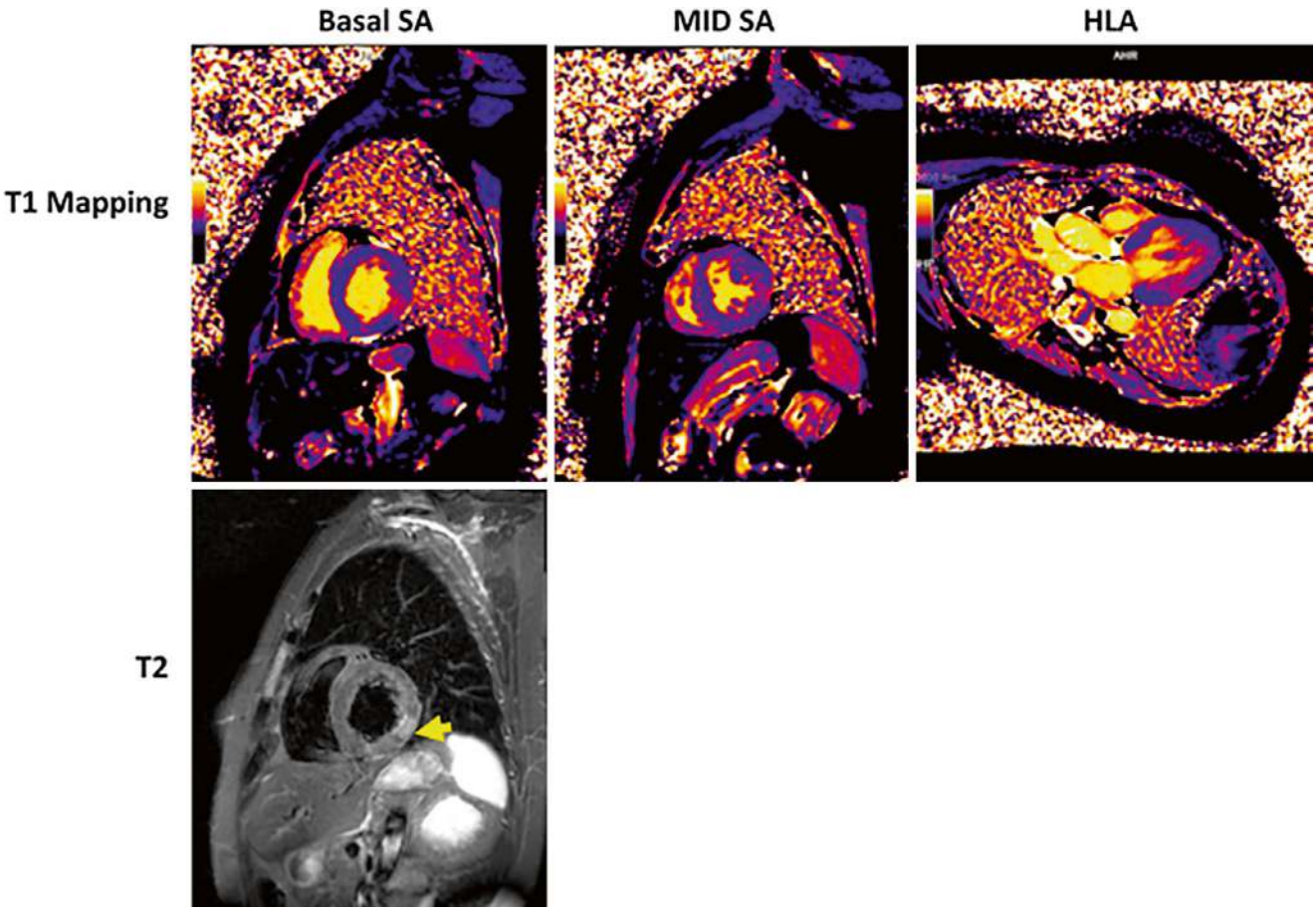


Fig. 7.34 Cardiac MRI images with basal and mid short-axis (SA) and horizontal long-axis images (HLA). T1-mapping demonstrated abnormally short T1 velocity (< 800 msec), consistent with glycosphingolipid accumulation. T2-weighted images demonstrated increased signal in keeping with edema

7.7 Amyloidosis

7.7.1 Amyloidosis: Case 62

Key Points

- Perfusion defects in a nonvascular distribution with a pattern that involves the base with relative sparing of the LV apex should raise the suspicion of microvascular dysfunction and nonischemic cardiomyopathy.
- Coronary angiography should always be considered to exclude obstructive coronary artery disease.
- Coronary microvascular dysfunction is prevalent in patients with cardiac amyloidosis.

History

- A 61-year-old man with progressive dyspnea on exertion and atypical chest pain was referred for a myocardial perfusion PET.
- He had a strong family history of coronary artery disease.
- His cardiac risk factors include hypertension and dyslipidemia.
- He also had a report of thickened left ventricular walls and diastolic dysfunction on an echocardiogram (not shown) (Figs. 7.35 and Table 7.5).

PET/CT Images

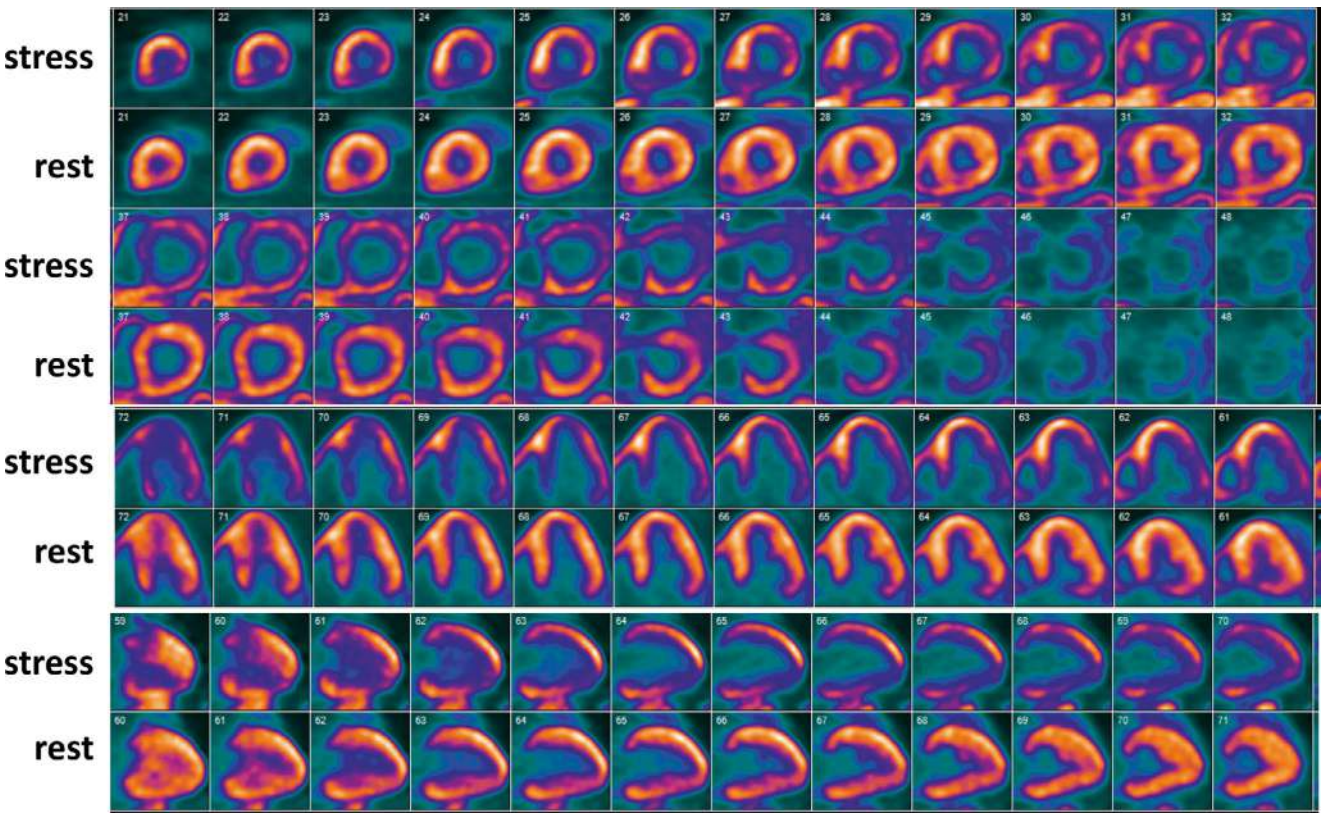


Fig. 7.35 Rest and adenosine stress ^{13}N-ammonia myocardial perfusion PET/CT images. There is marked TID (ratio: 1.43, normal: 1.05) of the LV cavity during stress. The stress myocardial perfusion images demonstrate large perfusion defects of severe intensity throughout the mid and basal LV segments in a noncoronary distribution, showing complete reversibility

Table 7.5 Summary of the quantitative blood flow data demonstrating a severe reduction in stress MBF (normal value >1.8 mL/min/g) and MFR (normal value >2.0) in all coronary artery territories and globally

	MBF rest (ml/min/g)	MBF stress (ml/min/g)	MFR (stress/rest)
LAD	0.79	0.97	1.23
LCX	0.82	1.14	1.39
RCA	0.73	1.02	1.39
Global LV	0.78	1.03	1.32

Findings

- There is marked TID (ratio: 1.43, normal: 1.05) of the LV cavity during stress.
- The stress myocardial perfusion images demonstrate a large-sized perfusion defect of severe intensity throughout the mid and basal LV segments, showing complete reversibility.
- The stress MBF and MFR are markedly reduced both regionally and globally.
- Non-contrast ECG gated cardiac CT: The Agatston CACS was 0.

Imaging Diagnosis

- Large areas of severe stress induced ischemia along non-coronary distributions.

Differential Diagnosis

- Infiltrative cardiomyopathy.
- Multivessel obstructive coronary artery disease.

Correlative Imaging

- Invasive coronary angiography.
- Cardiac MRI (Figs. 7.36 and 7.37).

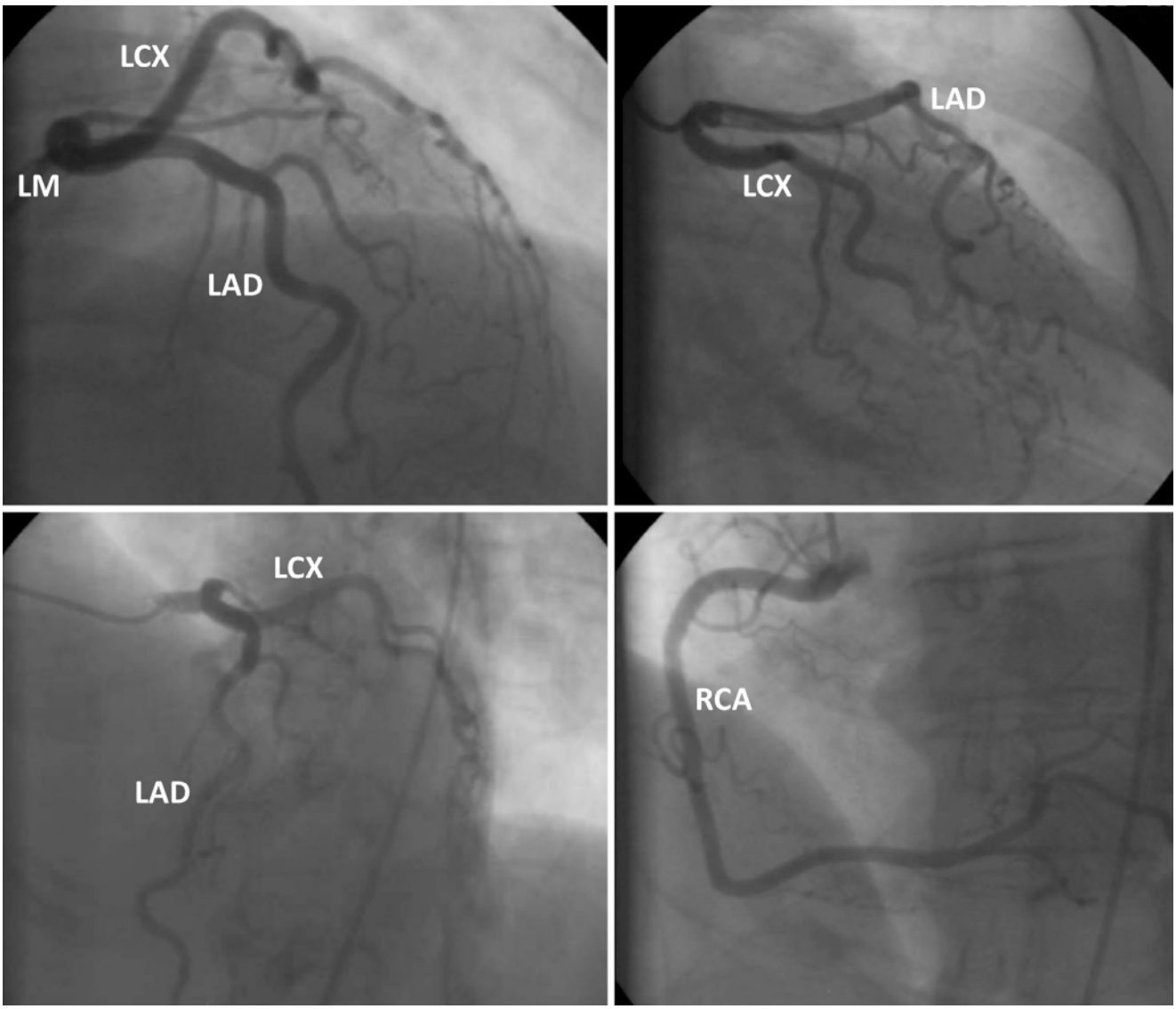


Fig. 7.36 Selective views of the invasive coronary angiography demonstrated no evidence of coronary artery disease

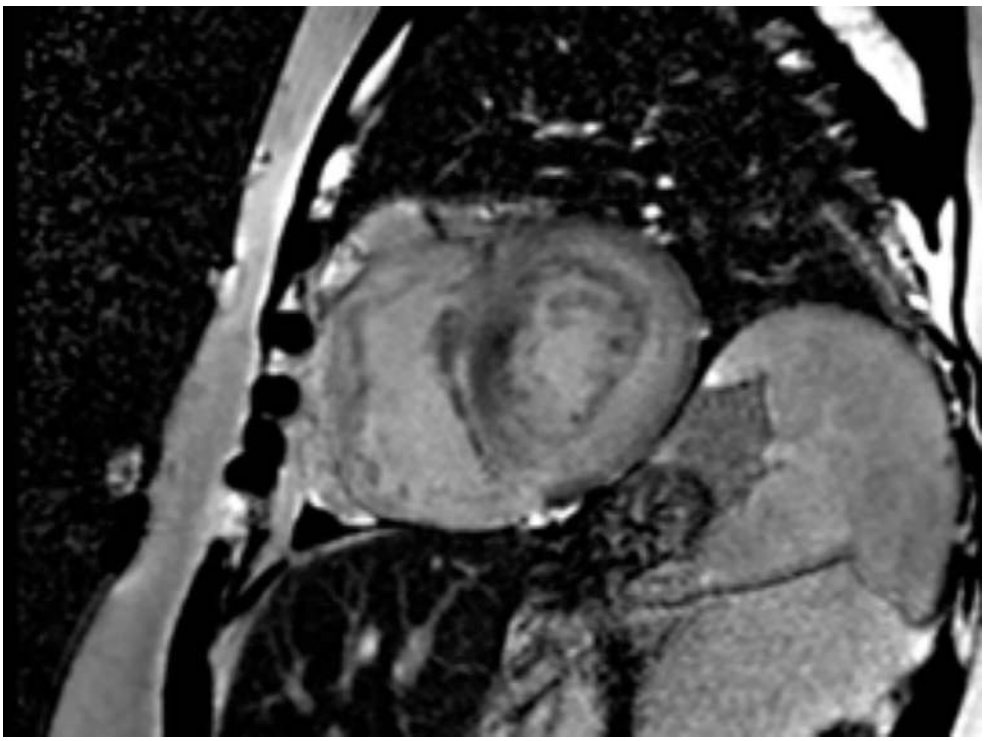


Fig. 7.37 Short-axis view of the cardiac MRI showing diffuse subendocardial late gadolinium enhancement in the base of the left ventricle

Management

- Subsequent investigations included serum free light chain levels, serum and urine immunofixation, and a fat pad biopsy, which confirmed light chain amyloidosis.
- Patient underwent chemotherapy.

Further Reading

- Dorbala S, Vangala D, Bruyere J, Quarta C, Kruger J, Padera R, et al. Coronary Microvascular Dysfunction Is Related to Abnormalities in Myocardial Structure and Function in Cardiac Amyloidosis. JACC: Heart Failure. 2014;2:358–367.
- Bravo P, Di Carli M, Dorbala S. Role of PET to evaluate coronary microvascular dysfunction in non-ischaemic cardiomyopathies. Heart Failure Reviews. 2017;22:455–464.
- Cecchi F, Olivotto I, Gistri R, Lorenzoni R, Chiriatti G, Camici P. Coronary Microvascular Dysfunction and Prognosis in Hypertrophic Cardiomyopathy. New England Journal of Medicine. 2003;349:1027–1035.

The opinions expressed in this chapter are those of the author(s) and do not necessarily reflect the views of the IAEA: International Atomic Energy Agency, its Board of Directors, or the countries they represent.

Open Access This chapter is licensed under the terms of the Creative Commons Attribution 3.0 IGO license (http://creativecommons.org/licenses/by/3.0/igo/), which permits use, sharing, adaptation, distribution and reproduction in any medium or format, as long as you give appropriate credit to the IAEA: International Atomic Energy Agency, provide a link to the Creative Commons license and indicate if changes were made.

Any dispute related to the use of the works of the IAEA: International Atomic Energy Agency that cannot be settled amicably shall be submitted to arbitration pursuant to the UNCITRAL rules. The use of the IAEA: International Atomic Energy Agency's name for any purpose other than for attribution, and the use of the IAEA: International Atomic Energy Agency's logo, shall be subject to a separate written license agreement between the IAEA: International Atomic Energy Agency and the user and is not authorized as part of this CC-IGO license. Note that the link provided above includes additional terms and conditions of the license.

The images or other third party material in this chapter are included in the chapter's Creative Commons license, unless indicated otherwise in a credit line to the material. If material is not included in the chapter's Creative Commons license and your intended use is not permitted by statutory regulation or exceeds the permitted use, you will need to obtain permission directly from the copyright holder.

Infection

8

Marcelo Di Carli, Raffaele Giubbini, Paolo Raggi, Michelle Williams, Elisa Milan, Ayaz Aghayev, Nazarena Pizzi, Albert Roque, Paola Anna Erba, Roberto Boni, Antonio Celestino, Elena Busnardo, Marianna Spallino, Irene Gotuzzo, Diana Paez, and Maurizio Dondi

Objectives

- To learn how to use PET imaging to exclude infection or inflammation.
- To recognize imaging patterns that may indicate infection rather than inflammation.
- To learn how to integrate correlative imaging findings into the interpretation of PET images.
- To learn how to use PET imaging to guide management.

Infection and inflammation are critical considerations in the management of patients with cardiovascular conditions, particularly those with implanted devices or prosthetic valves. Positron emission tomography (PET) imaging has emerged as a powerful tool in distinguishing between these two entities, guiding clinical decision-making and management. This chapter focuses on the application of PET imaging in the evaluation of suspected infections, including prosthetic valve endocarditis (PVE) and device-related infections. Through a series of detailed case studies, we will explore the imaging patterns that indicate infection versus inflammation, the integration of correlative imaging findings, and the use of PET imaging to guide therapeutic strategies.

8.1 Suspected Prosthetic Valve Endocarditis (PVE)

8.1.1 Prosthetic Valve Endocarditis: Case 63

Key Points

- In case of suspected infective endocarditis arising on prosthetic valves, Fluorodeoxyglucose (^{18}F-FDG PET)/computed tomography (CT) can be used to confirm the diagnosis, adding a major criterion of the ESC 2023 diagnostic criteria or a minor criterion of the MAGIC classification.
- The pattern of uptake of ^{18}F-FDG PET/CT can be used to differentiate chronic postsurgical remodeling (mild diffuse uptake) from active sites of infection (focal and intense uptake).

All authors have no conflict of interest to disclose.

M. Di Carli · A. Aghayev
Brigham and Women's Hospital, Boston, MA, USA
e-mail: mdicarli@bwh.harvard.edu; aaghayev@bwh.harvard.edu

R. Giubbini
Nuclear Medicine, International Specialized Hospital of Uganda (ISHU), Kampala, Uganda
e-mail: raffaele.giubbini@unibs.it

P. Raggi
Division of Cardiology, University of Alberta, Edmonton, AB, Canada

M. Williams
British Heart Foundation Centre for Research Excellence, Institute for Neuroscience and Cardiovascular Research, University of Edinburgh, Edinburgh, United Kingdom
e-mail: michelle.williams@ed.ac.uk

E. Milan
Nuclear Cardiology Lab and PET Centre, Treviso Hospital, Treviso, Italy
e-mail: elisa.milan@aulss2.veneto.it

N. Pizzi · A. Roque
Vall d'Hebron University Hospital, Barcelona, Spain

P. A. Erba · R. Boni · A. Celestino · M. Spallino · I. Gotuzzo
Nuclear Medicine, ASST Papa Giovanni XXIII Bergamo and University of Milano Bicocca, Milan, Italy
e-mail: paolaanna.erba@unimib.it; robertoboni.erba@unimib.it; antoniocelestino.erba@unimib.it; mariannaspallino.erba@unimib.it; irenegotuzzo.erba@unimib.it

E. Busnardo
Nuclera Medicine Department – San Raffaele Hospital, Milan, Italy
e-mail: busnardo.elena@hsr.it

D. Paez · M. Dondi (✉)
Division of Human Health, International Atomic Energy Agency, Vienna, Austria
e-mail: d.paez@iaea.org; m.dondi@iaea.org

© The Author(s) 2027
M. Di Carli et al. (eds.), *IAEA Atlas of Cardiac PET/CT*, https://doi.org/10.1007/978-3-662-74188-7_8

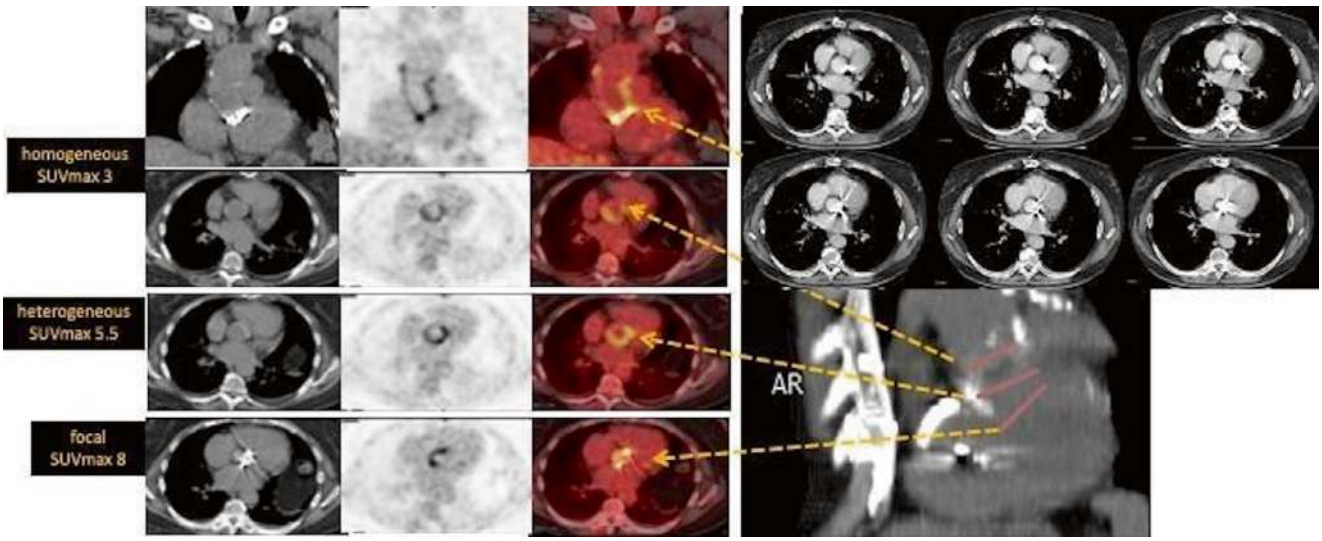


Fig. 8.1 ^{18}F-FDG PET/CT images with CT, PET, fused PET/CT, coronary computed tomography angiography (CCTA), and attenuation correction CT images. These show diffuse uptake along the ascending aorta graft which is nonspecific. There is also diffuse and intense focal uptake in the aortic valve suspicious for infection

History

- A 63-year-old woman was admitted to hospital with the diagnosis of acute enteritis after a week of fever with WBC = 7400/ul (N = 82,9%) CRP = 3.93 mg/dl. Empirical treatment with phosphomycin was followed by ciprofloxacin.
- Despite treatment, on day 10, she developed an episode of fever with gastric pain and finger paresthesia. She was admitted to the hospital.
- Her past medical history included a Bental procedure 4 years earlier for severe aortic stenosis and an ascending aorta aneurysm (beginning root). She also had an undifferentiated connective tissue disease with associated neutropenia.
- She had reduced respiratory sounds which were absent at the left base, a normal cardiac rhythm, and normal intensity heart sounds with a 3/6 systolic murmur over the base area.
- Lab tests: ESR = 35 mmHg, CRP = 3.95 mg/dl, normal WBCs, α1-globulin = 6.6%, LDH = 352 U/L. Blood culture positive for *Streptococcus infantarius*.
- She underwent transthoracic and transesophageal echocardiography; these showed nonspecific thickening of the aortic valve prosthesis with areas of hypoechoic areas of unknown significance and a possible small mobile hypoechoic mass on the aortic valve of uncertain significance.
- She was referred for ^{18}F-FDG PET/CT to assess for possible endocarditis (Fig. 8.1).

PET/CT Images

Findings

- ^{18}F-FDG PET/CT showed diffuse bilateral symmetric uptake at the site of the ascending aorta graft, consistent with nonspecific postsurgical inflammation.
- At the aortic valve, there was a pattern of intense focal uptake on a background of diffuse uptake, suspicious for infection.

Imaging Diagnosis

- Intense focal uptake on a background of diffuse uptake associated with the aortic valve suspicious for aortic valve endocarditis.

Differential Diagnosis

- Infection.
- Inflammation.
- Artifact.

Correlative Imaging

- None.

Management

- After PET/CT, the patient was started on antimicrobial therapy and was referred for a surgical assessment.

Further Reading

- Victoria Delgado, Nina Ajmone Marsan, Suzanne de Waha, et al. 2023 ESC Guidelines for the management of endocarditis: Developed by the task force on the management of endocarditis of the European Society of Cardiology (ESC). *European Heart Journal*, Volume 44, Issue 39, 14 October 2023, Pages 3948–4042, https://doi.org/10.1093/eurheartj/ehad193

- M Sollini, F Bartoli, R Boni, R Zanca, Role of multimodal imaging in patients with suspected infections after the Bentall procedure. Front. Cardiovasc. Med., 01 December 2021 Sec. Cardiovascular Imaging Volume 8–2021 | https://doi.org/10.3389/fcvm.2021.745556
- Nabil Chakfé, Holger Diener, Anne Lejay, et al. Editor's Choice - European Society for Vascular Surgery (ESVS) 2020 Clinical Practice Guidelines on the Management of Vascular Graft and Endograft Infections. Eur J Vasc Endovasc Surg 2020 Mar;59(3):339–384. https://doi.org/10.1016/j.ejvs.2019.10.016. Epub 2020 Feb 5.
- Johan Wassélius 1, Jonas Malmstedt, Bo Kalin et al. High ^{18}F-FDG Uptake in synthetic aortic vascular grafts on PET/CT in symptomatic and asymptomatic patients J Nucl Med 2008 Oct;49(10):1601–5. https://doi.org/10.2967/jnumed.108.053462. Epub 2008 Sep 15.

8.1.2 Prosthetic Valve Endocarditis with Contrast CT: Case 64

Key Points

- ^{18}F FDG PET/CT has proven to be useful to confirm the presence of prosthetic valve endocarditis. ^{18}F-FDG PET, associated with CT angiography (^{18}F-FDG PET/CTA) can help in the detection of periprosthetic complications such as abscesses or pseudoaneurysms, which are relevant for prognosis and decision-making and can be missed by echocardiography in some cases.
- Dedicated cardiac PET/CT has demonstrated to provide the maximum information (both metabolic and anatomic) for the diagnosis of PVE and its complications, but entails important technical considerations, which include ECG-gated acquisitions and contrast-enhanced cardiac CT.

History

- A 76-year-old man with a bioprosthetic aortic valve replacement 13 years ago referred for a PET/CTA study in the setting of fever and bacteremia due to *Enterococcus faecalis*.
- Transoesophageal echocardiography (TOE) showed marked leaflet thickening of the aortic prosthesis but no clear images of vegetations.
- The patient also had a recently implanted axillo-femoral bypass graft for treating obstructive peripheral artery disease (Figs. 8.2 and 8.3).

PET/CTA Images

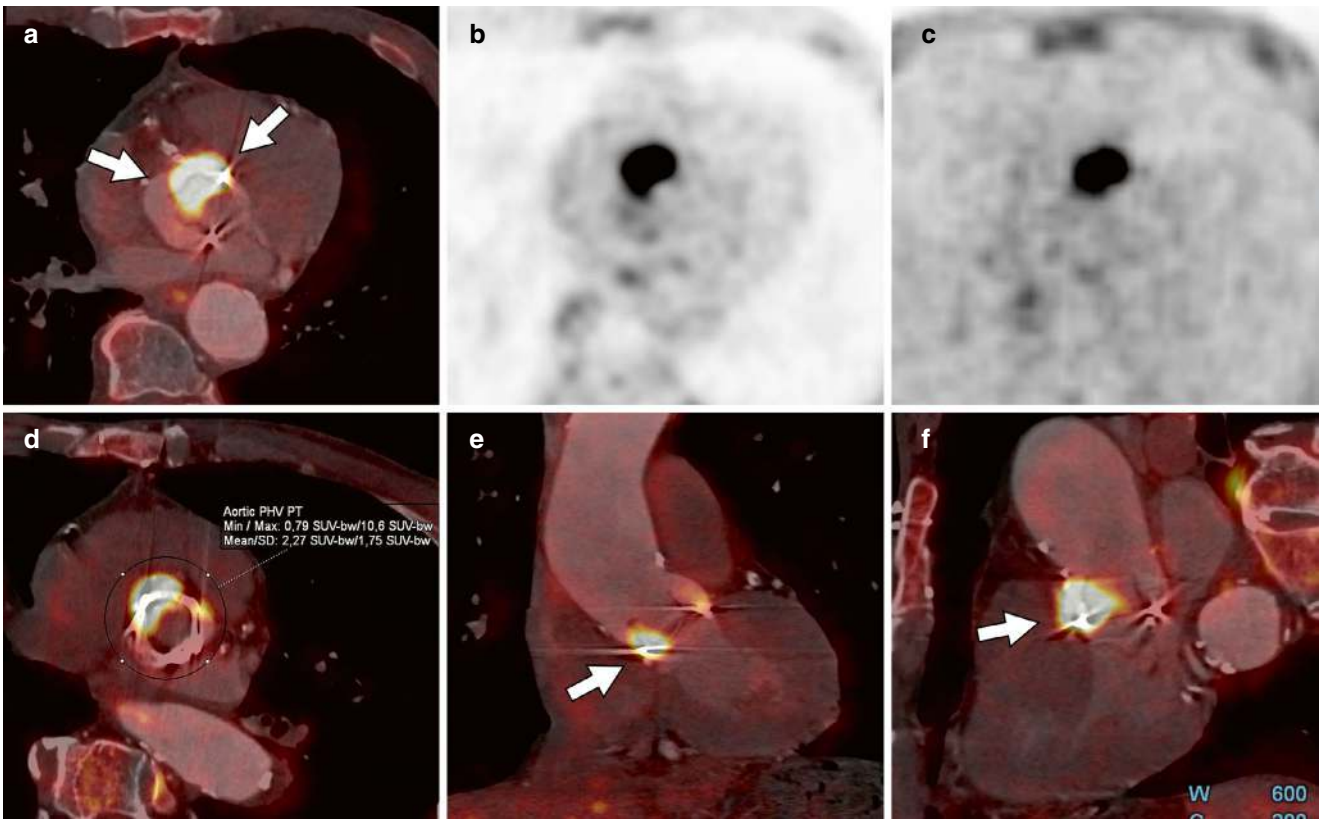


Fig. 8.2 Cardiac ^{18}F-FDG PET/CT. Fusion (**a**), attenuation-corrected (**b**), and non-attenuation-corrected PET (**c**) axial views showing focal and intense (SUVmax 11, SUVmean 2.3) ^{18}F-FDG uptake at the aortic prosthetic ring. Fusion transverse (**d**), coronal (**e**), and 3-chamber (**f**) views of the aortic prosthetic valve better delineate the ^{18}F-FDG uptake and suggest periprosthetic extension of the metabolic activity (arrows)

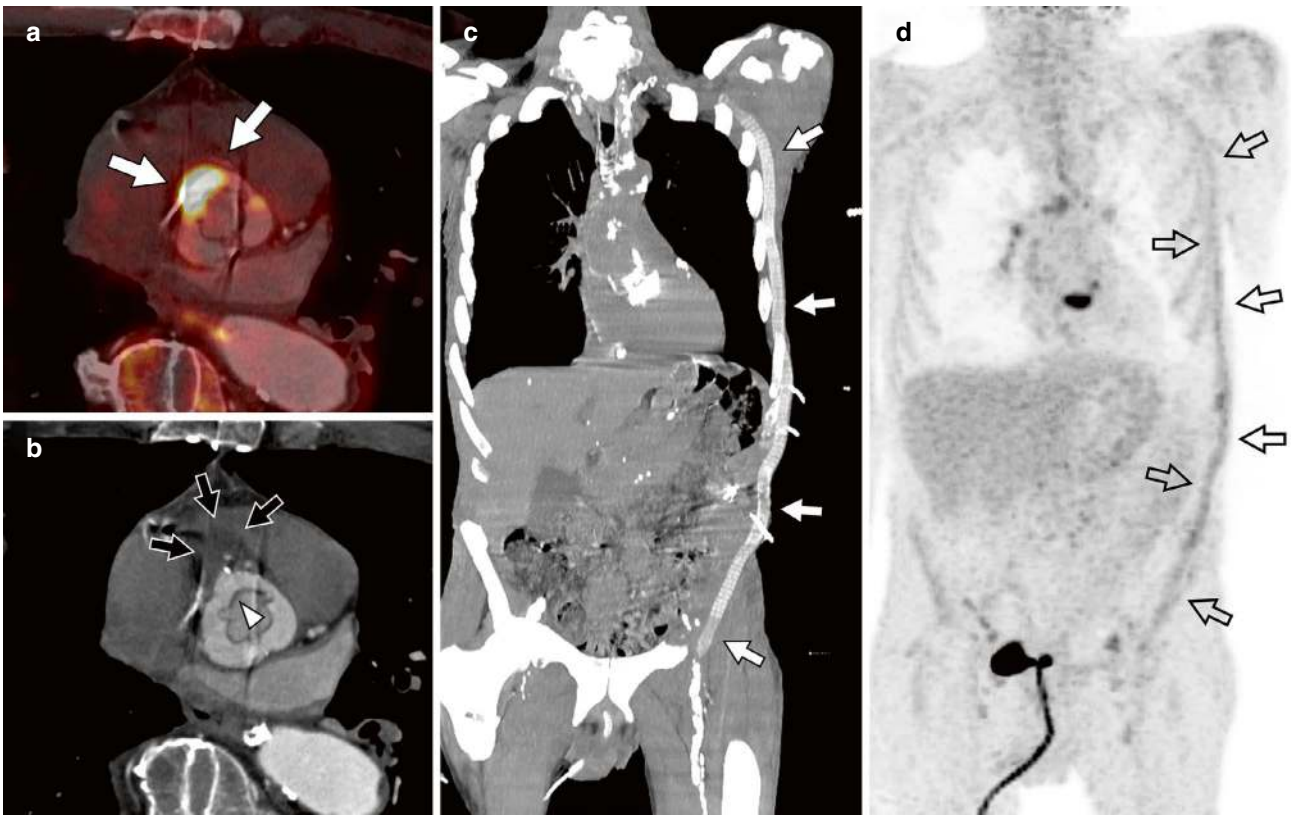


Fig. 8.3 ^{18}F-FDG-PET/CTA. Fusion (**a**) and CTA (**b**) transverse valve plane images of the aortic bioprosthesis. Intense focal FDG uptake at the right coronary sinus (**a**, white arrows). Thickened right aortic leaflet (**b**, arrowhead) without images of vegetations. Periprosthetic soft tissue lesion (10-mm thick) consistent with a periprosthetic abscess (**b**, black arrows). Whole-body CT (**c**) and PET (**d**) images showed no distant lesions related to PVE and depicted mild and diffuse FDG uptake at the peripheral left axillo-femoral bypass, ruling-out infection of the graft

Findings Summary
- Intense focal ^{18}F-FDG uptake at the aortic prosthetic ring, confirming the diagnosis of PVE.
- Periprosthetic hypermetabolic soft tissue lesion (periprosthetic abscess).

Imaging Diagnosis
- Prosthetic aortic valve endocarditis (PVE) with periprosthetic extension (abscess).
- No evidence of distant lesions or sources of the bacteremia detected by PET/CT.
- Infection of the peripheral bypass ruled out.

Correlative Imaging
- Transoesophageal echocardiography (TOE): leaflet thickening, but no clear images of vegetations.
- Colonoscopy: normal.

Differential Diagnosis: Discussion
- Visualization of prosthetic ^{18}F-FDG uptake does not always imply infection. ^{18}F-FDG uptake distribution must be properly interpreted to differentiate normal from infection patterns.
- Likewise, the presence of anatomical lesions characteristic of endocarditis detected by CTA significantly increases the diagnostic specificity.

Management
- Enterococcal prosthetic valve endocarditis with periprosthetic abscess.
- Periprosthetic abscess is considered as locally uncontrolled infection and indication for surgery.
- New aortic valve replacement with good result and clinical outcome.

Further Reading

- Fowler VG, Durack DT, Selton-Suty C, Athan E, Bayer AS, Chamis AL, et al. The 2023 Duke-ISCVID Criteria for Infective Endocarditis: Updating the Modified Duke Criteria. Clin Infect Dis 2023;77:518–526. https://doi.org/10.1093/cid/ciad271.
- Oliveira M, Guittet L, Hamon M, Hamon M. Comparative Value of Cardiac CT and Transesophageal Echocardiography in Infective Endocarditis: A Systematic Review and Meta-Analysis. Radiol Cardiothorac Imaging 2020;2:e190189.

8.1.3 Prosthetic Valve Endocarditis After Mechanical Valve Replacement: Case 65

Key Points

- ^{18}F-FDG-PET/CT has demonstrated a significant improvement in the diagnostic yield of prosthetic valve endocarditis (PVE).
- This hybrid imaging technique has proven to be useful to confirm the diagnosis in cases of high clinical suspicion of PVE when echocardiography is negative or inconclusive, which is its main and widely accepted indication.
- An optimal cardiac PET/CT scan implies a proper acquisition and interpretation of both metabolic and anatomic images (PET/CTA).

History

- A 47-year-old woman who underwent mechanical aortic and mitral valve replacement 7 years ago was referred for a cardiac PET/CTA in the setting of fever and persistent positive blood cultures (*Staphylococcus epidermidis)* after a venous thrombophlebitis episode.
- Echocardiography had been inconclusive (visualization of a small 2-mm mobile mass on the mitral valve indistinguishable between small vegetation or thrombus) (Fig. 8.4).

PET/CTA Images

Imaging Findings

- Intense multifocal ^{18}F-FDG uptake at the aortic prosthetic valve, confirming the diagnosis of PVE.
- A valve uptake index (VUI) value of 0.62 correlates with an abnormal FDG uptake pattern.
- Hypermetabolic soft tissue lesion at the mitral-aortic fibrosa consistent with a periprosthetic abscess.

Imaging Diagnosis

- Prosthetic valve endocarditis (PVE) with periprosthetic extension (abscess) at the mitral-aortic union.
- No evidence of distant lesions or sources of the bacteremia detected by PET/CT.

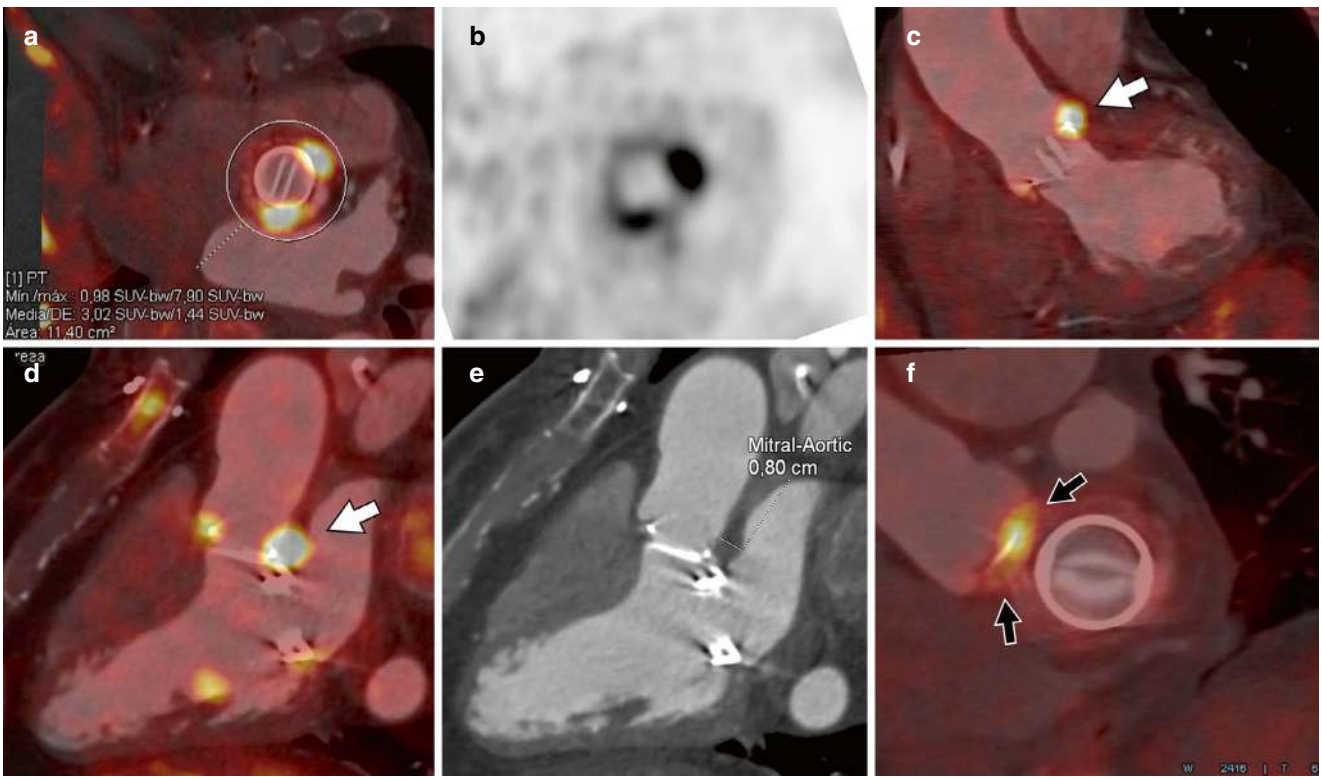


Fig. 8.4 ^{18}F-FDG-PET/CTA scan. Fusion (**a**) and attenuation-corrected PET (**b**) transverse view of the aortic prosthesis showing intense (SUVmax 8, SUVmean 3) and multifocal (VUI 0.62) FDG uptake at the aortic prosthetic ring. Coronal-oblique view confirms focal ^{18}F-FDG uptake (**c**, arrow), normal opening of both discs, and no evidence of vegetations by CTA. Three-chamber fusion (**d**) and CT (**e** and **f**) images showing hypermetabolic thickening of the mitral-aortic fibrosa (8-mm thick) associated with soft tissue lesion, findings consistent with a periprosthetic abscess (arrow). Fusion transverse view of the mitral prosthetic valve that is in close contact with the involved mitral-aortic fibrosa but with no other significant FDG uptake. There are no images of vegetations in any of the prostheses. (Legend: SUVmax and SUVmean, maximum and mean standardized uptake value; VUI, valve uptake index)

Correlative Imaging
- Transesophageal echocardiography (TOE):
- Small 2-mm mobile mass on the mitral valve indistinguishable between small vegetation or thrombus.

Differential Diagnosis
- Prosthetic ^{18}F FDG uptake can be secondary to sterile inflammatory activity (postsurgical reactive and healing process) or infection, and the differential diagnosis between these two situations relies on the adequate interpretation of the ^{18}F FDG uptake pattern (distribution and intensity) and the presence of underlying anatomical lesions.

Management
- Staphylococcal prosthetic endocarditis with periprosthetic extension (locally uncontrolled infection).
- High surgical risk patient (fragile patient, history of mucopolysaccharidosis). Moreover, there was no evidence of prosthetic disfunction, no persistent fever, limited periprosthetic extension and no symptomatic embolic events.
- The patient was managed medically (unlimited antibiotic treatment). A control PET scan after 6 weeks of antibiotic treatment showed persistent focal FDG uptake but no additional periprosthetic complications.

Further Reading

- Delgado V, Ajmone Marsan N, de Waha S, Bonaros N, Brida M, Burri H, et al. 2023 ESC Guidelines for the management of endocarditis. ESC Scientific Document Group. Eur Heart J 2023 14; 44:3948–4042.
- Pizzi MN, Roque A, Fernández-Hidalgo N, et al. Improving the diagnosis of infective endocarditis in prosthetic valves and intracardiac devices with ^{18}F-FDG-PET/CT-Angiography: initial results at an infective endocarditis referral center. Circulation 2015; 132:1113–1126.
- Roque A, Pizzi MN, Fernandez-Hidalgo N, Romero-Farina G, Burcet G, Reyes-Juarez JL, et al. The valve uptake index: improving assessment of prosthetic valve endocarditis and updating [18F]FDG PET/CT(A) imaging criteria. Eur Heart J Cardiovasc Imaging 2022;23: 1260–1271.

8.1.4 Prosthetic Valve Endocarditis in TAVI: Case 66

Key Points
- ^{18}F-FDG-PET/CT and cardiac CT have demonstrated diagnostic utility for the detection of endocarditis in the population of patients with transcatheter aortic valve implantation (TAVI) valves.
- TAVI-infective endocarditis (IE) is a growing medical issue, and its diagnosis can also be challenging for echocardiography due to quite frequent atypical manifestations.

History
- An 88-year-old man with a TAVI implantation 3 months ago was referred for fever and multiple blood cultures positive for *Enterococcus faecalis*. Echocardiography was negative, but clinical suspicion of endocarditis remained high, and a cardiac ^{18}F-FDG PET/CTA was performed (Figs. 8.5 and 8.6).

PET/CTA Images

Findings Summary
- Initial (diagnostic) cardiac PET/CT.
- Valve leaflet thickening and vegetations.
- Hypermetabolic periprosthetic soft tissue thickening (abscess).

Follow-Up PET/CT
- Contrast-filled cavity (pseudoaneurysm).
- Persistent prosthetic ^{18}F-FDG uptake.

Imaging Diagnosis
- Transcatheter aortic valve implantation endocarditis (TAVI-IE) complicated with a periprosthetic abscess which evolved to pseudoaneurysm.

Correlative Imaging
- Transesophageal echocardiography (TOE): negative.

Differential Diagnosis: Discussion
As in surgically implanted prosthetic valves, FDG uptake in TAVI must be carefully evaluated to differentiate non-infection from infection. Focal or heterogeneous uptake suggests endocarditis, especially if associated with infective endocarditis-related anatomical lesions.

Leaflet thickening secondary to thrombus deposition could mimic vegetations. The presence or absence of abnormal FDG uptake and the correlation with blood cultures will help avoid misdiagnosis.

Management
- The patient was considered of high risk for surgery (age, fragility, TAVI procedures).
- He was managed medically and continues follow-up of the pseudoaneurysm by echocardiography and cardiac CTA.

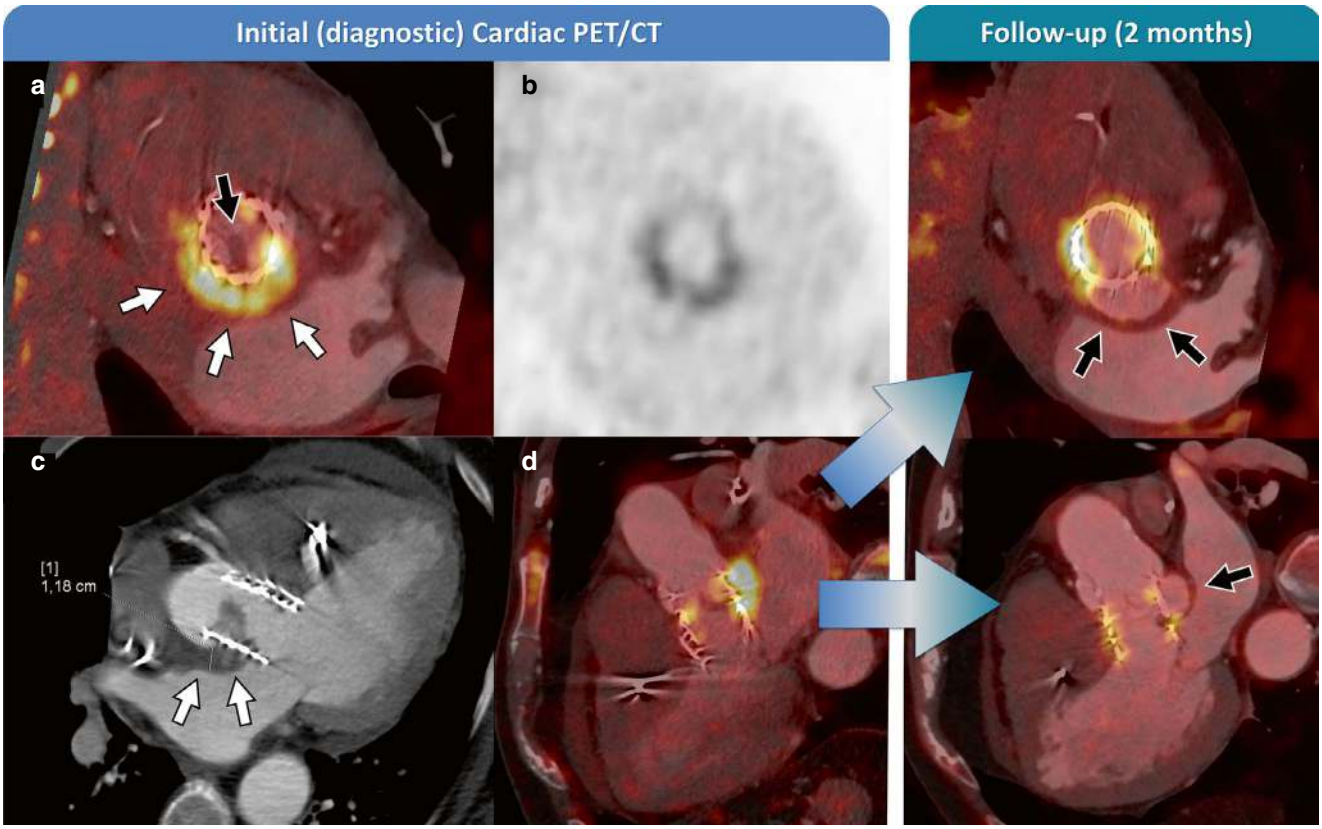


Fig. 8.5 ^{18}F-FDG-PET/CTA scan. Fusion (**a**) and attenuation-correction PET (**b**) transverse views of the aortic prosthesis show severe thickening of the noncoronary valve leaflet with vegetations (black arrow) and intense (SUVmax 6.5) heterogeneous (VUI 0,67) FDG uptake (white arrows) at the posterior aspect of the aortic prosthetic stent. Cardiac CTA (**c**) and fusion (**d**) three-chamber view/projection showing a periprosthetic hypermetabolic soft tissue lesion (15-mm thick, arrows) affecting the mitral-aortic fibrosa which corresponds to a peri-TAVI periprosthetic abscess. The patient was considered high risk for surgery, and medical treatment was decided. A follow-up PET/CT scan 2 months later revealed the presence of a contrast-filled cavity at previous location of the periprosthetic abscess, indicating its evolution into a pseudoaneurysm. Regarding metabolism, there was a significant decrease of the FDG uptake extension and intensity (SUVmax 4.2) (extension and intensity) although not complete resolution. Legend: *SUVmax*, maximum standardized uptake value, *VUI* valve uptake index

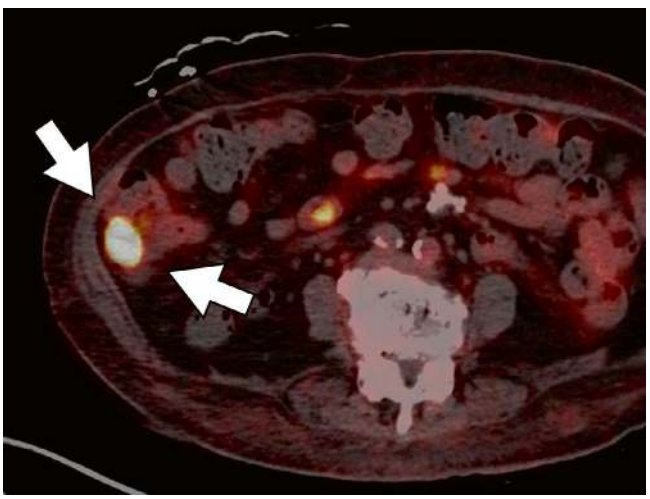


Fig. 8.6 Fusion axial view of the whole-body acquisition shows focal and intense ^{18}F-FDG uptake in the ascending colon (arrows), suggesting the portal of entry of the infection. A subsequent colonoscopy confirmed a colonic polypoid lesion

Further Reading

- San S, Abulizi M, Moussafeur A, Oliver L, Lepeule R, Nahory L, et al. Characterization of 18-Fluorodeoxyglucose Uptake Pattern in Infective Endocarditis After Transcatheter Aortic Valve Implantation. JACC Cardiovasc Imaging 2019;12:930–932.
- Del Val D, Trottier M, Alperi A, Muntané-Carol G, Faroux L, Delarochellière R, et al. 18F-Fluorodeoxyglucose Uptake Pattern in Noninfected Transcatheter Aortic Valves. Circ Cardiovasc Imaging. 2020;13:e011749.

8.1.5 Bioprosthetic Pulmonary-Valved Graft Infection in a Patient with CHD: Case 67

Key Points

- Surgical treatment of patients with congenital heart disease (CHD) often requires implantation of a large amount of prosthetic material, thus making these a recognized

risk group for endocarditis and especially complex for evaluation by echocardiography.
- ^{18}F-FDG-PET/CT has proven to be a very useful technique in reaching a conclusive diagnosis of cardiac infection when the clinical suspicion is high, and echocardiography is negative or inconclusive.

History
- A 38-year-old man, with a history of pulmonary atresia and ventricular septal defect (VSD) repaired in infancy with a bioprosthetic pulmonary-valved tube (a graft connecting the right ventricle to the pulmonary arteries) and a VSD closure patch.
- He was admitted due to septic shock, and blood cultures were positive for *Staphylococcus aureus*. A transthoracic echocardiography showed mild gradient increase in the pulmonary prosthesis, without lesions definitive for endocarditis.
- Transesophageal echocardiography (TOE) was not performed, since it would probably not improve visualization of right-sided structures.
- A cardiac ^{18}F-FDG PET/CTA was performed to complete evaluation due to the high clinical suspicion of infection (Fig. 8.7).

PET/CTA Images

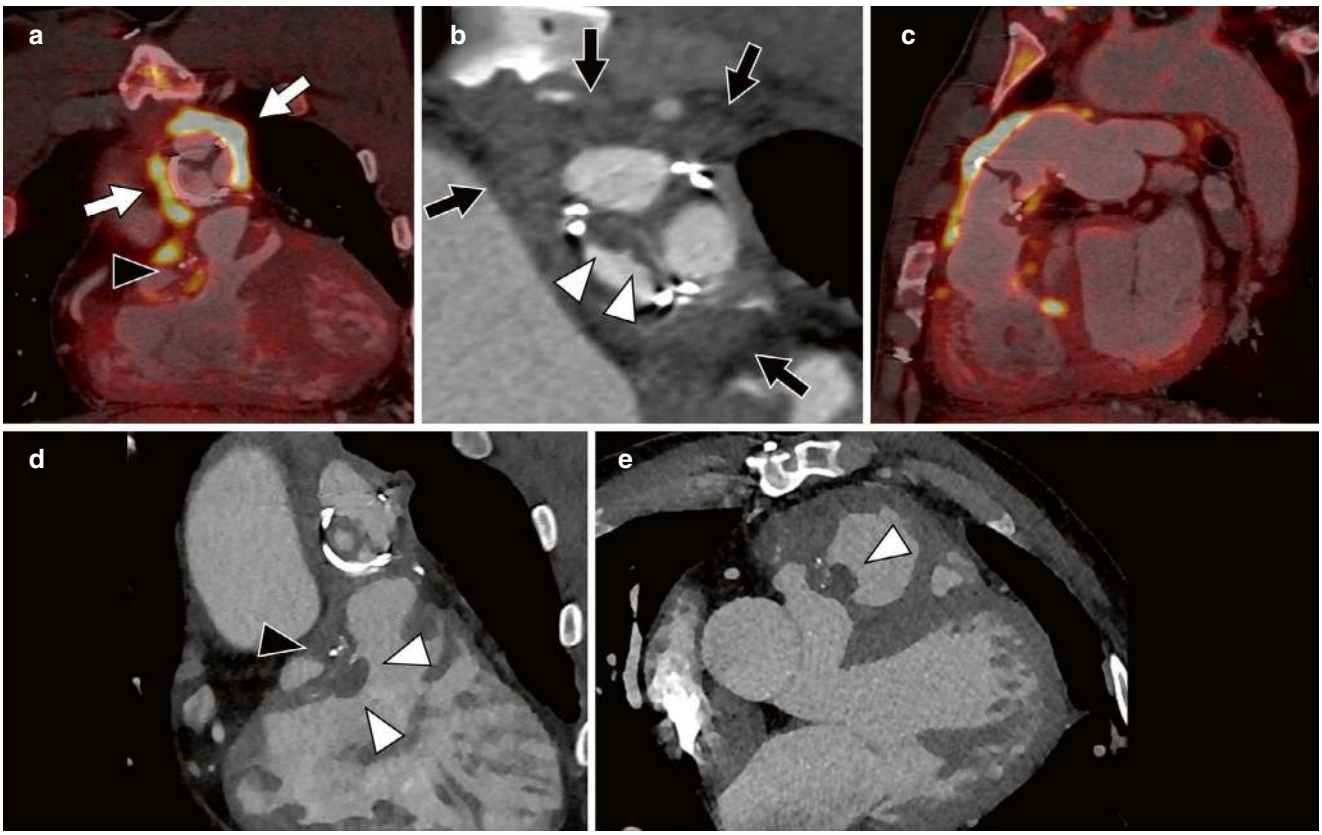


Fig. 8.7 ^{18}F-FDG PET/CTA. Fusion (**a**) and CTA (**b**) transverse view images of the bioprosthetic pulmonary graft at the valvular plane showing marked nodular thickening of the valvular leaflets consistent with multiple vegetations (**b**, arrowheads). Intense and heterogeneous perivalvular FDG uptake (**a**, arrows) associated with an underlying ill-defined soft tissue perivalvular and perigraft lesion (**b**, arrows) compatible with a periprosthetic abscess. In addition, there was focal FDG uptake at the VSD patch (**a**, arrowhead). Sagittal view (**c**) at the pulmonary graft showing the cranio-caudal extension of the peritubular abscess and improving the visualization of vegetations. A follow-up CTA (**d** and **e**) revealed a large vegetation (hypodense soft tissue lesion, white arrowheads) which appeared on the infected VSD patch (black arrowhead)

Findings Summary
- Marked thickening and multiple vegetations of the valvular leaflets.
- Periprosthetic soft tissue lesion with intense and heterogeneous FDG uptake (periprosthetic abscess).
- Focal FDG uptake at the VSD patch, where later arose a large vegetation (hypodense soft tissue lesion).

Imaging Diagnosis
- Bioprosthetic pulmonary-valved graft infection, involving the VSD patch.
- No evidence of pulmonary septic embolic lesions.

Correlative Imaging
- Transthoracic echocardiography (not shown): increased pulmonary gradients and significant leaflet thickening but no clear images of vegetations.

Differential Diagnosis
- None.

Management
PET/CTA allowed correct evaluation of all the prosthetic materials confirming the diagnosis of cardiac infection. The patient underwent surgery with a pulmonary-valved graft and VSD patch replacement.

Further Reading

- Olivella A, Pizzi MN, Dos-Subirà L, et al. Right-sided endocarditis on Contegra tube in a complex cianotic congenital heart disease. J Nucl Cardiol. 2019 https://doi.org/10.1007/s12350-019-01708-w.
- Meyer Z, Fischer M, Koerfer J, et al. The role of FDG-PET-CT in pediatric cardiac patients and patients with congenital heart defect. Int J Cardiol. 2016;220:656–60.
- Pizzi MN, Dos-Subirà L, Roque A, et al. ^{18}F-FDG-PET/CT angiography in the diagnosis of infective endocarditis and cardiac device infection in adult patients with congenital heart disease and prosthetic material. International Journal of Cardiology 2017;248:396–402.

8.1.6 Aortic Graft Infection: Case 68

Key Points
- ^{18}F-FDG-PET/CT and CT can be useful imaging techniques for assessing prosthetic aortic graft infections.
- Infected grafts usually show intense, multifocal, or heterogeneous peritubular ^{18}F-FDG uptake along the entire graft, associated with peritubular soft tissue lesions (abscess) or poorly delimited collections.
- As in PVE cases, vegetations or pseudoaneurysms can also be found affecting the valved portion of the graft. ^{18}F-FDG uptake circumscribed/limited to the graft sutures or other surgical adhesive materials can be a normal finding, and homogeneous peritube fluid accumulation can be found after recent graft surgery and should not be considered infection.

History
- A 52-year-old man with a Bentall-Bono procedure and a pacemaker due to A type aortic dissection and postsurgical AV-block 8 years previously.
- He was hospitalized due to severe anemia, constitutional syndrome, and 3 months of fever.
- Blood cultures were positive for *Streptococcus mutans*.
- Transthoracic echocardiography showed vegetations at the mechanic aortic valve.
- He was urgently transferred to a third-level hospital with an endocarditis heart team and possibility of cardiac surgery (Fig. 8.8).

PET/CTA Images

Findings Summary
- Intense and heterogeneous peritube FDG uptake associated with a soft tissue lesion around the whole graft consistent with a peri-Bentall abscess.
- Contrast-enhanced cavity compatible with a pseudoaneurysm.

Imaging Diagnosis
Aortic graft infection.

Correlative Imaging
Transthoracic echocardiography (not shown): vegetations at the prosthetic mechanical aortic valve. Unable to visualize the tubular portion of the graft.

Differential Diagnosis: Discussion—Teaching Points
- Low-grade diffuse peritube FDG uptake with accumulation at the sutures rather than around the tube and no pathological anatomic changes in the CTA images should be considered normal findings.
- Homogeneous fluid and well-delimited perigraft collections can be found after recent graft surgery and should not be considered infection.

Management
Aortic graft and pacemaker replacement. Although a high-risk surgery, the patient underwent well.

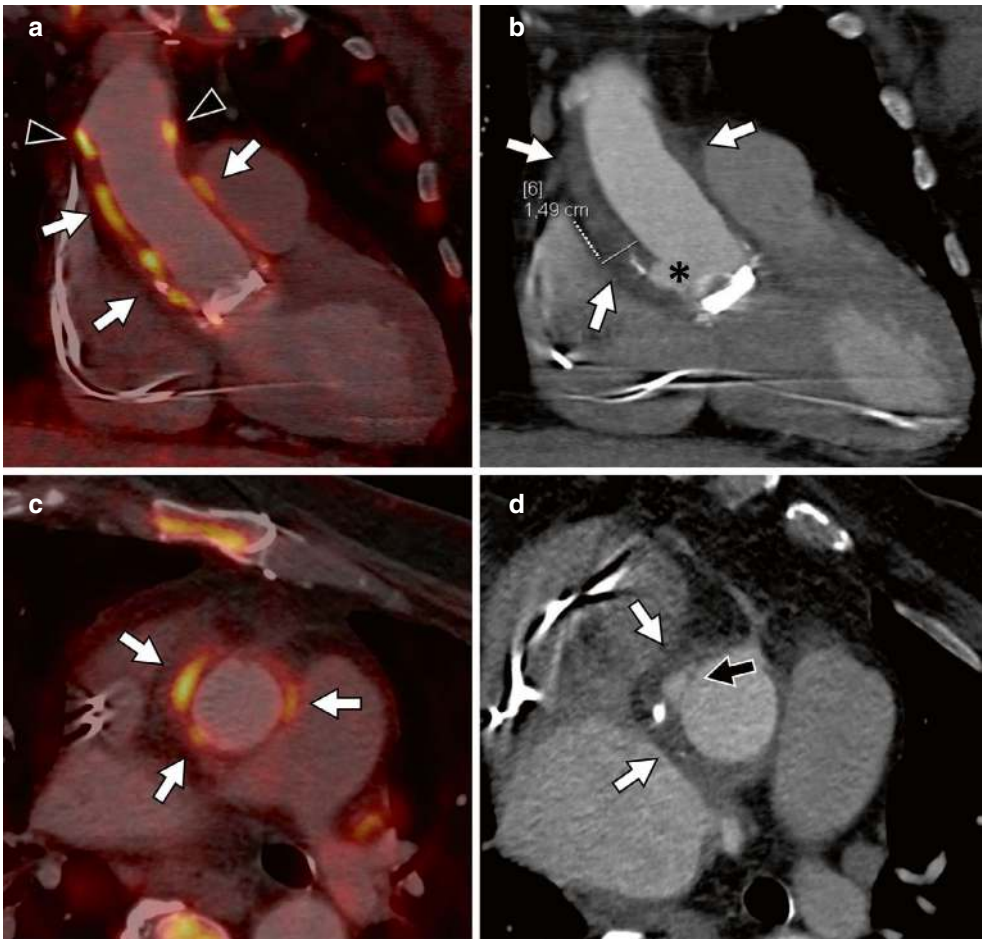


Fig. 8.8 ^{18}F-FDG-PET/CTA. Coronal and cross-sectional fusion (**a**, **c**) and CT (**b**, **d**) images. Intense (SUVmax 12) and heterogeneous perigraft FDG uptake (**a**, **c**, arrows), along the whole-body tube (**a**, black arrowheads) and associated with an underlying soft tissue lesion depicted by CTA (**b**, arrows). The described findings are consistent with a perigraft infection and abscess. Contrast-enhanced images also allowed the visualization of a small pseudoaneurysm at right coronary sinus level (**b**, asterisk; **d**, arrows)

Further Reading

- Lyons OT, Baguneid M, Barwick TD, Bell RE, Foster N, Homer-Vanniasinkam S, et al. Diagnosis of Aortic Graft Infection: A Case Definition by the Management of Aortic Graft Infection Collaboration (MAGIC). Eur J Vasc Endovasc Surg 2016 Dec;52:758–763.
- Ramos-Martínez A, Blanco-Alonso S, Calderón-Parra J, Rodríguez-Alfonso B, Martínez-López D, Cobo-Marcos M, et al. Endocarditis in Patients With Ascending Aortic Prosthetic Graft: A Series From a National Referral Hospital. J Am Coll Cardiol 2020 May 12;75:2380–2382.
- Pizzi MN, Roque A, Cuéllar-Calabria H, Fernández-Hidalgo N, Ferreira-González I, González-Alujas MT et al. Infective versus inflammatory patterns in ^{18}F-FDG-PET/CTA of prosthetic cardiac valves and valve-tube grafts. J Am Coll Cardiol Img 2016;9:1224–27.
- Wahadat AR, Tanis W, Mulders TA, Graven LH, Bekker MWA, Bekkers JA, et al. Normal imaging findings after ascending aorta prosthesis implantation on 18F-Fluorodeoxyglucose Positron Emission Tomography with computed tomography. J Nucl Cardiol 2022;29:2938–2948.

8.1.7 Native Valve Endocarditis: Case 69

Key Points

- Echocardiography and blood cultures are the cornerstone for diagnosing native valve endocarditis (NVE).
- The reported sensitivity of ^{18}F-FDG PET/CT in NVE is low, and its systematic use in this clinical scenario is not currently recommended by guidelines.
- C*ardio-dedicated* ECG-gated PET/CT examinations, which include cardiac CTA (already recommended in the evaluation of NVE) can help achieve the diagnosis of endocarditis and its complications in some cases.

History

- An 80-year-old man admitted due to prostatitis causing persistent bacteremia by *Enterococcus faecalis*.
- An echocardiogram was performed because of heart failure and a significant aortic murmur, and it showed severe aortic regurgitation but no clear vegetations on the aortic native valve. Conversely, a possible vegetation on the mitral native valve was described/identified (Fig. 8.9).

PET/CTA Images

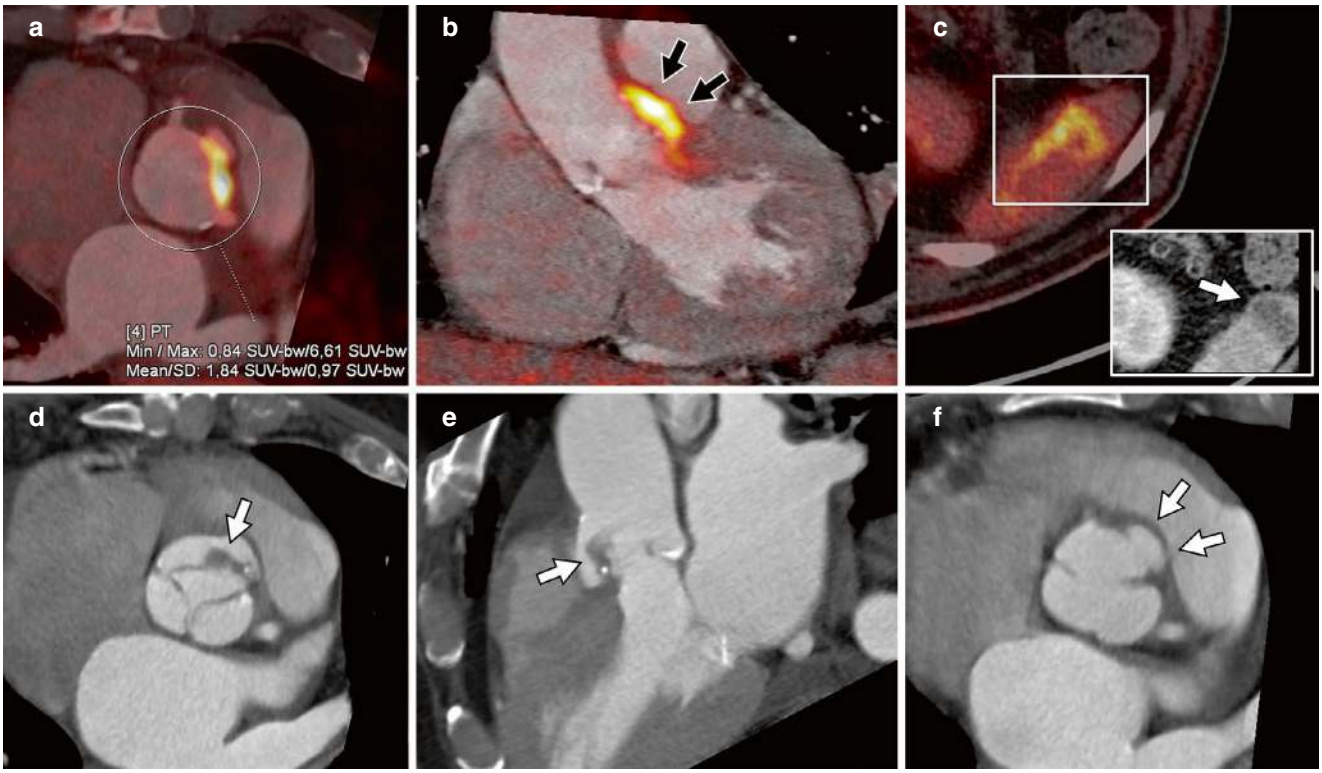


Fig. 8.9 Cardiac ^{18}F-FDG-PET/CTA. Transverse (**a**) and coronal (**b**) fusion images of the aortic valve showing focal and intense (SUVmax 6.6) valve FDG uptake (and probably periaortic extension). (**c**) CTA images showing a mobile hypodense soft tissue lesion at the aortic right leaflet compatible with vegetation (**d**, **e**, arrows) and a contrast-filled cavity arising from the right coronary sinus corresponding with a pseudoaneurysm (**f**, arrows). Fusion and CT upper abdominal images depicting a peripheral hypodense spleen lesion with hypermetabolic walls consistent with splenic embolism. Legend: SUVmax and SUVmean, maximum and mean standardized uptake value

Findings Summary
- Mobile hypodense soft tissue leaflet lesion (vegetation).
- Intense focal aortic and periaortic ^{18}F-FDG uptake (suggests perivalvular extension of the infection, probably abscess).
- Contrast-filled cavity arising from the right coronary sinus (pseudoaneurysm).
- Hypodense spleen lesion with hypermetabolic walls (splenic embolism).

Imaging Diagnosis
- Aortic native valve endocarditis.
- Perivalvular extension of the infection with pseudoaneurysm and probable abscess (locally uncontrolled infection).
- Splenic embolism (distant infective endocarditis related lesion).

Correlative Imaging
- Transoesophageal echocardiography (TOE).
- Severe aortic regurgitation.
- Possible mitral vegetation.

Differential Diagnosis
- Although remote and infrequent, certain entities can eventually affect the aortic root and could be consider differential diagnostics. Among others, take into account vasculitis or other inflammatory processes, IgG4-related disease, tumors, and aortic hematomas.

Management
- NVE with locally uncontrolled infection, embolism, and persistent bacteremia.
- The patient underwent aortic valve replacement with good results.
- Also completed 6-week antibiotic treatment.

Further Reading

- Fowler VG, Durack DT, Selton-Suty C, Athan E, Bayer AS, Chamis AL, et al. The 2023 Duke-ISCVID Criteria for Infective Endocarditis: Updating the Modified Duke Criteria. Clin Infect Dis 2023;77:518–526.
- [18F]FDG-PET CT for the evaluation of native valve endocarditis. Abikhzer G, Martineau P, Grégoire J, Finnerty V, Harel F, Pelletier-Galarneau M.J Nucl Cardiol. 2022 Feb;29(1):158–165.

8.1.8 Native Valve Endocarditis in a Pediatric Patient: Case 70

Key Points

- ^{18}F-FDG PET/CT can be a useful diagnostic tool in the evaluation of children with fever of unknown origin.
- ^{18}F-FDG PET/CT can detect septic emboli such as in the lungs.
- ^{18}F-FDG PET/CT can differentiate between endocarditis and other infective processes. However, the sensitivity of ^{18}F-FDG PET/CT for native valve endocarditis is low.

History

- A 6-year-old girl with a congenital perimembranous ventricular septal defect presented with fever, positive blood cultures (abiotrophia).
- A transthoracic echocardiogram showed moderate tricuspid insufficiency but was otherwise negative for vegetations.
- She was referred for ^{18}F-FDG PET/CT to rule out possible endocarditis and to identify foci of distant infection (Fig. 8.12).

PET/CT Images

Imaging Diagnosis

Focal ^{18}F-FDG uptake in the tricuspid valve and right lung consistent with infection.

Differential Diagnosis

- Infection.
- Inflammation.

Correlative Imaging

- None.

Findings

- Optimal suppression of physiological myocardial uptake with high intensity focal uptake of ^{18}F-FDG in the tricuspid valve (Fig. 8.10).
- Focal intense ^{18}F-FDG uptake in the periphery of the right lung associated with an area of consolidation (Fig. 8.11).
- Diffuse and intense uptake in the spleen and bone marrow are likely reactive to the sepsis (Fig. 8.13).

Management

- The patient was treated with antibiotic therapy for two weeks with initial clinical response, followed by recur-

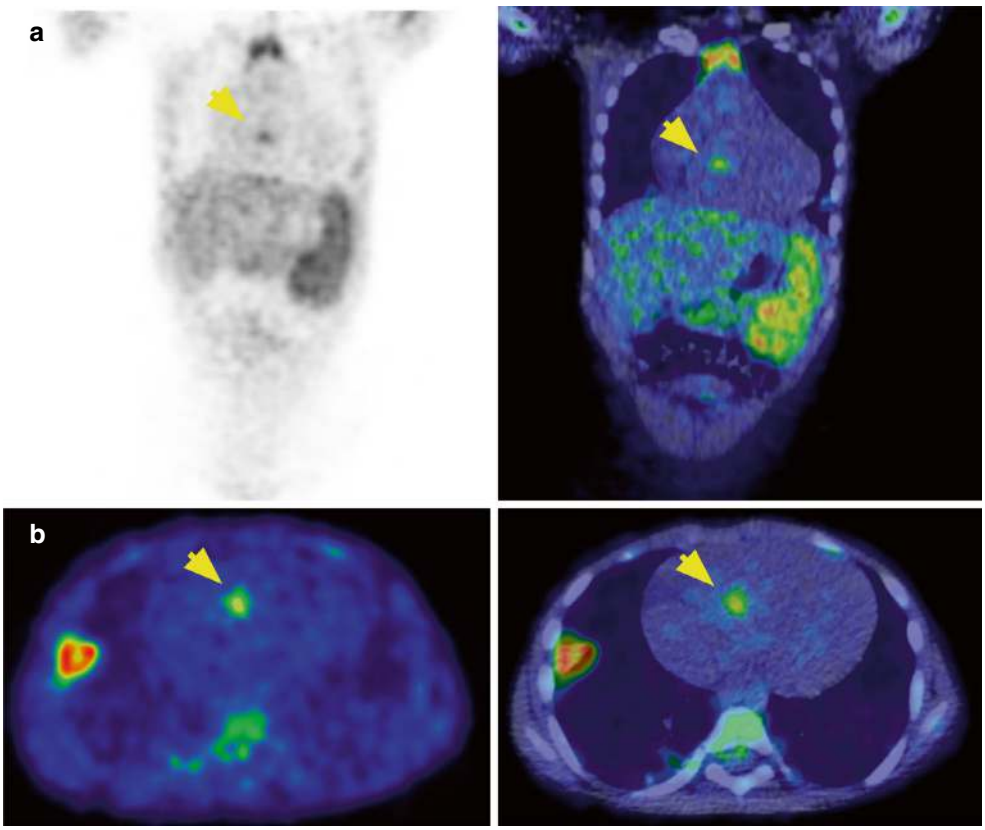


Fig. 8.10 ^{18}F-FDG PET/CT images showed focal uptake at the tricuspid valve (yellow arrow) in coronal (**a**) and axial (**b**) reconstructions

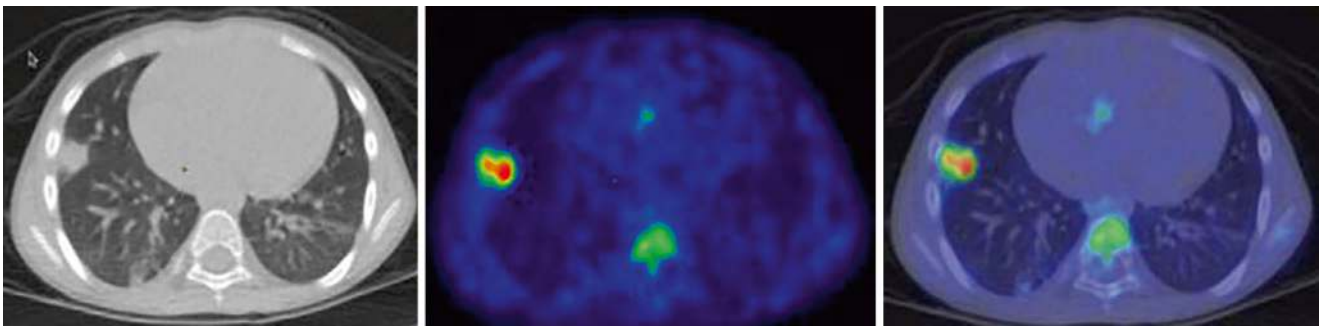


Fig. 8.11 ^{18}F-FDG PET/CT images showed focal increase of ^{18}F-FDG associated with an area of consolidation in the periphery of the right lung (yellow arrows)

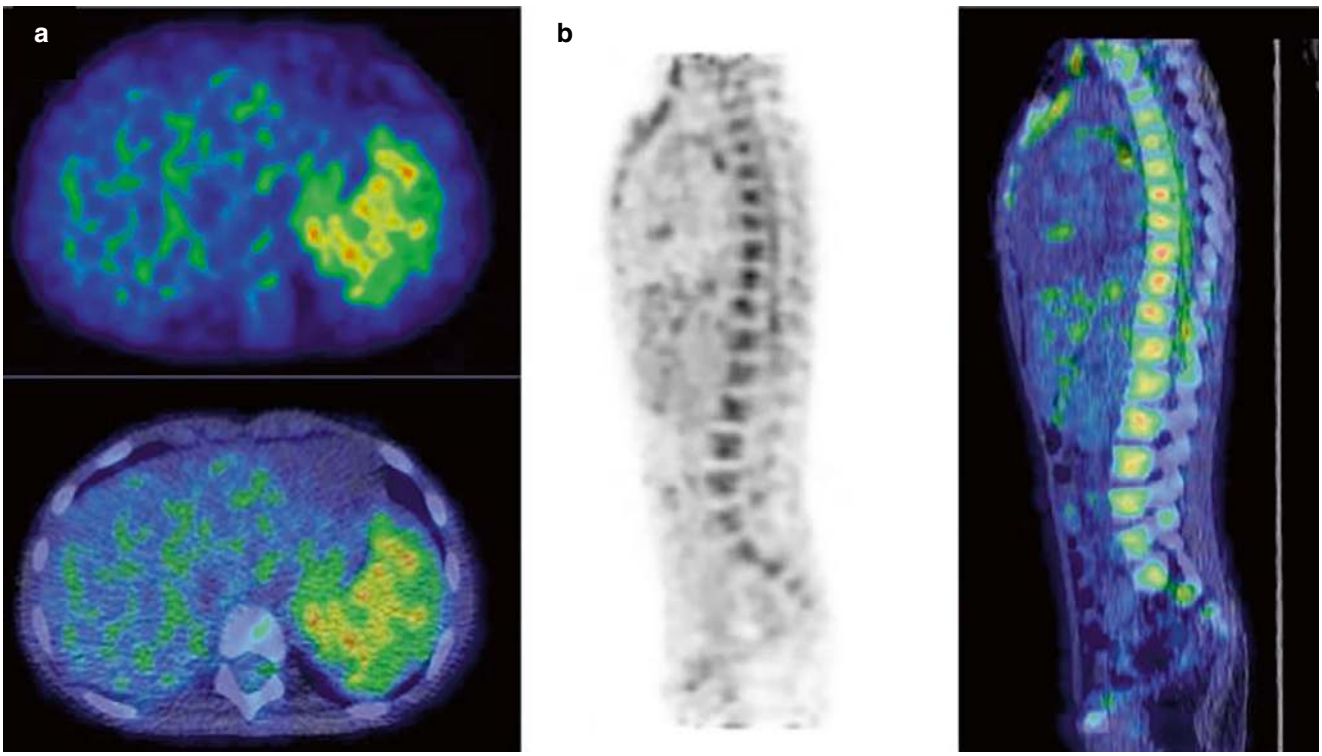


Fig. 8.12 ^{18}F-FDG PET/CT images of the abdomen and spine showing diffuse uptake in the spleen and bone marrow which are likely reactive

rence of fever after discontinuation of therapy, with evidence of vegetations on the tricuspid valve on echocardiogram. For these reasons, the patient underwent surgery, with vegetation removal of the anterior tricuspid flap and commissural repair.

- Histological examination confirmed the presence of endocarditis.

Further Reading

- J.P. Pijl, T C. Kwee, G.E. Legger, et. Al. Role of FDG-PET/CT in children with fever of unknown origin. Eur J Nucl Med Mol Imaging 2020, 47:1596–1604.
- Walter, C.; Zuccarino, F.; Carretero Bellón, J.M. PET/CT Role in the Diagnosis of Infective Endocarditis in Patients with Congenital Heart Disease. Anales de Pediatría 2022, 96: 260–263.

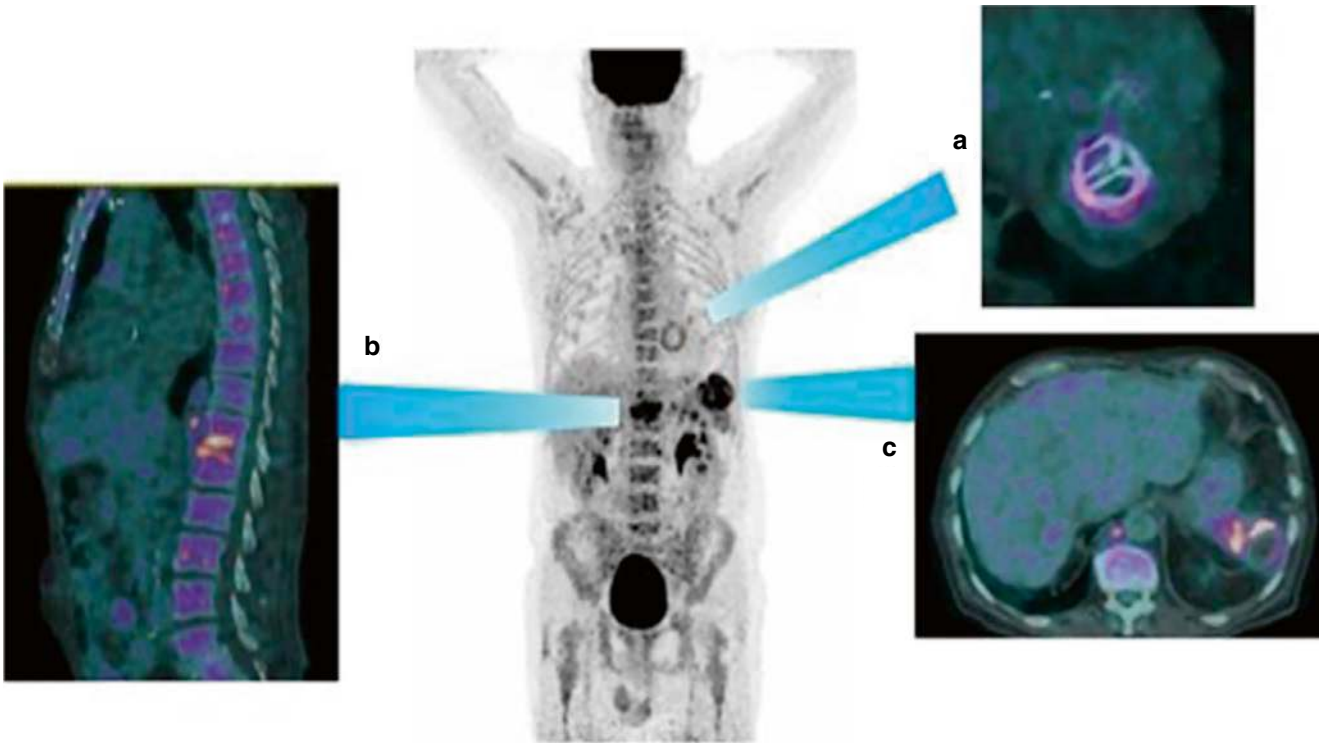


Fig. 8.13 ^{18}F-FDG PET/CT shows intense diffuse uptake at the mitral valve (A); intense uptake involving the lower aspect of the vertebral body of D12 and the upper aspect of the vertebral body of L1 (B); rim of intense uptake at the left hypochondrium level (C)

8.1.9 Focal Abscess Before and After Antibiotic Therapy: Case 71

Key Points

- ^{18}F-FDG PET/CT is complementary in patients with high risk for infectious endocarditis to detect valve involvement.
- The detection of metastatic infections impacts the subsequent treatment management.
- ^{18}F-FDG PET/CT can be used in patients with infective endocarditis and metastatic infections to assess antimicrobial therapy response and guide clinical management.

History

- A 71 year-old man reported to the emergency room with abdominal pain and vomiting; no fever, CRP 10.45 (normal <2 mg/L).
- History of mitral valve and aortic valve replacement, both with a mechanical prosthesis. Pacemaker implantation for paroxysmal atrial flutter. Negative blood cultures.
- Previous splenectomy for hemorrhagic shock for splenic artery pseudoaneurysm.
- Transthoracic echocardiogram was performed showing only mild aortic valve regurgitation.

Baseline PET/CT

Findings

- ^{18}F-FDG PET/CT: intense diffuse uptake at the mitral valve as for the presence of IE.
- Whole-body workout shows intense uptake involving the lower aspect of the vertebral body of D12 and the upper aspect of the vertebral body of L1, typical pattern of spondylodiscitis.
- Encapsulated lesion at the left hypochondrium adjacent to the pancreatic tail, characterized by rim of intense uptake and mild contrast enhancement surrounding a wide photopenic area with air bubbles inside, compatible with an abscess.
- Whole-body images also showed diffuse increase of ^{18}F-FDG uptake in the bone marrow, indirect sign of acute infection.

Differential Diagnosis

- Transesophageal echocardiography (TEE) was also performed confirming the presence of vegetation at the mitral valve in the absence of pathological findings at the aortic valve.

Management

- The patient was hospitalized.
- After a blood culture positive for *Enterococcus faecalis*, amoxicillin and ceftriaxone for 6 weeks followed by oral therapy with amoxicillin are initiated.

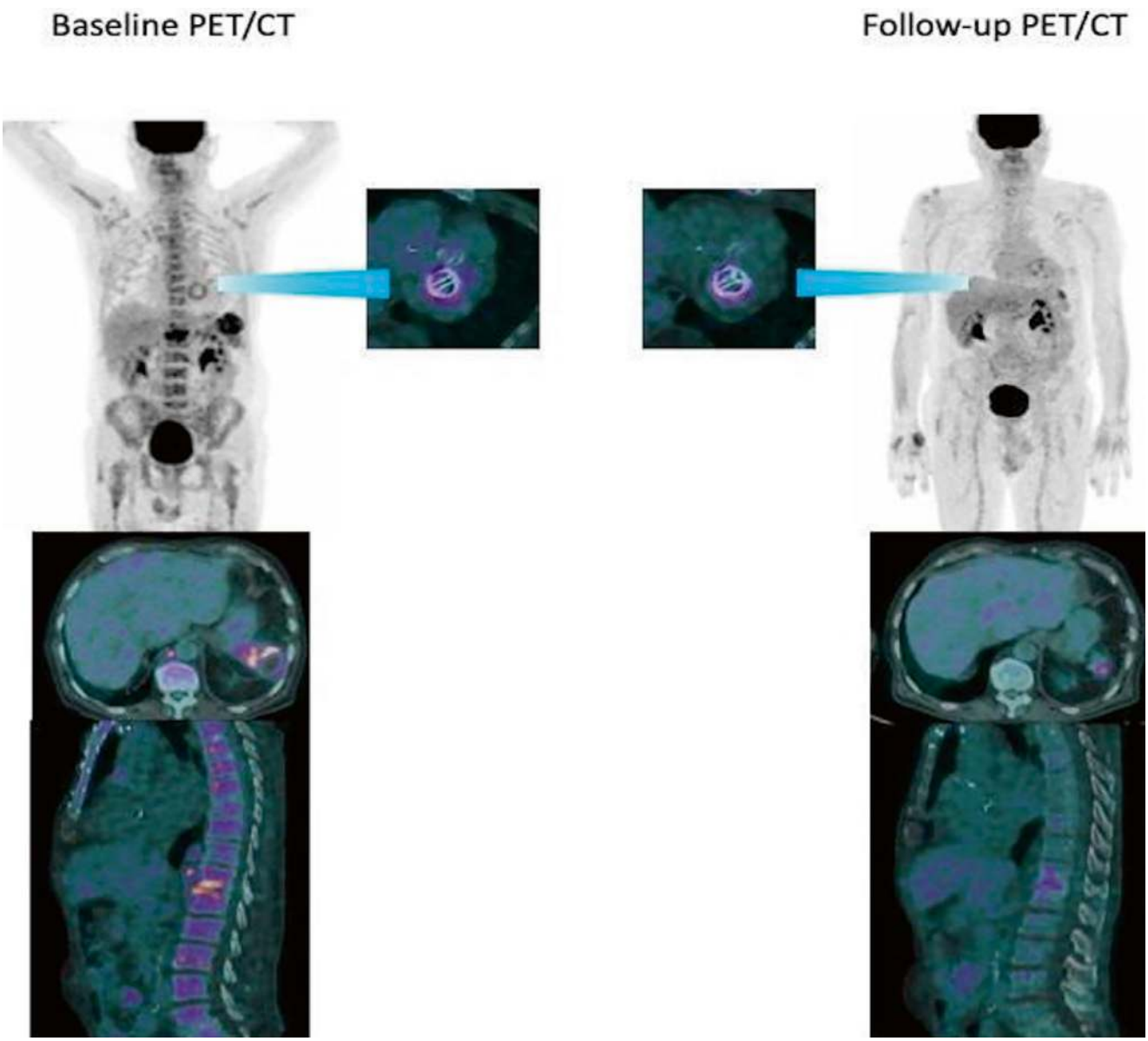


Fig. 8.14 Significant reduction of the uptake at the mitral valve prosthesis, slightly persistent on the posterior aspect; reduced uptake at D12-L1 level; reduced but persistent hyperactivity at the level of left hypochondrium

- Blood culture becomes negative after 10 days of treatment.
- 3 months after the baseline scan, a follow-up study was performed (Fig. 8.14).

Follow-Up PET/CT Study

Findings

- ^{18}F-FDG PET/CT performed at 3 months after the baseline under treatment with oral amoxicillin showed significant reduction of the uptake both at the mitral valve prosthesis (persistent at the posterior aspect).
- The metastatic sites of infections at the vertebral body demonstrated reduced uptake.
- Persistent active lesions at the left hypochondrium adjacent to the pancreatic tail, despite reduction.

Management

- Based on the PET/CT findings, treatment continuation was planned, and surgery postponed.

Further Reading

- Delgado V, Ajmone Marsan N, de Waha S, Bonaros N, Brida M, Burri H, et al. ESC Scientific Document Group. 2023 ESC Guidelines for the management of endocarditis. Eur Heart J. 2023 Aug 25: ehad193.

- Sambola A, Lozano-Torres J, Boersma E, Olmos C, Ternacle J, Calvo F, et al. ESC EORP EURO-ENDO Registry Investigator Group. Predictors of embolism and death in left-sided infective endocarditis: the European Society of Cardiology EURObservational Research Programme European Infective Endocarditis registry. Eur Heart J. 2023 Aug 18:ehad507.
- Ferro P, Boni R, Bartoli F, Lazzeri F, Slart RHJA, Erba PA. Radionuclide Imaging of Infective Endocarditis. Cardiol Clin. 2023 May;41(2):233–249.
- Ferro P, Boni R, Slart RH, Erba PA. Imaging of Endocarditis and Cardiac Device-Related Infections: An Update. Semin Nucl Med. 2023 Mar;53(2):184–198. https://doi.org/10.1053/j.semnuclmed.2023.01.001.

8.2 Device Infection

8.2.1 Generator Pocket and Lead Infection: Case 72

Key Points

- ^{18}F-FDG PET is a useful technique to evaluate pacemaker infection, especially within the pacemaker generator pocket.
- The diagnostic accuracy of PET/CT is very high in generator pocket infection, but lower for the assessment of pacemaker leads.

History

- A 74-year-old man with a previous pacemaker/ICD implant was admitted with fever.
- He underwent ^{18}F-FDG PET/CT for suspected infective endocarditis (Fig. 8.15).

PET/CT Images

Findings

- There is a focus of intense ^{18}F-FDG uptake (SUVmax: 4.8) in the pacemaker generator pocket, which persists in the non-attenuation corrected images.
- The diffuse cardiac uptake is due to inadequate patient preparation and limits the assessment for associated valvular endocarditis.

Imaging Diagnosis

- Intense focal ^{18}F-FDG uptake in the pacemaker generator pocket suspicious for infection.

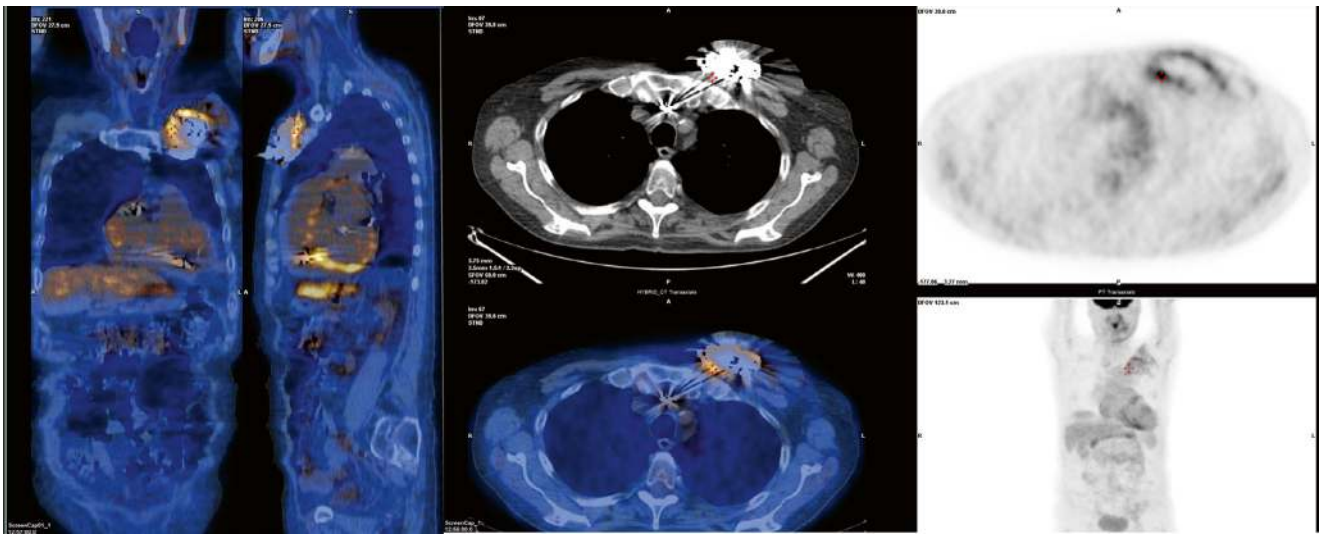


Fig. 8.15 Coronal, sagittal, and axial ^{18}F-FDG PET/CT images (left and middle panels), non-attenuation corrected axial (right upper panel), and PET image (right lower panel), showing a focus of intense ^{18}F-FDG uptake in the pacemaker generator pocket

Differential Diagnosis
- Pacemaker generator pocket infection.
- Nonspecific inflammation in pacemaker pocket.

Correlative Imaging
- None.

Management
- The focality and intensity of the ^{18}F-FDG uptake was considered indicative of an infection focus in the pacemaker generator pocket. The patient started antibiotic therapy and a pocket surgical revision was considered.

Further Reading

- Arnon-Sheleg E, Israel O, Keidar Z. PET/CT Imaging in Soft Tissue Infection and Inflammation—An Update. Seminars in Nuclear Medicine. 2020;50:35–49.
- Chen W, Sajadi M, Dilsizian V. Merits of FDG PET/CT and Functional Molecular Imaging Over Anatomic Imaging With Echocardiography and CT Angiography for the Diagnosis of Cardiac Device Infections. JACC: Cardiovascular Imaging. 2018;11:1679–1691.

8.2.2 Device Infection in Patient with Amyloidosis: Case 73

Key Points
- ^{18}F-FDG PET is a useful diagnostic tool for excluding or identifying device infection.
- The sensitivity of ^{18}F-FDG for pacemaker lead infection is low, but specificity is high.

History
- An 87-year-old woman with a history of transthyretin amyloid (ATTR) cardiomyopathy and pacemaker implantation for heart block presented with fever and cachexia.
- Transthoracic echocardiography was nondiagnostic for infective endocarditis.
- She underwent ^{18}F-FDG PET/CT to assess for infection (Figs. 8.16 and 8.17).

PET/CT Images

Findings
- PET/CT images demonstrate intense focal ^{18}F-FDG uptake along the pacemaker lead in the right ventricle, which persisted in the non-attenuation corrected images. There was no ^{18}F-FDG uptake in the pacemaker pocket.

Imaging Diagnosis
- Focal uptake associated with the pacemaker lead in keeping with infected pacemaker lead.

Differential Diagnosis
- Infection.
- Inflammation.
- Artifact.

Correlative Imaging
- None.

Management
- The images are consistent with an infected intracardiac section of the pacemaker lead.
- The patient was started on broad-spectrum antibiotic therapy and transferred to a rehabilitation center.

Further Reading

- Arnon-Sheleg E, Israel O, Keidar Z. PET/CT Imaging in Soft Tissue Infection and Inflammation—An Update. Seminars in Nuclear Medicine. 2020; 50:35–49.
- Chen W, Sajadi M, Dilsizian V. Merits of FDG PET/CT and Functional Molecular Imaging Over Anatomic Imaging With Echocardiography and CT Angiography for the Diagnosis of Cardiac Device Infections. JACC: Cardiovascular Imaging. 2018; 11:1679–1691.

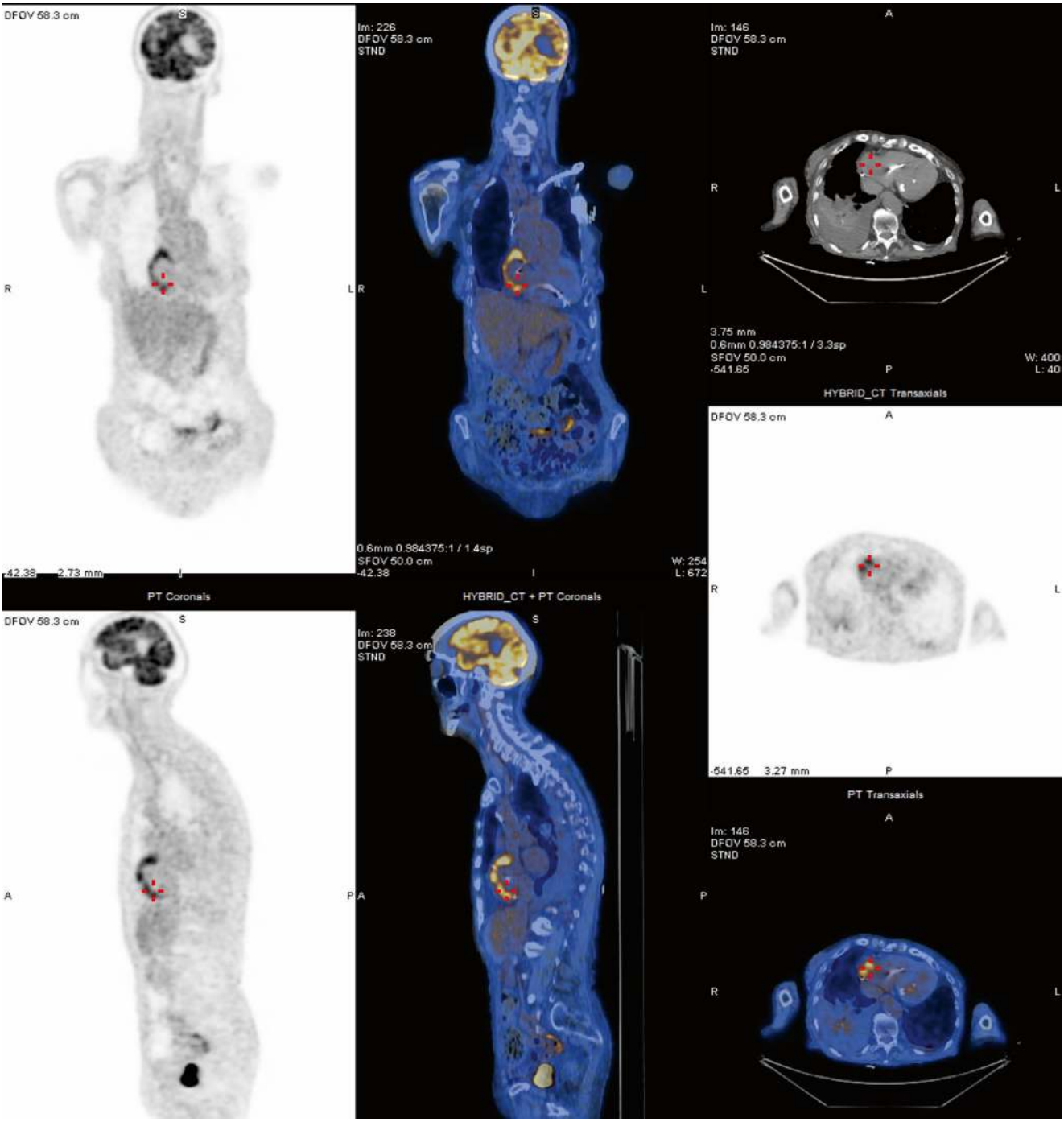


Fig. 8.16 PET/CT images demonstrating intense focal ^{18}F-FDG uptake along the pacemaker lead in the right ventricle. There was no ^{18}F-FDG uptake in the pacemaker generator pocket

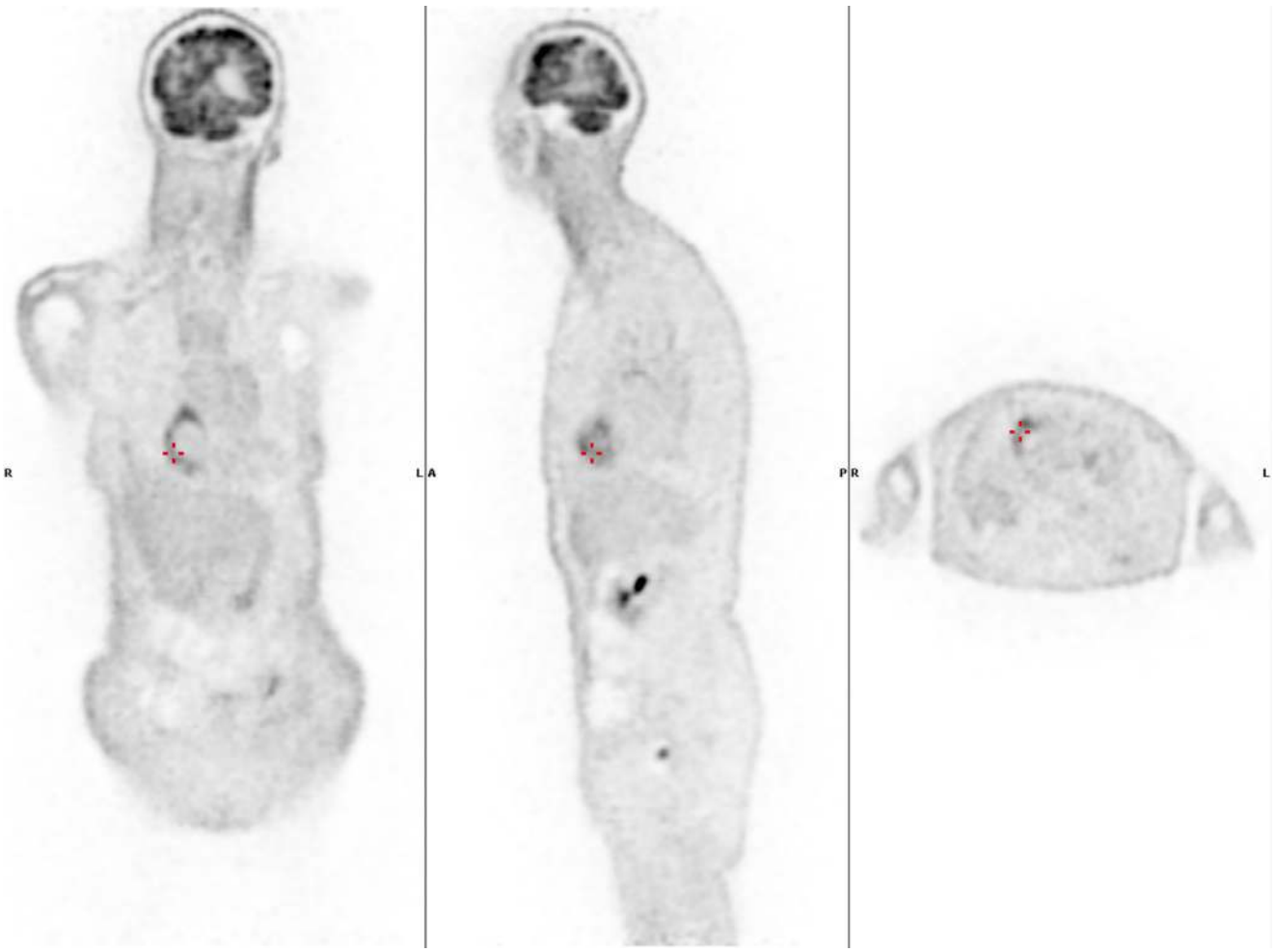


Fig. 8.17 PET images without attenuation correction demonstrating persistence of intense focal ^{18}F-FDG uptake along the pacemaker lead in the right ventricle

8.2.3 Generator Pocket Infection, Cardiac Device Infection: Case 74

Key Points

- Beyond valvular infective endocarditis, [18F]FDG-PET/CT has also proven to be useful in the diagnosis of cardiac device infections (CDI).
- Echocardiography is usually the first technique in the evaluation of these patients, but its visualization is mainly restricted to the intracardiac leads, while PET/CT can assess the whole device.
- However, the diagnostic yield is different regarding the site of the suspected infection. The reported accuracy is very high for the generator/pocket infection and the extravascular segments of the leads, while the assessment of the intravascular and intracardiac portion is less profitable.
- The association of a venous phase ECG-gated CTA may allow the detection of vegetations or thrombi and provide information about venous access permeability, useful in case of planning device replacement.

History

- A 71-year-old woman with an implantable cardioverter defibrillator (ICD) implanted 10 years previously presented with pain and local signs of inflammation at the generator pocket.
- Blood cultures and transesophageal echocardiography were negative. Due to persistent high suspicion of device infection (CDI), a PET/CTA examination was indicated (Figs. 8.18 and 8.19).

PET/CTA Images

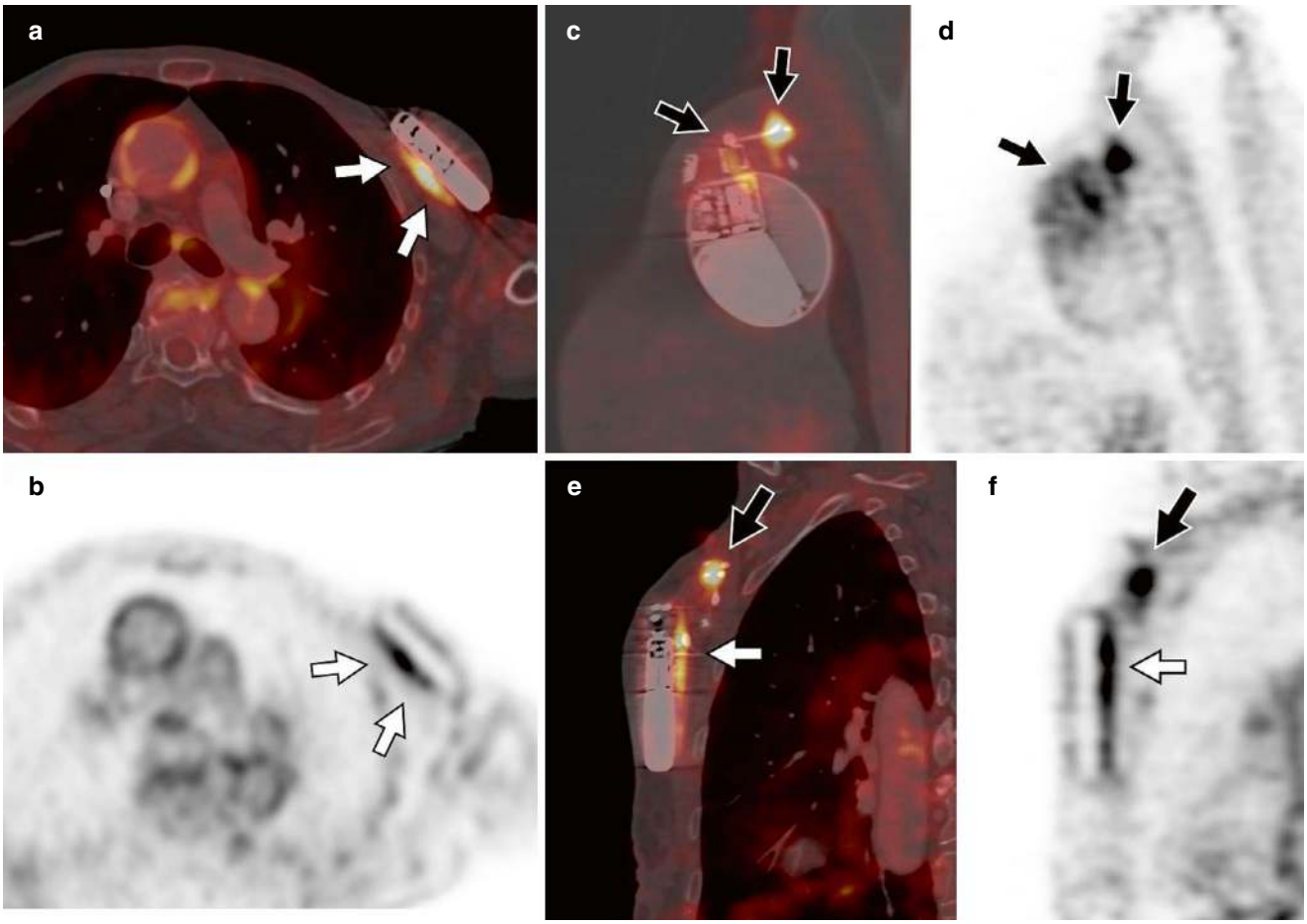


Fig. 8.18 ^{18}F-FDG-PET/CTA. Fusion (**a**, **c**, **e**) and attenuation-corrected PET (**b**, **d**, **f**) images showing intense ^{18}F-FDG-uptake (SUVmax 5) around the device generator (white arrows), mainly in its posterior side, and focal uptake along the initial extravascular lead segments (black arrows). There was mild anterior subcutaneous fat stranding with no other significant soft tissue alterations

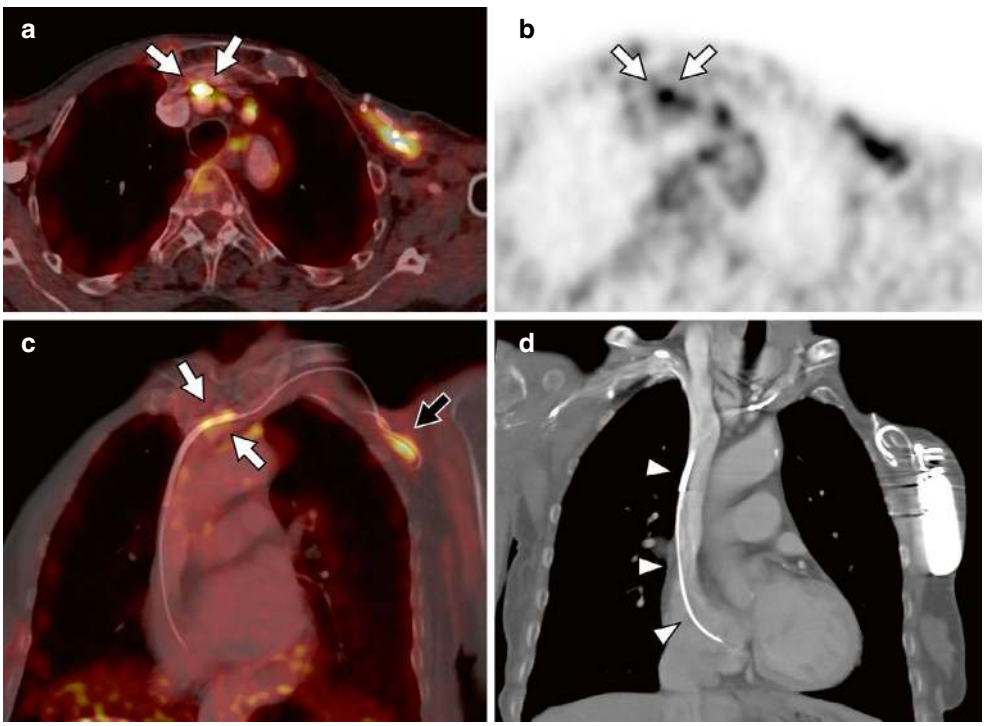


Fig. 8.19 ^{18}F-FDG-PET/CTA. Fusion (**a**) and attenuation-corrected PET (**b**) axial view showing intense and focal (SUVmax 3.7) FDG uptake on the intravascular segment of the lead at the innominate vein. (**c**) Oblique-coronal reformation depicts uptake on the extravascular (pocket, black arrow) and intravascular (white arrows) leads. Note how the intravascular lead is nicely depicted in its course along the superior vena cava and right atrium in the ECG-gated CT coronal image (**d**, arrowheads), with no thrombi or vegetations. In addition, permeability of the right/contralateral upper venous access is checked/assessed

Findings Summary
- Heterogeneous and intense FDG uptake at the generator/pocket.
- Mild soft tissue reaction.
- Focal and intense FDG uptake on the extravascular segment of the leads.
- Focal and intense FDG uptake on the intravascular segment of the leads.

Imaging Diagnosis
Cardiac device infection with involvement of both the generator and intravascular system (known as cardiac device related infective endocarditis—CDRIE).

Correlative Imaging
- Transesophageal echocardiography (not shown): negative.

Differential Diagnosis: Discussion
- In cases of recent implantation, reactive FDG uptake can be seen around the generator in the pocket, up to approximately 6 weeks post-procedure.
- On the other hand, uptake on the leads is highly suggestive of infection, with a very high positive predictive value.

Management
- Cardiac device infection with intravascular involvement.
- The device was removed, and cultures were positive for *Staphylococcus epidermidis*.

Further Reading

- Sarrazin JF, Philippon F, Tessier M, et al. Usefulness of Fluorine-18 Positron Emission Tomography/Computed Tomography for Identification of Cardiovascular Implantable Electronic Device Infections. J Am Coll Cardiol 2012;59:1616–1625.
- Juneau D, Golfam M, Hazra S, et al. Positron emission tomography and single-photon emission computed tomography imaging in the diagnosis of cardiac implantable electronic device infection: a systematic review and meta-analysis. Circ Cardiovasc Imaging 2017;10:e005772.
- Blomstrom-Lundqvist C, Traycov V, Erba P, et al. European Heart Rhythm Association (EHRA) international consensus document on how to prevent, diagnose, and treat cardiac implantable electronic device infections-endorsed by the Heart Rhythm Society (HRS), the Asia Pacific Heart Rhythm Society (APHRS), the Latin American Heart Rhythm Society (LAHRS), International Society for Cardiovascular Infectious Diseases (ISCVID) and the European Society of Clinical Microbiology and Infectious Diseases (ESCMID) in collaboration with the EACTS. Eur Heart J 2022;41:2012–32.

8.2.4 Identifying Source of Infection with Whole-Body PET/CT (False Positive with and Without Attenuation Correction): Case 75

Key Points
- ^{18}F-FDG PET/CT is a useful imaging technique in the evaluation of patients with fever of unknown origin. It is considered highly sensitive, but specificity is moderate. In equivocal cases, radiolabeled white blood cell imaging can be considered.
- Dense calcification and metal can lead to artificially high ^{18}F-FDG uptake on attenuation correction images. It is always recommended that both the attenuation corrected and non-attenuation corrected images be evaluated.

History
- An 85-year-old woman with chronic atrial fibrillation and pacemaker implantation had a recent fall with displacement of the left hip and a peritrochanteric hematoma.
- She was evaluated for fever of unknown origin and positive blood cultures which identified *Staphylococcus aureus*.
- Transesophageal echocardiography was negative for endocarditis.
- She was referred for ^{18}F-FDG PET/CT for identification of possible infectious foci (Figs. 8.20, 8.21 and 8.22).

PET/CT Images

Findings
- The ^{18}F-FDG PET/CT showed high tracer uptake in the left hip suggestive of peritrochanter infection or inflammation.
- There is a second focus of focal ^{18}F-FDG uptake at the level of the left subclavian vein, corresponding to the pacemaker lead. This is present on both the attenuation-corrected and uncorrected PET images.
- There is an additional focus of intense ^{18}F-FDG accumulation in the area of dense mitral annular calcification, which almost completely disappears in the non-attenuation correction PET images.

Imaging Diagnosis
- Focal areas of increased ^{18}F-FDG uptake consistent with infection including the left hip and pacemaker lead.

Differential Diagnosis
- Infection.
- Nonspecific inflammation.
- Artifact.



Fig. 8.20 Coronal ^{18}F-FDG PET image demonstrating intense glucose uptake around the left hip

Management

- The presence of focal ^{18}F-FDG uptake in the pacemaker lead that persisted in the uncorrected PET images in the clinical context of a patient with fever and bacteremia with positive blood cultures is consistent with an infected pacemaker lead.
- The pacemaker lead was removed. Culture of the device was positive for *Staphylococcus aureus*.
- Systemic broad-spectrum antibiotic therapy was initiated.
- The ^{18}F-FDG focus around the dense mitral annular calcification was an attenuation correction artifact.

Further Reading

- Kouijzer I, Mulders-Manders C, Bleeker-Rovers C, Oyen W. Fever of Unknown Origin: the Value of FDG-PET/CT. Seminars in Nuclear Medicine. 2018;48:100–107.
- Diemberger I, Bonfiglioli R, Martignani C, Graziosi M, Biffi M, Lorenzetti S, et al. Contribution of PET imaging to mortality risk stratification in candidates to lead extraction for pacemaker or defibrillator infection: a prospective single center study. European Journal of Nuclear Medicine and Molecular Imaging. 2018;46:194–205.

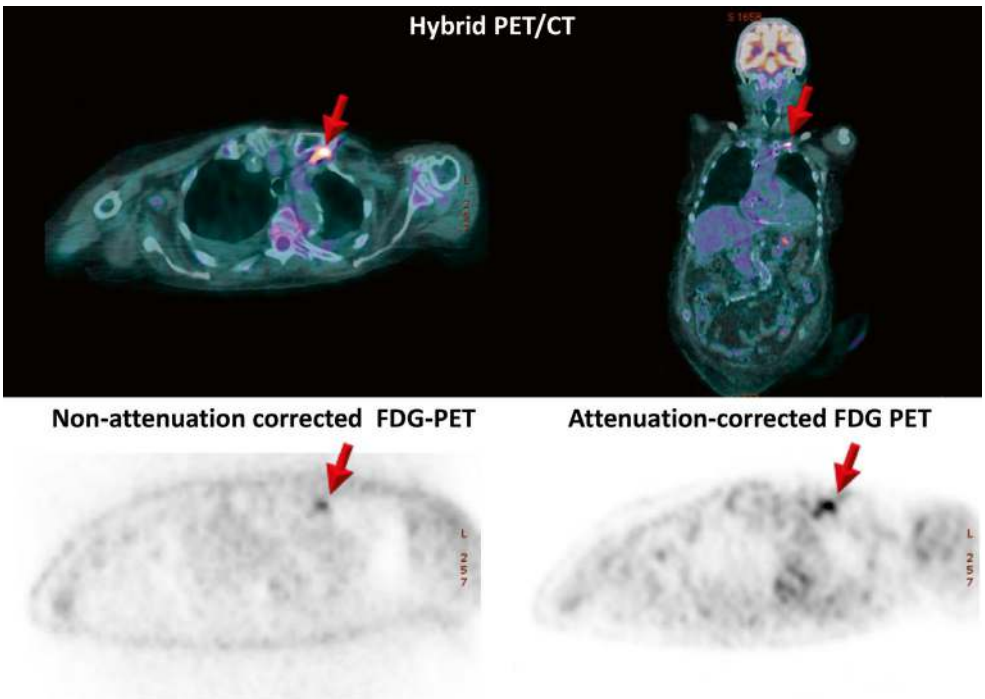


Fig. 8.21 ^{18}F-FDG PET/CT images demonstrating intense focal uptake around the pacemaker lead on attenuation corrected images (arrow, top panel), which persists on the non-attenuation corrected images (arrow, lower panel)

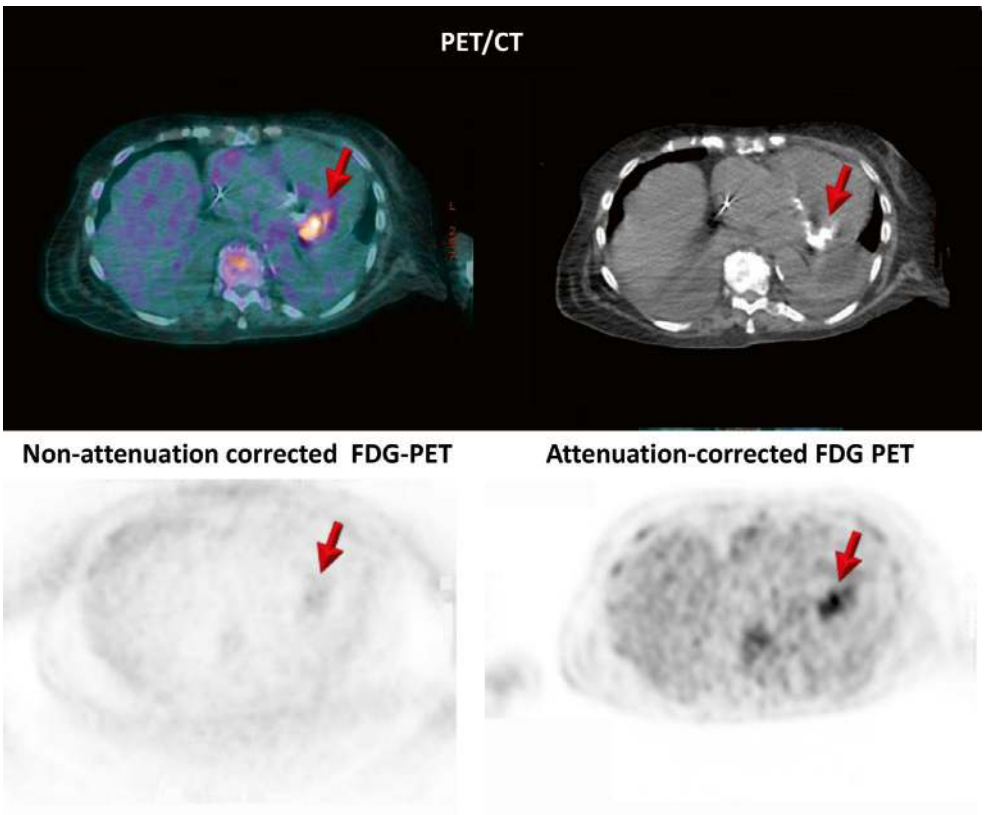


Fig. 8.22 ^{18}F-FDG PET/CT images showing intense ^{18}F-FDG accumulation in the area corresponding to intense mitral annular calcification (arrow, top panel). This almost completely disappears on non-attenuation correction images suggesting that it is an artifact (arrow, Lower panel)

8.2.5 Left Ventricular Assist Device (LVAD) Driveline Infection: Case 76

Key Points

- ^{18}F-FDG PET/CT is a valuable diagnostic tool in the suspicion of LVAD infection, helping to differentiate between infected and noninfected LVAD patients and to further localize the site of the infection as peripheral (percutaneous exit site and/or drive line) versus central (exterior cannula and/or pump pocket).
- It is essential to evaluate both the attenuation-corrected and non-attenuation-corrected images in the LVAD infection to ensure that the focus of uptake persists.
- Early detection of LVAD infection on ^{18}F-FDG PET/CT has relevant clinical, therapeutic, and prognostic implications.

History

- A 66-year-old male with ischemic cardiomyopathy status post-HeartMate II-LVAD implantation, was referred to ^{18}F-FDG PET/CT for fever and purulent discharge from the driveline exit site. Patient performed ^{18}F-FDG PET/CT scans before and during therapy (Figs. 8.23 and 8.24).

PET/CT Images

Differential Diagnosis

- Peripheral (percutaneous exit site and/or drive line) versus central (cannula exterior and/or pump pocket) infection.

Management

- The patient started surgical vacuum-assisted closure therapy (VAC-therapy) on the exit and the abdominal tract of driveline and performed aggressive systemic antibiotic treatment.

Further Reading

- J. Kim, ED Feller et Al. FDG PET/CT imaging for LVAD associated infection JACC: Cardiovasc imaging. 2014, 8: 83942.
- J. Kim, ED. Feller et Al. FDG PET/CT for early detection and localization of left ventricular assist device infection. JACC: Cardiovasc imaging. 2019, 12: 722–9.
- MC Tam, VN Patel et Al. Diagnostic Accuracy of FDG PET/CT in Suspected LVAD Infections: A Case Series, Systematic Review, and Meta-Analysis JACC Cardiovasc Imaging. 2021, 13: 1191–1202.

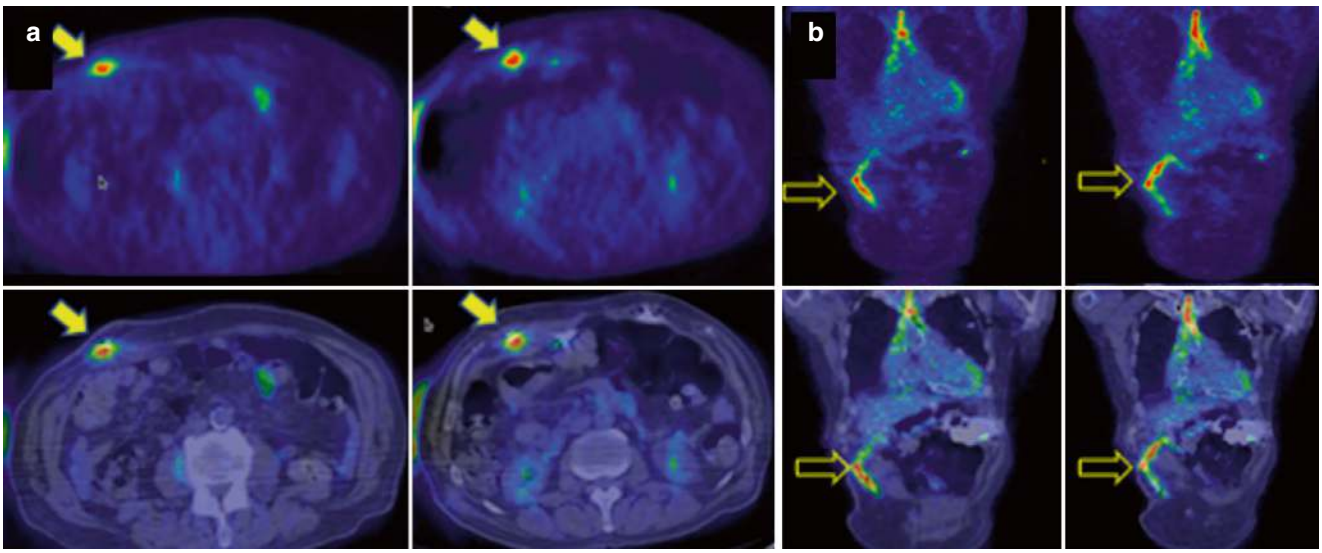


Fig. 8.23 Baseline ^{18}F-FDG PET/CT showed intense ^{18}F-FDG uptake on axial (**a**) and coronal (**b**) images within the subcutaneous soft tissue along the course of the LVAD driveline from the exit point through the right lower abdominal wall

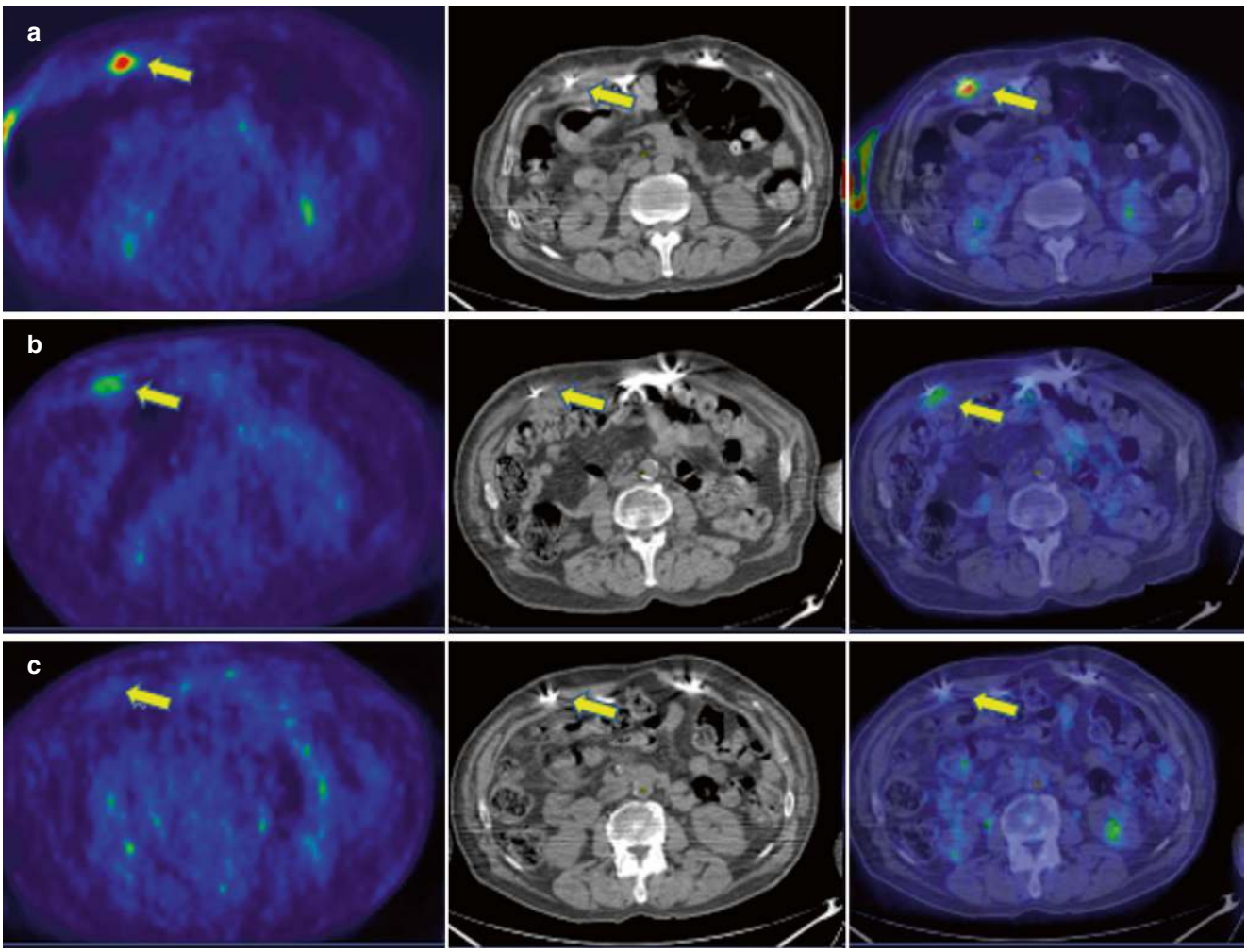


Fig. 8.24 Baseline ^{18}F-FDG PET/CT showed intense ^{18}F-FDG uptake within the subcutaneous soft tissue along the LVAD driveline (**a**); ^{18}F-FDG uptake decreased after 4 weeks of therapy (**b**) and disappeared at the end of therapy (**c**)

8.2.6 Assessing Infection in a Left Ventricular Assist Device: Case 77

Key Points

- Left ventricular assist device (LVAD) infection is a severe condition with high mortality, and its diagnosis is challenging.
- ^{18}F-FDG-PET/CT may help in the evaluation of these complex devices where infection can affect different portions of the system and that are very difficult to assess using other diagnostic techniques.
- Contrast-enhanced CT images (CTA) are also advisable for a better evaluation of vascular structures, the presence of thrombosis and perivascular lesions.
- Knowledge of the findings that should be considered normal is important to avoid misdiagnosis.

History

A 70-year-old man with an LVAD (Heartmate-3) due to advanced ischemic cardiomyopathy implanted 6 months before who is referred for a PET/CTA study under suspicion of infection (serous fluid from the driveline insertion site and mild fever) (Fig. 8.25).

PET/CTA Images

Findings Summary

- Circumferential FDG uptake at the pump (considered a normal finding—reactive).
- Mild and diffuse FDG uptake of the outflow graft, which was patent, ruling out infection.
- Focal FDG uptake at the driveline suggestive of infection.

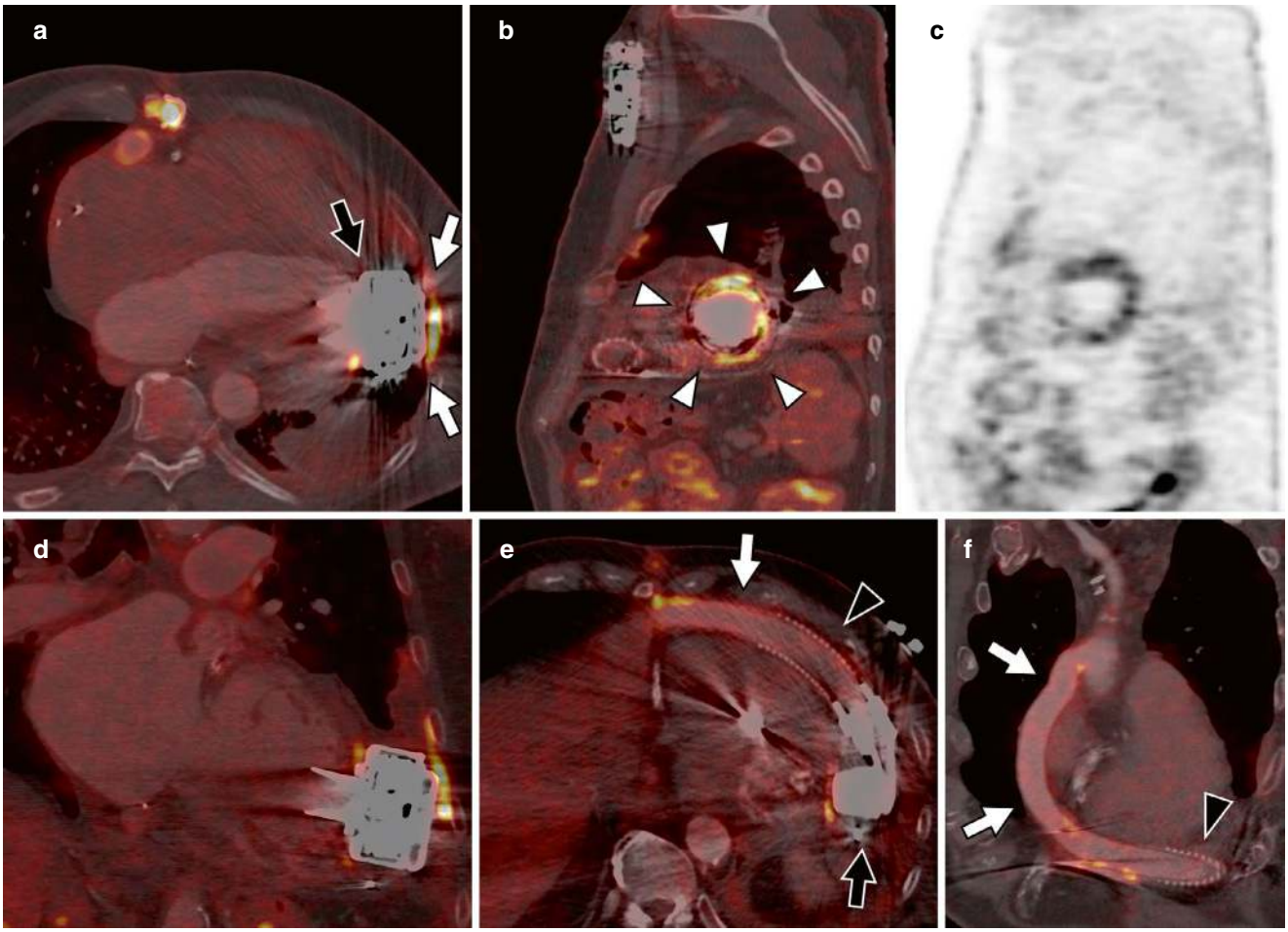


Fig. 8.25 ^{18}F-FDG-PET/CTA images showing the pump and the outflow cannula of the left ventricular assist device (LVAD). Fusion (**a**, **b**, **d**) and attenuation-corrected PET (**c**) images focused on the pump (**a**, black arrow). Axial (**a**), oblique-coronal (**d**), and transverse views (**b**, **c**) showing circumferential reactive FDG uptake around the myocardial union of the pump (**a**, **b**, arrowheads). Fusion multiplanar reformations (**e**, **f**) depicting the full extent of the outflow cannula (**e**, black arrow). Two parts of the graft can be differentiated, a first segment that comes out of the pump covered by a rigid polytetrafluoroethylene tube to prevent kinks (black arrowheads), and a bare segment anastomosed to the native aorta (white arrows). The graft was patent, with no evidence of thrombi, and mild diffuse FDG uptake in the wall that did not suggest infection (Fig. 8.26)

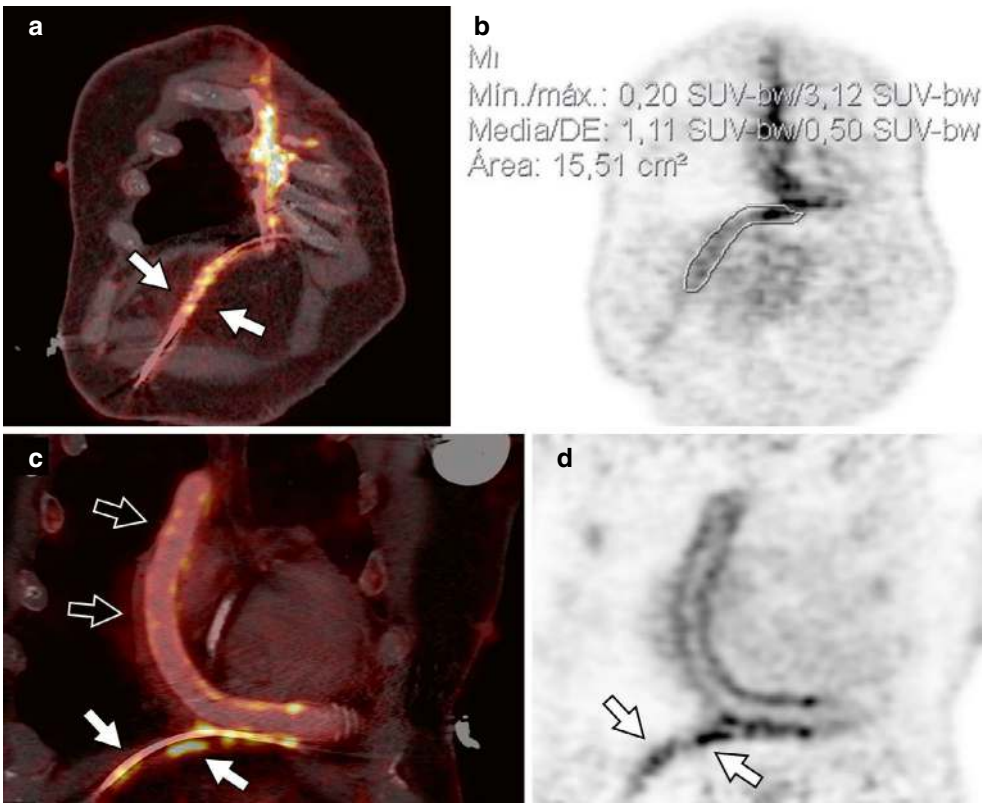


Fig. 8.26 ^{18}F-FDG-PET/CTA. Fusion (**a**) and attenuation-corrected PET (**b**) coronal images of the driveline tunneled through the anterior abdominal wall (white arrows) and connected to the electronic controller showing multifocal FDG uptake (SUVmax 6) associated with peripheral fat stranding at its prehepatic and intrathoracic segment, findings highly suggestive of infection. Fusion (**c**) and attenuation-corrected PET (**d**) multiplanar reformations depicting the driveline with abnormal uptake at its intrathoracic segment (white arrows) and its close relationship with the outflow graft, which was considered not directly infected

Imaging Diagnosis

- Driveline infection.

Correlative Imaging

- Transesophageal echocardiography (not shown): small 2-mm mobile mass on the mitral valve indistinguishable between small vegetation or thrombus.

Differential Diagnosis

- Circumferential FDG uptake around the myocardial pump junction and mild and diffuse FDG uptake on the walls of the outflow cannula are the sites in an LVAD system where metabolic activity can be considered non-pathologic.
- Focal or heterogeneous uptakes should be considered highly suggestive of infection.
- Any tracer uptake in the driveline should be suspicious of infection.

Management

- Antibiotic treatment with good clinical response.
- A control PET scan after 8 weeks of antibiotics showed resolution of the FDG uptake at the driveline.

Further Reading

- Kim J, Feller ED, Chen W, Liang Y, Dilsizian V. FDG PET/CT for Early Detection and Localization of Left Ventricular Assist Device Infection: Impact on Patient Management and Outcome. JACC Cardiovasc Imaging. 2019 Apr;12(4):722–729.
- Tam MC, Patel VN, Weinberg RL, Hulten EA, Aaronson KD, Pagani FD, Corbett JR, Murthy VL. Diagnostic Accuracy of FDG PET/CT in Suspected LVAD Infections: A Case Series, Systematic Review, and Meta-Analysis. JACC Cardiovasc Imaging. 2020 May;13(5):1191–1202.
- Ten Hove D, Wahadat AR, Slart RHJA, Wouthuyzen-Bakker M, Mecozzi G, Damman K, Witteveen H, Caliskan K, Manintveld OC, Sinha B, Budde RPJ, Glaudemans AWJM. Added value of semi-quantitative analysis of [18F]FDG PET/CT for the diagnosis of device-related infections in patients with a left ventricular assist device. Eur Heart J Cardiovasc Imaging. 2023 May 31;24(6):819–828.

The opinions expressed in this chapter are those of the author(s) and do not necessarily reflect the views of the IAEA: International Atomic Energy Agency, its Board of Directors, or the countries they represent.

Open Access This chapter is licensed under the terms of the Creative Commons Attribution 3.0 IGO license (http://creativecommons.org/licenses/by/3.0/igo/), which permits use, sharing, adaptation, distribution and reproduction in any medium or format, as long as you give appropriate credit to the IAEA: International Atomic Energy Agency, provide a link to the Creative Commons license and indicate if changes were made.

Any dispute related to the use of the works of the IAEA: International Atomic Energy Agency that cannot be settled amicably shall be submitted to arbitration pursuant to the UNCITRAL rules. The use of the IAEA: International Atomic Energy Agency's name for any purpose other than for attribution, and the use of the IAEA: International Atomic Energy Agency's logo, shall be subject to a separate written license agreement between the IAEA: International Atomic Energy Agency and the user and is not authorized as part of this CC-IGO license. Note that the link provided above includes additional terms and conditions of the license.

The images or other third party material in this chapter are included in the chapter's Creative Commons license, unless indicated otherwise in a credit line to the material. If material is not included in the chapter's Creative Commons license and your intended use is not permitted by statutory regulation or exceeds the permitted use, you will need to obtain permission directly from the copyright holder.



Vasculitides

9

Paolo Raggi, Marcelo Di Carli, Michelle Williams, Raffaele Giubbini, Diana Paez, Maurizio Dondi, Erick Alexanderson, Isabel Carvajal, Ayaz Aghayev, Alison Clifford, Dan Pugh, and Neeraj Dhaun

Objectives

- To learn the pattern of vascular inflammation on positron emission tomography (PET) in different large vessel vasculitides.
- To learn how to integrate correlative imaging findings into the interpretation of PET images.
- To learn how to use PET imaging to guide management.

The vasculitides are a group of rare diseases characterized by inflammation of the blood vessel walls. At the tissue level, inflammatory cells (consisting of lymphocytes, neutrophils, macrophages, and others) infiltrate the wall and produce inflammatory cytokines resulting in tissue necrosis. Macroscopically, the inflamed vessel typically responds by becoming either thickened, stenotic, occluded, or potentially aneurysmal and susceptible to dissection/rupture. Depending on the size and distribution of affected vessels, patients with vasculitis have the potential to quickly develop organ- or life-threatening ischemia, and therefore rapid recognition and diagnosis of these diseases is essential.

Vasculitides can be classified as primary (idiopathic) or secondary (triggered by another process), and by the size of blood vessel affected. See Tables 9.1 and 9.2 for a broad overview of the classification of vasculitides. Small vessel vasculitides (SVV) predominantly affect the arterioles, capillaries, and venules, with occasional medium or large vessel overlap. Typical SVV manifestations include ear, nose, and throat (ENT) features (scleritis, sinusitis, sensorineural hearing loss), as well as pulmonary (diffuse alveolar hemorrhage or inflammatory nodules), renal (glomerulonephritis), and neurological (mononeuritis multiplex). In contrast, medium vessel vasculitides (MVV) are characterized by inflammation restricted to the medium vessels, for example, the renal arteries (causing hypertension), mesenteric arteries (producing ischemic bowel), or coronary arteries (resulting in myocardial ischemia). Large vessel vasculitides (LVV), by definition, target the aorta and major branch vessels. Classic features of LVV include cranial symptoms (headache, vision loss, or stroke); however, those with aortitis alone may be minimally symptomatic. Untreated, patients with aortitis are at increased risk for aortic dissection.

All authors have no conflict of interest to disclose.

P. Raggi
Division of Cardiology, University of Alberta, Edmonton, AB, Canada

M. Di Carli · A. Aghayev
Brigham and Women's Hospital, Boston, MA, USA
e-mail: mdicarli@bwh.harvard.edu; aaghayev@bwh.harvard.edu

M. Williams
British Heart Foundation Centre for Research Excellence, Institute for Neuroscience and Cardiovascular Research, University of Edinburgh, Edinburgh, United Kingdom
e-mail: michelle.williams@ed.ac.uk

D. Pugh · N. Dhaun
British Heart Foundation Centre for Research Excellence, University of Edinburgh, Edinburgh, UK
e-mail: dpugh2@exseed.ac.uk; bean.dhaun@ed.ac.uk

R. Giubbini
Nuclear Medicine, International Specialized Hospital of Uganda (ISHU), Kampala, Uganda
e-mail: raffaele.giubbini@unibs.it

D. Paez · M. Dondi (✉)
Division of Human Health, International Atomic Energy Agency, Vienna, Austria
e-mail: d.paez@iaea.org; m.dondi@iaea.org

E. Alexanderson · I. Carvajal
Instituto Nacional de Cardiologia Ignacio Chavex, Mexico City, Mexico

A. Clifford
University of Alberta, Edmonton, AB, Canada
e-mail: alison5@ualberta.ca

© The Author(s) 2027
M. Di Carli et al. (eds.), *IAEA Atlas of Cardiac PET/CT*, https://doi.org/10.1007/978-3-662-74188-7_9

Table 9.1 Primary systemic vasculitides, grouped according to vessel size

Vessel size	Vasculitis nomenclature
Large vessel vasculitides (LVV)	Giant cell arteritis (GCA)
	Takayasu arteries (TAK)
Medium vessel vasculitides (MVV)	Polyarteritis nodosa (PAN)
	Kawasaki's disease (KD)
Small vessel vasculitides (SVV)	Antineutrophil cytoplasmic antibody (ANCA)-associated vasculitis (AAV)
	-Microscopic polyangiitis (MPA)
	-Granulomatosis with polyangiitis (GPA)
	-Eosinophilic granulomatosis with polyangiitis (EGPA)
	Immune complex SVV
	-Anti-glomerular basement membrane (anti-GBM) disease
	-Cryoglobulinemic vasculitis (CV)
	-IgA vasculitis
	-Hypocomplementemic urticarial vasculitis (HUV)
Variable vessel vasculitides (VVV)	Behcet's disease (BD)
	Cogan's syndrome
Single organ vasculitides (SOV)	Cutaneous leukocytoclastic angiitis
	Cutaneous arteritis
	Primary central nervous system vasculitis
	Isolated aortitis
	Others

Table 9.2 Potential secondary causes of vasculitis and their typical vessel targets

Etiology	Examples and typical targets
Infection related	
Viral	Hepatitis B, C, HIV (small, medium, or large vessel)
Bacterial	*Staphylococcus*, *Streptococcus*, *Salmonella*, *Coxiella burnetti*, syphilis, *Mycobacteria* (large vessel)
Fungal	Mycotic aneurysm (large vessel)
Medication-induced	
	Hydralazine (small vessel)
	Methimazole (small vessel)
	Propylthiouracil (small vessel)
	Anti-TNF agents (small vessel)
	Levamisole (small or medium vessel)
	Minocycline (medium vessel)
	Immune checkpoint inhibitors (small, medium, or large vessel)
	G-CSF (large vessel)
	Other agents
Other systemic autoimmune rheumatic diseases	
	Systemic lupus erythematosus (small and medium vessel)
	Sarcoidosis (small, medium, or large vessel)
	Relapsing polychondritis (small, medium, or large vessel)
	Rheumatoid arthritis (medium vessel)
	Spondyloarthritis (large vessel)
	IgG4-related disease (large vessel)

Abbrev: *TNF* tumor necrosis factor, *G-CSF* granulocyte colony stimulating factor

Treatment of primary systemic vasculitis usually requires urgent immunosuppression. Glucocorticoids are used initially to control the disease, with subsequent taper over months, followed by early introduction of additional immunosuppressive agents (e.g., rituximab, tocilizumab, or cyclophosphamide) to achieve remission and allow prednisone taper. Due to the myriad of serious side effects associated with prednisone exposure, securing the most accurate diagnosis is essential.

Diagnosing vasculitis requires consideration of clinical features, inflammatory markers, serological tests, and, importantly, imaging. Histological confirmation of vasculitis may be secured through tissue biopsy; however, in patients with predominantly LVV or aortitis, this is usually not feasible. In these cases, ^{18}F-fluorodeoxyglucose (FDG)-positron emission tomography/computed tomography (PET/CT) imaging may play a critical role in early diagnosis. FDG PET can depict the increased metabolic activity occurring in the large vessels as a result of active inflammation, potentially allowing for a sooner diagnosis of vasculitis, before structural vessel wall changes (such as stenosis or aneurysm) occur, with reported high sensitivity (90%) and specificity (98%). Although glucocorticoid use reduces the sensitivity of FDG PET/CT for detecting LVV, it has been shown that scans obtained <3 days of initiating glucocorticoids maintain their test characteristics. International consensus criteria have been established to standardize the acquisition and interpretation of FDG PET/CT in LVV (Slart). It is recommended that visual FDG uptake in the vessels be compared to that of the liver (with 0 = no uptake, 1 < less than liver uptake, 2 = liver uptake, 3 > liver uptake). Grade 2 vascular FDG uptake is considered possibly positive and grade 3 uptake positive for vasculitis.

9.1 Assess Response to Therapy in Vasculitis: Case 78

Key Points

- ^{18}F-FDG PET/CT is a very effective tool for monitoring treatment response in inflammatory diseases, including sarcoidosis and vasculitis.

History

- A 63-year-old woman with a history of pulmonary sarcoidosis admitted for fever, vomiting, and headache.
- She was referred for ^{18}F-FDG PET/CT to assess for vasculitis before and after therapy (Figs. 9.1 and 9.2).

PET/CT Images

Findings

- The whole-body PET/CT images confirmed multiple areas of active inflammation including mediastinal and hilar lymph nodes consistent with her history of known sarcoidosis and vascular inflammation involving the abdominal aorta and iliac arteries.

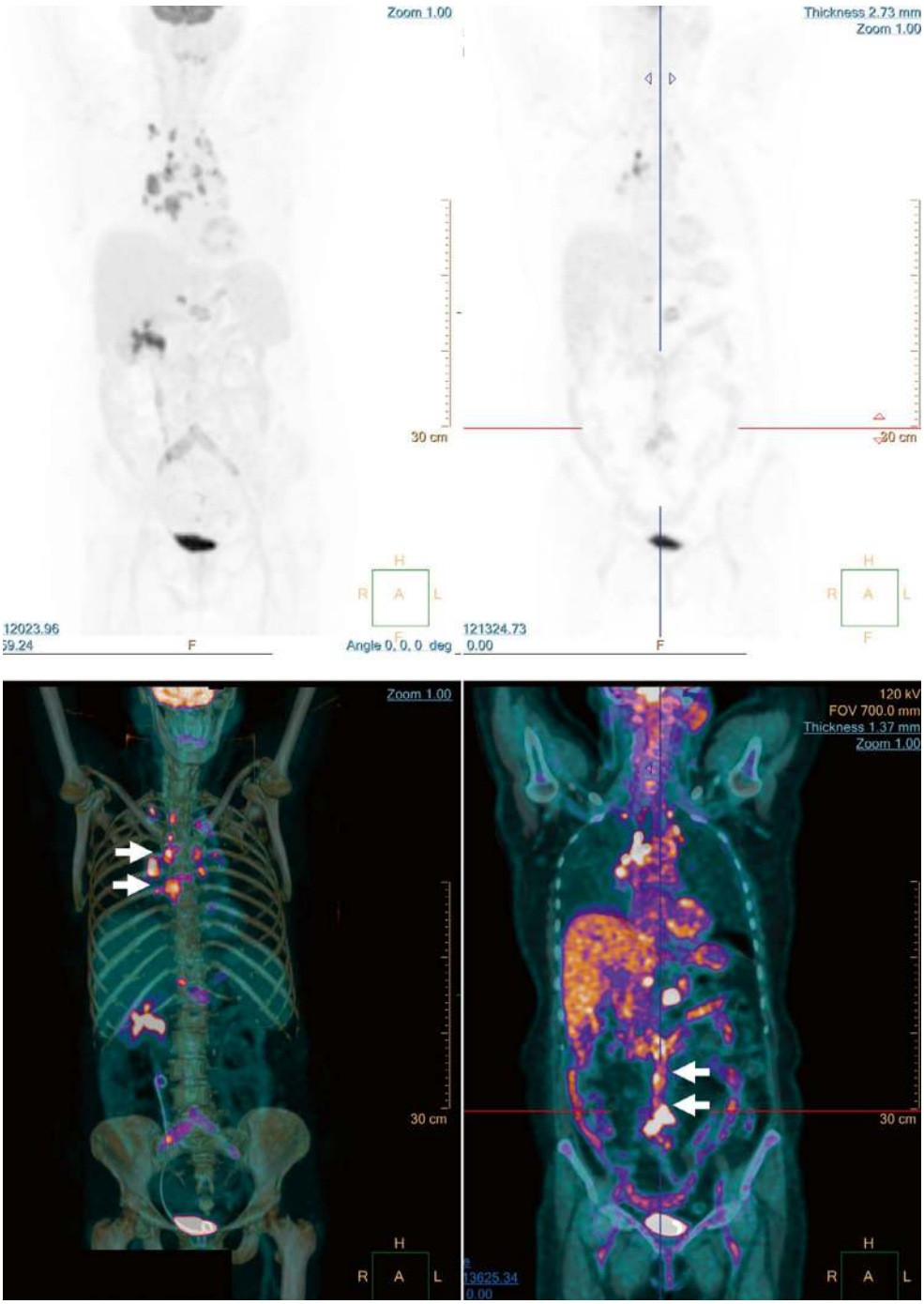


Fig. 9.1 Whole-body PET/CT images during the index admission showing multiple foci of intense ^{18}F-FDG uptake in the mediastinum and hilar regions (arrows) and in the abdominal aorta and iliac arteries (arrows)

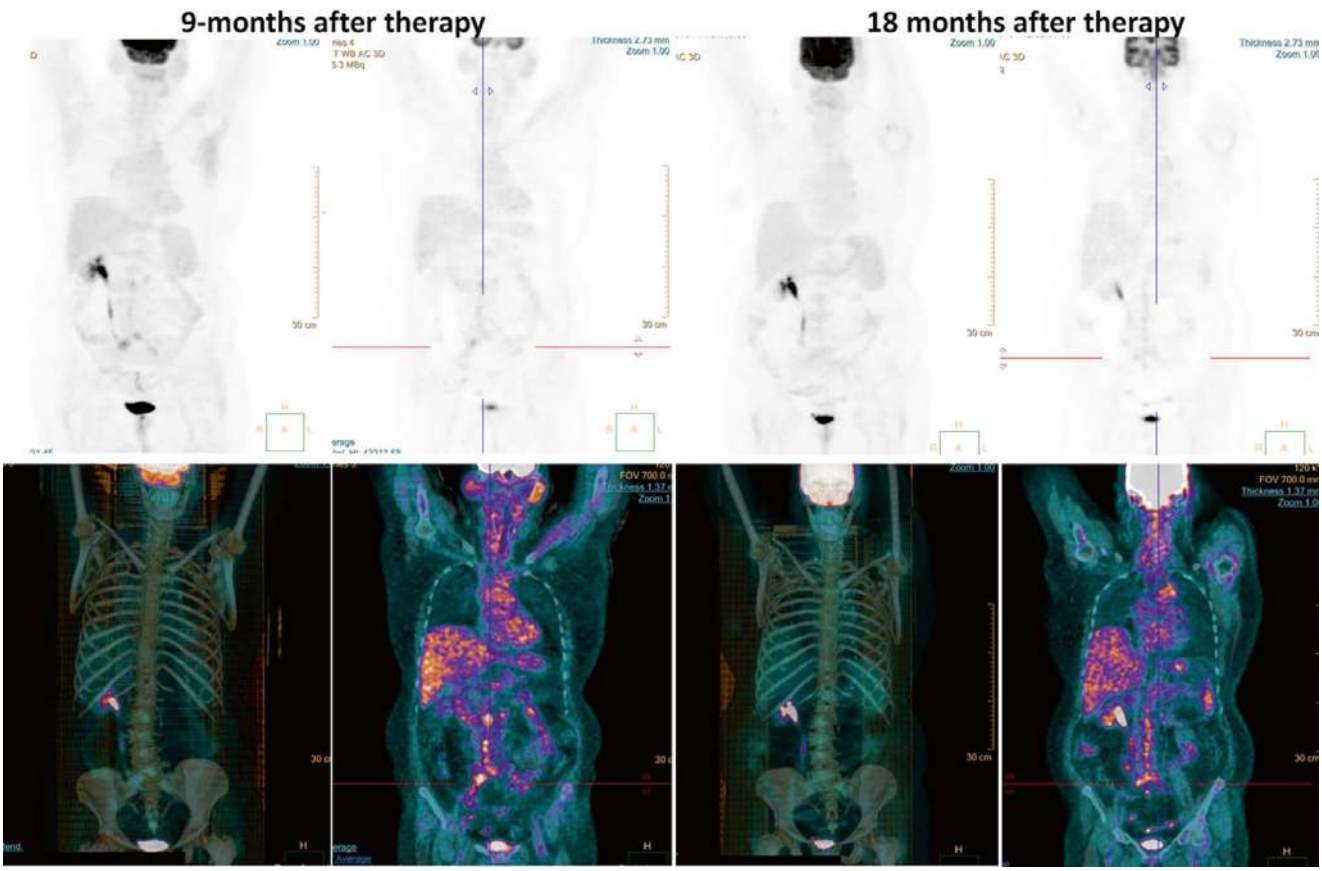


Fig. 9.2 Baseline and follow-up whole-body PET maximum intensity projection (MIP) images obtained at 6, 9, and 18 months after the initial scan demonstrate complete resolution of ^{18}F-FDG uptake in the thoracic lymph nodes and markedly reduced but still active inflammation in the abdominal aorta and proximal iliac arteries

- The 9- and 18-month follow-up whole-body ^{18}F-PET/CT images demonstrate interval resolution of inflammatory foci in the chest and marked improvement in the abdominal aorta and iliac arteries.

Imaging Diagnosis

- Systemic vasculitis secondary to sarcoidosis.

Differential Diagnosis

- Pulmonary sarcoidosis.
- Takayasu arteritis.
- Giant cell arteritis.
- Sarcoid vasculitis.

Correlative Imaging

- Whole-body contrast CT angiography was performed during initial hospital admission. It showed dilation of the abdominal aorta with aneurysm of the right iliac artery and several ulcerations (Fig. 9.3).

Management

- The patient was initiated on immunosuppressive therapy with corticosteroids. Tocilizumab was added after the 9-month ^{18}F-FDG-PET/CT study.

Further Reading

- Piekarski E, Benali K, Rouzet F. Nuclear Imaging in Sarcoidosis. Seminars in Nuclear Medicine. 2018;48:246–260.
- Versari A, Pipitone N, Casali M, Jamar F, Pazzola G. Use of imaging techniques in large vessel vasculitis and related conditions. The Quarterly Journal of Nuclear Medicine and Molecular Imaging. 2018;62:34–39.

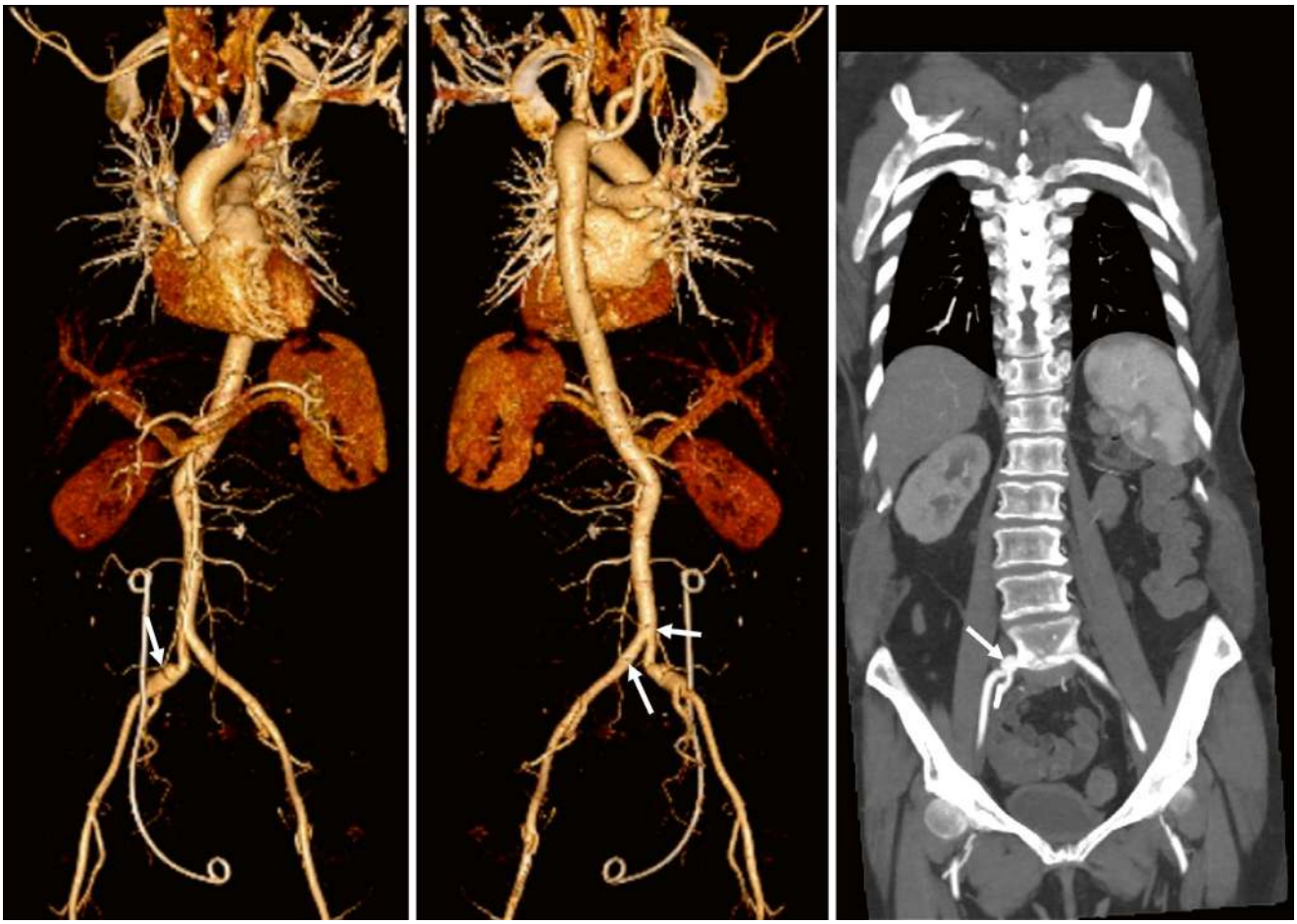


Fig. 9.3 Contrast CT angiography showing dilation of the abdominal aorta with aneurysm of the right iliac artery and several ulcerations

9.2 Large Vessel Vasculitis: Case 79

Key Points

- ^{18}F-FDG PET/CT is useful to assess the presence and extent of arterial inflammation and provides important information that can inform initiation and monitoring of treatment as discussed in case 64.

History

- A 65 -year-old woman with a history of diabetes and hypertension presented with sudden onset renal dysfunction secondary to bilateral renal artery stenosis for which she underwent bilateral renal artery angioplasty with subsequent improvement of renal function.
- She underwent thoracic, abdominal, and pelvic CT angiography and ^{18}F-FDG PET/CT (Fig. 9.4).

PET/CT Images

Findings

- The CT angiogram demonstrates diffuse thickening of the thoracic and abdominal aorta.
- The PET images demonstrate increased ^{18}F-FDG uptake throughout the thoracic and abdominal aorta and iliac arteries.

Differential Diagnosis

- Takayasu arteritis.
- Giant cell arteritis.

Correlative Imaging

- None.

Management

- The patient was started on immunosuppression with good clinical response. No follow-up imaging was available.

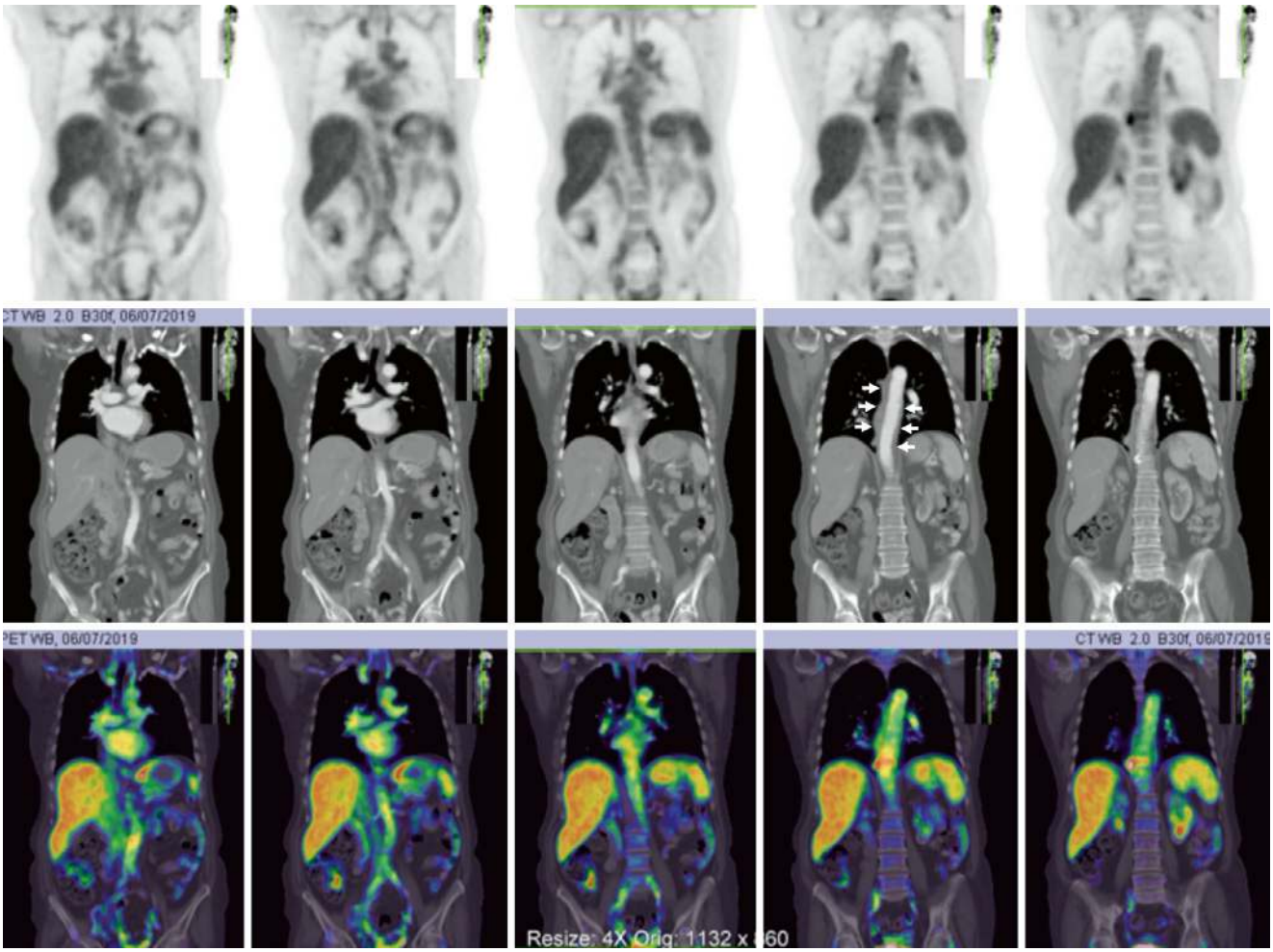


Fig. 9.4 ^{18}F-FDG PET (top), CT angiography (middle), and fused limited whole-body PET/CT images

Further Reading

- Tezuka D, Haraguchi G, Ishihara T, Ohigashi H, Inagaki H, Suzuki J, et al. Role of FDG PET-CT in Takayasu Arteritis. JACC: Cardiovascular Imaging. 2012;5:422–429.
- Slart R, et al. FDG-PET/CT(A) imaging in large vessel vasculitis and polymyalgia rheumatica: joint procedural recommendation of the EANM, SNMMI, and the PET Interest Group (PIG), and endorsed by the ASNC. European Journal of Nuclear Medicine and Molecular Imaging. 2018;45:1250–1269.
- Prieto-González S, Depetris M, García-Martínez A, Espígol-Frigolé G, Tavera-Bahillo I, Corbera-Bellata M, et al. Positron emission tomography assessment of large vessel inflammation in patients with newly diagnosed, biopsy-proven giant cell arteritis: a prospective, case–control study. Annals of the Rheumatic Diseases. 2014;73:1388–1392.

9.3 Immunoglobulin G4 Vasculitis: Case 80

Key Points

- IgG4-related disease is a common cause of retroperitoneal fibrosis and periaortitis, and may present with a normal C-reactive protein despite active disease.
- About 60% of patients with IgG4-related disease have multiorgan involvement. PET/CT is useful for identifying additional, and sometimes asymptomatic, sites of inflammation which may be amenable to biopsy for confirmation of diagnosis. Most frequently affected organs are the pancreas, salivary glands, kidneys, lacrimal glands, and periaortic tissues.
- PET/CT can be used to assess the activity of retroperitoneal inflammation and fibrosis and to monitor response to immunosuppression.

History

- A 70 -year-old man presented to the hospital with severe right-sided flank pain. Abdominal ultrasound and abdominal CT revealed right ureter obstruction with hydronephrosis due to extensive retroperitoneal fibrosis.
- The patient also reported 10 lb weight loss, dry eyes, and dry mouth. Physical exam was significant only for firm, nontender enlargement of both submandibular salivary glands.
- Blood testing revealed normal complete blood count (CBC), normal creatinine, C-reactive protein 2.1 mg/L (normal <5.0), and serum lipase slightly above the upper limits of normal. Antinuclear antibodies (ANA) was positive, with normal complement levels and negative anti-dsDNA. Serum IgG4 level was elevated at 2.56 g/L (normal 0.07–0.74 g/L), as was serum IgE at 731 kU/L (normal <120 KU/L). Syphilis serology and TB skin testing were negative.
- PET/CT was requested to assess retroperitoneal inflammation and to identify potential sites for tissue biopsy to confirm the suspected diagnosis of IgG4-related disease (Figs. 9.5 and 9.6).

PET/CT Images

Findings

Intense retroperitoneal hypermetabolism along the anterior wall of the abdominal aorta, extending from L2 level caudally throughout the length of the entire infrarenal abdominal aorta and into both common iliac arteries, in keeping with active retroperitoneal fibrosis.

Moderate hypermetabolism in both submandibular glands, suggesting active sialadenitis.

Small focus of uptake in the uncinate process of the pancreas.

Imaging Diagnosis

- Intense aortic and iliac FDG uptake consistent with IgG4 vasculitis.

Differential Diagnosis

- IgG4-related disease with submandibular, pancreatic, and retroperitoneal/periaortic involvement.
- Idiopathic retroperitoneal fibrosis.

Correlative Imaging

- None.

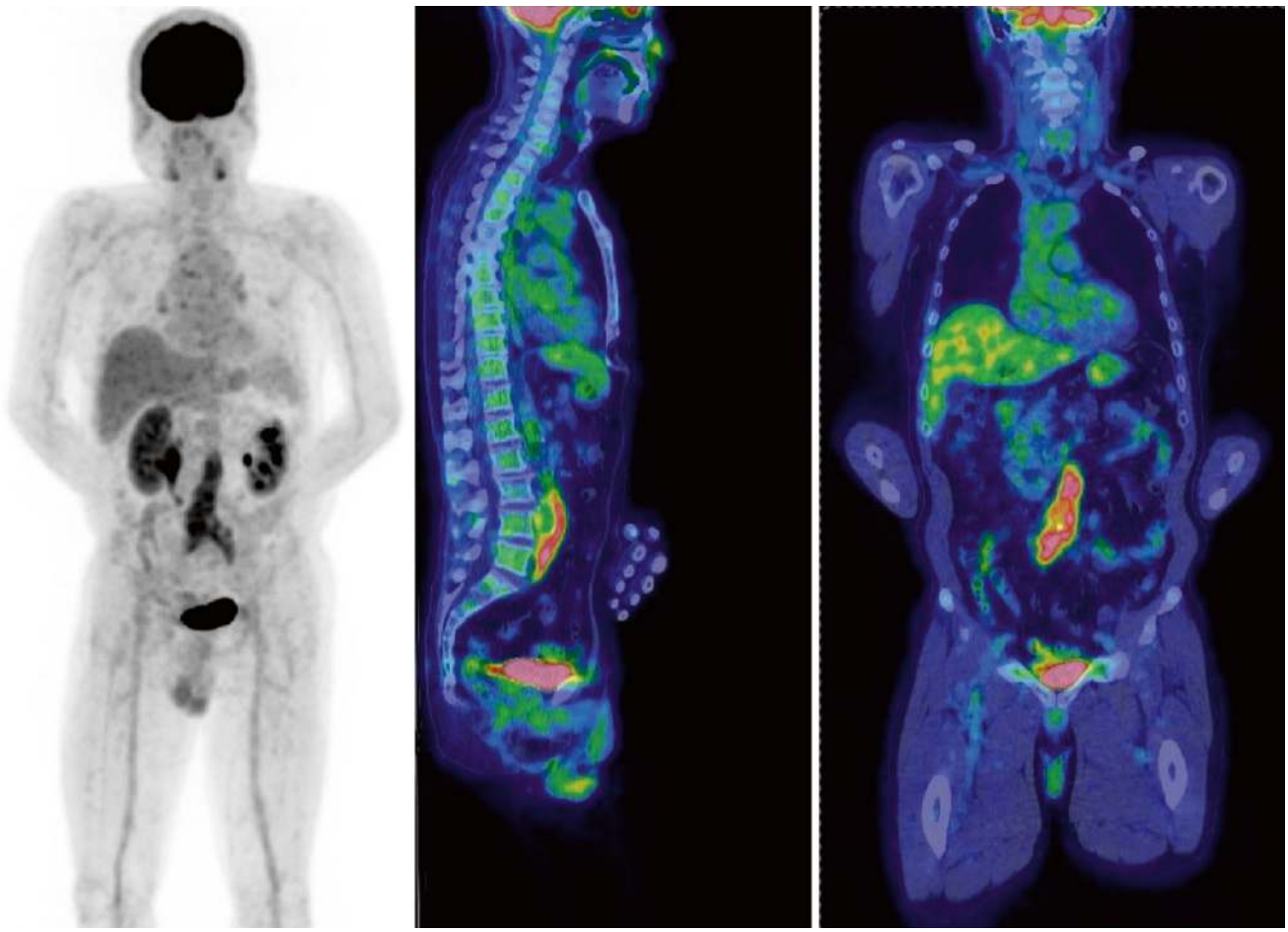


Fig. 9.5 Increased uptake throughout the abdominal aorta extending to the iliac arteries. Moderate uptake at the level of uncinate process of the pancreas



Fig. 9.6 Moderate uptake at the level of the salivary glands

Management

- Excisional biopsy of the left submandibular gland revealed a dense lymphoplasmacytic infiltrate with storiform fibrosis. IgG4 + plasma cells were increased (>30/hpf overall with foci up to 100/hpf), confirming the diagnosis.
- The patient was treated with prednisone 40 mg po daily with tapering over several months, but ultimately required rituximab to achieve complete response (Fig. 9.7).

Follow-Up Imaging

Findings

- Follow-up PET/CT posttreatment showed resolution of ^{18}F-FDG uptake in the periaortic tissue with mild residual thickening around the distal infrarenal aorta, and normalization of uptake in the pancreas and submandibular glands in keeping with good treatment response.

Further Reading

- Inoue D, Yoshida K, Yoneda N, Ozaki K, Matsubara T, Nagai K et al. IgG4-related disease: dataset of 235 consecutive patients. Medicine (Baltimore),2e.

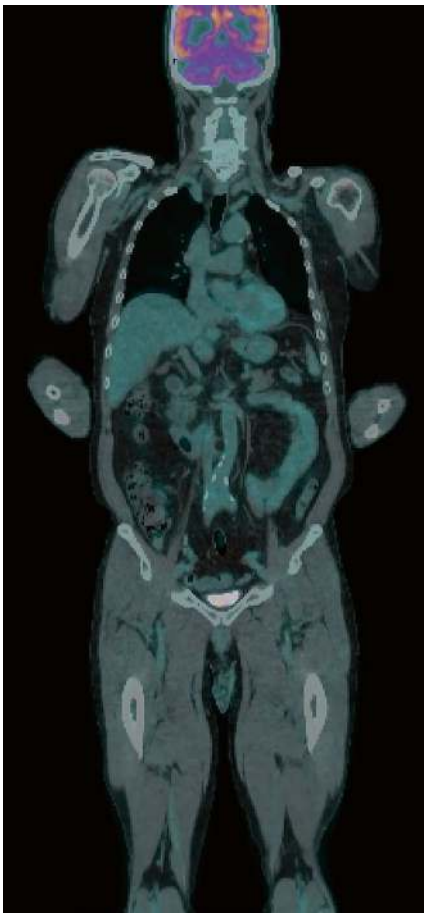


Fig. 9.7 Mild residual thickening around the distal infrarenal aorta

9.4 Takayasu Arteritis: Case 81

Key Points

- Takayasu arteritis is a chronic inflammatory disease of the large arteries and predominantly affects young women. The clinical course varies—while some patients achieve long-term remission, relapse may occur in between 30 and 80% of patients, with progressive development of critical vascular stenoses and occlusions. The clinical assessment of Takayasu arteritis is limited, as symptoms are often subtle or nonspecific, and inflammatory markers are neither sensitive nor specific for this disease; therefore, routine imaging of the entire aorta and all branch vessels is required for disease monitoring.
- ^{18}F-FDG PET/CT can be used to help gauge disease activity or quiescence in Takayasu arteritis. The pattern of uptake in large vessel vasculitis (diffuse) differs from that

seen in atherosclerosis (focal, patchy) as does the distribution of affected vessels.
- Interpretation of ^{18}F-FDG PET/CT is most reliable in patients who are not taking glucocorticoids.

History
- A 57-year-old woman with a history of hypertension and diabetes presented with a 1 year history of progressive weight loss, fatigue, myalgia, exertional chest pain and dyspnea, and right worse than left arm claudication. She also had a history of Takayasu arteritis, diagnosed at age 45, initially treated with high-dose prednisone and tapered over 1 year. She then stopped all immunosuppression and was lost to follow-up.
- On exam, blood pressure was 99/56 mmHg in the right arm and 128/56 mmHg in the left arm. Heart sounds were regular, with a loud diastolic murmur. Right radial and brachial pulses were absent, and there was a right carotid bruit. All other peripheral pulses were present.
- Laboratory finds: normal complete blood count and differential, C-reactive protein 33 mg/L (normal<5.0 mg/L); erythrocytes sedimentation rate (ESR) 43 mm/Hr. ANA, extractable nuclear antigens (ENA), anti-dsDNA, ANCA, syphilis, and tuberculosis testing were negative.
- CT angiogram: wall thickening and enhancement of the ascending aorta and innominate artery; 70% stenosis of right subclavian artery; and 50% stenosis of right common carotid artery. The wall of superior mesenteric and right renal arteries is also thickened.
- PET/CT was requested to differentiate active versus quiescent large vessel vasculitis (Figs. 9.8 and 9.9).

PET/CT images

Imaging Diagnosis
- Intense FDG uptake consistent with Takayasu arteritis in the ascending aorta, aortic arch, innominate artery, bilateral subclavian and bilateral carotid arteries, and abdominal aorta.

Differential Diagnosis
- Active Takayasu arteritis.
- Quiescent Takayasu arteritis.
- Atherosclerosis.
- Giant cell arteritis.

Correlative Imaging
- None.

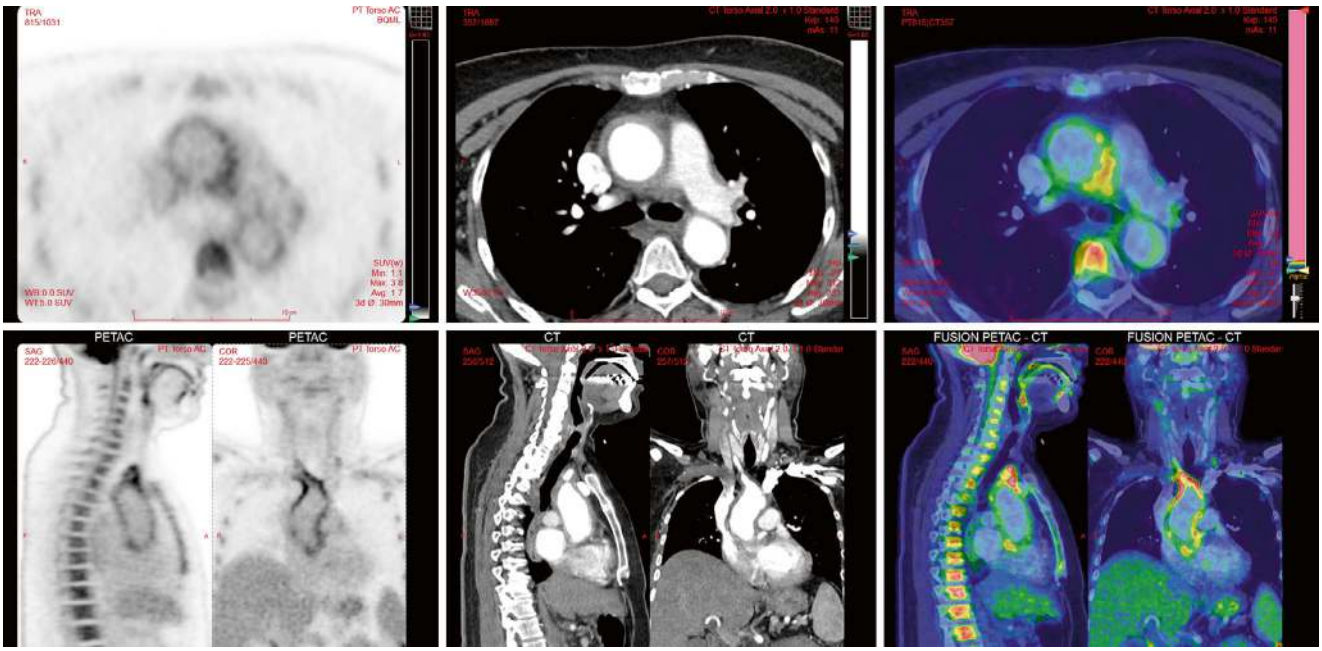


Fig. 9.8 Diffuse grade 3 vascular uptake in the ascending aorta, aortic arch, innominate, bilateral subclavian and carotid arteries

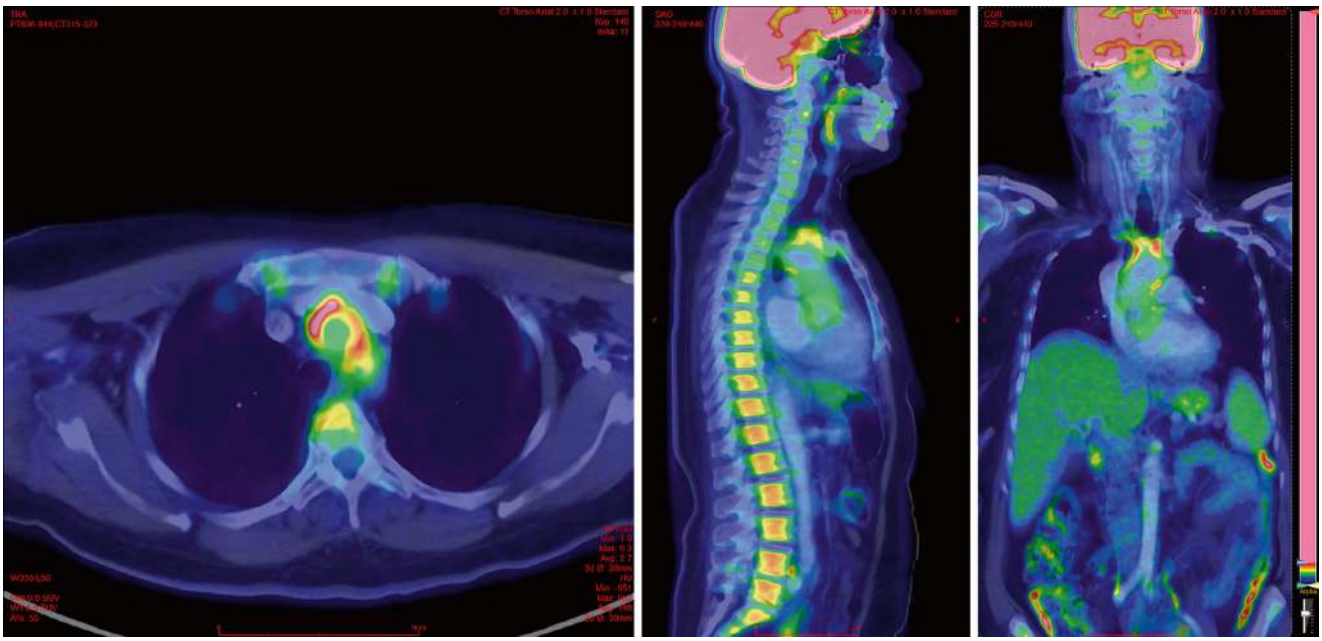


Fig. 9.9 Uptake in the abdominal aorta

Management

- Given the presence of worsening symptoms, elevated inflammatory markers and high FDG uptake in the large vessels with a distribution and pattern typical of large vessel vasculitis, the patient's Takayasu arteritis was deemed active. High-dose prednisone and methotrexate were initiated.

Further Reading

- Kerr GS. Takayasu arteritis. Curr Opin Rheumatology, 1994;6(1):32–8.
- Tombetti E, Mason JC. Takayasu arteritis: advanced understanding leading to new.
- horizons. Rheumatology (Oxford), 2019;58(2):206–19.
- Slart RHJA; Writing group; Reviewer group; Members of EANM Cardiovascular; Members of EANM Infection and Inflammation; Members of Committees, SNMMI Cardiovascular Members of Council, PET Interest Group; Members of ASNC; EANM Committee Coordinator. FDG-PET/CT(A) imaging in large vessel vasculitis and polymyalgia rheumatica: joint procedural recommendations of the EANM, SNMMI, and the PET Interest Group (PIG), and endorsed by the ASNC. Eur J Nucl Med Mol Imaging, 2018; 45(7):1250–1269.
- Banerjee S, Quinn K, Gribbons K, Rosenblum J, Civelek A, Novakovich E et al. Effect of treatment on imaging, clinical, and serologic assessments of disease activity in large vessel vasculitis. J Rheumatol, 2020;47(1):99–107.

9.5 Giant Cell Arteritis: Case 82

Key Points

- ^{18}F-FDG PET/CT can be used to confirm a new diagnosis of giant cell arteritis and may help document the extent of vascular involvement.
- Vascular uptake is graded visually in comparison to liver uptake, and the scores of individual vascular territories can be summed to provide a total vascular score.

History

- A 77-year-old woman with a past history of polymyalgia rheumatica presented with 3 months of new bilateral headache, scalp tenderness, drenching night sweats, and 5 kg weight loss. She was on no immunosuppression. The scalp was tender on the left side of the head, and the left temporal artery pulse was absent. C-reactive protein was 95 mg/L (normal <5.0) and ESR was 94 mm/hr. She was started empirically on prednisone 60 mg po daily and PET/CT was requested to screen for large vessel involvement with suspicion for giant cell arteritis (Figs. 9.10 and 9.11).

PET/CT Images

Findings

- Diffuse, grade 3 FDG uptake was seen in the bilateral common carotids, subclavian, axillary arteries, thoracic and abdominal aorta, and femoral/popliteal arteries, diagnostic of active large vessel vasculitis.
- ^{18}F-FDG uptake in interspinous ligaments suggestive of active polymyalgia rheumatica.

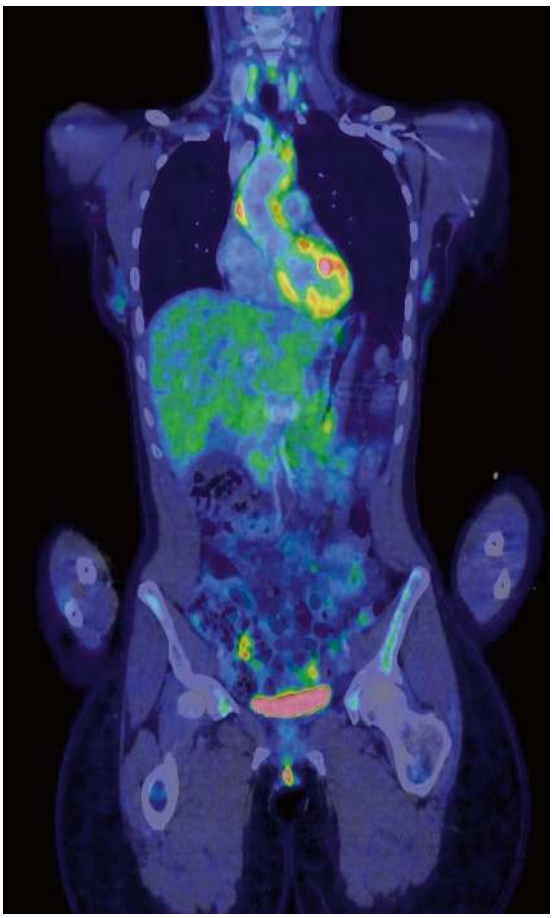


Fig. 9.10 Intense uptake involving common carotids bilaterally, subclavian, axillary arteries, thoracic and abdominal aorta, and femoral/popliteal arteries

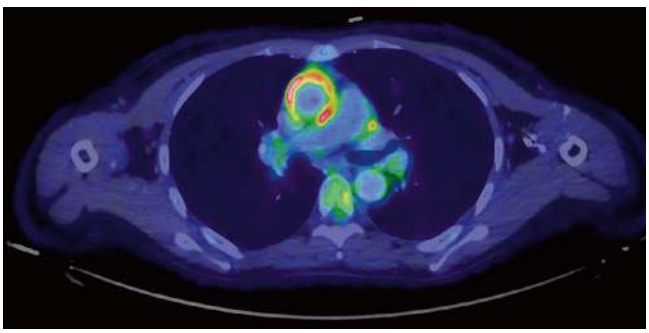


Fig. 9.11 ^{18}F-FDG uptake in interspinous ligaments

Differential Diagnosis
- Active giant cell arteritis.

Correlative Imaging
None.

Management
- The patient was treated with oral prednisone 60 mg daily with taper and weekly subcutaneous tocilizumab.
- Repeat PET/CT performed 6 months later showed only minimal residual inflammation in the ascending aorta.

Further Reading

- Dejaco C, Ramiro S, Duftner C, Besson F, Bley T, Blockmans D et al. EULAR recommendations for the use of imaging in large vessel vasculitis in clinical practice. Ann Rheum Dis, 2018;77(5):636–43.
- Slart R, Writing group; Reviewer group; Members of EANM Cardiovascular; Members of EANM Infection & Inflammation; Members of Committees, SNMMI Cardiovascular; Members of Council, PET Interest Group; Members of ASNC; EANM Committee Coordinator. FDG-PET/CT(A) imaging in large vessel vasculitis and polymyalgia rheumatica: joint procedural recommendations of the EANM, SNMMI, and the PET Interest Group (PIG), and endorsed by the ASNC. Eur J Nucl Med Mol Imaging, 2018; 45(7):1250–1269.

9.6 Multimodality Imaging in Giant Cell Arteritis: Case 83

Key Points
- The diagnostic workup of large vessel vasculitis with FDG PET/CT often requires whole-body imaging (at least top of head to below the knees or top of head to toes).
- Dedicated head imaging is useful to examine extracranial/cranial arteries when giant cell arteritis is suspected.
- FDG PET/CT has excellent diagnostic accuracy for the identification of large vessel vasculitis, especially giant cell arteritis.
- The associated halo sign on vascular ultrasound is highly specific for vascular inflammation.

History
An 85-year-old male patient with a history of anemia, fatigue, weight loss, and headaches with elevated inflammatory markers and clinical suspicion of large vessel vasculitis was referred for FDG PET/CT (Fig. 9.12).

FDG PET/CT

Correlative Imaging (Ultrasound)
Given the suspicion of giant cell arteritis, the patient underwent ultrasound of the head and neck and extremities (Fig. 9.13).

The diagnosis of giant cell arteritis was further affirmed through a temporal artery biopsy.

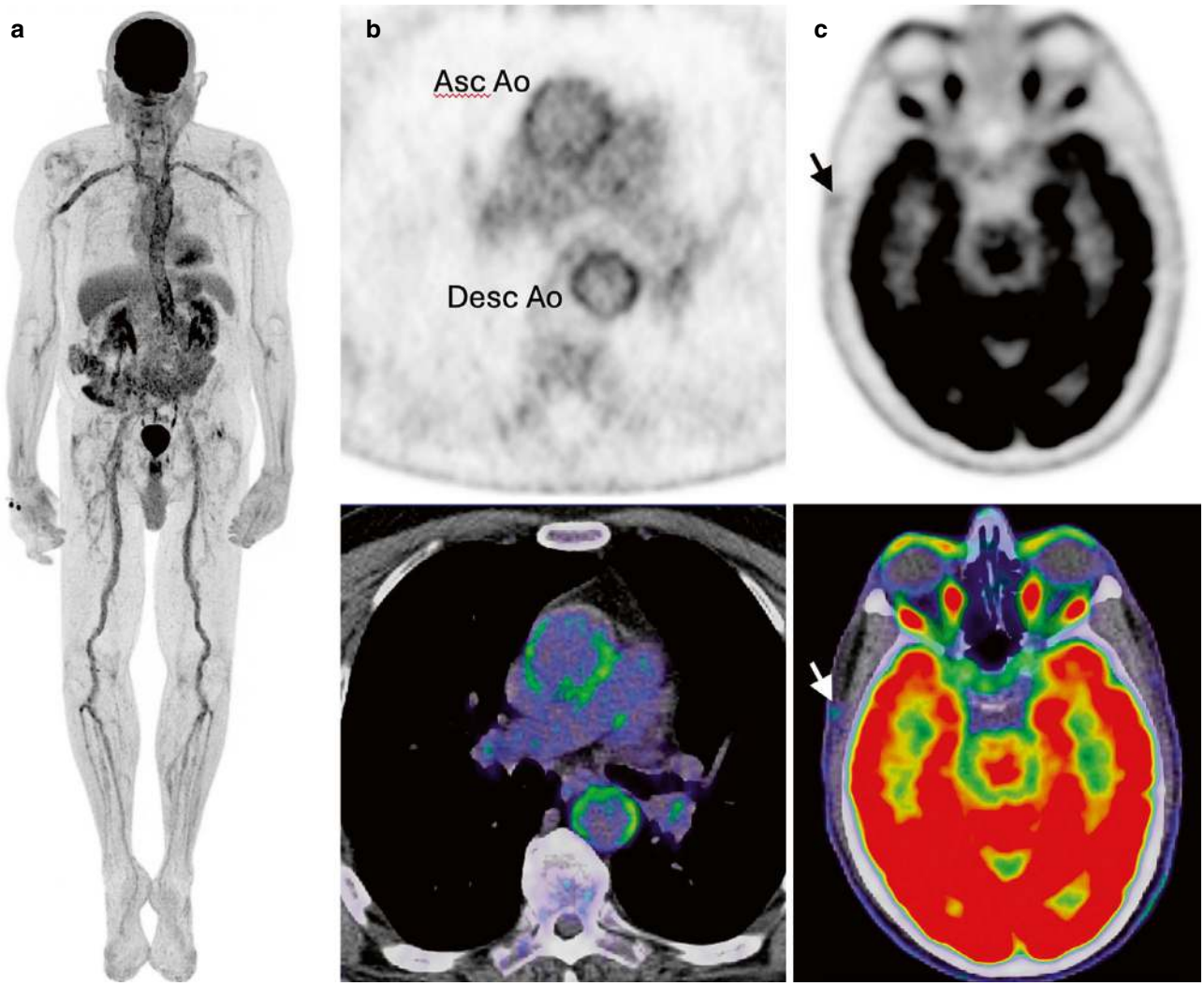


Fig. 9.12 Whole-body FDG PET scan demonstrated diffuse and intense FDG uptake throughout the aorta and its major branches (panel A), particularly on the aorta itself (panel B). Additionally, there was moderate FDG uptake in the right temporal artery (arrow, panel C)

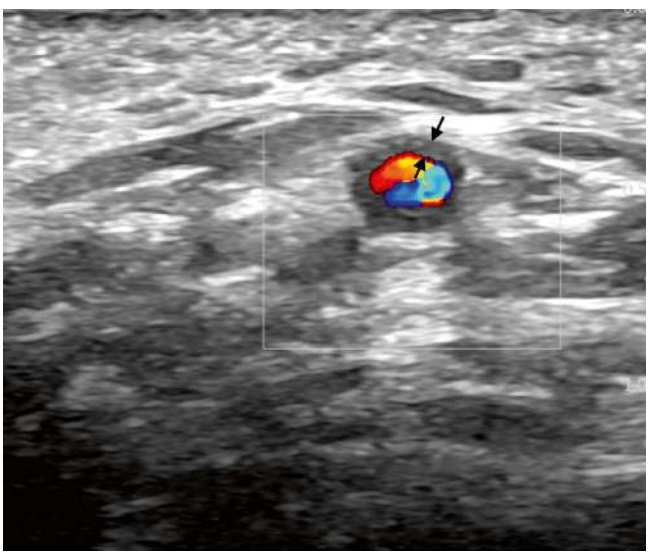


Fig. 9.13 Ultrasound image displaying the "halo sign" in the subclavian artery. The "halo sign" describes an inflamed, edematous, and thickened vessel wall that appears as a hypoechoic rim around the vessel lumen (arrows)

Findings
The FDG PET and ultrasound findings are consistent with a large vessel vasculitis.

Imaging Diagnosis
Large vessel vasculitis consistent with giant cell arteritis (GCA).

Differential Diagnosis
1. Giant cell arteritis (most likely).
2. Takayasu arteritis (rare).
3. Atherosclerosis (no halo sign on vascular ultrasound).

Management
The patient underwent temporal artery biopsy that confirmed the diagnosis of giant cell arteritis. Initially managed with steroid treatment; then tocilizumab was added, achieving complete remission of symptoms and improvement of inflammatory markers.

Further Reading

- Abikhzer G, Treglia G, Pelletier-Galarneau M, et al. EANM/SNMMI guideline/procedure standard for [(18)F] FDG hybrid PET use in infection and inflammation in adults v2.0. *Eur J Nucl Med Mol Imaging*. Jan 2025;52(2):510–538. https://doi.org/10.1007/s00259-024-06915-3
- Dejaco C, Ramiro S, Bond M, et al. EULAR recommendations for the use of imaging in large vessel vasculitis in clinical practice: 2023 update. *Ann Rheum Dis*. May 15 2024;83(6):741–751. https://doi.org/10.1136/ard-2023-224543
- Slart R, Writing g, Reviewer g, et al. FDG-PET/CT(A) imaging in large vessel vasculitis and polymyalgia rheumatica: joint procedural recommendation of the EANM, SNMMI, and the PET Interest Group (PIG), and endorsed by the ASNC. *Eur J Nucl Med Mol Imaging*. Jul 2018;45(7):1250–1269. https://doi.org/10.1007/s00259-018-3973-8

9.7 PET/MRI for Diagnosis and Monitoring of Large Vessel Vasculitis: Case 84

Key Points
- ^{18}F-FDG-PET/magnetic resonance imaging (MRI) is a promising tool for monitoring disease activity in large vessel vasculitis.
- Hybrid, whole-body scanning can identify areas of active vascular inflammation as well as the sequelae of "burnt out" disease, e.g., stenosis, occlusion, or aneurysm.
- ^{18}F-FDG-PET/MRI for large vessel vasculitis is currently a research technique, but, in the future, it could be used to guide clinical management decisions, including the escalation and de-escalation of treatment, something which is currently significantly challenging.

History
- A 38-year-old woman presented with several months of nonspecific abdominal discomfort in addition to vague constitutional symptoms including fatigue, malaise, and loss of appetite.
- Initial investigations demonstrated a serological inflammatory response.
- CT scanning demonstrated a stenosis in the superior mesenteric artery as well as subtle aortic wall thickening. This raised the possibility of Takayasu arteritis.
- She underwent ^{18}F-FDG PET/MRI (Figs. 9.14 and 9.15).

PET/MRI Images

Findings
- ^{18}F-FDG PET/MRI imaging showed radiotracer uptake within the wall of the thoracic and abdominal aorta as well as at the origin of the superior mesenteric artery.
- Quantitative analysis demonstrated an SUVmax of 6.5 within the abdominal aortic wall.
- The MRI component of the scan demonstrated increased T2-weighted mural signal within the same aortic territories.
- The magnetic resonance angiography (MRA) demonstrated stenosis at the origin of the superior mesenteric artery.

Imaging Diagnosis
- Active large vessel vasculitis, likely Takayasu arteritis.

Differential Diagnosis
- Alternative causes of aortitis, including infection.

Correlative Imaging
- None.

Management
- The patient was treated with high-dose prednisolone in addition to the IL-6 receptor antagonist tocilizumab.
- The patient went on to have a follow-up research ^{18}F-FDG-PET/MRI scan which demonstrated resolution of the ^{18}F-FDG uptake in the superior mesenteric artery, though persistence of the changes within the aorta. There was no change in the degree of superior mesenteric artery stenosis. Following this, her treatment was escalated to infliximab.

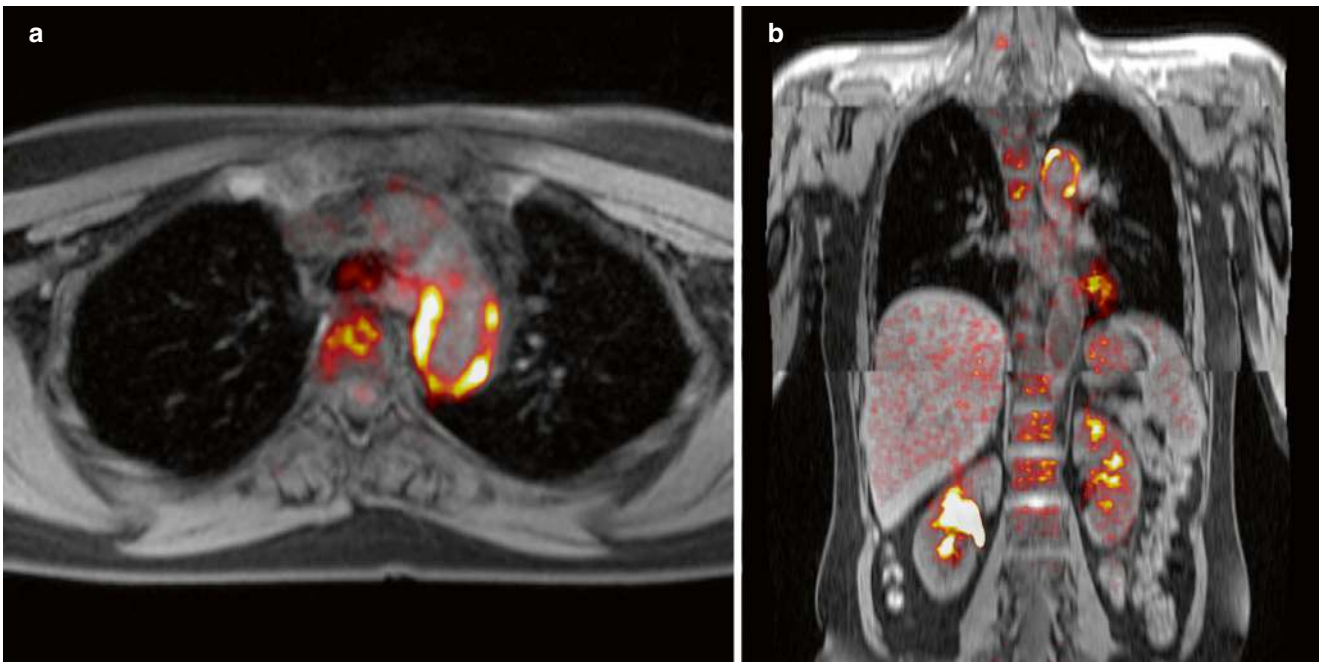


Fig. 9.14 ^{18}F-FDG PET/MRI of the aorta with axial (**a**) and coronal (**b**) images demonstrating radiotracer uptake within the ascending thoracic aorta

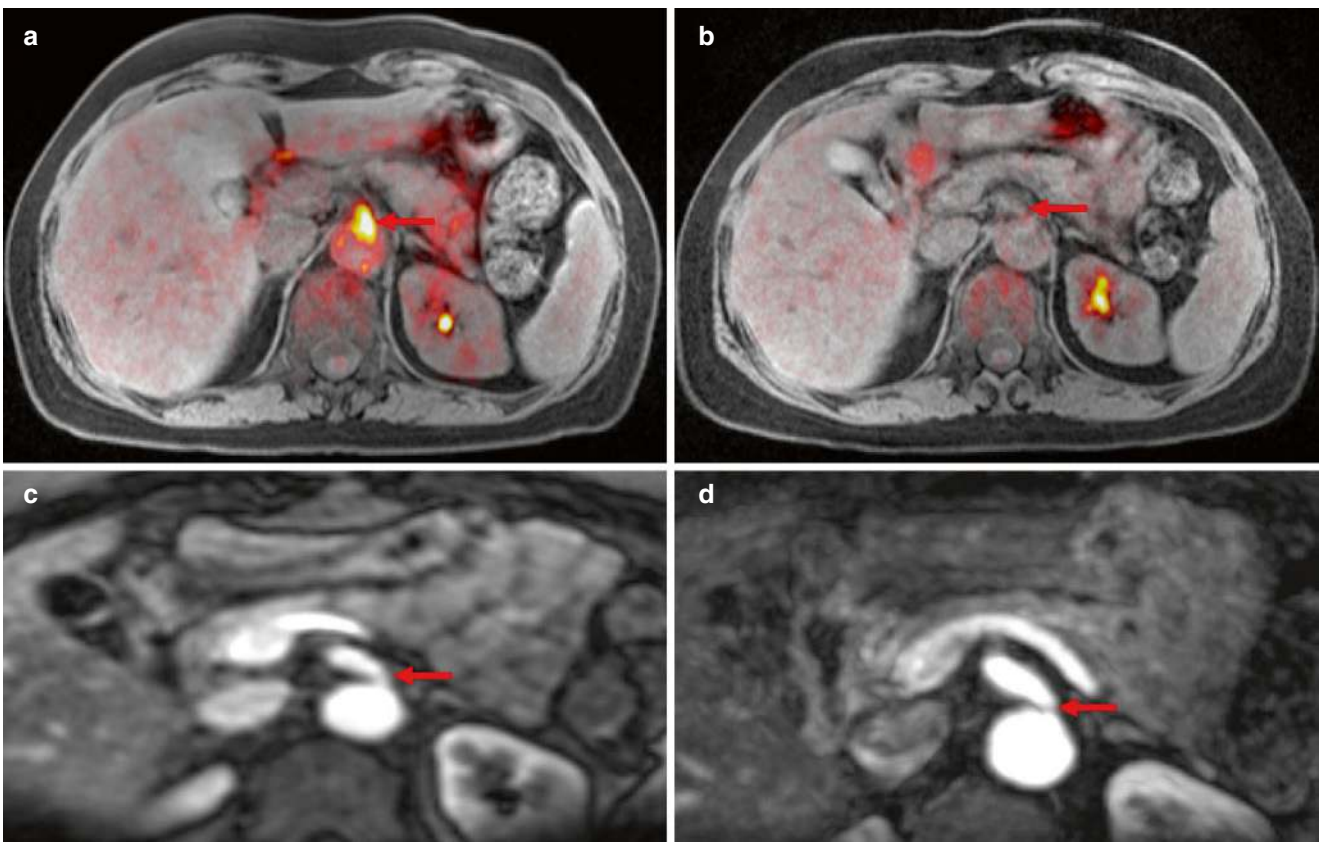


Fig. 9.15 ^{18}F-FDG PET/MRI at the time of presentation (**a**, **c**) and after 6 months of treatment with prednisolone and tocilizumab (**b**, **d**). The images show radiotracer uptake at the origin of the superior mesenteric artery at the time of presentation associated with a severe stenosis (**a**, **c**). After treatment 6 months later, the stenotic lesion was unchanged, but the radiotracer uptake had resolved, in keeping with resolution of the active inflammation

Further Reading

- Pugh D, Karabayas M, Basu N, Cid MC, Goel R, Goodyear CS, Grayson PC, McAdoo SP, Mason JC, Owen C, Weyand CM, Youngstein T, Dhaun N. Large-vessel vasculitis. Nat Rev. Dis Primers. 2022 Jan 6;7(1):93. https://doi.org/10.1038/s41572-021-00327-5.
- Pugh D, Dhaun N. Comment on: A novel model to assess disease activity in Takayasu arteritis based on 18F-FDG PET/CT: a Chinese cohort study. Rheumatology (Oxford). 2022 Apr 18;61(SI):SI97-SI98. https://doi.org/10.1093/rheumatology/keab802.

The opinions expressed in this chapter are those of the author(s) and do not necessarily reflect the views of the IAEA: International Atomic Energy Agency, its Board of Directors, or the countries they represent.

Open Access This chapter is licensed under the terms of the Creative Commons Attribution 3.0 IGO license (http://creativecommons.org/licenses/by/3.0/igo/), which permits use, sharing, adaptation, distribution and reproduction in any medium or format, as long as you give appropriate credit to the IAEA: International Atomic Energy Agency, provide a link to the Creative Commons license and indicate if changes were made.

Any dispute related to the use of the works of the IAEA: International Atomic Energy Agency that cannot be settled amicably shall be submitted to arbitration pursuant to the UNCITRAL rules. The use of the IAEA: International Atomic Energy Agency's name for any purpose other than for attribution, and the use of the IAEA: International Atomic Energy Agency's logo, shall be subject to a separate written license agreement between the IAEA: International Atomic Energy Agency and the user and is not authorized as part of this CC-IGO license. Note that the link provided above includes additional terms and conditions of the license.

The images or other third party material in this chapter are included in the chapter's Creative Commons license, unless indicated otherwise in a credit line to the material. If material is not included in the chapter's Creative Commons license and your intended use is not permitted by statutory regulation or exceeds the permitted use, you will need to obtain permission directly from the copyright holder.



Cardiac Toxicity After Chemo/Radiation

10

Raffaele Giubbini, Paolo Raggi, Marcelo Di Carli, Michelle Williams, Diana Paez, Maurizio Dondi, Elisa Milan, Francesco Lanfranchi, Matteo Bauckneht, and Gianmario Sambuceti

Objectives

- To understand the complexities of cardiac toxicity arising from chemotherapy and radiation therapy through detailed case studies.
- To emphasize the importance of early detection and comprehensive management of cardiac toxicity to improve patient outcomes.
- To equip healthcare professionals with advanced imaging techniques and clinical observations to identify, monitor, and mitigate cardiac toxicity in patients undergoing cancer therapies.

The intersection of oncology and cardiology presents unique challenges, particularly in the context of cardiac toxicity following chemotherapy and radiation therapy. As cancer treatments advance, so does our understanding of their potential adverse effects on the heart. This chapter delves into the complexities of cardiac toxicity, offering insights through a series of detailed case studies.

This chapter explores the multifaceted nature of cardiac complications that can arise posttreatment, emphasizing the importance of early detection and comprehensive management. From the aftermath of chemotherapy in Hodgkin's Lymphoma to the incidental findings of cardiac masses, each case provides a unique perspective on the cardiac risks associated with cancer therapies.

Through advanced imaging techniques and clinical observations, this chapter aims to equip healthcare professionals with the knowledge to identify, monitor, and mitigate cardiac toxicity, ultimately improving patient outcomes.

10.1 After Chemotherapy for Hodgkin's Lymphoma: Case 85

Key Points

- The presence of myocardial ^{18}F-FDG uptake following chemotherapy is a common finding.
- While this finding could represent myocardial injury secondary to chemotherapy in some patients, the finding

All authors have no conflict of interest to disclose.

R. Giubbini
Nuclear Medicine, International Specialized Hospital of Uganda (ISHU), Kampala, Uganda

P. Raggi
Division of Cardiology, University of Alberta, Edmonton, AB, Canada

M. Di Carli
Brigham and Women's Hospital, Boston, MA, USA
e-mail: mdicarli@bwh.harvard.edu

M. Williams
British Heart Foundation Centre for Research Excellence, Institute for Neuroscience and Cardiovascular Research, University of Edinburgh, Edinburgh, United Kingdom
e-mail: michelle.williams@ed.ac.uk

D. Paez · M. Dondi (✉)
Division of Human Health, International Atomic Energy Agency, Vienna, Austria
e-mail: d.paez@iaea.org; m.dondi@iaea.org

E. Milan
Nuclear Cardiology Lab and PET Centre, Treviso Hospital, Treviso, Italy
e-mail: elisa.milan@aulss2.veneto.it

F. Lanfranchi · M. Bauckneht · G. Sambuceti
Department of Health Sciences (DISSAL), University of Genova, Genoa, Italy
e-mail: studenti@unige.it; matteo.bauckneht@unige.it; gianmario.sambuceti@unige.it

© The Author(s) 2027
M. Di Carli et al. (eds.), *IAEA Atlas of Cardiac PET/CT*, https://doi.org/10.1007/978-3-662-74188-7_10

must be interpreted in the context of clinical symptoms and cardiac function.
- In patients with LV dysfunction and heart failure, the heart switches substrate metabolism from preferential fatty acid utilization to glucose.

History
- A 56-year-old man with Hodgkin's lymphoma (HL) was referred for staging purposes with ^{18}F-FDG PET/CT.
- After the baseline evaluation, the patient started treatment with doxorubicin, bleomycin, vinblastine, and dacarbazine (Fig. 10.1).

^{18}F-FDG PET/CT Images

Findings
- The baseline scan showed intense tracer uptake in supradiaphragmatic lymph nodes.
- In the follow-up ^{18}F-FDG PET/CT scan, a complete treatment response was observed (Deauville score 1).
- However, intense myocardial uptake was noted in the follow-up scan.

Imaging Diagnosis
- Complete treatment response with resolution of FDG uptake in all diseased areas.

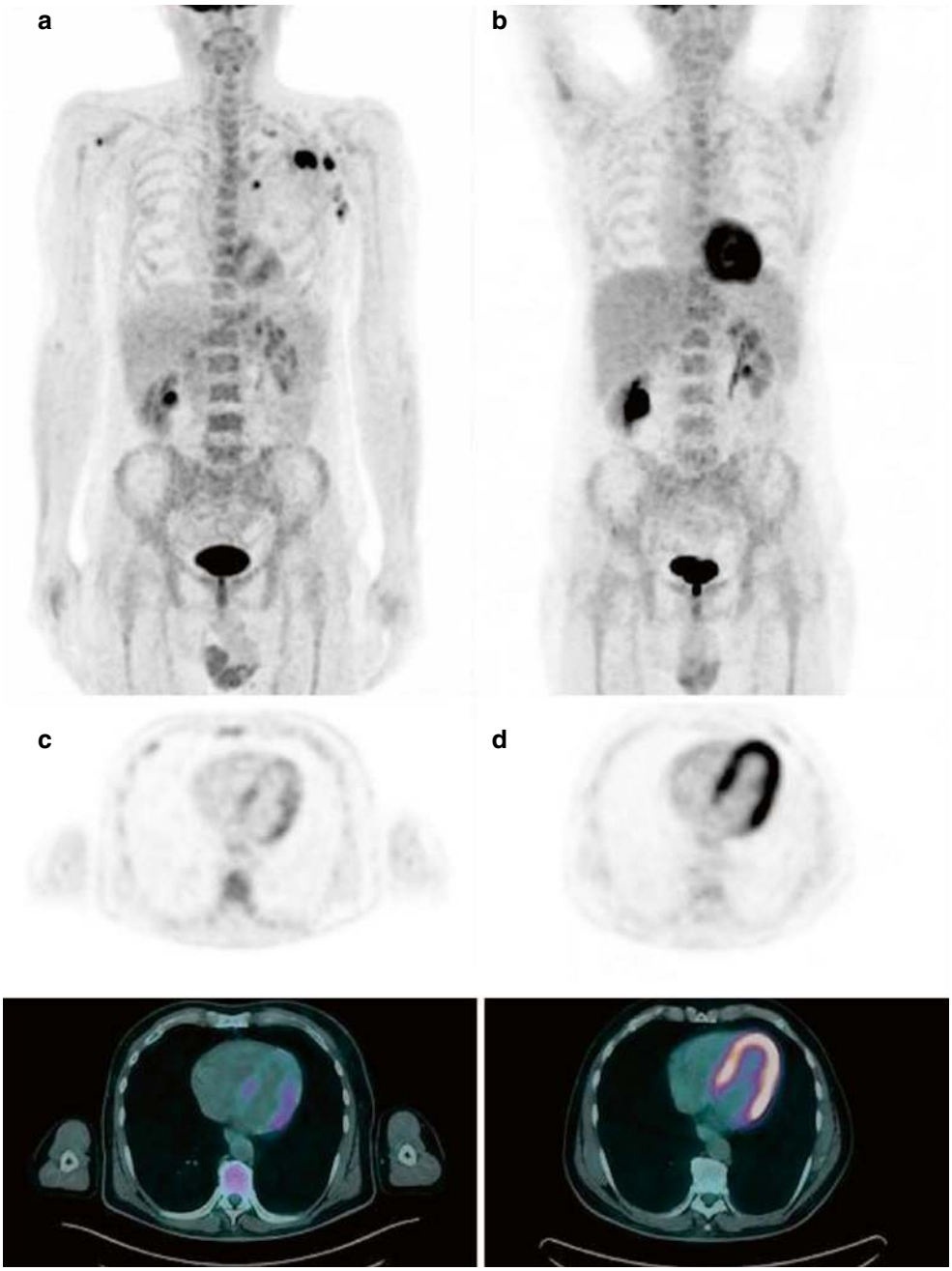


Fig. 10.1 Basal (**a** and **c**) and follow-up ^{18}F-FDG PET/CT images. Maximum intensity projection images at baseline (**a**) showed several nodal localizations of the disease, while on the follow-up evaluation, (**b**) no ^{18}F-FDG-active lesion was detected (Deauville score 1). The myocardial ^{18}F-FDG uptake appeared remarkably increased in the follow-up compared to the baseline images. The same finding is highlighted when comparing (**c**) baseline and (**d**) follow-up transaxial PET only (above) and fused images (bottom row)

- Interim development of intense myocardial FDG uptake is noted.

Differential Diagnosis
- None.

Correlative Imaging
- None.

Management
- The patient completed the treatment protocol, and the final ^{18}F-FDG PET/CT showed a complete metabolic response according to the Lugano criteria.
- During the standard cardiological follow-up, the patient developed an asymptomatic moderate left ventricular dysfunction, potentially associated with the previous chemotherapy treatment.

Further Reading

- Baucknehtt M, Pastorino F, Castellani P, et al. Increased myocardial 18F-FDG uptake as a marker of Doxorubicin-induced oxidative stress. J Nucl Cardiol. 2020;27(6):2183–2194. https://doi.org/10.1007/s12350-019-01618-x
- Kim J, Cho SG, Kang SR, et al. Association between FDG uptake in the right ventricular myocardium and cancer therapy-induced cardiotoxicity. J Nucl Cardiol. 2020;27(6):2154–2163. https://doi.org/10.1007/s12350-019-01617-y.
- Baucknehtt M, Ferrarazzo G, Fiz F, et al. Doxorubicin Effect on Myocardial Metabolism as a Prerequisite for Subsequent Development of Cardiac Toxicity: A Translational 18F-FDG PET/CT Observation. J Nucl Med. 2017;58(10):1638–1645. https://doi.org/10.2967/jnumed.117.191122.

10.2 Pericarditis After Chemotherapy: Case 86

Key Points
- Pericarditis can be a late, dose-dependent complication of mediastinal irradiation. It can also be an adverse effect from chemotherapy (e.g., doxorubicin). While it can also result from heart failure, this patient had normal LV systolic function.
- The presence of ^{18}F-FDG uptake is consistent with active pericardial inflammation.

History
- A 66-year-old woman with Hodgkin's lymphoma undergoing interim ^{18}F-FDG PET/CT (Fig. 10.2) to monitor treatment response after two cycles of doxorubicin, bleomycin, vinblastine, and dacarbazine.

Findings
- The ^{18}F-FDG PET/CT images showed no evidence of uptake in mediastinal lymph nodes.
- There was a small pericardial effusion with moderate ^{18}F-FDG uptake in the pericardium.

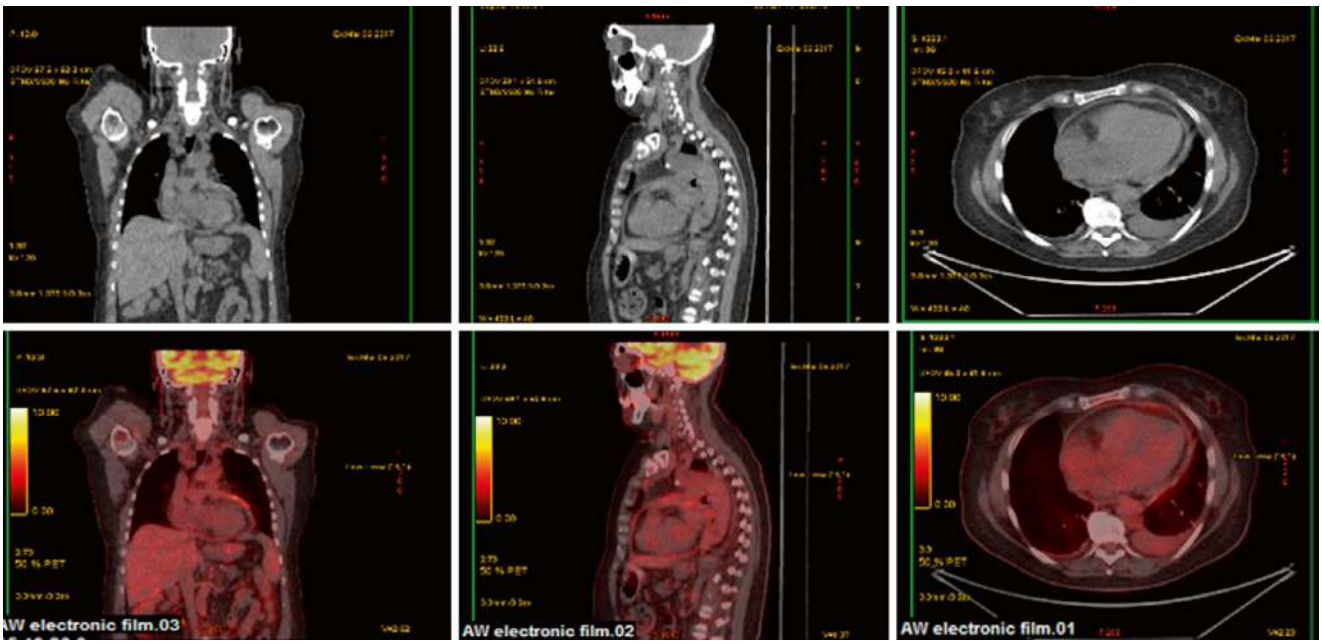


Fig. 10.2 Limited whole-body ^{18}F-FDG PET/CT demonstrated a small pericardial effusion with moderate uptake in the pericardium

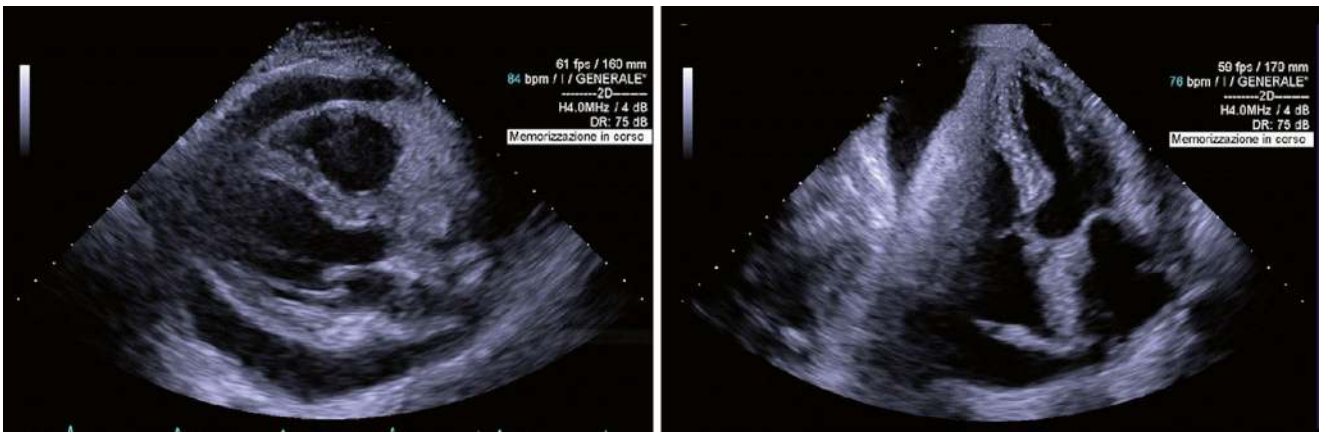


Fig. 10.3 Transthoracic echocardiogram confirming the presence of a moderate pericardial effusion

- Transthoracic echocardiography performed 4 days after ^{18}F-FDG PET/CT scan showed an interval increase in pericardial effusion.

Imaging Diagnosis
- Moderate ^{18}F-FDG uptake in the pericardium suggesting active inflammation.

Differential Diagnosis
- None.

Correlative Imaging
- Transthroracic echocardiogram (Fig. 10.3).

Management
- The patient received anti-inflammatory therapy.

Further Reading

- Floyd J, Nguyen D, Lobins R, Bashir Q, Doll D, Perry M. Cardiotoxicity of Cancer Therapy. Journal of Clinical Oncology. 2005;23:7685–7696.
- Laursen AH, Elming MB, Ripa RS, Hasbak P, Kjær A, Køber L, Marott JL, et al. Rubidium-82 positron emission tomography for detection of acute doxorubicin-induced cardiac effects in lymphoma patients. J Nucl Cardiol. 2018 Oct 8. doi:10.1007/s12350-018-1458-6. [Epub ahead of print].
- Bauckneht M, Pastorino F, Castellani P, Cossu V, Orengo A, Piccioli P, et al. Increased myocardial 18F-FDG uptake as a marker of Doxorubicin-induced oxidative stress. J Nucl Cardiol. 2019 Feb 8. doi:10.1007/s12350-019-01618-x. [Epub ahead of print].
- Plana JC, Thavendiranathan P, Bucciarelli-Ducci C, Lancellotti P. Multi-Modality Imaging in the Assessment of Cardiovascular Toxicity in the Cancer Patient. JACC Cardiovasc Imaging. 2018 Aug;11(8):1173–1186. doi:10.1016/j.jcmg.2018.06.003. Review. Erratum in: JACC Cardiovasc Imaging. 2019 Jan;12(1):224.

10.3 Incidental Findings of Cardiac Masses

10.3.1 Cardiac Metastasis from Prostate Cancer Detected with 18F-PSMA-1007: Case 87

Key Points
- ^{18}F-PSMA-1007 PET/CT is a valuable tool for restaging purposes in prostate cancer patients.
- Considering the high specificity of this radiotracer, this atypical finding was still defined as a possible metastatic site after the multidisciplinary.
- However, some benign conditions that may lead to the accumulation of this tracer at the cardiac level and this finding could also reflect benign tracer uptake in the setting of lipomatous hypertrophy of the interatrial septum.

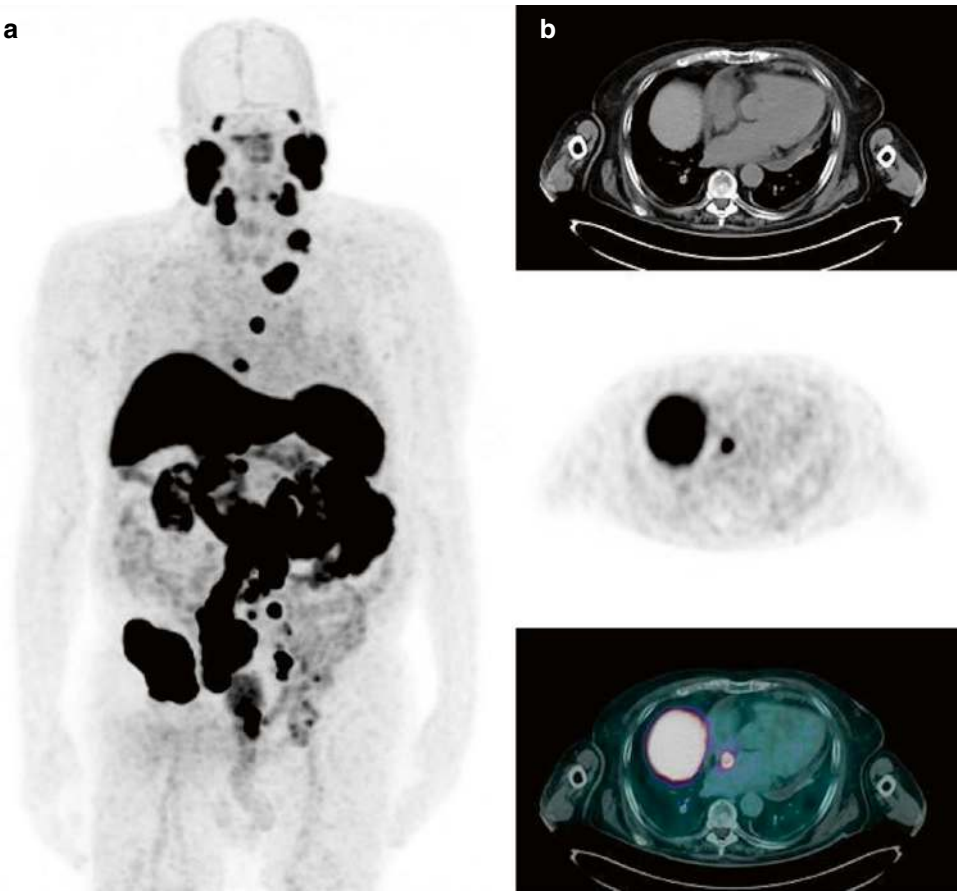


Fig. 10.4 Maximum intensity projection images of ^{18}F-PSMA-1007 PET/CT (**a**). In the right half of the picture CT only (top), PET only (middle), and fused images (bottom) at the level of the interatrial septum (**b**), showing a focal area of high tracer uptake in the interatrial septum

History

- A 90-year-old man with a diagnosis of metastatic hormone-sensitive prostate cancer (Gleason Score 5 + 4 at biopsy; diffuse skeletal lesions on bone scan and CT) undergoing treatment with androgen deprivation therapy was referred for restaging purposes (biochemical recurrence, prostate-specific antigen = 69 ng/mL).
- The patient could not receive CT contrast agents because of reduced kidney function, and thus he underwent ^{18}F-PSMA-1007 PET/CT.

PET/CT Images

Findings

- The exam demonstrated a nodal and skeletal progression of disease (Fig. 10.4a).
- In addition, ^{18}F-PSMA-1007 PET/CT showed a focal area of high tracer uptake at the interatrial septum, with a SUVmax of 20 (Fig. 10.4b).

Imaging Diagnosis

- Possible cardiac metastasis.

Differential Diagnosis

- Benign uptake in lipomatous hypertrophy of the interatrial septum.

Correlative Imaging

- None.

Management

- The patient was referred to cardiac MRI and cardiological evaluation.
- Unfortunately, within a few months, the patient died because of a sudden worsening of his general conditions.

Further Reading

- Das JP, Yeh R. Prostate cancer cardiac metastasis detected on serial imaging with [68Ga] PSMA-11 PET/CT. Eur J Nucl Med Mol Imaging. 2022;49(11):3952–3953. https://doi.org/10.1007/s00259-022-05815-8.
- Barbosa FG, Queiroz MA, Nunes RF, et al. Revisiting Prostate Cancer Recurrence with PSMA PET: Atlas of Typical and Atypical Patterns of Spread. Radiographics. 2019;39(1):186–212. https://doi.org/10.1148/rg.2019180079.

• Vinjamoori AH, Jagannathan JP, Shinagare AB, et al. Atypical metastases from prostate cancer: 10-year experience at a single institution. AJR Am J Roentgenol. 2012;199(2):367–372. https://doi.org/10.2214/AJR.11.7533.

10.4 ^{68}Ga-DOTATOC PET/CT in Metastatic Neuroendocrine Tumors: Case 88

Key Points

- PET/CT imaging with ^{68}Ga-DOTA-conjugated peptides is useful in the diagnostic workup of neuroendocrine neoplasms.
- This tool is capable of predicting the response to therapies with somatostatin analogs.
- This technique plays a key role in the selection of patients for radioligand therapy.

History

- A 66-year-old woman with a new diagnosis of a neuroendocrine tumor of the ileum (Ki67 5–10%, G2).
- Contrast-enhanced CT showed a lesion in the right lung and supraclavicular lymph nodes suspicious for neuroendocrine tumor metastases. Brain CT was normal.
- The patient was referred for staging purposes with ^{68}Ga-DOTATOC PET/CT.

PET/CT Images

Findings

- There is intense ^{68}Ga-DOTATOC uptake in the ileum with associated metastases in the lymph nodes, pancreas and right pleura (Fig. 10.5a).
- ^{68}Ga-DOTATOC PET/CT identified a focal area of uptake in the myocardium of the left ventricle with a SUVmax of 12 (Fig 10.5b), suspicious for cardiac metastasis.

Correlative Imaging

- Cardiac MRI identified signal alterations in the area identified on ^{68}Ga-DOTATOC PET/CT in the left ventricular myocardium (Fig. 10.6), which were suspicious for a neuroendocrine tumor metastasis.

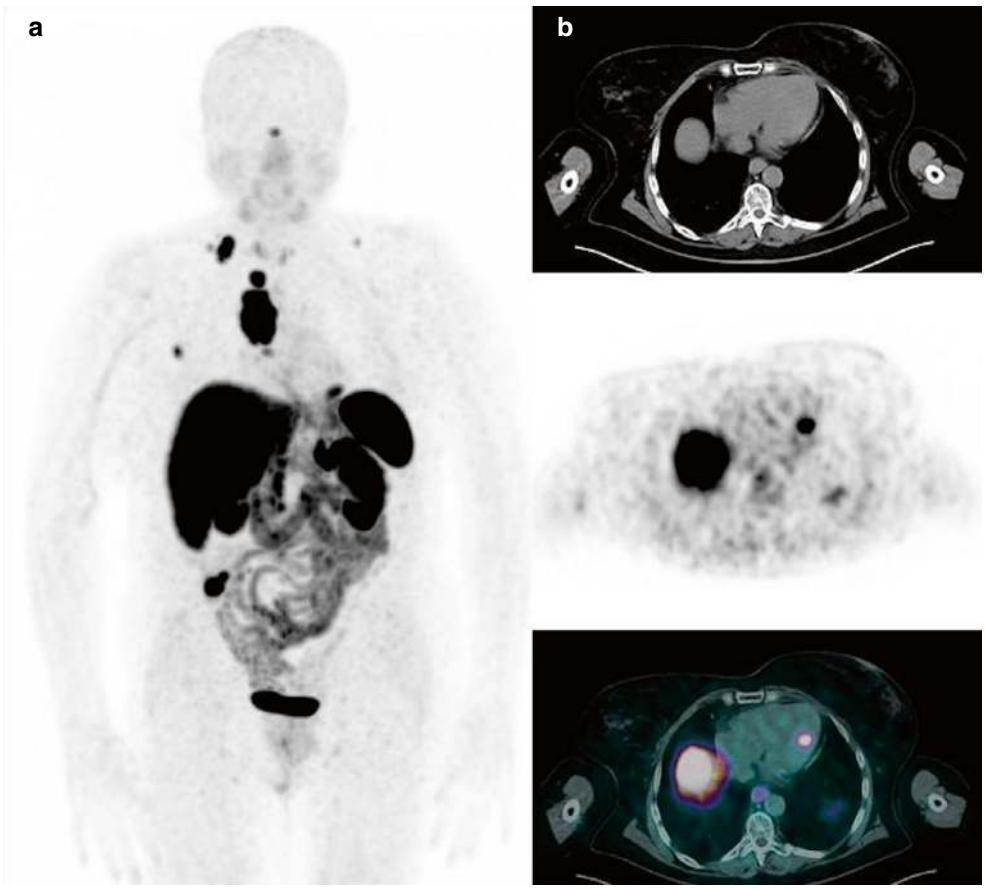


Fig. 10.5 Maximum intensity projection images of ^{68}Ga-DOTATOC PET/CT (**a**). Transaxial CT only (top), PET only (middle), and fused images (bottom) at the level of the left ventricle (**b**), showing a focal area of high uptake suspicious for a cardiac metastasis from the neuroendocrine tumor

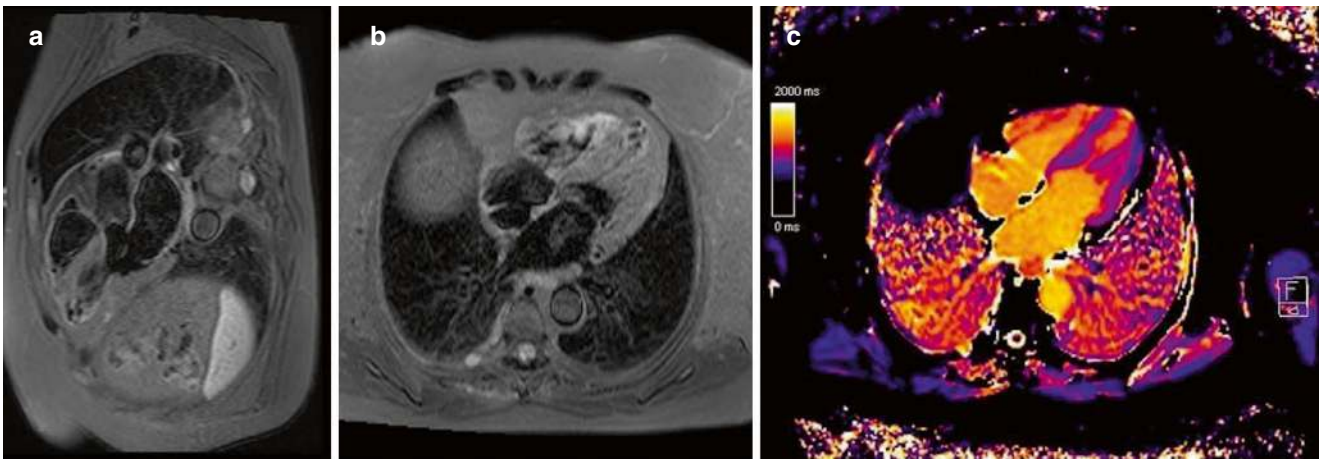


Fig. 10.6 Cardiac MRI sagittal (**a**) and transaxial images (**b**) showed hyperintensity in short-tau-inversion-recovery (STIR) T2-weighted fat-suppressed sequences. T1 mapping sequences detected increased native T1 values (1024 ms) (**c**). These two findings were detected in the area identified on ^{68}Ga-DOTATOC PET/CT in the left ventricle myocardium

Imaging Diagnosis

- ^{68}Ga-DOTATOC PET/CT uptake in the myocardium of the left ventricle suspicious for a cardiac metastasis.

Differential Diagnosis

- None.

Management

- A treatment with somatostatin analogs was chosen by the neuroendocrine tumor -dedicated multidisciplinary disease management team.
- Considering that both ^{68}Ga-DOTATOC PET/CT and cardiac MRI were suspicious for a cardiac metastasis from NET, no biopsy was required.
- The patient was referred to cardiologic evaluation and underwent ECG, dynamic ECG monitoring, and echocardiography, which were all normal.

Further Reading

- Herrera-Martínez Y, Vercher-Conejero JL, Martín-Marcuartu JJ, Telué Vega A, Guerrero-Pérez F, Cortés Romera M. [68Ga]-DOTATOC PET/CT in myocardial metastases of neuroendocrine neoplasms. J Nucl Cardiol. 2023;30(4):1706–1708. https://doi.org/10.1007/s12350-022-03014-4.
- Kunz WG, Eschbach RS, Stahl R, et al. Identification and characterization of myocardial metastases in neuroendocrine tumor patients using 68Ga-DOTATATE PET-CT. Cancer Imaging. 2018;18(1):34. Published 2018 Sep 20. https://doi.org/10.1186/s40644-018-0168-2.
- Calissendorff J, Sundin A, Falhammar H. ^{68}Ga-DOTATOC-PET/CT detects heart metastases from ileal neuroendocrine tumors. Endocrine. 2014;47(1):169–176. https://doi.org/10.1007/s12020-013-0108-7.

The opinions expressed in this chapter are those of the author(s) and do not necessarily reflect the views of the IAEA: International Atomic Energy Agency, its Board of Directors, or the countries they represent.

Open Access This chapter is licensed under the terms of the Creative Commons Attribution 3.0 IGO license (http://creativecommons.org/licenses/by/3.0/igo/), which permits use, sharing, adaptation, distribution and reproduction in any medium or format, as long as you give appropriate credit to the IAEA: International Atomic Energy Agency, provide a link to the Creative Commons license and indicate if changes were made.

Any dispute related to the use of the works of the IAEA: International Atomic Energy Agency that cannot be settled amicably shall be submitted to arbitration pursuant to the UNCITRAL rules. The use of the IAEA: International Atomic Energy Agency's name for any purpose other than for attribution, and the use of the IAEA: International Atomic Energy Agency's logo, shall be subject to a separate written license agreement between the IAEA: International Atomic Energy Agency and the user and is not authorized as part of this CC-IGO license. Note that the link provided above includes additional terms and conditions of the license.

The images or other third party material in this chapter are included in the chapter's Creative Commons license, unless indicated otherwise in a credit line to the material. If material is not included in the chapter's Creative Commons license and your intended use is not permitted by statutory regulation or exceeds the permitted use, you will need to obtain permission directly from the copyright holder.

Future Directions

11

Michelle Williams, Marcelo Di Carli, Paolo Raggi, Raffaele Giubbini, Diana Paez, Maurizio Dondi, Mouaz Al-Mallah, Olivier Clerc, Sharmila Dorbala, Jason Zelt, Christiane Wiefels, Rob de Kemp, Yoshito Kadoya, Neil Craig, Marc R. Dweck, Beth Whittington, Anna Barton, Marta Peverelli, Christopher Wall, Jason M. Tarkin, Andrej Ćorović, Craig Balmforth, and David Newby

Objectives

- To learn about emerging applications of molecular imaging with positron emission tomography (PET) in cardiovascular disease.
- To understand the potential applications of PET in the diagnosis and management of patients with cardiac amyloidosis.
- To learn about the potential utility of PET in the diagnosis of myocarditis.
- To learn about the potential utility of novel radiotracers for PET imaging to assess thrombosis, fibrosis, calcification, and inflammation in cardiovascular disease.

In this chapter, we explore the state-of-the-art techniques which have the potential to change how we use PET imaging in cardiovascular disease. Research is underway into a variety of novel radiotracers which can identify specific biological processes which are important in cardiovascular disease. This includes assessment of microcalcification, thrombosis, fibrosis, innervation, and subtypes of inflammation.

Atherosclerosis is an important target for molecular PET imaging. It is an immune-inflammatory disease of the arterial wall characterized by build-up of cholesterol, fat, calcium, and other substances that migrate from the blood into the vessel intima. It is a slow and progressive disease that ultimately narrows the vessel lumen, limiting the flow of oxygen-rich blood to the tissues. During different stages of atherosclerosis microcalcification, thrombosis, inflamma-

All authors have no conflict of interest to disclose.

M. Williams
British Heart Foundation Centre for Research Excellence, Institute for Neuroscience and Cardiovascular Research, University of Edinburgh, Edinburgh, United Kingdom
e-mail: michelle.williams@ed.ac.uk

N. Craig · M. R. Dweck · B. Whittington · C. Balmforth · D. Newby
British Heart Foundation Centre for Research Excellence, University of Edinburgh, Edinburgh, UK
e-mail: neil.craig@ed.ac.uk; Marc.dweck@ed.ac.uk; bwhittin@exseed.ed.ac.uk; craig.balmforth@ed.ac.uk; d.e.newby@ed.ac.uk

M. Di Carli · O. Clerc · S. Dorbala
Brigham and Women's Hospital, Boston, MA, USA
e-mail: mdicarli@bwh.harvard.edu; oclerc@bwh.harvard.edu; sdorbala@bwh.harvard.edu

P. Raggi
Division of Cardiology, University of Alberta, Edmonton, AB, Canada

R. Giubbini
Nuclear Medicine, International Specialized Hospital of Uganda (ISHU), Kampala, Uganda
e-mail: raffaele.giubbini@unibs.it

D. Paez · M. Dondi (✉)
Division of Human Health, International Atomic Energy Agency, Vienna, Austria
e-mail: d.paez@iaea.org; m.dondi@iaea.org

M. Al-Mallah
De Bakey Heart and Vascular Center, Houston, TX, USA
e-mail: mal-mallah@houstonmethodist.org

J. Zelt
Department of Medicine, University of Ottawa, Ottawa, ON, Canada
e-mail: jazelt@toh.ca

C. Wiefels · R. de Kemp · Y. Kadoya
University of Ottawa Heart Institute, Ottawa, ON, Canada
e-mail: cwiefels@toh.ca; radekemp@ottawaheart.ca; ykadoya@ottawaheart.ca

A. Barton · M. Peverelli · C. Wall · J. M. Tarkin · A. Ćorović
Heart & Lung Research Institute, University of Cambridge, Cambridge, UK
e-mail: abarton3@exseed.ed.ac.uk; mp2068@cam.ac.uk; cw463@cam.ac.uk; jt545@cam.ac.uk; ac476@cam.ac.uk

© The Author(s) 2027
M. Di Carli et al. (eds.), *IAEA Atlas of Cardiac PET/CT*, https://doi.org/10.1007/978-3-662-74188-7_11

tion, and fibrosis occur and are potential targets for molecular PET imaging.

Molecular imaging with PET can provide new insights into the mechanisms involved in the development of cardiovascular diseases. In future, it may be possible to target these biological processes with novel treatments and use PET imaging to optimize and monitor therapies.

In addition, total-body PET scanners provide the opportunity to simultaneously image the entire body, enhancing the assessment of vascular disease throughout the body and systemic interactions. These scanners have improved sensitivity, enabling improved image quality and/or faster or lower radiation dose imaging. Other hardware and software improvements, including the use of artificial intelligence, will continue to improve PET imaging. This includes improving reconstruction, time of flight resolution, signal-to-noise, and image analysis.

The cases in this chapter illustrate the promising potential of new PET techniques for cardiovascular imaging. However, this is a rapidly evolving area of research. It is currently uncertain which developments will be used primarily in research to enhance our understanding of disease and which will translate into clinical practice to improve patient outcomes.

11.1 NEW TRACER for Myocardial Perfusion Imaging

11.1.1 ^{18}F-Flurpiridaz

^{18}F-Flurpiridaz is a new radiopharmaceutical agent targeting mitochondrial complex I, primarily developed for myocardial perfusion imaging (MPI) using positron emission tomography (PET), for CAD diagnosis. Compared to single-photon emission computed tomography (SPECT) MPI, it provides high-resolution images due to PET's superior imaging.

11.1.2 Example of Case with Flurpiridaz: Case 89

Key Points

^{18}F-Flurpiridaz demonstrates a higher sensitivity than sestamibi for the detection of perfusion abnormalities on stress nuclear testing, and its extraction curve shows superior dynamics compared with ^{99}Tc- and ^{82}Rb-based tracers, with greater extraction at each flow increment.

^{18}F-Flurpiridaz allows acquiring perfusion images and calculating myocardial blood flow with half the radiation dose of a typical ^{99}Tc-sestamibi rest-stress protocol (approximately 6 vs 12–18 mSv).

The half-life of ^{18}F-flurpiridaz is approximately 2 hours compared to 6 hours for ^{99}Tc and 80 seconds for ^{82}Rb.

History

- A 65-year-old man with a history of systemic hypertension, diabetes mellitus, obstructive sleep apnea, and new onset chest pain was referred for MPI SPECT with ^{99m}Tc-Sestamibi, using vasodilator stress. Low dose CCB were in use to control his Afib. Due to his obstructive sleep apnea, patient never tolerated beta blockers.
- Baseline and post-stress electrocardiogram (ECG) showed atrial fibrillation and he did not develop electrocardiographic signs of ischemia during the stress portion of the test.

ECG (Fig. 11.1)
SPECT study (Fig. 11.2)

Findings

SPECT scan was interpreted as showing uniform tracer uptake with no evidence of ischemia or scar. A ^{18}F-Flurpiridaz stress scan was obtained as part of a research protocol (Figs. 11.3 and 11.4).

Interpretation

Sestamibi SPECT study shows no perfusion abnormalities.

^{18}F-Flurpiridaz PET/computed tomography (CT) shows an anterior wall defect reversible at rest, consistent with ischemia, confirmed by myocardial flow reerve (MFR) results; apical defect only minimally reversible, possibly related to apical thinning. Moderately enlarged left ventricle (LV) with normal LV systolic function both at rest and after stress.

Differential Diagnosis

None.

Correlative Imaging

Coronary angiography (Fig. 11.5).

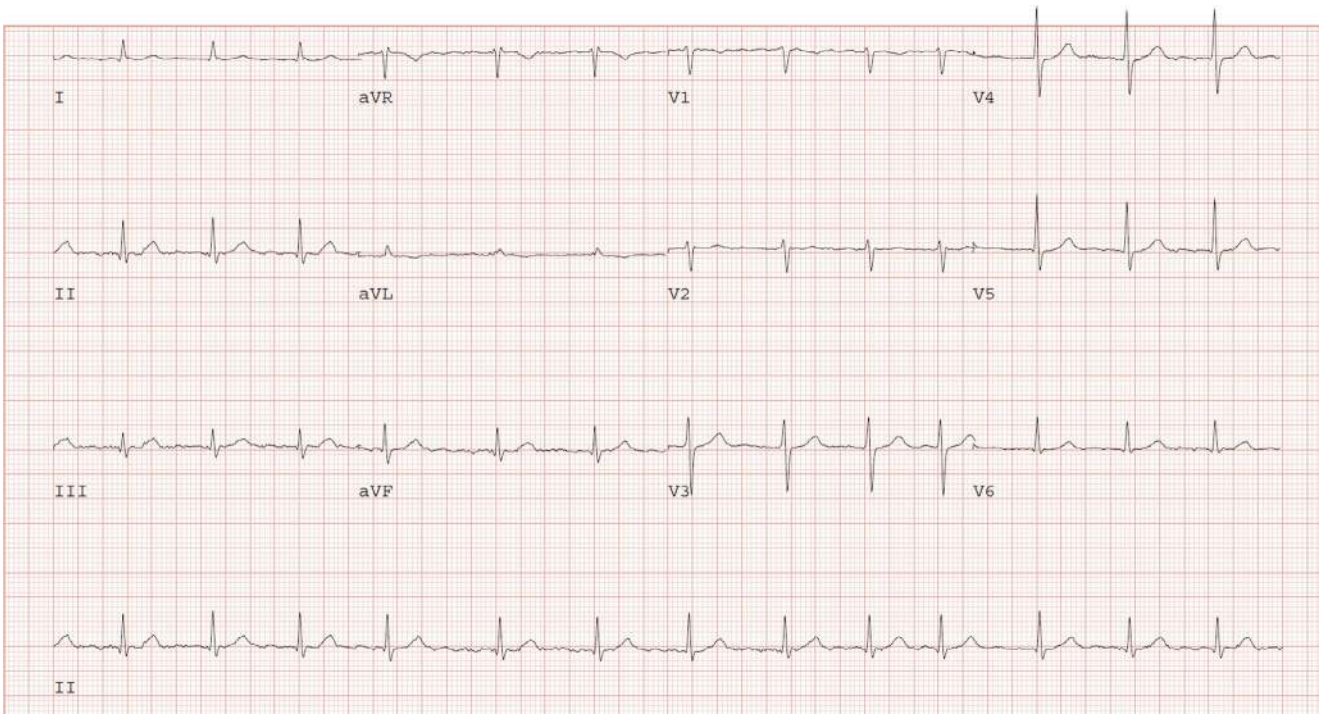


Fig. 11.1 Stress ECG showing atrial fibrillation with no other abnormalities

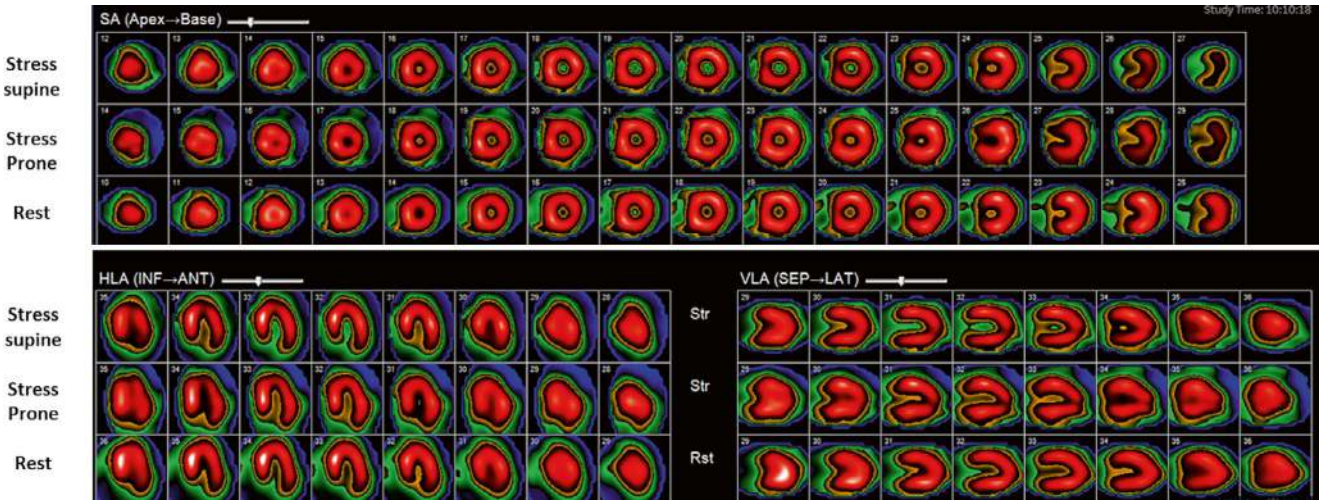


Fig. 11.2 ^{99m}Tc-Sestamibi stress SPECT acquisition conducted in both supine and prone position (first two rows, respectively). Both stress and rest showed uniform tracer uptake with no evidence of ischemia or scar

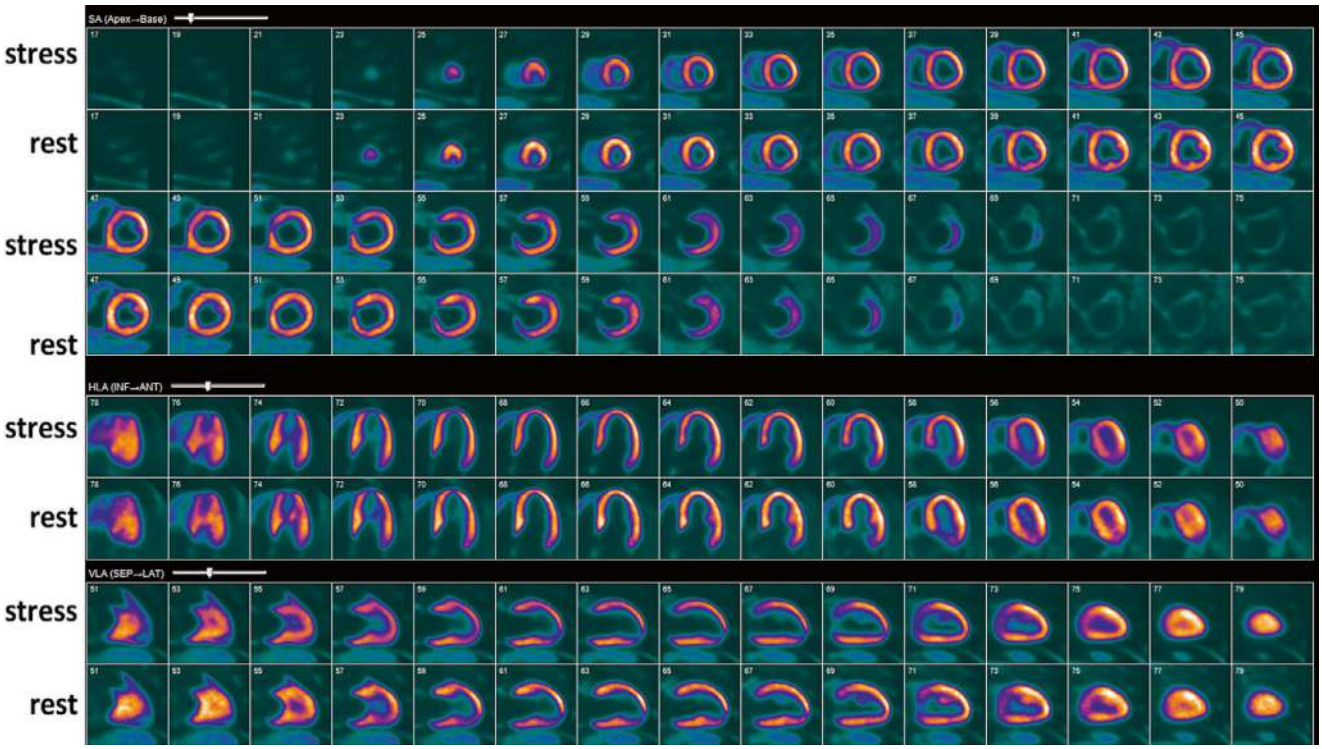


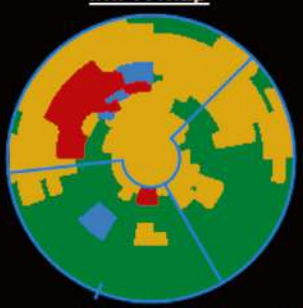
Fig. 11.3 ^{18}F-Flurpiridaz PET/CT. During stress, there was a moderate-size perfusion defect of mild severity in the mid to distal anterior wall, and a small perfusion defect of the apex of the LV

Fig. 11.4 The MFR confirmed reduced perfusion of the anterior wall and apex of the LV in the LAD territory

Global Results

Region	Mean Flow (ml/min/g) MC Str	MC Rst	MC Str	MC Rst	Ratio
LAD	70%	80%	1.83	1.01	1.80
LCX	88%	87%	2.17	1.04	2.09
RCA	71%	70%	1.93	0.87	2.22
TOT	75%	79%	1.94	0.96	2.02

iMFR Map



Normal MFR: 2.23

Diffusely Impaired MFR: 1.79

Focally Impaired MFR: 1.72



Region	Normal Perf MFR>=2.0	Normal Perf MFR<2.0	Str Defect MFR>=2.0	Str Defect MFR<2.0
LAD	14 % (2.11)	69 % (1.75)	3 % (2.04)	13 % (1.70)
LCX	65 % (2.20)	35 % (1.91)	0 % (--)	0 % (--)
RCA	80 % (2.29)	11 % (1.86)	5 % (2.41)	5 % (1.79)
TOT	46 % (2.23)	43 % (1.79)	3 % (2.21)	7 % (1.72)

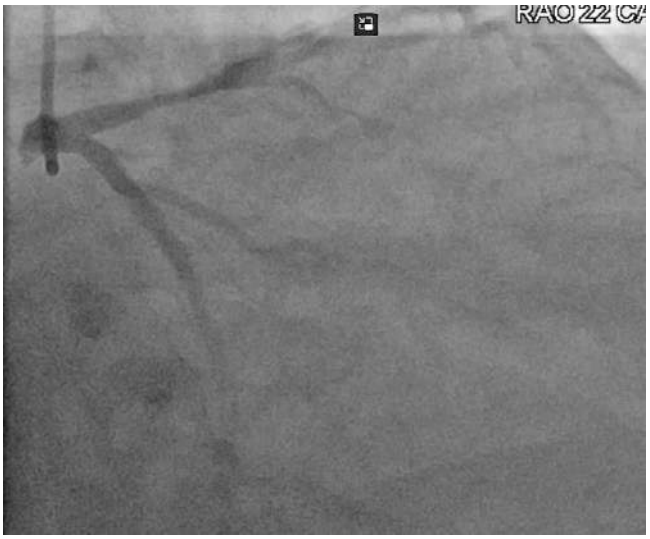


Fig. 11.5 Selective view of coronary angiogram showing normal LM, 70% stenosis of proximal to mid LAD. Left circumflex artery (LCX) and right coronary artery (RCA) showed nonobstructive CAD (not shown)

Management
Percutaneous coronary intervention (PCI) to left anterior descending artery (LAD)

Further Reading

- N. Matsumoto Update of ^{18}F-flurpiridaz Ann Nucl Cardiol. 2024; 10(1): 49–50.
- D.S. Berman, J. Maddahi, B. K. Tamarappoo, J-Czernin, R. Taillefer, J.E. Udelson, et al. Flurpiridaz F 18 PET: Phase II Safety and Clinical Comparison with SPECT Myocardial Perfusion Imaging for Detection of Coronary Artery Disease. J Am Coll Cardiol. 2013 Jan 29; 61(4): 469–477.
- Poitrasson-Rivière, J.B. Moody, J.M. Renaud, T. Hagio, L. Arida-Moody, C.J. Buckley, Integrated myocardial flow reserve (iMFR) assessment: optimized PET blood flow quantification for diagnosis of coronary artery disease. Eur J Nucl Med Mol Imaging. 2023 Dec; 51(1): 136–146.
- R.A. Werner, X. Chen, S.P. Rowe, C. Lapa, M.S. Javadi, T. Higuchi Moving into the next era of PET myocardial perfusion imaging: introduction of novel 18F-labeled tracers. Int J Cardiovasc Imaging. 2019; 35(3): 569–577. Published online 2018 Oct 17.

11.2 Molecular Radiotracers for Cardiovascular Imaging

11.2.1 ^{18}F-Sodium Fluoride

^{18}F-Sodium fluoride (^{18}F-NaF) is a well-known bone avid radiotracer that binds to hydroxyapatite, a key structural component of bones and vascular calcification. As an oncology tracer, ^{18}F-NaF has been used to assess increased bone metabolism, such as bony metastases and fracture healing. On the surface of calcifications, fluoride ions are exchanged with hydroxyl groups to form fluoroapatite. ^{18}F-NaF uptake is particularly associated with areas of active microcalcification, rather than larger more stable macro-calcifications. In cardiovascular disease research it has been used to assess microcalcification associated with aortic, coronary, carotid, and valvular heart disease.

11.2.2 ^{68}Gallium-DOTATATE

^{68}Gallium-DOTATATE (^{68}Ga-DOT) is routinely used for the investigation of neuroendocrine tumors. It binds to somatostatin receptor subtype 2 ($SSTR_2$), a transmembrane receptor involved in a broad range of functions, which is typically overexpressed in neuroendocrine cancers. In addition, $SSTR_2$ receptors are expressed on activated macrophages, suggesting that ^{68}Ga-DOT may help detect areas with active inflammation. Several other radiolabeled somatostatin analogs are also available, including ^{68}Ga-DOTATOC and ^{68}Ga-DOTANOC. Research studies have assessed the ability of radiolabeled somatostatin analogs to assess vasculitis, atherosclerosis, myocardial inflammation, and cardiac sarcoidosis. ^{18}Fluoride radiolabeled octreotide has also been developed for research use (e.g., ^{18}F-fluoroethyltriazole-βAG-TOCA).

11.2.3 ^{18}Fluoride-GP1

^{18}Fluoride-GP1 (^{18}F-GP1) is a PET radiotracer with high affinity for the activated glycoprotein IIb/IIIa receptor. This receptor is present on activated platelets which form a central component of acute thrombosis. ^{18}F-GP1 has been used in research studies to assess thrombosis throughout the body, including in coronary arteries, carotid arteries, cardiac valves, and brain parenchyma. It has also been used to assess thrombosis associated with prosthetic cardiac valves, implanted cardiac devices, and aortic grafts and stents. Other thrombus or platelet targeting radiotracers have been used in pilot studies for PET and SPECT imaging.

11.2.4 ^{68}Gallium-FAPI

Fibroblast activation protein-specific inhibitors (FAPI) were initially developed for the treatment of cancer. They bind to activated fibroblasts which express fibroblast activation protein (FAP) and can be radiolabeled with ^{68}gallium or ^{18}fluoride. ^{68}Ga-FAPI is being actively investigated in a variety of oncological conditions. In addition, in cardiovascular disease,

research is exploring the use of ^{68}Ga-FAPI in myocardial infarction, chemotherapy induced cardiotoxicity, cardiomyopathies, heart failure, pulmonary artery hypertension, aortic disease, atherosclerosis, and valvular heart disease.

11.2.5 ^{11}Carbon-Meta-hydroxyephedrine

^{11}Carbon-meta-hydroxyephedrine (^{11}C-HED) is a PET radiotracer which is a structural analog of norepinephrine, sharing similar neuronal kinetics. It binds strongly to the norepinephrine reuptake transporter (NET-1). ^{11}C-HED PET imaging is widely recognized as the gold standard for noninvasive evaluation of sympathetic innervation and function. Research studies have assessed the extent of sympathetic denervation in conditions such as diabetic cardiomyopathy and heart failure. As it is an ^{11}carbon labeled radiotracer (T/2 20.4 min), it is primarily confined to research and centers with cyclotron facilities. To overcome these logistic constraints, similar radiotracers with ^{18}F labeling are currently in development.

Further Reading

- N. Matsumoto Update of ^{18}F-flurpiridaz Ann Nucl Cardiol. 2024; 10(1): 49–50.
- D.S. Berman, J. Maddahi, B. K. Tamarappoo, J-Czernin, R. Taillefer, J.E. Udelson, et al. Flurpiridaz F 18 PET: Phase II Safety and Clinical Comparison with SPECT Myocardial Perfusion Imaging for Detection of Coronary Artery Disease. J Am Coll Cardiol. 2013 Jan 29; 61(4): 469–477.
- Moss A, Daghem M, Tzolos E, et al. Coronary Atherosclerotic Plaque Activity and Future Coronary Events. JAMA Cardiol. 2023;8(8):755–764.
- Hoilund-Carlsen PF, Piri R, Gerke O, et al. NaF PET Imaging of atherosclerosis burden. J Imaging, 2023, 9(2):31.
- Rominger A, Saam T, Vogl E, et al. In vivo imaging of macrophage activity in the coronary arteries using 68Ga-DOTATATE PET/CT: correlation with coronary calcium burden and risk factors. J Nucl Med, 2010, 51:193–197.
- Tarkin JM, Joshi FR, Evans NR, et al. Detection of atherosclerotic inflammation by 68Ga-DOTATATE PET compared to [18F]FDG PET imaging. J Am Coll Cardiol, 2017, 69:1774–91.
- Bing R, Deutsch M-A, Sellers SL, et al. 18F-GP1 Positron Emission Tomography and Bioprosthetic Aortic Valve Thrombus. JACC: Cardiovascular Imaging. 2022;15(6):1107–1120.
- Barton AK, E. Tzolos, R. Bing, et al. Emerging molecular imaging targets and tools for myocardial fibrosis detection. Eur Heart J Cardiovasc Imaging 2023;24(3):261–75.
- Zelt JGE, deKemp RA, Rotstein BH, et al. Nuclear Imaging of the Cardiac Sympathetic Nervous System: A Disease-Specific Interpretation in Heart Failure. JACC: Cardiovascular Imaging. 2020/04/01/ 2020;13(4):1036–1054.

11.3 Cardiac Amyloidosis

11.3.1 Differentiating Transthyretina Amyloidosis (ATTR) from Light Chain Amyloidosis (AL) Amyloidosis with SPECT/CT and PET/CT: Case 90

Key Points

- Cardiac amyloidosis SPECT imaging with ^{99m}Tc-3,3-diphosphono-1,2-propanodicarboxylic acid (DPD), hydroxymethylene diphosphonate (HMDP), or pyrophosphate (PYP) has high sensitivity and specificity for cardiac transthyretin (ATTR) amyloidosis. It can be used to diagnose cardiac ATTR amyloidosis when a monoclonal gammopathy is excluded.
- ^{18}F-targeted amyloid tracers such as Florbetapir have high sensitivity for detection of cardiac amyloidosis, but as they are pan-amyloid tracers, they therefore cannot differentiate AL from ATTR.

History

- A 72-year-old male with worsening dyspnea on exertion, lower leg swelling and fatigue, and an abnormal echocardiogram was referred for a ^{99m}Tc pyrophosphate (PYP) scan and ^{18}F-florbetapir PET/CT imaging to evaluate for cardiac amyloidosis (Figs. 11.6 and 11.7).

Findings

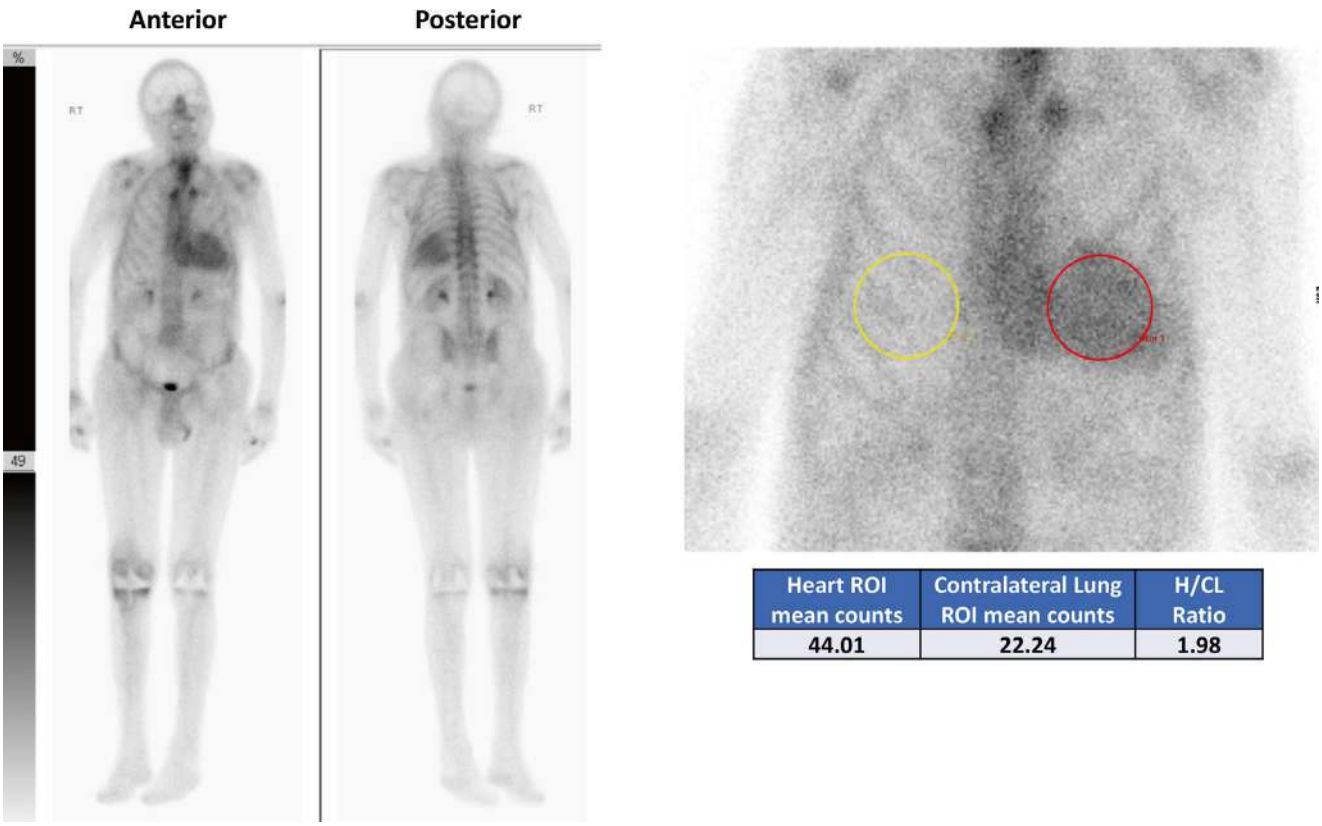
- ^{18}F-Florbetapir PET/CT imaging showed intense cardiac uptake of the radiotracer.
- The apical four-chamber view on echocardiography (Fig. 4.29) demonstrates thickened left ventricular walls and biatrial enlargement. There is also an increased echogenicity of the myocardium.
- The 17-segment polar map of global longitudinal strain (GLS) quantification demonstrates the typical appearance of cardiac amyloidosis with reduced global reduced GLS at the mid and base of the LV with sparing of the apical LV segments.

Differential Diagnosis

- Light chain (AL) cardiac amyloidosis.

Correlative Imaging

- Echocardiography (Figs. 3.29 and 11.8).



Heart ROI mean counts	Contralateral Lung ROI mean counts	H/CL Ratio
44.01	22.24	1.98

Fig. 11.6 Whole-body study using ^{99m}Tc PYP

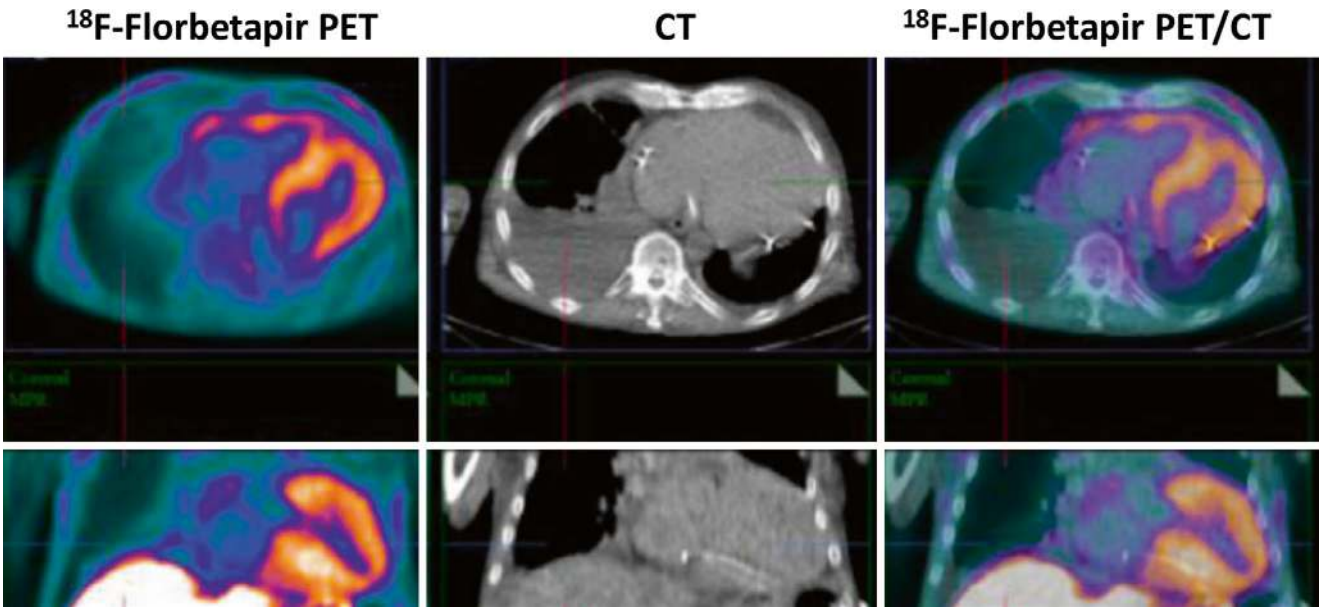


Fig. 11.7 ^{18}F-Florbetapir PET/CT imaging

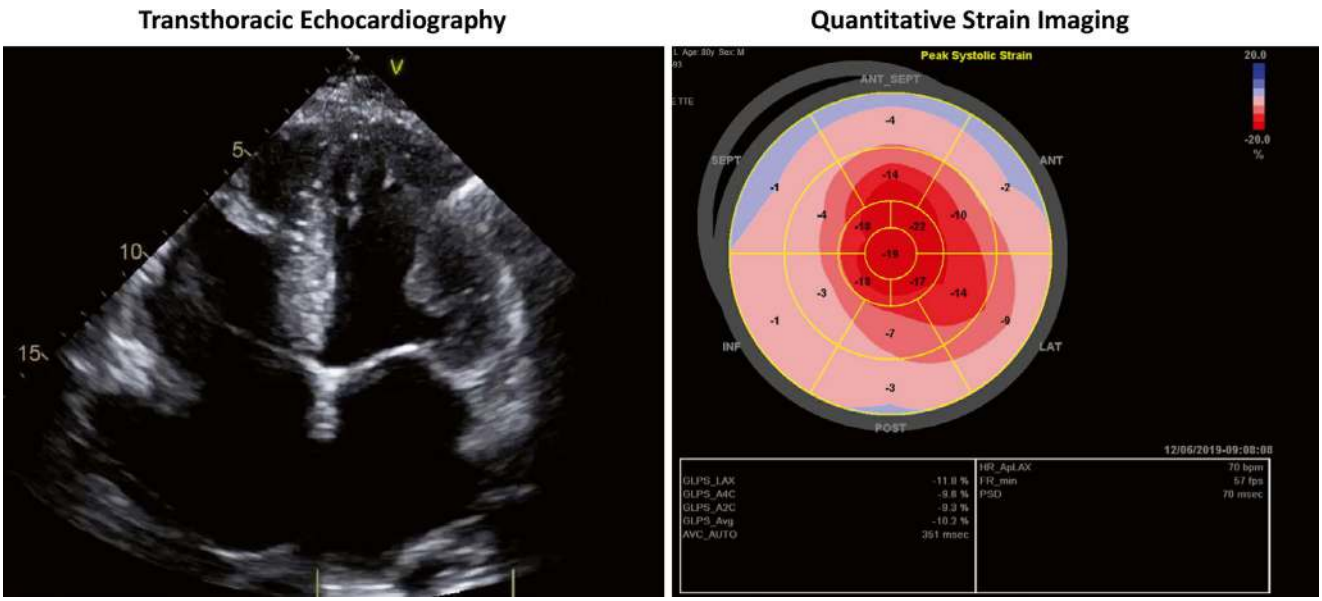


Fig. 11.8 2D echocardiography images and systolic strain map. The apical four-chamber view (left panel) on echocardiography demonstrates thickened left ventricular walls and biatrial enlargement. There is also an increased echogenicity of the myocardium. A 17-segment polar map (right panel) of global longitudinal strain (GLS) values demonstrates the typical appearance of cardiac amyloidosis with reduced global GLS (−10.2%; normal < −16%), and reduced GLS at the mid and base, and preserved apical GLS

Management

- The patient's heart failure medications were optimized. He was started on a recently approved transthyretin (TTR) stabilizer, tafamidis, to slow the progression of the disease.

Further Reading

- Chareonthaitawee P, Beanlands R, Chen W, Dorbala S, Miller E, Murthy V, et al. Joint SNMMI–ASNC Expert Consensus Document on the Role of 18 F-FDG PET/CT in Cardiac Sarcoid Detection and Therapy Monitoring. Journal of Nuclear Medicine. 2017;58:1341–1353.
- Dorbala S, Ando Y, Bokhari S, Dispenzieri A, Falk R, Ferrari V, et al. ASNC/AHA/ASE/EANM/HFSA/ISA/SCMR/SNMMI expert consensus recommendations for multimodality imaging in cardiac amyloidosis: Part 1 of 2—evidence base and standardized methods of imaging. Journal of Nuclear Cardiology. 2019;26:2065–2123.

11.3.2 Cardiac Imaging in AL Amyloidosis: Case 91

Key Points

- ^{18}F-targeted amyloid tracers have high sensitivity for the detection of cardiac amyloidosis. However, these are pan-amyloid tracers and therefore cannot differentiate AL from ATTR.

History

- A 67-year-old male presented to the emergency department following a syncopal episode. He was noted to have marked orthostatic hypotension.
- An ECG showed low voltage QRS complexes with anterior Q waves. An echocardiogram showed concentric left ventricular hypertrophy with an ejection fraction of 50%.
- A ^{99m}technetium pyrophosphate (PYP) scan showed myocardial uptake.
- A ^{18}F-florbetapir PET/CT was performed as part of a research protocol (Fig. 11.9).

^{99m}Tc PYP Scan
PET/CT Scan (Fig. 11.10)

Findings

- Intense retention of ^{18}F-florbetapir in the myocardium.

Differential Diagnosis

- Light chain (AL) cardiac amyloidosis.

Correlative Imaging

- Echocardiography.
- Contrast-enhanced cardiac MRI (Fig. 11.11).

Management

- Given the strong clinical and imaging evidence of cardiac amyloidosis, serum immunofixation and free light chain levels were performed. They revealed a markedly elevated free lambda light chain.

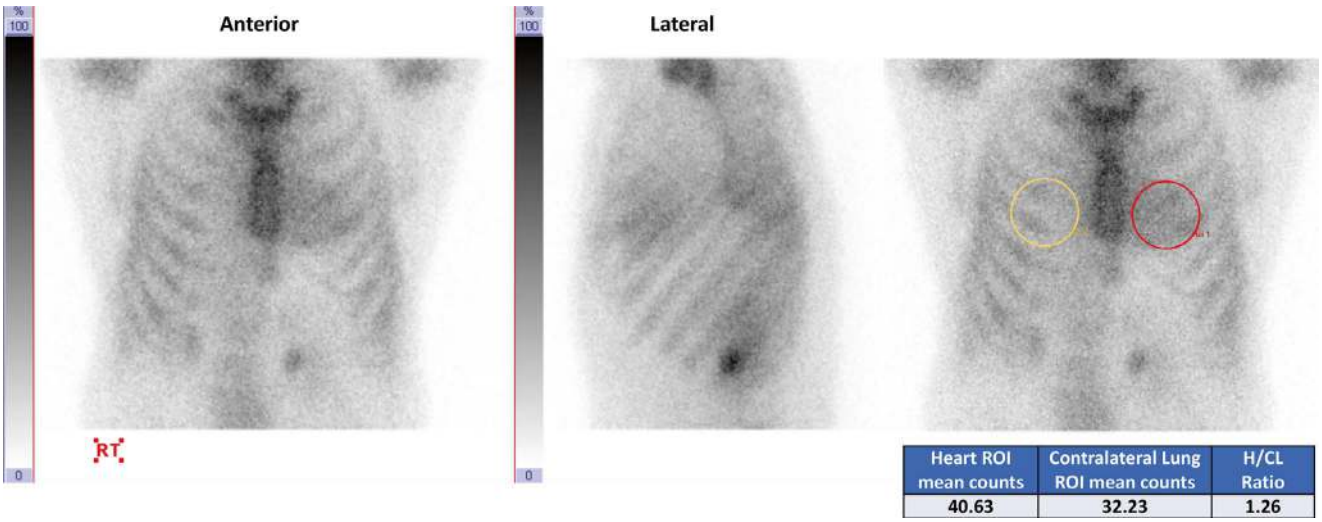


Fig. 11.9 ^{99m}Technetium PYP chest planar views demonstrate mildly increased uptake in the cardiac region



Fig. 11.10 ^{18}F-Florbetapir PET/CT imaging showing intense cardiac uptake of the radiotracer

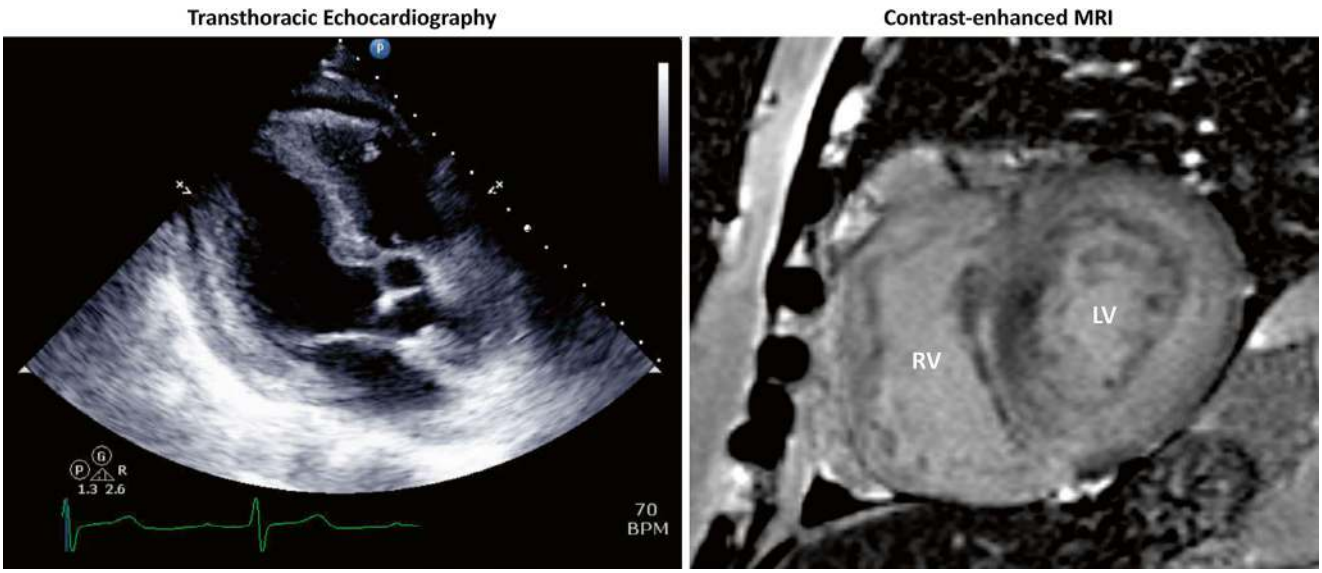


Fig. 11.11 Left panel: 2D echocardiography (left side) demonstrates mildly thickened left ventricular walls. There is also a small pericardial effusion seen best along the right ventricular free wall. Right side: Contrast-enhanced MRI (right side) images shows a typical appearance of diffuse transmural late gadolinium enhancement of the left ventricle and of the right ventricle

- A fat pad biopsy showed amyloid deposition, with a positive Congo red stain, with apple green birefringence under polarized light. Mass spectrometry showed a profile consistent with light chain (lambda) amyloid deposition.
- The patient underwent bone marrow biopsy. He was started on a chemotherapy regimen consisting of bortezomib, with cyclosporine and dexamethasone. He was also started on midodrine to improve his postural symptoms.

Further Reading

- Gillmore J, Maurer M, Falk R, Merlini G, Damy T, Dispenzieri A, et al. Nonbiopsy Diagnosis of Cardiac Transthyretin Amyloidosis. Circulation. 2016;133:2404–2412.
- Dorbala S, Ando Y, Bokhari S, Dispenzieri A, Falk R, Ferrari V, et al. ASNC/AHA/ASE/EANM/HFSA/ISA/SCMR/SNMMI expert consensus recommendations for multimodality imaging in cardiac amyloidosis: Part 1 of 2—evidence base and standardized methods of imaging. Journal of Nuclear Cardiology. 2019;26:2065–2123.

11.3.3 ^{124}I-Evumetazide Targeted Tracer: Case 92

Key Points

- Cardiac transthyretin (ATTR) amyloidosis can be diagnosed noninvasively with imaging.
- Bone-avid radiotracer SPECT/CT has become the standard method for this purpose, based on its high specificity, but its sensitivity remains somewhat limited, and true cases may be missed.
- Cardiac MRI can be useful given its high sensitivity for myocardial diseases, but its specificity is not sufficient to diagnose cardiac amyloidosis.
- ^{124}I-Evuzamitide PET/CT (previously named ^{124}I-p5 + 14 or AT-01) is a promising novel method, combining high sensitivity and high specificity for all types of cardiac amyloidosis.

History

This 73-year-old male presented with chest tightness, shortness of breath, and clinical signs of heart failure. He had a past medical history of bilateral carpal tunnel syndrome surgery, trigger finger and lower back decompressive surgeries, diabetes, and hypertension. Laboratory testing showed elevated NT-proBNP and high-sensitivity troponin T. The echocardiogram demonstrated asymmetric left ventricular (LV) hypertrophy more prominent in the septum, a mildly reduced LV ejection fraction of 42%, diastolic dysfunction grade 2, and an impaired LV global longitudinal strain of −11% without clear apical sparing. Cardiac amyloidosis was suspected.

^{99m}Tc-Pyrophosphate SPECT/CT (Fig. 11.12)

Cardiac MRI (Fig. 11.13)

^{124}I-Evuzamitide PET/CT (Fig. 11.14)

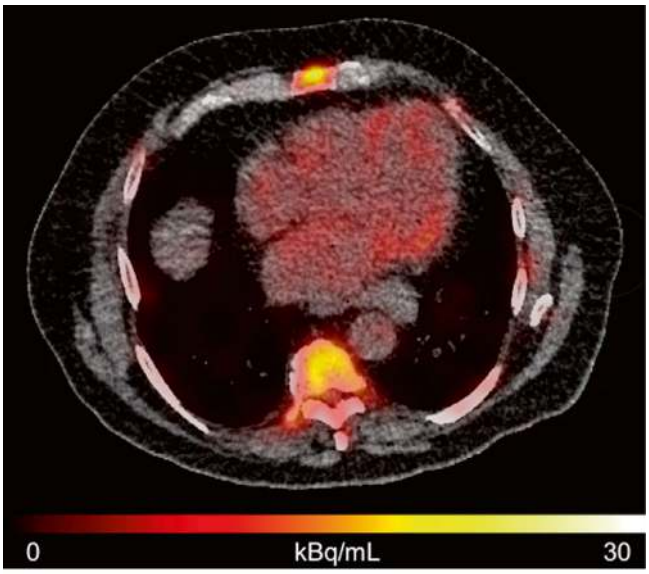


Fig. 11.12 ^{99m}Tc-pyrophosphate (PYP) SPECT/CT showed mild myocardial uptake (grade 1). This finding was considered as equivocal and not sufficient to undoubtedly confirm the diagnosis of cardiac amyloidosis. kBq/mL: kilobecquerel by milliliter

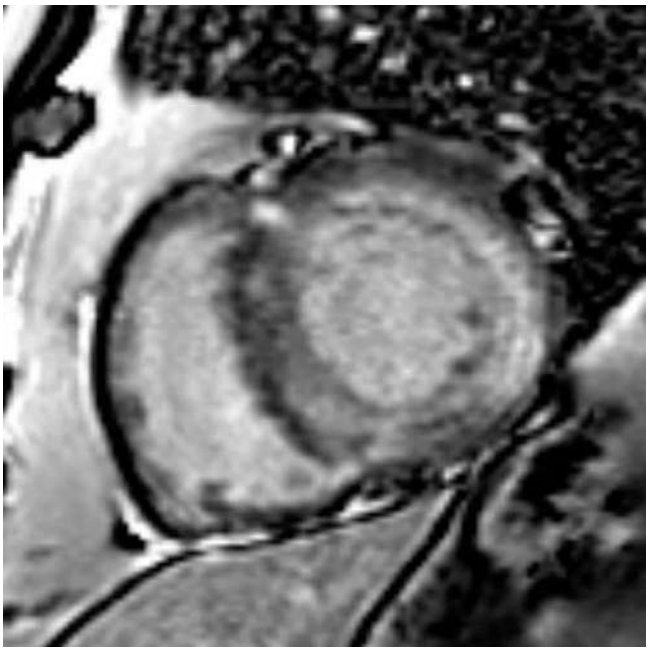


Fig. 11.13 Cardiac MRI showed basal and mid-ventricular subendocardial and mid-wall late gadolinium enhancement of the LV free wall and inferior septum, as well as of the left atrium, as seen on this short-axis mid-ventricular slice from a phase-sensitive inversion recovery (PSIR) sequence (in light gray). Although suggestive of cardiac amyloidosis, this finding was not specific enough to confirm the diagnosis

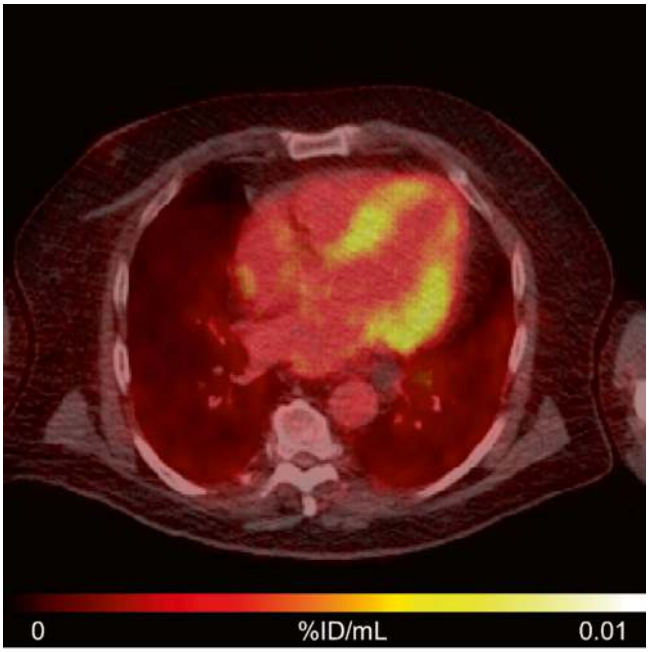


Fig. 11.14 ^{124}I-Evuzamitide is a specific pan-amyloid targeted radiotracer. His ^{124}I-Evuzamitide PET/CT showed definite intense myocardial uptake consistent with cardiac amyloidosis. %ID/mL: percent injected dose by milliliter

Diagnosis

While echocardiogram and MRI were suggestive of cardiac amyloidosis, the equivocal findings from ^{99m}Tc-pyrophosphate SPECT/CT did not clearly support this diagnosis. However, ^{124}I-Evuzamitide PET/CT demonstrated definite myocardial uptake, strongly suggestive of cardiac amyloidosis. Light-chain (AL) amyloidosis was excluded by electrophoresis, immunofixation, and free light chain assays. Endomyocardial biopsy showed amyloid deposits on staining with Congo red and sulfated alcian blue. Immunofluorescence was positive for transthyretin. Mass spectrometry confirmed the presence of transthyretin amyloid. Furthermore, transthyretin gene sequencing did not show any pathogenic variant. Hence, the diagnosis of wild-type ATTR amyloidosis was established.

Management

Transthyretin-stabilizing treatment with tafamidis was initiated, in addition to standard heart failure therapy. The clinical follow-up was favorable.

Further Reading

- Clerc OF, Cuddy SAM, Robertson M, et al. Cardiac Amyloid Quantification Using ^{124}I-Evuzamitide (^{124}I-P5 + 14) Versus ^{18}F-Florbetapir: A Pilot PET/CT Study. *JACC Cardiovasc Imaging*. 2023;16(11):1419–1432. https://doi.org/10.1016/j.jcmg.2023.07.007
- Wall JS, Martin EB, Lands R, et al. Cardiac Amyloid Detection by PET/CT Imaging of Iodine (^{124}I) Evuzamitide (^{124}I-p5 + 14): A Phase 1/2 Study. *JACC Cardiovasc Imaging*. 2023;16(11):1433–1448. https://doi.org/10.1016/j.jcmg.2023.08.009
- Kurian A, de Moraes A, Clerc OF, et al. ^{124}I-Evuzamitide PET/CT Diagnosis of Wild-Type Transthyretin Amyloid Cardiomyopathy in a Woman With Negative Diagnostic Evaluation. *Circ Cardiovasc Imaging*. Published online February 25, 2025. https://doi.org/10.1161/CIRCIMAGING.124.017807

11.4 Molecular Imaging

11.4.1 ^{18}F-Sodium Fluoride in Coronary Artery Disease: Case 93

Key Points

- ^{18}F-Sodium fluoride (^{18}F-NaF) is an established radiotracer which demonstrates areas of active bone turnover and can be used to identify bone metastasis.
- In cardiovascular disease, it can also identify areas of active coronary microcalcification.
- Research studies have shown that ^{8}F-NaF can identify the culprit coronary artery lesion in myocardial infarction and that assessment of the coronary microcalcification activity with ^{18}F-NaF PET can identify patients at increased risk of myocardial infarction.
- In cardiovascular disease, it is currently used as a research radiotracer, with potential future uses including the assessment of coronary artery, valvular heart, aortic aneurysm, and peripheral vascular diseases.

History

A 62-year-old male with a history of coronary artery disease took part in a research study where he underwent ^{18}F-NaF and contrast-enhanced CT coronary angiogram.

PET/CT Images (Figs. 11.15 and 11.16)

Findings

^{18}F-NaF PET showed uptake in the left anterior descending coronary artery. At this position on the coronary CT angiogram, there was calcified plaque causing less than 50% stenosis. In the left circumflex coronary artery, there were two patent stents. In the periphery of the proximal stent, there was further ^{18}F-NaF uptake on PET.

Imaging Diagnosis

^{18}F-NaF PET showed active coronary microcalcification in the left anterior descending coronary artery and in the periphery of the stent in the proximal left circumflex artery.

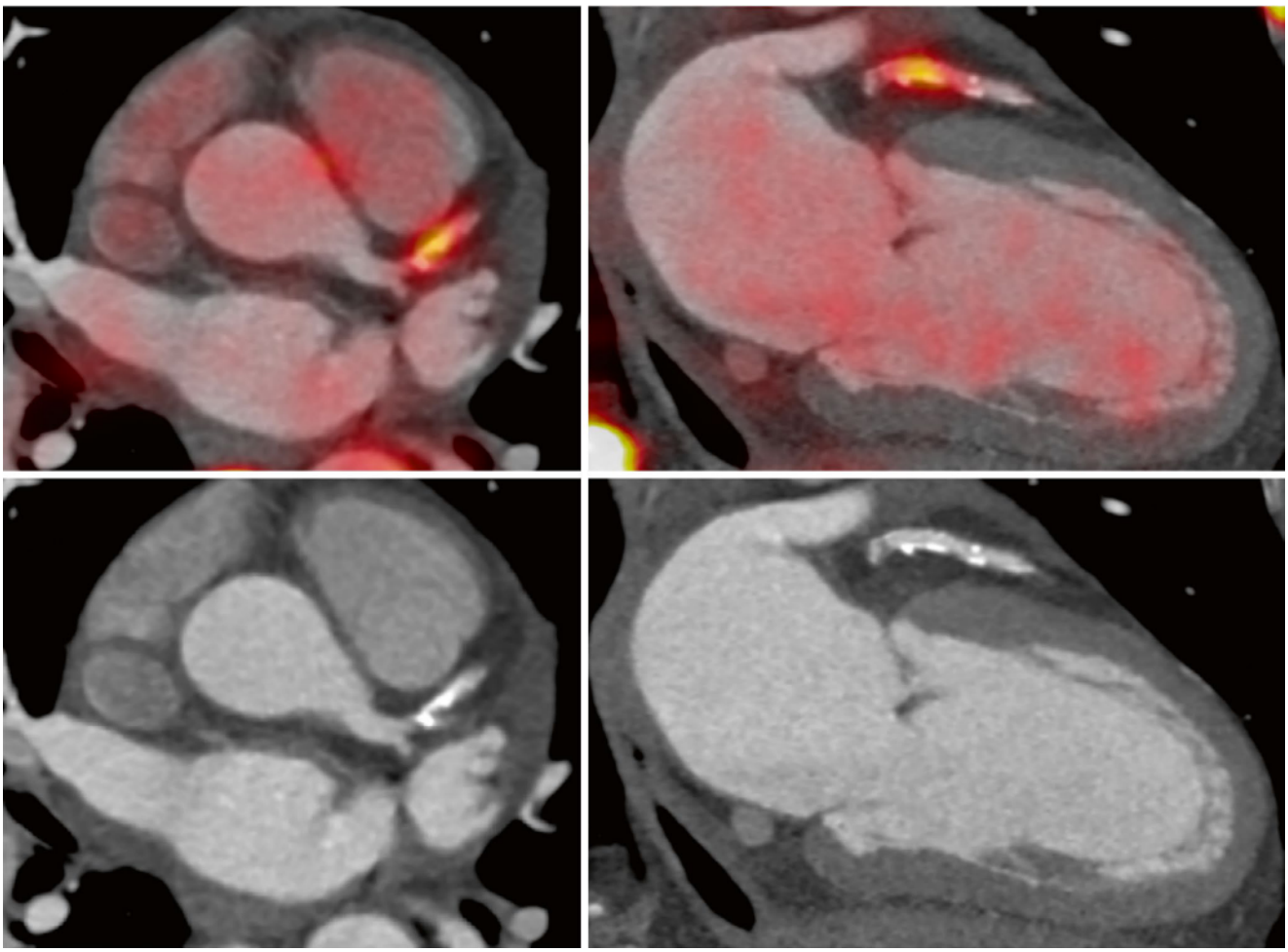


Fig. 11.15 ^{18}F-NaF PET CT images showing uptake in the proximal left anterior descending coronary artery associated with calcified plaque which causes less than 50% stenosis

Further Reading

- Dweck MR, Chow MW, Joshi NV, Williams MC, Jones C, Fletcher AM, et al. Coronary arterial 18F-sodium fluoride uptake: a novel marker of plaque biology. J Am Coll Cardiol. 2012 Apr 24;59(17):1539–48.
- Moss A, Daghem M, Tzolos E, Meah MN, Wang KL, Bularga A, et al.; PREFFIR Investigators. Coronary Atherosclerotic Plaque Activity and Future Coronary Events. JAMA Cardiol. 2023 Aug 1;8(8):755–764.

11.4.2 1^{18}F-Sodium Fluoride in Aortic Valve Disease: Case 94

Key Points

- ^{18}F-Sodium fluoride (^{18}F-NaF) is a novel radiotracer which acts as a marker of microcalcification that has been identified in arteries and valves.
- It is a research radiotracer in cardiovascular disease, but higher ^{18}F-NaF uptake in aortic valves has been independently associated with more rapid disease progression and is used in clinical trials to assess potential impact on disease activity.

History

- A 75-year-old man with moderate aortic stenosis, hypertension, and previous coronary artery bypass grafting presented with unexplained shortness of breath.
- As part of a research study, he underwent ^{18}F-NaF PET/CT at baseline, and 7 years later, he underwent follow-up CT.

PET/CT Images (Fig. 11.17)

Findings

- ^{18}F-NaF PET/CT at baseline showed radiotracer uptake in the aortic valve. CT shows that this is predominantly localized to the left and noncoronary cusps.
- Subsequent CT 7 years later demonstrated an increase in calcification, localized to the region of increased ^{18}F-NaF uptake on PET.

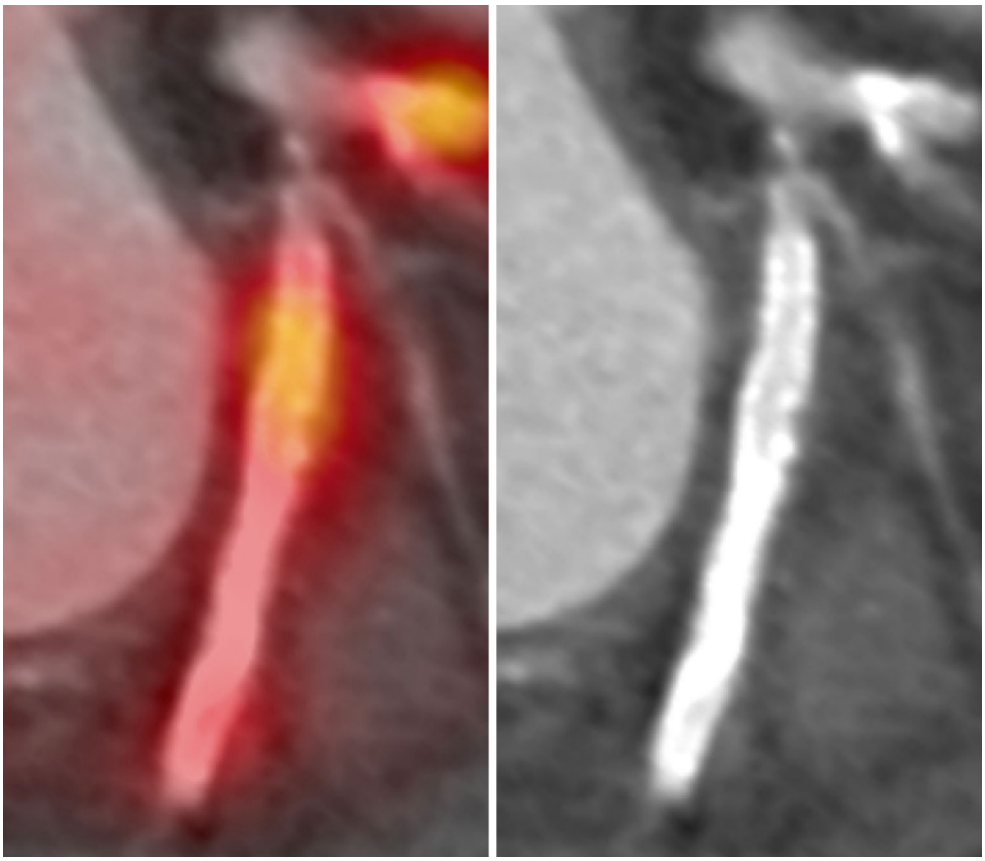


Fig. 11.16 ^{18}F-NaF PET CT images showing uptake in the proximal stent in the left circumflex artery which is patent on coronary CT angiogram images

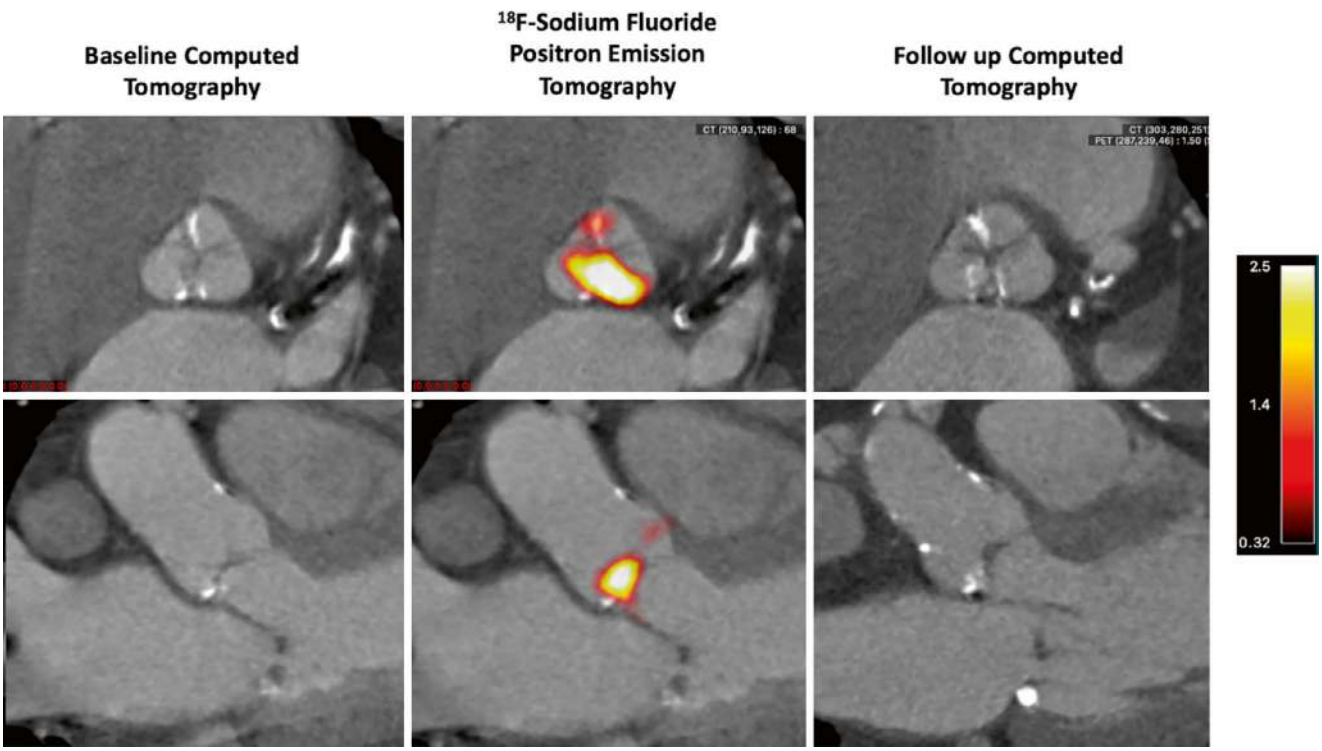


Fig. 11.17 Images of the aortic valve on the baseline CT angiogram, fused baseline CT angiogram, and ^{18}F-NaF PET/CT and follow-up CT 7 years later. At baseline, he had mild aortic valve calcification and high uptake of radiotracer in the aortic valve, predominantly located in the left and noncoronary cusps. On the follow-up CT 7 years later, there was an increase in the density and volume of calcification in this region

Correlative Imaging
- Transthoracic echocardiography confirmed the progression from moderate to severe aortic stenosis.

Imaging Diagnosis
- Severe aortic stenosis.

Differential Diagnosis
- None.

Management
- He was referred for aortic valve replacement surgery.

Further Reading
- Dweck MR, Jenkins WSA, Vesey AT, Pringle MAH, Chin CWL, Malley TS, Cowie WJA, Tsampasian V, Richardson H, Fletcher A, Wallace WA, Pessotto R, Beek EJRv, Boon NA, Rudd JHF, Newby DE. 18F-Sodium Fluoride Uptake Is a Marker of Active Calcification and Disease Progression in Patients With Aortic Stenosis. Circulation: Cardiovascular Imaging. 2014;7(2):371–8.

11.5 Thrombus Imaging

11.5.1 Thrombus Imaging of Pulmonary Embolism: Case 95

Key Points
- ^{18}F-GP1 uptake is a marker of activated platelets and thrombus formation on PET.
- It is currently a research radiotracer, but future uses could include identification and quantification of cardiac, vascular, valvular, and other thrombus.

History
- A 52-year-old man presented with a three-week history of breathlessness.
- He had a family history of venous thrombosis but no other past medical history.
- His DDimer was elevated, and he was referred for a CT pulmonary angiogram.
- The CT pulmonary angiogram showed bilateral pulmonary emboli in the right middle lobe, right lower lobe, left lower lobe, and lingula. There was associated straightening of the interventricular septum in keeping with right heart strain.
- As part of a research study, they underwent PET imaging with the radiotracer ^{18}F-GP1.

PET/CT Images (Fig. 11.18)

Findings
- Pulmonary embolism with ^{18}F-GP1 uptake on PET/CT images.

Imaging Diagnosis
- Pulmonary embolism.

Differential Diagnosis
- None.

Correlative Imaging
- None.

Management
- Lifelong anticoagulation.

Further Reading
- Bing R, Andrews JPM, Williams MC, van Beek EJR, Lucatelli C, MacNaught G, et al. In Vivo Thrombosis Imaging in Patients Recovering from COVID-19 and Pulmonary Embolism. Am J Respir Crit Care Med. 2021 Oct 1;204(7):855–856.

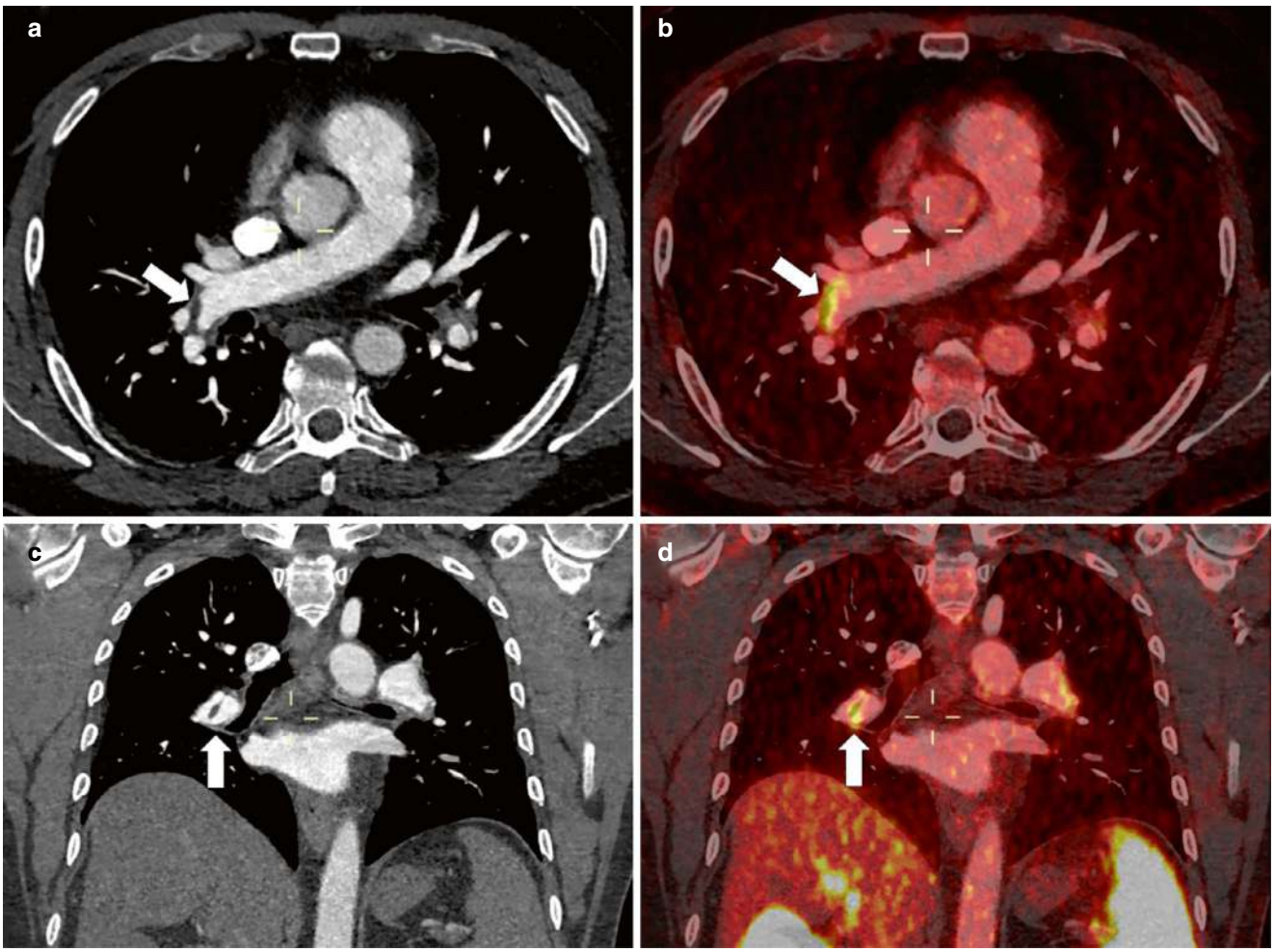


Fig. 11.18 ^{18}F-GP1 PET/CT images showing (A, B) a CT pulmonary angiogram with thrombus in the right lower lobe pulmonary artery (arrows) and (C, D) corresponding ^{18}F-GP1 uptake on fused PET/CT images

11.5.2 Apical Left Ventricle Thrombus Post-Myocardial Infarction: Case 96

Key Points

- ^{18}F-GP1 can identify thrombus which may be challenging to identify with other imaging modalities.
- It is currently a research radiotracer, but future uses could include identification and quantification of cardiac, valvular, and coronary thrombus.

History

- A 64 year-old man with a previous history of coronary artery disease, myocardial infarction, and PCI to the LAD presented to the emergency department with chest pain. He had an inferior ST elevation myocardial infarction and was treated with an RCA stent.
- His cardiovascular risk factors included smoking and a strong family history of coronary artery disease.
- As part of a research study, they underwent PET imaging with the radiotracer ^{18}F-GP1.

PET/CT Images (Fig. 11.19)

Findings

- ^{18}F-GP1 uptake in a thrombus situated at the left ventricle apex.

Imaging Diagnosis

- Thrombus in the left ventricle apex.

Differential Diagnosis

- None.

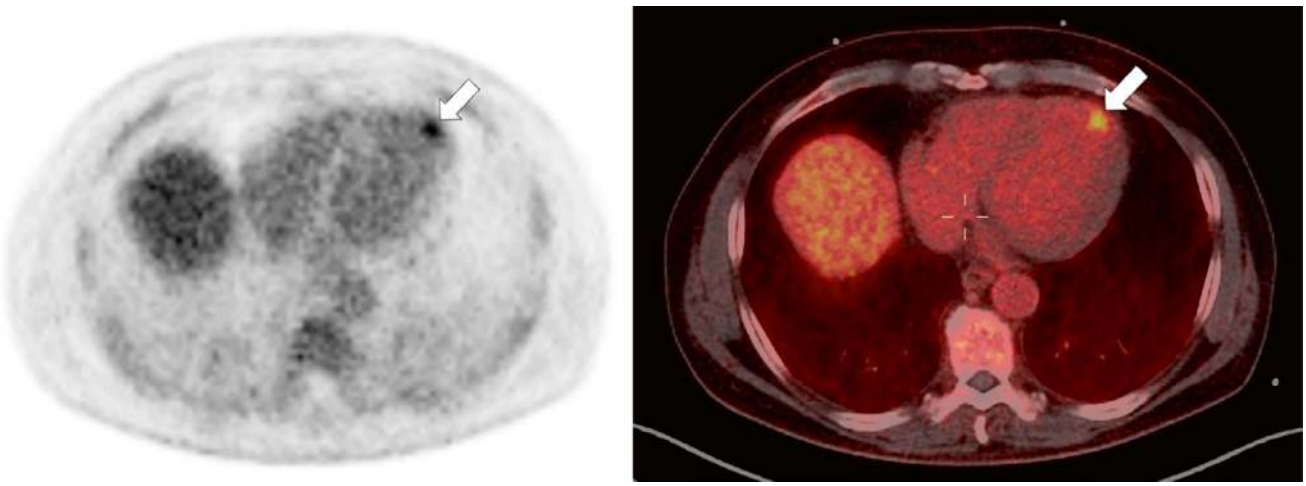


Fig. 11.19 ^{18}F-GP1 PET image and fused PET/CT images. These show focal radiotracer uptake adjacent to the apex of the left ventricle (arrows)

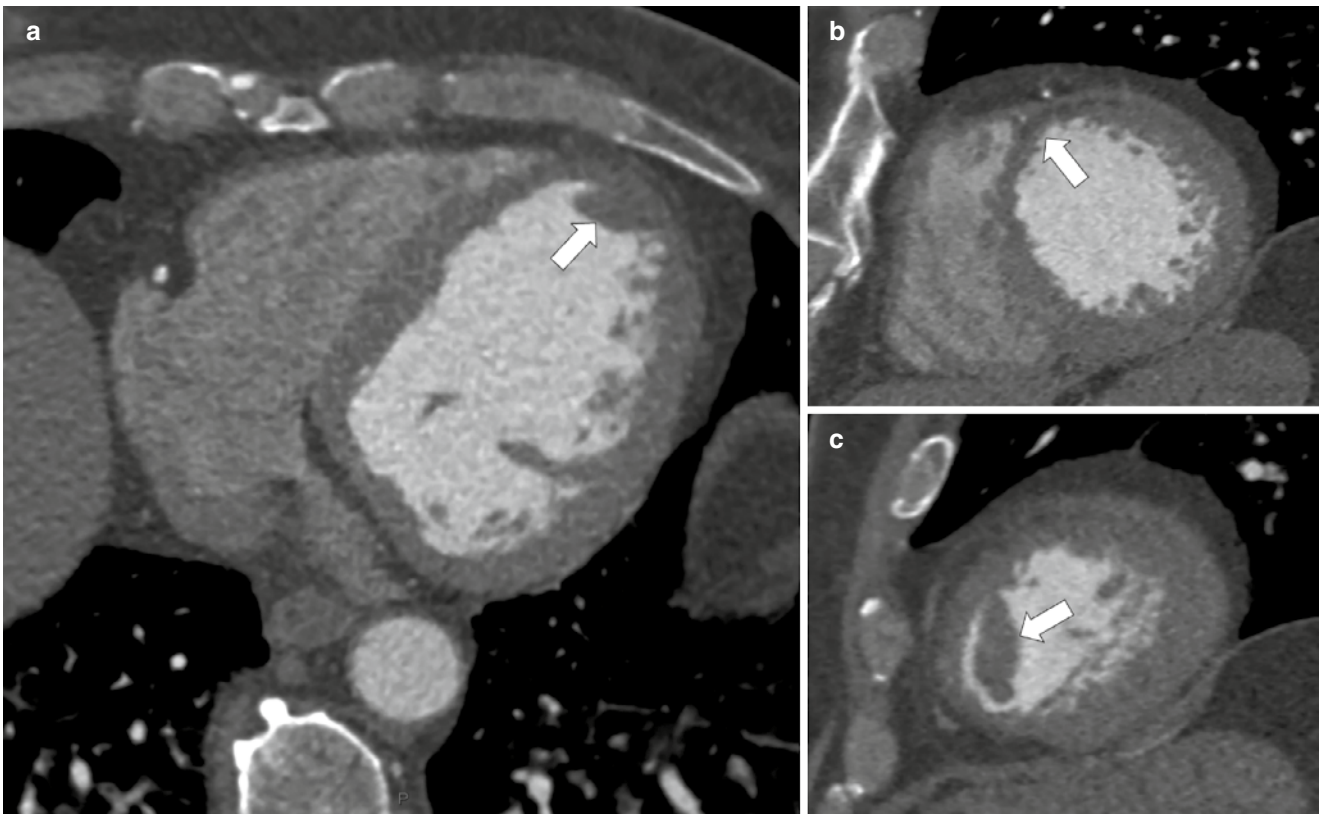


Fig. 11.20 Cardiac CT angiogram images acquired at the same time as the PET/CT showing axial and oblique images. There is an old LAD territory infarct with mural thinning and fatty infiltration (arrow). The thrombus is seen within the LV cavity adjacent to an area of inferior/inferoseptal mural thinning associated with the recent STEMI

Correlative Imaging

- CT coronary angiogram (Fig. 11.20).

Management

- Lifelong anticoagulation.

Further Reading

- E Tzolos, R Bing, J Andrews, M Macaskill, A Tavares, G MacNaught, T Clarke, M C Williams, E J R Van Beek, N Koglin, A Stephens, M R Dweck, D E Newby, In vivo coronary artery thrombus imaging with 18F-GP1 PET-CT,

European Heart Journal, Volume 42, Issue Supplement_1, October 2021.
- Camaj A, Fuster V, Giustino G et al. Left Ventricular Thrombus Following Acute Myocardial Infarction. J Am Coll Cardiol 2022; 79:1010–1022.

11.5.3 Thrombus Imaging of Prosthetic Material: Case 97

Key Points
- ^{18}F-GP1 is a novel radiotracer which detects thrombus formation.
- It is a radiotracer based on elarofiban which binds to the glycoprotein IIb/IIIa receptor on activated platelets.
- It is currently a research radiotracer, but future uses could include identification and quantification of cardiac, valvular, and coronary thrombus.

History
- A 77-year-old patient presented with symptoms of an acute left temporal lobe ischemic stroke.
- They had a past medical history of left ventricle systolic dysfunction with a cardiac resynchronization therapy device (CRT-D) pacemaker in situ.
- As part of a research study, they underwent PET imaging with the radiotracer ^{18}F-GP1.

PET/CT Images

Findings
- ^{18}F-GP1 PET shows radiotracer uptake in activated platelets on thrombus in several positions on the right ventricle and superior vena cava (Fig. 11.21b, d).
- Corresponding CT shows that this was in the location of the pacemaker lead (Fig. 11.21a, c).

Imaging Diagnosis
- ^{18}F-GP1 uptake demonstrated thrombus formation on the pacemaker lead.
- Left temporal lobe ischemic stroke.
- The patent foramen ovale and pacemaker lead-related thrombus suggests a cardioembolic source of the ischemic stroke.

Differential Diagnosis
- None (Fig. 11.22).

Correlative Imaging
- ^{18}F-GP1 PET of the brain shows focal radiotracer uptake in the region of the left temporal lobe infarction (Fig. 11.22b).
- Corresponding CT of the brain showed mild contrast hyperenhancement in this region, in keeping with the sub-

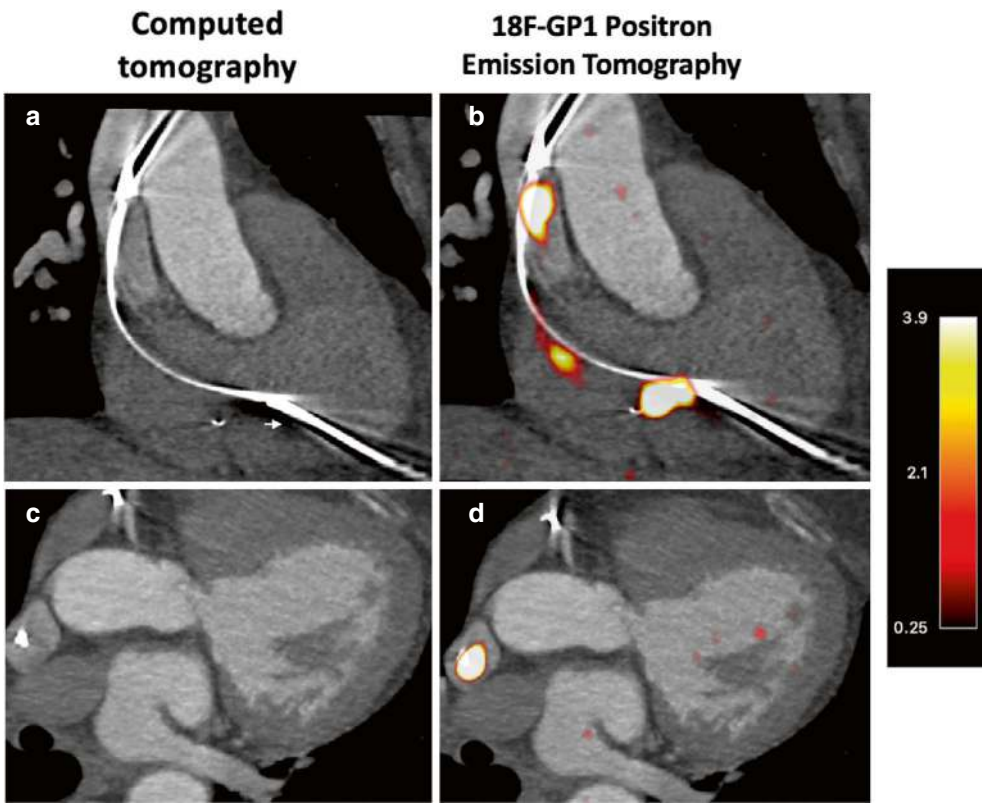


Fig. 11.21 ^{18}F-GP1 PET/CT of the heart. ^{18}F-GP1 PET/CT shows radiotracer uptake in several regions of the right ventricle and in the superior vena cava in keeping with activated platelets and thrombus formation (**b**, **d**). Corresponding electrocardiogram gated contrast enhanced coronary CT angiography showed that this radiotracer uptake was associated with the CRT-D pacemaker lead (**a**, **c**)

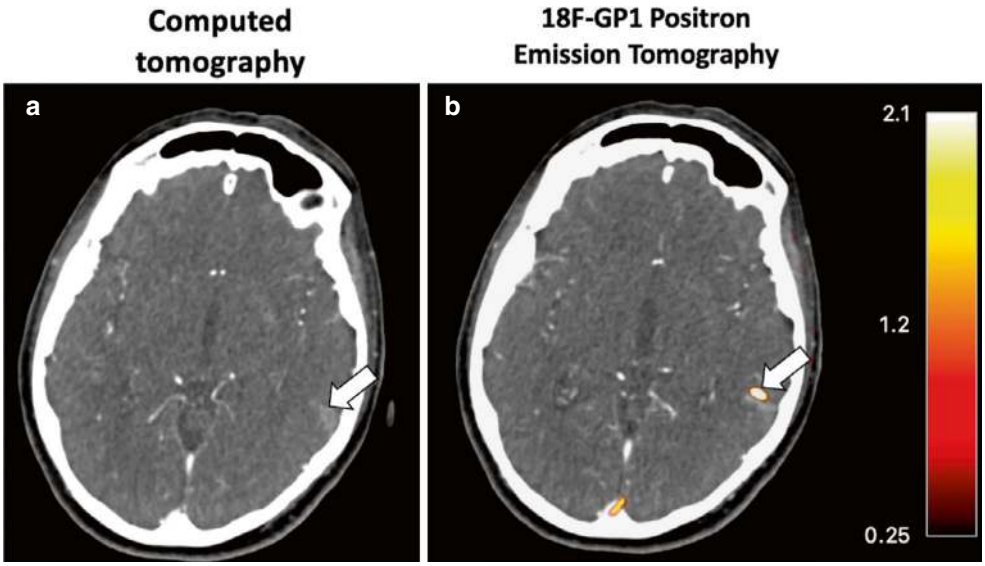


Fig. 11.22 CT of the brain with iodinated contrast showed a left temporal ischemic stroke (**a**, arrow). ^{18}F-GP1 PET/CT shows radiotracer uptake associated with the left temporal ischemic stroke (**b**, arrow) in keeping with activated platelets and thrombus formation associated with the ischemic stroke

acute nature of the stroke at the time of imaging (Fig. 11.22a).
- Cardiac CT showed that the patient had a patent foramen ovale, suggesting a cardioembolic etiology of stroke.
- Subsequent bubble echocardiography demonstrated a patent foramen ovale.

Management
- Lifelong antigoagulation.

Further Reading
- Whittington B, Tzolos E, Bing R, et al. Noninvasive In Vivo Thrombus Imaging in Patients With Ischemic Stroke or Transient Ischemic Attack-Brief Report. Arterioscler Thromb Vasc Biol. 2023 Sep;43(9):1729–1736.

11.5.4 Thrombus Imaging of Prosthetic Valves with ^{18}F-GP1: Case 98

Key Points
- ^{18}F-GP1 is currently a research radiotracer, but future uses could include identification and quantification of cardiac, valvular, and coronary thrombus.

History
- A 65-year-old man underwent a tissue aortic valve replacement and aortic root repair for a bicuspid aortic valve, severe aortic stenosis, and a dilated ascending thoracic aorta.
- He had a history of a transient ischemic attack and was taking clopidogrel, bisoprolol, and simvastatin.
- As part of a research study, he underwent PET/CT imaging with the radiotracer ^{18}F-GP1 6 months after surgery.

PET/CT Images (Figs. 11.23 and 11.24)

Findings
- PET imaging with ^{18}F-GP1 showed radiotracer uptake associated with the prosthetic aortic valve and ascending thoracic aorta in keeping with activated platelet activity and thrombus formation.

Imaging Diagnosis
- Activated platelets and thrombus formation on the prosthetic aortic valve and ascending thoracic aorta.

Differential Diagnosis
- None.

Correlative Imaging
- None.

Management
- There was no change in management based on this research PET/CT.

Further Reading
- Bing R, Deutsch MA, Sellers SL, Corral CA, Andrews JPM, van Beek EJR, et al. 18F-GP1 Positron Emission Tomography and Bioprosthetic Aortic Valve Thrombus. JACC Cardiovasc Imaging. 2022 Jun;15(6):1107–1120.

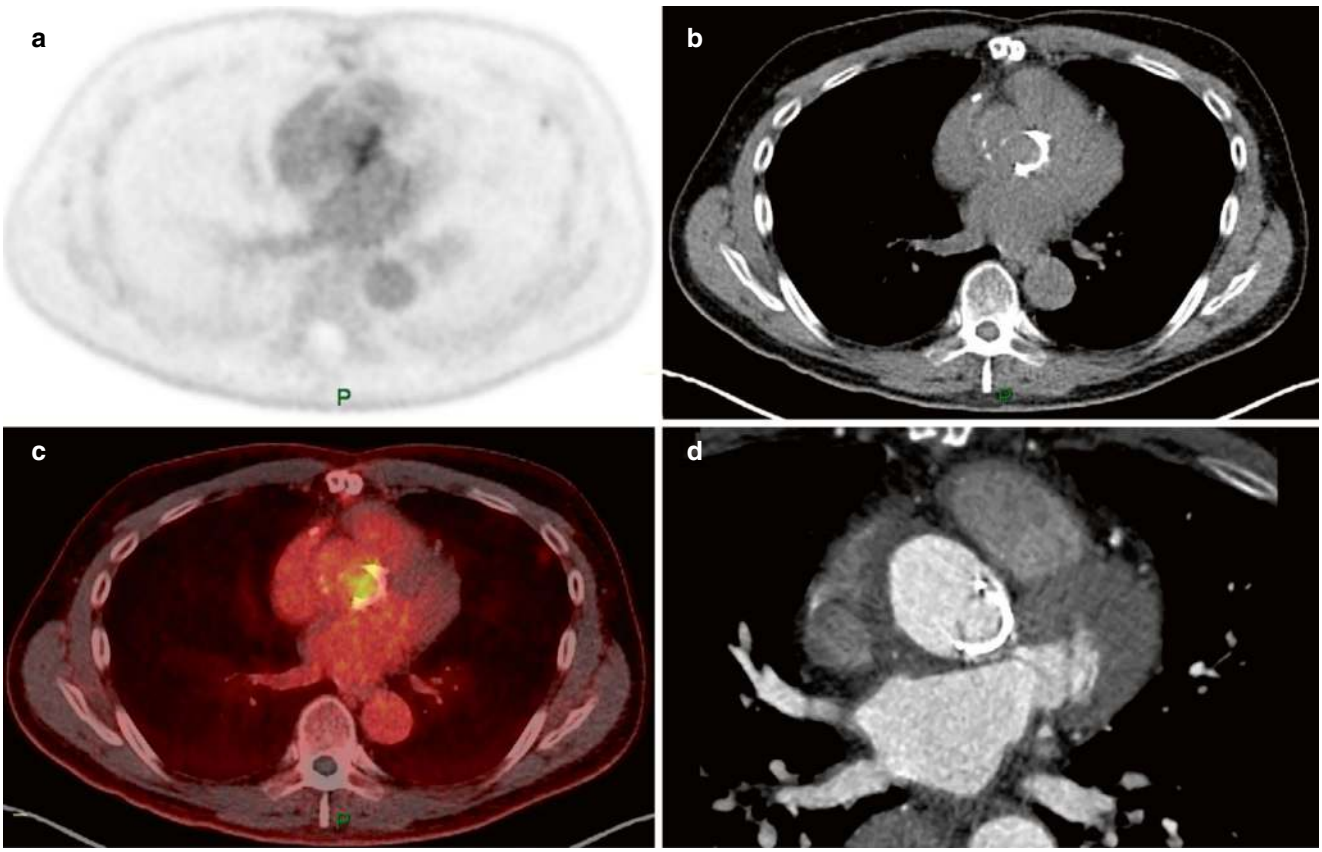


Fig. 11.23 ^{18}F-GP1 PET/CT and CT coronary angiography with axial images of the prosthetic aortic valve. Radiotracer uptake is seen on the PET image (**a**) and fused PET and CT images (**c**) which corresponds to the location of the prosthetic aortic valve seen on non-contrast and contrast-enhanced images (**b**, **d**). SUVmax in the prosthetic valve was 4.65 and in the ascending aorta was 3.67

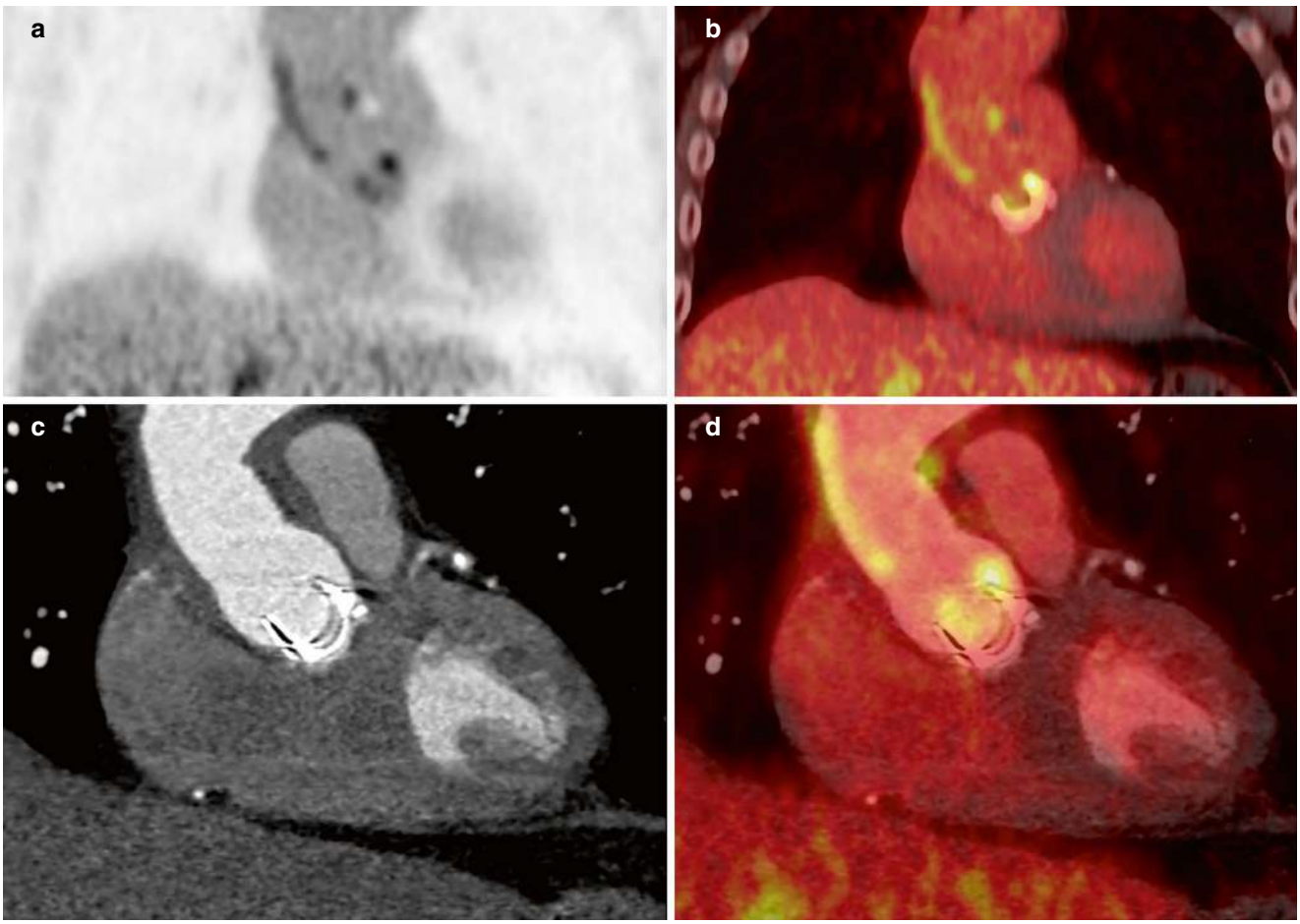


Fig. 11.24 ^{18}F-GP1 PET/CT and CT coronary angiography with coronal images of the prosthetic aortic valve and aortic root repair. Radiotracer uptake is seen on the PET image (**a**), fused PET and non-contrast attenuation correction CT image (**b**) and fused PET and contrast-enhanced CT image (**d**). This corresponds to the location of the prosthetic aortic valve and aortic root repair seen on the contrast-enhanced CT (**c**)

11.6 Fibrosis Imaging

11.6.1 ^{68}Ga-FAPI Fibrosis Imaging in Aortic Valve Disease: Case 99

Key Points

- FAPI binds to fibroblast activation protein which is expressed on the cell surface of activated fibroblasts, the key effector cell of fibrosis formation.
- It is currently a research radiotracer, but future uses in valvular heart disease could include prediction of disease progression and assessment of risk for valve intervention.

History

- A 77-year-old man with hypertension presented with mild exertional chest discomfort and was found to have a systolic murmur.
- A transthoracic echocardiogram confirmed severe aortic stenosis with preserved LV systolic function.
- As part of a research study, he underwent ^{68}Ga-FAPI PET/CT and cardiac MRI.

PET/CT Images (Figs. 11.25 and 11.26)

Findings

- ^{68}Ga-FAPI PET shows radiotracer uptake in the aortic valve. CT shows that this is localized to the right and noncoronary cusps and is in keeping with active fibroblast activity.
- ^{68}Ga-FAPI PET also shows radiotracer uptake in the left ventricular myocardium in keeping with active fibroblast activity.

Correlative Imaging

- Cardiac MRI confirmed presence of preserved LV systolic function, with no areas of late gadolinium enhance-

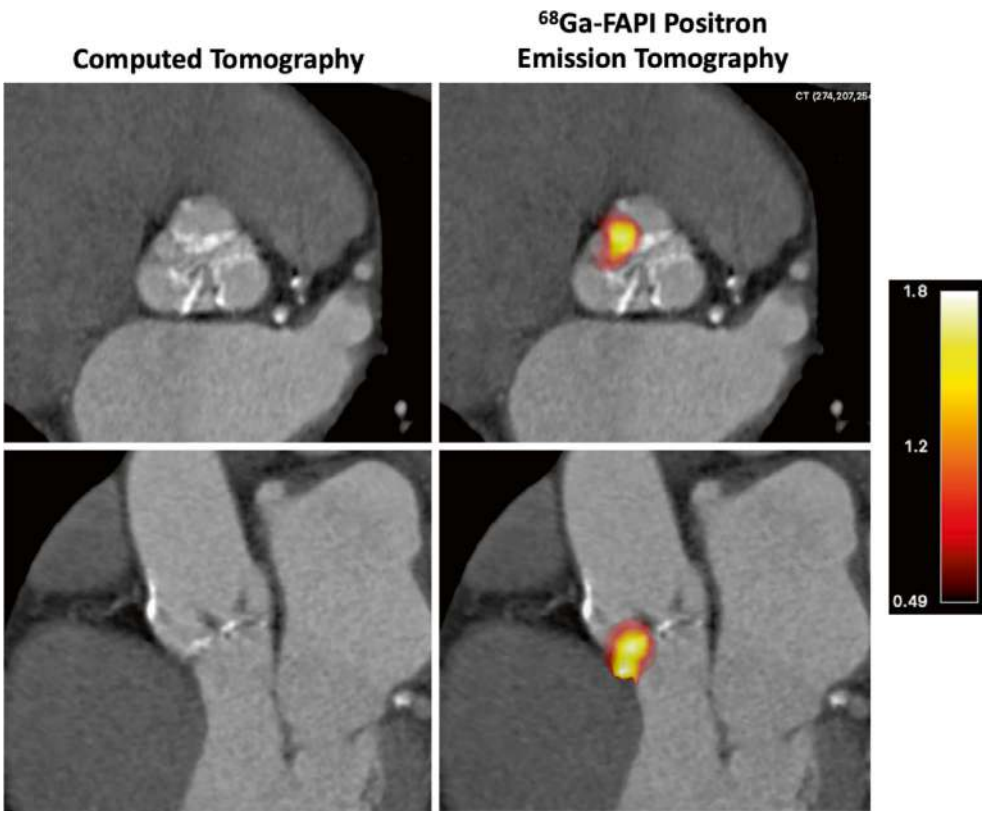


Fig. 11.25 ^{68}Ga-FAPI PET/CT showed radiotracer uptake in the aortic valve. CT shows that this is localized to the right and noncoronary cusps

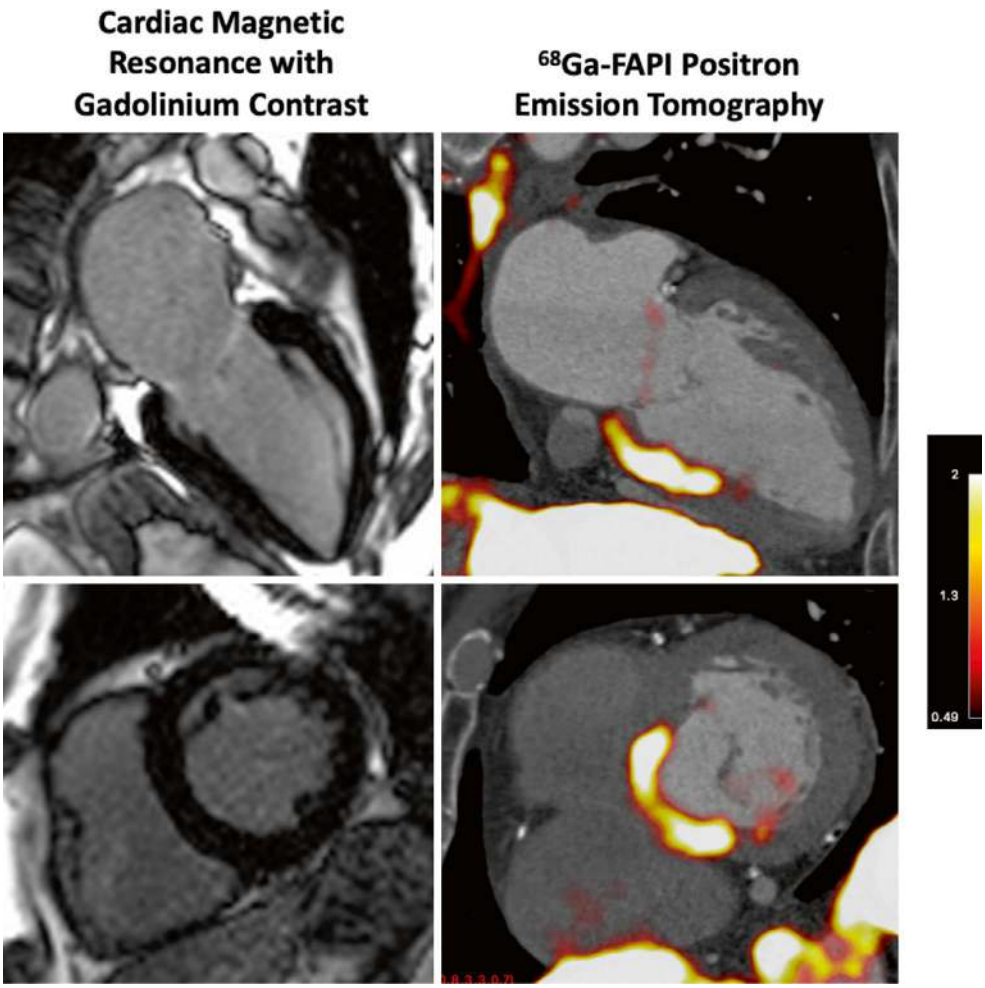


Fig. 11.26 Cardiac MRI and ^{68}Ga-FAPI PET/CT with two chamber and short-axis views of the LV myocardium. ^{68}Ga-FAPI PET/CT showed radiotracer uptake in the LV myocardium. Cardiac MRI showed preserved LV systolic function and no evidence of late gadolinium enhancement in these areas

ment identified. Thus, the ^{68}Ga-FAPI myocardial uptake indicates active early fibroblast activity rather than established fibrosis and scar formation.

Imaging Diagnosis
- Severe aortic stenosis.

Differential Diagnosis
- None.

Management
- The patient was referred for aortic valve replacement surgery.

Further Reading
- Barton AK, Tzolos E, Bing R, Singh T, Weber W, Schwaiger M, et al. Emerging molecular imaging targets and tools for myocardial fibrosis detection, *European Heart Journal - Cardiovascular Imaging 2023:* 24 (3); 261–275.
- Diekmann J, Neuser J, Röhrich M, Derlin T, Zwadlo C, Koenig T, et al. Molecular Imaging of Myocardial Fibroblast Activation in Patients with Advanced Aortic Stenosis Before Transcatheter Aortic Valve Replacement: A Pilot Study. J Nucl Med. 2023 Aug;64(8):1279–1286.

11.6.2 ^{68}Ga-FAPI Imaging of Fibrosis Post-Myocardial Infarction: Case 100

Key Points
- ^{68}Ga-FAPI is currently a research radiotracer with potential in cancer and other disease imaging. Future cardiovascular uses could include identification and quantification of fibrosis in myocardial infarction, infiltrative cardiomyopathies, and other cardiovascular diseases.

History
- A 66-year-old man experienced an anterior ST elevation myocardial infarction 2 years previously.
- He presented with recurrent exertional chest pain and was treated with a stent to his left anterior descending coronary artery.
- As part of a research study, he underwent PET/MRI imaging with the radiotracer ^{68}Ga-FAPI.

PET/CT Images

Findings
- ^{68}Ga-FAPI PET showed radiotracer uptake in the apical anterior segment of the left ventricle myocardium. This is seen on a long-axis view of the left ventricle (Fig. 11.27b) and on the polar map of the left ventricle (Fig. 11.28).
- Quantitative analysis demonstrated a maximum tissue to background ratio (TBRmax) within the infarct of 3.0.

Imaging Diagnosis
- Previous myocardial infarction with ongoing fibroblast activity.

Differential Diagnosis
- Other causes of myocardial fibrosis, such as infiltrative diseases and malignancy.

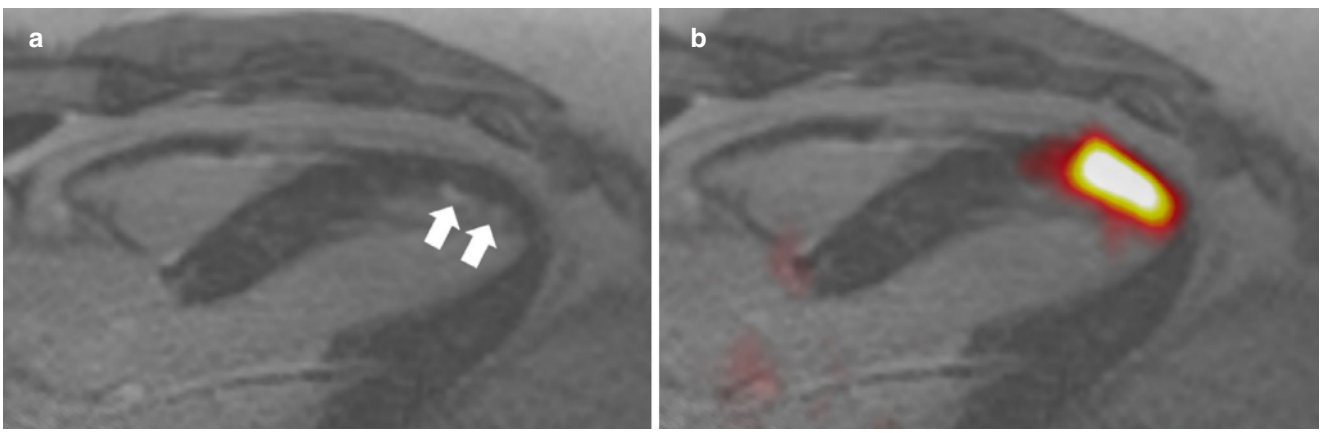


Fig. 11.27 ^{68}Ga-FAPI PET/MRI images from a patient with previous myocardial infarction. Late gadolinium enhancement MRI (**a**) showed a small area of subendocardial late enhancement in the apical anterior segment. Fused PET/MRI (**b**) images showed ^{68}Ga-FAPI radiotracer uptake in the corresponding region

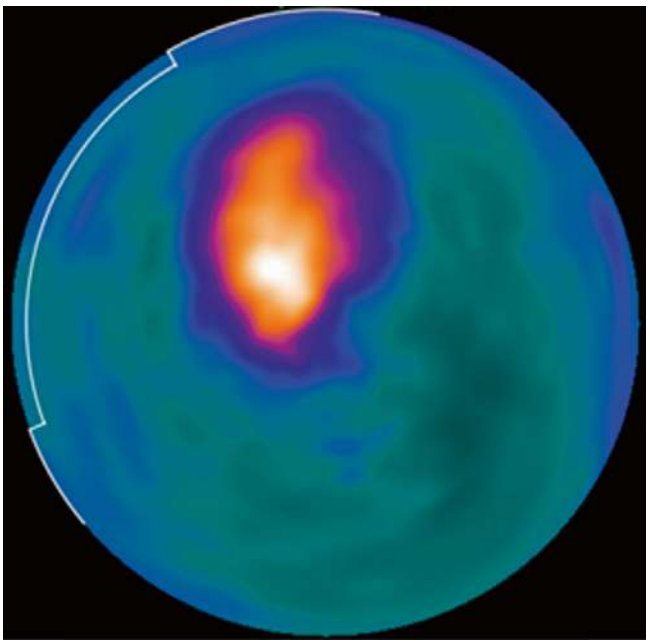


Fig. 11.28 Polar map of the left ventricle PET showing ^{68}Ga-FAPI radiotracer uptake in the apical anterior segments

Correlative Imaging

- Cardiac magnetic resonance imaging (MRI) showed subendocardial late gadolinium enhancement in the apical anterior segment of the left ventricle at the same position as the ^{68}Ga-FAPI PET uptake (Fig. 11.27a).

Management

- There was no change in management based on these findings as part of the research study.
- Ongoing research aims to assess the temporal change in fibrosis additivity after myocardial infarction and its prognostic implications.

Further Reading

- Barton AK, Tzolos E, Bing R, et al. Emerging molecular imaging targets and tools for myocardial fibrosis detection. *Eur Heart J Cardiovasc Imaging*. 2023;24(3):261–275.
- Diekmann J, Koenig T, Thackeray JT, Derlin T, Czerner C, Neuser J, et al. Cardiac Fibroblast Activation in Patients Early After Acute Myocardial Infarction: Integration with MR Tissue Characterization and Subsequent Functional Outcome. J Nucl Med. 2022 Sep;63(9):1415–1423.

11.7 Vascular Inflammation Imaging

11.7.1 Takayasu Arteritis PET/MRI Imaging: Case 101

Key Points

- ^{18}F-FET-bAG-TOCA is a somatostatin receptor binding PET radiotracer.
- Research studies have shown that macrophage expression of somatostatin receptor 2 (SSR_2) is a novel inflammation imaging target for cardiovascular disease.

History

- A 44-year-old woman with a past medical history of Takayasu arteritis, systemic hypertension, and type 2 diabetes mellitus presented with fatigue and night sweats.
- C-reactive protein (CRP) was elevated at 83 (normal range < 3.0 mg/L) and erythrocyte sedimentation rate (ESR) was elevated at 120 mm/hr. (normal range < 35 mm/hr).
- The Indian Takayasu Clinical Activity Score-CRP was 4, indicating clinically active vasculitis.
- ^{18}F-FET-bAG-TOCA PET/MRI imaging was performed as part of a research study.

PET/MR Images

Findings

- ^{18}F-FET-bAG-TOCA PET imaging showed avid radiotracer uptake in the aortic root and ascending thoracic aorta (Fig. 11.29).
- Quantification showed a maximum SUV of 3.3.

Imaging Diagnosis

- Active Takayasu arteritis.

Differential Diagnosis

- Other causes of large vessel vasculitis.

Correlative Imaging

- MRI showed fusiform dilatation of the aorta measuring 4.4 cm in maximum diameter with marked para-aortic thickening (Fig. 11.29).

Management

- Immunosuppression was escalated following clinical assessment.

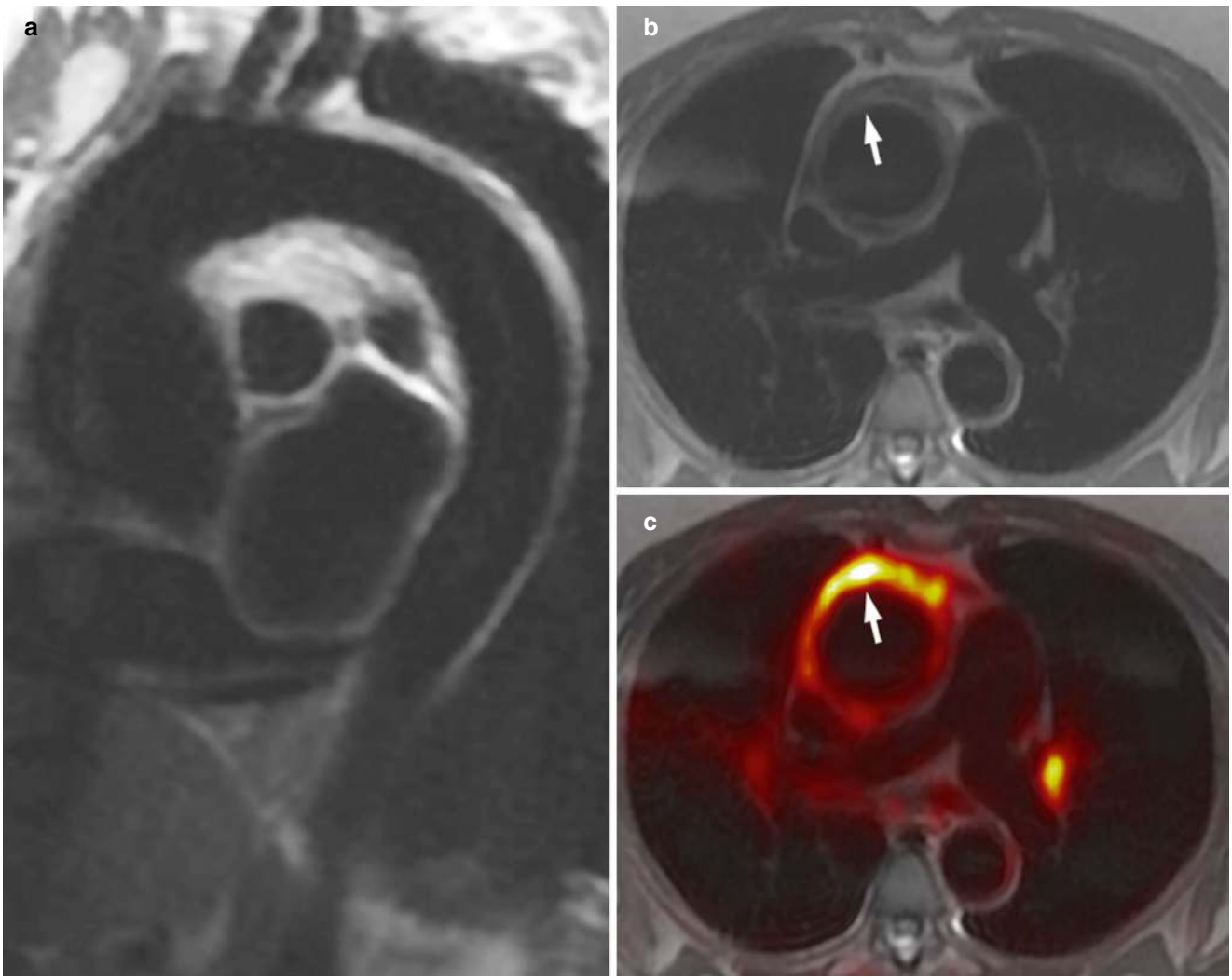


Fig. 11.29 ^{18}F-FET-bAG-TOCA PET/MRI images from a patient with active Takayasu arteritis. Sagittal (**a**) and axial (**b**) views of the thoracic aorta showing dilation and thickening of the ascending thoracic aorta. Fused PET/MRI image (**c**) showing ^{18}F-FET-bAG-TOCA uptake associated with this area of dilation and thickening

- Ongoing research aims to evaluate the clinical efficacy of SST_2 imaging for diagnosis and therapeutic monitoring in large vessel vasculitis.

Further Reading

- Ćorović A, Wall C, Nus M, Gopalan D, Huang Y, Imaz M, Zulcinski et al. Somatostatin Receptor PET/MR Imaging of Inflammation in Patients With Large Vessel Vasculitis and Atherosclerosis. J Am Coll Cardiol 2023;81(4):336–354.

11.7.2 Inflammation After Myocardial Infarction: Case 102

Key Points

- Research studies have shown that targeting macrophage expression of somatostatin receptor 2 (SST_2) with ^{68}Ga-DOTATATE PET can provide a novel marker of cardiovascular inflammation.

History

- A 70-year-old man presented with chest pain and was diagnosed with a late-presentation anterior ST segment elevation myocardial infarction.
- Emergency percutaneous coronary intervention was performed with insertion of a drug-eluting stent to an occluded left anterior descending artery.
- ^{68}Ga-DOTATATE PET/CT imaging and CT coronary angiography was subsequently performed as part of a research study.

PET/MRI Images

Findings

- PET/CT images acquired at 13 days post-infarct demonstrated increased ^{68}Ga-DOTATATE uptake in the infarcted myocardial segments in the mid to apical interventricular septum and anterior walls (Fig. 11.30b, d).

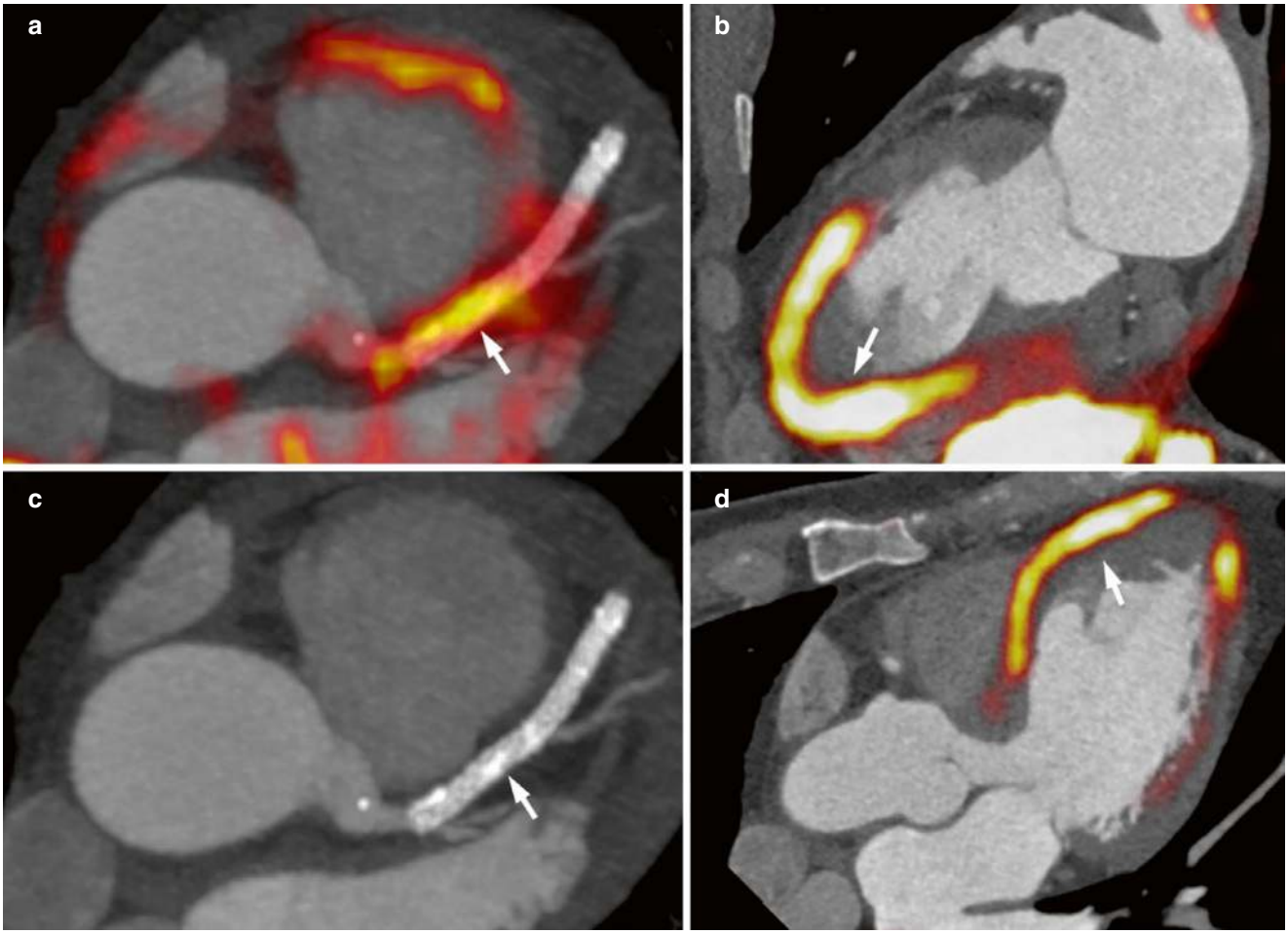


Fig. 11.30 ^{68}Ga-DOTATATE PET/CT images showing increased signal (arrows) in the (**a**, **c**) culprit stented left anterior descending coronary artery and the (**b**, **d**) infarcted left ventricular myocardium

- Quantification of radiotracer uptake in the infarcted myocardial segments showed a maximum SUV of 2.4.
- ^{68}Ga-DOTATATE uptake was also demonstrated in the stented culprit coronary artery (Fig. 11.30a, c).

Imaging Diagnosis
- Recent myocardial infarction with evidence of microvascular obstruction.
- Coronary stent implantation with evidence of ongoing inflammation.

Differential Diagnosis
- None.

Correlative Imaging
- Cardiac MRI showed impaired left ventricular function, with full thickness late gadolinium enhancement in the mid to apical interventricular septum and anterior walls (Fig. 11.31). There was also patchy mid-wall hypoenhancement consistent with microvascular obstruction, and an aneurysmal apex with a small apical thrombus.

Management
- Management was as per the usual clinical care for the treatment of an acute myocardial infarction with associated left ventricle systolic impairment. In addition, the patient received anticoagulation for the left ventricular thrombus.
- There was no change in the clinical management based on ^{68}Ga-DOTATATE PET/CT imaging findings performed for purposes of research.
- Ongoing research is evaluating the use of ^{68}Ga-DOTATATE for detecting residual coronary and infarct-related inflammation after myocardial infarction and its association with longer-term adverse imaging outcomes.

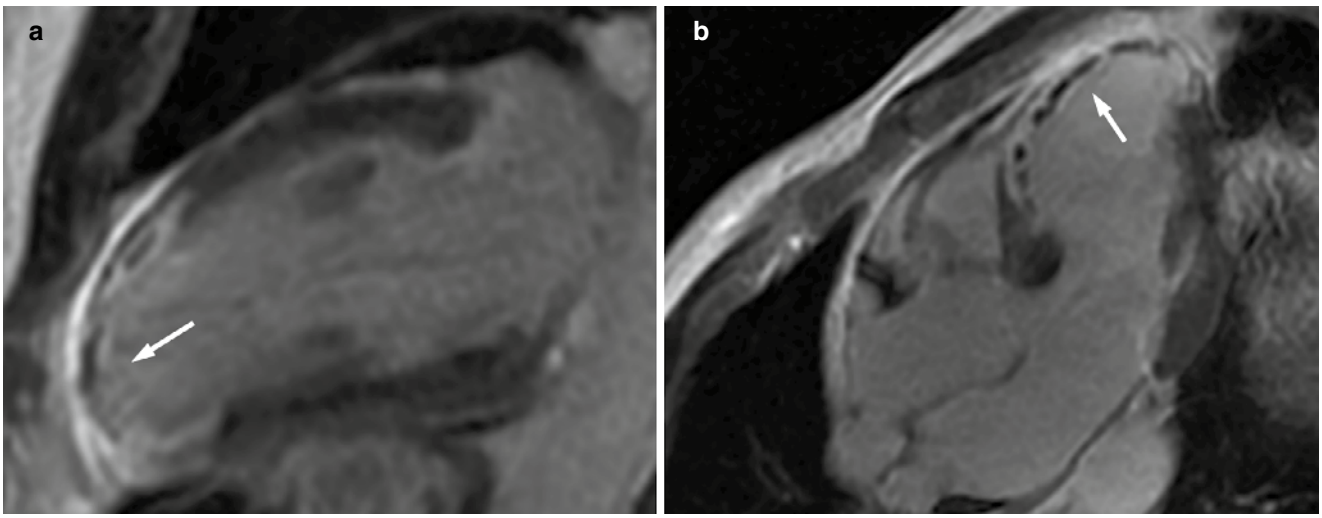


Fig. 11.31 Corresponding late gadolinium enhancement MRI images showing full thickness late gadolinium enhancement in the apical interventricular septum and anterior walls, patchy mid-wall hypoenhancement consistent with microvascular obstruction, and an aneurysmal apex with a small apical thrombus

Further Reading

- Tarkin JM, Joshi FR, Evans NR, Chowdhury MM, Figg NL, Shah AV, et al. Detection of atherosclerotic inflammation by 68Ga-DOTATATE PET compared to 18F-FDG PET imaging. J Am Coll Cardiol 2017;69(14):1774–91.
- Ćorović A, Gopalan D, Wall C, Peverelli M, Hoole SP, Calvert PA, et al. Novel Approach for Assessing Postinfarct Myocardial Injury and Inflammation Using Hybrid Somatostatin Receptor Positron Emission Tomography/Magnetic Resonance Imaging. Circ Cardiovasc Imaging 2023;16(1):e014538.

11.7.3 Lymphocitic Myocarditis: Case 103

Key Points

- Myocarditis should almost always be in the differential diagnosis when cardiac sarcoidosis is suspected as both the clinical presentation (heart failure, ventricular tachycardia) and imaging findings can be similar.

History

- A 47-year-old woman with a history of lymphocytic myocarditis with restrictive cardiomyopathy and chronotropic incompetence requiring dual chamber pacemaker placement was referred for ^{18}F-FDG PET for the evaluation of cardiac sarcoidosis and rest ^{99m}Tc-sestamibi SPECT myocardial perfusion.

PET/CT Images (Figs. 11.32 and 11.33)

Findings

- The rest myocardial perfusion images demonstrated no regional defects.
- The cardiac ^{18}F-FDG images demonstrated intense glucose uptake throughout the anterior and lateral walls of the left ventricular myocardium with less ^{18}F-FDG uptake in the inferior wall and the apex.
- The ECG-gated images demonstrated normal LV systolic function with a rest LVEF of 67% and normal regional wall motion and thickening.
- On the whole-body PET/CT images, there was diffuse increased ^{18}F-FDG uptake in the spleen, but no other areas of abnormal extracardiac ^{18}F-FDG uptake.

Imaging Diagnosis

- Possible active myocardial inflammation.

Differential Diagnosis

- Myocarditis.
- Cardiac sarcoidosis.
- Arrhythmogenic cardiomyopathy.
- Partial suppression of ^{18}F-FDG uptake.

Correlative Imaging

- None.

Management

- The patient eventually underwent biventricular ventricular assist device placement and subsequent successful cardiac transplantation for end-stage restrictive cardio-

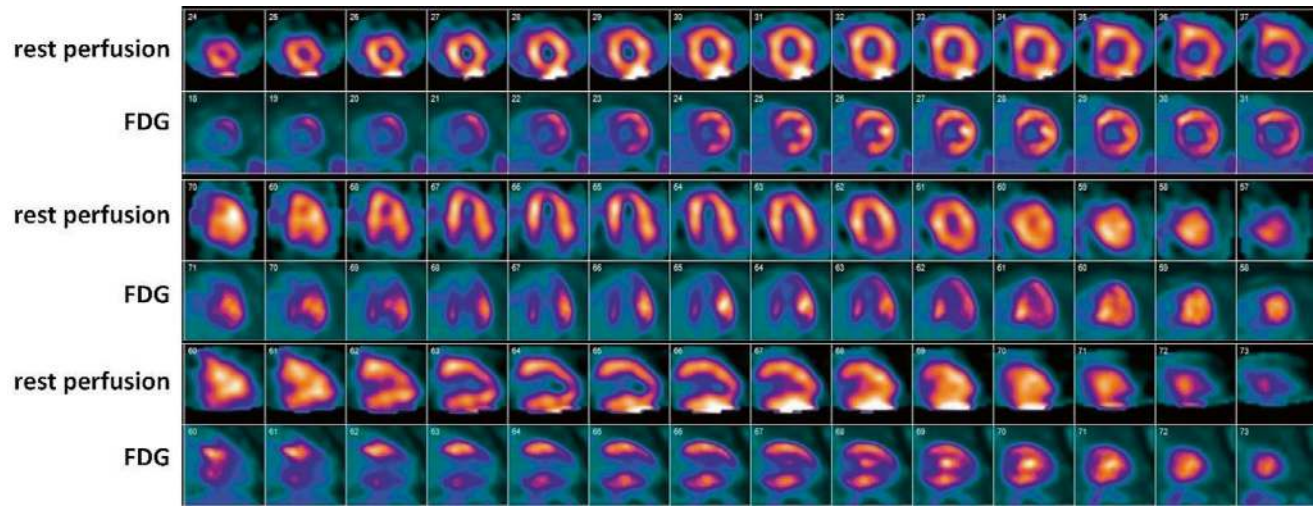


Fig. 11.32 Rest ^{99m}Tc-sestamibi SPECT myocardial perfusion and ^{18}F-FDG PET/CT images. The rest myocardial perfusion images demonstrated no regional defects. The cardiac ^{18}F-FDG images demonstrated intense glucose uptake throughout the anterior and lateral walls of the left ventricular myocardium with less ^{18}F-FDG uptake in the inferior wall and the apex

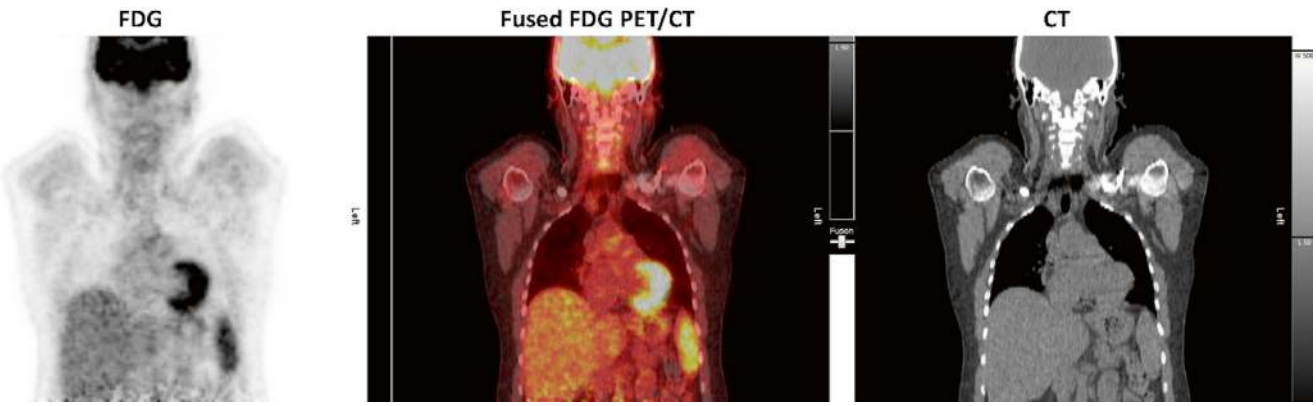


Fig. 11.33 Limited whole-body PET/CT images demonstrating diffuse increased ^{18}F-FDG uptake in the spleen

myopathy. Histology of the explanted heart revealed restrictive cardiomyopathy with biventricular hypertrophy and active myocarditis.

Further Reading

- Vita T, Okada D, Veillet-Chowdhury M, Bravo P, Mullins E, Hulten E, et al. Complementary Value of Cardiac Magnetic Resonance Imaging and Positron Emission Tomography/Computed Tomography in the Assessment of Cardiac Sarcoidosis. Circulation: Cardiovascular Imaging. 2018;11.
- Divakaran S, Stewart G, Lakdawala N, Padera R, Zhou W, Desai A, et al. Diagnostic Accuracy Of Advanced Imaging In Cardiac Sarcoidosis: An Imaging-Histologic Correlation Study In Patients Undergoing Cardiac Transplantation. Journal of the American College of Cardiology. 2019;73:934.

11.8 Imaging of Cardiac Sympathetic Innervation

11.8.1 Denervation in Large Anterior Infarction and Ischemic Cardiomyopathy: Case 104

Key Points

- Cardiac sympathetic nervous dysfunction plays a crucial role in the pathogenesis of several conditions, including myocardial ischemia, arrhythmias, and heart failure.
- Cardiac sympathetic innervation can be investigated by nuclear cardiology imaging by SPECT and PET tracers.
- The extent of sympathetic denervation assessed via 11C-HED PET imaging predicts the risk of sudden cardiac arrest in patients with ischemic cardiomyopathy (see PAREPET trial).

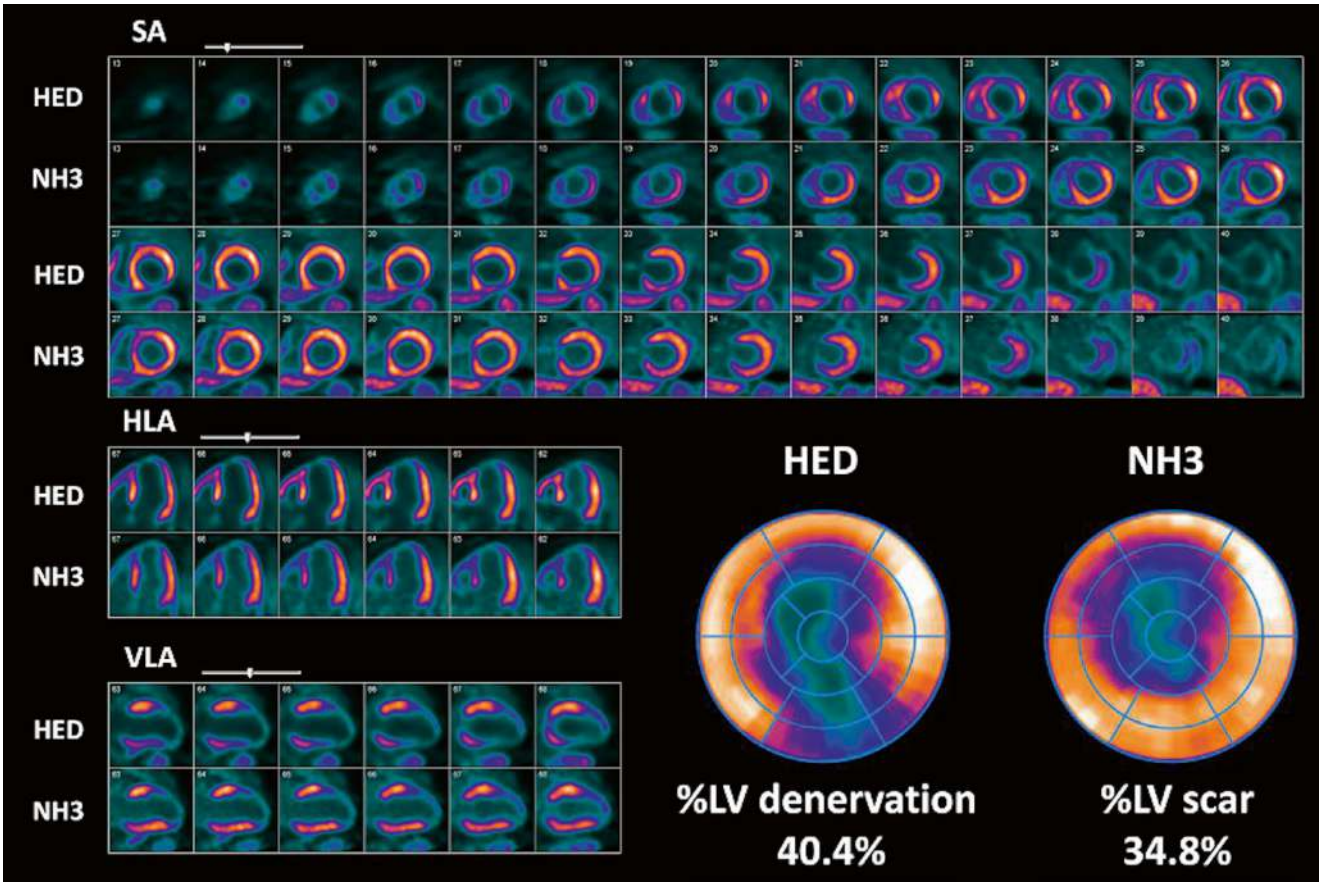


Fig. 11.34 $^{13}NH_3$ PET shows reduced perfusion in the mid to apical anterior segment, mid anteroseptal segment, apical septal and inferior segments, and apex. Uptake defect in the HED study matches perfusion defect

History

A 67-year-old male presented with dyspnea (NYHA class II). Past medical history included myocardial infarction, percutaneous coronary intervention with stenting to LAD and RCA, congestive heart failure, and ICD implantation. Patient medication included ACE inhibitor, beta blocker, aspirin, spironolactone, statin, DPP-4 inhibitor, and metformin.

Transthoracic echocardiography showed LVEF of 38% and an LVEDV (left ventricular end-diastolic volume) (index) of 81 mL/m^2. Coronary angiogram showed patent LAD and RCA stents and severe stenosis in the ramus intermedius artery.

The patient underwent dynamic ^{11}C meta-hydroxyephedrine (^{11}C-HED) and ^{13}N-ammonia ($^{13}NH3$) PET imaging as part of a clinical research study (Fig. 11.34).

PET Imaging Findings

In $^{13}NH3$ PET imaging, there is reduced perfusion in the mid to apical anterior segment, mid anteroseptal segment, apical septal and inferior segments, and apex. This perfusion abnormality has a matching HED defect, consistent with a prior MI.

The RCA territory shows normal myocardial perfusion but reduced HED uptake, suggesting regional functional denervation in an area of viable myocardium.

Clinical Course

Patient experienced VT storm and ICD shock 5 years after the PET imaging.

Further Reading

- Fallavollita JA, Heavey BM, Luisi AJ Jr., Michalek SM, Baldwa S, Mashtare TL Jr., Hutson AD, Dekemp RA, Haka MS, Sajjad M, Cimato TR, Curtis AB, Cain ME, Canty JM Jr. Regional myocardial sympathetic denervation predicts the risk of sudden cardiac arrest in ischemic cardiomyopathy. J Am Coll Cardiol. 2014 Jan 21;63(2):141–9. https://doi.org/10.1016/j.jacc.2013.07.096.

- Wang JZ, Zelt JGE, Kaps N, Lavallee A, Renaud JM, Rotstein B, Beanlands RSB, Fallavollita JA, Canty JM Jr., deKemp RA. Does quantification of [11C]meta-hydroxyephedrine and [13 N]ammonia kinetics improve risk stratification in ischemic cardiomyopathy. J Nucl Cardiol. 2022 Apr;29(2):413–425. doi:10.1007/s12350-021-02732-5. Epub 2021 Aug 2. Erratum in: J Nucl Cardiol. 2021 Oct;28(5):2419–2420. https://doi.org/10.1007/s12350-021-02779-4.

11.8.2 Denervation in Medium-Size Inferolateral Myocardial Infarction: Case 105

Key Points

See previous case.

History

A 91-year-old male presented with shortness of breath (NYHA class II). Past medical history included myocardial infarction treated with stent to the LAD, congestive heart failure, and atrial fibrillation. Cardiac risk factors included hypertension, dyslipidemia, and family history of coronary artery disease. Patient medication included ACE inhibitor, beta blocker, apixaban, furosemide, and statin. Transthoracic echocardiography demonstrated LVEF of 30%. Coronary angiogram showed mild stenoses in the left main (LM), LAD, and RCA.

Patient underwent dynamic ^{11}C meta-hydroxyephedrine (^{11}C-HED) and ^{13}N-ammonia (^{13}NH3) PET imaging as part of a clinical research study (Fig. 11.35).

Findings

There is reduced ^{11}C-HED retention in the inferior and inferolateral walls from apex to base, representing partially viable but denervated myocardium.

Clinical Course

Patient had no episodes of sudden cardiac arrest until he passed away from noncardiac reasons.

Further Reading

- Zelt JGE, Wang JZ, Mielniczuk LM, Beanlands RSB, Fallavollita JA, Canty JM Jr., deKemp RA. Positron

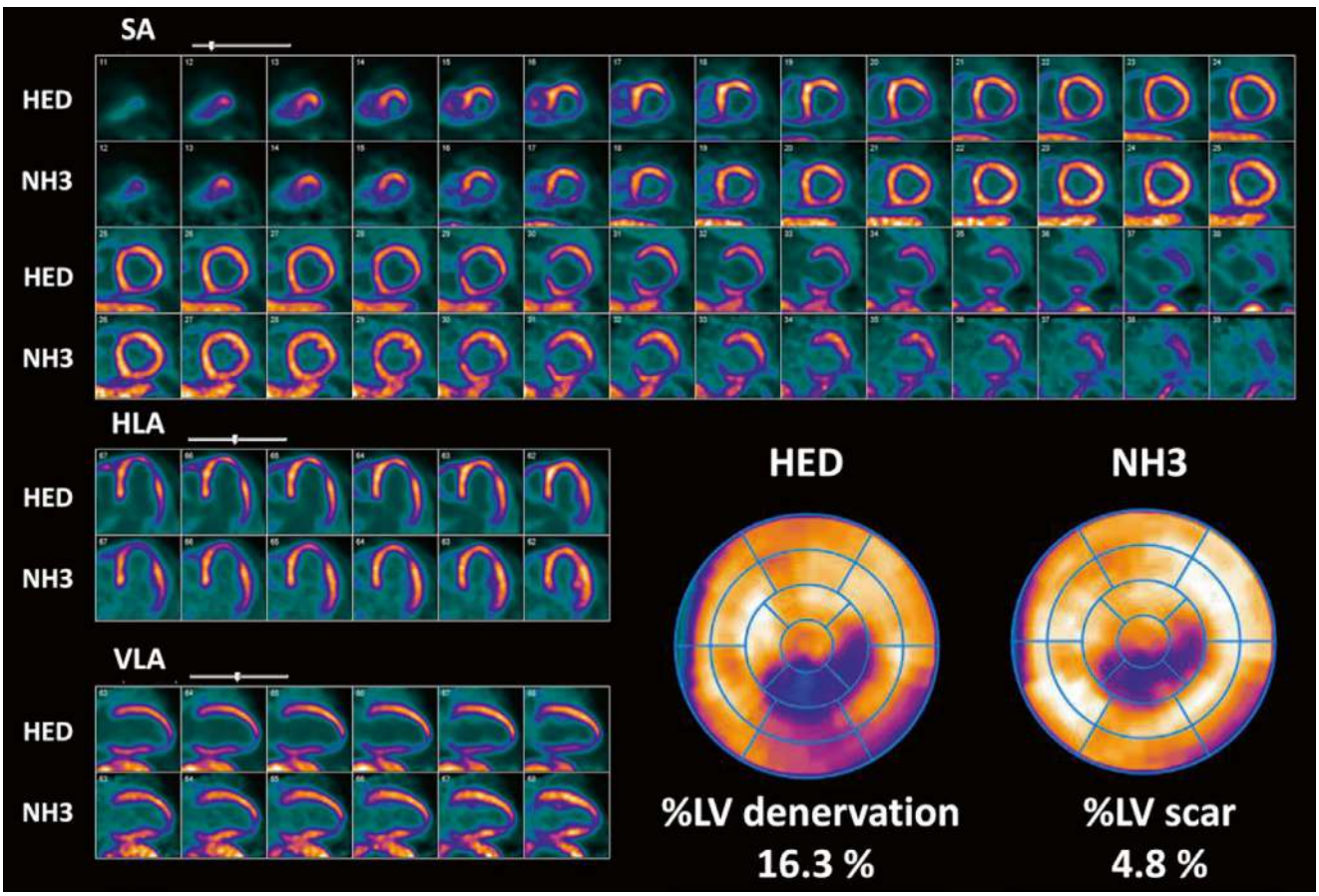


Fig. 11.35 Study with ^{11}C-HED shows reduced retention in the inferior and inferolateral walls from apex to base

Emission Tomography Imaging of Regional Versus Global Myocardial Sympathetic Activity to Improve Risk Stratification in Patients With Ischemic Cardiomyopathy. Circ Cardiovasc Imaging. 2021 Jun;14(6):e012549. https://doi.org/10.1161/CIRCIMAGING.121.012549.

- Fallavollita JA, Heavey BM, Luisi AJ Jr., Michalek SM, Baldwa S, Mashtare TL Jr., Hutson AD, Dekemp RA, Haka MS, Sajjad M, Cimato TR, Curtis AB, Cain ME, Canty JM Jr. Regional myocardial sympathetic denervation predicts the risk of sudden cardiac arrest in ischemic cardiomyopathy. J Am Coll Cardiol. 2014 Jan 21;63(2):141–9. https://doi.org/10.1016/j.jacc.2013.07.096.
- Zelt JGE, Britt D, Mair BA, Rotstein BH, Quigley S, Walter O, Garrard L, Robinson S, Mielniczuk LM, deKemp RA, Beanlands RS. Regional Distribution of Fluorine-18-Flubrobenguane and Carbon-11-Hydroxyephedrine for Cardiac PET Imaging of Sympathetic Innervation. JACC Cardiovasc Imaging. 2021 Jul;14(7):1425–1436. https://doi.org/10.1016/j.jcmg.2020.09.026.
- Wang JZ, Zelt JGE, Kaps N, Lavallee A, Renaud JM, Rotstein B, Beanlands RSB, Fallavollita JA, Canty JM Jr., deKemp RA. Does quantification of [11C]meta-hydroxyephedrine and [13 N]ammonia kinetics improve risk stratification in ischemic cardiomyopathy. J Nucl Cardiol. 2022 Apr;29(2):413–425. doi:10.1007/s12350-021-02732-5. Epub 2021 Aug 2. Erratum in: J Nucl Cardiol. 2021 Oct;28(5):2419–2420. https://doi.org/10.1007/s12350-021-02779-4.

11.9 Total Body PET

11.9.1 Cardioembolic Stroke: Case 106

Key Points

- Total-body PET imaging has the potential to improve assessment of multi-territory cardiovascular diseases.

History

A 63-year-old female with infective endocarditis developed symptoms of ischemic stroke and multiple emboli. She took part in a research study where she underwent total-body PET/CT with the thrombus radiotracer ^{18}F-GP1, along with CT head, carotid CT carotid angiogram, coronary CT angiogram, and CT lower limb venogram.

Imaging Findings (Figs. 11.36 and 11.37)

Imaging Diagnosis

- Infective endocarditis with multiple emboli including the brain and digits.
- Deep vein thrombosis.

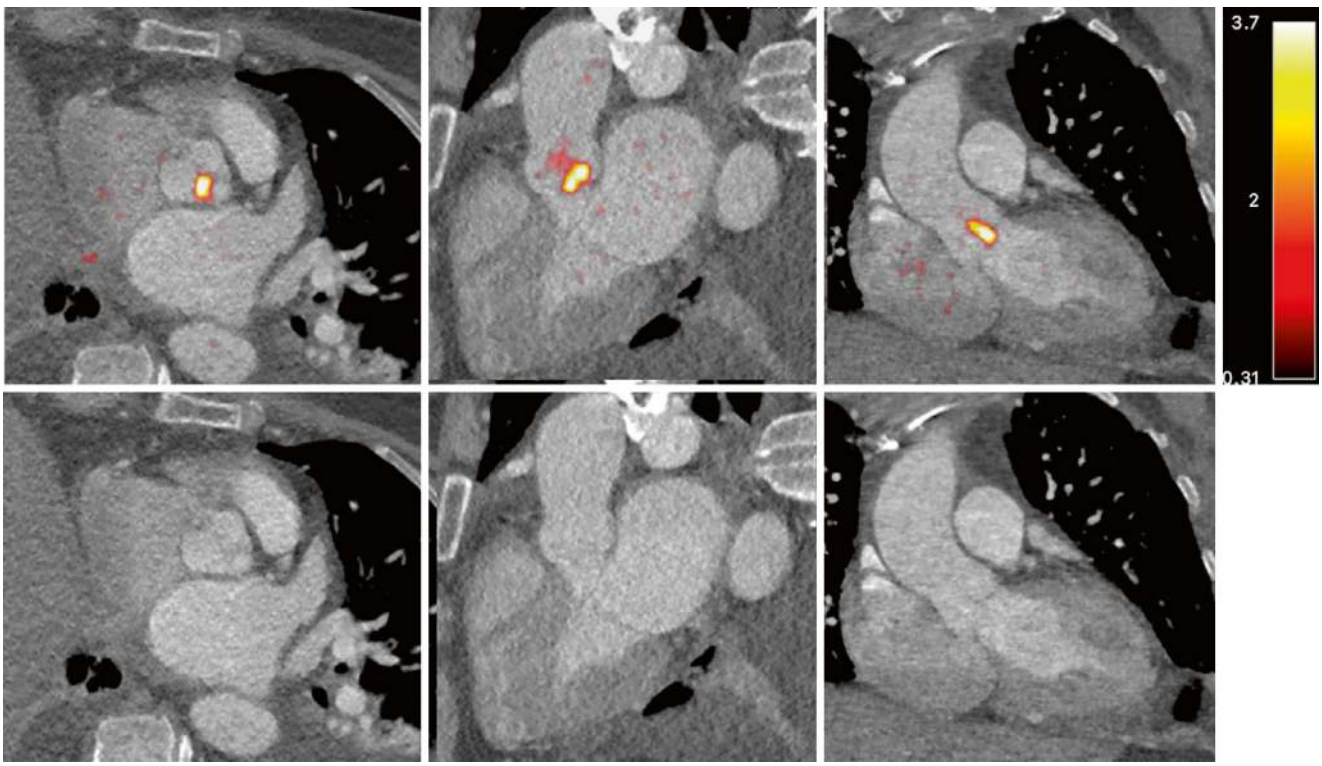


Fig. 11.36 Fused ^{18}F-GP1 PET/CT images (top line) and coronary CT angiogram images (bottom line) showing radiotracer uptake associated with the aortic valve

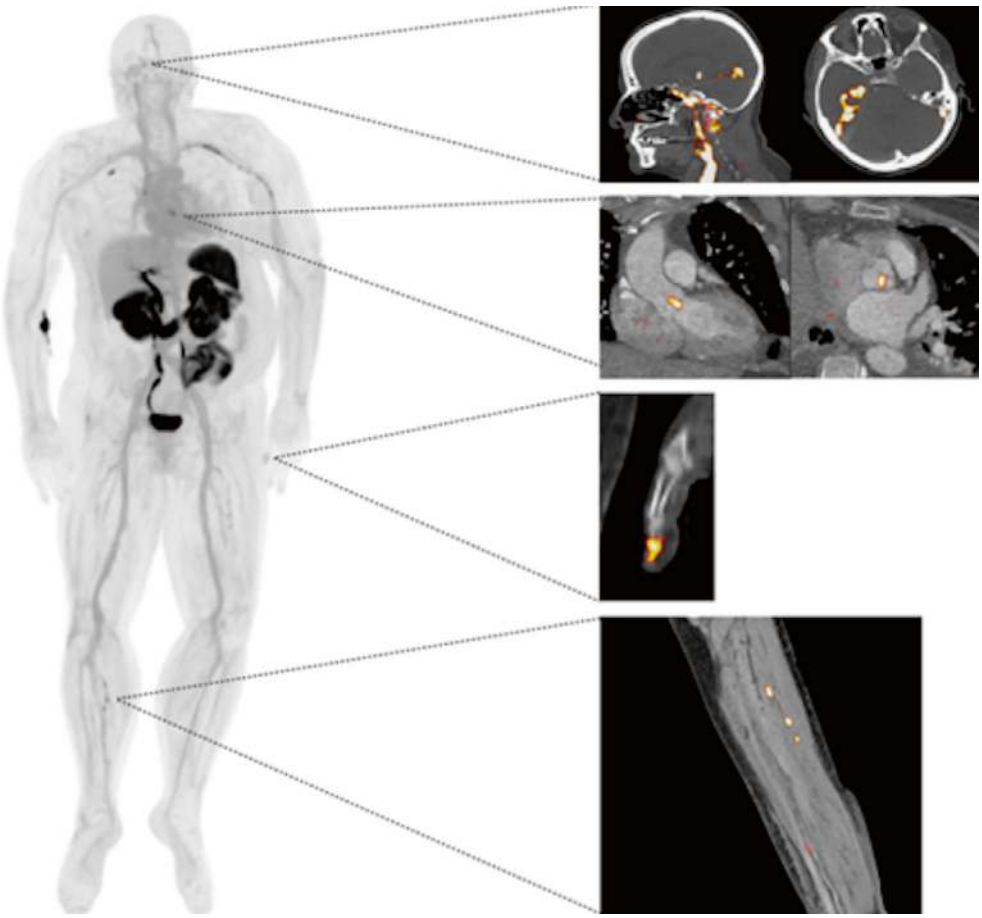


Fig. 11.37 Total-body PET imaging identified radiotracer uptake in keeping with thrombus associated with the ischemic stroke, aortic valve, digital embolus, and a deep vein thrombosis

Differential Diagnosis

None.

Further Reading

- Slart RHJA et al. Total-Body PET/CT Applications in Cardiovascular Diseases: A Perspective Document of the SNMMI Cardiovascular Council. Journal of Nuclear Medicine Apr 2024, 65 (4) 607–616.

The opinions expressed in this chapter are those of the author(s) and do not necessarily reflect the views of the IAEA: International Atomic Energy Agency, its Board of Directors, or the countries they represent.

Open Access This chapter is licensed under the terms of the Creative Commons Attribution 3.0 IGO license (http://creativecommons.org/licenses/by/3.0/igo/), which permits use, sharing, adaptation, distribution and reproduction in any medium or format, as long as you give appropriate credit to the IAEA: International Atomic Energy Agency, provide a link to the Creative Commons license and indicate if changes were made.

Any dispute related to the use of the works of the IAEA: International Atomic Energy Agency that cannot be settled amicably shall be submitted to arbitration pursuant to the UNCITRAL rules. The use of the IAEA: International Atomic Energy Agency's name for any purpose other than for attribution, and the use of the IAEA: International Atomic Energy Agency's logo, shall be subject to a separate written license agreement between the IAEA: International Atomic Energy Agency and the user and is not authorized as part of this CC-IGO license. Note that the link provided above includes additional terms and conditions of the license.

The images or other third party material in this chapter are included in the chapter's Creative Commons license, unless indicated otherwise in a credit line to the material. If material is not included in the chapter's Creative Commons license and your intended use is not permitted by statutory regulation or exceeds the permitted use, you will need to obtain permission directly from the copyright holder.

